e-ISSN 2149-6366

Cilt 11, Sayı 2, Haziran 2022
Volume 11, Number 2, June 2022

# TDFD
## TÜRK DOĞA ve FEN DERGİSİ

**TURKISH JOURNAL OF NATURE AND SCIENCE**

# TJNS

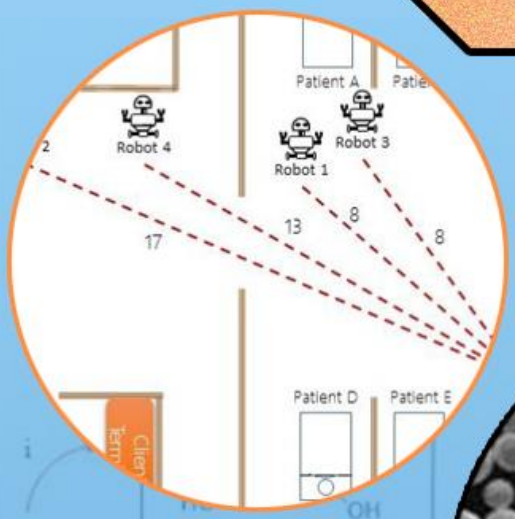


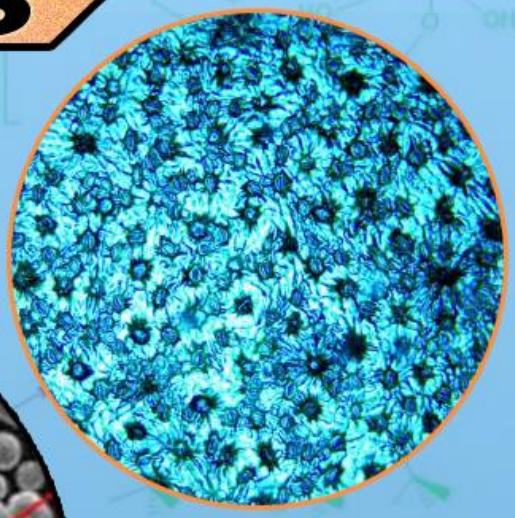

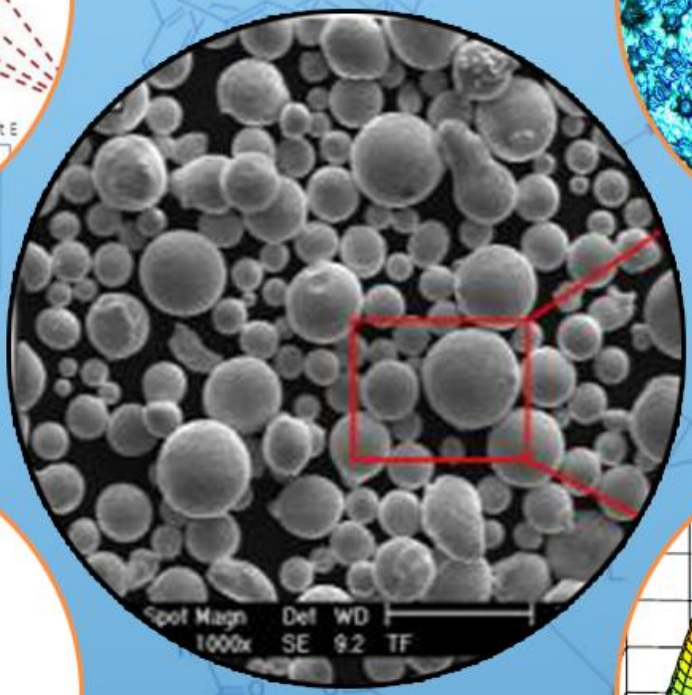


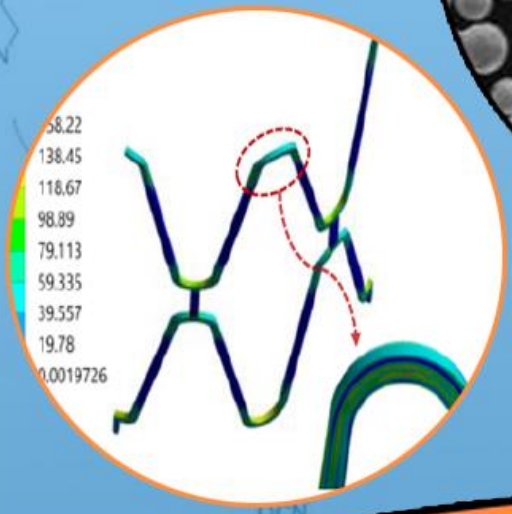


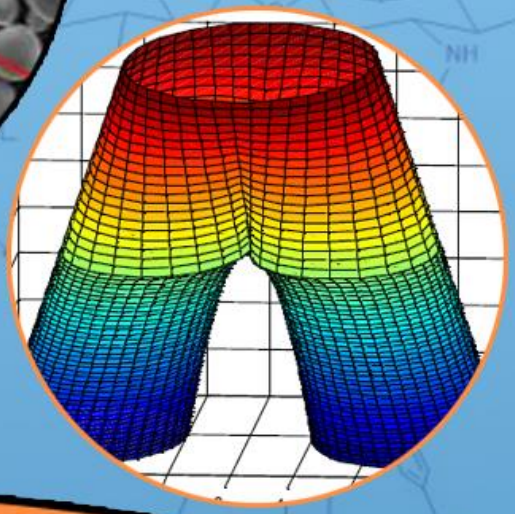

www.dergipark.gov.tr/tdfd

Bingöl Üniversitesi Fen Bilimleri Enstitüsü tarafından yayımlanmaktadır.
Published by Bingol University Institute of Science

# TÜRK DOĞA VE FEN DERGİSİ

## Amaç

Türk Doğa ve Fen Dergisi, Dergipark tarafından yayınlanan Bingöl Üniversitesi Fen Bilimleri Enstitüsüne ait ulusal ve hakemli bir dergidir. Türk Doğa ve Fen Dergisi, Türkiye ve dünyanın her yerinden gelen doğa ve fen bilimlerinin her alanında özgün, yayımlanmamış, yayımlanmak üzere başka yere gönderilmemiş makale, derleme ve sempozyum değerlendirmesi gibi çalışmaların bilim alemine sunulması amacıyla kurulmuştur.

## Kapsam

Türk Doğa ve Fen Dergisinde Mühendislik, Ziraat, Veterinerlik, Fen ve Doğa Bilimleri alanlarından olmak üzere Türkçe ve İngilizce hazırlanmış orijinal makale, derleme ve sempozyum değerlendirmesi gibi çalışmalar yayımlanır. Türk Doğa ve Fen Dergisi sadece online sistemde yayınlanmakta olup ayrıca kağıt baskısı bulunmamaktadır.

## *Merhaba…*

Türk Doğa ve Fen Dergisi, Dergipark tarafından yayınlanmakta olup Bingöl Üniversitesi Fen Bilimleri Enstitüsüne aittir. Bahar ve güz dönemi olmak üzere yılda iki defa çıkarılan ulusal hakemli bir dergi olarak ilk sayısını 2012 bahar döneminde yayımlamıştır. Türk Doğa ve Fen Dergisi, Türkiye ve dünyanın her yerinden gelen doğa ve fen bilimlerinin her alanında özgün, yayımlanmamış, yayımlanmak üzere başka yere gönderilmemiş makale, derleme ve sempozyum değerlendirmesi gibi çalışmaların bilim alemine sunulması amacıyla kurulmuştur. İlk sayısından bugüne kesintisiz olarak faaliyetlerini sürdürmektedir.

Türk Doğa ve Fen Dergisi sadece online sistemde yayınlanmakta olup ayrıca kağıt baskısı bulunmamaktadır. Dergimize gelen her çalışma öncelikle Turnitin intihal programında taranmaktadır. Dergimizde editörlerin, hakemlerin ve yazarların, uluslararası yayım etik kurallarına uyması ve makalelerin yazım kurallarına uyumlu olması zorunluluğu vardır.

Yazarlar yayımlanmak üzere dergimize gönderdikleri çalışmaları ile ilgili telif haklarını zorunlu olarak Bingöl Üniversitesi Türk Doğa ve Fen Dergisi'ne devretmiş sayılırlar. Yazarlardan herhangi bir ücret talep edilmemektedir. Yazarların değerlendirmeleri, dergimizin resmi görüşü olarak kabul edilemez. Çalışmaların her türlü sorumluluğu yazarlarına aittir. Araştırma ürünleri için etik kurul raporu gerekli ise, çalışma üzerinde bu raporun alınmış olduğu belirtilmeli ve kurul raporu sisteme kaydedilmelidir. Araştırma ile ilgili intihal, atıf manipülasyonu, sahte veri uydurma vb. suistimallerin tespit edilmesi halinde yayım ve etik ilkelerine göre davranılır. Bu durumda çalışmanın yayımlanmasını önlemek, yayımdan kaldırmak ya da başka işlemler yapmak için gerekli işlemler takip edilmektedir.

Dergimizde, kaynak gösteriminde uluslararası Vancouver sistemine geçilmiştir. Ayrıca dergimiz, Creative Commons ile lisanslanmak suretiyle dergimizde yayımlanan makalelerin paylaşımı, kaynak gösterimi ve yayımlanmasında dergi ve yazar haklarını korumaya almıştır. 2018 yılı güz döneminden itibaren makaleler, uluslararası yazar kimlik numarası ORCID No'su ile yayımlanmaktadır.

Dergi ekibi, dergimizin ulusal ve uluslararası indekslerce taranan bir dergi olması yönünde çalışmalarını titizlikle sürdürmektedir. Dergimize gösterilen ilgi bu yönde bizleri teşvik etmeye devam edecektir.

Bingöl Üniversitesi Fen Bilimleri Enstitüsü tarafından yayımlanmaktadır

# EDİTÖRLER (YAYIN) KURULU

**Prof. Dr. Zafer ŞİAR**

Bingöl Üniversitesi, Fen-Edebiyat Fakültesi, Matematik Bölümü
E-Mail: zsiar@bingol.edu.tr

**Prof. Dr. Uğur ÇAKILCIOĞLU**

Munzur Üniversitesi, Pertek Sakine Genç Meslek Yüksekokulu, Bitki Morfolojisi ve Anatomisi Bölümü
E-Mail: ucakilcioglu@yahoo.com

**Doç. Dr. Kamuran DİLSİZ**

Bingöl Üniversitesi, Fen-Edebiyat Fakültesi, Fizik Bölümü
E-Mail: kdilsiz@bingol.edu.tr

**Doç. Dr. Şükran KONCA**

Bakırçay Üniversitesi, Mühendislik ve Mimarlık Fakültesi, Temel Bilimler, Matematik Bölümü
E-Mail: sukran.konca@bakircay.edu.tr

**Doç. Dr. İdris YAZGAN**

Kastamonu Üniversitesi, Fen Edebiyat Fakültesi, Biyoloji

E-Mail: idrisyazgan@gmail.com

**Doç. Dr. Abdulcabbar YAVUZ**

Gaziantep Üniversitesi, Mühendislik Fakültesi, Metalurji ve Malzeme Mühendisliği
E-Mail: ayavuz@gantep.edu.tr

**Doç. Dr. Bünyamin ALIM**

Bayburt Üniversitesi, Teknik Bilimler Meslek Yüksekokulu, Elektrik ve Enerji Bölümü
E-Mail: balim@bayburt.edu.tr

**Dr. Öğr. Üyesi Mustafa Şükrü KURT**

Erzurum Teknik Üniversitesi, Fen Fakültesi, Temel Bilimler
E-Mail: mustafa.kurt@erzurum.edu.tr

**Dr. Öğr. Üyesi Sinan SAĞIR**

Karamanoğlu Mehmetbey Üniversitesi, Fizik

E-Mail: sinansagir@kmu.edu.tr / sinan.sagir@cern.ch

**Dr. Öğr. Üyesi Murat AYDEMİR**

Erzurum Teknik Üniversitesi, Fen Fakültesi, Temel Bilimler

E-Mail: murat.aydemir@erzurum.edu.tr

## Mühendislik Bilimleri

**Doç. Dr. Özgür ÖZGÜN**

Bingöl Üniversitesi, Sağlık Bilimleri Fakültesi, İş Sağlığı ve Güvenliği Bölümü
E-Mail: oozgun@bingol.edu.tr

**Prof. Dr. Figen KOREL**

İzmir Yüksek Teknoloji Enstitüsü, Gıda Mühendisliği Bölümü
E-Mail: figenkorel@iyte.edu.tr

**Prof. Dr. Kubilay ASLANTAŞ**

Afyon Kocatepe Üniversitesi, Teknoloji Fakültesi, Makine Mühendisliği Bölümü
E-Mail: aslantas@aku.edu.tr

**Prof. Dr. Hamit Özkan GÜLSOY**

Marmara Üniversitesi, Teknoloji Fakültesi, Metalurji ve Malzeme Mühendisliği Bölümü
E-Mail: ogulsoy@marmara.edu.tr

**Prof. Dr. Ali Adnan HAYALOĞLU**

İnönü Üniversitesi, Mühendislik Fakültesi, Gıda Mühendisliği Bölümü
E-Mail: adnan.hayaloglu@inonu.edu.tr

**Prof. Dr. Barbara SAWICKA**

University of Life Sciences in Lublin, Department of Plant Production Technology and Commodities Sciences
E-Mail: barbara.sawicka@gmail.com

**Prof. Dr. İbrahim GÜNEŞ**

Giresun Üniversitesi, Mühendislik Fakültesi, İnşaat Mühendisliği Bölümü
E-Mail: ibrahim.gunes@giresun.edu.tr

**Doç. Dr. Sırma YEĞİN**

Ege Üniversitesi, Mühendislik Fakültesi, Gıda Mühendisliği Bölümü
E-Mail: sirma.yegin@ege.edu.tr

**Doç. Dr. Hasan OĞUL**

Sinop Üniversitesi, Mimarlık ve Mühendislik Fakültesi, Nükleer Enerji Mühendisliği
E-Mail: hogul@sinop.edu.tr

**Doç. Dr. Murat YILMAZTEKİN**

İnönü Üniversitesi, Mühendislik Fakültesi, Gıda Mühendisliği Bölümü
E-Mail: murat.yilmaztekin@inonu.edu.tr

**Doç. Dr. Ferhat AYDIN**

Sakarya Uygulamalı Bilimler Üniversitesi, Teknoloji Fakültesi, İnşaat Mühendisliği Bölümü
E-Mail: ferhata@subu.edu.tr

**Dr. Öğr. Üyesi Nurullah DEMİR**

Bingöl Üniversitesi, Mühendislik ve Mimarlık Fakültesi, Gıda Mühendisliği Bölümü
E-Mail: ndemir@bingol.edu.tr

**Dr. Öğr. Üyesi Ahmet GÜNER**

Bingöl Üniversitesi, Mühendislik ve Mimarlık Fakültesi, Elektrik ve Elektronik Mühendisliği Bölümü
E-Mail: aguner@bingol.edu.tr

**Dr. Öğr. Üyesi Tahir AKGÜL**

Sakarya Uygulamalı Bilimler Üniversitesi, Teknoloji Fakültesi, İnşaat Mühendisliği Bölümü
E-Mail: tahirakgul@subu.edu.tr

**Dr. Erhan Sulejmani**

University of Tetova, Faculty of Food Technology and Nutrition
E-Mail: erhan.sulejmani@unite.edu.mk

**Dr. Hacène Medjoudj**

Larbi Ben M'Hidi University of Oum El Bouaghi, Food Science Department
E-Mail: medjoudjh@yahoo.com

**Dr. Avinash Lakshmikanthan**

Nitte Meenakshi Institute of Technology, Department of Mechanical Engineering, Karnataka, India
E-Mail: avinash.laks01@gmail.com

**Dr. Manjunath Patel GC**

PES Institute of Technology and Management, Department of Mechanical Engineering, Karnataka, India
E-Mail: manju09mpm05@gmail.com

## Sağlık Bilimleri

**Doç. Dr. Aydın Şükrü BENGÜ**

Bingöl Üniversitesi, Sağlık Hizmetleri Meslek Yüksekokulu, Tıbbi Hizmetler ve Teknikler
E-Mail: abengu@bingol.edu.tr

**Dr. Öğr. Üyesi Dilhun Keriman ARSERİM UÇAR**

Bingöl Üniversitesi, Sağlık Bilimleri Fakültesi, Beslenme ve Diyetetik Bölümü
E-Mail: dkucar@bingol.edu.tr

**Dr. Öğr. Üyesi Abdullah TUNÇ**

Bingöl Üniversitesi, Sağlık Bilimleri Fakültesi, İş Sağlığı ve Güvenliği Bölümü
E-Mail: atunc@bingol.edu.tr

**Dr. Öğr. Üyesi Ramazan GÜNDOĞDU**

Bingöl Üniversitesi, Sağlık Hizmetleri Meslek Yüksekokulu, Eczane Hizmetleri
E-Mail: rgundogdu@bingol.edu.tr

**Dr. Alexander HERGOVICH**

UCL Cancer Institute, Faculty of Medical Sciences, Department of Cancer Biology, UCL, London, UK
E-Mail: a.hergovich@uc.ac.uk

**Dr. Valenti GOMEZ**

UCL Cancer Institute, Faculty of Medical Sciences, Department of Oncology, UCL, London, UK
E-Mail: valentin.gomez@ucl.ac.uk

## Veterinerlik Bilimleri

**Doç. Dr. Cüneyt ÇAĞLAYAN**

Bingöl Üniversitesi, Veteriner Fakültesi, Temel Bilimler Bölümü
E-Mail: ccaglayan@bingol.edu.tr

**Prof. Dr. Fatih Mehmet KANDEMİR**

Atatürk Üniversitesi, Veteriner Fakültesi, Veteriner Hekimliği Temel Bilimler
E-Mail: fmehmet.kandemir@atauni.edu.tr

**Doç. Dr. Akın KIRBAŞ**

Bozok Üniversitesi, Veteriner Fakültesi, Klinik Bilimler Bölümü
E-Mail: akindahiliye55@yahoo.com

**Doç. Dr. Emrah Hicazi AKSU**

Atatürk Üniversitesi, Veteriner Fakültesi, Klinik Bilimler Bölümü
E-Mail: emrahaksu@atauni.edu.tr

## Ziraat Bilimleri

**Prof. Dr. Kağan KÖKTEN**

Bingöl Üniversitesi, Ziraat Fakültesi, Tarla Bitkileri Bölümü
E-Mail: kahafe1974@yahoo.com

**Prof. Dr. Mustafa SÜRMEN**

Adnan Menderes Üniversitesi, Ziraat Fakültesi, Tarla Bitkileri Bölümü
E-Mail: mustafa.surmen@adu.edu.tr

**Prof. Dr. Banu YÜCEL**

Ege Üniversitesi, Ziraat Fakültesi, Hayvan Yetiştirme Anabilim Dalı, Zootekni Bölümü
E-Mail: banu.yucel@ege.edu.tr

**Doç. Dr. Hakan İNCİ**

Bingöl Üniversitesi, Ziraat Fakültesi, Zootekni Bölümü
E-Mail: hinci@bingol.edu.tr

## TEKNİK EDİTÖRLER

**Dr. Mücahit ÇALIŞAN**

Bingöl Üniversitesi, Teknik Bilimler Meslek Yüksekokulu, Bilgisayar Teknolojileri
E-Mail: mcalisan@bingol.edu.tr

**Dr. Ersin KARAKAYA**

Bingöl Üniversitesi, Ziraat Fakültesi, Tarım Ekonomisi Bölümü
E-Mail: karakayaersin1982@gmail.com

**Dr. Nimetullah KORKUT**

Bingöl Üniversitesi, BİNUZEM, Bilgisayar Teknolojileri
E-Mail: nkorkut@bingol.edu.tr

## DİL EDİTÖRÜ

**Öğr. Gör. Ahmet KESMEZ**
Bingöl Üniversitesi, Yabancı Diller Yüksekokulu, İngilizce Bölümü
E-Mail: akesmez@bingol.edu.tr

Türk Doğa ve Fen Dergisi
Turkish Journal of Nature and Science
www.dergipark.gov.tr/tdfd

## İÇİNDEKİLER/CONTENTS

| | |
|---|---|
| **Kanser Dostu MEIS Proteinleri**<br><br>**Büşra ÇİMEN[1], Abdullah ASLAN[1*]**<br><br>[1] Fırat Üniversitesi, Fen Fakültesi, Biyoloji Bölümü, Moleküler Biyoloji ve Genetik Programı, Elazığ, Türkiye<br>Büşra ÇİMEN ORCID No: 0000-0003-3415-3390<br>Abdullah ASLAN ORCID No: 0000-0002-6243-4221<br><br>**Sorumlu yazar: aaslan@firat.edu.tr*<br><br>(Alınış: 15.09.2021, Kabul: 21.03.2022, Online Yayınlanma: 29.06.2022) | **156** |

Araştırma Makalesi https://doi.org/10.46810/tdfd.954171 Research Article

Türk Doğa ve Fen Dergisi
Turkish Journal of Nature and Science
www.dergipark.gov.tr/tdfd

# Bilecik Koşullarında Yetiştirilen Sofralık Domateste Farklı Sulama Seviyeleri ve Malç Uygulamasının Net Gelire Etkisi

**Murat KARAER[1*], Hayrettin KUŞÇU[2], Hüseyin T. GÜLTAŞ[1]**

[1]Bilecik Şeyh Edebali Üniversitesi, Ziraat ve Doğa Bilimleri Fakültesi, Biyosistem Mühendisliği Bölümü, Bilecik, Türkiye
[2]Bursa Uludağ Üniversitesi, Ziraat Fakültesi, Biyosistem Mühendisliği Bölümü, Bursa, Türkiye
Murat KARAER ORCID No: 0000-0002-1920-181X
Hayrettin KUŞÇU ORCID No: 0000-0001-9600-7685
Hüseyin T. GÜLTAŞ ORCID No: 0000-0002-4987-8522

**Sorumlu yazar: murat.karaer@bilecik.edu.tr*

(Alınış: 18.06.2021, Kabul: 09.03.2022, Online Yayınlanma: 29.06.2022)

**Anahtar Kelimeler**
Domates, Malç, Ekonomik su kullanım etkinliği, Net gelir

**Öz:** Bu çalışma, 2017 yetiştirme döneminde Bilecik Şeyh Edebali Üniversitesi Araştırma ve Uygulama alanında, sofralık domateste farklı sulama seviyeleri ve malç uygulamasının ekonomik su kullanım etkinliği ile net gelire olan etkilerini araştırmak için yapılmıştır. Araştırma, tesadüf bloklarında bölünmüş parseller deneme desenine göre 3 tekrarlı olarak ana parselleri 2 malç uygulaması [malç (M) ve malçsız (NM)], alt parselleri ise 4 sulama konusu oluşturacak şekilde kurulmuştur. Sulamalar A-Sınıfı Buharlaşma Kabı'na göre 4 farlı pan katsayısı (1,00, 0,75, 0,50, 0,25 ×A pan) uygulanarak yapılmıştır. Çalışma sonucunda en yüksek verim I100×M konusundan 72.56 t ha-1, en yüksek ekonomik su kullanım etkinliği ise 22,52 TL m-3 olarak elde edilmiştir. Birim hacim sulama suyuna karşılık elde edilen net gelir 8,53 TL m-3 ve birim alandan elde edilen net gelir ise 40662,4 TL ha-1 olarak hesaplanmıştır. Çalışma sonucunda sulama suyu seviyelerinden bağımsız olarak malç uygulanan konulardan daha yüksek ekonomik su kullanım etkinliği ve net gelir elde edilmiştir.



# The Effect of Different Irrigation Levels and Mulch Application on Net Income in Table Tomatoes Grown in Bilecik Conditions

**Keywords**
Tomatoes, Mulch, Economic water use efficiency, Net income

**Abstract:** This study was carried out to investigate the effects of different irrigation levels and mulch application on economic water use efficiency and net income in table tomatoes in Bilecik Şeyh Edebali University Research and Application area during the 2017 growing season. The research was designed as a split-plot design with 3 replications and the main plots were consist of two mulch application [mulch(M) and no mulch (NM)] and sub-parcels were consist of four irrigation levels. Irrigation was done according to Class A evaporation pan and four different pan coefficient were used (1.00, 0.75, 0.50, 0.25 ×Epan). As a result of the study, the highest yield was obtained from I100×M parcels as 72.56 t ha-1. The highest economic water use efficiency was obtained as 22.52 TL m-3. The highest net income obtained from the unit area was calculated as 40662.4 TL ha-1 and the net income obtained against the unit volume of irrigation water was calculated as 8.53 TL m-3. As a result of the study, higher economic water use efficiency and net income were obtained mulched parcels regardless of irrigation water levels.

## 1. GİRİŞ

Domates (Solanum lycopersicum L.), patlıcangiller (Solanoceae) familyasından, anavatanı Güney ve Orta Amerika olan ve insan beslenmesinde yaygın olarak kullanılan tek yıllık bir sebze türüdür. Domates yüksek besin özelliklerinin yanı sıra tarımsal sanayiye entegre olan önemli bir ticari üründür. Taze tüketimi yanında farklı kullanım alanlarıyla işlenmiş gıda ürünü olarak da tüketilmekte ve bu ürünlerin hammaddeleri olarak kullanılmaktadır. Önemli bir ticari ürün olan domates dünyada da en çok üretimi yapılan yaş sebze olarak 1.

sırada yer almaktadır. Domatesin yaklaşık 4,7 milyon ha alanda tarımı yapılmakta ve 182,3 milyon tonluk bir verim elde edilmektedir. Domatesten sonra dünyada en çok üretimi yapılan sebzeler olarak kuru soğan, hıyar, lahana ve patlıcan gelmektedir [1].

Dünyada olduğu gibi Türkiye'de de domates en çok üretimi yapılan yaş sebzedir. Dünyada Çin ve Hindistan'dan sonra en çok üretim alanına sahip 3. ülke, üretim miktarı olarak ise Çin, Hindistan ve ABD'den sonra 4. sırada yer almaktadır [1]. Türkiye'nin hemen hemen her bölgesinde yetiştiriciliği yapılan domateste, 2019 yılında 173 bin ha alanda yaklaşık 12,8 milyon ha'lık üretim yapılmıştır [2].

Türkiye'de domates üretimi her bölgede yapılmakla birlikte yoğun olarak Akdeniz ve Ege bölgelerinde yetiştirilmekte ve bunu Marmara bölgesi izlemektedir. Sofralık domates yetiştiriciliği daha çok Akdeniz bölgesinde, sanayilik domates üretimi ise Marmara ve Ege bölgesinde yaygın bir şekilde yapılmaktadır. Türkiye'nin sanayilik domates ihtiyacının yaklaşık %84'lük kısmı da Marmara ve Ege bölgesinden karşılanmaktadır [3].

Su, birçok tarımsal ürünün en önemli girdisidir ve bitki verim ve kalitesini doğrudan etkileyebilmektedir. Kış aylarında bitkiler su isteklerini yağışlarla karşılamakta fakat yaz aylarında düşen yağışlar çoğunlukla bitkiler için yeterli olmamakta ve bitkinin su isteğini karşılamamaktadır. Bu nedenle, karlı bir üretim yapmak için sulama zorunlu bir gereksinim haline dönüşmektedir. Fakat son yıllardaki küresel su sıkıntısı da göz önüne alındığında; sulama yaparken verimde önemli kayıplar yaşamadan, tarımsal su kullanım etkinliğini arttırmak için uygun bir sulama programının hazırlanması ve sulama suyunda kısıtlamaya gidilmesi gerektiği zorunlu olmaktadır. Kısıntılı sulama uygulamaları, domateste olduğu gibi bazı meyve kalitesi özelliklerini artırırken verim kayıplarına da neden olabilmektedir. Kısıntılı sulamanın yanında uygulanacak farklı yöntemlerle su kullanım etkinliğini de arttırmak mümkün olmaktadır. Bu uygulamalardan birisi de malç uygulamasıdır.

Malç uygulaması toprak yüzeyinde oluşan buharlaşmayı azaltarak su kullanım randımanını yükseltebilmektedir. Malçlamanın, topraktaki nemin muhafaza etmesi, erkencilik sağlaması, yabancı ot kontrolünün daha kolay yapılması ve daha temiz meyve elde edilmesi ve buna benze birçok önemli faydaları vardır [4]. Malç malzemesi olarak inorganik ve organik materyaller kullanılabilmektedir. Malç uygulamasıyla birlikte topraktaki su muhafaza edilmekte ve suyun buharlaşmasını %10-50 arasında veya daha fazla oranda azaltabilmektedir [5-6].

Sebze yetiştiriciliğinde kullanılan malçların hem toprakta hem de yetiştirilen ürünlerde birçok yönden fayda sağladığı yapılan bilimsel araştırmalarda ortaya konulmuştur [4,7,8,9,10,11,12-13]. Malç uygulamasının verimi arttırmasıyla gelirde önemli bir oranda artış elde edilirken, girdi maliyetlerinin önemli bir kısmında da azalma meydana gelebilmektedir.

Birçok araştırmacıda yaptıkları çalışmalarda kısıntılı sulamanın verim kayıplarına neden olabileceğini fakat malç uygulamasıyla birlikte verimin arttığını ve eksik sulamanın neden olduğunu kayıpların malç uygulamasıyla birlikte giderilebileceğini ortaya koymuşlardır [14,15,16,17,18-19].

Bu çalışma, Bilecik koşullarında 2017 yılında sofralık domates üzerinde yapılmıştır. Araştırmada, damla sulama ile farklı sulama seviyeleri ve malç uygulamasının ekonomik su kullanım etkinliği ile birim sulama suyu hacmine göre net gelir üzerine olan etkilerinin karşılaştırması yapılmıştır..

## 2. MATERYAL VE METOT

Tarla denemeleri Bilecik ilinde yer alan Bilecik Şeyh Edebali Üniversitesi, Tarımsal Uygulama ve Araştırma Merkezine bağlı alanda 2017 yetiştirme döneminde yürütülmüştür. Araştırma alanı killi-tınlı bir toprak yapısına sahiptir. Bilecik bölgesi iklimi geçit tipi özelliği göstermekte ve Marmara ile İç Anadolu iklimi karışık halde görülmektedir. Uzun yıllık meteorolojik verilere göre, yağış ortalaması 453,9 mm, sıcaklık ortalaması ise 12,5 °C'dir. Denemenin yapıldığı aylarda toplam yağış 94,7 mm, ortalama sıcaklık ise 21,06 °C olarak gerçekleşmiştir.

Araştırma bölünmüş bloklar deneme desenine göre 3 tekrarlı olarak kurulmuştur. Ana konuları malç uygulamaları alt konuları da sulama suyu seviyeleri oluşturmuştur. Sulama konuları tablo 1'de verilmiştir. Çalışmada, sulama suyunun hesaplanmasında, A-Sınıfı Buharlaşma Kabı'ndan yararlanılmış ve sulamalar 5 gün aralıklarla düzenli olarak damla sulama yöntemiyle yapılmıştır. Sulama suyu miktarı, konulu sulama uygulamalarının başlamasını takiben her sulama öncesinde Eşitlik 1 yardımıyla hesaplanmıştır [20].

$$I = kc \times kp \times Ep \times P \times A \quad (1)$$

Eşitlikte, I: Sulama suyu miktarı (lt), kp: Deneme konusuna ilişkin katsayı, kc: Bitki katsayısı, Ep: A-Sınıfı Buharlaşma Kabı'nda meydana gelen yığışımlı buharlaşma miktarı (mm), P: Islatılan alan, A: Parsel alanı (m2) değerlerini göstermektedir.

Eşitlikteki kc katsayı gelişme dönemlerine göre farklılık göstermiştir. Başlangıç periyodunda 0,6, gelişme periyodunda 0,6-1,15 arasında, orta periyotta 1.15 ve son periyotta ise 1,15-0,80 arasında katsayılar alınmıştır. Bununla birlikte, malçın parselleri örtme oranı %80 olduğundan, malçlı koşullarda yetiştirilen parsellerdeki domates bitkilerinin bitki su tüketimi değerlerinin belirlenmesinde yağış değeri, düşen yağışın %20'si alınarak (P×0,20) hesaplanmıştır.

**Tablo 1.** Denemeye ilişkin sulama konuları

| Sulama Konuları | Sulama Konusunun Tanımı | kp |
|---|---|---|
| **I100** | A-Sınıfı Buharlaşma Kabı'nda meydana gelen yığışımlı buharlaşmanın %100'ünün uygulandığı konu | 1.00 |
| **I75** | A-Sınıfı Buharlaşma Kabı'nda meydana gelen yığışımlı buharlaşmanın %75'inin uygulandığı konu | 0,75 |
| **I50** | A-Sınıfı Buharlaşma Kabı'nda meydana gelen yığışımlı buharlaşmanın %50'sinin uygulandığı konu | 0,50 |
| **I25** | A-Sınıfı Buharlaşma Kabı'nda meydana gelen yığışımlı buharlaşmanın %25inin uygulandığı konu | 0,25 |

Çalışmada Zahide F1 sırık domates çeşidi kullanılmıştır. Domatesler fide olarak temin edilmiş ve 23 Mayıs tarihinde parsellere dikilmiştir. Her parsel sıra arası 80 cm ve sıra üzeri 40 cm olacak şekilde 4 sıradan oluşturulmuş ve her bitki sırasına 1 lateral çekilmiştir. Parseller 6,4 m boyunda ve 3,2 m genişliğinde (20,48 m2) oluşturulmuştur. Her parselde tekerrürler arasında 2 metre, bloklar arasında ise 3 metre boşluk bırakılmıştır. Toprak analizi sonuçlarına göre gübrelemede azotlu, fosforlu ve potaslı gübreler kullanılmıştır. Dikimden önce 20 kg da-1 15:15:15 kompoze gübresi dikimden sonra 7 kg da-1 13-0-46 potasyum nitrat ve dekara 5 kg da-1 MAP gübreleri damla sulama sistemi ile bitkilere verilmiştir.

Toprak suyu gözlemleri gravimetrik yöntem kullanılarak yapılmıştır. Bitki kök bölgesi toprak su içeriği gravimetrik yöntemle yetişme mevsimi boyunca konulu sulamalar öncesi, sonrası ve sulamalar arasında izlenmiştir. Örnekler her 30 cm'lik katman için I100 deneme konusunda 120 cm derinliğe kadar diğer sulama konularında ise 90 cm derinlikteki toprak katmanlarından örnekler alınmıştır. Her sulama konusu için bitki su tüketimi (ET) su dengesi eşitliği kullanılarak Eşitlik 2'deki gibi hesaplanmıştır [21].

$$ET = I + P - R - D \pm \Delta S \quad (2)$$

Eşitlikte; ET: Bitki su tüketimi (mm), I: Uygulanan sulama suyu miktarı (mm), P: Sulama dönemi içerisinde düşen yağış miktarı (mm), R: Yüzey akışı ve kılcal yükselme (mm), D: Derine sızma , ΔS: Toprak profilindeki ne değişim miktarı (mm/90cm) değerini göstermektedir. Damla sulama yönteminde yüzey akışı ve alanda taban suyu da olmadığı için kılcal yükselme (R) sıfır kabul edilmiştir. Tarla kapasitesini aşacak bir şekilde sulama konusu olmadığından dolayı derine sızma (D) değeri de sıfır alınmıştır [22]. Mevsimlik bitki su tüketimi, iki sulama aralığı için hesaplanan evapotranspirasyon değerlerinin yığışımlı toplamları alınarak belirlenmiştir. Bununla birlikte, malçın parselleri örtme oranı %80 olduğundan, malçlı koşullarda yetiştirilen parsellerdeki domates bitkilerinin bitki su tüketimi değerlerinin belirlenmesinde yağış değeri, düşen yağışın %20'si alınarak (P×0,20) hesaplanmıştır.

Ekonomik su kullanım etkinliği brüt gelirin gerçek evapotranspirasyona bölünmesiyle belirlenmiştir (Eşitlik 3) [23]. Birim sulama suyuna karşılık elde edilen net geliri hesaplamak için ise birim alandan elde edilen net gelir toplam sulama suyu miktarına bölünmüştür (Eşitlik 4).

$$ESKE = BG/ET \quad (3)$$

$$NGS = NG/SS \quad (4)$$

Eşitliklerde; ET: Gerçek evapotranspirasyon miktarını (m-3 ha-1), ESKE: Ekonomik su kullanım etkinliğini (TL m-3), BG: Brüt geliri (TL ha-1), NGS: Birim sulama suyu hacmine göre net geliri (TL m-3), NG: Net geliri (TL ha-1), SS: Sulama suyu miktarını (m-3 ha-1) ifade etmektedir.

### 2.1. Net Gelir Hesabı

Birim alandan elde edilen net gelir (TL ha-1), brüt gelirden toplam üretim masraflarının çıkarılmasıyla bulunmuştur. Brüt gelir, her deneme konusu için, verim değerleriyle domatesin tarladaki yerel satış fiyatının (1 TL kg-1) çarpılmasıyla belirlenmiştir. Toplam üretim masrafı sabit ve değişken masrafların toplanmasıyla belirlenmiştir. Sabit masraflar, malç uygulanan ve malçsız tüm deneme konuları için ayrı ayrı hesaplanmış ve kendi içlerinde eşit kabul edilmiştir. Değişken masraflar hariç sabit masraflar malç uygulanan konular için 30365 TL ha-1 malç uygulanmayan konular için 30825 TL ha-1 olarak belirlenmiştir. Su ve sulamaya ilişkin masraflar değişken masraflar olarak alınmıştır. Kullanılan suyun maliyeti (TL ha-1), birim hacim su fiyatı (0,18 TL m-3) ile deneme konusuna göre birim alana uygulanan sulama suyu miktarının (m3 ha-1) çarpılmasıyla bulunmuştur. Çalışma alanında, sulama suyu su kuyusundan damla sulama sistemine basılmasında elektrik enerjisiyle çalışan bir pompa (15 kW) kullanılmıştır. Elektrik enerji masrafı (TL ha-1), bu çalışmada kullanılan damla sulama sistemi özellikleri dikkate alınarak her deneme konusu için belirlenen sulama süresi (saat ha-1), tarımsal elektrik enerji maliyeti (0,88 TL kW-1) ve 15 kW değerlerinin çarpılması suretiyle hesaplanmıştır. Böylece, kullanılan suyun maliyeti ile enerji maliyeti toplanarak değişken masraflar elde edilmiştir.

### 2.2. İstatistiksel analiz

Meyve verimlerine ilişkin veri Minitab 19 programında varyans analizi (ANOVA) ile değerlendirilmiş ve ortalama değerler arasında $p<0,01$ düzeyinde önemli farklılıkları belirlemek için Duncan'ın çoklu dağılım testi kullanılmıştır.

## 3. BULGULAR

Uygulanan sulama suyu miktarı, verim üzerinde %1 olasılık düzeyinde önemli bir etkiye sahip olmuştur. Uygulanan sulama suyu, bitki su tüketimi, verim ve ekonomik su kullanım etkinliği değerleri Tablo 2'de verilmiştir. En yüksek verim I100×M konusundan elde edilirken, en düşük verim I25×NM konusundan elde edilmiştir. En yüksek verim I100 sulama konusundan elde edilmiş olmasına rağmen I100×NM ve I75×M konuları arasında verim açısından istatistiksel olarak önemli bir fark bulunmamıştır. Ayrıca, malç uygulanan tüm sulama

suyu seviyelerinde verim ve ekonomik su kullanım etkinliği açısından daha yüksek sonuçlar vermiştir. Daha önce yapılan çalışmalarda da araştırmacılar sulama suyu seviyesi azaldıkça meyve veriminin düştüğünü bildirmişlerdir [24,25,26,27,28,29,30-31]. Malç uygulamasıyla ilgili yapılan çalışmalarda da malç uygulamasının sulama konularından bağımsız olarak bütün sulama suyu seviyelerinde verim ve ekonomik su kullanım etkinliğinin malç uygulanmayan konulara göre daha yüksek değerler orta koymuşlardır [14,16,32,33-34]. Malç uygulamasıyla birlikte yapılan su kısıtı ekonomik açıdan domates üretimini olumlu etkilemiştir.

**Tablo 2.** Uygulanan sulama suyu, bitki su tüketimi, verim ve ekonomik su kullanım etkinliği

| Deneme konusu | Uygulanan sulama suyu (mm) | Bitki su tüketimi (mm) | Verim (t ha$^{-1}$) | Ekonomik su kullanım etkinliği (TL m$^{-3}$) |
|---|---|---|---|---|
| I100×M | 512,3 | 482 | 72,56 a | 15,05 |
| I100×NM | 512,3 | 570 | 68,95 ab | 12,10 |
| I75×M | 395,47 | 375 | 65,3 b | 17,41 |
| I75×NM | 395,47 | 488 | 58,74 c | 12,04 |
| I50×M | 278,65 | 298 | 51,62 d | 17,32 |
| I50×NM | 278,65 | 326 | 44,44 ef | 13,63 |
| I25×M | 161,82 | 190 | 42,79 ef | 22,52 |
| I25×NM | 161,82 | 247 | 38,92 f | 15,76 |

Çalışmada deneme konularından elde edilen meyve verimlerinin parasal değeri belirlenerek bitki su tüketimine oranlanmış ve böylece ekonomik su kullanım etkinliği (ESKE) belirlenmiştir. En yüksek ekonomik su kullanım etkinliği değerleri sulama konularından bağımsız olarak malç uygulaması uygulanan konulardan elde edilmiştir. Elde edilen değerler 12.04-22.52 TL m-3 arasında değişmiştir (Tablo 2).

En yüksek ekonomik su kullanım etkinliği değeri I25×M konusundan elde edilmiş ve bunu I75×M ve I50×M konuları izlemiştir.

Çiftçiler sulama suyundan elde edilecek tasarrufun yanında optimum girdi kullanımı ile sadece verimlerini değil, net gelirlerini de en yüksek düzeye çıkarmayı hedeflemektedir. Buradan yola çıkarak ekonomik analiz gerçekleştirilmiş ve sonuçları Tablo 3'de verilmiştir.

**Tablo 3.** Deneme konularının domates verimi ve net gelir üzerine etkisi

| Deneme Konusu | Sabit Masraf (TL ha$^{-1}$) | Toplam Sulama Masrafı (TL ha$^{-1}$) | Toplam Masraf (TL ha$^{-1}$) | Brüt Gelir (TL ha$^{-1}$) | Net Gelir (TL ha$^{-1}$) | Birim Sulama Suyu Hacmine Göre Net Gelir (TL m$^{-3}$) |
|---|---|---|---|---|---|---|
| I100×M | 30365 | 1532,6 | 31897,6 | 72560 | 40662,4 | 7,94 |
| I100×NM | 30825 | 1532,6 | 32357,6 | 68950 | 36592,4 | 7,14 |
| I75×M | 30365 | 1183,1 | 31548,1 | 65300 | 33751,9 | 8,53 |
| I75×NM | 30825 | 1183,1 | 32008,1 | 58740 | 26731,9 | 6,76 |
| I50×M | 30365 | 833,6 | 31198,6 | 51620 | 20421,4 | 7,33 |
| I50×NM | 30825 | 833,6 | 31658,6 | 44440 | 12781,4 | 4,59 |
| I25×M | 30365 | 484,1 | 30849,1 | 42790 | 11940,9 | 7,38 |
| I25×NM | 30825 | 484,1 | 31309,1 | 38920 | 7610,9 | 4,70 |

Tablo 3'te verilen net gelir hesabında kullanılan üretim maliyetleri, sofralık domates yetiştiriciliği için tüm üretim giderleri (fide maliyeti, çapa, gübre, hasat, malçlama vb.) dikkate alınarak hesaplanmıştır. Malç uygulanan konularda malç masrafı ortaya çıkarken malç kullanımdan dolayı yabancı otlanma olmadığı için çapalama masrafı olmamıştır. Malç uygulanmayan konularda ise çapalama masrafları hesaplanarak sabit masraflara eklenmiştir. Uygulanan sulama suyu miktarı ve sulama süresine bağlı olarak birim su maliyeti, suyun sisteme pompalanması için gerekli enerji maliyeti ve sulama işçiliği maliyeti de artmıştır. Tablo 3'de görüldüğü gibi en yüksek net gelir en fazla sulama suyunun uygulandığı konulardan elde edilmiş ve sulama suyu miktarı azaldıkça elde edilen net gelirde azalmıştır. Birim alan başına en yüksek net gelir 40662,4 TL ha-1 olarak I100×M konusundan, en düşük net gelir ise 7610,9 TL ha-1 olarak I25×NM konusundan elde edilmiştir. Bütün sulama suyu sevilerinde malç uygulanan konulardan malç uygulanmayan konulara göre daha yüksek net gelir elde edilmiştir. Birim sulama suyu hacmine göre net gelir hesabı her uygulama için kullanılan toplam sulama suyu miktarının net gelire oranlanmasıyla hesaplanmış ve 8,53-4,59 TL m-3 arasında değişmiştir. Sulama konularından bağımsız olarak değerlendirdiğimizde malç uygulanan konulardan birim sulama suyundan daha yüksek net gelir elde edilmiştir. En yüksek birim sulama suyu hacmine göre net gelir ise 8,53 TL m-3 olarak %25 su kısıntısının uygulandığı I75×M konusundan belirlenmiştir. En düşük değer ise 4,59 TL m-3 olarak I50×NM konusundan elde edilmiştir. En yüksek sulama suyu miktarı uygulanan I100 konusuyla en yüksek birim sulama suyu hacmine göre net gelir elde edilen I75×M konusu kıyaslandığında, I75×M konusuna 116,83 mm daha az su uygulanmış ve daha yüksek birim sulama suyu hacmine göre net gelir belirlenmiştir. Bu durum, sezonda uygulanan %25 su kısıntısıyla hem sudan tasarruf edilebileceğini hem de uygulanan birim sudan daha yüksek kar elde edileceğini göstermiştir.

## 4. SONUÇ

Çalışmada, malç uygulanan konulardan bütün sulama suyu seviyelerinde daha yüksek verim ve net gelir elde edildiğini göstermiştir. Su kaynaklarının sürdürülebilirliği ve optimum işletmecilik açısından %25 su kısıntısının uygulandığı malçlı I75×M (395,47 mm) konunun uygun olduğu belirlenmiştir. Buna göre, 5 günde bir pan buharlaşma miktarının 0,75 katının uygulandığı malçlı konular önerilebilir. Bu uygulamada domates verimi 65,3 t ha-1, fiziksel su kullanım etkinliği 18,08 kg m-3 ekonomik su kullanım etkinliği ise 17,41 TL m-3 olarak hesaplanmıştır. En uygun birim sulama suyu hacmine göre net gelir 8,53 TL m-3 ve net gelir 33751,9 olarak belirlenmiştir.

## KAYNAKLAR


[1] FAO. Food and Agriculture Organization of the United Nations,2018; [cited 2018 March 05]. Available from: http://www.fao.org/faostat/en/#data/QC

[2] Anonim. Bitkisel üretim istatistikleri. TC. Başbakanlık Türkiye İstatistik Kurumu; 2019.

[3] Abak, K. Türkiye'de domatesin dünü, bugünü ve yarını. Türktob Dergisi. 2016; 17: 8-13.

[4] Ekinci, M., Dursun, A. Sebze yetiştiriciliğinde malç kullanımı. Derim. 2006; 23(1), 20-27.

[5] Splittstoesser, W.E. Vegetable growing handbook, organic and traditional methods, Plant physiology in horticulture university of Illinois, Urbana, Illinois; 1990.

[6] Swiader, J.M., Ware, G.W., Collum, J.P. Producing vegetable crops. Interstate publishes, Inc. Danville, Illinois;1992.

[7] Koçer, G., Eltez, S. Serada domates yetiştiriciliğinde farklı renkte malç kullanımının verim, kalite ve sera beyaz sineği Trialeurodes vaporariorum (Westw.)(Homoptera: Aleyrodidae) nimf populasyonuna olan etkileri üzerine araştırmalar. Alatarım. 2004; 3(2): 36-42.

[8] Kurtar, E. Isıtmasız cam serada sonbahar dönemi yazlık kabak (Cucurbita pepo L.) yetiştiriciliğinde malç uygulamalarının etkileri. Harran Tarım ve Gıda Bilimleri Dergisi. 2010; 14(2), 69-76.

[9] Aksakal, E. Toprak Yüzey Malçının Yüzey Akış ve Toprak Kayıpları Üzerine Etkisi. Atatürk Üniversitesi Ziraat Fakültesi Dergisi. 2012; 42(2), 139-144.

[10] Lushi, I.M., Haxhınasto, L., Balaj, N., Hasani, F. Comparison of different mulch materials on some tomato (Solanum lycopersicum) cultivars under controlled environment conditions. Research Journal of Agricultural Science. 2012; 44(1), 99-103.

[11] Uzun S., Kandemir D., Özkaraman F., Özer H. Açıkta ve serada organik sebze yetiştiriciliği. Doğu Karadeniz 1. Organik Tarım Kongresi, 26-28 Haziran, Kelkit, Gümüşhane.

[12] Kosterna, E. The effect of soil mulching with straw on the yield and selected components of nutritive value in broccoli and tomatoes. Folia Horticulturae. 2014; 26(1), 31-42.

[13] Mu, L., Liang, Y., Zhang, C., Wang, K., Shi, G. Soil respiration of hot pepper (Capsicum annuum L.) under different mulching practices in a greenhouse, including controlling factors in China. Acta Agriculturae Scandinavica, Section B-Soil & Plant Science. 2014; 64(1), 85-95.

[14] Berihun, B. Effect of mulching and amount of water on the yield of tomato under drip irrigation. J. Hort. For. 2011; 3: 200-206.

[15] Kumar, A. V., Moulı, G. C., Ramulu, V., Kumar, K. A. Effect of drip irrigation levels and mulches on growth, yield and water use efficiency of tomato. Part I: Plant Science. 2012; 104: 121-127.

[16] Biswas, S. K., Akanda, A. R., Rahman, M. S., Hossain, M. A. Effect of drip irrigation and mulching on yield, water-use efficiency and economics of tomato. Plant Soil and Environment. 2015; 61(3), 97-102.

[17] Alebachew, K. Evaluation of deficit ırrigation and mulching on water productivity of tomato (Lycopersicon esculentum Mill) under drip irrigation system at kallu woreda, south wollo, Ethiopia [Master Thesis]. Ethiopia: Haramaya University; 2017.

[18] Wadatkar, S. B., Deshmukh, M. M., Mankar, A. N., Kale, M. U., Kale, V. S. Response of tomato to polyethylene mulch under drip fertigation. Journal of Agriculture Research and Technology. 2017; 42(3), 220.

[19] Aliabadi, B. T., Hassandokht, M. R., Etesami, H., Alikhani, H. A., Dehghanisani, H. Effect of mulching on some characteristics of tomato (Lycopersicon esculentum Mill.) under deficit irrigation. Journal of Agricultural Science & Technology. 2019; 21(4).

[20] Kanber, R. Irrigation of first and second product peanuts by utilizing open water surface evaporation in Çukurova conditions. Regional Groundwater Research Institute Publications; 1984.

[21] Garrity, D. P., Watts, D. G., Sullivan, C. Y., Gilley, J. R. Moisture deficits and grain sorghum performance: evapotranspiration-yield relationships. 1. Agronomy Journal. 1982; 74(5), 815-820.

[22] Hanks, R. J. Model for predicting plant yield as ınfluenced by water use. 1. Agronomy journal. 1974; 66(5), 660-665.

[23] Pereira LS, Cordery I, Iacovides I. Improved indicators of water use performance and productivity for sustainable water conservation and saving. Agricultural Water Management. 2012; 108: 39-51.

[24] Patanè, C., Tringali, S., Sortino, O. Effects of deficit irrigation on biomass, yield, water productivity and fruit quality of processing tomato under semi-arid Mediterranean climate conditions. Sci. Hort. 2011; 129: 590-596.

[25] Özbahçe, A, Tarı, A.F., Çetin, Ö. Toprak nemi izlenerek oluşturulan sulama programından uygun pan katsayısının tahmini: domates örneği. 9. Sebze Tarımı Sempozyumu, 12-14 Eylül, Konya, 2012.

[26] Kuscu, H., Turhan, A., Ozmen, N., Aydinol, P., Demir, A.O. Optimizing levels of water and nitrogen

applied through drip irrigation for yield, quality, and water productivity of processing tomato (Lycopersicon esculentum Mill.). Horticulture, Environment, and Biotechnology. 2014; 55(2), 103-114.

[27] Lahoz, I., Pérez-de-Castro, A., Valcárcel, M., Macua, J.I., Beltrán, J., Roselló, S, et al. Effect of water deficit on the agronomical performance and quality of processing tomato. Scientia Horticulturae. 2016; 200, 55-65.

[28] Agbna, G.H., Dongli, S., Zhipeng, L., Elshaikh, N.A., Guangcheng, S.,Timm, L. C. Effects of deficit irrigation and biochar addition on the growth, yield, and quality of tomato. Scientia Horticulturae. 2017; 222, 90-101.

[29] Tarı, A.F., Sapmaz, M. Farklı sulama düzeylerinin serada yetiştirilen domatesin verim ve kalitesine etkisi. Toprak Su Dergisi. 2017; 6(2), 11-17.

[30] Zhang, H., Xiong, Y., Huang, G., Xu, X., Huang, Q. Effects of water stress on processing tomatoes yield, quality and water use efficiency with plastic mulched drip irrigation in sandy soil of the Hetao Irrigation District. Agricultural Water Management. 2017; 179, 205-214.

[31] Çebi, U. K., Selçuk, Ö., Altıntaş, S., Yurtseven, E., Öztürk, O. Farklı sulama suyu kalitesi ve su düzeylerinin serada yetiştirilen domates bitkisinin verim ve su kullanım etkinliği üzerine etkisi. Harran Tarım ve Gıda Bilimleri Dergisi. 2018; 22(1), 33-46.

[32] Singh, R., Kumar, S., Nangare, D. D., Meena, M. S. Drip irrigation and black polyethylene mulch influence on growth, yield and water-use efficiency of tomato. African Journal of Agricultural Research. 2009; 4(12), 1427-1430.

[33] Mukherjee, A., Kundu, M., Sarkar, S. Role of irrigation and mulch on yield, evapotranspiration rate and water use pattern of tomato (Lycopersicon esculentum L.). Agric. Water Management. 2010; 98:182-189.

[34] Rajablariani, H., Rafezi, R., Hassankhan, F. Using colored plastic mulches in tomato (Lycopersicon esculentum L.) production. International Proceedings of Chemical, Biological and Environmental Engineering. 2012; 47(3), 12-16

Araştırma Makalesi https://doi.org/10.46810/tdfd.867991 Research Article

Türk Doğa ve Fen Dergisi
Turkish Journal of Nature and Science
www.dergipark.gov.tr/tdfd

# Kuru Koşullarda Yetiştirilen Bazı Kavuzsuz Arpa Genotiplerinde (*Hordeum vulgare* L. var. *nudum* Hook. f.) Verim ile Verime Etkili Karakterler Arasındaki İlişkiler

**Soner YÜKSEL[1*], Saime ÜNVER İKİNCİKARAKAYA[2]**

[1] Geçit Kuşağı Tarımsal Araştırma Enstitüsü Müdürlüğü, Eskişehir, Türkiye
[2] Ankara Üniversitesi, Ziraat Fakültesi, Tarla Bitkileri Bölümü, Ankara, Türkiye
Soner YÜKSEL ORCID No: 0000-0002-0984-0765
Saime ÜNVER İKİNCİKARAKAYA ORCID No: 0000-0001-8561-9002

**Sorumlu yazar: soner.yuksel@tarimorman.gov.tr*

(Alınış: 25.01.2021, Kabul: 09.03.2022, Online Yayınlanma: 29.06.2022)

**Anahtar Kelimeler**
Kavuzsuz arpa,
Hat,
Verim,
Kuru koşullar,
Korelasyon

**Öz:** Bu araştırmada; 9 adet kavuzsuz arpa hattı ile tescilli kavuzsuz arpa çeşidi Özen'in kuru koşullarda verim ile verime etkili karakterler arasındaki ilişkilerin belirlenmesi amacıyla 2013 ve 2014 yetiştirme sezonunda Eskişehir Geçit Kuşağı Tarımsal Araştırma Enstitüsü Müdürlüğü arazisinde yürütülmüştür. Verim ile bayrak yaprağı alanı, bayrak yaprağı yeşil kalma süresi, sap uzunluğu, üst boğum arası uzunluğu, başak boyu, metrekarede başak sayısı, hasat indeksi, birim alan tane verimi, başakta tane sayısı, metrekarede biyolojik verim, başakta tane verimi, steril başakçık sayısı, fertil başakçık sayısı, toplam başakçık sayısı, bin tane ağırlığı, hektolitre ağırlığı, protein oranı, 2.5 mm elek üstü, çıkış süresi ve başaklanma gün sayısı arasındaki ilişkiler incelenmiştir. Korelasyon analizi sonuçlarına göre; başakta tane sayısı ile başakta tane verimi, hektolitre ağırlığı ve başaklanma gün sayısı arasında olumlu ve önemli ilişki saptanırken protein oranı (r=-0.743**) ile olumsuz ve önemli ilişki tespit edilmiştir. Tane verimi ile metrekarede biyolojik verim, metrekarede başak sayısı ve hasat indeksi özellikleri arasında olumlu ve önemli ilişkiler belirlenmiştir.



# Relationships Between Yield and Yield Characters of Some of Hulless Barley Genotypes (*Hordeum vulgare* L. var. *nudum* Hook. f.) Grown in Dry Conditions

**Keywords**
Hulless barley,
Genotype,
Yield,
Dry conditions,
Correlation

**Abstract:** This study was conducted at the experimental fields of Eskişehir Transitional Zone Agricultural Research Institute in growing seasons of 2013 and 214 in order to determine the to relationships between seed yield and yield components of nine hulless barley lines and one registered hulless barley variety -Özen- in rainfall conditions. Flag leaf area, flag leaf staying green time, stem length, upper internode length, spike length, number of spikes per square meter, harvest index, grain yield per unit area, biological yield per square meter, grain number per spike, grain yield per spike, sterile spikelet number, fertile spikelet number, total spikelet number, thousand grain weight, hectoliter weight, protein ratio, 2.5 mm above sieve and relationships between emergence time and number of days to earing were examined. According to the correlation analysis results; there was a positive and significant relationship between grain number per spike and grain yield per spike, hectoliter weight and number of days to spike. However, a negative and significant relationship was determined in terms of protein ratio (r =-0.743**). As a result of this study, important relationships were determined between grain yield and biological yield per square meter, number of ears per square meter and harvest index.

## 1. GİRİŞ

Türkiye; arpanın (*Hordeum vulgare* L.) gen merkezlerinden birisidir ve dünya arpa üreticisi ülkeler arasında ilk 10 içerisinde yer almaktadır. Daha çok kışlık olarak tarımı yapılmaktadır. Türkiye'de ekiliş alanı ve üretim miktarı bakımından ikinci sırada, dünya genelinde tahıllar içerisinde dördüncü sırada yer almaktadır. Arpanın 2019 yılında 2,8 milyon hektar ekiliş alanı ve üretimi 7,6 milyon ton ve verimi 293 kg da$^{-1}$ düzeyindedir [1].

Kavuzsuz arpa ile ilgili gerek üretimi gerek ıslahı gerekse gıda, yem ve endüstriyel alanlarda değerlendirilmesi hususlarında araştırmalar yapılmaya devam etmektedir. Besinsel lif kaynakları ve β-glukan değerleri yönüyle kavuzsuz arpa oldukça zengindir [2]. Enerji içeriği ve yüksek sindirilebilir protein miktarı [3], ekmek imalatında paçalda kullanılabilmesi, içerdiği çözünebilir lifler ile plazma kolesterolünü azaltıcı özelliği sebebiyle kavuzsuz arpaya olan ilgi artmaktadır [4]. Kavuz bulunmaması öğütme teknolojisi açısından kolaylık sağlamaktadır. Kepek ve una kolaylıkla ayrılabilmesi klasik buğday öğütme ekipmanları ve metotları ile daha kolay olmaktadır [5]. Ülkemizde yürütülen kavuzsuz arpa ıslah çalışmaları sonucunda 2012 yılında Özen ve 2014 yılında Yalın isimli iki çeşit Ankara Tarla Bitkileri Merkez Araştırma Enstitüsü Müdürlüğü tarafından tescil edilmiştir.

Bu çalışmada, Eskişehir kuru koşullarında Özen çeşidi ile 9 adet kavuzsuz arpa hattının verim ile verime etkili karakterler arasındaki ilişkilerin belirlenmesi hedeflenmiştir.

## 2. MATERYAL VE METOT

Araştırma, Eskişehir Geçit Kuşağı Tarımsal Araştırma Enstitüsü deneme arazisinde, 2012–2013 ve 2013–2014 üretim yıllarında kuru koşullarda gerçekleştirilmiştir. Denemenin yürütüldüğü alanın denizden yüksekliği 780 m olup, 39° 46” doğu boylamında ve 30° 31” kuzey enlemleri arasında yer almaktadır.

Karasal iklimin hâkim olduğu Eskişehir’de uzun yıllar ortalamasına göre yağış miktarı 326.8 mm’dir. Denemenin yürütüldüğü 2013 ve 2014 yıllarındaki yetiştirme dönemlerine ve uzun yıllara ait aylık yağış ve sıcaklık verileri Tablo 1’de verilmiştir. İklim verileri değerlendirildiğinde, iki yıl arasında yağış miktarı açısından yaklaşık 45 mm’lik bir farklılık meydana gelmiş, ilk yıl mayıs ayında başaklanma dönemindeki yetersiz yağış yıllar arasında iklimsel açıdan farklılıklar meydana getirmiştir.

**Tablo 1.** Denemenin yürütüldüğü yıllar ve uzun yıllara ait meteorolojik veriler [6]

| Aylar | 2012-2013 | | | 2013-2014 | | | Uzun Yıllar | |
|---|---|---|---|---|---|---|---|---|
| | Yağış (mm) | Ort. Nem (%) | Ort. Sıcaklık (°C) | Yağış (mm) | Ort. Nem (%) | Ort. Sıcaklık (°C) | Yağış (mm) | Ort. Sıcaklık (°C) |
| Ekim | 16,1 | 78,1 | 14,2 | 65,0 | 65,6 | 9,8 | 25,0 | 11.4 |
| Kasım | 14,5 | 92,3 | 7,3 | 15,0 | 73,5 | 6,7 | 30,3 | 5,7 |
| Aralık | 73,2 | 95,1 | 2,2 | 1,5 | 76,0 | 1,7 | 45,7 | 1,4 |
| Ocak | 18,5 | 93,6 | 1,7 | 21,0 | 81,0 | 3,6 | 38,3 | -1,3 |
| Şubat | 25,4 | 88,0 | 5,6 | 5,0 | 62,3 | 5,5 | 32,3 | 0,2 |
| Mart | 30,6 | 59,8 | 7,6 | 19,1 | 69,0 | 7,9 | 33,1 | 4,6 |
| Nisan | 26,8 | 63,2 | 11,5 | 51,4 | 63,7 | 13,0 | 35,1 | 9,2 |
| Mayıs | 5,8 | 51,5 | 18,6 | 31,2 | 63,3 | 16,3 | 43,3 | 14,1 |
| Haziran | 36,5 | 53,6 | 20,2 | 63,7 | 64,1 | 19,8 | 29,1 | 18,6 |
| Temmuz | 0,8 | 52,8 | 21,6 | 20,4 | 57,8 | 23,7 | 13,8 | 21,9 |
| Toplam | 248,2 | | | 293,3 | | | 326,8 | |
| Ortalama | | | 11,05 | | | 10,80 | | 8,58 |

Ekim öncesinde deneme alanının 3 farklı derinliklerden alınan toprak örneklerinin analizleri, Eskişehir Geçit Kuşağı Tarımsal Araştırma Enstitüsü, Toprak-Su Araştırmaları Laboratuvarlarında yapılmış ve bu analizlere ait sonuçlar Tablo 2’de verilmiştir.

**Tablo 2.** Deneme alanı topraklarının analiz sonuçları

| | Derinlik (cm) | pH | Toplam Tuz (%) | Kireç (%) | Organik Madde (%) | Yarayışlı $P_2O_5$ (kg $da^{-1}$) | Yarayışlı $K_2O$ (kg $da^{-1}$) |
|---|---|---|---|---|---|---|---|
| 1.YIL | 0-30 | 8,1 | 0,30 | 7,49 | 1,7 | 5,31 | 103,4 |
| | 30-60 | 8,0 | 0,28 | 8,91 | 1,0 | 1,67 | 77,3 |
| | 60-90 | 8,1 | 0,25 | 9,62 | 0,9 | 0,95 | 63,4 |
| | **Derinlik (cm)** | **pH** | **Toplam Tuz (%)** | **Kireç (%)** | **Organik Madde (%)** | **Yarayışlı $P_2O_5$ (kg $da^{-1}$)** | **Yarayışlı $K_2O$ (kg $da^{-1}$)** |
| 2.YIL | 0-30 | 7,4 | 0,131 | 8,1 | 1,7 | 4,7 | 97,9 |
| | 30-60 | 7,5 | 0,089 | 9,0 | 0,9 | 2,2 | 75,2 |
| | 60-90 | 7,6 | 0,048 | 10,52 | 0,4 | 2,5 | 55,4 |

Denemenin birinci yıl kurulduğu alandan alınan toprak örneklerinde yapılan analiz sonuçlarına göre, toprak bünyesi killi, kireç ve organik madde içeriği bakımından orta, yarayışlı fosfor bakımından zayıf ve yarayışlı potasyum bakımından ise zengin özelliğe sahiptir (Tablo 2). Denemenin ikinci yıl kurulduğu alanda ise toprak bünyesi tınlı, kireç ve organik madde içeriği bakımından orta, yarayışlı fosfor bakımından zayıf ve yarayışlı potasyum bakımından ise zengin özelliğe sahiptir.

Bu çalışmada, tescilli kavuzsuz arpa çeşidi Özen ile Tarla Bitkileri Merkez Araştırma Enstitüsü Müdürlüğü tarafından yürütülen ıslah programında ileri çıkan dokuz

adet kavuzsuz arpa hattı deneme materyali olarak kullanılmıştır. Standart olarak kullanılan Özen çeşidi denemenin yürütüldüğü yıl Türkiye'de tescil edilmiş ilk kavuzsuz arpa çeşidi olma özelliğine sahiptir. Denemelerde kullanılan kavuzsuz arpa genotipleri Tablo 3'de verilmiştir.

**Tablo 3.** Denemelerde kullanılan kavuzsuz arpa genotipleri

| Sıra No | Genotipler |
|---|---|
| 1 | SB90704 |
| 2 | ICB 100811 |
| 3 | MOLA/BERMEJO"S"//NISPERO |
| 4 | ICB 100819 |
| 5 | Bugar |
| 6 | K-247/2401-13//Radikal/Vavilon LF7 |
| 7 | Roho/Masurka//ICB-103020 |
| 8 | CYCLONE/4/YAA560.2//LUTHER/BK259/3/NGYAK-8/PLAISANT |
| 9 | CYCLONE/4/YAA560.2//LUTHER/BK259/3/NGYAK-8/PLAISANT |
| 10 | ÖZEN |

Her iki yılda tarla denemeleri nadastan sonra ekilmiştir. Ekim öncesi dekara 6 kg saf N ve 7,6 kg saf $P_20_5$ gelecek şekilde taban gübresi olarak 16,5 kg $da^{-1}$ diamonyum fosfat (18.46.0) ve üst gübre olarak 14,3 kg $da^{-1}$ amonyum sülfat (%21 Azot) gübreleri kullanılmıştır. Denemede metrekareye 450 tohum kullanılmıştır. Ekim işlemi ekim mibzeri ile sıra arası 20 cm (6 sıra) ve parsel boyutu 5x1,2= 6 $m^2$ olarak gerçekleştirilmiştir.

Genotiplerin verim ile; bayrak yaprağı alanı, bayrak yaprağı yeşil kalma süresi, sap uzunluğu, üst boğum arası uzunluğu, başak boyu, metrekarede başak sayısı, hasat indeksi, birim alan tane verimi, metrekarede biyolojik verim, başakta tane sayısı, başakta tane verimi, steril başakçık sayısı, fertil başakçık sayısı, toplam başakçık sayısı, bin tane ağırlığı, hektolitre ağırlığı, protein oranı, 2,5 mm elek üstü, çıkış süresi ve başaklanma gün sayısı değerleri incelenmiştir.

Ekimler ilk yıl 06 Mart 2013 tarihinde ve ikinci yıl ise 18 Şubat 2014 tarihinde gerçekleştirilmiştir.

Araştırma, Tesadüf Blokları Deneme Deseninde 3 tekrarlamalı olarak yürütülmüştür. Korelasyon analizinde iki yıllık denemelerin tekerrür ortalamaları kullanılmış ve çalışmadan elde edilen verilerin istatistiki analizleri SAS yazılımı JMP Pro 13.0.0 (64 bit) paket programı [7] kullanılarak yapılmıştır.

## 3. BULGULAR

Araştırmamızda kullanılan 10 kavuzsuz arpa genotipi ile kuru koşullarda 2013 ve 2014 yıllarında yürütülen çalışma sonucunda, incelenen özellikler arasındaki ilişkiler korelasyon analizi ile belirlenmiş ve sonuçları Tablo 4'de özetlenmiştir. Korelasyon analizi sonuçlarına göre; bayrak yaprağı alanı ile sap uzunluğu, üst boğum arası uzunluğu, başakta tane verimi, bin tane ağırlığı, hektolitre ağırlığı ve başaklanma gün sayısı arasında olumlu ve önemli ilişki hesaplanmıştır. Bayrak yaprağı yeşil kalma süresi, protein oranı ve çıkış süresi yönünden ise olumsuz ve önemli ilişki belirlenmiştir.
Bayrak yaprağı yeşil kalma süresi ile metrekarede biyolojik verim ve protein oranı (r=0,895**) arasında olumlu ve önemli ilişki saptanmıştır. Sap uzunluğu, üst boğum arası uzunluğu, başak boyu, hasat indeksi, başakta tane sayısı, başakta tane verimi, bin tane ağırlığı, hektolitre ağırlığı, 2,5 mm elek üstü ve başaklanma gün sayısı arasında ise olumsuz ve önemli ilişki elde edilmiştir.

Sap uzunluğu ile önemli ve pozitif korelasyonlar üst boğum arası uzunluğu, başak boyu, hasat indeksi, başakta tane sayısı, başakta tane verimi, bin tane ağırlığı, hektolitre ağırlığı, elek üstü ve başaklanma gün sayısı arasında belirlenmiştir. Olumsuz ve önemli ilişki protein oranında r=-0,864** hesaplanmıştır. Sekiz lokasyonda yürütülen bir çalışmada bitki boyu ile başak boyu (r=0.184*), protein oranı (r=0.282**), tane verimi (r=0.631**) arasında olumlu ve önemli, başakta tane sayısı (r=-0.252**) arasında olumsuz ve önemli, bin tane ağırlığı (r=0.145) arasında olumlu ve önemli ilişkiler bulunmuş [8] elde edilen tüm bu veriler, çalışmamız sonucunda alınan değerler ile başakta tane sayısı hariç benzerlik göstermektedir.

Üst boğum arası uzunluğu, başak boyu, başakta tane sayısı, başakta tane verimi (r=0,868**), bin tane ağırlığı, hektolitre ağırlığı, 2,5 mm elek üstü ve başaklanma gün sayısı arasında olumlu ve önemli ilişki saptanmıştır. Metrekarede biyolojik verim ve protein oranı yönünden ise olumlu ve önemsiz ilişki belirlenmiştir. Yürütülen bir araştırmada 13 maltlık arpa çeşidi 5 lokasyonda verim ve tanede protein kapsamı yönünden denenmiş protein-verim korelasyon katsayısı 0.4306 olarak bulunmuştur [9].

Başak boyu ile metrekarede biyolojik verim, başakta tane sayısı, başakta tane verimi, fertil başakçık sayısı, toplam başakçık sayısı, hektolitre ağırlığı ve başaklanma gün sayısı arasında olumlu ve önemli ilişki saptanmıştır. Protein oranı arasında ise olumsuz ve önemli ilişki belirlenmiştir. Arpada daha önce yapılan bir çalışmada [8] bulgularımızın aksine başak boyu ile başakta tane sayısı (r=-0.252**) arasında olumsuz ve önemli, protein oranı (r=0.206*) arasında olumlu ve önemli, tane verimi (r=-0.144) arasında olumsuz ve önemsiz ilişkiler tespit edilmiştir.

Metrekarede başak sayısı ile birim alan tane verimi arasında önemli ve pozitif korelasyon belirlenmiştir. Olumsuz ve önemli ilişki bin tane ağırlığında hesaplanmıştır. Yapılan bir çalışmada, kışlık ve yazlık olarak denenen arpa çeşitlerinin tane veriminin $m^2$'deki başak sayısından etkilendiğini, bin tane ağırlığının ise sadece yazlık arpada önemli olduğu vurgulanmıştır [10].

Korelasyon analizi sonuçlarına göre; hasat indeksi ile birim alan tane verimi, başakta tane sayısı, başakta tane verimi, hektolitre ağırlığı ve başaklanma gün sayısı arasında olumlu ve önemli ilişki saptanmıştır. Protein oranı yönünden ise olumsuz ve önemli ilişki belirlenmiştir. Çukurova koşullarında 25 adet iki sıralı arpa çeşit ve hatları ile yürütülen bir araştırmada, tane verimi ile başaktaki tane sayısı arasında önemli ve olumsuz, başakta tane sayısı ve bin tane ağırlığı ile bitki boyu arasında önemli ve olumlu ilişkiler elde edilmiştir [11].

Birim alan tane verimi ile metrekarede biyolojik verim (r=0,544**) arasında olumlu ve önemli ilişki saptanmıştır. Metrekarede biyolojik verim ile önemli ve pozitif korelasyonlar fertil başakçık sayısı ve toplam başakçık sayısı arasında belirlenmiştir. Olumsuz ve önemli ilişki hektolitre ağırlığında bulunmuştur. Korelasyon analizi sonuçlarına göre; başakta tane sayısı ile başakta tane verimi, hektolitre ağırlığı, elek üstü ve başaklanma gün sayısı arasında olumlu ve önemli ilişki tespit edilmiştir. Protein oranı (r=-0,743**) yönünden ise olumsuz ve önemli ilişki belirlenmiştir. 1000 tane ağırlığının diğer 8 karakterle ilişkisini belirlemek üzere, 50 adet arpa çeşidi kullanarak 10 yerde yapılan araştırmada, arpaların 1000 tane ağırlığı ile bitki boyu, tane, sap verimi ve toplam biyolojik verim arasında olumlu, kardeş başına tane ve $m^2$'deki kardeş sayısı arasında olumsuz ilişkiler olduğu görülmüştür [12].

Başakta tane verimi ile bin tane ağırlığı, hektolitre ağırlığı, 2,5 mm elek üstü ve başaklanma gün sayısı arasında (r=0,822**) olumlu ve önemli ilişki saptanmıştır. Protein oranı arasında ise (r=-0,807**) olumsuz ve önemli ilişki belirlenmiştir. Bu durum özellikle tane veriminin artması ile protein oranının azalmasını ifade etmektedir. Genel olarak taneye besin maddesi birikimi sırasında önce proteinler daha sonra da nişastalar birikmektedir. Nişasta birikimi fazla olduğunda tanedeki protein oranı azalmakta ancak bin tane ağırlığı ve bitkide tane verimi artmaktadır. Bu nedenle protein oranı ile bitkide tane verimi arasında belirlenen olumsuz ve önemli ilişki bu sonuçları destekler nitelikte bulunmuştur. Fertil başakçık sayısı ile önemli ve pozitif korelasyonlar toplam başakçık sayısı arasında (r=0,959**) bulunmuştur. Olumsuz ve önemli ilişki 2,5 mm elek üstü arasında hesaplanmıştır. Toplam başakçık sayısı ile 2,5 mm elek üstü arasında olumsuz ve önemli ilişki tespit edilmiştir. Erzurum şartlarında 30 yerli ve yabancı buğday çeşidiyle 2 yıl süreyle yürütülen bir araştırmada, $m^2$'deki fertil başak sayısı ile bitki boyu arasında olumlu ve önemli bir korelasyon bulunduğu, çeşitlerin bitki boyu ile tanenin protein oranı ve tane verimi arasında olumsuz ve önemli; başaktaki tane sayısı ile bin tane ağırlığı, protein oranı ve bitki boyu arasında olumsuz ve önemsiz korelasyonlar elde edilmiştir [13].

Korelasyon analizi sonuçlarına göre; bin tane ağırlığı ile hektolitre ağırlığı, 2,5 mm elek üstü ve başaklanma gün sayısı arasında olumlu ve önemli ilişki saptanmıştır. Yapılan bir çalışmada bin tane ağırlığı ile yatma, başak sapı uzunluğu ve verim arasında pozitif önemli bir ilişki bulunduğu belirtilmiştir [14]. Hektolitre ağırlığı ile 2,5 mm elek üstü ve başaklanma gün sayısı (r=0,717**) arasında olumlu ve önemli ilişki bulunmuştur. Protein oranı ile arasında ise (r=-0,702**) olumsuz ve önemli ilişki elde edilmiştir. Protein oranı ile olumsuz ve önemli korelasyonlar 2,5 mm elek üstü ve başaklanma gün sayısı (r=-0,821) arasında hesaplanmıştır. Korelasyon analizi sonuçlarına göre; 2,5 mm elek üstü ile başaklanma gün sayısı arasında olumlu ve önemli ilişki tespit edilmiştir.

## 4. SONUÇ

Kavuzsuz arpa genotiplerinde kuru koşullarda iki yıl süre ile yürütülen araştırmadan elde edilen verilerle korelasyon analizi yapılmış ve tane verimi ile ilişkili özelliklerin belirlenmesi amaçlanmıştır. Analiz sonuçlarına göre özellikler arası ilişkiler saptanmıştır.

Sonuç olarak, birim alan tane verimi ile metrekarede biyolojik verim, metrekarede başak sayısı ve hasat indeksi özellikleri arasında olumlu ve önemli ilişkiler belirlenmiştir. Özellikle son yıllarda ülkemizde gıda endüstrisinde önem kazanan kavuzsuz arpa ile kuru koşullarda yürütülmesi planlanan çalışmalarda denememizden elde edilen verilerin ıslahçılara yol gösterebileceği düşünülmektedir.

## Teşekkür

Bu çalışma Tarım ve Orman Bakanlığı, Tarımsal Araştırmalar ve Politikalar Genel Müdürlüğü tarafından (Proje No: TAGEM/TBAD/13/A12/P05/005) desteklenmiştir. Desteklerinden dolayı Tarımsal Araştırmalar ve Politikalar Genel Müdürlüğü'ne teşekkür ederiz.

*Prof. Dr. Saime ÜNVER İKİNCİKARAKAYA danışmanlığında Soner YÜKSEL'in tamamlamış olduğu "Bazı Kavuzsuz Arpaların (*Hordeum vulgare* L. var. *nudum* Hook. f.) Gelişme Dönemleri İle Verim ve Verim Öğelerinin Belirlenmesi" isimli doktora tezinden üretilmiştir.

## KAYNAKLAR

[1] TÜİK 2020. Türkiye İstatistik Kurumu. http://tuik.gov.tr [Ziyaret Tarihi: 21.09.2020]
[2] Yalçın E, Çelik S, Akar T, Sayım İ, Köksel H. Kavuzsuz arpanın önemi, β-glukan ve besinsel lif içeriği. Hububat Ürünleri Teknolojisi Kongresi, Bildiriler Kitabı, s.399-403, Gaziantep. 2006
[3] Anonymous. Cereal Programme, ICARDA Annual Report. 1994; 172 pp, Aleppo/Syria.
[4] Ottekin A, Akar T, Tosun H, Ozan AN, Demir Z. Kavuzsuz arpanın tarımsal ve teknolojik özelliklerinin belirlenmesi. IV. Ulusal Nükleer Tarım ve Hayvancılık Kongresi, Tebliğ Özetleri, s.29, Bursa. 1996.
[5] Karaduman Y. Kavuzsuz Arpa Potansiyeli. Unlu Mamuller Tek. Dergisi. 2006; 74: 21-26.
[6] Anonim. Eskişehir, Orman ve Su İşleri Bakanlığı Meteoroloji 3. Bölge Müdürlüğü Aylık Hava Raporu Verileri. 2014.

[7] Anonymous. JMP® Pro 13.0.0, Copyright © 2016, SAS Institute Inc., Cary, NC, USA.
[8] Tosun H, Ottekin A, Akar T. The Relations Between Yield and Some Characters Affecting Yield in Some Barley Cultivars. Tarla Bitkileri Merkez Araştırma Enstitüsü Dergisi. 1993; 2 (4).
[9] Tong Y, and Yan BX. A Preliminary Report on the Yield and Quality of Malting Barley and Their stability. Ningxia J. of. Agro-Forestry Science and Tech. 1989; (3), 4-7.
[10] Stock HG, Wıcke HJ, and Fuchs W. Determination of Optimum Ranges of Yield Structure in Different Cereals Grown on a D5 site. Field Crops. 1988; 32 (11): 721-729.
[11] Kılınç M, Kırtok Y, Yağbasanlar T. Çukurova Koşullarına Uygun Arpa Çeşitlerinin Geliştirilmesi Üzerinde Araştırmalar. 2. Arpa-Malt Semineri Tebliğleri. 1992; 205-218.
[12] Hadjıchrıstodoulou A. Stability of 1000 Grain Weight and Its Relaton with Other Traits of Barley In Dry Areas. Plant Breed. Abs., Vol: 61, No:5 (4314), May, 1991.
[13] Köycü C, Yılmaz B. Yield, Yield Components, and Quality of Foreing and Nature Wheat Varieties Grown at Erzurum, Turkey. 1977; 1-7.
[14] Kıran A.K. Bazı Arpa (Hordeum vulgare L.) Genetik Kaynakları Materyalinin Karakterizasyonu. Anadolu J. of AARI. 1999; 9(2); 72-90

.

**Ekler**
**Ek A Tablo 4.**

**Tablo 4.** 2013 ve 2014 yıllarında kuru koşullarda yetiştirilen kavuzsuz arpa genotiplerinin incelenen özelliklere ilişkin korelasyon katsayıları

| | BYA (1) | BYYKS (2) | SAPU (3) | UBAU (4) | BB (5) | $m^2$BS (6) | HI (7) | BATV (8) | $m^2$BV (9) | BTS (10) | BTV (11) | SBS (12) | FBS (13) | TBS (14) | BTANE (15) | HLT (16) | PO (17) | EÜ (18) | ÇS (19) |
|---|---|---|---|---|---|---|---|---|---|---|---|---|---|---|---|---|---|---|---|
| 2 | -0,324* | 1 | | | | | | | | | | | | | | | | | |
| 3 | 0,396** | -0,890** | 1 | | | | | | | | | | | | | | | | |
| 4 | 0,413** | -0,846** | 0,874** | 1 | | | | | | | | | | | | | | | |
| 5 | 0,230 | -0,263* | 0,429** | 0,378** | 1 | | | | | | | | | | | | | | |
| 6 | -0,168 | 0,069 | -0,165 | -0,202 | -0,201 | 1 | | | | | | | | | | | | | |
| 7 | 0,025 | -0,343** | 0,283* | 0,202 | -0,128 | 0,245 | 1 | | | | | | | | | | | | |
| 8 | -0,148 | -0,085 | 0,110 | 0,025 | 0,206 | 0,481** | 0,408** | 1 | | | | | | | | | | | |
| 9 | -0,103 | 0,296* | -0,195 | -0,264* | 0,254* | 0,248 | -0,069 | 0,544** | 1 | | | | | | | | | | |
| 10 | 0,181 | -0,729** | 0,748** | 0,614** | 0,398** | -0,055 | 0,362** | 0,230 | -0,110 | 1 | | | | | | | | | |
| 11 | 0,369** | -0,881** | 0,872** | 0,868** | 0,360** | -0,221 | 0,261* | 0,092 | -0,230 | 0,734** | 1 | | | | | | | | |
| 12 | -0,061 | -0,002 | 0,011 | 0,090 | 0,088 | 0,015 | -0,076 | 0,118 | 0,079 | -0,057 | 0,019 | 1 | | | | | | | |
| 13 | 0,131 | 0,037 | 0,138 | 0,001 | 0,598** | -0,093 | -0,079 | 0,108 | 0,388** | 0,205 | 0,001 | -0,165 | 1 | | | | | | |
| 14 | 0,118 | 0,027 | 0,160 | -0,001 | 0,635** | -0,051 | -0,059 | 0,161 | 0,420** | 0,203 | 0,002 | -0,075 | 0,959** | 1 | | | | | |
| 15 | 0,403** | -0,398** | 0,382** | 0,558** | 0,202 | -0,377** | -0,145 | -0,148 | -0,165 | 0,137 | 0,510** | 0,225 | -0,238 | -0,197 | 1 | | | | |
| 16 | 0,292* | -0,850** | 0,786** | 0,740** | 0,401** | -0,163 | 0,253* | -0,031 | -0,279* | 0,711** | 0,791** | -0,064 | 0,035 | 0,024 | 0,363** | 1 | | | |
| 17 | -0,285* | 0,895** | -0,864** | -0,794** | -0,287* | -0,073 | -0,461** | -0,243 | 0,106 | -0,743** | -0,807** | 0,009 | -0,065 | -0,067 | -0,273 | -0,702** | 1 | | |
| 18 | 0,099 | -0,604** | 0,461** | 0,579** | -0,183 | -0,106 | 0,132 | 0,030 | -0,195 | 0,297* | 0,616** | 0,084 | -0,436** | -0,455** | 0,582** | 0,412** | -0,529** | 1 | |
| 19 | -0,336** | -0,070 | 0,034 | -0,092 | -0,013 | 0,247 | 0,150 | 0,240 | 0,046 | 0,156 | 0,040 | -0,236 | 0,047 | 0,047 | -0,326** | 0,136 | -0,124 | 0,000 | 1 |
| 20 | 0,316* | -0,857** | 0,871** | 0,762** | 0,289* | -0,033 | 0,331** | 0,183 | -0,236 | 0,680** | 0,822** | -0,033 | 0,040 | 0,083 | 0,312* | 0,716** | -0,821** | 0,437** | 0,035 |

%5, %1 seviyesinde önemli. 1:BYA: Bayrak yaprağı alanı, 2:BYYKS: Bayrak yaprağı yeşil kalma süresi, 3:SAPU: Sap uzunluğu, 4:ÜBAU: Üst boğum arası uzunluğu, 5:BB: Başak boyu, 6:m2BS: Metrekarede başak sayısı, 7:HI: Hasat indeksi, 8:BATV: Birim alan tane verimi, 9:$m^2$BV: Metrekarede biyolojik verim, 10:BTS: Başakta tane sayısı, 11:BTV: Başakta tane verimi, 12:SBS: Steril başakçık sayısı, 13:FBS: Fertil başakçık sayısı, 14:TBS: Toplam başakçık sayısı, 15:BTANE: Bin tane ağırlığı, 16:HLT: Hektolitre ağırlığı, 17:PO: Protein oranı, 18:EÜ: 2.5 mm elek üstü, 19:ÇS: Çıkış süresi, 20:BGS: Başaklanma gün sayısı

Cilt 11, Sayı 2, Sayfa 13-16, 2022 Volume 11, Issue 2, Page 13-16, 2022

Araştırma Makalesi https://doi.org/10.46810/tdfd.765794 Research Article

Türk Doğa ve Fen Dergisi
Turkish Journal of Nature and Science
www.dergipark.gov.tr/tdfd

# Bingöl İli Açık Yeşil Alanlarında Kullanılan Peyzaj Bitkilerinin Arıcılık Açısından Önemi

**Ahmet CAF[1*], Deniz CANLI[2], Mihriban AHISKALI[2], Rıdvan POLAT[3]**

[1]Bingöl Üniversitesi, Teknik Bilimler Meslek Yüksekokulu Park ve Bahçe Bitkileri Bölümü, Bingöl, Türkiye
[2] Bingöl Üniversitesi, Gıda Tarım Ve Hayvancılık Meslek Yüksekokulu Bitkisel ve Hayvansal Üretim Bölümü, Bingöl, Türkiye
[3]Bingöl Üniversitesi, Ziraat Fakültesi Peyzaj Mimarlığı Bölümü, Bingöl, Türkiye

Ahmet CAF: 0000-0002-4295-7703
Deniz CANLI: 0000-0001-9794-8911
Mihriban AHISKALI: 0000-0003-0580-7594
Rıdvan POLAT: 0000-0003-0261-3671
**Sorumlu yazar: acaf@bingol.edu.tr*

(Alınış: 07.07.2020, Kabul: 21.03.2022, Online Yayınlanma: 29.06.2022)

**Anahtar Kelimeler**
Arıcılık,
Bal,
Bingöl,
Nektar,
Peyzaj Bitkileri,

**Öz:** Bingöl ili ülkemizde arıcılık açısından en önemli noktaların başında gelmektedir. Bu önemin asıl nedeni ilin doğal bitki örtüsü çeşitliliği ve yoğunluğudur. Sulak alanların çeşitliliği, bolluğu ve kısa mesafelerde artan rakım farklılıkları da bunu etkileyen unsurlardandır. Bingöl %28,4'lük orman varlığı ile ülkemizin en yeşil şehirlerinden biridir. Bu çalışmada, Bingöl ilinde yer alan açık ve yeşil alanlarda bitkisel tasarım çalışmalarında kullanılan bitkisel materyal tespit edilerek çeşitlilik belirlenmiş ve arıcılık açısından önemine değinilmiştir. Arıcılık açısından değerlendirmeler yapılırken; kullanılan bitkilerin nektar ve polen açısından önemine değinilerek eser, minör, sekonder ve dominant olmak üzere hangi oranlarda önemli olduğu tespit edilmiş ve önerilere yer verilmiştir. Araştırma sonucunda 41 familyaya ait 81 cins ve 102 taksonun ilin açık yeşil alanlarında peyzaj çalışmalarında kullanıldığı tespit edilmiştir. Polen açısından incelendiğinde; 14 taksonun eser, 12 taksonun minör, 8 taksonun sekonder ve 3 taksonun ise dominant olduğu toplam 37 takson tespit edilmiştir. Nektar açısından incelendiğinde ise; 9 takson eser, 10 takson minör, 5 takson sekonder ve 4 takson da dominant olmak üzere toplamda 28 takson belirlenmiştir. Polen açısından dominant olan cinsler; *Cornus*, *Cotoneaster* ve *Salix'*tir. Nektar açısından ise; *Pyrus*, *Robinia*, *Salix* ve *Tilia* cinsleri dominant derecede öneme sahiptir.



# The Importance of Landscape Plants Used in the Open Green Areas of Bingöl in Terms of Beekeeping

**Keywords**
Beekeeping,
Honey,
Bingöl,
Nectar,
Landscape Plants

**Abstract:** Bingöl is one of the most important points in terms of beekeeping in our country. The main reason for this importance is the natural vegetation diversity and density of the province. Diversity, abundance of wetlands and increasing altitude differences over short distances are also factors affecting this. Bingöl is one of the greenest cities of our country with a forest presence of 28.4%. In this study, diversity was determined by determining the vegetal material used in vegetation design studies in open and green areas in Bingöl province and its importance in terms of beekeeping was mentioned. Again, by mentioning the importance of the plants used in relation to the subject in terms of nectar and pollen, it was determined which proportions are important as works, minor, secondary and dominant and suggestions are given. As a result of the research, it was determined that 81 genera and 102 taxa belonging to 41 families were used in landscape studies in the open green areas of the province. In terms of pollen preferences of honey bees a total of 37 taxa were identified, of which 14 were rare, 12 were minor, 8 were secondary and 3 were dominant. In terms of nectar; a total of 29 taxa were determined, 9 taxa rare, 10 minor, 5 secondary and 4 taxa dominant. Dominant taxa in terms of pollen; *Cornus*, *Cotoneaster*, and *Salix*. In terms of nectar*; Pyrus*, *Robinia*, *Salix* and *Tilia* have a dominant degree**.**

## 1. GİRİŞ

Bitkiler insanlık tarihinin ilk gününden beri önemini korumaktadır. İnsanoğlu bitkileri başta besin kaynağı olmak üzere birçok amaç için doğrudan kullanmışlardır. Canlılar yaşamak için ekolojik olarak birbirlerine ihtiyaç duyarlar. Bitkilerin büyük bir çoğunluğu tozlaşmak için başka bir canlıya ihtiyaç duyarlar. Bu canlılar içerisinde; kelebekler böcekler ve en önemlisi arıların rolü büyüktür [1]. Arılardan ise bal arıları (*Apis melifera* L.) ile bitkiler arasındaki ortak ilişkinin her iki canlı için önemi son derece büyüktür [2]. Arılar beslenmek ve bal depolamak için bitkileri ziyaret ettikleri sırada onlardan polen, nektar ve salgı maddesi toplarlar[3].

Süs bitkileri renk, şekil, form ve estetik özellikleri ile dikkat çeken ilgi uyandıran otsu ve odunsu bitkiler olup, insanoğlunun acılarını ve sevinçlerini sembolize etmiş ve aynı zamanda teselli kaynağı olmuşlardır [4]. Bitkiler sürekli gelişen ve değişen canlılar oldukları için statik olmayıp dinamik özellikler gösteren varlıklardır. Bitkiler hem fonksiyonel hem de estetik özellikleri ile insanoğlu için çok önemli bir yere sahiptir [5]. Artan nüfus artışı ve buna bağlı olarak artan arazi kullanımı sonucunda doğa tahrip olmaktadır. Kişi başına düşen yeşil alan miktarı gelişmiş ülkelerle kıyaslandığında ülkemiz arka sıralarda yer almaktadır [6]. Kentsel yeşil alanlar insanların daima ihtiyaç duyduğu ortamlar olup, onlara; temiz hava, bol oksijen ve serbest hareket etme duygusu kazandıran, sağlıklı ruhsal ve bedensel açıdan faydalı bir ortam oluşturan yerlerdir [7].

Bu araştırmada; Bingöl ilinin açık ve yeşil alanlarında kullanılan peyzaj bitkileri tespit Ayrıca arıcılık açısından çok önemli bir noktada bulunan Bingöl ilinde gelecekte yapılması planlanan bal orman eylem planlarına katkı sağlayacağı ve ilerleyen dönemlerde yapılacak olan kentsel açık ve yeşil alanlarda kullanılan bitkisel materyale yön verebileceği düşünülmektedir.

## 2. MATERYAL VE METOT

Çalışma alanına konu olan Bingöl ili Doğu Anadolu bölgesinin yukarı Fırat bölümünde, Çapakçur ve Gayt derelerinin Bingöl ovasına ulaştığı alanda kurulmuştur. Daha sonra çeşitli nedenlerden dolayı bu alanın kuzeyinde, doğusunda ve güneyinde yer alan yüksek düzlüklere taşınmıştır. Doğu Anadolu Bölgesi'nin Yukarı Fırat bölümünde yer alan Bingöl ili 38° 27' ve 40°27' doğu boylamlarıyla 41°20' ve 39°54' kuzey enlemleri arasında bulunmaktadır (Şekil 1). Şehrin en alçak yeri 1050 metre olup ortalama 1150 metre rakıma sahiptir. Etrafındaki dağların ortalama yüksekliği 1700 metredir [8].

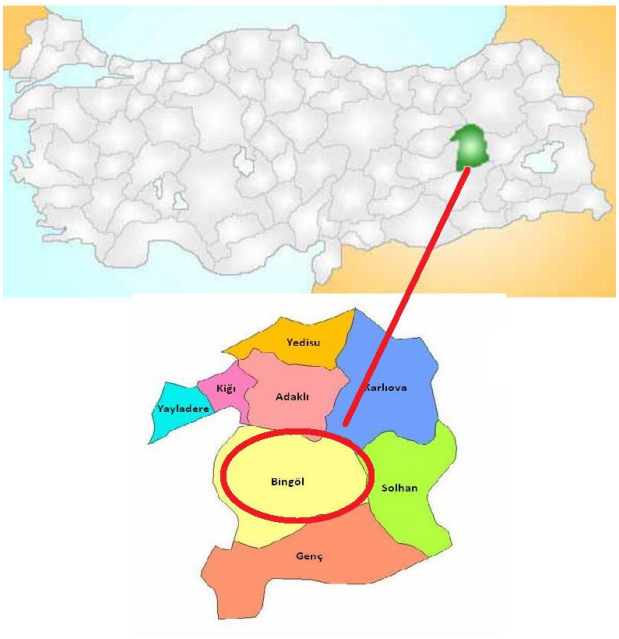


**Şekil 1.**Çalışma alanının genel görüntüsü

Bingöl ili, coğrafi konumu nedeniyle karasal iklim özelliklerinin hüküm sürdüğü bir yerleşim alanıdır. Bu durum; bölgede kuzey doğuya gidildikçe daha belirgin hal almaktadır. Bölgede kışlar karlı, uzun ve şiddetli yaz ayları ise genel anlamda sıcak ve nispeten kısadır. Fakat çalışma yapılan alan kendine özgü nedenlerden dolayı farklılıklar göstermektedir. Bölgede yapılan barajlar küresel ısınma ve şehrin etrafının dağlarla çevrili olup çanak biçiminde olmasından kaynaklanan yöresel bir klima söz konusudur.

Çalışmada ülkemizde arı bitkileri üzerine yapılmış literatürlerden faydalanılmıştır [9, 10]. Bunlara ek olarak kent merkezindeki açık ve yeşil alanlar gezilmiş gözlemler yapılmış, tespit edilen bitki türleri fotoğraflanmış ve teşhis edilmiştir. Çalışma yapılan alanlar haritalandırılırken uydu fotoğraflarından yararlanılmıştır.

## 3. BULGULAR

Araştırma sonucunda 41 familyaya ait 81 cins ve 102 taksonun ilin açık yeşil alanlarında peyzaj çalışmalarında (süsleme, gölgelik, yer örtücü, vurgu vb.) kullanıldığı tespit edilmiştir (Ek A). Peyzaj açısından en çok tercih edilen familyalar; Rosaceae (18 takson), Fabaceae (8 takson), Pinaceae (8 takson), Asteraceae (6 takson) ve Oleaceae (5 takson) olarak belirlenmiştir. En fazla taksona sahip cins ise; 5 taksonla *Prunus* olup bunu ve 3 taksonla *Cedrus* takip etmektedir. Alanda tespit edilen bitkiler hayat formu üzerinden değerlendirildiğinde % 48 ağaç, % 26 çalı, % 20 otsu, % 4 çalı veya ağaççık, % 2'i ise tırmanıcı formda oldukları belirlenmiştir.

Arıcılık açısından bakıldığında 18 familya ve 33 cinse ait toplam 37 taksonun önemli bir potansiyel taşıdığı tespit edilmiştir. Arı bitkileri bakımından ön plana çıkan familyalar; Rosaceae (10 takson), Sapindaceae, Oleaceae ve Astereceae (3'er takson)'dir (Şekil 2). Bu taksonlar literatür verileri ışığında polen ve nektar verimleri

açısından incelendiğinde [9,10]; 14 taksonun polen açısından eser, 12 taksonun minör, 8 taksonun sekonder ve 3 taksonun dominant olmak üzere toplam 37 taksonun arı ürünlerinde farklı kategorilerde etkiye sahip olabileceği görülmektedir. Nektar açısından bakıldığında ise; 9'u eser, 10'u minör, 5'i sekonder ve 4'ü de dominant etkiye sahip toplamda 29 takson belirlenmiştir. Polen açısından dominant etki gösterebilecek olan cinsler; *Cornus, Cotoneaster,* ve *Salix*'tir. Nektar açısından ise; *Pyrus, Robinia, Salix* ve *Tilia* dominant öneme sahiptir.

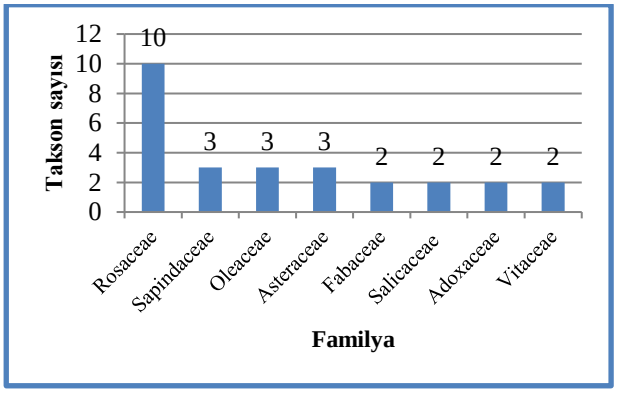


**Şekil 2.** Arıcılık açısından önemli familyalar ve takson sayıları

## 4. SONUÇ

Bingöl ili gerek konumu ve doğal koşulları gerekse de bal üretim miktarı açısından arıcılık faaliyetleri için önemli bir yere sahiptir. İran-Turan flora bölgesinin içinde yer alan ve topografik bakımdan farklılıklar gösteren alan, sahip olduğu floristik zenginlik ve çiçeklenme dönemindeki farklılıklar nedeniyle ülkemiz arıcılığı için zengin bir potansiyele sahiptir [11, 12]. Bingöl ilinde yapılan çalışmalar; arıcılık açısından önemli bitkilerin nisan ayında çiçeklenmeye başlayıp temmuz sonuna kadar devam ettiği gözlemlendiği ve doğal floranın arıcılık için uygun olduğu belirtilmiştir [12-15].

Bingöl ili açık yeşil alanlarında kullanılan peyzaj bitkilerinin genel durumuna bakıldığında egzotik türlerin bulunma yoğunluğu dikkat çekmektedir. Çalışma alanında doğal bitkilerin peyzajda kullanılması yok denecek kadar az bir seviyededir. Tarihi kayıtlara göre, insan aktivitesinin olduğu alan içine giren bitki türleri kent alanlarında kendini çoğaltmaya, yayılmaya başlamaktadır. Kent flora ve vejetasyonundaki bu değişimler, doğal türlerin yok olması ve doğal olmayan türlerin doğallaşması eğilimi ile sonuçlanır [16]. Peyzaj çalışmalarında öncelikli amaç ağaçlandırma ve yeşil alan oluşturmaktır. Bununla beraber alan peyzajında tercih edilen 102 bitkiden 37 (%36) taksonun taksonun arıcılık açısından önemli potansiyele sahip olduğu belirlenmiştir. Arıcılık açısından önemli görülen taksonlardan 10'unun Rosaceae ve 3'er taksonun ise Sapindaceae, Oleaceae ve Asteracea familyalarına ait olduğu görülmektedir. Polen açısından incelendiğinde 3 taksonun dominant, nektar açısından bakıldığında ise 4 taksonun ballarda dominant oranlarda önemli olduğu tespit edilmiştir. Polen açısından bakıldığında *Cornus, Cotoneaster, Salix* ve *Brassica* taksonları ön plana çıkarken, nektar açısından değerlendirme yapıldığında *Pyrus, Robinia, Salix* ve *Tilia* taksonlarının önemli bir yere sahip olduğu görülmektedir.

Öztürk vd. (2017) tarafından yapılan çalışmada, muhtemel peyzaj düzenlemelerinde arıcılık faktörünün göz önünde bulundurulmasının bölge arıcılığına katkı sağlayabileceği vurgulanmıştır [17]. Bingöl Üniversitesi'nin Tarım ve Havza Bazlı Kalkınma alanında pilot üniversite olarak seçilmesi ve ihtisaslaşma alanlarının "Arı ve Arı Ürünleri" ile "Ekonomik Değeri Yüksek Bitkilerin Tespiti ve Değerlendirilmesi" olarak belirlenmesinin ardından; üniversite bünyesinde arıcılık ile alakalı birçok proje yürütülmeye başlanmıştır. İlin arıcılığının gelişimi açısından açık ve yeşil alanlarda kullanılacak bitkisel peyzaj materyalleri seçilirken arıcılık faktörünün de göz önünde bulundurulmasının önemi ortaya çıkmaktadır. Yapılan çalışmada arıcılık açısından önemli olan bazı doğal süs bitkilerinin sonraki dönemlerde yapılacak açık ve yeşil alan bitkisel tasarımlarında kullanılmaları, bölge iklimine uygunluk ve arıcılık açısından oldukça önem taşımaktadır.

## KAYNAKLAR

[1] Özbek H. Kültür bitkilerinin tozlaşmalarında bal arısı (*Apis mellifera* L.). Atatürk Üniversitesi, Ziraat Fakültesi Dergisi, 1979, 10: 1-2.

[2] Yücel B, Duman I. Effects of foraging activity of honeybees (Apis mellifera L.) on onion (Allium cepa) seed production and quality. Pakistan Journal of Biological Sciences, 2005, 8: 123–126.

[3] Fıratlı Ç, Gençer HV. Dünya arıcılığı ve Türkiye'nin yeri, Türkiye II. Teknik Arıcılık Kongresi (8-9 Şubat 1994), T.C. Ziraat Bankası Kültür Yayınları, 1995, 28: 20-28, Ankara.

[4] Kılıç Ö. Bingöl'de süs bitkisi olarak kullanılabilme potansiyeli olan bazı doğal bitkiler. Peyzaj ve Süs Bitkiciliği Dergisi, 2018.

[5] Güçlü K. Erzurum'da kültürel çevrenin güzelleştirilmesinde kullanılabilecek süs ağaç ve ağaççıklarının yetiştirilmesi. Atatürk Üniversitesi Ziraat Fakültesi Dergisi, 1994, 25: 461-468.

[6] Ekici B, Sarıbaş M. Bartın kenti peyzaj düzenlemelerinde kullanılan bitki materyalleri üzerine bir araştırma. ZKÜ Bartın Orman Fakültesi Dergisi, 2006, 8(9): 1-9.

[7] Smardon R C. Perception aesthetics of the urban environment: Review of the role of vegetation, landscape and urban planning, Elsevier Science Publication, B.V., Amsterdam, 1990, 105-120.

[8] Caf A, Irmak MA, Yılmaz H. Woody plants used in green spaces of Bingöl city and their use aims. Iğdır Üniversitesi Fen Bilimleri Dergisi, 2016, 6(2): 103 – 110.

[9] Sorkun K. Türkiye'nin nektarlı bitkileri, polenleri ve balları, Palme Yayıncılık, 2010. Ankara.

[10] Özhatay N, Koçyiğit M, Bona M. İstanbul'un ballı bitkileri, Bal-Der Yayıncılık, 2010, İstanbul.

[11] Sandal E K, Kan C. Bingöl ilinde arıcılık faaliyetleri. Türk Coğrafya Dergisi, 2013, 60: 1-12.

[12] Behçet L, Yapar Y. Matan dağı (Bingöl) florasında arıcılık açısından önemli bitkiler. Biyolojik Çeşitlilik ve Koruma Dergisi, 2019, 12(1), 149-159.

[13] Bakoğlu A, Kutlu M A, Kökten K. Bingöl yöresinde bal arısı (*Apis mellifera* L.) için önemli olan

bitkilerin tespiti, ömür uzunlukları ve çiçeklenme tarihleri. Türkiye 10. Tarla Bitkileri Kongresi Ankara, 2011.

[14] Polat R, Esim N, Ürüşan Z, Caf A, Ahıskalı M, Canlı D. Solhan (Bingöl) florasının arıcılık açısından değerlendirilmesi. Türk Doğa ve Fen Dergisi 2020;9:1-10. doi:10.46810/tdfd.772388.

[15] Polat R, Canlı D, Selvi S, Esim N, Çakılcıoğlu U, et al. Bingöl arı florası ve polen atlası. Ankara,Türkiye. Akademisyen Yayınevi; 2021.

[16] Sukkop H (ed), Urban ecology: Plants and plant communities in urban environments, SPB Publishing, The Hague, 2004, 45-74

[17] Öztürk F, Erkan C, Ölçücü C, Çiriğ N, Özok N, Öğün E. Van ili peyzaj bitkilerinin arıcılık açısından değerlendirilmesi. Yüzüncü Yıl Üniversitesi Tarla Bilimleri Dergisi, 2017, 27(4): 601-607.

## Ekler

**Ek A.** Bingöl İli Açık ve Yeşil Alanlarında Kullanılan Peyzaj Bitkilerinin Arıcılık Açısından Önemi

| | Bilimsel Adı | Familyası | Yöresel İsimleri | Kökeni | Çiçeklenme Dönemi | Formu | Arıcılık Açısından Önemi |
|---|---|---|---|---|---|---|---|
| 1 | *Sambucus nigra* L. | Adoxaceae | Mürver, Çındar | Avrupa, Hindistan | Haziran | Çalı | Polen*/Nektar* |
| 2 | *Viburnum opulus* L. | Adoxaceae | Kartopu | Avrupa, Kuzey Afrika | Nisan-Ağustos | Çalı | Polen*/Nektar*** |
| 3 | *Celosia argentea* L. | Amaranthaceae | Horozibiği | Asya | Haziran-Kasım | Otsu | |
| 4 | *Bellis perennis* L. | Asteraceae | Koyungözü | Avrupa Sibirya | Mart-Temmuz | Otsu | Polen* |
| 5 | *Callistephus chinensis* (L.) Nees | Asteraceae | Çin Asteri | Çin | Nisan-Mayıs | | |
| 6 | *Gaillardia aristata* Pursh | Asteraceae | Gaylardia | Amerika | Haziran-Ekim | Otsu | Polen**/Nektar** |
| 7 | *Gazania rigens* (L.) Gaertn. | Asteraceae | Gazanya | Güney Afrika | Haziran-Ekim | Otsu | |
| 8 | *Dahlia variabilis* (Willd.) Desf | Asteraceae | Yıldız Çiçeği | Meksika | Haziran-Kasım | Otsu | |
| 9 | *Zinnia elegans* L. | Asteraceae | Zinya | Meksika | Mayıs-Ekim | Otsu | Polen**/Nektar** |
| 10 | *Begonia cucullata* Willd. | Begoniaceae | Begonya | Brezilya | Mayıs-Eylül | Otsu | |
| 11 | *Berberis thunbergii* DC. | Berberidaceae | Berberis, Kadıntuzluğu | Asya, Avrupa ve Kuzey Amerika | Nisan - Mayıs | Çalı | Polen*/Nektar* |
| 12 | *Mahonia japonica* (Thunb.) DC. | Berberidaceae | Mahonya | Güney Asya | Mayıs | Çalı | |
| 13 | *Betula pendula* Roth | Betulaceae | Huş ağacı | Kuzey Avrupa, Asya Türkiye | Mart-Nisan | Ağaç | |
| 14 | *Catalpa bignonioides* Walter | Bignoniaceae | Katalpa | Güneydoğu Amerika | Mayıs-Temmuz | Ağaç | |
| 15 | *Catalpa bungei* C.A.Mey. | Bignoniaceae | Top katalpa | Amerika | Haziran-Temmuz | Ağaç | |
| 16 | *Brassica oleracea* L. | Brassicaceae | Lahana | Akdeniz | Haziran-temmuz | Otsu | Polen***/ Nektar*** |
| 17 | *Alyssum maritimum* (L.) Lam. | Brassicaceae | Kuduzotu | Avrupa | Nisan-Mayıs | Otsu | |
| 18 | *Buxus sempervirens* L. | Buxaceae | Şimşir | İngiliz adaları | Ocak-Nisan | Çalı | |
| 19 | *Abelia grandifolia* Villarreal | Caprifoliaceae | Abelya | Doğu Asya, Meksika | Mayıs-Kasım | Çalı | |
| 20 | *Lonicera caprifolium* L. | Caprifoliaceae | Hanimeli | Avrupa | Mayıs-Temmuz | Çalı | Polen*/Nektar* |
| 21 | *Symphoricarpos albus* (L.) S.F.Blake | Caprifoliaceae | İnci Çalısı | Kuzey Amerika | Nisan-Mayıs | Çalı | |
| 22 | *Weigela florida* (Bunge) A. DC. | Caprifoliaceae | Vangelya, Gelintacı | Doğu Asya, Çin, Kore | Nisan | Çalı | |
| 23 | *Dianthus barbatus* L. | Caryophyllaceae | Hüsnüyusuf | Anadolu, Kuzey ve Orta Avrupa, Balkanlar, Doğu Asya | Mayıs-Haziran | Otsu | |
| 24 | *Dianthus chinensis* L. | Caryophyllaceae | Çin Karanfili | Çin | Nisan-Mayıs | Çok yıllık yarı odunsu bitki | |
| 25 | *Euonymus japonicus* Thunb. | Celastraceae | Japon papaz külahı, taflan | Japonya | Mayıs-Ağustos | Çalı | |
| 26 | *Cornus alba* L. | Cornaceae | Kızılcık | Türkiye, Orta Güney Avrupa Kafkaslar | Mart-Nisan | Ağaç | Polen****/ Nektar** |
| 27 | *Cupressus arizonica* Greene | Cupressaceae | Mavi servi | Meksika ve Arizona | Mart | Ağaç | Polen* |
| 28 | *Juniperus chinensis* Roxb. | Cupressaceae | Yayılıcı ardıç | Çin | Mart-Nisan | Çalı | |
| 29 | *Platycladus orientalis* (L.) Franco | Cupressaceae | Doğu mazısı | Çin, Hindistan | Haziran-Temmuz | Çalı | |
| 30 | *Thuja orientalis* L. | Cupressaceae | Mazı | Doğu Asya | Mayıs-Haziran | Çalı | |
| 31 | *Elaeagnus angustifolia* L. | Elaeagnaceae | İğde | Asya | Nisan-Haziran | Çalı veya Ağaç | Polen*/Nektar** |
| 32 | *Albizia julibrissin* Durazz. | Fabaceae | Gülbirişim | Japonya, Batı Asya | Mayıs-Ağustos | Ağaç | |
| 33 | *Cercis siliquastrum* L. | Fabaceae | Erguvan | Güney ve Orta Avrupa | Nisan-Mayıs | Çalı veya Ağaç | Polen*/Nektar* |
| 34 | *Chaenomeles japonica* (Thunb.) Lindl. ex Spach | Fabaceae | Japon ayvası | Japonya | Mart-Nisan | Çalı | |
| 35 | *Gleditschia triacanthos* L. | Fabaceae | Gledіçya, yalancı keçiboynuzu | Orta ve Doğu Amerika | Nisan-Haziran | Ağaç | |
| 36 | *Laburnum anagyroides* Medik. | Fabaceae | Sarısalkım | Güney Avrupa | Nisan-Mayıs | Ağaç | |
| 37 | *Robinia hispida* L. | Fabaceae | Kıllıakasya | Kuzey Amerika | Mayıs | Ağaç | |
| 38 | *Robinia pseudoacacia* L. | Fabaceae | Akasya, Yalancı Akasya | Doğu ve Orta İngiltere | Nisan-Haziran | Ağaç | Polen*/Nektar**** |
| 39 | *Wisteria sinensis* (Sims) Sweet | Fabaceae | Mor salkım | Çin | Nisan-Haziran | Çalı | |
| 40 | *Quercus rubra* L. | Fagaceae | Meşe | Anadolu, Avrupa, Kuzey Amerika | Nisan - Mayıs | Ağaç | |
| 41 | *Pelargonium zonale* (L.) L'Hér. ex Aiton | Geraniaceae | Sardunya | Güney Afrika | Haziran-Kasım | Otsu | |
| 42 | *Ribes nigrum* L. | Grossulariaceae | Karagat | Avrupa, Asya | Nisan | Çalı | |
| 43 | *Juglans regia* L. | Juglandaceae | Ceviz | Orta Asya | Nisan-Mayıs | Ağaç | Polen** |
| 44 | *Salvia splendens* Sellow ex Schult. | Lamiaceae | Ateş çiçeği | Güney Amerika | Haziran-Ekim | Otsu | |
| 45 | *Fritillaria imperialis* L. | Liliaceae | Ağlayan gelin | Orta Doğu, Türkiye | Mart- Nisan | Otsu | |
| 46 | *Hibiscus syriacus* L. | Malvaceae | Hatmi çalısı | Çin | Mayıs-Haziran | Otsu | |
| 47 | *Tilia tomentosa* Moench | Malvaceae | Ihlamur | Güneydoğu Avrupa | Mayıs-Haziran | Ağaç | Polen***/ Nektar**** |

**Ek A (Devamı).** Bingöl İli Açık ve Yeşil Alanlarında Kullanılan Peyzaj Bitkilerinin Arıcılık Açısından Önemi

| | Bilimsel Adı | Familyası | Yöresel İsimleri | Kökeni | Çiçeklenme Dönemi | Formu | Arıcılık Açısından Önemi |
|---|---|---|---|---|---|---|---|
| **48** | *Maclura pomifera* (Raf.) C.K.Schneid. | Moraceae | Ayı dutu, yalancı, Portakal ağacı | | Mayıs-Haziran | Ağaç | |
| **49** | *Morus alba* L. | Moraceae | Dut | Çin, Japonya | Mayıs | Ağaç | Polen* |
| **50** | *Forsythia* × *intermedia* Zabel | Oleaceae | Altınçanak, altınçan | Kuzey İrlanda | Mart-Mayıs | Çalı | Polen* |
| **51** | *Fraxinus americana* L. | Oleaceae | Amerikan dişbudağı | | Mart- Nisan | Ağaç | |
| **52** | *Fraxinus excelsior* L. | Oleaceae | Dişbudak | | Mart- Nisan | Ağaç | Polen*/Nektar* |
| **53** | *Ligustrum vulgare* L. | Oleaceae | Adi kurtbağrı | Avrupa, Kuzey Afrika, Asya | Mayıs-Haziran | Çalı | Polen**/Nektar* |
| **54** | *Syringa vulgaris* L. | Oleaceae | Leylak | Güneydoğu Avrupa | Mart-Haziran | Çalı veya Ağaç | |
| **55** | *Paulownia tomentosa* Steud. | Paulownaceae | Pavlonya | Doğu Asya | Nisan-Haziran | Ağaç | |
| **56** | *Abies nordmanniana* (Steven) Spach * | Pinaceae | Kafkas göknarı | | Nisan | Ağaç | |
| **57** | *Cedrus atlantica* (Endl.) Manetti ex Carrière | Pinaceae | Atlas sediri | Himalayalar, Afganistan, Kuzey Afrika | Kasım-Aralık | Ağaç | |
| **58** | *Cedrus deodara* (Roxb. ex D.Don) G.Don | Pinaceae | Himalaya sediri | Himalayalar | Kasım-Aralık | Ağaç | |
| **59** | *Cedrus libani* A.Rich. | Pinaceae | Sedir | Lübnan | Kasım-Aralık | Ağaç | |
| **60** | *Picea abies* (L.) H.Karst. | Pinaceae | Avrupa lâdini | Kuzey Yarım Küre | Nisan-Mayıs | Ağaç | |
| **61** | *Pinus nigra* J.F.Arnold | Pinaceae | Karaçam | Asya, Kırım, Balkanlar | Nisan- Mayıs | Ağaç | |
| **62** | *Pinus sylvestris* L. | Pinaceae | Sarıçam | Avrupa, Sibirya | Temmuz -Eylül | Ağaç | |
| **63** | *Picea pungens* Engelm. | Pinaceae | Mavi ladin | Kuzey Amerika | Nisan-Mayıs | Ağaç | |
| **64** | *Antirrhinum majus* L. | Plantaginaceae | Aslanağzı | Akdeniz | Haziran-Eylül | Otsu | |
| **65** | *Platanus acerifolia* (Aiton) Willd. | Platanaceae | Akçaağaç yapraklı çınar | İngiltere | Nisan-Mayıs | Ağaç | |
| **66** | *Platanus orientalis* L. | Platanaceae | Çınar | Anadolu, Asya | Mart-Nisan | Ağaç | |
| **67** | *Portulaca grandiflora* Hook. | Portulacaceae | İpek tırnağı | Güney Amerika | Nisan-Haziran | Otsu | |
| **68** | *Chaenomeles sinensis* (Dum.Cours.) Koehne | Rosaceae | Ayva | Doğu Asya, Çin | Nisan-Mayıs | Ağaç | |
| **69** | *Cotoneaster horizontalis* Decne. | Rosaceae | Dağ muşmulası | Avrupa, Güney Afrika ve Asya | Nisan-Mayıs | Çalı | Polen****/ Nektar*** |
| **70** | *Cotoneaster dammeri* C.K.Schneid. | Rosaceae | Medik | Çin | Nisan-Mayıs | Çalı | |
| **71** | *Crataegus monogyna* Jacq. | Rosaceae | Sinz, Sez, Yemişen, Alıç | Kuzeydoğu Anadolu ile Avrupa, Kıbrıs, Suriye ve Kuzey Irak | Mayıs-Haziran | Çalı veya Ağaç | Polen**/Nektar*** |
| **72** | *Kerria japonica* (L.) DC. | Rosaceae | Kanarya gülü, kerya | Çin, Japonya | Mart-Ağustos | Çalı | |
| **73** | *Malus pumila* Mill. | Rosaceae | Elma | Avrupa, Türkiye | Nisan-Mayıs | Ağaç | |
| **74** | *Malus hupehensis* (Pamp.) Rehder | Rosaceae | Süselması | Çin | Nisan-Mayıs | Ağaç | |
| **75** | *Prunus armeniaca* L. | Rosaceae | Kayısı | Çin | Mart-Nisan | Ağaç | Polen**/Nektar** |
| **76** | *Prunus avium* (L.) L. | Rosaceae | Kiraz | | Nisan-Mayıs | Ağaç | Polen**/Nektar** |
| **77** | *Prunus cerasus* L. | Rosaceae | Vişne | | Nisan-Mayıs | Ağaç | |
| **78** | *Prunus divaricata* var. *pissardi* Koch. | Rosaceae | Erik | Güneydoğu Avrupa ve Batı Asya | Nisan | Ağaç | Polen**/Nektar** |
| **79** | *Prunus dulcis* (Mill.) D.A.Webb | Rosaceae | Badem | | Mart-Nisan | Ağaç | Polen* |
| **80** | *Pyracantha coccinea* M.Roem. | Rosaceae | Ateş dikeni | Güneydoğu Avrupa | Nisan-Haziran | Çalı | Polen***/Nektar* |
| **81** | *Pyrus communis* L. | Rosaceae | Armut | Kuzey ve Güneybatı Anadolu ile Kafkasya | Mayıs-Haziran | Ağaç | Polen***/ Nektar**** |
| **82** | *Pyrus salicifolia* Pall. | Rosaceae | Dadaş armudu | Orta Doğu | Mayıs-Haziran | Ağaç | |
| **83** | *Rosa canina* L. | Rosaceae | İt gülü, Kuşburnu | Avrupa, Kuzey Afrika, Batı Asya | Mayıs-Temmuz | Çalı | Polen**/Nektar* |
| **84** | *Rosa hybrida* Vill | Rosaceae | Gül | Asya, Avrupa | Nisan-Mayıs | Çalı | |
| **85** | *Spiraea* × *vanhouttei* (Briot) Zabel | Rosaceae | Bahçe ispiryası | Avrupa, Asya, Kuzey Amerika, Meksika | Nisan-Temmuz | Çalı | Polen**/Nektar** |
| **86** | *Populus alba* L. | Salicaceae | Akkavak | Avrupa, Sibirya, Batı Asya ve Kuzey Amerika | Nisan-Mayıs | Ağaç | Polen*** |
| **87** | *Populus nigra* L. | Salicaceae | Karakavak | Asya, Kırım, Balkanlar | Nisan | Ağaç | |
| **88** | *Salix alba* L. | Salicaceae | Söğüt | Kuzey Afrika, Avrupa ve Asya, Türkiye | Nisan-Mayıs | Ağaç | Polen****/ Nektar**** |
| **89** | *Salix babylonica* L. | Salicaceae | Salkım söğüt | Çin | Nisan | Ağaç | |
| **90** | *Acer negundo* L. | Sapindaceae | İsfendan, akçaağaç | Kuzey Amerika | Mart-Nisan | Ağaç | Polen***/Nektar** |
| **91** | *Acer pseudoplatanus* L. | Sapindaceae | Dağ akçaağacı, Çınar yapraklı akçaağaç | Avrupa, Sibirya, Türkiye | Mart-Nisan | Ağaç | Polen***/Nektar** |
| **92** | *Aesculus hippocastanum* L. | Sapindaceae | At kestanesi | Kuzey Amerika | Nisan-Mayıs | Ağaç | Polen**/Nektar* |
| **93** | *Koelreuteria paniculata* Laxm. | Sapindaceae | Güvey feneri | Çin, Kore | Haziran-Ağustos | Ağaç | |
| **94** | *Buddleja davidii* Franch. | Scrophulariaceae | Kelebek çalısı | Orta ve Batı Çin | Mayıs-Kasım | Çalı | |
| **95** | *Ailanthus altissima* (Mill.) Swingle | Simaroubaceae | Kokar ağaç | Çin | Mayıs-Haziran | Ağaç | |
| **96** | *Petunia hybrida* Vilm. | Solanaceae | Petunya | Güney Amerika | Haziran-Kasım | Otsu | |
| **97** | *Tamarix tetrandra* Pall. ex M.Bieb. | Tamaricaceae | Ilgın, gezik | Güneydoğu Avrupa, Asya | Nisan-Mayıs | Çalı | |
| **98** | *Taxus baccata* L. | Taxaceae | Porsuk | Avrupa ile Akdeniz, Türkiye ve Kafkasya | Nisan-Mayıs | Ağaç | Polen* |
| **99** | *Ulmus glabra* Huds. | Ulmaceae | Dağ karaağacı | Avrupa, Sibirya | Nisan | Ağaç | |
| **100** | *Viola wittrockiana* Gams ex Nauenb. & Buttler | Violaceae | Menekşe | Avrupa | Ekim-Mayıs | Otsu bitki | |
| **101** | *Parthenocissus quinquefolia* (L.) Planch. | Vitaceae | Amerikan sarmaşığı | Kuzey Amerika | Haziran-Temmuz | Tırmanıcı | Polen**/Nektar*** |
| **102** | *Vitis vinifera* L. | Vitaceae | Asma | Akdeniz | Mayıs | Tırmanıcı | Polen*** |

EK

Araştırma Makalesi https://doi.org/10.46810/tdfd.1017787 Research Article

Türk Doğa ve Fen Dergisi
Turkish Journal of Nature and Science
www.dergipark.gov.tr/tdfd

# Effects of Regular and Continuous Exercise on Oxidative Stress and Apoptosis

**Fatih ÇAKAR[1*], Abdurrauf YÜCE[2], Gözde ARKALI[2]**

[1] Bingol University, Vocational School of Health Services, Department of Therapy and Rehabilitation, Bingöl, Türkiye
[2] Fırat University, Faculty of Veterinary Medicine, Department of Physiology, Elaziğ, Türkiye
Fatih ÇAKAR ORCID No: 0000-0002-7551-4087
Abdurrauf YÜCE ORCID No: 0000-0003-2928-5970
Gözde ARKALI ORCID No: 0000-0002-0850-7557

**Corresponding author: fcakar@bingol.edu.tr*

(Received: 02.11.2021, Accepted: 06.04.2022 Online Publication: 29.06.2022)

**Keywords**
Exercise, Oxidative stress, Apoptosis, BAX / BCL-2

**Abstract:** This study, it was aimed to investigate the effects of intense acute exercise and regular and continuous exercise on oxidative stress parameters and apoptosis-related Bax and Bcl-2 protein levels in rats. In the study, 1 control and 4 experimental groups were formed from 35 male Wistar-Albino rats, 7 in each group. The control group was not exercised, the other four groups exercised at a speed of 1.5 km/h for 1 hour on a 20-degree incline treadmill every day. Control and 1st, 2nd, 3rd, and 4th groups at the end of the 1st, 7th, 15th, and 30th day, respectively, were sacrificed. Malondialdehyde (MDA) as an indicator of lipid peroxidation, and Glutathione (GSH), Catalase (CAT), Glutathione Peroxidase (GSH-Px) activity as an antioxidant indicators in muscle and plasma were measured. BAX and BCL-2 protein expression levels were also checked for apoptosis in skeletal muscle. According to the results obtained, skeletal muscle and plasma MDA values increased after acute exercise ($P<0.05$), while skeletal muscle and plasma GSH-Px and CAT values increased significantly after regular and continuous exercise ($P<0.01$). It was observed that BAX protein expression level increased, BCL-2 protein expression level decreased and BAX/BCL-2 ratio increased in acute exercise ($p<0.05$). As a result, it was concluded that regular and continuous exercise has a protective effect against oxidative stress and, apoptosis triggered by acute exercise can be suppressed by regular and continuous exercise.



# Düzenli ve Sürekli Egzersizin Oksidatif Stres ve Apoptozise Etkisi

**Anahtar Kelimeler**
Egzersiz, Oksidatif stres, Apoptozis, BAX/BCL-2

**Özt:** Bu çalışmada, ratlarda zorlayıcı veya yoğun bir şekilde yapılan akut egzersiz ile düzenli ve sürekli olarak yapılan egzersizin oksidatif stres parametreleri ve apoptozis ile ilişkili Bax ve Bcl-2 protein düzeyleri üzerine etkisinin araştırılması amaçlandı. Çalışmada 35 adet Wistar-Albino ırkı erkek sıçanlardan, her grupta 7 adet olacak şekilde 1 kontrol ve 4 deney grubu oluşturuldu. Kontrol grubuna egzersiz yaptırılmadı, diğer dört gruba her gün 20 derece eğimli koşu bandında 1 saat boyunca 1,5 km/h hızında egzersiz yaptırıldı. 1., 7., 15. ve 30. gün sonunda sırasıyla kontrol ve 1., 2., 3. ve 4. gruplar sakrifiye edildi. Kas ve plazmada, lipid peroksidasyonunun göstergesi olarak Malondialdehit(MDA) seviyelerine, antioksidan göstergesi olarak Glutatyon(GSH), Katalaz(CAT), Glutatyon Peroksidaz(GPx) aktivitelerine bakıldı. İskelet kasındaki apoptozis için de BAX ve BCL-2 protein ekspresyon düzeylerine bakıldı. Elde edilen sonuçlara göre, akut egzersiz sonrası iskelet kası ve plazma MDA değerleri yükselirken ($P<0,05$), düzenli egzersize devam ettikten sonra, iskelet kası ve plazma GPx, CAT değerlerinde anlamlı artış olduğu belirlendi ($P<0,01$). Akut egzersizde BAX protein eksprasyon düzeyinin arttığı, BCL-2 protein eksprasyon düzeyinin azaldığı ve BAX/BCL-2 oranın arttığı ($p<0,05$) görüldü. Sonuç olarak, düzenli ve sürekli egzersizin oksidatif strese karşı koruyucu etkisinin olduğu ve akut egzersizle tetiklenen apoptozisin düzenli ve sürekli egzersizle baskılanabileceği kanısına varıldı.

## 1. INTRODUCTION

Physical activities carried out within a certain plan and program to develop or protect one or more structures of the body are called exercise [1]. A healthy and productive life depends on individuals exercising regularly [2], but the type, and intensity of exercise have different effects on human metabolism. It has been determined that acute, intense exercise triggers the formation of free radicals, affects the antioxidant defense system in different ways, and causes programmed cell death by activating apoptotic mechanisms in the cell, thus causing cellular damage. In cases where exercise is applied regularly for a long time, it has been determined that the level of oxidative damage is reduced, antioxidant enzyme activity is increased and apoptotic mechanisms are not significantly affected [3,4].

Both at rest and during contraction, skeletal muscles produce reactive oxygen (ROS) and nitrogen species (RNS). Physiologically, low levels of ROS are produced in the muscles to regulate muscle tone and maintain their contractility, but excessive ROS formation occurs as a result of intense and long-term exercises, which causes muscle damage, limitations in muscle function, and dysfunction in muscle contractions [5]. This is the result of intense and prolonged exercise inflicting oxidative damage to both proteins and lipids in contracted muscle fibers [6]. Regular exercise causes changes in both enzymatic and non-enzymatic antioxidants in skeletal muscle. Numerous studies in both animals and humans have shown that after aerobic exercise, antioxidant enzyme activity increases in blood and tissues [7,8].

In addition to acute resistance exercise, endurance exercises cause an increase in apoptosis [4,9,10], while moderate exercise does not significantly affect apoptosis. The intensity of potential mediators of apoptosis increases with exercise intensity and, after exceeding a certain level, they trigger apoptosis [11].

This study, it was aimed how acute exercise affects oxidative stress in skeletal muscle and plasma and how it shapes some protein expressions related to apoptosis. At the same time, it is aimed to investigate how these two mechanisms will be affected when exercise is continued regularly and continuously.

## 2. MATERIAL AND METHOD

This study was conducted with the permission of Fırat University Animal Experiments Local Ethics Committee (Meeting: 2019/06, Decision No: 58). In the study, 35 Wistar Albino breed male rats, 3-6 months old and weighing 250-300 grams, were used. Experimental applications were carried out in accordance with the conditions of care and use of laboratory animals (12 hours light: 12 hours dark and 24±3°C). During the experimental applications, standard commercial rat food (pellet food) and tap water were given to the rats. After a one-week adaptation period, the rats were divided into 5 groups, 7 in each group, as indicated below. The application of exercise on the groups is as the following: Control Group: No exercise was applied. 1. Experimental Group: One day, acute exercise was done at a speed of 1.5 km h-1 for 1 hour on a 20-degree incline treadmill. 2. Experimental Group: Acute exercise was done for 1 hour at a speed of 1.5 km h-1 on a 20-degree incline treadmill every day for a week. 3. Experimental Group: Acute exercise was done at a speed of 1.5 km h-1 for 1 hour on a 20-degree incline treadmill every day for 15 days. 4. Experimental Group: Acute exercise was done at a speed of 1.5 km h-1 for 1 hour on a 20-degree incline treadmill every day for a month. After intraperitoneal administration of the xylazine (10 mg kg-1)/ketamine (60 mg kg-1) combination, the rats were sacrificed under anesthesia and tissue samples were taken from the biceps femoris muscle and blood samples from the vena cava caudalis. The samples were stored in deep freeze at -20°C until analysis. MDA and GSH levels, CAT and GSH-Px enzyme activity in biceps femoris muscle and plasma were measured spectrophotometrically. BAX and BCL-2 protein expression levels, which are markers of apoptosis in skeletal muscle, were measured by western blot technique [12,13].

The spectrophotometric method of Placer et al.[14] was used for the determination of lipid peroxidation. The level of GSH-Px activity in tissue and plasma was measured as stated by Lawrence et al.[15] GSH level in tissue and plasma was measured as stated by Sedlak and Lindsay [16]. Working principle, all non-protein sulfhydryl groups in the samples were found in the form of GSH. Tissue and plasma CAT activity was determined by the method described by Goth [17]. The Lowry [18] method was used for protein determination. A purple-blue color was formed by treating the phenol reagent with copper and adding it to the mixture. Protein determination was made by reading the resulting mixture in a spectrophotometer at 650 nm.

Whether the values obtained as a result of the study were normally distributed or not was determined by Shapiro-Wilk normality analysis. To compare the group means, it was determined by ONE WAY ANOVA test whether there was a significant difference in the arithmetic means of more than two independent groups. Differences between groups were determined by the DUNCAN test. The significance level was accepted as $p<0.05$. IBM SPSS Statistics 22 package program was used to perform statistical analyzes and data are given as X±SD.**2.1.**

## 3. RESULTS

### 3.1. Oxidative Stress Parameters

Plasma MDA levels of the 1st group increased compared to the control group, 3rd and 4th groups ($p<0.05$). Skeletal muscle MDA levels of the 1st and 2nd groups were higher than the control group ($p<0.05$). The plasma CAT activity of the 4th group was higher than the 1st and 2nd groups and control group ($p<0.01$). The skeletal muscle CAT activity of the 3rd and 4th groups were found to be significantly higher in the control group and 1st group ($p<0.01$). An increase was observed in the

plasma GSH-Px activity of the 4th group compared to the control and 1st and 2nd groups ($p<0.05$). The skeletal muscle GSH-Px activity of the 4th group was found to be significantly higher than the control and 1st group ($p<0.05$). (Table 1)

**Table 1.** Oxidative Stress Parameters (a,b: The statistical difference between different letters in the same column is important).

| Oxidative Stress Parameters | | | | | | | | |
|---|---|---|---|---|---|---|---|---|
| **Groups** | **MDA (nmol/g)** | | **GSH (nmol/g)** | | **GSH-Px (IU/g protein)** | | **Catalaz (kU/g protein)** | |
| | **Muscle** | **Plasma** | **Muscle** | **Plasma** | **Muscle** | **Plasma** | **Muscle** | **Plasma** |
| **Control** | $14.69\pm1,98^{b}$ | $21.95\pm4.08^{b}$ | $3.42\pm0.11$ | $2.35\pm0.22$ | $18.94\pm5.39^{b}$ | $22.64\pm4.30^{b}$ | $21.43\pm2.91^{c}$ | $10.93\pm2.16^{b}$ |
| **1st group** | $16.84\pm1.18^{a}$ | $29.69\pm5.72^{a}$ | $3.88\pm0.35$ | $2.41\pm0.13$ | $18.88\pm4.89^{b}$ | $21.32\pm5.94^{b}$ | $24.22\pm3.48^{bc}$ | $11.33\pm2.91^{b}$ |
| **2nd group** | $16.76\pm0.67^{a}$ | $26.45\pm2.01^{ab}$ | $3.82\pm0.45$ | $2.48\pm0.32$ | $22.78\pm6.95^{ab}$ | $21.31\pm9.59^{b}$ | $27.32\pm1.53^{ab}$ | $11.34\pm4.80^{b}$ |
| **3rd group** | $16.15\pm1.60^{ab}$ | $24.78\pm1.13^{b}$ | $3.72\pm0.54$ | $2.63\pm0.51$ | $23.90\pm5.08^{ab}$ | $28.02\pm10.55^{ab}$ | $30.00\pm5.04^{a}$ | $12.57\pm3.05^{ab}$ |
| **4th group** | $15.85\pm1.13^{ab}$ | $24.51\pm4.48^{b}$ | $3.74\pm0.28$ | $2.73\pm0.64$ | $26.88\pm4.51^{a}$ | $33.41\pm8.76^{a}$ | $30.62\pm3.06^{a}$ | $16.66\pm1.85^{a}$ |
| **Significance Level** | $P<0.05$ | $P<0.05$ | $P>0.05$ | $P>0.05$ | $P<0.05$ | $P<0.05$ | $P<0.001$ | $P<0.05$ |

### 3.2. BAX-BCL-2 Protein Expression Levels

Skeletal muscle BAX protein expression levels of the 1st group were higher than the control group and 4th group ($p<0.05$). (Figure 1). It was observed that the skeletal muscle BCL-2 protein expression levels of the first group was lower than the control group and 4th group ($p<0.05$). (Figure2). It was determined that the skeletal muscle BAX/BCL-2 ratio of the 1st group was higher than the control group ($p<0.05$). When the experimental groups were compared among themselves: The skeletal muscle BAX/BCL-2 ratio of the 1st group was found to be significantly higher than that of the 3rd and 4th groups ($p<0.05$).(Figure3).

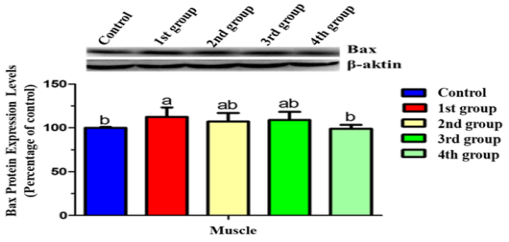


**Figure 1.** Muscle BAX Protein Expression Levels, Mean, SD, $p<0.05$.(a,b: The statistical difference between different letters in the same column is significant).

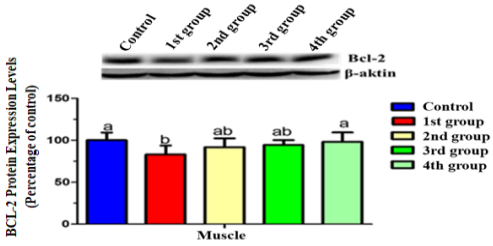


**Figure 2.** Muscle BCL-2 Protein Expression Levels, Mean, SD, $p<0.05$.(a,b: The statistical difference between different letters in the same column is significant).

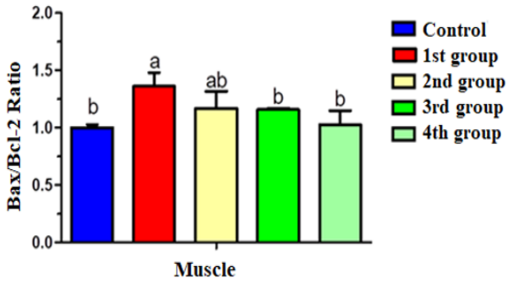


**Figure 3.** Muscle BAX/BCL-2 Ratio Mean, SD, $p<0.05$.(a,b: The statistical difference between different letters in the same column is significant).

## 4. DISCUSSION

Our study demonstrates that acute intense exercise increases lipid peroxidation in muscle and plasma, while regular and continuous exercise decreases lipid peroxidation. While it was seen that acute exercise did not make a significant contribution to the antioxidant defense system, it was found that regular and continuous exercise contributed significantly to the antioxidant defense mechanism. At the same time, it was determined that apoptosis triggered by acute exercise was suppressed after regular and continuous exercise.

It has been observed that muscle and plasma MDA levels, which increase with acute intense exercise, decrease when exercise is continued regularly [19,20,21,22,23]. Although these results are in parallel with many studies, there are studies indicating that resistance exercise significantly increases ROS production [24,25,26]. We can think that the reason for this difference in studies is related to the type, intensity and duration of the exercise. Although muscle and plasma GSH activity were found to be higher in the exercise groups compared to the control group, this increase was not statistically significant. Muscle and plasma GP-X and CAT activities in all exercise groups were higher than the control group ($p<0.05$). Specific studies on the type, intensity and intensity of exercise in shaping the antioxidant mechanism are not sufficient [24]. The high GP-X and CAT activities in all groups in our study indicate that both acute and regular exercise

positively affect the antioxidant mechanism. In their study, Chadorneshin et al.[23] showed that intense exercise increases CAT and GP-X activities. Lambertucci et al.[27] reported that aerobic exercise increased antioxidant enzyme activity in both old and young rats.

The formation of exercise-induced free radicals varies with the type, intensity and duration of physical exercise [28]: therefore, oxidative stress has been associated with decreased physical performance, muscle fatigue, muscle damage and overtraining [29]. It has been hypothesized that the body's physiological amount of antioxidants is not sufficient to prevent exercise-induced oxidative stress and that additional antioxidants are needed to reduce oxidative stress and muscle damage [30]. In many studies, the effects of exercise duration on this situation have been revealed [31]. The intensity, duration and type of exercise determine the direction in which the balance of oxidant and antioxidant defense mechanisms will shift [32]. While the balance is deteriorated towards oxidative stress in acute strenuous exercises [33,34], regular, short-term and non-vigorous exercises shift the balance towards antioxidant defense systems.

When the findings were evaluated, skeletal muscle and plasma BAX protein expression values were increased in the 1st group and decreased in the 2nd, 3rd and 4th groups, respectively. On the other hand, BCL-2 values decreased in the 1st group and increased in the 2nd, 3rd and 4th groups. The ratio of BAX/BCL-2 decreased, respectively. These results show that acute exercise-induced apoptosis is suppressed with regular exercise [35,36,37].

As a result, it shows that while acute exercise does not significantly contribute to the antioxidant defense system in plasma and muscle tissue, regular exercise provides a significant contribution to the antioxidant defense mechanism by increasing the GSH-Px and CAT activities. The gradual decrease of MDA level, which increases significantly in muscle and plasma during acute exercise, shows that regular exercise strengthens the antioxidant defense system, on the contrary, it reduces free radicals and lipid peroxidation. It can be said that the critical balance between exercise-induced apoptosis signal, prosurvival and proapoptotic factors and intracellular protection systems that contribute to apoptosis resistance depends on the intensity and duration of exercise. At the same time, after regular exercise, the apoptotic process in muscle tissue can be inactivated. Both ROS production and apoptosis increased in the acute period after exercise. During periods of regular exercise, the decrease in ROS level and the decrease in apoptosis show parallelism. This shows that there is a strong relationship between apoptosis and oxidative stress.

**Funding:** This study was supported by the Fırat University Scientific Research Projects (FUBAP). This article was prepared from the master thesis

## REFERENCES

[1] Rodriguez-Ayllon M, Cadenas-Sánchez C, Estévez-López F, Muñoz NE, Mora-Gonzalez J, Migueles J, et al. Role of physical activity and sedentary behavior in the mental health of preschoolers, children and adolescents: a systematic review and meta-analysis. Sports medicine. 2019;49(9):1383-1410.

[2] Parr EB, Heilbronn LK, Hawley JA. A time to eat and a time to exercise. Exercise and sport sciences reviews. 2020;48(1):4.

[3] Thirupathi A, Pinho RA. Effects of reactive oxygen species and interplay of antioxidants during physical exercise in skeletal muscles. Journal of physiology and biochemistry. 2018;74(3):359-367.

[4] Lin JY, Kuo WW, Baskaran R, Kuo CH, Chen YA, Chen WST, et al. Swimming exercise stimulates IGF1/PI3K/Akt and AMPK/SIRT1/PGC1α survival signaling to suppress apoptosis and inflammation in aging hippocampus. Aging (albany NY). 2020;12(8):6852.

[5] Kruk J, Kotarska K, Aboul-Enein BH. Physical exercise and catecholamines response: benefits and health risk: possible mechanisms. Free Radical Research. 2020;54(2-3):105-125.

[6] Thirupathi A, Pinho RA. Effects of reactive oxygen species and interplay of antioxidants during physical exercise in skeletal muscles. Journal of physiology and biochemistry. 2018;74(3):359-367.

[7] Fernandes MS DS, Kubrusly MS, Lima TRLDA, Muller CR, Américo ALV, Fernandes MP, et al. Aerobic exercise training exerts beneficial effects upon oxidative metabolism and non-enzymatic antioxidant defense in the liver of leptin deficiency mice. Frontiers in Endocrinology. 2020;11:898.

[8] D'Angelo S, Rosa R. Oxidative stress and sport performance. Sport Sci. 2020;13:18-22.

[9] Ghajari H, Hosseini SA, Farsi S. The effect of endurance training along with cadmium consumption on Bcl-2 and bax gene expressions in heart tissue of rats. Annals of Military and Health Sciences Research. 2019;17(1):e86795.

[10] Habibi P, Alihemmati A, Ahmadiasl N, Fateh A, Anvari E. Exercise training attenuates diabetes-induced cardiac injury through increasing miR-133a and improving pro-apoptosis/anti-apoptosis balance in ovariectomized rats. Iranian journal of basic medical sciences. 2020;23(1):79.

[11] Andreotti DZ, Silva JDN, Matumoto AM, Orellana AM, De Mello PS, Kawamoto EM. Effects of physical exercise on autophagy and apoptosis in aged brain: Human and animal studies. Frontiers in Nutrition. 2020;7:94.

[12] Bass JJ, Wilkinson DJ, Rankin D, Phillips BE, Szewczyk NJ, Smith K, et al. An overview of technical considerations for Western blotting applications to physiological research. Scand J Med Sci Sports. 2017;27:4–25. https://doi.org/10.1111/sms.12702.

[13] Kielkopf CL, Bauer W, Urbatsch I. Expressing Cloned Genes for Protein Production, Purification, and Analysis. Mol. Cloning A Lab. Man. 4th ed.

New York: Cold Spring Harbor Laboratory Press: 2012. p. 1599–625.
[14] Placer ZA, Cushman LL, Johnson BC. Estimation of product of lipid peroxidation (malonyl dialdehyde) in biochemical systems. Anal Biochem. 1966;16:359–64. https://doi.org/10.1016/0003-2697(66)90167-9.
[15] Lawrence RA, Burk RF. Glutathione peroxidase activity in selenium-deficient rat liver. Biochem Biophys Res Commun. 1976;71:952–8.
[16] Sedlak J, Lindsay RH. Estimation of total, protein-bound, and nonprotein sulfhydryl groups in tissue with Ellman's reagent. Anal Biochem. 1968;25:192–205. https://doi.org/https://doi.org/10.1016/0003-2697(68)90092-4.
[17] Goth L. A simple method for determination of serum catalase activity and revision of reference range. Clin Chim Acta. 1991;196:143–51. https://doi.org/10.1016/0009-8981(91)90067-m.
[18] Lowry OH, Rosebrough NJ, Farr AL, Randall RJ. Protein measurement with the Folin phenol reagent. J Biol Chem. 1951;193:265–75.
[19] Souissi W, Bouzid MA, Farjallah MA, Ben Mahmoud L, Boudaya M, Engel FA, et al. Effect of different running exercise modalities on post-exercise oxidative stress markers in trained athletes. International journal of environmental research and public health. 2020;17(10):3729.
[20] Wang X, Wang Z, Tang D. Aerobic exercise alleviates inflammation, oxidative stress, and apoptosis in mice with chronic obstructive pulmonary disease. International Journal of Chronic Obstructive Pulmonary Disease. 2021;16:1369.
[21] Carru C, Da Boit M, Paliogiannis P, Zinellu A, Sotgia S, Sibson R, et al. Markers of oxidative stress, skeletal muscle mass and function, and their responses to resistance exercise training in older adults. Experimental Gerontology. 2018;103:101-106.
[22] Alikhani S, Sheikholeslami-Vatani D. Oxidative stress and anti-oxidant responses to regular resistance training in young and older adult women. Geriatrics & Gerontology International. 2019;19(5):419-422.
[23] Chadorneshin HT, Nayebifar S, Abtahi-Eivary SH, Nakhaei H. Comparison of Effects of High-Intensity Interval Training and Continuous Training on Memory and Correlation with Antioxidant Enzyme Activity in the Rat Brain. Ann Mil Health Sci Res. 2021;19(2):e113888.
[24] Thirupathi A, Wang M, Lin JK, Fekete G, István B, Baker JS, et al. Effect of different exercise modalities on oxidative stress: a systematic review. BioMed Research International. 2021. https://doi.org/10.1155/2021/1947928
[25] Kawamura T, Muraoka I. Exercise-induced oxidative stress and the effects of antioxidant intake from a physiological viewpoint. Antioxidants. 2018;7(9):119.
[26] Powers SK, Deminice R, Ozdemir M, Yoshihara T, Bomkamp MP, Hyatt H. Exercise-induced oxidative stress: Friend or foe?. Journal of sport and health science. 2020;9(5):415-425.
[27] Lambertucci RH, Levada-Pires AC, Rossoni LV, Curi R, Pithon-Curi TC. Effects of aerobic exercise training on antioxidant enzyme activities and mRNA levels in soleus muscle from young and aged rats. Mechanisms of ageing and development. 2007;128(3):267-275.
[28] Wang F, Wang X, Liu Y, Zhang Z. Effects of Exercise-Induced ROS on the Pathophysiological Functions of Skeletal Muscle. Oxidative Medicine and Cellular Longevity. 2021. https://doi.org/10.1155/2021/3846122
[29] Cheng AJ, Jude B, Lanner JT. Intramuscular mechanisms of overtraining. Redox biology. 2020; 35:101480.
[30] Taherkhani S, Suzuki K, Castell L. A short overview of changes in inflammatory cytokines and oxidative stress in response to physical activity and antioxidant supplementation. Antioxidants. 2020;9(9):886.
[31] Aguilo A, Tauler P, Pilar Guix M, Villa G, Cordova A, Tur JA, et al. Effect of exercise intensity and training on antioxidants and cholesterol profile in cyclists. J Nutr Biochem 2003;14:319–25. https://doi.org/10.1016/s0955-2863(03)00052-4.
[32] Lu Y, Wiltshire HD, Baker JS, Wang Q. Effects of High Intensity Exercise on Oxidative Stress and Antioxidant Status in Untrained Humans: A Systematic Review. Biology. 2021;10(12):1272.
[33] Bosco G, Paganini M, Giacon TA, Oppio A, Vezzoli A, Dellanoce C, et al. Oxidative stress and inflammation, microRNA, and hemoglobin variations after administration of oxygen at different pressures and concentrations: A randomized trial. International journal of environmental research and public health. 2021;18(18):9755.
[34] Kruk J, Aboul-Enein BH, Duchnik E. Exercise-induced oxidative stress and melatonin supplementation: current evidence. The Journal of Physiological Sciences. 2021;71(1):1-19.
[35] Song SH, Jee YS, Ko IG, Lee SW, Sim YJ, Kim DY, et al. Treadmill exercise and wheel exercise improve motor function by suppressing apoptotic neuronal cell death in brain inflammation rats. Journal of exercise rehabilitation. 2018;14(6):911.
[36] Darband SG, Sadighparvar S, Yousefi B, Kaviani M, Mobaraki K, Majidinia M. Combination of exercise training and L-arginine reverses aging process through suppression of oxidative stress, inflammation, and apoptosis in the rat heart. Pflügers Archiv-European Journal of Physiology. 2020;472(2):169-178.
[37] Wu F, Li Z, Cai M, Xi Y, Xu Z, Zhang Z, et al. Aerobic exercise alleviates oxidative stress-induced apoptosis in kidneys of myocardial infarction mice by inhibiting ALCAT1 and activating FNDC5/Irisin signaling pathway. Free Radical Biology and Medicine. 2020;158:171-180.

Cilt 11, Sayı 2, Sayfa 22-26, 2022 Volume 11, Issue 2, Page 22-26, 2022

Araştırma Makalesi https://doi.org/10.46810/tdfd.1086012 Research Article

Türk Doğa ve Fen Dergisi
Turkish Journal of Nature and Science
www.dergipark.gov.tr/tdfd

# A Real-time Video Measurement System for Quality Control Applications

**Fatih AKKOYUN**[1*]

[1] Karadeniz Technical University, Trabzon Voc. Ed., Mechanical and Metal Technologies Dept., Trabzon, Türkiye
Fatih AKKOYUN ORCID No: 0000-0002-1432-8926

**Corresponding author: fatihakkoyun@ktu.edu.tr*

(Received: 10.03.2022, Accepted: 08.04.2022, Online Publication: 29.06.2022)

**Keywords**
Video measurement system, Non-contact measuring, Quality control, Image processing, Computer vision

**Abstract:** Quality control is extremely important for manufacturing compatible parts to supply products that meet production requirements. It provides track and control of the stages of the process and minimizes waste by supporting high levels of productivity. In industrial quality control applications, most manufacturers prefer a video measurement system (VMS), which offers non-contact high accurate measurement results, for evaluating machined parts and products. However, due to the advanced technology and low competition, the price of non-contact measurement devices is high. Besides some facilities and some research laboratories couldn't reach these high-cost devices. Today, with the help of evolving technology and open-source image processing libraries, it is possible to offer cost-effective and accurate non-contact measurement systems for industrial measuring applications. This study aims to put forward a VMS to measure parts/products in two dimensions with swift and accurate results. The proposed system has an error below 1% and the linear regression coefficient ($r^2$) was found over 0.95. It works in real-time and the minimum frequency was found 10 Hz for repetitive measurements, real-time measurement applications. The proposed cost-effective device can be adapted into various quality control applications in industrial manufacturing.



# Kalite Kontrol Uygulamaları için Gerçek Zamanlı Bir Video Ölçüm Sistemi

**Anahtar Kelimeler**
Video ölçüm sistemi, Temassız ölçüm, Kalite kontrol, Görüntü işleme, Bilgisayarlı görü

**Öz:** Kalite kontrol, imalat aşamalarına uyumlu parçaların üretimi sağlamak açısından oldukça büyük bir öneme sahiptir. İmalat aşmalarının takibi ve denetimini, bunun yanında imalat atıklarının azaltılarak üretim veriminin yükseltilmesini sağlamaktadır. Endüstriyel kalite kontrol uygulamalarında genellikle video ölçüm sistemleri (VMS), temassız ölçüm ve yüksek doğruluk sonuçları sağlaması nedeniyle, çoğu üretici tarafından tercih sebebidir. Ancak, ileri teknoloji barındıran bu cihazlar ve rekabetin az olmasın nedeniyle bu ölçüm sistemlerinin piyasa fiyatları yüksektir. Bunun yanında sadece bazı araştırma merkezleri ve laboratuvarlar bu cihazlardan faydalanabilmektedir. Günümüzde, gelişen teknoloji ve açık kaynaklı görüntü işleme kütüphaneleri sayesinde, düşük maliyetli ve yüksek doğruluğa sahip temassız ölçüm sistemlerinin endüstriyel uygulamalarda kullanımı mümkün hale gelmektedir. Bu çalışmada, imalat parçaları ve ürünlerin boyutsal ölçümlerinde hızlı ve yüksek doğruluklu bir VMS ortaya çıkarılmıştır. Sunulmakta olan sistemin %1'in altında hata oranı bulunmaktadır. Doğrusal regresyon katsayısı ($r^2$) 0.95 olarak bulunmuştur. Bu sistem gerçek-zamanlı olarak 10 Hz frekans ile tekrarlı ölçümlere uygun olarak alışmaktadır. Önerilen bu düşük-maliyetli cihaz, endüstriyel uygulamalarda birçok kalite kontrol aşamasına uyarlanabilmektedir.

## 1. INTRODUCTION

A VMS offers a fast and accurate solution for quality control applications. Manufacturing processes, especially mass production lines are sequentially required quality-checking processes [1,2]. There are various techniques with the help of contact and non-contact measurement devices for controlling the quality of a work material, which are used to measure the dimensions of the work material [3]. For example, a mechanical caliper requires contact with the work material to accomplish the measurement duty [4]. Besides, it requires a labor force of the quality control expert to complete the measuring process [5,6]. In many industries, the quality of a work material depends on contactless procedures for

evaluating the possible dimensional error and surface properties [7].

Today, advanced technology offers a wide range of contactless, non-destructive evaluation (NDE), techniques for quality control procedures [8]. In the literature, there are sound, light, and displacement-based surface and dimension measurement devices referring to NDE applications. Typically, an NDE device is used with an active or passive sensing method according to the application area [9–11]. Most of the active sensing applications, infrared light sources are preferred for non-contact measuring duties in many studies [12–14]. There are also ultrasonic approaches for active sensing NDE methods using sound-based devices for quality control applications [15–19]. In one example, ultrasonic sources are used as sound-based devices for quality control applications [19]. A VMS is proper for both active and passive sensing methods that are suitable for NDE quality control applications [8,20–22].

The NDE approaches are offering a fast and accurate option when compared to the mechanical contact-based measurement approaches [23,24]. In addition to contactless operation, the NDE approaches are minimizing the user-dependent measurement errors. For most measurement applications, concerning the accuracy and performance of the quality control devices, a VMS is a good example of an NDE quality control application using light reflectance for measuring processes. [25,26].

In this study, a cost-effective VMS is developed for NDE quality control applications to measure parts/products with the capacity of two-dimensional measurements. The proposed system provides fast, accurate, and automated measurements. The system has an accuracy of around 98% and the linear regression coefficient (r2) was found over 0.95. The presented VMS accomplishes measurements in real-time with a minimum 10 Hz measuring frequency. The proposed cost-effective device can be adapted into various quality control applications in industrial manufacturing, especially for real-time measurement applications.

## 2. MATERIAL VE METHODS

The VMS is composed of an imaging device, a light table, and image processing software with a Personal Computer (PC). The block diagram of VMS used for image capturing and processing duties is shown in Figure 1.

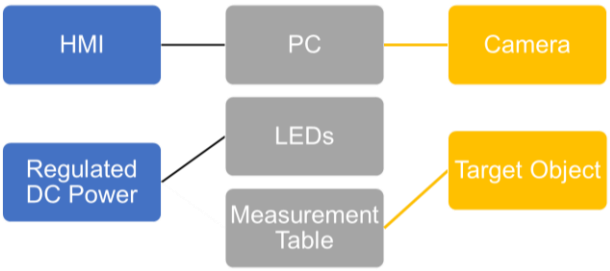


**Figure 1.** The block diagram of VMS

### 2.1. Experimental setup

The actual image of VMS with assemble is shown in Figure 2. The figure presents the actual image of the VMS, the imaging device, and the light table. The light table also determines the limits of the measurement area of the system. It is a combination of a light source and a transparent plexiglass material. The surface of this material is filled with white dots to distribute the light in a uniform structure.

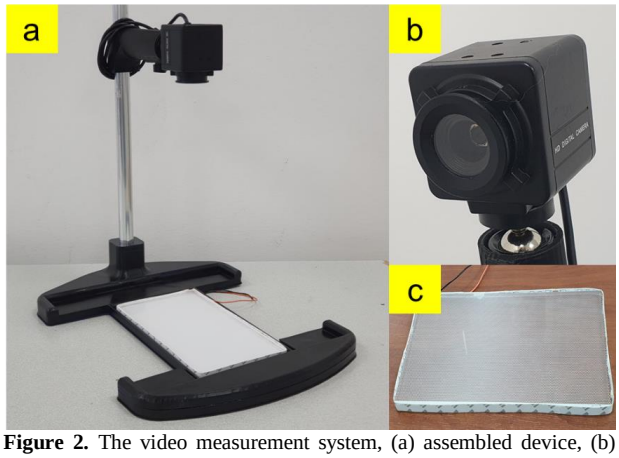


**Figure 2.** The video measurement system, (a) assembled device, (b) CCD camera, (c) light table

The camera (Figure 2 (b)) with CMOS image sensor (Imx214, Sony exmor rs, Japan) is connected to a PC via USB function. The images are captured with the camera device using custom-written computer vision (CV) software.

The light table (Figure 2 (c)) consists of an LED series that surrounded a transparent measurement table [27]. Thus, the illuminated light table provides a smooth white background for the measuring area. A regulated 12-volt power source is supplied to the light table.

Here, the CV software uses image-processing techniques for detecting the edges of the work material and calculating the distances for two axes. To achieve these duties the Open Source Computer Vision Library (OpenCV) is used as an image processing library [28,29], which is suitable for real-time CV applications. The software is written with the C++ programming language using this image processing library [30].

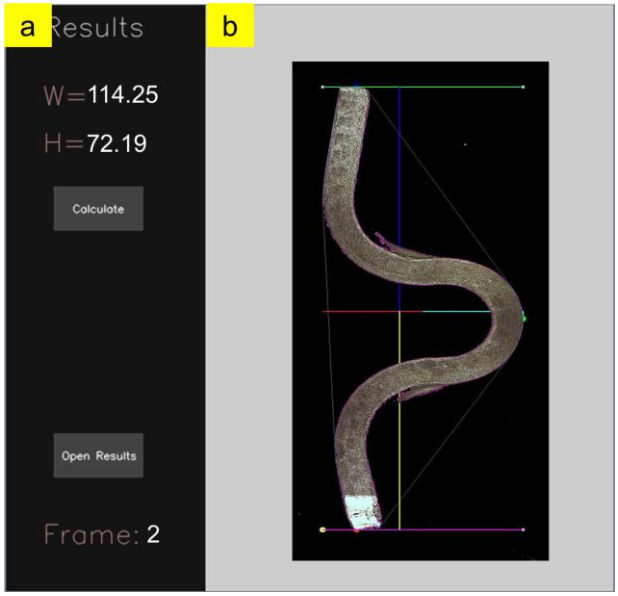


**Figure 3.** The graphical user interface, (a) result screen, (b) monitoring screen

The graphical user interface (GUI) of the software is shown in Figure 3. This interface has two screening areas, the first one is used to show the measurand and the second one is for screening the measured material in real-time. Additionally, with the help of custom-written software, users have the ability to conduct both automated and manual measurements together.

The spatial calibration of the imaging device is conducted by referring to the pixels and a known sample [31]. A square material is used as a sample and both axes of the sample are measured using a precise caliper (0.01 mm). The VMS software is calculated the pixel numbers of the sample for these two axes. In the last stage, a ratio is determined to determine the slope formula from both axes. Thus, a relationship is obtained for the X and Y axes of the measurement are for converting pixel numbers to meter units. The equations (Eqn. 1 and Eqn. 2) are representing the conversion of pixels into millimeters.

$$X_l = m_x\,(X_{max} - X_{min}) + n_x \qquad (1)$$

$$Y_l = m_y\,(Y_{max} - Y_{min}) + n_y \qquad (2)$$

The VMS software uses image processing procedures in addition to Eqn. 1 and Eqn. 2. for calculating the length and width of the work material, which is placed into the measuring area. The image processing procedures are starting with the image capturing step. In the next stage, the image is cropped to the region of interest (ROI) area. Next, the ROI is converted to hue saturation value (HSV) and grayscale colors. A threshold is applied to the grayscale image to obtain a black-white (BW) colored image. In the next stage, the contour detection process is applied. The work material on the light table is detected in this stage and contouring points are recorded. The minimum and maximum values for the X and Y axes are extracted from the contour numbers to calculate the width and height of the work material. The distances are obtained in pixel numbers for both the X and Y axes. In the last stage, the distances in pixel numbers are converted from the pixel numbers to meter units using the equations (Eqn. 1 and Eqn. 2).

## 3. RESULTS AND DISCUSSION

The spatial calibration results show that there is a linear relationship between length and pixel numbers. Four different lengths from five to fifteen mm. are measured for both X and Y-axes using the image processing software of the VMS. The result of the obtained relationship between pixel number and the actual length is shown in Figure 4.

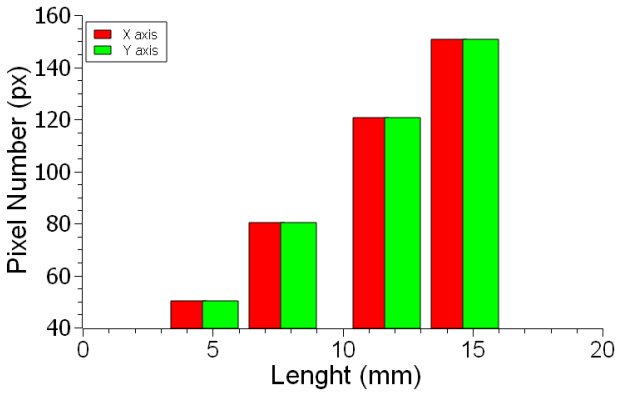


**Figure 4.** The relationship between pixel number and actual length

In the next stage, a test material was placed in the measurement area for correction. Four repetitive measurements are conducted for both axes. The actual value of the test material and the measurand for X and Y-axes are shown in Figure 5.

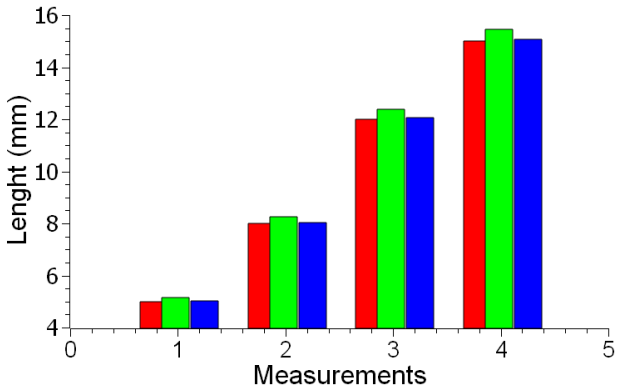


**Figure 5.** The test material and the measurement results for X and Y-axes

The VMS is evaluated after the calibration and correction stages using different work materials. The work materials with different lengths are placed in the measurement area. In Figure 6 the results of the measurements are shown for these work materials. In total 8 different material lengths are measured with four-time repetitions. The error bar obtained from repetitive measurements and linear fit values are shown in Figure 6. The VMS error is found below 1%. The linear regression coefficient (r2) was found over 0.95 while the VMS is tested in real-time.

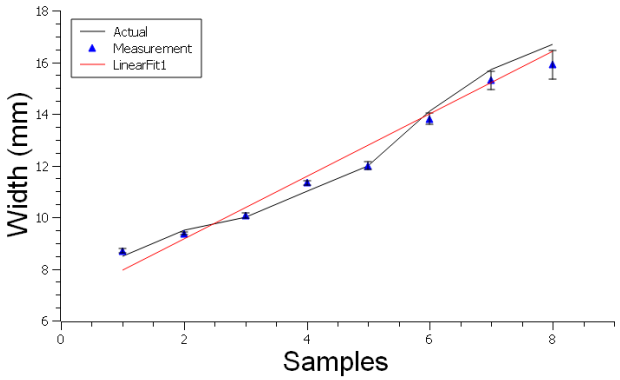


**Figure 6.** The measurements of work materials.

## 4. CONCLUSIONS

In industrial applications, it is a necessity to evaluate the outputs of the manufacturing process. In the present study, a VMS using an image-acquiring device and a light table is demonstrated. The VMS produces fast and accurate results while it is working in real-time. It accomplishes measurements in real-time with a minimum 10 Hz measuring frequency.

The cost-effective system achieves measuring a work material with the capacity of two-dimensional measurements. It also provides automated measurements in addition to the fast, accurate measuring process.

The system successfully operated with an accuracy of around 98% and the linear regression coefficient (r2) was found over 0.95. The proposed cost-effective device can be adapted into various quality control applications in industrial manufacturing, especially for real-time measurement applications.

Manufacturers in industrial applications and researchers in the laboratories can use the proposed VMS for evaluating the quality of a produced work material in real-time using an inexpensive, fast, and accurate measuring device. Thus, the offered VMS is a cost-effective and accurate quality control system with the help of advanced CV systems.

### Acknowledgments

We thank Sena Sezen and Mert Hatipoglu for their suggestions and recommendations.

## REFERENCES

[1] Akkoyun F, Ozcelik A. Rapid Characterization of Cell and Bacteria Counts using Computer Vision. Tr J Nat Sci 2021;10:269–74. https://doi.org/10.46810/tdfd.902441.

[2] Ozcelik A, Aslan Z. A simple acoustofluidic device for on-chip fabrication of PLGA nanoparticles. Biomicrofluidics 2022;16:014103. https://doi.org/10.1063/5.0081769.

[3] Akkoyun F, Ercetin A. Automated Grain Counting for the Microstructure of Mg Alloys Using an Image Processing Method. J Mater Eng Perform 2021. https://doi.org/10.1007/s11665-021-06436-2.

[4] Erçetin A, Aslantaş K, Perçin M. Micro milling of tungsten-copper composite materials produced through powder metallurgy method: Effect of composition and sintering temperature. J Fac Eng Archit Gazi Univ 2018;33:1369–81. https://doi.org/10.17341/gummfd.43569.

[5] Dwivedi SK, Vishwakarma M, Soni PA. Advances and Researches on Non Destructive Testing: A Review. Mater Today Proc 2018;5:3690–8. https://doi.org/10.1016/j.matpr.2017.11.620.

[6] Kilic K, Boyaci IH, Koksel H, Kusmenoglu I, Kılıç K, Boyacı İH, et al. A classification system for beans using computer vision system and artificial neural networks. J Food Eng 2007;78:897–904. https://doi.org/10.1016/j.jfoodeng.2005.11.030.

[7] Seifi M, Gorelik M, Waller J, Hrabe N, Shamsaei N, Daniewicz S, et al. Progress Towards Metal Additive Manufacturing Standardization to Support Qualification and Certification. JOM 2017;69:439–55. https://doi.org/10.1007/s11837-017-2265-2.

[8] Teagle PR. The quality control and non-destructive evaluation of composite aerospace components. Composites 1983;14:115–28. https://doi.org/10.1016/S0010-4361(83)80007-X.

[9] Xie H, Tian YQ, Granillo JA, Keller GR. Suitable remote sensing method and data for mapping and measuring active crop fields. Int J Remote Sens 2007;28:395–411. https://doi.org/10.1080/01431160600702673.

[10] Paap A, Askraba S, Alameh K, Rowe J. Photonic-based spectral reflectance sensor for ground-based plant detection and weed discrimination. Opt Express 2008;16:1051. https://doi.org/10.1364/oe.16.001051.

[11] Arimoto H, Egawa M. Non-contact skin moisture measurement based on near-infrared spectroscopy. Appl Spectrosc 2004;58:1439–46. https://doi.org/10.1366/0003702042641218.

[12] El Masri Y, Rakha T. A scoping review of non-destructive testing (NDT) techniques in building performance diagnostic inspections. Constr Build Mater 2020;265:120542. https://doi.org/10.1016/j.conbuildmat.2020.120542.

[13] Hawkins SA, Jones DR. Prediction modelling of storage time and quality measurements using visible-near infrared spectra of pasteurized shell eggs. J Food Meas Charact 2013;7:101–6. https://doi.org/10.1007/s11694-013-9144-5.

[14] Cho C, Kim J, Kim J, Lee SJ, Kim KJ. Detecting for high speed flying object using image processing on target place. Cluster Comput 2016;19:285–92. https://doi.org/10.1007/s10586-015-0525-x.

[15] Kouche A El, Hassanein HS. Ultrasonic Non-Destructive Testing (NDT) Using Wireless Sensor Networks. Procedia Comput Sci 2012;10:136–43. https://doi.org/10.1016/j.procs.2012.06.021.

[16] Medeossi F, Sorgato M, Bruschi S, Savio E. Novel method for burrs quantitative evaluation in micro-milling. Precis Eng 2018;54:379–87. https://doi.org/10.1016/j.precisioneng.2018.07.007.

[17] Yaqoob M, Sharma S, Aggarwal P. Imaging techniques in Agro-industry and their applications, a review. J Food Meas Charact 2021;15:2329–43. https://doi.org/10.1007/s11694-021-00809-w.
[18] Khoyutanov EA, Gavrilov VL. Coal Quality Control in Mining Complex-Structure Deposits. J Min Sci 2019;55:399–406. https://doi.org/10.1134/S1062739119035721.
[19] Herakovic N, Simic M, Trdic F, Skvarc J. A machine-vision system for automated quality control of welded rings. Mach Vis Appl 2011;22:967–81. https://doi.org/10.1007/s00138-010-0293-9.
[20] Ghaderi M, Banakar A, Masoudi AA. Using dielectric properties and intelligent methods in separating of hatching eggs during incubation. Measurement 2018;114:191–4. https://doi.org/10.1016/j.measurement.2017.09.038.
[21] Nyalala I, Okinda C, Nyalala L, Makange N, Chao Q, Chao L, et al. Tomato volume and mass estimation using computer vision and machine learning algorithms: Cherry tomato model. J Food Eng 2019;263:288–98. https://doi.org/10.1016/j.jfoodeng.2019.07.012.
[22] Prijatna D, Muhaemin M, Wulandari RP, Herwanto T, Saukat M, Sugandi WK. A Study of Light Level Effect on the Accuracy of Image Processing-based Tomato Grading. IOP Conf Ser Earth Environ Sci 2018;147:012005. https://doi.org/10.1088/1755-1315/147/1/012005.
[23] Çevik ZA, Özsoy K, Erçetin A. The Effect of Machining Processes on the Physical and Surface Morphology of Ti6al4v Specimens Produced Through Powder Bed Fusion Additive Manufacturing. Int J 3D Print Technol Digit Ind 2021;5:187–94. https://doi.org/10.46519/ij3dptdi.947650.
[24] Erçetin A, Aslantaş K. The effect of different cutting parameters on cutting force, tool wear and burr formation in micro milling WCu composite material fabricated via powder metallurgy. Turkish J Nat Sci 2016;5:1–5.
[25] Akkoyun F, Ercetin A, Aslantas K, Pimenov DY, Giasin K, Lakshmikanthan A, et al. Measurement of Micro Burr and Slot Widths through Image Processing: Comparison of Manual and Automated Measurements in Micro-Milling. Sensors 2021;21:4432. https://doi.org/10.3390/s21134432.
[26] Ercetin A, Akkoyun F, Şimşir E, Pimenov DY, Giasin K, Gowdru Chandrashekarappa MP, et al. Image Processing of Mg-Al-Sn Alloy Microstructures for Determining Phase Ratios and Grain Size and Correction with Manual Measurement. Materials (Basel) 2021;14:5095. https://doi.org/10.3390/ma14175095.
[27] Akkoyun F, Gucluer S, Ozcelik A. Potential of the acoustic micromanipulation technologies for biomedical research. Biomicrofluidics 2021;15:061301. https://doi.org/10.1063/5.0073596.
[28] Bradski G, Kaehler A. Learning OpenCV, Computer Vision with OpenCV Library. 2008. https://doi.org/10.1109/MRA.2009.933612.
[29] Akkoyun F. Inexpensive multispectral imaging device. Instrum Sci Technol 2022:1–17. https://doi.org/10.1080/10739149.2022.2047061.
[30] Stroustrup B. The C++ Programming Language 3rd Edition. 1989.
[31] Laliberte AS, Goforth MA, Steele CM, Rango A. Multispectral remote sensing from unmanned aircraft: Image processing workflows and applications for rangeland environments. Remote Sens 2011;3:2529–51. https://doi.org/10.3390/rs3112529.

Araştırma Makalesi https://doi.org/10.46810/tdfd.1017499 Research Article

Türk Doğa ve Fen Dergisi
Turkish Journal of Nature and Science
www.dergipark.gov.tr/tdfd

# Application of Blockchain Powered Mobile Robots in Healthcare: Use Cases, Research Challenges and Future Trends

**Mehmed Oğuz ŞEN[1*], Fatih OKUMUŞ[2], Adnan Fatih KOCAMAZ[1]**

[1] İnönü University, Faculty of Engineering, Department of Computer Engineering, Malatya,Türkiye
[2] İnönü University, Faculty of Engineering, Department of Software Engineering, Malatya, Türkiye
Mehmed Oğuz ŞEN ORCID No: 0000-0002-0533-1859
Fatih OKUMUŞ ORCID No: 0000-0003-3046-9558
Adnan Fatih KOCAMAZ ORCID No: 0000-0002-7729-8322

**Corresponding author: oguz.sen@inonu.edu.tr*

(Received: 10.03.2022, Accepted: 08.04.2022, Online Publication: 29.06.2022)

**Keywords**
Blockchain, Mobile robots, Multi robot systems, Hyperledger Fabric, Blockchain in healthcare, Medical robots

**Abstract:** Using service robots in healthcare is gaining importance in case of emergent situations like pandemics where human labour is considered risky. Multi robot systems of mobile robots have the potential to perform simple but vital tasks in healthcare. However, centralized control with a server computer of these systems carry the risks of single point of failure and ineffective operation of robots, thus decentralized control with blockchain integration offers a better solution. We mention research challenges regarding blockchain powered multi robot systems of mobile robots from use case, blockchain technology and its integration into current computing systems used in medical centers aspects. Then we propose a method for decentralized management and task distribution in a multi robot system by using Hyperledger Fabric as a permissioned blockchain platform and give common use case scenarios. In this system, tasks are assigned to robots depending on the selection of nearest available robots to the task target. Each robot runs the smart contract containing the task assignment method, so that data traffic for the task assignment process is distributed among the network, instead of stacking up on a single line as in a centralized system. Future research issues and directions for future works are also stated as a conclusion.



# Blokzincir Destekli Mobil Robotların Sağlık Hizmetinde Uygulanması: Kullanım Örnekleri, Araştırma Zorlukları ve Gelecek Trendler

**Anahtar Kelimeler**
Blokzincir, Hareketli robotlar, Çoklu robot sistemleri, Hyperledger Fabric, Sağlık hizmetlerinde blokzincir, Tıbbi robotlar

**Öz:** İnsan emeğinin riskli görüldüğü pandemi gibi acil durumlarda hizmet robotlarının sağlık hizmetlerinde kullanılması önem kazanmaktadır. Mobil robotlardan oluşan çoklu robot sistemleri, sağlık hizmetlerinde basit ama hayati görevleri yerine getirme potansiyeline sahiptir. Ancak bu sistemlerin bir sunucu bilgisayar ile merkezi kontrolü, tek arıza noktası ve robotların etkisiz çalışması risklerini taşır, bu nedenle blok zincir entegrasyonu ile merkezi olmayan kontrol daha iyi bir çözüm sunar. Bu çalışmada blokzincir destekli çoklu mobil robot sistemleri ile ilgili araştırma zorlukları; örnek kullanım durumları, blokzincir teknolojisi ve tıp merkezlerinde kullanılan mevcut bilgi işlem sistemlerine entegrasyonu açılarından ele alınmıştır. Ardından, izne bağlı erişimli bir blok zinciri platformu olan Hyperledger Fabric kullanarak çoklu robot sistemlerinde merkezi olmayan yönetim ve görev dağıtımı için bir yöntem önerilmekte ve ortak kullanım senaryoları verilmektedir. Söz konusu sistemde, görev hedefine en yakın faal robotların seçimine bağlı olarak robotlara görevler atanmaktadır. Her robot, görev atama fonksiyonunu içeren akıllı sözleşmeyi çalıştırmakta; böylece görev atama işlemi için veri trafiği, merkezi bir sistemde olduğu gibi tek bir hatta yığılmak yerine ağ üzerine dağıtılmaktadır. Gelecekteki araştırma konuları ve gelecekteki çalışmalar için yönelimler de sonuç kısmında belirtilmiştir.

## 1. INTRODUCTION

Pandemics like COVID-19 reminded the importance of utilization of service robots in healthcare not only to protect medical personnel from being infected but also to lower the contagion of viruses. There already exist some applications of service robots being used in medical centers as distribution of patients' bare necessities (food,

medicine etc.), diagnosis requiring close contact and sanitization of critical places (surgery rooms, laboratories etc.). In most of these applications, management and task distribution of service robots is performed using centralized systems; the robots are remotely connected to server computers that are integrated into the medical center's automation system. In this paper we present an application framework for multiple mobile medical robots in healthcare, introducing the decentralized approach using blockchain systems.

Using static systems for the communication between mobile robots in a multi robot system becomes a hampering factor when new robots are added to the system. Protocols, procedures and hardware used in the communication needs to be different when there are 2, 3, … or n robots operating in the multi robot system. With its decentralized network structure, blockchain makes dynamic communication between robots possible by providing a smooth communication infrastructure which is able to operate fluently, independent from the number of robots.

This study aims to show how a network of mobile service robots for healthcare can communicate and perform tasks assigned to them via a blockchain platform by stating its advantages over centralized systems. Contrary to centralized systems where a robot is expected to communicate only with a server for receiving orders or sending data, a medical service robot can propagate its current state by sharing its position information, status and data acquired from its sensor suite over the blockchain network to the rest of the robots. Therefore, it can inform other robots of its presence as to be distinguished from static obstacles and can be accessed at any time via other robots instead of setting multiple Wi-Fi routers for a seamless connection with a server. In a centralized system, task assignment and robot control are performed on the central server-side, and robots are considered dumb machines. However dynamic task distribution regarding efficient task assignment and autonomous behaviour of robots without the need of a server can be accomplished in a decentralized system. Users can connect to a decentralized network via a client, see the progress of robots, create tasks for robots and request task assignments. This should not be confused with in a server manner; robots are not directly being intervened at client side, only monitoring and task definitions are done here. By increasing dynamism in the robot system, downstream and upstream load decreases significantly thus easing the computation at client side. In addition to this, a blockchain system inherently provides a decent medium for execution of distributed intelligence. We also indicate that Hyperledger Fabric is a more feasible solution than Ethereum as a blockchain platform by stating advantages and disadvantages.

Remainder of this paper is structured as follows: In Section 2 we give background knowledge about blockchain technology and systems of mobile robots in healthcare with related studies. Research challenges regarding blockchain and integration of blockchain powered mobile robots into current medical systems are discussed in Section 3. Our proposed method with example use cases is explained in Section 4. A projection about blockchain applications of medical robot swarms and future directions are presented in Section 5. Finally, we make a conclusion and state our future work in Section 6.

## 2. BACKGROUND

### 2.1. Blockchain Technology

Blockchain can be defined as an immutable list of records (i.e. blocks of data) where each record is mapped from the previous one by cryptographic hash functions. Before the production of the first record, a genesis block containing the metadata and block structure is generated by the blockchain network according to the blockchain platform's algorithm. A blockchain network is generally defined as a distributed system which can be accessed publicly or with a permission that is responsible for running the blockchain platform and execution of constantly running and ready-to-be-triggered decentralized programs (defined as smart contracts). Public blockchain networks mostly work in a trustless medium (i.e. malignant nodes trying to capture the network's control or spam with redundant actions to render it unusable) and thus must achieve consensus regarding this situation.



Most known for financial applications like cryptocurrencies, blockchain technology in fact presents a much broader concept; decentralization of network systems, data persistence and immutability in distributed databases, consensus in a trustless distributed system. Introduced in 2008 with the declaration of Bitcoin [1], blockchain technology is a hot research area promising decentralized solutions for various problems.

Successful management of collaboration of mobile robots in healthcare is essential for safe and secure medical treatments to patients. Server computers dedicated for controlling mobile robots are used in current applications. As an alternative to this approach, decentralization with blockchain technology eliminates the necessity of deploying and maintaining a server. In this paper we deal with the benefits of applying blockchain as a decentralized solution for mobile robots in healthcare.

### 2.2. Mobile Robots in Healthcare

Current studies on mobile robots centric applications include several research domains such as indoor logistics [2], search and rescue [3,4], molecular robotics [5,6] and health [7-9]. Among these research domains, healthcare related studies gained much attention and popularity since the beginning of ongoing COVID-19 pandemic. Common applications of mobile robots in healthcare include medical examination, patient surveillance [7,8] and medical transportation [9] but these applications mostly deal with single robots. Multi robot systems can

provide an efficient way to perform healthcare services fluently.

In the centralized management of multiple mobile robots, a server computer's computational workload is going to increase when new service robots are connected to the server. However, if a decentralized approach is preferred then the workload created by the new robots will be distributed among the decentralized network instead of taxing a single point in the multiple mobile robot system.

Specific adaptations of blockchain systems to multi robot systems for multi robot collaboration in fighting COVID-19 pandemic are stated in [10] and [11], but an application for general healthcare services hasn't been proposed yet. Our paper focuses on using a permissioned blockchain platform as a decentralized management for mobile service robots in healthcare.

### 2.3. Hyperledger Fabric as a Decentralized Solution

Several applications of mobile robots with blockchain for managing both a single robot and multi robot systems including swarm robots [12] have been proposed, with the majority of studies conducted in the literature dated in 2020 and 2021. They can be classified as consensus proposals [13] [14], path planning [15], cooperative working [16], information sharing [17], collective decision making [18], robot partitioning [19], task allocation [20-21]. Ethereum is the preferred blockchain network in most these applications with the mention of tradeoffs in smart contract development.

One of the projects within the Hyperledger consortium, Hyperledger Fabric was proposed as a private and permissioned blockchain platform for enterprise level decentralized application development [22]. There are applications proposed for secure and efficient record tracking in the pharmaceutical industry [23], healthcare [24], energy trading [25] and food industry [26] where Fabric is used as a blockchain platform.

Hyperledger Fabric provides a modular system for developers, that means ledger data can be stored in multiple formats and other deterministic consensus algorithms can be set to be used by peers. Channels are mandatorily created for members connected to a Fabric network to join for initiating a ledger to store transactions between members of it.

Blockchain technology and decentralization is the underlying logic of the Bitcoin network operating worldwide, but Bitcoin network uses smart contracts for simple transactions of cryptocurrency, which can't be programmed as demanded, and thus can't be adjusted to provide a decentralized solution for robots in healthcare. Ethereum allows smart contract customization and provides tools to set up a test network [27]. With these characteristics Ethereum is the preferred blockchain platform by most of the developers working in decentralized applications. However, transaction cost in ETH cryptocurrency stands as a tradeoff for decentralized applications running in the main Ethereum network, so developers need to consider code optimizations in their smart contracts [28]. There is another catch that public blockchain networks like the main Ethereum network are not suitable for operating systems of multiple mobile robots, since the consensus algorithm used may demand higher computational power and energy than the robot's limited hardware and power units. Setting a private Ethereum network can solve this issue but Ethereum wallets of the robots connected to the blockchain network must be checked to deal with running out of cryptocurrency and failing to operate. Hence a blockchain platform which can be modified with respect to requirements of a mobile robot system would provide an efficient decentralized solution.

Considering these advantages, Fabric provides a more feasible and customizable blockchain platform than Ethereum. Our proposed method is based on a blockchain network of mobile robots operating Fabric.

## 3. RESEARCH CHALLENGES

Despite recent advancements in blockchain technology and medical service robots there are still problems regarding the use case scenarios, seamless execution of blockchain systems and integration into current medical systems.

- Robots must be accessorized with specific equipment for treatment.
- In case of an emergency situation, a contingency plan for the robots must be well defined and put into action when need arises. (failure of a specific robot, power outage etc.)
- Each task and its sub tasks for the robots must be defined with utmost clarity and consist of solid and concrete steps.
- Entire system must be secure from external tampering and Byzantine robot behaviours.
- Sanitization of the robots must be included as a post mission step for next tasks.

After stating the challenges at the use case level, we discuss the challenges stemming from the technical aspects of blockchain and robots' integration to current medical infrastructure.

### 3.1. Challenges in Blockchain

Blockchain systems have been improved to satisfy the varying demands of miscellaneous decentralized applications, but much work is needed to make a full substitution of current centralized systems. First of all, most blockchain platforms provide APIs that are too generic to develop complicated (in terms of complex data types) decentralized applications. For instance, an instantiated object of a custom defined class can't be directly stored to the ledger database in Fabric, it needs to be marshalled to JSON string before storing. Considering robotics (swarm or multi robot systems), there doesn't exist a blockchain platform dedicated to it or tool to integrate blockchain with a middleware (ROS etc.) for various robots. Hence developers must make

software designs for decentralized applications simplified enough to match the API of the blockchain platform they choose. Blockchain platforms are also designed for storing data with smaller size; if larger files are needed to be stored in a blockchain, an external distributed storage protocol like IPFS [29] must be integrated with the blockchain system used. Another challenge current blockchain platforms are expected to meet in the future is the ongoing development of quantum computing. SHA-256 is the preferred cryptographic hashing method in popular blockchain platforms and is expected to be rendered unusable with cryptanalytic attacks by quantum computers. Therefore, development of quantum resistant cryptographic hash algorithms and their implementations in blockchain platforms stands as research topics for researchers.

### 3.2. Challenges in Mobile Robots Integration to Medical Systems

Contemporary medical automation systems used in medical centers are centralized systems which can be developed by different companies but need to include protocols and services for reporting to government officials when requested and interoperability with auxiliary facilities (pharmacy, medical logistics etc.). For instance, the Ministry of Health is responsible for defining the standards of medical treatments and diagnosis algorithms, monitoring the clinical activity in all medical centers including private clinics and public hospitals in Turkey. Integration of the blockchain network as a decentralized system into centralized systems used in medical infrastructure must meet the standards and procedural requirements.

Another challenge arises when data modelling of the chosen blockchain platform needs to comply with data model used in the content management system (CMS) of the medical center. While synchronizing data between robots with blockchain records in their storage and CMS, conversion of complex data types must be committed elaborately to avoid accidental data loss or overwrites. Relational database management systems (RDBMS) are preferred in most CMS applications and thus type standards must be set out to match or at least to be easily convertible while exchanging data between RDBMS of the medical center and ledger databases of the robots connected to the blockchain platform.

## 4. PROPOSED METHOD

Due to its decentralized nature, blockchain systems can provide a decent solution for management of multi robot systems. The advantages of autonomous multi-robot collaboration include easily scalable, better fault tolerance against any possible failure of robots, better adaptability to the environment, less memory, less processing power, better options for exception controlling, and less capability for individual robots. A use case scenario for a multi robot system using Fabric is demonstrated in Figure 1. As it is seen in the figure there are five mobile service robots operating in a blockchain powered multi robot system at a healthcare facility. Robot 1 is appointed to deliver medicine to Patient A and proceeds to the medical supplies room to pick it up. As a post task objective, Robot 2 goes to the nearest sanitization unit to be sanitized for the next task. Robot 3 is appointed to deliver food to Patient C and is serving food to patient. After gathering samples from Patient B, Robot 4 brings them to doctors in the examination room. Robot 5 is appointed to a physical examination of Patient D and is carrying it out. While the robots are at work, they all have the same copies of ledgers containing robot and task information (namely RobotLedger and TaskLedger) at the same time and update the ledgers by committing new information records after achieving consensus. Medical personnel can connect to the Fabric network via an application at client side to create tasks and send a request for assignment of them to available robots. Since all of the peers in a Fabric network share the same ledger database, each robot in the system has the position and task information of other robots and updates its position and status regularly.

Since locations of facility areas (cafeteria, sanitization etc.) and patient beds remain static during robot operations; their position information can be stored in both client side and robots, there is no need to store this data in blockchain.

### 4.1. Definition of a Robot for Robot Ledger

A robot is recorded on blockchain with following attributes as shown in Table 1.



**Table 1.** Attributes of a robot definition in blockchain

| Attribute Type | Attribute Name |
|---|---|
| Integer | RobotID |
| Integer | TaskCategoryID |
| Integer | TaskCounter |
| Integer | AssignedTaskID |
| Floating-point | Position_x |
| Floating-point | Position_y |
| String | Status |

RobotID: Each robot has a unique identifier as a positive integer value.
TaskCategoryID**:** Stores which type of task the robot is assigned to and currently carries out. Its value is limited to the values (as shown in Table 2) enumerated for task categories.

**Table 2.** Enumeration of task categories

| TaskCategoryID | Task Category |
|---|---|
| 1 | Medical supply delivery |
| 2 | Food delivery |
| 3 | Medical Textile Delivery |
| 4 | Physical examination |
| 5 | Sanitization |
| 6 | Charging |

TaskCounter: Stores the total number of tasks successfully completed by the robot since initial deployment. This variable can be reset to zero at the end of the day after archiving its value to track the robot's performance.

AssignedTaskID: Stores the unique identifier of the task the robot is carrying on. This variable is used for querying task details on the task ledger on demand. If unassigned its value is 0 or null.

Position_x: Stores the horizontal (x coordinate) position of the robot.

Position_y: Stores the vertical (y coordinate) position of the robot.

Status: Shows the current status of the robot. If a task is assigned to the robot or the robot is getting sanitized, it is set to BUSY. If the robot is being charged at a charging station, it is set to CHARGING. Otherwise it is set to IDLE.

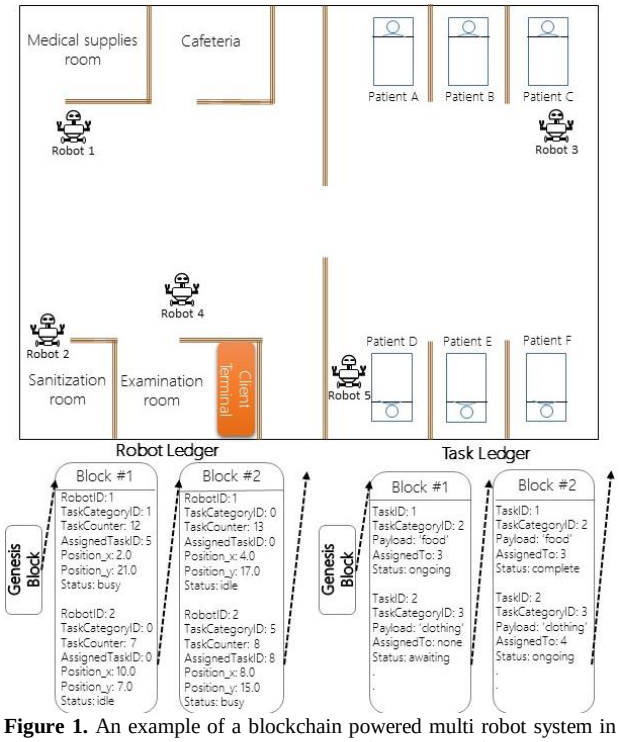


**Figure 1.** An example of a blockchain powered multi robot system in action. Robot 1 moves to gather medicine for the task of delivering it to Patient A. After completing a task, Robot 2 arrives at the nearest sanitization unit to be sanitized for the next task. Robot 3 delivers food to Patient C. Robot 4 brings the samples gathered from Patient B to doctors in the examination room while Robot 5 is conducting a routine physical examination of Patient D. Each robot has the same copies of RobotLedger and TaskLedger records at any time. Medical personnel in the examination room can create tasks and send a request for assignment of the task at the client terminal connected to the Fabric network.

After setting up and deploying the Fabric network with robots as peers, each robot in the system is expected to carry out tasks, which can be generated on demand by medical staff.

### 4.2. Definition of a Task for Task Ledger

A task is recorded on blockchain with following attributes as shown in Table 3.

**Table 3**. Attributes of a task definition in blockchain

| Attribute Type | Attribute Name |
|---|---|
| Integer | TaskID |
| Integer | TaskCategoryID |
| String | Payload |
| Integer | AssignedTo |
| String | Status |

TaskID: Each task has a unique identifier as a positive integer value.
TaskCategoryID: Stores which type of task the robot is assigned to and currently carries out. Its value is limited to the values enumerated for task categories.

Payload: Used to define what robot is carrying to target. Can be food, clothing, medicine etc. If the robot is not carrying anything it is set to NONE.

AssignedTo: Used to determine which robot the task is assigned to. If unassigned its value is 0 or null.

Status: Shows the current status of the task, if task is not assigned to a robot, it is set to AWAITING. If the task is assigned, it is set to ONGOING. If it is completed, then it is set to COMPLETE.

Tasks (shown in Figure 2) to be carried out by the robots can be categorized as follows:

1. *Medical supply delivery*: Robot goes to the initial position (pharmacy, nurse room etc.) of the requested item (medicine, scrubs etc.) and picks it up. Then the robot is ordered to move to the patient's location as the target position and delivers the requested item(s). Finally, the robot is ordered with the sanitization task before accepting new tasks.

2. *Food or clothing delivery*: Robot goes to the initial position (cafeteria, laundry room) of the requested item (food, scrubs etc.) and picks it up. Then the robot is ordered to move to the patient's location as the target position and delivers the requested item(s). If anything needs to be carried away from the patient (empty dishes, dirty clothing etc.), the robot picks it up and moves to where it needs to be dropped (cafeteria, laundry room etc.). Finally, the robot is ordered with the sanitization task before accepting new tasks.

3. *Physical examination*: Being equipped with required tools for close examination of the patient (stethoscope etc.), robots are ordered to go to the patient's location (bed, examination chair or couch etc.) as the target position. After the examination the robot moves to medical personnel to bring the samples gathered from the patient if necessary. Finally, the robot is ordered with the sanitization task before accepting new tasks.

4. *Sanitization*: After the completion of any other tasks, the robot is ordered to go to the nearest sanitization unit to be ready for the next tasks. The robot's status needs to be busy in order not to be accidentally ordered for a new task. After the sanitization process is completed, the robot gets ready to await new tasks.

5. *Charging*: When a robot's battery life is below a threshold value (e.g. 10% of total) the robot might not be able to complete a task successfully, so after checking its battery life, a robot is appointed to be charged at the nearest possible charging station automatically. While being charged, a robot's status is assigned to `CHARGING` and it won't be considered among available robots.


**Figure 2.** Task definitions for robots. Steps to be performed are explained for each task category.

### 4.3. Task Assignment Procedure

Using the client application running on the terminal depicted in Figure 1, authorized medical personnel can connect to the Fabric blockchain network of the robots and oversee its operation. Functions that a user can perform in the client application are as follows:

- *Create a Task*: The user can define tasks for the robots on demand. Details of a task are determined by the user according to the data model described in Section 4.2. After entering task information, the task is submitted to the blockchain network to be committed to the task ledger.
- *Send Task Assignment Request*: The user can select a task stored in the task ledger and request it to be carried out. Since the blockchain network operates decentralized, assignment of a task to a robot is first submitted to the network as a request, then assignment is done after execution of the task assignment algorithm. First, available robots are determined by checking the status of each robot in the network (step 1). Then for each available robot, its current position is gathered and Euclidean distance to the target position of the task is calculated. (step 5) Finally, the robot with the nearest Euclidean distance is selected for assigning the task. (step 6) If more than one robot has the same distance, the robot which demanded the task earlier by completing execution of smart contract faster is chosen (step 8). Pseudocode of this task assignment algorithm is as follows.
-

**ALGORITHM 1:** Task assignment to robots

```
1 availableRobots = CheckRobotStatus();
2 nearestRobotID=0;
3 for each availableRobot in availableRobots
4   initialPosition = getPosition();
5   distance = EuclideanDistance(initialPosition, targetPosition);
6   if (distance < nearestDistance)
7       then nearestRobotID = RobotID
8  if (distance = nearestDistance)
9       then if(TimeUnit.nearestRobotID > TimeUnit.RobotID)
10          then nearestRobotID = RobotID
```

- *Network Status*: The user can see the current status of the robots (i.e. performing a task, standing idle), number of blocks committed and the block data in both robot and task ledgers.

For the blockchain network shown in Figure 3, a medical personnel logins to the client application and requests a swab sample of Patient F. For this, the medical personnel creates a task in the physical examination category and determines the payload and sets Patient F as the target position. The task is stored in the task ledger with the status set to `AWAITING` (demonstrated in Figure 3(c)). Then the medical personnel sends a task assignment request to the blockchain network. For the assignment of the task, status of each robot is checked and Robot 1, Robot 2, Robot 3 and Robot 4 (which already have swab kits) are found as the available robots at that moment. While running the task assignment algorithm described above, Euclidean distances of Robot 1, Robot 2, Robot 3 and Robot 4 are computed as 8, 13, 8 and 17 respectively. Having the least Euclidean distance to Patient F, Robot 1 and Robot 3 are both candidates for appointment but since Robot 1 runs the smart contract faster and broadcasts its availability earlier, it is assigned with the task the medical personnel just created and the confirmation message of successful task assignment is returned to the user.

It should be noted that the client application is only responsible for providing the interface for task generation and request of task assignment to an available robot. The task assignment algorithm described above is implemented as a method (i.e. `AssignTaskToRobot`) in Java source code of smart contract defined for robots. When requesting a task assignment, the client application actually makes a remote procedure call (with `SubmitTransaction` method in Fabric Java API) for invoking the method in the smart contract running on the Fabric network (as shown in Figure 4). Since the position of the robots can be accessed from the robot ledger, Euclidean distances are computed at each robot and the nearest robot is appointed in a distributed way. Since the outcome of this invocation might require a ledger update (a successful assignment needs to be recorded), consensus of the peers (robots in this case) must be achieved first. For this, robots execute the smart contract deployed on the network and send their appointment requests to other robots over the network. Since each robot in the network is involved in achieving consensus, data transition is distributed among the network, instead of overloading the bandwidth of a single node (i.e. a server node). Hence utilizing

decentralization with distribution of the whole task assignment process over the network mitigates the burden of a server in a centralized system.

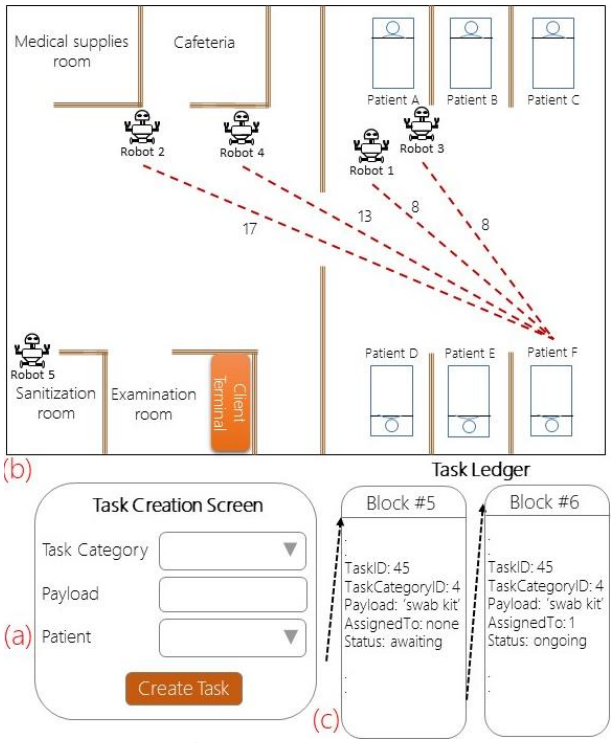


**Figure 3.** Creation of a task and its assignment to Robot 1. Medical personnel creates the task by entering task details in the client application connected to Fabric network which is demonstrated in (a). Execution of the task assignment yields that Robot 1, Robot 2, Robot 3 and Robot 4 are the available robots in the network at that moment with Euclidean distances shown in (b) to Patient F. Robot 1 and Robot 3 have the least Euclidean distance to Patient F but since Robot 1 acted first, it is appointed to the task and task information is stored in the task ledger as shown in (c). It can be seen that the `AssignedTo` attribute now has the robot ID value of Robot 1 and the `Status` attribute is set to `ONGOING` in the sixth block of the task ledger.

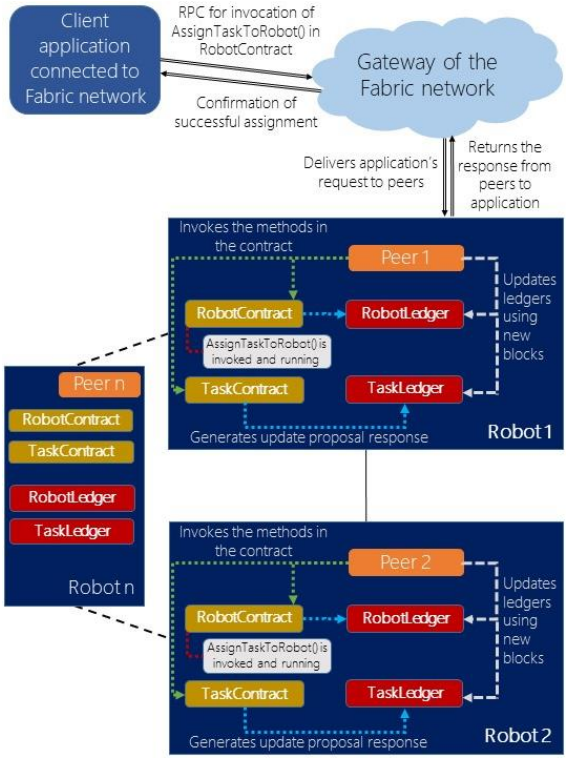


**Figure 4.** Simplified overview of robots as peers in the Fabric network. Each peer (i.e. robot) runs the smart contracts (RobotContract and TaskContract) deployed on the network. Along with other method definitions for CRUD transactions, RobotContract contains `AssignTaskToRobot` method which is the actual implementation of the task assignment algorithm described above. Users can request the assignment of the task they created by invoking AssignTaskToRobot remotely via client application. Invocation requests from client app and their responses are transmitted to the peers via the gateway of the network. Interactions depicted inside a robot are the same for 2nd, 3rd … nth robots.

## 5. FUTURE TRENDS

Automatisation and robotics applications in healthcare services provides not only protection of patients against contagion of diseases but also decreases the cost and manpower requirements in medical centers. Service robots being developed come with more powerful hardware thus they can run their sensor suite and still operate in a blockchain network. Blockchain systems overcome trust problems in distributed networks of mobile robots. Since Hyperledger project aims to provide enterprise level decentralized solutions besides cryptocurrencies, a project dedicated for management of systems of mobile robots with its integration into popular robotics middlewares like Robot Operating System could be launched as a specialized form of Fabric for robotics. In addition to the application framework we propose in here, more detailed and complicated task definitions and robot integrations with experiments on simulations and real robots are planned for future work.

## 6. CONCLUSION

Using autonomous systems of mobile robots in healthcare is a beneficial approach thanks to not only human resource management but also decreasing the contagious risks of human labour in medical centers. Blockchain systems provide distributed data storage while preserving integrity and immutability in the execution and management of multi robot systems. Also communication between robots such as sharing position, orientation and sensor data is simplified through blockchain infrastructure. However, public blockchain networks like Ethereum aren't feasible for operating multi robot systems since limited hardware capabilities of the robots can't compete with the powerful cluster systems while running the Proof of Work consensus algorithm. Setting a private Ethereum network can be suggested but robots need to be checked for not to be drained out of cryptocurrency. We introduce the idea of using Hyperledger Fabric as a permissioned blockchain platform to eliminate these disadvantages and state use case scenarios where task categories with definitions for service robots are explained. Being in nascent stages, blockchain integration into multi robot systems has the potential to be a golden standard in management and operation of distributed intelligence for mobile robots. As the service robots in healthcare continue to improve, various applications of blockchain in medical services are expected to emerge and become widespread.

## REFERENCES


[1] Nakamoto S. Bitcoin: A peer-to-peer electronic cash system. Decentralized Business Review. 2008;21260.

[2] Okumuş F, Dönmez E, Kocamaz AF. A cloudware architecture for collaboration of multiple agvs in indoor logistics: Case study in fabric manufacturing enterprises. Electronics. 2020;9(12): 2023.

[3] Dadgar M, Couceiro MS, Hamzeh A. RbRDPSO: Repulsion-Based RDPSO for Robotic Target Searching. Iranian Journal of Science and Technology - Transactions of Electrical Engineering. 2020;44(1): 551–563.

[4] Trotta A, Montecchiari L, Felice MD, Bononi L. A GPS-Free Flocking Model for Aerial Mesh Deployments in Disaster-Recovery Scenarios. IEEE Access. 2020;8: 91558–91573.

[5] Kabir AMR, Inoue D, Kakugo A. Molecular swarm robots: recent progress and future challenges. Science and Technology of Advanced Materials. 2020;21(1): 323–332.

[6] Keya JJ, Kabir AMR, Inoue D, Sada K, Hess H, Kuzuya A, Kakugo A. Control of swarming of molecular robots. Scientific Reports. 2018;8(1): 1–10.

[7] Holland J, Kingston L, McCarthy C, Armstrong E, O'Dwyer P, Merz F, et al. Service Robots in the Healthcare Sector. Robotics. 2021;10(1): 47.

[8] Farkh R, Marouani H, Al Jaloud K, Alhuwaimel S, Quasim MT, Fouad Y. Intelligent autonomous-robot control for medical applications. Computers, Materials and Continua. 2021;68(2): 2189-2203.

[9] Fang B, Mei G, Yuan X, Wang L, Wang Z, Wang J. Visual SLAM for robot navigation in healthcare facility. Pattern Recognition. 2021;113: 107822.

[10] Alsamhi SH, Lee B. Blockchain-Empowered Multi-Robot Collaboration to Fight COVID-19 and Future Pandemics. IEEE Access. 2021;9: 44173–44197.

[11] Alsamhi SH, Lee B, Guizani M, Kumar N, Qiao Y, Liu X. Blockchain for decentralized multi-drone to combat COVID-19 and future pandemics: Framework and proposed solutions. Transactions on Emerging Telecommunications Technologies. 2021;32: e4255.

[12] Strobel V, Ferrer EC, Dorigo M. Blockchain technology secures robot swarms: a comparison of consensus protocols and their resilience to byzantine robots. Frontiers in Robotics and AI. 2020;7: 54.

[13] Liu J, Xie M, Chen S, Ma C, Gong Q. An improved DPoS consensus mechanism in blockchain based on PLTS for the smart autonomous multi-robot system. Information Sciences. 2021;575: 528-541.

[14] Singh PK, Singh R, Nandi SK, Ghafoor KZ, Rawat DB, Nandi S. An efficient blockchain-based approach for cooperative decision making in swarm robotics. Internet Technology Letters. 2020;3(1): e140.

[15] Mokhtar A, Murphy N, Bruton J. Blockchain-based multi-robot path planning. 5th World Forum on Internet of Things, WF-IoT 2019. Limerick: IEEE; 2019. p. 584-589.

[16] Karthik S, Chandhar NP, Akil M, Chander S, Amogh J, Aditya R. Bee-Bots: A Blockchain Based Decentralised Swarm Robotic System. 6th International Conference on Control, Automation and Robotics, ICCAR 2020. Singapore: IEEE; 2020. p. 145-150.

[17] Nishida Y, Kaneko K, Sharma S, Sakurai K. Suppressing chain size of blockchain-based information sharing for swarm robotic systems. 6th International Symposium on Computing and Networking Workshops, CANDARW 2018. Hida Takayama: IEEE; 2018. p. 524-528.

[18] Nguyen TT, Hatua A, Sung AH. Blockchain approach to solve collective decision making problems for swarm robotics. International Congress on Blockchain and Applications, BLOCKCHAIN'22 2019. Ávila: Springer; 2019. p. 118-125.

[19] Tran JA, Ramachandran GS, Shah PM, Danilov CB, Santiago RA, Krishnamachari B. SwarmDAG: A partition tolerant distributed ledger protocol for swarm robotics. Ledger. 2019;4(1): 25-31.

[20] Basegio TL, Michelin RA, Zorzo AF, Bordini RH. A decentralised approach to task allocation using blockchain. International Workshop on Engineering Multi-Agent Systems, EMAS 2017. Sao Paulo: Springer; 2019. p. 75-91.

[21] Grey J, Godage I, Seneviratne O. Swarm Contracts: Smart Contracts in Robotic Swarms with Varying Agent Behavior. 2020 IEEE International Conference on Blockchain (Blockchain). Rhodes Island: IEEE; 2020 p. 265-272.

[22] Androulaki E, Barger A, Bortnikov V, Cachin C, Christidis K, De Caro A, et al. Hyperledger Fabric: A distributed operating system for permissioned blockchains. Proceedings of the Thirteenth EuroSys Conference, EuroSys'18 2018. Porto: ACM; 2018. p. 1-15.

[23] Uddin M. Blockchain Medledger: Hyperledger fabric enabled drug traceability system for counterfeit drugs in pharmaceutical industry. International Journal of Pharmaceutics. 2021;597: 120235.

[24] Uddin M, Memon MS, Memon I, Ali I, Memon J, Abdelhaq M, et al. Hyperledger fabric blockchain: Secure and efficient solution for electronic health records. Computers, Materials and Continua. 2021;68(2): 2377–2397.

[25] Lohachab A, Garg S, Kang BH, Amin M B. Performance evaluation of Hyperledger Fabric-enabled framework for pervasive peer-to-peer energy trading in smart Cyber–Physical Systems. Future Generation Computer Systems. 2021;118: 392–416.

[26] Surjandari I, Yusuf H, Laoh E, Maulida R. Designing a Permissioned Blockchain Network for the Halal Industry using Hyperledger Fabric with multiple channels and the raft consensus mechanism. Journal of Big Data. 2021;8(1): 10.

[27] A Next-Generation Smart Contract and Decentralized Application Platform. Ethereum

Project White Paper. Technical Report. V Buterin; 2014 [cited 2021 Oct 18]. Available from: https://ethereum.org/en/whitepaper/

[28] Zarir AA, Oliva GA, Jiang ZM, Hassan AE. Developing Cost-Effective Blockchain-Powered Applications: A Case Study of the Gas Usage of Smart Contract Transactions in the Ethereum Blockchain Platform. ACM Transactions on Software Engineering and Methodology (TOSEM). 2021;30(3): 1-38.

[29] InterPlanetary File System [Internet]. 2021 [cited 2021 Oct 18]. Available from: https://github.com/ipfs/ipfs

Araştırma Makalesi https://doi.org/10.46810/tdfd.1095624 Research Article

Türk Doğa ve Fen Dergisi
Turkish Journal of Nature and Science
www.dergipark.gov.tr/tdfd

# Prediction of Covid-19 Disease with Resnet-101 Deep Learning Architecture Using Computerized Tomography Images

**Bekir AKSOY[1*], Osamah Khaled Mulseh SALMAN[1]**

[1] Isparta University of Applied Sciences, Faculty of Technology, Department of Mechatronics Engineering, Isparta, Türkiye
Bekir AKSOY ORCID No: 0000 0001 8052 9411
Osamah Khaled Musleh SALMAN ORCID No: 0000-0001-6526-4793

**Corresponding author: bekiraksoy@isparta.edu.tr*

(Received: 30.03.2022, Accepted: 26.04.2022, Online Publication: 29.06.2022)

**Keywords**
Covid-19, Deep Learning, ResNet-101, Computerized Tomography Images

**Abstract:** Many pandemics have caused the deaths of millions of people in world history from past to present. Therefore, the measures to be taken in the prevention of pandemics are of great importance. In addition to the precautions, it is very important to be able to diagnose the disease early. The most recent pandemic occurred in the world is the COVID-19 outbreak that emerged in China in late 2019. In this study, Computerized Tomography images of 746 patients taken from an open source (GitHub) website were used. The data set was made ready for training by performing sizing and normalization operations on the data set. Images were analyzed using the Resnet-101 model, which is one of the deep learning architectures. Classification process was carried out with the created Resnet-101 model. With the Resnet-101 model, individuals with Covid-19 disease were tried to be identified. The Resnet-101 model detected individuals with Covid-19 disease with an accuracy rate of 94.29%.



# Resnet-101 Derin Öğrenme Mimarisi ile Bilgisayarlı Tomografi Görüntüleri Kullanılarak Covid-19 Hastalığının Tahminlenmesi

**Anahtar Kelimeler**
Covid-19, Derin Öğrenme, ResNet-101, Bilgisayarlı Tomografi Görüntüleri

**Öz:** Geçmişten günümüze dünya tarihinde birçok salgın milyonlarca insanın ölümüne neden olmuştur. Bu nedenle salgınlardan korunmada alınacak önlemler büyük önem taşımaktadır. Önlemlere ek olarak, hastalığın erken teşhis edilebilmesi çok önemlidir. Dünyada en son yaşanan salgın 2019 yılının sonlarında Çin'de ortaya çıkan COVID-19 salgınıdır. Bu çalışmada 746 hastanın açık kaynaklı (GitHub) bir web sitesinden alınan Bilgisayarlı Tomografi görüntüleri kullanılmıştır. Görüntüler, derin öğrenme mimarilerinden Resnet-101 modeli kullanılarak analiz edilmiştir. Oluşturulan Resnet-101 modeli ile sınıflandırma işlemi gerçekleştirilmiştir. Resnet-101 modeli ile Covid-19 hastalığı olan bireyler tespit edilmeye çalışılmıştır. Resnet-101 modeli, Covid-19 hastalığı olan bireyleri %94,29 doğruluk oranıyla tespit ettiği belirlenmiştir

## 1. INTRODUCTION

Health is one of the most important factors affecting societies today. Undoubtedly, pandemics are one of the factors that significantly affect human health. The first known pandemic in history is the Plague of Justinian that emerged in 541 [1]. Many pandemics, such as the black death [2], the modern plague [3], which occurred between 1346 and 1353 in world history after the Plague of Justinian, killed thousands of people. The last pandemic in the world is the COVID-19 pandemic. The COVID-19 pandemic first appeared in Wuhan, China in late December, and it has influenced the whole world and has been declared a pandemic by the world health organization [4,5]. In order to prevent the spread of the SARS-CoV-2 virus, a serious isolation was attempted around the world. Another important point to prevent the spread of the SARS-CoV-2 virus is the early detection of the virus. The COVID-19 test kit is often used to detect the virus. The fact that Covid-19 test kits are low in number and the results obtained from those test kits took time caused people to look for different alternatives. One of the alternative ways explored recently is Computerized Tomography (CT) images. CT images consist of data

obtained by solid state detectors using a fan-shaped x-ray that rotates around the patient [6].

Doctors, virologists, epidemiologists, other public health officials and policy developers observed the spread of the SARS-CoV-2 virus together on CT imaging models. Many medical professionals, healthcare authorities, and policy makers have used CT images to monitor Covid-19 spread [7- 18]. When CT images of Covid-19 patients were examined, it was found that the posterior and peripheral parts of the patients were affected and these regions appeared as frosted glass on the CT images [13, 19]. However, it is not always possible to detect Covid-19 using CT images. For this reason, as in many fields, artificial intelligence methods are used in analyzing the CT images. For example, deep learning methods have been used on CT images to differentiate SARS-CoV-2 virus from viral pneumonia [20].

Deep learning is a sub-branch of machine learning and consists of data model layers for feature extraction and pattern recognition [21]. Deep learning is structurally a combination of high and low level hierarchy [20]. In deep learning, models such as Convolutional Neural Networks (CNN), Generative Adversarial Networks / GAN, Recurrent Neural Networks / RNN, CapsNet, Auto Encoder, HitNet are frequently used. These deep learning models are frequently used in many areas such as education [22, 23], facial recognition [24, 25] voice and emotion recognition [26, 27], cyber security [28] and health [29, 30].

In this study, a dataset containing 746 Covid-19 CT images created and shared on open source websites [31] by Zhao et al. (2020) was used. The data set was made ready for training by performing sizing and normalization operations on the data set. 349 Covid-19 positive CT images and 397 Covid-19 negative CT images were taken from this data set. Using the Resnet-101 deep learning method on the data set, Covid-19 patients were identified with an accuracy of 94.29%.

## 2. RELATED WORKS

When the academic studies that reviewed Covid-19 using CT images and Deep learning methods were examined; Li et al. (2020b) used CNN model for Covid-19 detection on lung CT images. The model created has been determined as 96% accurate according to AUC (Area Under Curve) performance evaluation criteria [20]. In another study, a model that helps radiologists to control the Covid-19 pandemic was created using the data set created by using CT images of MERS, SARS and ARDS from github, Open-i and Kaggle, and the CNN model [32]. In their study, Apostolopoulos et al. (2020) used X-ray images for the CNN network, which automatically detects features for the diagnosis of Covid-19 [33].

They obtained the best result in the study with MobilNet v2. In another study, they detected 90% accurate according to AUC performance evaluation criteria by using deep learning methods on CT images of patients diagnosed with viral pneumonia [34]. In another study, deep learning methods were used on the CT images of patients diagnosed with viral pneumonia, and they found 90% accurate according to the AUC performance evaluation criteria [35]. In their study, Wang and Wong (2020) proposed the Covid-NET model for Covid-19 detection on Chest CT images. Three results were obtained with the proposed model: normal 91.3%, covid-19 93.8% and non-Covid-19 88.9%. In another study, they created a diagnostic system based on CNN model for the diagnosis of COVID-19. The established diagnostic model has been determined as 97% accurate according to AUC performance evaluation criteria. In their study, Shan et al. (2020) developed a deep learning model to automatically measure the amount of infection occurring in the lungs of patients carrying the SARS-CoV-2 virus [36]. In Narin et al.'s (2020) study, 98% accuracy was achieved with the CNN-based ResNet50 model using CT images of Covid-19 patients using the transfer learning technique [37].

## 3. MATERYAL VE METOT

### 3.1. Materyal

In this study, Covid-CT-dataset created by [38], which includes a total of 746 CT images, 397 Non-Covid and 349 Covid-19, shared on an open-source site [31] has been used. This data set was modeled using the Resnet-101 deep learning method with a software prepared in Python programming language. Information about the data set used in the study is given in Section 3.1.1 and the structure of Resnet-101 architecture is given in section 3.1.2.



#### 3.1.1. Dataset

The properties of the data set used in this study are given in Table 1. When the table is examined, it is seen that a total of 746 images are selected from the Covid-CT-dataset in a way that the number of Covid and Non Covid is balanced. The Covid-19 dataset consists of 349 images and this dataset is divided into two datasets as 279 training and 70 test. The Non- Covid-19 dataset consists of 397 images and this dataset is divided into two datasets as 327 training and 70 tests.

**Table 1.** Covid-19 CT dataset distribution used in this study

| Dataset | Non-Covid-19 | Covid-19 | Total |
|---|---|---|---|
| Test | 70 | 70 | 140 |
| Train | 327 | 279 | 606 |
| Total | 397 | 349 | 746 |

#### 3.1.2. ResNet-101 network architecture

The Resnet-101 structure consists of 101 layers. Based on the Residual neural network learning method, this architecture is one of the deepest proposed architectures for ImageNet [39]. The biggest feature of Resnet-101 that differs from other architectures is that it optimizes the residues between input and desired convolution properties. Desired features are obtained more easily and efficiently compared to other architectures. Thus, residual optimization can be applied to reduce the number of parameters in a deeper network. By reducing the number

of parameters, the number of layers can be reduced to an effective number [40].

In ResNet architecture, information that cannot be learned in the previous layer is applied from the old layer to the new layer with the ResBlock layer. The Resblock layer is the blocks that feed residual values to the next layer in the Resnet architecture. This value added by this skip, which occurs between the weight layers and the Relu activation code at every two-layer activation, changes the system account [41].

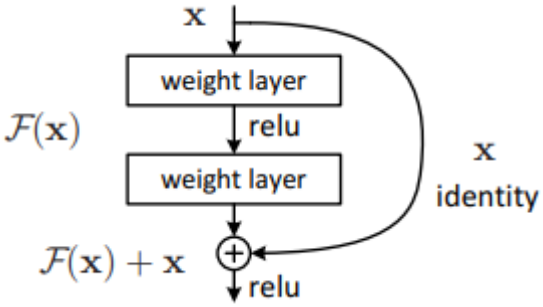


**Figure 1.** Residual Block [41]

The Residual Block structure has two layers and represents the nonlinear Relu function.

$$F = w_{2\sigma}(w_1 x) \quad (1)$$

By adding the second Relu value to this result, y output is obtained.

$$y = F(x, \{w_i\}) + x \quad (2)$$

In Eq. 2, x represents the input vector and y represents the output vector.

### 3.1.3. Performance evaluation criteria

Different evaluation criteria such as Area Under the ROC Curve (AUC), Receiver Operating Characteristic Curve (ROC), sensitivity, specificity, accuracy and F1 score are used to detect diseases in medical images. AUC value and ROC curve are generally used in performance evaluation of classification processes in deep learning. These two performance evaluation criteria are often used when data sets are not balanced. The ROC curve is a probability curve created for classes. Normally, in an ideal ROC curve, the x-axis contains False Positive Rate (FPR) values, and the y-axis contains True Positive Rate (TPR) values. The AUC value is calculated by calculating the area under the ROC curve. The calculated field value is a value ranging from 0 to 1. If the calculated value is close to 1, the model created is so close to success. In Table 2, cross-classification table is given for sensitivity, F1 score, accuracy and specificity according to estimation and reference test results. In the table, True Positive is expressed as TP, False Negative as FN, False Positive as FP and True Negative as TN. TP represents the correctly predicted positive class, FN, the false predicted negative class, FP represents the false predicted positive class, and TN represents the correctly predicted negative class [42-46].

**Table 2.** Cross-classification table according to estimation and reference test results

| | | **Predicted** | |
|---|---|---|---|
| | | Positive | Negative |
| **Actual** | Positive | TP | FN |
| | Negative | FP | TN |

Using Table 2, the mathematical expressions of sensitivity, specificity, accuracy and F1 score are given between Eq. 3-6 [42-46].

$$Sensitivity = \frac{TP}{TP+FN} \quad (3)$$

$$\text{Specificity} = \frac{TN}{TN+FP} \quad (4)$$

$$\text{Accuracy} = \frac{TP+TN}{\text{TP+FN}+TN+FP} \quad (5)$$

$$\text{F1 Score} = \frac{2*TP}{2*\text{TP+FN}+FP} \quad (6)$$

### 3.2. Methods

The work block diagram of the study carried out is given in Fig.2. In the first stage of the study, a data set was created using a total of 746 Covid-CT-dataset data taken from open source websites [31]. This dataset contains a total of 349 CT images carrying SARS-CoV-2 virus and 397 CTS that do not carry SARS-CoV-2 virus. In the second stage, the images in Covid-CT-dataset were divided into two classes and labeled as Covid-19 and Non Covid-19. Images belonging to Covid-19 class are divided into three as 234 training, 45 validation and 70 test. Non-Covid-19 class data are divided into three as 282 training, 45 validation and 70 tests. After the data sets were categorized, all images were converted to 296x296 dimensions. All images were normalized after conversion was performed. In the third stage, the learning rate of the Resnet-101 model used in the study has been optimized by training. According to the learning rate determined in the optimization process, the training process was carried out using the Resnet-101 model with 30 epochs. As the number of epochs increases, the performance of the model increases, but overfitting may occur. Therefore, it is necessary to choose an appropriate number of epochs. In the study, the number of epochs was chosen in areas where it increased in very small units, based on the performance and loss of the model. Batch size 16 and adam optimization method was used in the training phase of the ResNet-101 model. The model obtained at the end of each epoch operation was validated with validation data. At the last stage, the final Resnet-101 model was tested with 140 CT images and the model accuracy was determined.

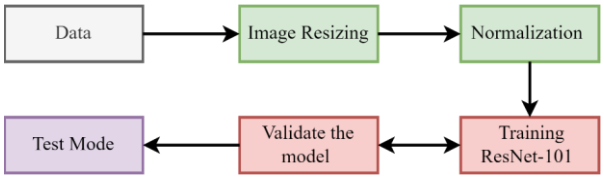


**Figure 2.** Work Block Diagram

## 4. RESEARCH FINDINGS

In this study, 746 Covid-CT-dataset images were modeled with one of the deep learning models Resnet-101. In Figure 3, the learning rate graph of the Resnet-101 model is given. When the graphic is analyzed, the learning rate for the Resnet-101 model was taken as 0.002 and the training process was carried out.

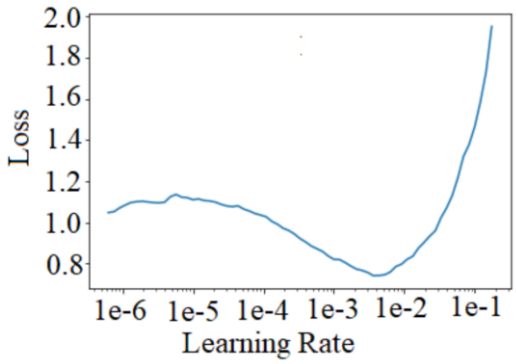


**Figure 3.** Learning rate effect graphic of Resnet-101 architecture

Choose an appropriate number of epochs and learning rate to avoid over fitting during the training phase. In order to check that there is no over fitting in the trained model, it was verified with the validation dataset during the training phase and tested using different data at the end of the training.

The confusion matrix of the model is given in Fig. 4 to determine the accuracy of the trained Resnet-101 architecture. It can be seen from the confusion matrix that 70 of 140 CT images used in the testing phase of the model are Covid-19 positive and the remaining 70 images are Covid-19 negative. As seen in the confusion matrix, the model created with Resnet-101 has classified 65 of 70 Covid-19 positive patients accurately and 5 patients inaccurately. In addition, the created model has classified 67 of 70 Covid-19 negative patients accurately and 3 patients inaccurately. The results obtained from the Confusion matrix show that the created model gives successful results in Covid-19 detection.

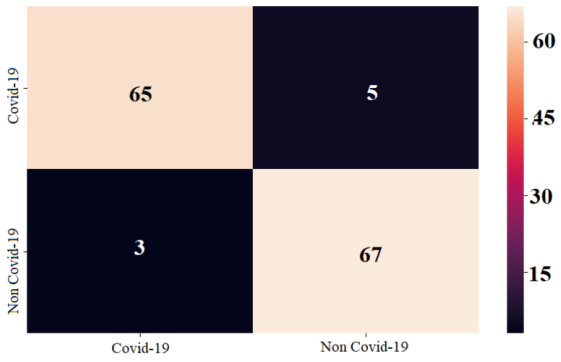


**Figure 4.** Confusion matrix

Following the successful results obtained from the confusion matrix, the sensitivity, specificity, accuracy and F1 score values for the Covid-CT data that the Resnet-101 model predicted correctly and incorrectly were calculated according to the values in the cross-classification table given in table 3. Sensitivity, specificity, accuracy, and F1 score values are showed in table 4 by using equations given between Eq. 3-6.

**Table 3.** Cross classification table for Resnet-101 model

| | | Predicted | |
|---|---|---|---|
| | | Covid-19 (Positive) | Non Covid-19 (Negative) |
| Actual | Covid-19 (Positive) | 65(TP) | 5(FN) |
| | Non Covid-19 (Negative) | 3(FP) | 67(TN) |

**Table 4.** Performance Evaluation Results of the Model

| Evaluation criteria | Sensitivity | Specificity | Accuracy | F1 score |
|---|---|---|---|---|
| Values | 92.86 | 95.71 | 94.29 | 94.2 |

When the values obtained from the calculations are examined, the sensitivity value is 92.86%, the specificity is 95.71%, the accuracy is 94.29% and the F1 Score value is 94.20%. The Resnet-101 model used in the study was evaluated with the ROC curve. In Figure 5, the ROC curve was drawn using the reference test and prediction data of the Resnet-101 model. As seen in the figure, it is seen that the Resnet-101 model gives a high successful result in the detection of Covid-19 virus.

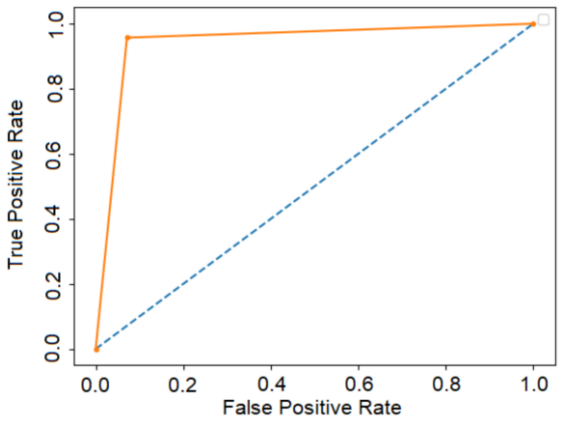


**Figure 5.** ROC Curve for Trained ResNet-19 model

The AUC value of the area under the ROC curve drawn according to the Resnet-101 model used in the study was determined as 0.943 using the ROC_AUC_score function of the scikit-learn library in the Python programming language. It was determined that the Resnet-101 model used to detect the SARS-CoV-2 virus by using the images in Covid-CT-Dataset detected the virus with an accuracy rate of 94.29%.

## 4. CONCLUSIONS

The SARS-CoV-2 virus, which appeared in China in December 2019, quickly spread and turned into a pandemic. Various measures have been taken in the world to prevent this pandemic. Many measures were taken, such as forbidding elderly people and children from going out, applying social distance rules, forbidding mass events. In addition to these precautions, isolating the individuals carrying the virus and personal cleaning are one of the most important measures to prevent the spread of the SARS-CoV-2 virus. Therefore, early diagnosis of patients with the SARS-CoV-2 virus is extremely important. Different methods are used to detect the SARS-CoV-2 virus. Among these methods, different methods such as Covid-19 blood test, chest x-ray are used.

In the study, 746 COVID-CT-dataset images taken from open access websites (GitHub) were used to determine COVID-19 disease. The reliability of the Resnet-101 model has been increased by taking an equal number of images with and without the SARS-CoV-2 virus in the data set. The Resnet-101 model used in the study was evaluated according to four different performance evaluation criteria. As a result of the evaluation;

- The Resnet-101 model was evaluated according to the Confusion matrix, the first performance evaluation criterion. As a result of the evaluation, 65 of 70 patients with SARS-CoV-2 virus and 67 of 70 patients without SARS-CoV-2 virus were determined correctly.
- Resnet-101 model was secondly evaluated according to sensitivity, specificity, accuracy and F1 score. As a result of the evaluation, it was found that the SARS-CoV-2 virus was detected with 92.86% sensitivity value, 95.71% specificity, 94.29% accuracy and 94.20% F1 Score value.
- When the Resnet-101 model is evaluated according to the ROC curve, it has been determined that it gives a highly successful result.
- In the last stage of the study, the Resnet-101 model was evaluated according to the AUC evaluation method. As a result of the evaluation, the AUC value was determined to be 0.943.

According to the four different evaluation criteria used in the study, the Resnet-101 model used to identify people with COVID-19 disease by using Covid-CT-dataset images detected the people with the disease with 94.3% accuracy. In future studies, it is thought that it would be appropriate to carry out different studies by using different deep learning methods or by enlarging the data set.

## ACKNOWLEDGES

We would like to thank Zhao et al. who opened the data set used in the study for open access.

## REFERENCES

[1] Çalışkan A. XIX. Yüzyıl ve XX. Yüzyıl başlarında Maraş ve kazalarında salgın hastalıklar ve salgın hastalıklara karşı alınan önlemler. Paradigma Akademi; 2019.
[2] Benedictow OJ, Benedictow OL. The Black Death, 1346-1353: the complete history. Boydell & Brewer; 2004.
[3] Condrau F. Samuel K. Cohn Jr., Epidemics: Hate and Compassion from the Plague of Athens to AIDS. Social History of Medicine. 2020; 33(4) : 1399–1401.
[4] Bung N, Krishnan SR, Bulusu G, Roy A. De novo design of new chemical entities (NCEs) for SARS-CoV-2 using artificial intelligence. Future medicinal chemistry. 2021;13(06): 575-585.
[5] Sevli O, Gülsoy VGB. Covid-19 salgınına yönelik zaman serisi verileri ile Prophet model kullanarak makine öğrenmesi temelli vaka tahminlemesi. Avrupa Bilim ve Teknoloji Dergisi. 2020; (19): 827-835.
[6] Macleod I, Heath N. Cone-beam computed tomography (CBCT) in dental practice. Dental update. 2008; 35(9): 590-598.
[7] Li X, Zeng X, Liu B, Yu Y. COVID-19 infection presenting with CT halo sign. Radiology: Cardiothoracic Imaging.2020; 2(1): e200026.
[8] Fang Y, Zhang H, Xu Y, Xie J, Pang P, Ji W. CT manifestations of two cases of 2019 novel coronavirus (2019-nCoV) pneumonia. Radiology. 2020; 295(1): 208-209.
[9] Xie X, Zhong Z, Zhao W, Zheng C, Wang F, Liu J. Chest CT for typical 2019-nCoV pneumonia: relationship to negative RT-PCR testing. Radiology, 2020; 296(2): 41-45.
[10] Kay F, Abbara S. The Many Faces of COVID-19: Spectrum of Imaging Manifestations. Radiology: Cardiothoracic Imaging. 2020; 2(1): e200037.
[11] Phelan AL, Katz R, Gostin LO. The novel coronavirus originating in Wuhan, China: challenges for global health governance. Jama. 2020; 323(8): 709-710.
[12] Nishiura H, Jung SM, Linton, NM, Kinoshita R, Yang Y, Hayashi K, et al. The extent of transmission of novel coronavirus in Wuhan, China, 2020. Journal of Clinical Medicine. 2020; 9(2): 330.
[13] Song F, Shi N, Shan F, Zhang Z, Shen J, Lu H, et al. Emerging 2019 novel coronavirus (2019-nCoV) pneumonia. Radiology, 2020; 295(1): 210-217.
[14] Liu T, Huang P, Liu H, Huang L, Lei M, Xu W, et al. Spectrum of chest CT findings in a familial cluster of COVID-19 infection. Radiology: Cardiothoracic Imaging. 2020; 2(1): e200025.

[15] Pan F, Ye T, Sun P, Gui, S, Liang B, Li L, et al. Time course of lung changes on chest CT during recovery from 2019 novel coronavirus (COVID-19) pneumonia. Radiology. 2020; 295(3), 715–721.
[16] Kong W, Agarwal PP. Chest imaging appearance of COVID-19 infection. Radiology: Cardiothoracic Imaging, 2020; 2(1): e200028.
[17] Ng MY, Lee EYP, Yang J, Yang F, Li X, Wang H, et al. Imaging profile of the COVID-19 infection: radiologic findings and literature review. Radiology: Cardiothoracic Imaging. 2020; 2(1): e200034.
[18] Wu Y, Xie YL, Wang X. Longitudinal CT findings in COVID-19 pneumonia: case presenting organizing pneumonia pattern. Radiology: Cardiothoracic Imaging.2020; 2(1): e200031.
[19] Ayan A, Kıraç S, Ayan UDA. COVID-19 Pandemisi Sürecinde Nükleer Tıp Uygulamaları İçin Kılavuz. Sağlık Bilimleri Üniversitesi. Ankara. 2020.
[20] Li L, Qin L, Xu Z, Yin Y, Wang X, Kong B, el al. Using Artificial Intelligence to Detect COVID-19 and Community-acquired Pneumonia Based on Pulmonary CT: Evaluation of the Diagnostic Accuracy. Radiology.2020; 296(2): 65–71.
[21] Azuaje F. Artificial intelligence for precision oncology: beyond patient stratification. NPJ precision oncology.2019; 3(1):1-5.
[22] Wang ZJ, Turko R, Shaikh O, Park H, Das N, Hohman F, et al. Cnn explainer: Learning convolutional neural networks with interactive visualization. IEEE Transactions on Visualization and Computer Graphics. 2020; 27(2): 1396-1406.
[23] Akour M, Al SH, Al Qasem O. The effectiveness of using deep learning algorithms in predicting students achievements. Indonesian Journal of Electrical Engineering and Computer Science. 2020; 19(1): 387-393.
[24] Khan S, Javed MH, Ahmed E, Shah SA, Ali SU. Facial Recognition using Convolutional Neural Networks and Implementation on Smart Glasses. In 2019 International Conference on Information Science and Communication Technology (ICISCT). Karachi: IEEE. 2019. p. 1-6.
[25] De Bortoli L, Guzzi F, Marsi S, Carrato S, Ramponi G. A fast face recognition CNN obtained by distillation. In International Conference on Applications in Electronics Pervading Industry, Environment and Society. Cham: Springer; 2019. p. 341-347.
[26] Amiriparian S, Awad A, Gerczuk M, Stappen L, Baird A, Ottl S, el al. Audio-based recognition of bipolar disorder utilising capsule networks. In 2019 International Joint Conference on Neural Networks (IJCNN). Budapest: IEEE; 2019. p.1-7.
[27] Chao H, Dong L, Liu Y, Lu B. Emotion recognition from multiband EEG signals using CapsNet. Sensors. 2019; 19(9): 2212.
[28] Choi YH, Liu P, Shang Z, Wang H, Wang Z, Zhang L, et al. Using deep learning to solve computer security challenges: a survey. Cybersecurity. 2020; 3(1):1-32.
[29] Khedkar S, Gandhi P, Shinde G, Subramanian V. Deep Learning and Explainable AI in Healthcare Using EHR. In: Dash S, Acharya BR, Mittal M, Abraham A, Kelemen A, editors. Deep Learning Techniques for Biomedical and Health Informatics. Cham: Springer; 2020. P. 129–148
[30] Uddin MZ. A wearable sensor-based activity prediction system to facilitate edge computing in smart healthcare system. Journal of Parallel and Distributed Computing. 2019; 123:46-53.
[31] Github (2020) UCSD-AI4H/COVID-CT. [Internet]. 2020 [cited 2020 May 12]. Available from: https://github.com/UCSD-AI4H /COVID-CT
[32] Salman FM, Abu-Naser SS, Alajrami E, Abu-Nasser BS, Alashqar BA. COVID 19 Detection using Artificial Intelligence. International Journal of Academic Engineering Research (IJAER). 2020; 4(3):18-25.
[33] Apostolopoulos ID, Mpesiana TA. Covid-19: automatic detection from x-ray images utilizing transfer learning with convolutional neural networks. Physical and engineering sciences in medicine. 2020; 43(2): 635-640.
[34] Wang S, Kang B, Ma J, Zeng X, Xiao M , Guo J, et al. A deep learning algorithm using CT images to screen for Corona Virus Disease (COVID-19). European radiology.2021; 31(8): 6096-6104.
[35] Wang L, Lin ZQ, Wong A. Covid-net: A tailored deep convolutional neural network design for detection of covid-19 cases from chest x-ray images. Scientific Reports.2020; 10(1): 1-12.
[36] Shan F, Gao Y, Wang J, Shi W, Shi N, Han M, et al. Lung infection quantification of covid-19 in CT images with deep learning. American Association of Physicists in Medicine. 2020; 48(4): 1633-1645.
[37] Narin A, Kaya C, Pamuk Z. Automatic detection of coronavirus disease (COVID-19) using X-ray images and deep convolutional neural networks. Pattern Analysis and Applications, 2021; 24(3), 1207-1220.
[38] Zhao J, Zhang Y, He X, Xie P. COVID-CT-Dataset: a CT scan dataset about COVID 19. 2020. arXiv preprint arXiv:2003.13865.
[39] He K, Zhang X, Ren S, Sun J. Deep residual learning for image recognition. In Proceedings of the IEEE conference on computer vision and pattern recognition. USA, Las Vegas: 2016. P. 770-778.
[40] Chung YM, Hu CS, Lawson A, Smyth C. Toporesnet: A hybrid deep learning architecture and its application to skin lesion classification. Mathematics.2021; 9(22): 2924.
[41] Koç M, Özdemir R. Enhancing Facial Expression Recognition in the Wild with Deep Learning Methods Using a New Dataset: RidNet. Bilecik Seyh Edebali University Journal of Science. 2019; 6(2): 384 - 396
[42] Šimundić AM. Measures of diagnostic accuracy: basic definitions. Ejifcc. 2009; 19(4): 203-211.
[43] Zhu W, Zeng N, Wang N. Sensitivity, specificity, accuracy, associated confidence interval and ROC analysis with practical SAS implementations. NESUG proceedings: health care and life sciences. Baltimore, Maryland. 2010. p.19:67.
[44] Lalkhen A, McCluskey A. Clinical tests: sensitivity and specificity. Continuing Education in

Anaesthesia Critical Care & Pain. 2008; 8(6): 221-223.
[45] Eusebi P. Diagnostic accuracy measures. Cerebrovascular Diseases. 2013; 36(4): 267-272.
[46] Chicco D, Jurman G. The advantages of the Matthews correlation coefficient (MCC) over F1 score and accuracy in binary classification evaluation. BMC genomics. 2004; 21(1): 1-13.

Araştırma Makalesi https://doi.org/10.46810/tdfd.1004408 Research Article

Türk Doğa ve Fen Dergisi
Turkish Journal of Nature and Science
www.dergipark.gov.tr/tdfd

# Farklı Aralıklarla Sulanan Gemlik Zeytin (*Olea europaea* L.) Çeşidinin Stoma Morfolojisindeki Plastisite

**Mehmet İlhan ODABAŞIOĞLU[1*], Ebru SAKAR[2], Meral ANLAĞAN TAŞ[3]**

[1] Adıyaman Üniversitesi, Ziraat Fakültesi, Bahçe Bitkileri Bölümü, Adıyaman, Türkiye
[2] Harran Üniversitesi, Ziraat Fakültesi, Bahçe Bitkileri Bölümü, Şanlıurfa, Türkiye
[3] GAP Tarımsal Araştırma Enstitüsü, Şanlıurfa, Türkiye
Mehmet İlhan ODABAŞIOĞLU ORCID No: 0000-0001-8060-3407
Ebru SAKAR ORCID No: 0000-0001-6622-6553
Meral ANLAĞAN TAŞ ORCID No: 0000-0002-5212-9039

**Sorumlu yazar: milhanodabasioglu@gmail.com*

(Alınış: 04.10.2021, Kabul: 26.04.2022, Online Yayınlanma: 29.06.2022)

**Anahtar Kelimeler**
Gemlik, Sulama Sıklığı, Zeytin Yaprağı, Yaprak Konumu, Stoma Özellikleri

**Öz:** Bu çalışma, yarı-kurak iklim koşullarına sahip Şanlıurfa ilinde yetiştirilen Gemlik zeytin çeşidine uygulanan farklı sulama aralıklarının, yapraklarda yer alan stomaların bazı özelliklerine etkilerini incelemek amacıyla yürütülmüştür. Bu amaçla; farklı aralıklarla (kontrol, 7, 14, 21, 28 ve 35 gün) sulanan 12 yaşındaki Gemlik zeytin çeşidi ağaçlarından hasat zamanı alınan yaprak örnekleri bitkisel materyal olarak kullanılmıştır. Yaprak örnekleri, sürgünlerin uç, orta ve bazal kısımlarından alınmış ve sürgün üzerinde yaprakların bulunduğu konuma bağlı olarak da stoma özelliklerinin değişimi incelenmiştir. Sulama aralıklarının; stoma yoğunluğu, stoma boyutları, stoma alanı, stoma şekil katsayısı, oransal stoma alanı ve potansiyel iletkenlik indeksinde farklılıklar oluşturduğu saptanmıştır. Stoma yoğunluğu en yüksek olan sulama aralığı 35 gün (413,05 adet $mm^{-2}$), en düşük olan sulama aralığı ise 28 gün (365,75 adet $mm^{-2}$) olarak saptanmıştır. Stoma yoğunluğunun genel olarak sulama aralığının artışına bağlı olarak arttığı, stoma boyu ve stoma alanının ise azaldığı saptanmıştır. Yaprakların sürgün üzerinde bulundukları konuma göre stoma özellikleri değişim göstermiş ancak bu durum stoma boyutlarında daha net görülmüştür. Sürgün ucundaki yaprakların, orta ve alt bölümdeki yapraklara göre daha küçük stomalara sahip olduğu belirlenmiştir. Çalışmada; stoma eni ile stoma boyu arasında kuvvetli bir ilişki olduğu belirlenmiştir.



# Plasticity in Stoma Morphology of Gemlik Olive (*Olea europaea* L.) Cultivar under Different Irrigation Intervals

**Keywords**
Gemlik, Irrigation İnterval, Olive Leaf, Leaf Position, Stoma Characteristics

**Abstract:** This study was carried out to examine the effects of different irrigation intervals applied to the Gemlik olive variety grown in Şanlıurfa, which has semi-arid climate conditions, on some characteristics of the leaf stomata. For this purpose, leaf samples taken at harvest time from 12-year-old Gemlik olive variety trees irrigated at different intervals (control, 7, 14, 21, 28, and 35 days) were used as plant material. Leaf samples were taken from the top, middle and basal parts of the shoots, and the changes in stomatal characteristics were also examined depending on the location of the leaves on the shoot. The analyses show that irrigation intervals were made significant differences in stoma density, stoma size, stoma area, stoma shape coefficient, relative stoma area, and potential conductivity index. Irrigation interval with the highest stomatal density was determined as 35 days (413.05 stoma $mm^{-2}$), and the lowest irrigation interval was determined as 28 days (365.75 stoma $mm^{-2}$). We show that the stomatal density generally increased with the increase of the irrigation interval, whereas the stomatal length and stomatal area decreased. The stomatal characteristics were changed according to the position of the leaves on the shoot, but this was more clearly in stomatal sizes. It was determined that the leaves at the top of the shoot have smaller stomata than the leaves in the middle and lower parts. It was determined that there was a strong relationship between stoma width and stoma length.

## 1. GİRİŞ

Bitkilerde su ve gaz alışverişinde kilit rol üstlenen stomaların, gerek hareketleri gerekse dağılımları pek çok araştırmanın konusunu oluşturmuştur. Özellikle kurak koşullarda, bitkilerde su kaybının azaltılmasıyla canlılığın ve gelişimin sürekliliğinin sağlanmasında stoma hareketlerinin önemli etkileri vardır. Nitekim kuraklık etkisi altındaki bitkilerde, stoma yoğunluğunun ve porlarının açıklığının değiştiğini bildiren araştırmalar; stomaların çevre şartlarına bağlı olarak plastisitelerinin (yoğunluklarının ve boyutlarının farklılaşma düzeylerinin) ne denli yüksek olduğuna da dikkat çekmektedir [1-4]. Stomaların dağılımları ve hareketleri üzerine etkili olan tek çevresel faktör kuraklık olmayıp; sıcaklık (yüksek ve düşük), şiddetli rüzgar, tuzluluk vb. stres kaynakları, yetiştiricilik yapılan ekoloji ve hatta kültürü yapılan türlerin yanı sıra anaçlar bile önemli değişimlere neden olabilmektedir [5-10]. Ayrıca stoma özelliklerinin bitki türüne göre değiştiği hatta aynı tür içerisinde yer alan farklı çeşitlerde dahi birbirinden farklı stoma özellikleri görüldüğünü bildiren araştırmalara literatürde sıklıkla rastlanmaktadır [11-14].

Bitkilerde yeşil olan tüm organların epidermal yüzeylerinde bulunan ancak yapraklarda daha yoğun olarak yer alan stomaların, yapraklarda yer aldığı konumlar da değişkenlik göstermektedir. Bazı türlerde yaprağın üst yüzeyinde (epistomatik), bazı türlerde yaprağın alt yüzeyinde (hipostomatik), bazı türlerde ise yaprağın her iki yüzeyinde de (amfistomatik) stomalar bulunmaktadır [15]. *Olea europea* L. türüne ait zeytin çeşitlerinin yapraklarının yalnızca abaxial yüzeyinde (yaprak alt yüzeyinde) stomaların bulunduğu, Beerling ve Chaloner [16] tarafından bildirilmiştir. Yener [17], zeytin yapraklarının alt yüzeyinde stoma bulunmasının nedeninin, bitkinin su kaybını azaltma stratejisinin bir parçası olduğunu bildirmiş ve zeytin yapraklarının alt yüzeyinde ortalama 625 adet $mm^{-2}$ stoma bulunduğunu aktarmıştır.

Literatürde, farklı bitki türlerinin yapraklarında stoma dağılımları ve özellikleri sıklıkla incelenmiş olmasına karşın; yaprak konumunun bu özellikler üzerine etkisi yeterince araştırılmamıştır. Sınırlı sayıdaki araştırmalarda da elde edilen bulgular birbirlerinden farklılık göstermektedir. Nitekim, Ataol Ölmez [18]'in farklı kayısı çeşitlerinde, Topsakal [19]'ın farklı Pistacia türlerinde yaptıkları çalışmalarda; yaprak örneklerinin alındığı yöneyin stoma yoğunluğu üzerinde etkili olmadığı saptanmıştır. Gokbayrak ve ark. [6] ise asma yapraklarında stoma yoğunluğu üzerine yöneyin etkili olduğunu ancak bu etkinin şiddetli rüzgarların neden olduğu yüksek transpirasyonu azaltmak için fenotipik bir düzenlemeden (ozmotik regülasyon) kaynaklanabileceğini bildirmişlerdir. Reich [20] ise yaprak konumunun etkisinin önemli olduğunu, kavaklarda yaprakların bitki üzerinde yer aldıkları bölgeye göre bu özelliklerin değişim gösterebileceğini bildirmiştir.

Her ne kadar farklı bitki türlerinde kuraklığın stomalar üzerine etkileri sıklıkla incelenmişse de sulama aralığının etkisi konusunda yeterli çalışma mevcut değildir. Bu çalışmada, daha önce yeterince araştırılmamış olan, farklı sulama aralıklarının bitkilerin yapraklarındaki stomaların özelliklerine etkilerini belirlemek amacıyla Gemlik zeytin (*Olea europaea* L.) çeşidi ağaçları kullanılmıştır. Farklı sulama aralıklarının yapraklarda, kuraklık stresinin neden olduğu değişimlere benzer değişimlere neden olup olmadığı saptanmaya çalışılmıştır. Bununla birlikte, yaprakların sürgün üzerindeki konumlarının da stomaların dağılımlarına ve plastisitesine etkileri belirlenmeye çalışılmıştır.

## 2. MATERYAL VE METOT

### 2.1. Materyal

Çalışma; Şanlıurfa'da, 2014 yılında yürütülmüştür. Bitkisel materyal olarak 6 m x 6 m dikim sıklığında yetiştirilmiş olan 12 yaşındaki Gemlik zeytin çeşidi ağaçları kullanılmıştır. Farklı sulama aralıklarının etkisini belirlemek için deneme 2010-2015 yılları arasında yürütülmüş olup 2 yıl ön verim alındıktan sonra 2012 yılında (ağaçlar 10 yaşında iken) sulama uygulamalarına başlanmıştır. Sulama konularının uygulanmaya başlamasının 2. yılında, zeytin hasadı döneminde (2014 yılı Kasım ayı) yaprak örnekleri alınmıştır. Denemenin yürütüldüğü bahçenin yer aldığı bölgenin iklim verileri Tablo 1'de sunulmuştur.



**Tablo 1.** Denemenin yürütüldüğü bölgenin 2014 yılına ait iklim verileri

| Parametreler | I | II | III | IV | V | VI | VII | VIII | IX | X | XI | XII |
|---|---|---|---|---|---|---|---|---|---|---|---|---|
| Ortalama Sıc. (°C) | 8,6 | 10,0 | 14,2 | 18,5 | 24,0 | 28,4 | 32,5 | 32,4 | 26,2 | 20,3 | 12,1 | 9,5 |
| En Yük. Sıc. (°C) | 13,5 | 16,2 | 20,0 | 24,9 | 30,8 | 34,8 | 39,6 | 39,3 | 32,9 | 26,3 | 17,8 | 12,9 |
| En Düş. Sıc. (°C) | 5,0 | 5,4 | 9,2 | 12,4 | 17,1 | 21,4 | 25,1 | 25,2 | 19,6 | 15,3 | 8,0 | 6,8 |
| Nisbi Nem (%) | 65,6 | 44,0 | 51,7 | 47,5 | 29,8 | 26,4 | 26,6 | 27,8 | 41,0 | 49,5 | 53,9 | 79,4 |
| Yağış Top. (kg $m^{-2}$) | 44,3 | 20,8 | 91,6 | 33,3 | 6,0 | 20,6 | - | 1,0 | 28,8 | 25,7 | 78,6 | 55,4 |

### 2.2. Yöntem

Sulamalara, topraktaki elverişli nem %60'a düştüğünde başlanmıştır. Deneme konularında yer alan tüm parsellerden gravimetrik yöntemle 4 farklı derinlikten (0-30, 30-60, 60-90, 90-120 cm) bozulmuş toprak örnekleri alınarak, mevcut nem düzeyi belirlenmiştir. Bütün konularda (0-35 gün sulama aralığı), toprak profilinin 0-90 cm derinliğindeki eksik nem tarla kapasitesine çıkarılacak şekilde (parsel alanı ve 0,40 örtü yüzdesi ile düzeltildikten sonra) ve su sayacı denetiminde sulamalar yapılmıştır. Sulamalar, mini spring yağmurlama sistemi (başlık debisi 200 lt $h^{-1}$ ve ıslatma çapı 6 m) kullanılarak yapılmıştır. Çalışmada, Gemlik zeytin çeşidi ağaçlarına uygulanan sulama aralıkları şu şekildedir; kontrol (susuz konu), 7 gün aralıkla sulama, 14 gün aralıkla sulama, 21 gün aralıkla sulama, 28 gün aralıkla sulama ve 35 gün aralıkla sulama. Ağaçlara, diğer kültürel işlemler

(gübreleme, budama, ilaçlama vb.) homojen olarak uygulanmıştır.

Tesadüf blokları deneme desenine göre 3 yinelemeli olarak yürütülmüş olan çalışmada; her parselde 3 ağaç yer almıştır. Yaprak örnekleri, deneme konularında yer alan ağaçların tamamından ve ağacı temsil edecek şekilde 4 farklı yöneyden (Kuzey, Güney, Doğu, Batı) eşit olarak, saat 8:00-10:00'da alınmıştır. Buna göre ağaçların her yöneyinden, tacın orta bölümünden 2'şer genç sürgün dipten kesilerek alınmış ve etiketlenerek, içerisinde buz kalıpları bulunan termosla stoma kalıplarının çıkarılması için laboratuvara nakledilmiştir.

Laboratuvara getirilen sürgünlerin uç, orta ve alt (bazal) kısımlarından 3'er yaprak alınmış ve stoma kalıpları Bekişli [21]'nin yöntemi modifiye edilerek, yaprakların alt yüzeyinden çıkarılmıştır (Şekil 1).

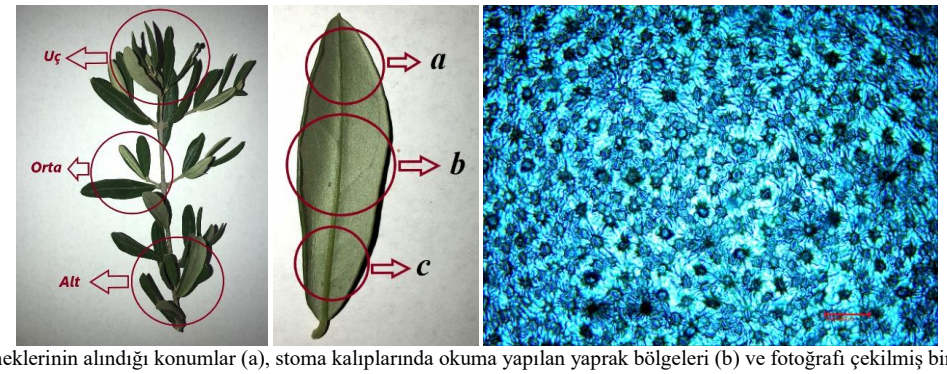


**Şekil 1.** Yaprak örneklerinin alındığı konumlar (a), stoma kalıplarında okuma yapılan yaprak bölgeleri (b) ve fotoğrafı çekilmiş bir stoma kalıbı (c)

Her sulama uygulaması için toplam 216 yaprak kalıbı alınmış ve her kalıbın 3 farklı bölgesinin fotoğrafları mikroskopta (Las Leica 1000) 10X/0,22 objektifte çekilmiştir. Daha sonra fotoğrafları çekilmiş olan kalıplarda (0,319 $mm^2$ görüş alanı) stoma sayım ve ölçümleri Las v4.3 bilgisayar programı kullanılarak yapılmıştır. Çalışmada incelenen stoma özellikleri; stoma yoğunluğu, stoma boyutları, stoma şekil katsayısı, stoma alanı, potansiyel iletkenlik indeksi ve oransal stoma alanıdır [22-23]. Elde edilen bulguların varyans analizi Minitab 18.0 programında yapılmış olup, grupların ortalama değerleri arasındaki anlamlı farklılıklar Tukey testi ile saptanmıştır.

## 3. BULGULAR VE TARTIŞMA

Farklı sulama aralıklarının, Gemlik zeytin çeşidinin yapraklarında stoma yoğunluğunun değişimine istatistiksel olarak $p \leq 0.01$ önem seviyesinde etki ettiği saptanmıştır. En yüksek stoma yoğunluğu (413,05 adet $mm^{-2}$) 35 gün aralıkla sulanan ağaçlardan alınan yapraklarda saptanırken, en düşük stoma yoğunluğu (365,75 adet $mm^{-2}$) 28 gün aralıkla sulanan ağaçlardan alınan örneklerde saptanmıştır (Şekil 2). Buna karşın 35 gün aralıkla sulanan ve kontrol grubunda yer alan ağaçlardan alınan örneklerde stoma yoğunluklarının, incelenen diğer gruplara göre daha yüksek bulunmuş olması; kuraklık stresinin etkisi ile zeytin ağaçlarının su kaybını azaltmak amacıyla stoma yoğunluklarını değiştirdiklerine işaret etmektedir.

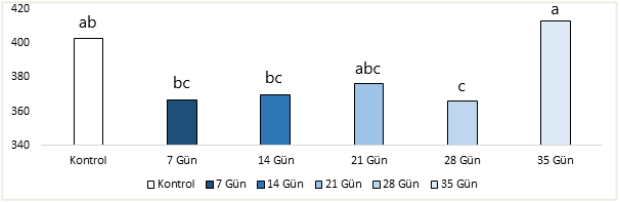


**Şekil 2.** Farklı sulama aralıklarının Gemlik zeytin çeşidinin yapraklarında stoma yoğunluğuna etkisi (adet $mm^{-2}$)

Gindel [24], kültürü yapılan 14 farklı bitki türünün yapraklarında stoma yoğunluğunun sulama koşullarına değiştiğini ve sulananlara göre sulanmayan bitkilerden alınan örneklerin daha fazla stomaya sahip olduklarını aktarmıştır. Farklı üzüm çeşitlerinde sulamanın yapraklarda stoma yoğunluğuna etkisini inceleyen Marasalı ve Aytekin [25], kuraklığın neden olduğu stresin şiddetine bağlı olarak stoma yoğunluğunun değişebileceğini, aşırı stres koşulları oluşmadıkça stoma yoğunluğunun çeşide özgü bir değişken olduğunu aktarmıştır. Palliotti ve ark. [2] ile Pekmezci ve Dardeniz [26] de stoma yoğunluğunun bitki türüne ve çeşide göre değişim göstermesine karşın kuraklık stresi altındaki bitkilerde stoma özelliklerinin farklılaşabileceğine ilişkin bulgulara ulaşmışlardır. Gomez Del-Campo ve ark. [27] ise stoma yoğunluğundaki söz konusu değişimlerin ancak belirli bir gelişme döneminde gerçekleşen kuraklık nedeniyle, fenotipik plastisitesi yüksek çeşitlerde adaptasyon yeteneğine bağlı olarak görüldüğünü bildirmiştir. Candar ve ark. [28] asma, Çalışkan ve ark. [29] ise limon fidanlarında kısıntılı sulamanın, stoma yoğunluğunu artış yönünde etkilediğini ancak bu değişimin istatistiksel olarak anlamlı olmadığını bildirmişlerdir. Çınar ve ark. [30], yer fıstığında kısıntılı sulamanın etkisiyle yapraklarda stoma yoğunluğunun arttığını bildirmiştir. Bosabalidis ve Kofidis [31] ile Guerfel ve ark. [32], kuraklık stresinin, zeytin fidanlarının yapraklarında stoma yoğunluğunun ve boyutlarının değişimine neden olduğunu saptamışlardır. Öncü [33] ise kısıntılı sulama uygulamalarına bağlı olarak Gemlik zeytin çeşidinin yapraklarında stoma yoğunluğunun değişiminin tek yönlü olmadığını ve tam sulanan konu ile 1/3 kısıntılı sulanana konudan alınan örneklerin stoma yoğunluğunun benzer olduğunu bildirmiştir. Buna karşın Al-Naqeeb [34], 6 farklı zeytin çeşidi üzerinde yaptığı araştırmada; %50 tarla kapasitesine kadar sulanan ağaçların yapraklarında, sulanmayan ağaçlara göre daha fazla stoma bulunduğunu bildirmiştir. Güler [35] ise farklı zeytin çeşitlerinin fidanları üzerinde yaptığı çalışmada, kuraklık stresinin yapraklarda stoma yoğunluğunu

arttırdığını ve stres koşulları ortadan kaldırıldığında bile bitkilerin stressiz koşullara nazaran anatomik yapılarındaki farklılığı bir süre daha sürdürdüklerini bildirmiştir.

Gemlik zeytin çeşidinin yapraklarında saptamış olduğumuz stoma yoğunluğu değerleri, daha önce bu çeşitte incelemeler yapan Öncü [33] ve Al-Naqeeb [34]'in belirtmiş oldukları alt/üst sınır değerleri içerisinde yer almaktadır. Çalışmada elde ettiğimiz; sulama aralığına bağlı olarak yapraklarda stoma yoğunluğunun sınırlı düzeyde değişim gösterebileceği bulgusu Roro ve Tesfaye [36] ile paralellik göstermektedir. Elde ettiğimiz bulgular ve bu alanda daha önce farklı araştırmacıların yapmış oldukları araştırmalar birlikte değerlendirildiğinde; bitkilerin yapraklarındaki stoma yoğunluğunu genotipin kontrol ettiği buna karşın kuraklık, kısmi kuralık ya da kesintili (dönemsel) kuraklık stresine maruz kalmış bitkilerin stoma yoğunluklarının değişebileceği kanaatine varılmıştır. Bununla birlikte, kuraklık stresinin neden olduğu; yapraklarda stoma morfolojisinde ve dağılımındaki değişimlerin, tek yıllık bitkilerde ve fidanlarda belirgin olarak görülmesine karşın kök sistemi gelişmiş olan çok yıllık bitkilerin ağaçlarında daha sınırlı olduğu söylenebilir [25; 37-42].

Sulama aralığı x yaprak konumu interaksiyonunda yer alan grupların ortalama stoma yoğunluğu değerleri arasında istatistiki olarak anlamlı bir farklılık saptanmamıştır. Bununla birlikte en fazla stoma (453,20 adet $mm^{-2}$), 35 gün aralıklarla sulanan ağaçların sürgünlerinin orta kısmında yer alan yapraklarında saptanmıştır (Tablo 2). En düşük stoma yoğunluğu (351,27 adet $mm^{-2}$) ise 14 gün aralıklarla sulanan ağaçların sürgünlerinin orta kısmında yer alan yapraklarında saptanmıştır. Yaprakların sürgün üzerindeki pozisyonlarının, stoma yoğunluğu üzerine etkisi istatistiki olarak önemsiz bulunmuştur. Buna karşın; sürgün büyümesini takiben olgunlaşan ve sürgünün alt kısımlarında konumlanan yaprakların, sürgünün uç kısmında yer alan genç yapraklara göre kısmen daha fazla stomaya sahip oldukları belirlenmiştir.

**Tablo 2.** Farklı sulama aralıkları ve yaprakların sürgün üzerindeki konumunun Gemlik zeytin çeşidinin yapraklarında stoma yoğunluğuna (adet $mm^{-2}$) etkileri

| Sulama Aralığı | Uç | Orta | Alt |
|---|---|---|---|
| Kontrol | 388,30 öd | 405,17 | 415,07 |
| 7 Gün | 358,60 | 361,53 | 379,13 |
| 14 Gün | 377,67 | 351,27 | 380,23 |
| 21 Gün | 370,33 | 361,29 | 397,64 |
| 28 Gün | 375,66 | 353,66 | 367,93 |
| 35 Gün | 393,43 | 453,20 | 392,51 |
| **Ortalama** | 377,33 ÖD | 381,02 | 388,75 |

ÖD ve öd: $p \geq 0.05$

Farklı bitki türlerinde yürütülen araştırmalarda; genç yaprakların, yaşlı yapraklara göre daha fazla stomaya sahip oldukları bildirmiştir [43-47]. Reich [20], hibrit kavak çeşitlerinde, yaprakların oluştuğu boğum düzeyinin artışına bağlı olarak stoma yoğunluğunun arttığını ancak değişim düzeyinin çeşide özgü olduğunu bildirmiştir. Farklı kayısı çeşitlerinde sürgünlerin uçlarında yer alan yaprakların, sürgünlerin dip ve orta kısımlarında yer alan yapraklara göre daha fazla stomaya sahip olduğunu bildiren Ataol Ölmez [18] ve Chardonnay üzüm çeşidinde boğum sayısı arttıkça yapraklarda stoma yoğunluğunun arttığını bildiren Rogiers ve ark. [48]'nın bulgularına karşılık; Topsakal [19] Pistacia türlerinde, Pekmezci ve Dardeniz [26] ise Yalova İncisi üzüm çeşidinde, yaprak konumunun (asmalarda boğum sayısının) stoma yoğunluğu üzerinde etkili olmadığını saptamıştır. Tetik ve Dardeniz [49] ile Yıldırım ve Dardeniz [50] ise üzüm çeşitlerinde, yaprakların sürgün üzerindeki konumunun stoma yoğunluğuna etkisinin önemli olduğunu ve sürgün ucundaki yaprakların daha az stomaya sahip olduğunu bildirmişlerdir. Sürücü [51] ise Stella kiraz çeşidinde farklı meyve dalı tiplerinin, yapraklarda stomaların yoğunluğuna etkisinin önemsiz olduğunu saptamıştır. Elde ettiğimiz bulgular; yapraklarda stoma yoğunluğunun, sürgünlerin bazal kısmından ucuna doğru gidildikçe azaldığını bildiren çalışmalar [49-50] ile benzerlik göstermektedir. Bununla birlikte; incelenen türlerin, örnek alınan dönemlerin, yetiştiricilik koşullarının, yaprak olgunluk düzeyinin ve yapraklarda inceleme yapılan bölgenin farklılığı da yaprak konumunun stoma yoğunluğu üzerine etkisini değiştirebilir.

Yaprakların sürgünden ayrıldığı erken dönemde epidermis büyümesini takiben stomalar da büyümekte ve sayıları artmaktadır, buna karşın yapraklar belirli bir büyüklüğe ulaştıktan sonra stoma sayısı artmamakta ancak epidermis hücreleri ve stomalar büyümektedir. Nitekim stoma boyutlarına (en ve boy) ve stoma yoğunluğuna ilişkin elde ettiğimiz bulgular bu durumu teyit etmektedir. Sulama aralıklarından bağımsız olarak, yaprakların sürgün üzerindeki konumlarının stoma boyu ve enine etkisi incelendiğinde; sürgünlerin ucundan bazal kısımlarına doğru, yapraklarda yer alan stomaların büyüdüğü saptanmıştır (Tablo 3). Sulama aralığı x yaprak konumu interaksiyonunda yer alan grupların, hem stoma eni hem de stoma boyu bakımından birbirlerinden, istatistiksel olarak anlamlı bir farklılık göstermedikleri belirlenmiştir. Sulama aralıklarının, her iki özelliğe de istatistiksel olarak $p \leq 0.01$ önem seviyesinde etki ettiği saptanmıştır. Daha sık sulanan ağaçların yapraklarında stomaların boyları daha uzun bulunmuştur. Buna karşın aynı değerlendirmeyi stoma eni için yapmak; ancak 7 gün aralıkla sulanan grup inceleme dışı bırakıldığında mümkündür.

Stoma boyutlarının sulama uygulamalarına bağlı olarak değişimlerini inceleyen araştırmacılar; sulamayla bitki su ihtiyacının karşılandığı bitkilere nazaran kısmi kuraklık ya da kısıntılı sulama uygulanan bitkilerin daha küçük stomalara sahip olduklarını saptamışlardır [2; 52-54]. Diğer bitki türlerinde saptanan bu değişim; zeytin çeşitleri için de geçerlidir. Nitekim Öncü [33], Güler [35] ve Mouna ve ark. [55] kuraklığa bağlı olarak zeytin yapraklarında stoma boyutlarının küçüldüğünü bildirmişlerdir. Bu çalışmada saptamış olduğumuz Gemlik zeytin çeşidinde stoma boyutlarının, sulama aralığının artışıyla bağlantılı olarak azaldığı bulgusu; farklı zeytin çeşitlerinde kuraklığın etkisiyle stoma boyutlarının azaldığına ilişkin sonuçlara ulaşan literatürdeki çalışmalarla paralellik göstermektedir.

**Tablo 3.** Farklı sulama aralıkları ve yaprakların sürgün üzerindeki konumunun Gemlik zeytin çeşidinin yapraklarında stoma boyutlarına etkileri

| Sulama Aralığı | Stoma Eni (µm) | | | | Stoma Boyu (µm) | | | |
|---|---|---|---|---|---|---|---|---|
| | Uç | Orta | Alt | Ortalama | Uç | Orta | Alt | Ortalama |
| Kontrol | 8,93 öd | 9,64 | 9,66 | 9,41 D** | 16,50 öd | 17,62 | 17,75 | 17,29 BC** |
| 7 Gün | 9,36 | 10,21 | 10,41 | 9,99 CD | 17,62 | 18,49 | 18,31 | 18,14 B |
| 14 Gün | 13,23 | 13,20 | 13,64 | 13,35 A | 18,69 | 20,13 | 20,26 | 19,69 A |
| 21 Gün | 10,85 | 10,52 | 11,03 | 10,80 BC | 16,95 | 17,26 | 18,13 | 17,45 BC |
| 28 Gün | 10,47 | 11,42 | 10,91 | 10,93 B | 16,63 | 18,46 | 18,21 | 17,77 BC |
| 35 Gün | 9,69 | 10,55 | 10,34 | 10,19 BCD | 16,59 | 17,37 | 17,22 | 17,06 C |
| **Ortalama** | 10,42 B* | 10,92 AB | 10,99 A | | 17,16 B** | 18,22 A | 18,31 A | |

öd: p≥0.05, *p≤ 0.05, **p≤ 0.01

Stoma şekil katsayısı (SŞK); stoma eninin boyuna oranını ifade eden bir değişkendir [23]. Stoma şekil katsayısının artışı; stoma porlarının açıklığının arttığına işaret etmektedir. Nazarian [56] da bu duruma dikkat çekmiş ve tuzluluk stresinin artışına bağlı olarak, kanola bitkisinin yapraklarında SŞK'nın azaldığını bildirmiştir. Gemlik zeytin çeşidinde, sulama aralığı x yaprak konumu interaksiyonunda yer alan gruplar arasında bu özellik bakımından istatistiki olarak anlamlı bir farklılık saptanmamıştır (Tablo 4). Yaprakların sürgün üzerindeki konumları da SŞK üzerinde etkili bulunmamıştır. Sulama aralıklarının etkisi ise istatistiksel olarak anlamlı (p≤0.01) bulunmuştur. En yüksek SŞK (67,78) 14 gün aralıkla sulanan grupta, en düşük SŞK (54,40) ise kontrol grubunda saptanmıştır. 21, 28 ve 35 gün aralıkla sulanan ağaçların SŞK birbirine benzer bulunmuştur.

Stoma boyutlarına ilişkin elde ettiğimiz bulgulara paralel olarak; sulama aralığının artışı, genel olarak (7 gün grubu dışında) stoma alanında küçülmeye neden olmuştur (Tablo 4). Kısa süreli stres koşullarında, bitkilerin stoma porlarını (kısmen veya tamamen) kapatması su kaybını sınırlandırmaktaysa da stres etmeninin ortadan kalkmaması nedeniyle strese maruz kalma süresi arttıkça bu düzenleme yeterli olmamaktadır. Kökleri vasıtasıyla, su ihtiyacını yeteri kadar karşılayamayan bitkilerin; stomadial transpirasyonla kaybettikleri su miktarını azaltmak ve bu sayede ozmotik regülasyonu sağlamak için anatomik yapılarında gerçekleştirdikleri değişimlerden biri de stoma alanını küçültmektir. Elde ettiğimiz bulgular; 14 gün aralıkla sulanan ağaçlarda, kuraklığın neden olduğu stresin görülmediğine işaret etmektedir. Ayrıca, yaprak konumunun da stoma alanı üzerinde etkili olduğu belirlenmiştir. Sürgünlerin uçlarında yer alan yaprakların, orta ve alt kısımlarda yer alan yapraklara göre daha düşük stoma alanına sahip olduğu saptanmıştır.

**Tablo 4.** Farklı sulama aralıkları ve yaprakların sürgün üzerindeki konumunun Gemlik zeytin çeşidinin yapraklarında stoma şekil katsayısına ve stoma alanına etkileri

| Sulama Aralığı | Stoma Şekil Katsayısı | | | | Stoma Alanı (µm$^2$) | | | |
|---|---|---|---|---|---|---|---|---|
| | Uç | Orta | Alt | Ortalama | Uç | Orta | Alt | Ortalama |
| Kontrol | 54,08 öd | 54,69 | 54,44 | 54,40 C** | 115,9 öd | 133,7 | 134,8 | 128,1 C** |
| 7 Gün | 53,11 | 55,34 | 56,81 | 55,09 C | 129,8 | 148,6 | 150,2 | 142,9 BC |
| 14 Gün | 70,73 | 65,43 | 67,19 | 67,78 A | 196,9 | 209,7 | 218,4 | 208,3 A |
| 21 Gün | 64,09 | 61,14 | 60,84 | 62,03 B | 144,7 | 142,8 | 157,2 | 148,3 BC |
| 28 Gün | 62,46 | 61,70 | 59,74 | 61,30 B | 138,4 | 166,7 | 156,7 | 154,0 B |
| 35 Gün | 58,56 | 60,78 | 60,04 | 59,79 B | 126,4 | 144,0 | 140,2 | 136,9 BC |
| **Ortalama** | 60,51 ÖD | 59,85 | 59,84 | | 142,0 B** | 157,6 A | 159,6 A | |

ÖD ve öd: p≥0.05, **p≤ 0.01

Potansiyel iletkenlik indeksi (Pİİ), yalnızca stoma porlarının açıklıklarına bağlı olmayıp aynı zamanda stoma yoğunluğuyla da ilişkili bir parametredir [23]. Genel olarak bitkilerde kuraklık, fizyolojik kuraklık ya da ağır metal stresi altında Pİİ azalmaktadır [22; 56-57]. Bu çalışmada incelediğimiz farklı sulama aralıklarının, Gemlik zeytin çeşidinde Pİİ üzerine etkisi istatistiki olarak önemli bulunmuştur (Tablo 5). Bununla birlikte 14 gün aralıkla sulanan ağaçlarda Pİİ'nin, incelenen diğer gruplara nazaran yüksek bulunmuş olması; en uygun sulama aralığının 14 gün olduğu değerlendirmesini desteklemektedir. Yaprak konumunun da Pİİ üzerine etkili olduğu ve sürgünlerin ucunda yer alan yapraklarda su kaybını önlemek amacıyla fenotipik bir düzenleme gerçekleştiği saptanmıştır. Yaprak konumu x sulama aralığı interaksiyonunda yer alan gruplar arasında ise bu özellik bakımından istatistiki olarak anlamlı bir farklılık olmadığı belirlenmiştir.

Yapraklarda belirli bir görüş alanında stomaların kapladığı alanın yüzde olarak ifadesini belirten oransal stoma alanı (OSA); yaprakların sürgün üzerindeki konumuna göre farklılık göstermektedir. Elde ettiğimiz bulgulara göre sürgünlerin ucunda yer alan yapraklarda OSA, sürgünlerin ortasında ve dip kısmında yer alan yapraklara göre daha düşük bulunmuştur (Tablo 5). Ceulemans ve ark. [58], iki farklı *Populus* klonunda yürüttükleri çalışmada; yaprak konumunun stoma indeksi (Sİ) üzerinde etkili olduğunu ve bitkinin üst kısımlarında konumlanan genç yaprakların, bitkinin orta ve alt bölümlerinde konumlanan olgun yapraklara göre daha düşük stoma indeksine sahip olduğunu bildirmişlerdir. OSA ve Sİ iki farklı parametre olmasına karşılık bu iki özellik birbirini destekleyecek bir değerlendirmeye işaret etmektedirler. Nitekim genç yapraklarda daha düşük Sİ ve OSA bulunması; yapraklar büyüdükçe stomalarının büyüdüğünü ancak bu büyümenin epidermis hücrelerine kıyasla fazla olduğuna işaret etmektedir. Ayrıca Sİ'nin bitki türüne göre değişim gösterdiğini bildiren Paul ve ark. [59]'nın bulguları; OSA 'nın da bitki türüne göre değişim gösterebileceğine işaret etmektedir. Nitekim Palliotti ve ark. [2] Sangiovese üzüm çeşidinde bu oranın, kuraklık uygulamalarına bağlı olarak 2,59-3,11 arasında, Odabasioglu ve Gursoz [23] ise farklı üzüm çeşitlerinde

5,4-7,5 arasında değişim gösterdiğini bildirmiştir. Bununla birlikte sulama aralıklarına bağlı olarak, OSA ilişkin saptamış olduğumuz değişim; yalnızca stoma porlarının açıklığı ile ilişkili olmayıp aynı zamanda stoma yoğunluğu ve stoma boyuyla da bağlantılıdır. İncelenen zeytin ağaçlarında, kuraklık stresine karşı erken gelişme döneminde oluşturulan ve süreklilik gösteren, su kaybı sınırlaması mekanizmasının bir parçası olarak OSA'da azalma görülmüştür.

**Tablo 5.** Farklı sulama aralıkları ve yaprakların sürgün üzerindeki konumunun Gemlik zeytin çeşidinin yapraklarında potansiyel iletkenlik indeksine ve oransal stoma alanına etkileri

| Sulama Aralığı | Potansiyel İletkenlik İndeksi | | | | Oransal Stoma Alanı (%) | | | |
|---|---|---|---|---|---|---|---|---|
| | Uç | Orta | Alt | Ortalama | Uç | Orta | Alt | Ortalama |
| Kontrol | 10,53 öd | 12,58 | 13,15 | 12,09 B** | 4,46 öd | 5,40 | 5,62 | 5,16 B** |
| 7 Gün | 11,14 | 12,38 | 12,80 | 12,11 B | 4,66 | 5,37 | 5,77 | 5,26 B |
| 14 Gün | 13,36 | 14,34 | 15,73 | 14,48 A | 7,43 | 7,39 | 8,32 | 7,71 A |
| 21 Gün | 10,73 | 10,78 | 13,08 | 11,53 B | 5,38 | 5,16 | 6,26 | 5,60 B |
| 28 Gün | 10,30 | 12,10 | 12,23 | 11,54 B | 5,08 | 5,87 | 5,78 | 5,57 B |
| 35 Gün | 11,01 | 13,70 | 11,71 | 12,14 B | 5,03 | 6,54 | 5,52 | 5,70 B |
| **Ortalama** | 11,18 B** | 12,65 A | 13,12 A | | 5,34 B** | 5,96 A | 6,21 A | |

öd: p≥0.05, **p≤ 0.01

Farklı sulama aralığı ve yaprakların sürgün üzerindeki konumlarına bağlı olarak incelenen örneklerde, stoma eni ile stoma boyu arasında kuvvetli ($R^2$=0,60 p≤0.01) bir ilişkinin olduğu saptanmıştır (Şekil 3). Stomaların boyunun artışına bağlı olarak stoma enleri de büyümüştür. Potansiyel iletkenlik indeksi ise hem stoma eninin ($R^2$=0,35 p≤0.01) hem de oransal stoma alanının ($R^2$=0,84 p≤0.01) artışına bağlı olarak artış göstermiştir. Stoma alanı ile stoma şekil katsayısı arasında da benzer bir ilişki saptanmıştır.

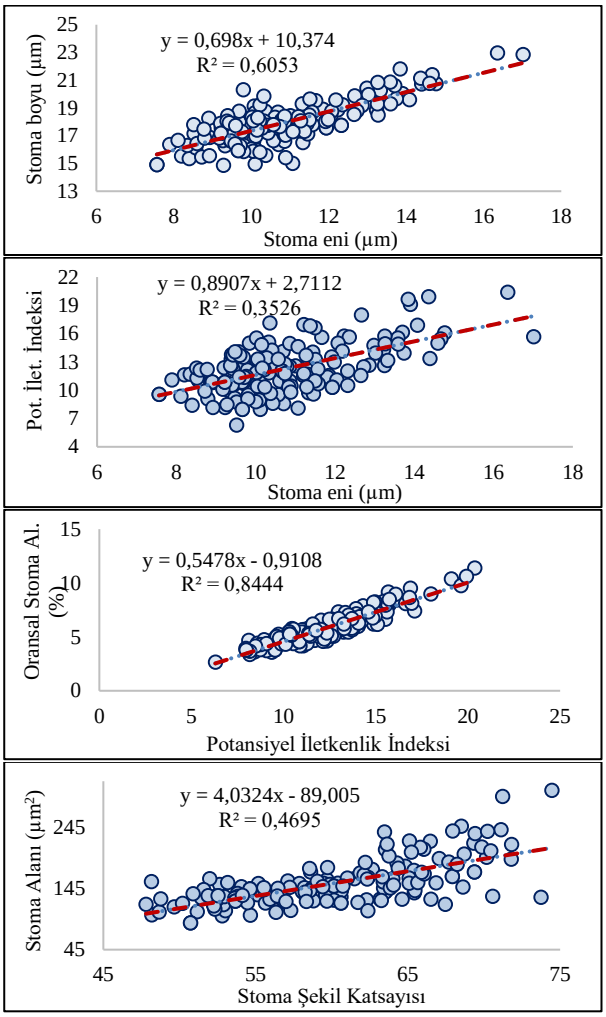


**Şekil 3.** Farklı sulama aralıkları ve yaprakların sürgün üzerindeki konumlarına bağlı olarak örneklenen Gemlik zeytin çeşidi yapraklarında bazı stoma özelliklerinin birbirleriyle ilişkisi

Genel olarak stoma özelliklerinin birbirleriyle ilişkileri incelendiğinde; stoma yoğunluğu ile stoma boyutları (en-boy) ve SŞK, SA arasında bir ilişkinin varlığından söz etmek mümkün değildir. Buna karşın; Pİİ ve OSA gibi stoma yoğunluğuna bağlı değişkenler üzerindeki etkisi istatistiki olarak anlamlı bulunmuştur (Tablo 6). Çalışmada incelenen diğer stoma özelliklerinin ise birbirleriyle ilişkileri p≤0.01 düzeyinde anlamlı bulunmuştur. Sevik ve ark. [60]'nın farklı türler üzerinde yürüttüğü çalışmada, stoma yoğunluğunun stoma boyutları ile ilişkili olmadığı saptanmıştır. Buna karşın, Yiğit ve ark. [61] *Aesculus hippocastanum* türünün yapraklarında stoma boyu ile stoma eni arasında güçlü bir ilişkinin varlığını saptamışlardır. Mert ve ark. [62] ise elma çeşitlerinde, stoma yoğunluğu ile stoma boyutları arasında negatif ilişki olduğunu ancak bu ilişkinin istatistiksel olarak önemsiz bulunduğunu bildirmişlerdir. Literatürde yer alan çalışmalar ve yürütmüş olduğumuz bu çalışmadan elde edilen bulgular birlikte değerlendirildiğinde; stoma boyutları ile stoma yoğunluğu arasındaki ilişkinin türlere bağlı olarak değişim gösterebileceği kanaatine varılmıştır.

**Tablo 6.** Gemlik zeytin çeşidi yapraklarında bazı stoma özelliklerinin birbirleriyle ilişkisi

| | SE | SB | SŞK | SA | Pİİ | OSA |
|---|---|---|---|---|---|---|
| **SY** | öd | öd | öd | öd | ** | ** |
| **SE** | | ** | ** | ** | ** | ** |
| **SB** | | | ** | ** | ** | ** |
| **SŞK** | | | | ** | ** | ** |
| **SA** | | | | | ** | ** |
| **Pİİ** | | | | | | ** |

öd: p≥0.05, **p≤ 0.01

## 4. SONUÇ

Bitkilerde stoma özellikleri birçok etkene bağlı olarak değişim gösterebilmektedir. Genotipin bu özellikler üzerindeki etkisi, diğer faktörlere kıyasla oldukça fazladır. Bu faktörlerden biri olan sulamanın etkisi, önceki çalışmalarda sulama düzeyi üzerinden değerlendirilmiş ancak sulama aralığının etkisi bu çalışmada daha detaylı incelenerek farklılıklar ortaya konmaya çalışılmıştır. Gemlik zeytin çeşidi ağaçlarında elde ettiğimiz bulgular; sulama aralığının, yaprakların stoma plastisitesi üzerindeki etkisinin önemli olduğunu göstermektedir. 14 gün aralıkla sulamanın, bitki fizyolojisinde kuraklık stresinin neden olduğu etkilerin

daha az görülmesine bu sayede anatomik yapıda da morfolojik olarak bu etkinin gözlemlenebildiğine işaret etmektedir. Bununla birlikte inceleme yapılan yaprakların bitki veya sürgün üzerindeki konumunun da stoma morfolojisi üzerinde etkili olduğu saptanmıştır. Hem yaprak gelişimine hem de yaprakların konumu nedeniyle çevresel strese maruz kalma düzeylerinin farklılığına bağlı olarak, stomalarda yüksek plastisite görüldüğü kanaatine varılmıştır. Bu alanda yapılacak yeni çalışmalarda farklı bitki türlerinin incelenmesi, elde ettiğimiz bulguların belirli bir tür veya çeşitle sınırlı kalıp kalmadığının anlaşılması açısından önemlidir.

## KAYNAKLAR


[1] Tobiessen P, Kana, TM. Drought-Stress Avoidance in Three Pioneer Tree Species. Ecology. 1974;55(3):667-670.

[2] Palliotti A, Silvestroni O, Petoumenou D, Vignaroli S, Berrios JG. Evaluation of Low-Energy Demand Adaptative Mechanisms in Sangiovese Grapevine During Drought. J. Int. Sci. Vigne Vin. 2008;42(1):41-47.

[3] Shekari F, Soltaniband V, Javanmard A, Abbasi A. The Impact of Drought Stress at Different Stages of Development on Water Relations, Stomatal Density and Quality Changes of Rapeseed (*Brassica napus* L.). Iran Agricultural Research. 2015;34(2):81-90.

[4] Wang SG, Jia SS, Sun DZ, Hua FAN, Chang XP, Jing RL. Mapping QTLs for Stomatal Density and Size under Drought Stress in Wheat (*Triticum aestivum* L.). Journal of Integrative Agriculture. 2016;15(9):1955-1967.

[5] Gülen H, Köksal N, Eriş A. Farklı Anaçlar Üzerine Aşılı Bazı Kiraz ve Elma Çeşitlerinde Stoma Yoğunluğu ve Stoma Boyutları. Bahçe. 2004;33(1-2):1-5.

[6] Gokbayrak Z, Dardeniz A, Bal M. Stomatal Density Adaptation of Grapevine to Windy Conditions. Trakia Journal of Sciences. 2008;6(1):18-22.

[7] Cárcamo HJ, Bustos MR, Fernández FE, Bastías EI. Mitigating effect of salicylic acid in the anatomy of the leaf of *Zea mays* L. lluteno ecotype from the Lluta Valley (Arica-Chile) under NaCl stress. Idesia. 2012;30(3):55-63.

[8] Babosha AV, Kumachova TK, Ryabchenko AS, Komarova GI. Stomata Polymorphism in Leaves of Apple Trees (*Malus domestica* Borkh.) Growing under Mountain and Plain Conditions. Biology Bulletin. 2020;47(4):352-363.

[9] Zhang S, Li J, Shen Y, Korkor LN, Pu Q, Lu J, et al. Physiological Responses of Dendrobium officinale under Exposure to Cold Stress with Two Cultivars. Phyton. 2020;89(3):599-617.

[10] Buckley CR, Caine RS, Gray JE. Pores for Thought: Can Genetic Manipulation of Stomatal Density Protect Future Rice Yields?. Frontiers in Plant Science. 2020;10: e1783.

[11] Green RL, Beard JB, Casnoff DM. Leaf Blade Stomatal Characterizations and Evapotranspiration Rates of 12 Cool-Season Perennial Grasses. HortScience. 1990;25(7):760-761.

[12] Shiraishi SI, Hsiung TC, Shiraishi M. Preliminary Survey on Stomatal Density and Lenght of Grapevine. Journal Faculty of Agriculture Kyushu University. 1996;41(1-2):11-15.

[13] Liao JX, Chang J, Wang GX. Stomatal Density and Gas Exchange in Six Wheat Cultivars. Cereal Research Communications. 2005;33(4):719-726.

[14] Rahemi M, Yazdani F, Sedaghat S. Evaluation of Freezing Tolerance in Olive Cultivars by Stomatal Density and Freezing Stress. International Journal of Horticultural Science and Technology. 2016;3(2):145-153.

[15] Çağlar S, Sütyemez M, Bayazit S. Seçilmiş Bazı Ceviz (*Juglans regia*) Tiplerinin Stoma Yoğunlukları. Akdeniz Üniversitesi Ziraat Fakültesi Dergisi. 2004;17(2):169-174.

[16] Beerling DJ, Chaloner WG. Stomatal Density Responses of Egyptian Olea europaea L. Leaves to CO2 Change Since 1327 BC. Annals of Botany. 1993;71(5):431-435.

[17] Yener SH. Türkiye'nin Değişik Yörelerinde Yetişen Zeytin Ağaçları Üzerinde Morfolojik ve Anatomik Araştırmalar. İstanbul: Marmara Üniversitesi; 1994.

[18] Ataol Ölmez H. Malatya Yöresinde Yetiştirilen Bazı Kayısı Çeşitlerinde Stomalar Üzerinde Araştırmalar. Şanlıurfa: Harran Üniversitesi; 1997.

[19] Topsakal B. Bazı Pistacia Türlerinin Yaprak Yapılarının ve Stoma Özelliklerinin Belirlenmesi. Şanlıurfa: Harran Üniversitesi; 2017.

[20] Reich PB. Leaf Stomatal Density and Diffusive Conductance in Three Amphistomatous Hybrid Poplar Cultivars. New phytologist. (1984);98(2):231-239.

[21] Bekişli Mİ. Harran Ovası Koşullarında Yetiştirilen Bazı Asma Çeşitleri ile Amerikan Asma Anaçlarının Yaprak ve Stoma Özelliklerinin Belirlenmesi. Şanlıurfa: Harran Üniversitesi; 2014.

[22] Orcen N, Nazarian G, Gharibkhani M. The Responses of Stomatal Parameters and SPAD Value in Asian Tobacco Exposed to Chromium. Polish Journal of Environmental Studies. 2013;22(5):1441-1447.

[23] Odabasioglu Mİ, Gursoz S. Leaf and Stomatal Characteristics of Grape Varieties (*Vitis vinifera* L.) Cultivated under Semi-Arid Climate Conditions. Fresenius Environmental Bulletin. 2019;28(11A):8501-8510.

[24] Gindel I. Stomatal Number and Size as Related to Soil Moisture in Tree Xerophytes in Israel. Ecology. 1969;50(2):263-267.

[25] Marasalı B, Aktekin A. Sulanan ve Sulanmayan Bağ Koşullarında Yetiştirilen Üzüm Çeşitlerinde Stoma Sayısının Karşılaştırılması. Tarım Bilimleri Dergisi. 2003;9(3):370-372.

[26] Pekmezci A, Dardeniz A. Yalova Çekirdeksizi Üzüm Çeşidinde Ben Düşme Döneminden İtibaren Yapılan Farklı Düzeylerdeki Sulama Uygulamalarının Çeşidin Stoma Özellikleri Üzerine Etkileri. ÇOMÜ Ziraat Fakültesi Dergisi. 2018;6(2):7-11.

[27] Gomez del Campo M, Ruiz C, Baeza P, Lissarrague JR. Drought Adaptation Strategies of Four Grapevine Cultivars (*Vitis vinifera* L.): Modification

of the Properties of the Leaf Area. J. Int. Sci. Vigne Vin. 2003;37:131-143.

[28] Candar S, Açıkbaş B, Korkutal İ, Bahar E. Trakya Bölgesi Şaraplık Üzüm Çeşitlerinde Kısıntılı Sulama Uygulamalarının Yaprak ve Stoma Morfolojik Özelliklerine Etkileri. Kahramanmaraş Sütçü İmam Üniversitesi Tarım ve Doğa Dergisi. 2021;24(4):766-776.

[29] Çalışkan T, Aydın A, Ortaş İ, Sezen M, Eken M. Kısıtlı Su ve Mikoriza Uygulamalarının Genç Kütdiken Limonunun Gelişimi Üzerine Etkileri. Alatarım. 2017;16(2):28-36.

[30] Çınar N, Aydinşakir K, Dinç N, Büyüktaş D, Işık M. Yerfıstığında (*Arachis hypogaea* L.) Su Stresinin Stoma Özellikleri Üzerine Etkisi. Mediterranean Agricultural Sciences. 2016;29(2):79-84.

[31] Bosabalidis AM, Kofidis G. Comparative Effects of Drought Stress on Leaf Anatomy of Two Olive Cultivars. Plant Science. 2002;163(2):375-379.

[32] Guerfel M, Baccouri O, Boujnah D, Chaïbi W, Zarrouk M. Impacts of Water Stress on Gas Exchange, Water Relations, Chlorophyll Content and Leaf Structure in the Two Main Tunisian Olive (*Olea europaea* L.) Cultivars. Scientia Horticulturae. 2009;119(3):257-263.

[33] Öncü B. Kısıntılı Sulama Koşullarında Yetiştirilen Gemlik Zeytin Fidanlarının Agronomik ve Fizyolojik Özellikleri ile Yüksek Sıcaklık Toleranslarının Belirlenmesi. Bursa: Bursa Uludağ Üniversitesi; 2021.

[34] Al-Naqeeb DAK. İzmir Koşullarında Sulanan ve Sulanmayan Bazı Zeytin Çeşitlerinin Yapraklarındaki Morfolojik ve Anatomik Farklılıkların Belirlenmesi. Ankara: Ankara Üniversitesi; 2020.

[35] Güler Z. Bazı Zeytin Çeşitlerinde Su Noksanlığı Stresinde Morfolojik-Anatomik, Fizyolojik ve Gen İfadesi Değişimlerin Belirlenmesi. Ankara: Ankara Üniversitesi; 2018.

[36] Roro AG, Tesfaye M. Morpho-physiological and Yield Responses of Sweet Potato (*Ipomoea batatas* (L.) Lam.) Genotypes to Frequency of Irrigation under Greenhouse Condition. International Journal of Plant & Soil Science. 2019;29(5):1-17.

[37] Buttery BR, Tan CS, Buzzell RI, Gaynor JD, MacTavish DC. Stomatal Numbers of Soybean and Response to Water Stress. Plant and Soil. 1993;149(2):283-288.

[38] Richardson AD, Berlyn GP, Ashton PM, Thadani R, Cameron IR. Foliar Plasticity of Hybrid Spruce in Relation to Crown Position and Stand Age. Canadian Journal of Botany. 2000;78(3):305-317.

[39] Klamkowski K, Treder W. Morphological and Physiological Responses of Strawberry Plants to Water Stress. Agriculturae Conspectus Scientificus. 2006;71(4):159-165.

[40] Sun Y, Yan F, Cui X, Liu F. Plasticity in Stomatal Size and Density of Potato Leaves Under Different Irrigation and Phosphorus Regimes. Journal of Plant Physiology. 2014;171(14):1248-1255.

[41] Küçükyumuk C, Sarısu H, Yıldız H, Kaçal E, Koçal H. Farklı Anaçlar Üzerine Aşılı 0900 Ziraat Kiraz Çeşidinde Su Stresinin Bazı Vejetatif Gelişim Parametrelerine Etkisi. Yüzüncü Yıl Üniversitesi Tarım Bilimleri Dergisi. 2015;25(2):180-192.

[42] Carignato A, Vázquez-Piqué J, Tapias R, Ruiz F, Fernández M. Variability and Plasticity in Cuticular Transpiration and Leaf Permeability Allow Differentiation of *Eucalyptus* Clones at an Early Age. Forests. 2020;11(1):9.

[43] Carlson JJR, Ditterline RL, Martin JM, Lund RE. Sampling Stomatal Density in Alfalfa. Crop Science. 1981;21(3):467-469.

[44] Sandanam S, Gee GW, Mapa RB. Leaf Water Diffusion Resistance in Clonal Tea (*Camellia sinensis* L.): Effects of Water Stress, Leaf Age and Clones. Annals of Botany. 1981;47(3):339-349.

[45] Xie S, Luo X. Effect of Leaf Position and Age on Anatomical Structure, Photosynthesis, Stomatal Conductance and Transpiration of Asian Pear. Botanical Bulletin of Academia Sinica. 2003;44:297-303.

[46] Adebooye OC, Hunsche M, Noga G, Lankes C. Morphology and Density of Trichomes and Stomata of *Trichosanthes cucumerina* (Cucurbitaceae) as Affected by Leaf Age and Salinity. Turkish Journal of Botany. 2012;36(4):328-335.

[47] Shabala L, Mackay A, Tian Y, Jacobsen SE, Zhou D, Shabala S. Oxidative Stress Protection and Stomatal Patterning as Components of Salinity Tolerance Mechanism in Quinoa (*Chenopodium quinoa*). Physiologia Plantarum. 2012;146(1):26-38.

[48] Rogiers SY, Hardie WJ, Smith JP. Stomatal Density of Grapevine Leaves (*Vitis vinifera* L.) Responds to Soil Tempera-ture and Atmospheric Carbon Dioxide. Australian Journal of Grape and Wine Research. 2011;17:147-152.

[49] Tetik Ç, Dardeniz A. Sofralık Üzüm Çeşitlerinde Farklı Boğumlardaki Yaprakların Farklı Dönemlerdeki Stoma Yoğunluk ve Büyüklüklerinin Belirlenmesi. ÇOMÜ Ziraat Fakültesi Dergisi. 2016;4(2):125-138.

[50] Yıldırım E, Dardeniz A. Farklı Anaçların 'Red Globe' Üzüm Çeşidinde Tüplü (Kaplı) Fidanların Stoma Özellikleri Üzerine Etkileri. ÇOMÜ Ziraat Fakültesi Dergisi. 2017;5(1):125-130.

[51] Sürücü Z. Kirazda Farklı Dal Tiplerinde Meyve Tutumu ile Bazı Meyve Ve Yaprak Özelliklerinin İncelenmesi. Şanlıurfa: Harran Üniversitesi; 2019.

[52] Cirillo C, De Micco V, Rouphael Y, Balzano A, Caputo R, De Pascale S. Morpho-Anatomical and Physiological Traits of Two Bougainvillea Genotypes Trained to Two Shapes Under Deficit Irrigation. Trees. 2017;31(1):173-187.

[53] Lei ZY, Han JM, Yi XP, Zhang WF, Zhang YL. Coordinated Variation Between Veins and Stomata in Cotton and Its Relationship with Water-Use Efficiency under Drought Stress. Photosynthetica. 2018;56(4):1326-1335.

[54] Özyurt İK, Akça Y. Mahlep Anaçlarında Kuraklık Stresinin Stoma ve Diğer Morfolojik Özellikler Üzerine Etkilerinin Belirlenmesi. Gaziosmanpaşa Üniversitesi Ziraat Fakültesi Dergisi. 2017;34(Ek Sayı):34-40.

[55] Mouna AM, Sahli A, Naziha G, Badii G, Ibtissem L. Growth, Yield Responses and Water Relations of

Different Varieties (*Olea europaea* L.) Cultivated Under Two Water Conditions in Semi-Arid Conditions of Tunisia. European Scientific Journal. 2014;10(15):468-489.

[56] Nazarian GR. Tuzluluk Stresinde Kanola Bitkisinin Morfolojik ve Fizyolojik Özellikleri Üzerine Salisilik Asidin Priming Uygulamasının Etkisi. İzmir: Ege Üniversitesi; 2016.

[57] Odabaşıoğlu, Mİ. Semi-Arid Koşullarda Farklı Anaçlar Üzerinde Yetiştirilen Sofralık Üzüm Çeşitlerinin Verim, Kalite ve Çekirdek Özellikleri ile Stoma Morfolojilerinin İncelenmesi. Şanlıurfa: Harran Üniversitesi; 2020.

[58] Ceulemans R, Van Praet L, Jiang XN. Effects of CO2 Enrichment, Leaf Position and Clone on Stomatal Index and Epidermal Cell Density in Poplar (*Populus*). New Phytologist. 1995;131(1):99-107.

[59] Paul V, Sharma L, Pandey R, Meena RC. Measurements of Stomatal Density and Stomatal Index on Leaf/Plant Surfaces. Physiological Techniques to Analyze the Impact of Climate Change on Crop Plants, Division of Plant Physiology, 2017. New Delhi: IARI; 2017. p. 27-30.

[60] Sevik H, Cetin M, Ozel HB, Erbek A, Cetin IZ. The Effect of Climate on Leaf Micromorphological Characteristics in Some Broad-Leaved Species. Environment, Development and Sustainability. 2021;23(4):6395-6407.

[61] Yigit N, Cetin M, Sevik H, Aricak B. Variation of Some Micro-Morphological Characters of Leaves of *Aesculus hippocastanum* Based on Growing Environment. Emergent Life Sciences Research. 2018;4(1):45-52.

[62] Mert C, Barut E, Uysal T. Farklı Anaçlar Üzerine Aşılı Elma Çeşitlerinde Stoma Morfolojilerinin Araştırılması. International Journal of Agricultural and Natural Sciences. 2009; 2(2): 61-64.

Araştırma Makalesi https://doi.org/10.46810/tdfd.1002192 Research Article

Türk Doğa ve Fen Dergisi
Turkish Journal of Nature and Science
www.dergipark.gov.tr/tdfd

# Pentilentetrazol ile Oluşturulan Akut Nöbet Modelinde Diazepamın Nitrik Oksit Sentaz ve Beyin Kaynaklı Nörotrofik Faktör Üzerine Etkisinin Araştırılması

**Bilal ŞAHİN[1*], Handan GÜNEŞ[1]**

[1] Sivas Cumhuriyet Üniversitesi, Tıp Fakültesi, Fizyoloji Bölümü, Sivas, Türkiye
Bilal ŞAHİN ORCID No: 0000-0002-4419-1385
Handan GÜNEŞ ORCID No: 0000-0003-3660-8264

**Sorumlu yazar: bilalsahin@cumhuriyet.edu.tr*

(Alınış: 29.09.2021, Kabul: 29.04.2022, Online Yayınlanma: 29.06.2022)

**Anahtar Kelimeler**
Nöbet,
Pentilentetrazol
Diazepam,
Nitrik Oksit
Sentaz,
Beyin Kaynaklı
Nörotrofik Faktör

**Öz:** Bu çalışmanın amacı, sıçanlarda pentilentetrazol (PTZ) ile oluşturulan nöbetlerde diazepamın antikonvülzan etkinliğinde nitrik oksit sentaz (NOS) ve beyin kaynaklı nörotrofik faktör (BDNF) üzerine etkisini araştırmaktır. Çalışmada 24 adet erkek Wistar Albino sıçan kullanılmıştır. Sıçanlar kontrol grubu, salin (1 mL $kg^{-1}$) +PTZ, diazepam (0,5 mg $kg^{-1}$)+PTZ ve diazepam (2 mg $kg^{-1}$)+PTZ grubu olarak 4 gruba ayrılmıştır (n=6). İntraperitoneal ilaç uygulamalarından 24 saat sonra biyokimyasal incelemeler için tüm sıçanların beyin dokuları çıkarılıp, korteks ve hipokampüs bölgeleri ayrılmıştır. Korteks ve hipokampüsteki NOS ve BDNF düzeyleri enzim bağlı immünosorbent analizi (ELISA) kitleri kullanılarak ölçülmüştür. Diazepam, salin+PTZ uygulanan grubuna göre istatistiksel açıdan anlamlı bir şekilde nöbet evresini azalttı ve ilk miyoklonik jerk (İMJ) süresini uzattı ($p<0.001$). Salin+PTZ, kontrol grubuna kıyasla hipokampüste NOS seviyelerini anlamlı olarak azalttı ($p<0.05$). Bununla birlikte diazepam+PTZ grupları, salin+PTZ grubuyla karşılaştırıldığında hipokampal NOS seviyesini anlamlı olarak artırdı ($p<0.001$). Ayrıca, salin+PTZ grubu kontrolle karşılaştırıldığında korteks ve hipokampüste BDNF seviyesini artırırken ($p<0.05$), diazepam+PTZ uygulanan gruplarda BDNF seviyesi salin+PTZ grubuna kıyasla düşüktü ($p<0.001$). Diazepam hipokampüste NOS seviyesini artırmış, korteks ve hipokampüste ise BDNF seviyelerini düşürmüştür. Sonuç olarak, diazepamın NOS ve BDNF üzerine düzenleyici etkisi antikonvülzan etkisiyle ilişkili olabilir.



# Investigation of the Effect of Diazepam on Nitric Oxide Synthase and Brain-Derived Neurotrophic Factor in Pentylenetetrazole-Induced Acute Seizure Model

**Keywords**
Seizure,
Pentylentetrazole
Diazepam,
Nitric Oxide
Syntase,
Brain Derived
Neurotrophic
Factor

**Abstract:** The aim of this study was to investigate the effect of diazepam on nitric oxide synthase (NOS) and brain-derived neurotrophic factor (BDNF) in the anti-convulsant activity of diazepam on pentylenetetrazole (PTZ) induced seizures in rats. 24 male Wistar Albino rats were used in the study. Rats were divided into 4 groups as control group, saline (1 mL $kg^{-1}$) +PTZ, diazepam (0.5 mg $kg^{-1}$) +PTZ and diazepam (2 mg $kg^{-1}$) +PTZ group (n=6). For biochemical studies, 24 hours after PTZ application, brain tissues of all rats were removed and cortex and hippocampus regions were isolated NOS and BDNF levels in the cortex and hippocampus were measured using ELISA kits. Diazepam significantly decreased the seizure stage and prolonged the first myoclonic jerk (IMJ) time compared to the saline group ($p<0.001$). Saline+PTZ significantly decreased NOS levels in the hippocampus when compared to the control group ($p<0.05$). However, the diazepam+PTZ groups significantly increased the hippocampal NOS level compared to the saline+PTZ group ($p<0.001$). In addition, the saline + PTZ group increased the BDNF level in the cortex and hippocampus compared to the control ($p<0.05$), while the BDNF level was lower in the diazepam+PTZ group compared to the saline+PTZ group ($p<0.001$). Diazepam increased NOS levels in the hippocampus and decreased BDNF levels in the cortex and hippocampus. In conclusion, the regulatory effect of diazepam on NOS and BDNF may be related to its anti-convulsant mechanisms.

## 1. GİRİŞ

Nöbet, merkezi sinir sisteminde belirli bir işlevi olan nöron topluluğunun ani, anormal ve hipersenkron deşarjları sonucu ortaya çıkmaktadır [1]. Nöbet oluşumu motor aktivitede, davranışlarda ve bilinç düzeyinde değişimlere yol açabilmektedir [2]. Epileptik nöbet için oluşturulan hayvan modelleri, nöbetlerin temel mekanizmalarının anlaşılması için önem arz etmektedir [3].

Pentilentetrazol (PTZ), $GABA_A$ klorür iyonofor kompleksinin seçici bir antagonistidir. PTZ, GABA aracılı transmisyonu bloke ederek nöbet aktivitesini stimüle etmektedir [4]. PTZ ile oluşturulan farklı nöbet modelleri, antiepileptik ilaç geliştirme çalışmalarında sıklıkla kullanılmaktadır [5]. Benzodiazepinler epileptik nöbetlerin tedavisinde kullanılan önemli bir ilaç grubudur [6]. Klasik olarak, benzodiazepinler $GABA_A$ reseptörü/kanalındaki benzodiazepin bağlama bölgesi aracılığıyla etki ederler ve klorür akışının artmasına ve nöronal membran potansiyelinin ve uyarılabilirliğinin (eksitabilite) azalmasına neden olurlar [7]. Benzodiazepinlerin $GABA_A$ reseptörü üzerindeki bağlanma yeri iyi bilinmesine rağmen [8], bu ilaç gruplarının antikonvülzan etki mekanizmaları henüz aydınlatılamamıştır.
Nitrik oksit (NO), bir enzim ailesi olan nitrik oksit sentaz (NOS) tarafından L-arginin'den sentezlenen ve guanilil siklazı güçlü bir şekilde uyaran, ikinci haberci cGMP seviyelerinin artmasına neden olan ve serbest radikale dönüşebilen bir gazdır. NO/cGMP sinyal yolağı, merkezi sinir sisteminde nörotransmitter/nöromodülatör olarak kilit rol oynar [9]. Literatürde, nitrik oksitin nöbetlerin türüne ve ilgili diğer nörotransmitter sistemlerine bağlı olarak antikonvülzan [10,11] ve prokonvülzan [3,12,13] etkilere sahip olduğu gösterilmiştir. Bununla birlikte, benzodiazepinlerin hipnotik [14], antinosiseptif [15] ve antikonvülzan [16] etkilerini NO'i modüle ederek gösterebileceği öngörülmüştür.

Beyin kaynaklı nörotrofik faktör (BDNF), nörotrofin ailesinin bir üyesidir ve nöronal gelişim ve sinaptik plastisitede önemli rol oynamaktadır [17]. Epilepsi ve BDNF arasındaki ilişki üzerine yapılan çalışmalarda, limbik nöbetlere katılan beyin bölgelerinde nöbet sonrası BDNF ekspresyonunun büyük ölçüde arttığı gösterilmiştir [18,19]. Ayrıca, nöbetlerden sonra hipokampal piramidal hücrelerde BDNF artışı tespit edilmiştir [20]. Buna ek olarak, BDNF'nin eksitabiliteyi artırdığı ve epileptogenezde rol oynadığı [21], BDNF sinyal transdüksiyonunun engellenmesinin ise epilepsi odağının gelişmesini inhibe ettiği gösterilmiştir [22].

Diazepamın antikonvülzan etkinliği ve olası mekanizmaları üzerine çeşitli çalışmalar yapılmıştır[23,24]. Fakat PTZ ile oluşturulan nöbet modelinde diazepamın NOS ve BDNF düzenlenmesi üzerine etkileri henüz tam olarak aydınlatılamamıştır. Bu çalışmada amacımız, sıçanlarda PTZ ile oluşturulan nöbet modelinde diazepamın kortikal ve hipokampal NOS ve BDNF üzerine etkisini araştırmaktır.

## 2. MATERYAL VE METOT

### 2.1. Deney Hayvanları

Bu çalışmada erişkin 24 adet erkek Wistar Albino sıçan (220-240 g) kullanıldı. Sıçanlar 22±1 °C oda sıcaklığında 12 saatlik aydınlık/karanlık siklusunun sağlandığı, sesten yalıtılmış odada ve %55±6 oranda nemli ortamda tutuldu ve uygun oranda beslenmeleri sağlandı. Deney uygulaması 09.00-15.00 saatleri arasında gerçekleşti ve deney ortamının ışık ile ses düzeyi sürekli kontrol altında tutuldu. Bu çalışma, Sivas Cumhuriyet Üniversitesi Hayvan Deneyleri Yerel Etik Kurulu Başkanlığının onayı ile yapıldı (Karar No: 65202830-050.04.04-512).

### 2.2. Çalışmada Kullanılan Kimyasallar

Pentilentetrazol ve diazepam (Sigma-Aldrich Co. St Louis, MO, ABD) üretici firmadan temin edildi. Kimyasallar serum fizyolojik (1 ml $kg^{-1}$) içinde çözülerek sıçanlara enjekte edildi.

### 2.3. Deney Protokolü

Çalışmada yer alan 24 sıçan her grupta 6 adet sıçan olacak şekilde rastgele 4 gruba ayrıldı.

Kontrol grubu: Sıçanlara 1 ml $kg^{-1}$ dozda serum fizyolojik (SF) intraperitoneal (i.p) olarak uygulandı.
Salin+PTZ grubu: Sıçanlara PTZ (45 mg $kg^{-1}$, i.p) ile nöbet indüklenmesinden 30 dakika önce 1 ml $kg^{-1}$ dozda serum fizyolojik (SF) intraperitoneal (i.p) olarak uygulandı.
Diazepam (0,5 mg $kg^{-1}$+PTZ grubu: Sıçanlara PTZ (45 mg $kg^{-1}$, i.p) ile nöbet indüklenmesinden 30 dakika önce 0,5 mg $kg^{-1}$ diazepam i.p olarak uygulandı [25].
Diazepam (2 mg $kg^{-1}$) +PTZ grubu: Sıçanlara PTZ (45 mg $kg^{-1}$, i.p) ile nöbet indüklenmesinden 30 dakika önce 2 mg $kg^{-1}$ diazepam i.p olarak uygulandı [25].
Nöbet modeli oluşturmak için sıçanlara önceki çalışmalardan referans alınarak 45 mg $kg^{-1}$ 'lık (1 mL $kg^{-1}$ hacim içerisinde) tek doz PTZ i.p olarak uygulandı [26]. Enjeksiyon sonrası hayvanlar üstü açık şeffaf pleksiglas (50x40x40 cm boyutlarında) kafeslere konuldu ve hayvanların davranışları 30 dakika boyunca gözlemlendi. Nöbet evresi modifiye Racine konvülziyon ölçeğine (RS) göre belirlendi. Nöbet aşamaları RS'a göre şu şekilde tanımlandı: 0=konvülziyon yok; 1=bıyık seğirmesi; 2=daha belirgin seğirme ile motor arrest; 3=miyoklonik seğirmeler; 4=düşme olmaksızın tonik-klonik nöbet; 5=düşme ile tonik-klonik nöbet; 6=vahşi sıçramalar ile tonik-klonik nöbet ve 7=ölümcül nöbet. [26]. Bununla birlikte, sıçanların PTZ sonrası ilk myoklonik jerk (İMJ) süreleri belirlendi (Şekil 1).

### 2.4. NOS ve BDNF Düzeylerinin Ölçümü

Hayvanların beyin dokusu örnekleri (korteks ve hipokampüs bölgesi) soğuk fosfat tamponlu salin (PBS) çözeltisi (pH 7.4) içinde homojenize edildi ve 12000 g'de 10 dakika boyunca 4 °C de santrifüj edildi. Daha sonra süpernatanlar NOS ve BDNF düzeylerinin ölçülmesi için -80 °C saklandı. Beyin süpernatanlarından NOS ve BDNF düzeylerinin belirlenmesinde ELISA ticari kiti (Sunredbio, Çin) kullanıldı. İşlem protokolleri, üreticinin talimatlarına göre yapıldı. Örneklerdeki toplam protein seviyelerini belirlemek için bir Bradford total protein ölçüm kiti (Merck Millipore, Darmstadt, Almanya) kullanıldı [27].

### 2.5. İstatistiksel Değerlendirme

Tüm deneysel sonuçlar ortalama ± ortalamanın standart hatası (SH) olarak ifade edildi. İstatistiksel analiz için SPSS istatistik programı (SPSS 23.0 for windows) kullanıldı. Veriler normal dağılıma uygunluk gösterdiğinden dolayı verilerin gruplar arası karşılaştırılması için varyans analizi (One way ANOVA), gruplar arası farklılığın hangi gruptan kaynaklandığı ise Tukey HSD (post-hoc test) ile tespit edildi. İstatistiksel anlamlılık p<0,05 düzeyinde tanımlandı.

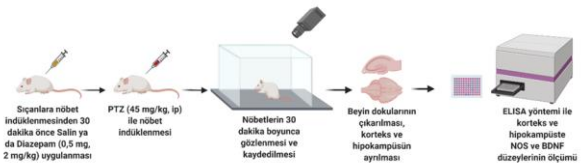


**Şekil 1**. Deney protokolü (BioRender.com lisanslı uygulaması kullanılarak oluşturulmuştur)

## 3. BULGULAR

### 3.1. Diazepamın Nöbet Parametreleri Üzerine Etkisi

Bu çalışmada, nöbet parametreleri, sıçanlara PTZ enjeksiyonundan sonra video kayıtları kullanılarak belirlendi. Şekil 2A'da gösterildiği gibi, diazepam+PTZ gruplarında nöbet evreleri salin+PTZ grubundaki hayvanlara göre anlamlı olarak daha düşük bulundu (p <0.001; Şekil 2A). Ayrıca, İMJ süreleri diazepam uygulanan sıçanlarda salin+PTZ grubuna kıyasla anlamlı olarak daha yüksekti (p<0.001; Şekil 2B).

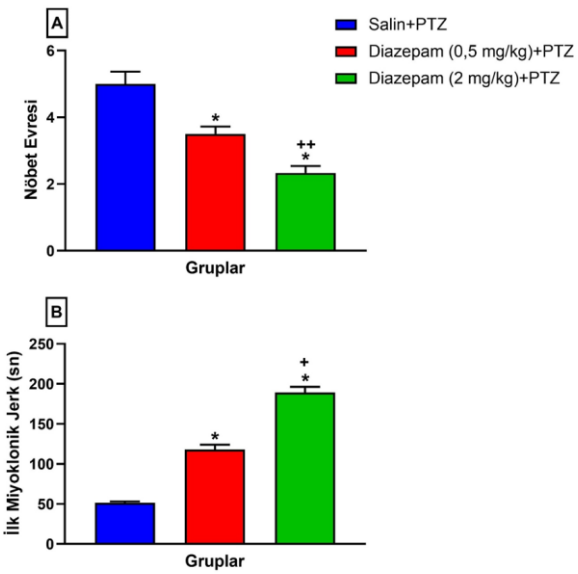


**Şekil 2.** Diazepamın sıçanlarda (n = 6) RS (A) ve İMJ (B) üzerine etkileri. Değerler ortalama ± SH olarak verilmiştir. * p<0.001, salin+PTZ grubu ile karşılaştırıldığında; $^{+}$ p<0.01, $^{++}$ p<0.001 Diazepam (0,5 mg $kg^{-1}$) +PTZ grubu ile karşılaştırıldığında.

### 3.2. Diazepamın Korteks ve Hipokampüste NOS ve BDNF Seviyeleri Üzerine Etkisi

Diazepamın nöbet sonrası kortikal NOS seviyeleri üzerine etkisi incelendiğinde gruplar arasında istatistiksel olarak anlamlı fark bulunmadı (p>0.05; Şekil 3A). Hipokampüste ise salin+PTZ grubunda kontrol grubuna göre NOS seviyeleri azaldı (p<0.001; Şekil 3B). Diazepam+PTZ gruplarında ise salin+PTZ grubuna göre NOS seviyeleri arttı (p<0.001; Şekil 3B).

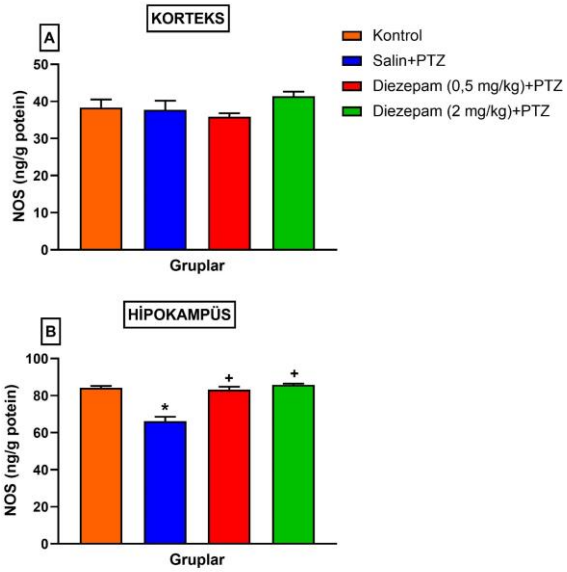


**Şekil 3.** Diazepamın sıçanlarda (n = 6) nöbet sonrası kortikal (A) ve hipokampal (B) NOS seviyeleri üzerine etkileri. Değerler ortalama ± SH olarak verilmiştir. * p<0.001 Kontrol grubu ile karşılaştırıldığında. $^{+}$ p<0.001 salin+PTZ grubu ile karşılaştırıldığında.

PTZ ile nöbet indüklenen grupta kontrol grubuna göre hipokampüs ve kortekste BDNF seviyesinde anlamlı olarak artış görüldü (p<0.001). Diğer yandan, diazepamın farklı dozları PTZ grubuna kıyasla kortekste BDNF seviyesinin düşmesine neden oldu (p<0.001; Şekil 4A). Benzer şekilde diazepamın 0,5 mg $kg^{-1}$ ve 2 mg $kg^{-1}$

dozları hipokampüste BDNF seviyelerini anlamlı olarak azalttığı görüldü ($p<0.01$, $p<0.001$; Şekil 4B).

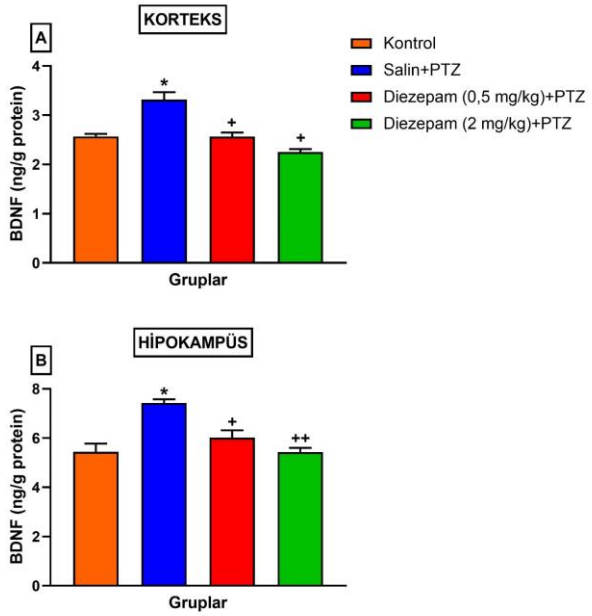


**Şekil 4.** Diazepamın sıçanlarda (n = 6) nöbet sonrası kortikal (A) ve hipokampal (B) BDNF seviyeleri üzerindeki etkileri. Değerler ortalama ± SH olarak verilmiştir. * $p<0.001$ kontrol grubu ile karşılaştırıldığında. $^{+}p<0.01$ ve $^{++}p<0.001$ salin+PTZ grubu ile karşılaştırıldığında.

## 4. TARTIŞMA

Bu çalışmada PTZ ile oluşturulan nöbet modelinde diazepamın korteks ve hipokampüste NOS ve BDNF üzerine etkileri araştırılmıştır. Diazepam nöbet sonrası kortikal NOS düzeylerine etki etmezken, hipokampal NOS seviyesini düşürmüştür. Buna ek olarak, diazepam uygulaması nöbet sonrası korteks ve hipokampüste artış gösteren BNDF seviyelerini düşürmüştür.

Sıçanlarda PTZ ile oluşturulan deneysel nöbet modellerinde PTZ'nin 45 mg $kg^{-1}$ akut enjeksiyonu miyoklonik jerk, klonus ve tonik-klonik kasılmalara neden olarak jeneralize nöbetlere yol açmaktadır [26,28]. Gholipour ve arkadaşları intravenöz PTZ enjeksiyonu ile oluşturdukları nöbet modelinde diazepamın klonik nöbete giriş süresini artırdığını belirtmişlerdir [29]. Benzer şekilde diazepam; sıçanlarda pilokarpinle indüklen status epileptikus modelinde toplam nöbet süresini azaltırken nöbete giriş süresini artırmıştır [30]. Mevcut çalışmada antikonvülzan özelliği bilinen diazepam, PTZ (45 mg $kg^{-1}$)ile oluşturulan nöbet modelinde nöbet evrelerinin azalmasına ve İMJ süresinin uzamasına neden olmuştur.

NO sinir sistemi için önemli bir nöromediyatördür, hipokampüs başta olmak üzere beynin birçok bölgesinde nöronal hücrelerde NOS tarafından L-arjininin L-sitrüline dönüştürülmesi sırasında oluşmaktadır [31]. PTZ ile oluşturulan nöbetlerde farklı beyin bölgelerinde NO miktarının arttığı gösterilmiştir [32]. NO ve epilepsi arasındaki ilişkiyi açıklayan çok sayıdaki farklı çalışmalarda NO hem prokonvülsan hem de antikonvülzan özellik göstermektedir [3, 33]. PTZ ile oluşturulan nöbet modellerinde nöbet sonrası korteks ve hipokampüsteki NO düzeylerindeki değişimler ile ilgili farklı sonuçlar bulunmaktadır. Nazıroğlu ve arkadaşları yaptıkları çalışmada PTZ ile indüklenen akut nöbet modelinde nöbetten sonra kortikal NO seviyesinin değişmediğini belirtmişlerdir [34]. Buna karşılık, Taşkıran ve arkadaşları ise PTZ ile oluşturulan nöbet sonrası hipokampüs ve kortekste PTZ uygulamasının nNOS, iNOS ve NO seviyelerini yükselttiğini, diazepamın ise bu değerleri düşürdüğünü tespit etmişlerdir [26]. Farklı bir çalışmada ise PTZ ile oluşturulan tonik klonik nöbetler sonrasında frontal kortekste nNOS düzeyi artmış, iNOS ve eNOS değişiklik göstermemiş; hipokampal nNOS, iNOS ve eNOS ekspresyonu ise azalmıştır [35]. Benzer şekilde Mazhar ve arkadaşları PTZ ile oluşturulan tutuşma modelinde nöbet sonrası NOS ekpresyonunun arttığını, diazepam uygulamasının ise NOS seviyesini düşürdüğünü belirtmişlerdir [36]. Öte yandan, diazepamın anksiyolotik etkilerini gösteren çalışmada kortikal ve hipokampal NOS üzerine etkisi olmadığı bulunmuştur [37]. Çalışmamızda ise PTZ ile oluşturulan nöbetler sonrası kortekste gruplar arası NOS seviyesinde değişiklik görülmemiştir. Bununla birlikte hipokampüste PTZ grubunda NOS seviyesinin düştüğü görülmüştür. Bunun nedeni epileptik nöbetlere bağlı olarak ortaya çıkan oksidatif stres olabilir. Hipokampüste yer alan NMDA reseptörlerinin kortekse göre aşırı aktivasyonu sonucu hücre içine aşırı kalsiyum girişi reaktif oksijen ürünlerinin oluşmasına neden olmaktadır. Bu oksidatif ürünlerin hipokampüste NOS ile reaksiyonu sonucu oksidatif peroksit ürünleri oluşturarak [38] NOS seviyesinin düşmesine neden olmuş olabilir. Diazepam ise hipokampüste nöbete bağlı azalan NOS seviyelerini artırmıştır. Diazepam oksidatif stres belirteçlerinin azalmasına neden olarak hipokampüste NOS seviyesini artırmış olabilir.

BDNF, merkezi sinir sisteminde görev alan büyüme faktörlerinden biridir [39] ve beyin plastisitesinde önemli yere sahiptir [40]. Yapılan deneysel çalışmalar BDNF'nin nöbet oluşumu ile ilişkili olabileceğini ortaya koymuştur [41]. Farklı epilepsi modellerinde BDNF ekpresyonunun arttığı görülmüştür [42-44]. Benzer şekilde farelerde PTZ ile oluşturulan nöbet modelinde nöbet sonrası BDNF seviyesi yüksek bulunmuştur [45]. Bunun aksine Şahin ve arkadaşları kainik asid ve PTZ ile oluşturdukları nöbet modellerinde nöbet sonrası BDNF seviyesinin azaldığını göstermişlerdir [46]. Benzer şekilde benzodiazepinlerin hipokampüste etki mekanizmasını araştıran bir çalışmada diazepamın BDNF seviyesini düşürdüğü gösterilmiştir [47]. Bu çalışmadan farklı olarak Regner ve arkadaşları PTZ ile oluşturulan tutuşma modelinde nöbet sonrası diazepam uygulan grubun PTZ grubuna göre kortikal ve hipokampal BDNF seviyeleri üzerine etki etmediğini belirtmişlerdir [48]. Çalışmamızda ise PTZ ile oluşturulan nöbet sonrasında korteks ve hipokampüste BDNF seviyesinin arttığı tespit edildi. Diazepam uygulaması ise hipokampal ve kortikal BDNF seviyelerini düşürdü.

## 5. SONUÇ

Diazepam, PTZ ile oluşturulan nöbet sonrası nöbet evrelerinin azalmasına ve ilk miyoklonik jerk süresinin artmasına neden olmuştur. Ayrıca diazepam, nöbet sonrası kortikal NOS seviyesi üzerine etki göstermezken hipokampal NOS seviyesini artırmıştır. Hipokampüste ve kortekste nöbet sonrası artan BDNF seviyeleri diazepam uygulaması sonrası düşmüştür. Diazepamın, NOS ve BDNF üzerine düzenleyici etkisi antikonvülzan etkisi ile bağlantılı olabilir. Ancak, bu hipotezin kanıtlanabilmesi için ileri moleküler çalışmalara ihtiyaç vardır.

## KAYNAKLAR


[1] Thomas R. Browne, Gregory L. Holmes. Epilepsy: Definitions and Background. Hanbook of Epilepsy. Third edition. USA; 2004. p. 6-7.

[2] Baykan B, Bebek N, Candan Gürses, Gökyiğit A. Epilepsi. Ed: Öge AE, Baykan B. Nöroloji. 2.Baskı. İstanbul: Nobel Tıp Kitabevleri; 2004. s. 279-309.

[3] Gunes H, Ozdemir E, Arslan. Coenzyme Q10 increases absence seizures in WAG/Rij rats: The role of the nitric oxide pathway. Epilepsy Res. 2019 Aug; 154:69-73.

[4] Zienowicz M, Wisłowska A, Lehner M. The effect of fluoxetine in a model of chemically induced seizures behavioral and immunocytochemical study. NeurosciLett. 2005; 373(3):226–231.

[5] E. Erkec, O. Arihan. Pentylenetetrazole kindling epilepsy model, Epilepsi. 2015; 21 (1): 6–12.

[6] Meierkord H, Boon P, Engelsen B, Gocke K, Shorvon S, Tinuper Holtkamp M. EFNS guideline on the management of status epilepticus. Eur. J. Neurol. 2006;13: 445–450.

[7] Rudolph U, Crestani F, Benke D, Brunig I, Benson JA, Fritschy JM, Martin JR, Bluethmann H, Mohler H, Benzodiazepine actions mediated by specific γ-aminobutyric acid (A) receptor subtypes. Nature.1999; 401:796–800.

[8] Hanson SM, Czajkowski C. Structural mechanisms underlying benzodiazepine modulation of the GABA(A) receptor. J. Neurosci. 2008; 28:3490–3499.

[9] Moncada S, Palmer RM, Higgs EA. Nitric oxide: physiology, pathophysiology, and pharmacology. Pharmacol. Rev. 1991; 43: 109–142.

[10] Nidhi G, Balakrishnan S, Pandhi P. Role of nitric oxide in electroshock and pentylenetetrazole seizure threshold in rats. Methods Find. Exp. Clin. Pharmacol. 1999;21: 609–612.

[11] Rajasekaran K, Jayakumar R, Venkatachalam K. Increased neuronal nitric oxide synthase (nNOS) activity triggers picrotoxin-induced seizures in rats and evidence for participation of nNOS mechanism in the action of antiepileptic drugs. Brain Res. 2003; 979: 85–97.

[12] Lizasoain I, Knowles RG, Moncada S. Inhibition by lamotrigine of the generation of nitric oxide in rat forebrain slices. J. Neurochem.1995; 64: 636–642.

[13] Nidhi G, Balakrishnan S, Pandhi P. Role of nitric oxide in electroshock and pentylenetetrazole seizure threshold in rats. Methods Find. Exp. Clin. Pharmacol.1999; 21: 609–612.

[14] Talarek S, Fidecka S. Involvement of nitricoxidergic system in the hypnotic effects of benzodiazepines in mice. Pol. J. Pharmacol. 2004;56: 719–726.

[15] Jimenez-Velazquez G, Lopez-Munoz FJ, Fernandez-Guasti A. Participation of the GABA/benzodiazepine receptor and the NO-cyclicGMP pathway in the “antinociceptive-like effects” of diazepam. Pharmacol. Biochem. Behav. 2008; 91:128–133.

[16] Talarek S, Fidecka S. Role of nitric oxide in anticonvulsant effects of benzodiazepines in mice. Pol. J. Pharmacol. 2003; 55: 181–191.

[17] Lee FS, Chao MV. Neurotrophic factors. Neural Sciences. 2008; 1: 96-102.

[18] Dugich-Djordjevic MM, Peterson C, Isono F, Widmer HR, Denton TL, Bennett GL, Hefti F. Immunohistochemical visualization of brain-derived neurotrophic factor in the rat brain. European Journal of Neuroscience. 1995; 7: 1831-1839.

[19] Phillips HS, Hains JM, Laramee GR, Rosenthal A, Winslow JW. Widespread expression of BDNF but not NT3 by target areas of basal forebrain cholinergic neurons. Science. 1990; 250: 290- 294.

[20] Huntley GW, Benson DL, Jones EG, Isackson PJ. Developmental expression of brain derived neurotrophic factor mRNA by neurons of fetal and adult monkey prefrontal cortex. Brain Research Developmental Brain Research. 1992;70: 53-63.

[21] Nawa H, Carnahan J, Gail C. BDNF protein measured by a novel enzyme immunoassay in normal brain and after seizure: partial disagreement with mRNA levels. European Journal of Neuroscience. 1995; 7: 1527- 1535.

[22] Wetmore C, Cao Y, Pettersson RF, Olson L. Brain-derived neurotrophic factor: subcellular compartmentalization and interneuronal transfer as visualised with antipeptide antibodies. Proceedings of the National Academy of Sciences. 1991;88: 9843-9847.

[23] Ochoa JG, Kilgo WA. The Role of Benzodiazepines in the Treatment of Epilepsy. CurrTreat Options Neurol 2016; 18:1–11. https://doi.org/10.1007/S11940-016-0401-X.

[24] Pitkänen A, Kharatishvili I, Narkilahti S, Lukasiuk K, Nissinen J. Administration of diazepam during status epilepticus reduces development and severity of epilepsy in rat. Epilepsy Res 2005; 63:27–42. https://doi.org/10.1016/J.EPLEPSYRES.2004.10.003.

[25] Albertson TE, Peterson SL, Stark LG. The anticonvulsant effects of diazepam and phenobarbital in prekindled and kindled seizures in rats. Neuropharmacology 1981; 20:597–603.

[26] Taskiran AS, Tastemur Y. The role of nitric oxide in anticonvulsant effects of lycopene supplementation on pentylenetetrazole-induced epileptic seizures in rats. Exp Brain Res. 2021;239(2):591-599.

[27] Ernst O, Zor T. Linearization of the Bradford protein assay. J Vis Exp. 2010; 12(38):1918.

[28] Sefil F, Kahraman I, Dokuyucu R, Gokce H, Ozturk A, Tutuk O, Aydin M, Ozkan U, Pinar N.

Ameliorating effect of quercetin on acute pentylenetetrazole induced seizures in rats. Int J Clin Exp Med. 2014 Sep 15;7(9):2471-7.

[29] Gholipour T, Rasouli A, Jabbarzadeh A, Nezami BG, Riazi K, Sharifzadeh M, Dehpour AR. The interaction of sildenafil with the anticonvulsant effect of diazepam. Eur J Pharmacol. 2009 Sep 1;617(1-3):79-83.

[30] Mante PK, Adongo DW, Woode E. Anticonvulsant effects of antiaris toxicaria aqueous extract: investigation using animal models of temporal lobe epilepsy. BMC Res Notes.2017; 10: 167.

[31] Ferraro G, Sardo P. Nitric oxide and brain hyperexcitability. In Vivo. 2004; 18:357–36615.

[32] Watanabe M, Miyai A, Danjo S, Nakamura Y, Itoh K. The threshold of pentylenetetrazole-induced convulsive seizures, but not that of nonconvulsive seizures, is controlled by the nitric oxide levels in murine brains. Exp Neurol. 2013; 247:645-52.

[33] Gotti S, Sica M, Viglietti-Panzica C, Panzica G. Distribution of nitric oxide synthase immunoreactivity in the Mouse brain. Microsc Res Tech. 2005;68(1):13-35.

[34] Naziroğlu M, Kutluhan S, Yilmaz M. Selenium and topiramate modulates brain microsomal oxidative stress values, $Ca^{2+}$-ATPase activity, and EEG records in pentylentetrazol-induced seizures in rats. J Membr Biol. 2008 Sep-Oct;225(1-3):39-49.

[35] Kapucu A. Effect of erythropoıetın on nıtrıc oxıde synthase types ın the hıppocampus and frontal cortex ın ptz ınduced seizure ın rats. Journal of Istanbul Faculty of Medicine. 2019;82(2):107-115.

[36] Mazhar F, Malhi SM, Simjee SU. Comparative studies on the effects of clinically used anticonvulsants on the oxidative stress biomarkers in pentylenetetrazole-induced kindling model of epileptogenesis in mice. J Basic Clin Physiol Pharmacol. 2017 Jan 1;28(1):31-42.

[37] Volke V, Soosaar A, Kõks S, Vasar E, Männistö PT. L-Arginine abolishes the anxiolytic-like effect of diazepam in the elevated plus-maze test in rats. Eur J Pharmacol. 1998 Jun 26;351(3):287-90.

[38] Standaert DG. NMDA receptors and nitric oxide synthase. Nature. 1999; 4:13-14.

[39] Lucini C, D'Angelo L, Cacialli P, Palladino A, de Girolamo P. BDNF, brain, and regeneration: Insights from zebrafish. Int J Mol Sci. 2018; 19(10): 3155.

[40] Autry AE, Monteggia LM. Brain-derived neurotrophic factor and neuropsychiatric disorders. Pharmacol Rev. 2012;64(2):238-58.

[41] Hong Z, Li W, Qu B, Zou X, Chen J, Sander J, et al. Serum brain derived neurotrophic factor levels in epilepsy. Eur J Neurol 2014;21(1): 57-64.

[42] Altar CA, Whitehead RE, Chen R, Wörtwein G, Madsen TM. Effects of electroconvulsive seizures and antidepressant drugs on brain-derived neurotrophic factor protein in rat brain. Biol Psychiatry. 2003; 54(7): 703-9.

[43] Falcicchia C, Paolone G, Emerich DF, Lovisari F, Bell WJ, Fradet T, et al. Seizure-suppressant and neuroprotective effects of encapsulated BDNF-producing cells in a rat model of temporal lobe epilepsy. Mol Ther Methods Clin Dev. 2018; 9: 211-24.

[44] Porcher C, Medina I, Gaiarsa J-L. Mechanism of BDNF modulation in GABAergic synaptic transmission in healthy and disease brains. Front Cell Neurosci. 2018; 12: 273.

[45] Malhi SM, Jawed H, Hanif F, Ashraf N, Zubair F, Siddiqui BS, Begum S, Kabir N, Simjee SU. Modulation of c-Fos and BDNF protein expression in pentylenetetrazole-kindled mice following the treatment with novel antiepileptic compound HHL-6. Biomed Res Int. 2014; 2014:876712.

[46] Şahin S, Gürgen SG, Yazar U, İnce İ, Kamaşak T, Acar Arslan E, Diler Durgut B, Dilber B, Cansu A. Vitamin D protects against hippocampal apoptosis related with seizures induced by kainic acid and pentylenetetrazol in rats. Epilepsy Res. 2019 Jan; 149:107-116.

[47] Licata SC, Shinday NM, Huizenga MN, Darnell SB, Sangrey GR, Rudolph U, Rowlett JK, Sadri-Vakili G. Alterations in brain-derived neurotrophic factor in the mouse hippocampus following acute but not repeated benzodiazepine treatment. PloS One. 2013 Dec; 19:8(12): e84806.

[48] Regner GG, Torres ILS, de Oliveira C, Pflüger P da Silva LS, Scarabelot VL, Ströher R, de Souza A, Fregni F, Pereira P. Transcranial direct current stimulation (tDCS) affects neuroinflammation parameters and behavioral seizure activity in pentylenetetrazole-induced kindling in rats. Neurosci Lett. 2020 Sep 14; 735:135162.

Cilt 11, Sayı 2, Sayfa 58-63, 2022 Volume 11, Issue 2, Page 58-63, 2022

Araştırma Makalesi https://doi.org/10.46810/tdfd.1107889 Research Article

Türk Doğa ve Fen Dergisi
Turkish Journal of Nature and Science
www.dergipark.gov.tr/tdfd

# Determination of Ibuprofen in Pharmaceutical Preparations by UPLC-MS/MS Method

**Ömer Faruk KOÇAK[1], Alptuğ ATİLA[2*]**

[1] Atatürk University, Vocational School, Department of Chemistry and Chemical Process Technologies, Erzurum, Türkiye

[2] Atatürk University, Faculty of Pharmacy, Department of Basic Pharmaceutical Sciences, Erzurum, Türkiye

Ömer Faruk KOÇAK ORCID No: 0000-0001-5873-0944

Alptuğ ATİLA ORCID No: 0000-0001-7027-809X

**Corresponding author: alptug@atauni.edu.tr*

(Received: 23.04.2022, Accepted: 09.05.2022, Online Publication: 29.06.2022)

**Keywords**
Ibuprofen, UPLC-MS/MS, Pharmaceutical analysis

**Abstract:** Ibuprofen (IBU) is a non-steroidal anti-inflammatory drug that is extensively prescribed. For the determination of IBU in pharmaceutical formulations, a sensitive, simple, accurate, and rapid ultra-performance liquid chromatography method in combination with tandem triple quadruple mass spectrometry (UPLC-MS/MS) has been used and validated. The chromatographic separation was accomplished using a $C_{18}$ UPLC column, 95 Å, 2.1 x 50 mm, 1.8 µm, and 0.1 percent formic acid in conjunction with acetonitrile (25:75 v/v. The flow rate was 0.15 ml $min^{-1}$, with a run duration of 2.0 minutes. The injection volume was 5 µL and the column temperature was held constant at 40 °C.The mass transitions of İbuprofen and IS were m/z 205.0 → 159.0 and 249.9 → 228.9, respectivelty. According to ICH guidelines, the approach was thoroughly verified. The linear range 1-5000 ng $mL^{-1}$ calibration curve has a strong correlation coefficient (0.9921). Within and between days precision were expressed as relative standard deviation and were lower than 6.24%. This method has been used to determine IBU in both pure form and pharmaceutical formulations with great success.



# İbuprofenin Farmasötik Preperatlarda UPLC-MS/MS Yöntemiyle Tayini

**Anahtar Kelimeler**
İbuprofen, UPLC-MS/MS, Farmasötik analiz

**Öz:** İbuprofen (IBU), yaygın olarak reçete edilen, steroid olmayan bir anti-inflamatuar ilaçtır. Farmasötik formülasyonlarda IBU'nun belirlenmesi için tandem üçlü dörtlü kütle spektrometrisi ile kombinasyon halinde hassas, basit, doğru ve hızlı ultra performanslı sıvı kromatografi yöntemi (UPLC-MS/MS) yöntemi kullanılmış ve doğrulanmıştır. Kromatografik ayırma, bir C18 UPLC kolonu, 95 Å, 2.1 x 50 mm, 1.8 µm ve asetonitril ile birlikte yüzde 0.1'lik formik asit (25:75 v/v) kullanılarak gerçekleştirildi. Akış hızı, 2.0 dakikalık bir çalışma süresi ile 0.15 ml $dak^{-1}$ idi. Enjeksiyon hacmi 5 µL ve kolon sıcaklığı 40 °C'de sabit tutuldu. İbuprofen ve IS kütle geçişleri sırasıyla m/z 205.0 → 159.0 ve 249.9 → 228.9 dur. ICH yönergelerine göre, yaklaşım tamamen doğrulandı. 1-5000 ng $mL^{-1}$ kalibrasyon eğrisi doğrusal aralığı, güçlü bir korelasyon katsayısına (0.9921) sahipti. Gün içi ve günler arası kesinlik, bağıl standart sapma olarak ifade edildi ve %6.24'ten düşüktü. Bu yöntem, hem saf formda hem de farmasötik formülasyonlarda IBU'yu büyük bir başarıyla belirlemek için kullanılmıştır.

## 1. INTRODUCTION

Ibuprofen (IBU) is a non-steroidal anti-inflammatory drug that is commonly used. By inhibiting the cyclooxygenase-2 enzyme, it primarily acts as an anti-inflammatory, antipyretic, and analgesic drug [1, 2]. IBU is commonly used to alleviate fever, pain, and inflammation in premature newborns, as well as to treat patent ductus arteriosus [3]. IBU takes 1-3 hours to achieve its apparent maximum concentration (Tmax), which is rapidly absorbed after oral intake, and maximum concentrations (Cmax) vary from 50-100 µg $mL^{-1}$. [4]. Ibuprofen has the chemical formula $C_{13}H_{18}O_2$ and the name (RS)-2-[4-(2-methylpropyl) phenyl] propanoic acid [5]. The chemical structure of IBU is shown in Figure 1. [6].

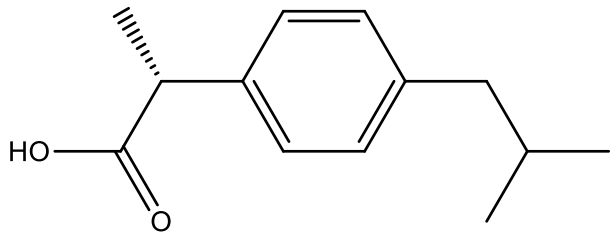


**Figure 1.** The chemical structure of Ibuprofen

According to a survey of the literature, no research have been done utilizing the UPLC-MS/MS technique to determine the quantity of IBU in pharmaceutical formulations. There have been research that used the LC-MS/MS approach to determine IBU from plasma. To determine the amount of IBU in pharmaceutical preparations, analytical studies have been conducted using the high-performance liquid chromatography (HPLC) method [7-9], capillary electrophoresis [10], HPTLC [2, 11, 12], and spectrofluorimetry [13, 14]. However, the analysis time in these research are lengthy, and the pre-analytical preparation procedures are time-consuming.

Ultra-high performance liquid chromatography (UPLC) is an upgraded derivative of HPLC systems with high-quality tiny porous packing material and the capacity to operate at extremely high pressures. Higher pressure capability and smaller particles in the stationary phase allow for enhanced efficiency and sensitivity, as well as quicker chromatographic analysis, thanks to sharper and higher peaks. As a result, the key benefits of UPLC systems include improved resolution and, more importantly, a large decrease in processing time [15-18]. Furthermore, compared to HPLC, mass spectrometric approaches can give higher sensitivity and specificity [3].

The study's goal was to develop a fast and sensitive ultra-performance liquid chromatography tandem mass spectrometer (UPLC-MS/MS) method for determining IBU in pharmaceutical preparations and pure form with high recovery and short run-time, as well as to validate the method according to ICH Q2(R1) guideline. The developed method was successfully applied in the analysis of IBU-containing tablet dosage forms after test scenarios were completed.

## 2. MATERIALS AND METHODS

### 2.1. Materials and Reagents

Novagenix Company (Ankara, Turkey) provided IBU with a purity of >99 percent and Erdostein (IS, purity>99 percent). Methanol and acetonitrile hyper grade for LC-MS systems were being provided by Merck (Darmstadt, Germany). Synergy® UV Water Purification System was used to make deionized water on a regular basis (Merck Millipore, Darmstadt, Germany). As a result, all of the other compounds were analytical grade and could be utilized without additional purification.

### 2.2. Instrumentation and Operation Conditions

An ultra-high-performance liquid chromatography system (UHPLC, 1290 Series, Agilent Technologies, Santa Clara, CA, USA) was employed to analyze the samples, which was linked to an Agilent 6490 Triple Quadrupole mass spectrometer (Agilent Technologies), which contained a triple quadrupole mass spectrometer, a degasser, an autosampler, a column compartment, as well as a binary pump. The autosampler tray temperature was kept at 10 degrees Celsius, and the reserved-phase C18 UPLC column (ZORBAX RRHD Eclipse Plus C18, 95, 2.1 x 50 mm, 1.8 m, Agilent Technologies, Loveland, CO, USA) was kept at 40 degrees Celsius was used to achieving Chromatographic separation. The samples were separated using isocratic elution with a mobile phase of 0.1 percent formic acid solution and acetonitrile (25:75, volume/volume). The mobile phase was processed using a 0.45 µm Millipore membrane filter before use. With a run time of 2.0 minutes, the flow velocity was 0.15 mL $min^{-1}$. The injection volume was 5 µL and the column temperature was kept fixed at 40°C for symmetrical peaks.

A mass spectrometer with a Jet Stream electrospray ion source interface was used in both negative and positive ionization mode in the mass range of 50–250 Da. The desolvation gas (1000 L $h^{-1}$) and cone gas (50 L $h^{-1}$) were both nitrogen. Capillary voltage of 2.0 kV, source temperature of 250 °C, and nebulizer pressure of 35 psi were used to determine the ion monitoring conditions. To conduct quantitative analysis, multiple reaction monitoring (MRM) modes of m/z 205.0→ 159.0 for IBU and 249.9→ 228.9 m/z for IS were used.

In methanol, stock solutions of IBU (1000 µg $mL^{-1}$) and IS (1000 µg $mL^{-1}$) were made. The IS 5000 ng/mL working standard solution was prepared by dilution with methanol from the IS stock solution; working solutions for calibration and controls were prepared similarly from stock solutions using methanol diluent. All of the solutions were kept at -20 degrees Celsius and warmed to room temperature before being used.

### 2.3. Selection of Internal Standard

We employed erdosteine as IS for IBU in a prior investigation. For both materials, mass and chromatographic settings were optimized [19]. We used erdosteine as an internal standard for IBU in this study and validated the approach we developed for IBU.

### 2.4. Preparation of Standards and Quality Control (QC) Samples

In methanol, IBU (1000 µg $mL^{-1}$) and IS (1000 µg $mL^{-1}$) stock solutions were produced. By diluting the stock solutions with methanol, the IBU and IS working standard solutions were created. Using methanol, further dilutions of working solutions for calibration and controls were generated from stock solutions. Working solutions were kept at -20 °C until they were needed and

then raised to room temperature. The solutions for quality control were produced on a daily basis.

### 2.5. Method Validation

Validation was conducted out in accordance with ICH Q2(R1) guidelines to ensure the analytical method's performance [20].

#### 2.5.1. Selectivity and specificity

Figure 2 shows representative MRM chromatograms of solutions derived from tablet formulations. It demonstrated that decent separation was acquired both standard and real sample conditions and no interfering peaks were discovered at the retention time of IBU and IS. [21] (Figure 2.).

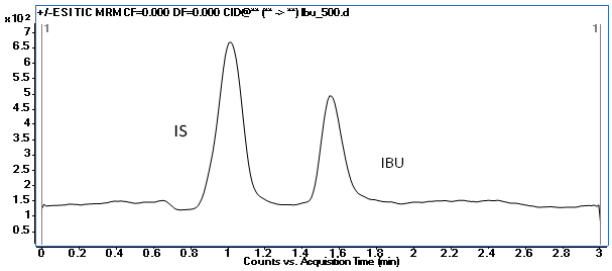


**Figure 2.** UPLC-MS/MS total ion current (TIC) chromatogram of IBU (500 ng $mL^{-1}$) and IS (500 ng $mL^{-1}$)

#### 2.5.2. Linearity and sensitivity

Standard working solutions at seven different concentrations of IBU and IS (500 ng $mL^{-1}$) were generated triplicate to obtain a calibration graph in the range of 0.1–5000 ng $mL^{-1}$. These samples were evaluated using the established approach, and the equation was constructed using least-squares weighted (1/x2) linear regression analysis. Continuous lower accumulations of standard solution were evaluated in sensitivity experiments. The LOD level was chosen as the lowest discernible and distinct peak. According to ICH recommendation, the detection and quantification limits were calculated based on the signal-to-noise ratio of 3:1 and 10:1, respectively [22].

#### 2.5.3. Precision and accuracy

The accuracy and precision of the UPLC-MS/MS technique were determined by analyzing quality control samples (QC's) in low, medium, and high concentrations within the calibration curve (4, 400, and 4000 ng $mL^{-1}$). Intraday precision and accuracy were determined by analyzing QC samples three times in one day, and inter-day precision and accuracy were determined by analyzing the same samples three times in three days following the intraday analysis. To calculate precision and accuracy, the RSD and RE are employed [22].

#### 2.5.4. Analysis of pharmaceuticals and recovery

The applicability of the methods for the determination of IBU in solid dosage forms (tablets) was examined by analyzing marketed medicinal products of BRUFEN (400 mg Abbott Pharmaceuticals Inc) and DOLVEN (600 mg Sanofi Pharmaceuticals Inc). The contents of each medication were extracted and weighed individually. Weighed and dissolved in methanol in an amount equivalent to one tablet. To ensure thorough dissolution, the solutions were sonicated for 15 minutes. The solutions were diluted with an optimum amount (150 and 400 ng $mL^{-1}$) and transmitted to an autosampler vial after being filtered through a microfilter. For analysis, 5 µL was injected into the UPLC-MS/MS system. By comparing the observed concentration to the notional concentration, average recoveries were computed.

## 3. RESULTS AND DISCUSSION

### 3.1. UPLC–MS/MS Method Development and Optimization

To attain the highest abundances of product and fragment ions, mass spectrometric settings were optimized. Direct injection of IBU and IS solutions into the mass spectrometer in both positive and negative ionization modes with an ESI source in the mass range of 80–300 Da resulted in full scan mass spectra and product ion scan spectra at 1000 ng $mL^{-1}$. IS had a greater peak intensity in negative ion mode than in positive mode, but IBU had a substantially higher peak intensity in negative mode. Using the multiple reaction monitoring mode, data for the two highest intense and/or different product ions for each precursor ion was obtained. MRM is a sensitive targeted mass spectrometry technique for identifying and quantifying particular chemicals by screening specific precursor molecule-to-fragment ion transitions [23]. IS transitioned to product at m/z 249.9→ 228.9, whereas IBU transitioned to product at m/z 205.0→ 159.0. However, there was only one product ion present for ibuprofen (IS), and there was no extra fragmentation product that could be chosen as the predictive ion (Figure 3.). For IBU and IS, the optimal collision energies were determined to be 2 and 1 eV, respectively. Further details about the optimum mass spectrometric conditions were shown in Table 1.

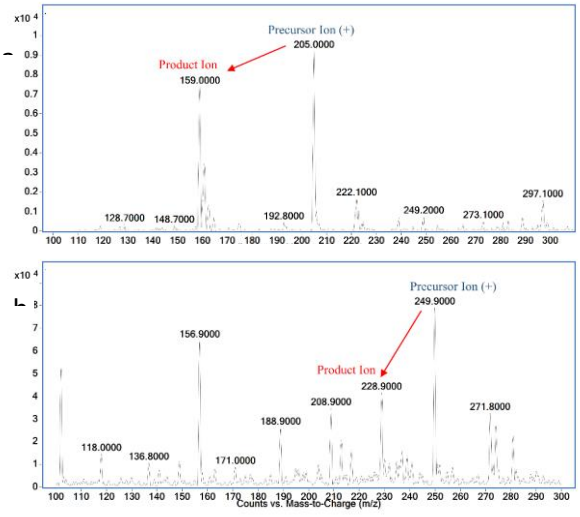


**Figure 3.** Product İon Mass Spectra for (A) Ibuprofen (m/z 205.0 → 159.0), (B) IS (Erdosteine) (m/z 249.9 → 228.9)

**Table 1.** Optimized MS/MS Parameters of the Method

| | IBU (Product Ion) | IS (Product Ion) |
|---|---|---|
| Ionization Mode | ESI+Agilent Jet Stream | |
| MRM Transitions (m/z) | 205.0 → 159.0 | 249.9 → 228.9 |
| Fragmentor Voltage (V) | 60 | 23 |
| Collision Energy (V) | 1 | 2 |
| Polarity | Negative | Positive |
| Dwell Time | 165 | 165 |
| Gas Temp (°C) | 250 | 250 |
| Gas Flow (l/min) | 8 | 8 |
| Nebulizer (psi) | 35 | 35 |
| SheathGasHeater | 250 | 250 |
| SheathGasFlow | 10 | 10 |
| Capillary (V) | 2000 | 2000 |

The mobile phase is optimized by testing a variety of solvents, ratios and flow programs to achieve good separation with good resolution of IBU and IS peaks in a short analysis time. It was found that the non-polar properties of IS became dominant during chromatographic separation and remained on the C18 column, requiring the use of acetonitrile for its elution. It was also found that the acidic aqueous solution significantly improved the resolution of IBU and minimized peak tailing compared to other solvents. Therefore, the optimal mobile phase consisting of water (0.1% formic acid) and acetonitrile was finally used at a flow rate of 0.15 mL $min^{-1}$. Under these specified conditions, IBU and IS retention times were approximately 1.554 and 1.017 for IBU and IS, respectively. Total analysis time was 2.0 minutes. This is a significantly faster execution time than the previous survey [24-28].

### 3.2. Selectivity and Specificity

Figure 5 shows representative MRM chromatograms of solutions derived from tablet formulations (150 and 400 ng $mL^{-1}$). It demonstrated that good separation was acquired both standard and real sample conditions and no intruding peaks were discovered at the retention time of IBU and IS [21].

### 3.3. Linearity and Sensitivity

The calibration curve was created by plotting the peak area ratio of IBU to IS to the concentration. The calibration curve was created by analysis in 7 different concentrations of IBU, the developed method was linear in the range of 1-5000 ng $mL^{-1}$, and the coefficient of determination (R2) exceeded 0.996 (Figure 4). LOD was calculated by injecting a continuous small accumulation of standard solution using the developed method, and values of 0.3 ng $mL^{-1}$and 3:1 S/N values were observed. The LOQ corresponding to the 10: 1 signal-to-noise ratio was determined to be 1 ng / mL. This shows that this method is sensitive enough.

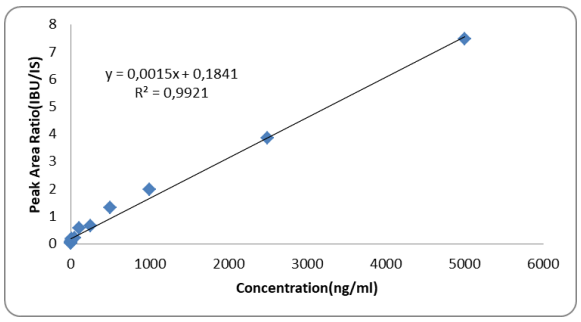


**Figure 4.** The Calibration Curve of the Method Obtained From Linear Regression Analysis of the Method (n=6).

### 3.4. Precision and Accuracy

The accuracy and precision values for QC solutions (4, 400, and 4000 ng $mL^{-1}$) were determined using percent relative error (percent RE) and percent relative standard deviations (percent RSD) over the same day (intra-day, n=3) and three consecutive days (inter-day), respectively. Table 2 shows the accuracy and precision findings. In every case, the intra-day and interday accuracy and precision values were within acceptable limits. With RE % (lower than 4.25 %) and % RSD (lower than 6.24 %) values, the approach demonstrated high accuracy and precision.

**Table 2.** Precision and Accuracy of the Method (n=6). x̄: Mean of the Six Replicated Analysis, SD: Standard Deviation, RE%: Relative Error, RSD: Relative Standard Deviations

| | Intra-day | | | Inter-day | | |
|---|---|---|---|---|---|---|
| Added (ng/mL) | Found x̄ (ng $mL^{-1}$) ± SD | Accuracy RE % | Precision RSD % | Found x̄ (ng $mL^{-1}$) ± SD | Accuracy RE % | Precision RSD % |
| 4 | 4.23 ± 0,13 | 5.75 | 3.07 | 4.17 ± 0.26 | 4.25 | 6.24 |
| 400 | 416.76 ± 14.85 | 4.19 | 3.56 | 395.40 ± 15.22 | -1.15 | 3.85 |
| 4000 | 3982.60 ± 84.59 | -0.44 | 2.02 | 3979.52 ± 77.20 | -0.51 | 1.94 |

### 3.5. Analysis of Pharmaceuticals and Recovery

The determination of IBU in tablet formulations was conducted to measure the applicability of the UPLCMS/MS method (Figure 5.). The amount of IBU in the selected commercial pharmaceuticals was found to be in good agreement with the IBU content of these formulations in experiments. For IBU six different lots of each drug, the drug content was found to be between 99.07 percent and 102.66 percent (Table 3.). These findings indicate that the method could be used to analyze IBU-containing tablet formulations on a regular basis.

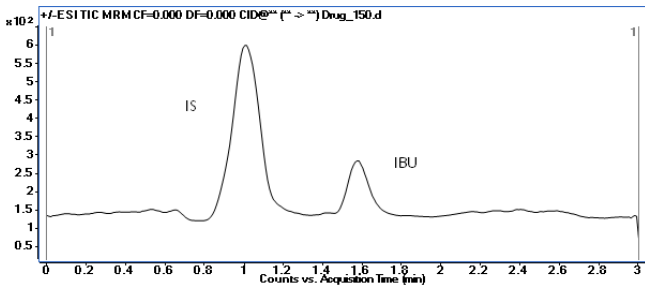


**Figure 5.** A Representative UPLC-MS/MS Chromatogram of IBU (150 ng $mL^{-1}$) Solutions Prepared from Tablet Formulations

**Table 3**. The Assay Results and Recovery of Pharmaceuticals Containing IBU in Two Different Concentration Levels (n=6)

| | BRUFEN 400 mg IBU | | DOLVEN 600 mg IBU | |
|---|---|---|---|---|
| | 150 ng $mL^{-1}$ | 400 ng $mL^{-1}$ | 150 ng $mL^{-1}$ | 400 ng $mL^{-1}$ |
| $\bar{x}$ (ng $mL^{-1}$) | 147.11 | 403.22 | 153.20 | 410.65 |
| SD | 5.04 | 7.49 | 7.47 | 9.78 |
| RSD % | 3.42 | 1.85 | 4.87 | 2,38 |
| Average Recovery % | 98.07 | 99.20 | 102.13 | 102.66 |

## 4. CONCLUSION

In the literature, the present approach was developed and validated for the determination of IBU from pharmaceutical formulations and pure form using the UPLC-MS/MS method. The linear range 1-5000 ng $mL^{-1}$ calibration curve has a strong correlation coefficient (0.9921). Within and between days precision were expressed as relative standard deviation and were lower than 6.24%. The findings showed that the suggested UPLC-MS/MS technique is a simple, precise, quick, accurate, and low-cost approach. This approach also offers a fast analytical time and a high sensitivity. In conclusion, this approach may be utilized to determine IBU in pure form and pharmaceutical formulations, routine analysis, pharmaceutical industry quality control laboratories, and stability monitoring.

## Acknowledgements

Ataturk University's East Anatolia High Technology Application and Research Centre handled sample preparation and mass spectrometric analysis (DAYTAM).

## Conflict of Interest

There are no conflicts of interest declared by any of the writers.

## REFERENCES

[1] Hong S, Xu K, Guo S, Yuan L, Wang H. Development and Validation of a New Simple HPLC Method for the Determination of 3-[4-(2-Methylpropyl)phenyl] Propanoic Acid as an Impurity of Ibuprofen and Ibuprofen Sodium. Chromatographia. 2017 Jul 1;80(7):1095–100.

[2] Ragab MAA, Abdel-Hay MH, Ahmed HM, Mohyeldin SM. Determination of ibuprofen and phenylephrine in tablets by high-performance thin layer chromatography and in plasma by high-performance liquid chromatography with diode array detection. J Chromatogr Sci. 2019;57(7):1–8.

[3] Puangpetch A, Limrungsikul A, Prommas S, Rukthong P, Sukasem C. Development and validation of a liquid chromatography-tandem mass spectrometry method for determination of ibuprofen in human plasma. Clin Mass Spectrom [Internet]. 2020;15:6–12. Available from: https://doi.org/10.1016/j.clinms.2019.10.002.

[4] Konstan MW, Byard PJ, Hoppel CL, Davis PB. Effect of High-Dose Ibuprofen in Patients with Cystic Fibrosis. N Engl J Med. 1995 Mar 30;332(13):848–54.

[5] Asif U, Sherwani AK, Akhtar N, Shoaib MH, Hanif M, Qadir MI, et al. Formulation Development and Optimization of Febuxostat Tablets by Direct Compression Method. Adv Polym Technol. 2016;35(2).

[6] Waraksa E, Wójtowicz-Zawadka M, Kwiatkowska D, Jarek A, Małkowska A, Wrzesień R, et al. Simultaneous determination of ibuprofen and its metabolites in complex equine urine matrices by GC-EI-MS in excretion study in view of doping control. J Pharm Biomed Anal. 2018;152:279–88.

[7] Padró JM, Osorio-Grisales J, Arancibia JA, Olivieri AC, Castells CB. Enantiomeric analysis of overlapped chromatographic profiles in the presence of interferences. Determination of ibuprofen in a pharmaceutical formulation containing homatropine. J Chromatogr A [Internet]. 2016;1467:255–60. Available from: http://dx.doi.org/10.1016/j.chroma.2016.05.094

[8] Ubale M, 1P.G.Dept. of Chemistry, Vasantrao Naik Mahavidyalaya A. RP-HPLC Method for Simultaneous Determination of Amlodipine Besylate and Atorvastatin Calcium : Application to Commerciallyavailable drug products. Int Arch App Sci Technol. 2014;5(1):22–7.

[9] Ali NW, Hegazy MA, Abdelkawy M, Abdelaleem EA. Simultaneous determination of methocarbamol and its related substance (guaifenesin) in two ternary mixtures with ibuprofen and diclofenac potassium by RP-HPLC method. J Liq Chromatogr Relat Technol. 2012;35(16):2229–42.

[10] Cunha RR, Chaves SC, Ribeiro MMAC, Torres LMFC, Muñoz RAA, Santos WTPD, et al. Simultaneous determination of caffeine, paracetamol, and ibuprofen in pharmaceutical formulations by high-performance liquid chromatography with UV detection and by capillary electrophoresis with conductivity detection. J Sep Sci. 2015;38(10):1657–62.

[11] Shah DA, Suthar DJ, Nagda CD, Chhalotiya UK, Bhatt KK. Development and validation of hptlc method for estimation of ibuprofen and famotidine in pharmaceutical dosage form. J Liq Chromatogr Relat Technol. 2014;37(7):941–50.

[12] Ragab MAA, Korany MA, Michail K, Issa AE, Daabees HM, Elkafrawy DS. Discrete fourier transform convoluted densitomteric peak responses for the determination of methocarbamol in different pharmaceutical mixtures in the presence of its degradation product. J Liq Chromatogr Relat Technol. 2014;37(14):1999–2020.

[13] El-Kimary EI, Ragab MAA. Derivative synchronous spectrofluorimetry: Application to the analysis of two binary mixtures containing codeine in dosage forms. Spectrochim Acta - Part A Mol Biomol Spectrosc [Internet]. 2018;204:677–84. Available from: https://doi.org/10.1016/j.saa.2018.06.102

[14] Damiani PC, Bearzotti M, Cabezón MA. Spectrofluorometric determination of ibuprofen in pharmaceutical formulations. J Pharm Biomed Anal. 2001;25(3–4):679–83.

[15] Nováková L, Matysová L, Solich P. Advantages of application of UPLC in pharmaceutical analysis. Talanta. 2006;68(3):908–18.

[16] Gumustas M, Kurbanoglu S, Uslu B, Ozkan SA. UPLC versus HPLC on drug analysis: Advantageous, applications and their validation parameters. Vol. 76, Chromatographia. 2013. 1365–1427 p.

[17] Kumar A, Saini G, Nair A, Sharma R. A preeminent technique in pharmaceutical analysis. Acta Pol Pharm. 2012;69(3):371–80.

[18] Mensch J, Noppe M, Adriaensen J, Melis A, Mackie C, Augustijns P, et al. Novel generic UPLC/MS/MS method for high throughput analysis applied to permeability assessment in early Drug Discovery. J Chromatogr B Anal Technol Biomed Life Sci. 2007;847(2):182–7.

[19] Yaman ME, Atila A. A rapid and sensitive UPLC – MS / MS method for quantification of erdosteine as bulk drug and in capsules as dosage forms. Maced Pharm Bull. 2021;67(2):23–31.

[20] Borman P, guidelines DE-IQ, 2017 undefined. Q2 (R1) validation of analytical procedures. books.google.com [Internet]. [cited 2022 Apr 23]; Available from: https://www.google.com/books?hl=tr&lr=&id=Wvk1DwAAQBAJ&oi=fnd&pg=PA127&dq=Borman,+P.,+Elder,+D.,+2017.+Validation+of+analytical+procedures:+text+and+methodology.+Q2+(R1).+++++++++++ICH+Quality+guidelines+5,+127-166.++&ots=pM8d8-hhC3&sig=p5XLtMsyb19nwZk69Gh6Xb0FQOU

[21] Method Validation in Pharmaceutical Analysis: A Guide to Best Practice - Google Kitaplar [Internet]. [cited 2022 Apr 23]. Available from: https://books.google.com.tr/books?hl=tr&lr=&id=HbBlyvlRgwkC&oi=fnd&pg=PR5&dq=Ermer,+J.,+Miller,+J.H.M.,+2006.+Method+validation+in+pharmaceutical+analysis:+A+guide+to+best+practice,+first+ed.+John+Wiley+%26+Sons.&ots=nWFpDMC5Oi&sig=1SoZdUvr6p2UBIFTI5z-IirtZBg&redir_esc=y#v=onepage&q&f=false

[22] (R1) IG-Q, 2005 undefined. Validation of analytical procedures: text and methodology. somatek.com [Internet]. 2014 [cited 2022 Apr 23]; Available from: https://somatek.com/wp-content/uploads/2014/06/sk140605h.pdf

[23] Sherwood CA, Eastham A, Lee LW, Risler J, Mirzaei H, Falkner JA, et al. Rapid optimization of MRM-MS instrument parameters by subtle alteration of precursor and product m/z targets. J Proteome Res. 2009;8(7):3746–51.

[24] Battu PR, MS Reddy. RP-HPLC Method for Simultaneous Estimation of Paracetamol and Ibuprofen in Tablets. Asian J Res Chem. 2009;2(1):70–2.

[25] Eraga SO, Arhewoh MI, Chibuogwu RN, Iwuagwu MA. A comparative UV−HPLC analysis of ten brands of ibuprofen tablets. Asian Pac J Trop Biomed [Internet]. 2015 Oct;5(10):880–4. Available from: http://linkinghub.elsevier.com/retrieve/pii/S2221169115001379

[26] Borahan T, Unutkan T, Şahin A, Bakırdere S. A rapid and sensitive reversed phase-HPLC method for simultaneous determination of ibuprofen and paracetamol in drug samples and their behaviors in simulated gastric conditions. J Sep Sci [Internet]. 2019 Feb;42(3):678–83. Available from: http://dx.doi.org/10.1016/j.apjtb.2015.06.005

[27] Sanchaniya PM, Mehta FA, Uchadadiya NB. Development and Validation of an RP-HPLC Method for Estimation of Chlorpheniramine Maleate, Ibuprofen, and Phenylephrine Hydrochloride in Combined Pharmaceutical Dosage Form. Chromatogr Res Int. 2013;2013:1–6.

[28] Arayne MS, Sultana N, Siddiqui FA, Naseem S, Qureshi F. Simultaneous determination of pyrimethamine, sulfadoxine, mefloquine, and ibuprofen in pharmaceutical formulations by RP-HPLC. Med Chem Res. 2010;19(9):1043–54.

Cilt 11, Sayı 2, Sayfa 64-69, 2022 Volume 11, Issue 2, Page 64-69, 2022

Araştırma Makalesi https://doi.org/10.46810/tdfd.1093356 Research Article

Türk Doğa ve Fen Dergisi
Turkish Journal of Nature and Science
www.dergipark.gov.tr/tdfd

# The Effects of Some Priming Applications on Seed Quality Parameters in Melon (*Cucumis melo* L.) Seeds Under Different Doses of NaCl Stress

**Tolga SARIYER[1*], Çağlar KAYA[2]**

[1] Çanakkale Onsekiz Mart University, Faculty of Agriculture, Department of Horticulture, Türkiye
[2] Çanakkale Onsekiz Mart University, Faculty of Agriculture, Department of Horticulture, Türkiye
Tolga SARIYER ORCID No: 0000-0002-1844-2996
Çağlar KAYA ORCID No: 0000-0002-7054-3081

**Corresponding author: tolgasariyer@comu.edu.tr*

(Received: 25.03.2022, Accepted: 10.05.2022, Online Publication: 29.06.2022)

**Keywords**
Priming, Melon, NaCl stress, Germination rate, Germination time

**Abstract:** Salinity of irrigation water and soil-based salinity is an important problem. Priming is an application that increases the germination rate by keeping the seeds in distilled water or different aqueous solutions for a certain period of time. Ipsala variety melon (*Cucumis melo* L.) seeds obtained from Manisa Kırkağaç region were used in the study to determine the effects of different NaCl stress and priming applications on seed quality. Melon seeds subjected to different priming applications were germinated in pure water (0 mM NaCl) and salt stress (140 mM NaCl) conditions. In the study, herbal origin thyme (*Origanum vulgare* L. subsp. *hirtum*), sage (*Salvia officinalis* L.) applications as well as $KNO_3$ (50 mM) and pure water applications were included as priming applications. In the study, it was determined that increase in the germination rate (%) and germination time (day) parameters which are important quality parameters in seeds, were more pronounced with priming applications. Priming with using sage and thyme plants were more effective respectively in increasing seed quality parameters.



# Farklı Dozlarda NaCl Stresi Uygulanan Kavun (*Cucumis melo* L.) Tohumlarında Bazı Priming Uygulamalarının Tohum Kalite Parametrelerine Etkileri

**Anahtar kelimeler**
Priming, Kavun, NaCl stresi, Çimlenme oranı, Çimlenme hızı

**Öz:** Sulama suları ve toprak kaynaklı tuzluluk, önemli bir sorun olarak karşımıza çıkmaktadır. Priming tohumların belli sürede saf su veya farklı sulu solüsyonlarda bekletilmesi şeklinde uygulanan ve çimlenme gücünü artıran bir uygulamadır. Farklı NaCl stresi ve priming uygulamalarının tohum kalitesine etkilerinin belirlenmesi amacı ile yapılan çalışmada Manisa Kırkağaç bölgesinden elde edilen İpsala çeşidi kavun (*Cucumis melo* L.) tohumları kullanılmıştır. Kavun tohumları farklı priming uygulamalarına tabi tutulmuş ardından, saf su (0 mM NaCl) ve tuz stresi (140 mM NaCl) koşullarında çimlendirilmiştir. Çalışmada priming uygulamaları olarak bitkisel kaynaklı kekik (*Origanum vulgare* L. subsp. *hirtum*), adaçayı (*Salvia officinalis* L.) uygulamalarının yanısıra $KNO_3$ (50 mM) ve saf su uygulamaları yer almıştır. Çalışmada, priming uygulamaları ile tohumda önemli kalite parametrelerinden olan çimlenme oranı (%) ve çimlenme hızı (gün) parametrelerinin artışı daha belirgin olmuştur. Çalışma değerlendirildiğinde, sırasıyla adaçayı ve kekik bitkisi kullanılarak yapılan priming uygulamaları, tohum kalite parametrelerini arttırmada daha etkili olmuştur.

## 1. INTRODUCTION

The salinity rate in our water resources is increasing day by day. Although there are salts in all surface and underground waters, this salt is transmitted to the soil by irrigation. Salinity affects the water uptake of plants negatively by increasing the osmotic pressure of soil water. Salt accumulation in the soil also negatively affects the physical and chemical properties of the soil [3]. Salt stress causes ion stress in plants as well as osmotic stress. Salt stress has a negative effect on plant growth as a result of the accumulation of ions such as $Na^+$ and $Cl^-$. The effect of salt stress varies depending on the type of salt, the level of stress, the type and genetic structure of the plant subjected to stress and the developmental stage of the plant [2].

Seeds germinate more easily in laboratory conditions than in farm conditions (farm or nursery). Because they are not exposed to the stress factors (salinity, drought, etc.) in laboratory conditions that they are exposed in farm while germinating. Therefore, it is inevitable that the germination rate will decrease in farm conditions compared to laboratory. This necessitates studies that expose seeds to various stress applications and include treatments that aimed at improving germination in stress conditions.

Various abiotic stresses lead to overproduction of reactive oxygen species (ROS), which are highly reactive and toxic in plants. These reactive oxygen species damage proteins, lipids, carbohydrates and DNA, resulting in oxidative stress [6]. According to the results of a different study [12] on the subject, reactive oxygen species increased in the cells of the elongation zone of the root tip of Arabidopsis with 200 mM NaCl application. Priming is an application that involves leaving the seeds in water under controlled conditions (imbibition) and drying the seed to its initial moisture content with the aim of improving the germination of seeds and initiating early events in germination. Primed seed is brought to a stage where metabolic processes begin with priming before planting. Therefore, primed seed is placed in a more advantageous position than unprimed seed. Primed seed can complete the remaining stages of the germination process (stage three-reimbibition of primed seed) more quickly than untreated seed [22].

Organic priming applications can be done such as using medicinal plants and can be an alternative priming method especially for producers and farmers who engaged in organic farming. Roby et al. [15], stated in their study that thyme (*Thymus vulgaris* L.), sage (*Salvia officinalis* L.), marjoram (Origanum majorana L.) plants have important antioxidant activities and they have a field of use as natural antioxidants. In the study [7], *Origanum vulgare* L. subsp. *hirtum* appears to have antioxidant activity.

Sen et al. [18], determined that NaCl and PEG applications decreased germination rate, increased reactive oxygen species and lipid peroxidation rate in three rice (*Oryza sativa*) cultivars (Neeraja, Vaisakh, Vyttila 6). In their study, they determined that the activities of metabolites as non-enzymatic antioxidant contents as well as antioxidant enzymes were significantly accelerated by different priming techniques. In a study [13], it was reported that priming applications using laurel fruit and moss had better results in pepper seeds while priming applications using dried black thyme and moss had better results in tomato seeds. In the study, it was observed that there was a high increase in germination rate with all priming applications on the third day of germination in tomato.

Özkaynak et al. [14], determined that priming applications had a positive effect on germination in their study using laurel, thyme, seaweed extracts and PEG 6000 in watermelon (*Citrullus lanatus* Thunb. cv. Toraman F1). In the study, it was stated that earlier, more homogeneous and stronger seedlings were obtained with priming applications, and it was stated that laurel, thyme and seaweed extracts could be successfully applied instead of chemical priming.

Rochalska et al. [16], have made priming applications using chamomile (30 and 100% concentration), sage (30 and 100% concentration), chamomile and sage mix (15%+15%) in beetroot (var. Czerwona Kula), sugar beet (var. Janosik) seeds. In the study, they determined that as a result of priming applications, there was an increase in germination ability (%) in both seeds 4 days after sowing, and priming applications had a positive effect on germination rate.

In study [17], with different potassium nitrate applications (0, 0.25, 0.50, 1.00, 1.50, 2.00 %) in rice varieties (KDML105 and RD15), germination percentage values were higher in the priming application with 1% $KNO_3$ than in the priming application with 2% $KNO_3$.

Priming applications made by Lara et al. [10], using polyethylene glycol (PEG 6000) -1.1MPa, 50 mM $KNO_3$, PEG+$KNO_3$ solutions in tomato. In their study, the priming application using $KNO_3$ solution had better results than other priming applications in increasing the germination power and germination rate values. The highest nitrate reductase activity was obtained as a result of priming with $KNO_3$. It was determined that priming with $KNO_3$ increased the antioxidant system activity, SOD and CAT activities by creating nitric oxide from nitrate reductase.

I another study [19], cumin seeds (*Cuminum cyminum* L.) were germinated in different salt solutions (NaCl, $CaCl_2$, $KNO_3$), at different concentrations (50, 100, 150 mM) and there was a decrease in the germination percentage under all salt stresses. In study the effect of salt stress was more pronounced with $KNO_3$ application than $CaCl_2$ and NaCl. In the study, they determined that there was no statistical difference in germination percentage as a result of 50 mM NaCl and $CaCl_2$ applications.

Aydın et al. [1], applied different levels (0, 75, 150, 250 mM) of salt stress (NaCl) in wheat (*Triticum aestivum* cv. Bezostaya), tomato (*Lycopersicon lycopersicum* cv. H55711), beans (*Phaseolus vulgaris* sp. sphearicus) and maize (*Zea mays* cv. Hido) cultivars. Germination rate, germination time, plant salt tolerance index, plant dry weight parameters were negatively affected in all varieties with 150 and 250 mM salt applications. Length of seedlings, root length, fresh weight parameters were negatively affected in all varieties with 75 mM salt application. Among the cultivars included in their study, they determined that the most tolerant cultivar was hybrid corn and the most susceptible cultivar was tomato.

Sivritepe et al. [20], applied priming for 3 days at 20 °C to Hasanbey (*Cucumis melo* L. Hasanbey'') and Kırkagac (*Cucumis melo* L. ''Kırkagac'') melon varieties with using 18 dS m-1 doses of NaCl. In their study, they

subjected the seeds to different stress applications by irrigating them with water containing NaCl at doses of 0.3, 4.5, 9.0, 13.5, 18 dS m-1. As a result of their study, when the subjects that were not primed were examined, the germination rate started to decrease at a dose of 4.5 dS m-1 NaCl in Hasanbey variety, while it started to decrease at a dose of 9.0 dS m-1 NaCl in Kırkagac variety. In their study they determined that melon seeds treated with NaCl stress at doses of 4,5, 9 dS m-1 NaCl with priming application and melon seeds treated with dose of 0,3 dS m-1 NaCl were in same statistical group in terms of germination rate. In addition, they determined that the mean germination time increased as the NaCl doses increased. In their studies, germination time decreased with priming application at all NaCl doses except 0.3 dS m-1 NaCl dose. In addition dry weight decreased in melon seedlings with increasing doses of NaCl in unprimed treatments.

The aim of the study is to determine the effects of different NaCl stress and some priming applications (pure water, herbal, chemical origin) on seed quality of melon (*Cucumis melo* L.) obtained from Manisa Kırkağaç region in Turkey where is an intense melon production.

## 2. MATERIAL AND METHOD

The research was carried out in the laboratory of Çanakkale Onsekiz Mart University, Faculty of Agriculture, Department of Horticulture in 2022. In the study, the seeds of Ipsala variety melon (*Cucumis melo* L.) grown in the Kırkagac region of Manisa province were used. Melon seeds, which were separated from the fruits harvested 50 days after full bloom in 2021, were dried using natural methods without any chemical treatment. The seeds were washed with distilled water for surface sterilization and dipped in 3% sodium hypochlorite solution for 10 seconds to disinfect the seed surface from fungi with the help of a sieve. The experiment was established according to the randomized plot design with 3 replications. 30 seeds were used in each replication in the experiment. The seeds were primed for 24 hours using solutions of dried thyme (*Origanum vulgare* subsp. hirtum), sage (*Salvia officinalis* L.) plants [16], $KNO_3$ (50 mM) and distilled water. The sage and thyme materials used in the study were obtained from a commercial store in the Çanakkale region. Primed and untreated seeds were germinated in purified water and high salinity (140 mM NaCl) conditions at 25°C. The seeds weighed before the priming application, were dried after the application in a shaded and ventilated environment until they reached their weight before the priming application. Seeds were arranged between 40×40 cm filter papers and watered with distilled water with or without NaCl in equal amounts on the first day and in equal amounts on the 7th day so that no dry areas were left on the filter papers. Seeds were kept in dark conditions in plastic bags for 14 days.

In the priming application using thyme, 5 g of dry thyme was put into 500 ml of water. The mixture was boiled and allowed to cool. 25 ml of the solution was taken, 175 ml of water was added and the application was made [13], [14]. The same application in [13], [14] was made using 5 g of sage. Sage *(Salviae folium)* was used in priming application by [16] as primed for 24 hours in red beet and sugar beet. Study consist of control, priming using 0 mM NaCl+dry thyme, priming using 0 mM NaCl+dry sage, priming using 0 mM NaCl+$KNO_3$, priming using 0 mM NaCl+pure water, priming using 140 mM NaCl, 140 mM NaCl+dry thyme, priming using 140 mM NaCl+dry sage, priming using 140 mM NaCl+$KNO_3$, priming using 140 mM NaCl+pure water applications. Thus, the study consisted of 10 subjects.

Analysis and measurements included in the study:

Germination Rate (%): Seeds that rooted out and reached 2 mm in length were stated as germinated. Seed lots were counted at the same time each day. Germination rate determined as = Number of germinated seeds Total number of seeds$^{-1}$.

Mean germination time (days): It was determined using the= $\sum \frac{n*D}{\sum n}$ formula [5].

n: Number of seeds germinated in D day hour$^{-1}$
D: Number of days from the start of germination
Σn: Total number of germinated seeds

Hypocotyl Length (mm): It was determined by measuring the length from the cotyledon leaves to the radicle thickness with the help of a caliper with a sensitivity of 0.01.

Radicle Length (mm): It was determined by measuring the length from the tip of the radicle to the end of the radicle with the help of a caliper with a sensitivity of 0.01.
Radicular Collar Thickness (mm): It was determined by measuring the thickness of the radicula just before the hypocotyl with the help of a caliper with a precision of 0.01.

Seed Vigor Index: [21].

SAS.8.0. programme was used in making statistical analyzes in the trial. Analysis of variance was performed, and the LSD (P<0.05) test was used to compare the differences between the means of the data.

## 3. RESULTS AND DISCUSSION

**Table 1.** Effects of Different NaCl and Priming Applications on Germination Rate (%)

| | Control[b] | Thyme[b] | Sage[b] | $KNO_3$[b] | Pure Water[b] |
|---|---|---|---|---|---|
| Control[a] | 91.11 [A] | 95.55 [A] | 94.44 [A] | 93.33 [A] | 92.22 [A] |
| 140 mM NaCl[a] | 61.11 [D] | 74.44 [C] | 85.55 [B] | 71.11 [C] | 73.33 [C] |

LSD P<0.05= 4.5247[c]
[a]: NaCl levels, [b]: Priming applications, [c]: LSD (P < 0.05) value

When the germination rate values were examined, it was seen that the germination rate values did not differ

statistically ($P < 0.05$) as a result of priming applications in the subjects that did not apply NaCl stress. When the unprimed subjects were examined, it was determined that the germination rate value decreased significantly ($P < 0.05$) as a result of NaCl application. It was concluded that priming application using sage plant had the highest value among the subjects to which NaCl was applied (Table 1). In a study [12], reactive oxygen species that cause oxidative stress increased with NaCl stress. In another study [18], it was determined that non-enzymatic antioxidant content and activities of antioxidant enzymes were accelerated by priming techniques. In a study, it was stated that priming applications affect germination positively in watermelon [14]. In another study [19], it was mentioned that the germination percentage of cumin decreased under different salt stresses (NaCl, $CaCl_2$, $KNO_3$).

**Table 2.** Effects of Different NaCl and Priming Applications on Germination Time (days)

| | Control[b] | Thyme[b] | Sage[b] | $KNO_3$[b] | Pure Water[b] |
|---|---|---|---|---|---|
| Control[a] | 5.35 $^{F}$ | 5.3 $^{F}$ | 5.48 $^{EF}$ | 5.33 $^{F}$ | 5.37 $^{F}$ |
| 140 mM NaCl[a] | 6.76 $^{A}$ | 5.94 $^{BC}$ | 5.66 $^{DE}$ | 6.15 $^{B}$ | 5.79 $^{CD}$ |

LSD P<0.05= 0.2562[c]
[a]: NaCl levels, [b]: Priming applications, [c]: LSD ($P < 0.05$) value

When the germination time values were examined, it was determined that the germination time increased slightly ($P < 0.05$) compared to control in the priming application using sage in subjects without NaCl stress. When the unprimed subjects were examined, it was observed that the germination time was increased statistically ($P < 0.05$) as a result of the NaCl application compared to the control application. When the subjects with NaCl application were examined, it was observed that the longest germination time was achieved in the subject that was not primed, the fastest germination was achieved in the application of priming using sage and this application was followed by pure water, thyme, and $KNO_3$ applications, respectively (Table 2). In a study [16], it was determined that priming applications had a positive effect on the germination rate of red beet and sugar beet.

**Table 3.** Effects of Different NaCl and Priming Applications on Hypocotyl Length (mm)

| | Control[b] | Thyme[b] | Sage[b] | $KNO_3$[b] | Pure Water[b] |
|---|---|---|---|---|---|
| Control[a] | 92.39 $^{C}$ | 113.97 $^{A}$ | 107.66 $^{B}$ | 91.81 $^{C}$ | 89.8 $^{C}$ |
| 140 mM NaCl[a] | 22.53 $^{E}$ | 28.73 $^{D}$ | 26.41 $^{DE}$ | 25.3 $^{DE}$ | 23.19 $^{E}$ |

LSD P<0.05= 4.7614[c]
[a]: NaCl levels, [b]: Priming applications, [c]: LSD ($P < 0.05$) value

When the hypocotyl length values were examined, it was observed that priming applications using thyme and sage had higher values than the control application ($P < 0.05$) and thyme application had the highest value in the subjects without NaCl stress. Hypocotyl length decreased significantly ($P < 0.05$) with 140 mM NaCl application. Hypocotil length of not primed seeds and seeds primed with pure water were in same statistical group ($P < 0.05$) in subjects which were treated with 140 mM NaCl. Priming application using thyme had highest hypocotyl length value in subjects treated with 140 mM NaCl (Table 3). In a study [1], 75 mM NaCl application in wheat, tomato, beans and corn reduces plant seedling and root length. In another study [14], early maturing, more homogeneous and stronger seedlings were obtained with priming applications.

**Table 4.** Effects of Different NaCl and Priming Applications on Radicle Length (mm)

| | Control[b] | Thyme[b] | Sage[b] | $KNO_3$[b] | Pure Water[b] |
|---|---|---|---|---|---|
| Control[a] | 98.17 $^{B}$ | 114.54 $^{A}$ | 112.64 $^{A}$ | 99.63 $^{B}$ | 115.73 $^{A}$ |
| 140 mM NaCl[a] | 36,39 $^{E}$ | 48,47 $^{C}$ | 40,09 $^{DE}$ | 49 $^{C}$ | 44.44 $^{DC}$ |

LSD P<0.05= 6,0948[c]
[a]: NaCl levels, [b]: Priming applications, [c]: LSD ($P < 0.05$) value

When the radicle length values were examined, it was determined that the values in the priming applications using thyme, sage and distilled water were in the same statistical group ($P < 0.05$) and were higher than the control application in the subjects without NaCl stress. It was observed that radicular length values decreased significantly ($P < 0.05$) with 140 mM NaCl application. When the subjects with 140 mM NaCl stress were examined, it was determined that the radicula length values of the subjects that were primed with thyme and $KNO_3$ were in the same statistical group ($P < 0.05$) and they had the highest values among the subjects at this NaCl stress level (Table 4). Radicle length decreased with increasing NaCl stress in some halophyte species (*Limonium sinense* Kuntze, *Glycine soja* sieb., *Sorghum sudanense* Stapf.) [11] and rice (*Oryza sativa*) genotypes [8].

**Table 5.** The Effects of Different NaCl and Priming Applications on Radicular Collar Thickness (mm)

| | Control[b] | Thyme[b] | Sage[b] | $KNO_3$[b] | Pure Water[b] |
|---|---|---|---|---|---|
| Control[a] | 1.57 $^{EF}$ | 1.53 $^{F}$ | 1.76 $^{ABCD}$ | 1.65 $^{DEF}$ | 1.68 $^{CDE}$ |
| 140 mM NaCl[a] | 1.85 $^{AB}$ | 1.86 $^{AB}$ | 1.72 $^{BCD}$ | 1.9 $^{A}$ | 1.8 $^{ABC}$ |

LSD P<0.05= 0.1442c
a: NaCl levels, b: Priming applications, c: LSD ($P < 0.05$) value

When the radicular collar thickness values were examined, fluctuations were observed and it was determined that the radicle thickness values mostly increased with priming applications (Table 5).

**Table 6.** The Effects of Different NaCl and Priming Applications on Seed Vigor Index

| | Control[b] | Thyme[b] | Sage[b] | $KNO_3$[b] | Pure Water[b] |
|---|---|---|---|---|---|
| Control[a] | 17358.9 $^{D}$ | 21841.2$^{A}$ | 20817.5 $^{B}$ | 17873.5 $^{D}$ | 18946.7 $^{C}$ |
| 140 mM NaCl[a] | 3599.1 $^{F}$ | 5745.6 $^{E}$ | 5688.1 $^{E}$ | 5278.2 $^{E}$ | 4954.9 $^{E}$ |

LSD P<0.05= 980.23
a: NaCl levels, b: Priming applications, c: LSD ($P < 0.05$) value

When the seed Vigor Index values were examined, it was determined that the $KNO_3$ application and the control application were in the same statistical group ($P < 0.05$)

in the subjects without NaCl stress. The highest seed vigor index value was determined in the priming application using thyme. It was observed that the seed vigor index decreased significantly with NaCl stress. Priming applications were significantly ($P < 0.05$) and equally effective in increasing the seed vigor index in 140 mM NaCl application (Table 6). It has been mentioned in some studies [9], [4], that priming applications in pepper (*Capsicum annuum* L.) and safflower (*Carthamus tinctorius*) are effective in reducing the negative effect of salt stress on the vigor index.

## 4. CONCLUSION

When the study was evaluated, it was determined that priming applications using thyme, sage, KNO3 and pure water were effective in reducing the negative effects of NaCl stress (140 mM) in all parameters except pure water application on hypocotyl length.

When evaluated statistically, priming applications did not affect the germination rate in subjects without NaCl stress. In subjects without NaCl application, priming applications did not affect positively to the germination time in subjects except sage application. When seed vigor index values were evaluated, thyme application had the highest value in subjects without NaCl stress.

When evaluated statistically, in reducing the negative effects of NaCl stress, sage application was more effective than other priming applications in terms of germination rate and time parameters and thyme application was more effective than other priming applications in terms of hypocotyl length. KNO3 and pure water applications never had the best effect on reducing the negative effects of NaCl stress statistically among priming applications but KNO3 application had better results against pure water application in terms of germination time, radicle length, hypocotyl length, radicular collar thickness applications.

When the data were evaluated, it was seen that sage and thyme applications were the most effective priming applications respectively.

## REFERENCES


[1] Aydın İ, Atıcı A. Tuz Stresinin Bazı Kültür Bitkilerinde Çimlenme ve Fide Gelişimi Üzerine Etkileri. Muş Alparslan Üniversitesi Fen Bilimleri Dergisi. 2015;3(2):1-15.

[2] Çulha Ş, Çakırlar H. Tuzluluğun Bitkiler Üzerine Etkileri ve Tuz Tolerans Mekanizmaları. AKU J. Sci. 2011;11(021002):11-34.

[3] Ekmekçi E, Apan M, Kara T. Tuzluluğun Bitki Gelişimine Etkisi. OMÜ Zir. Fak. Dergisi. 2005;20(3):118-125.

[4] Elouaner MA, Hannachi C. Seed priming to improve germination and seedling growth of safflower (*Carthamus tinctorius*) under salt stress. EurAsian Journal of BioSciences. 2012;6:76-84.

[5] Ellis RH, Roberts EH. Towards a Rational Basis for Testing Seed Quality. In: Hebblethwaite, P.D. (Ed.), Seed Production. Butterworths, London. 1980;605-635.

[6] Gill SS, Tuteja N. Reactive oxygen species and antioxidant machinery in abiotic stress tolerance in crop plants. Plant Physiology and Biochemistry. 2010;48:909-930.

[7] Karaboduk K, Karabacak O, Karaboduk H, Tekinay T. Chemıcal Analysıs And Antımıcrobıal Actıvıtıes Of The *Origanum vulgare* subsp. hirtum. Journal of Environmental Protection and Ecology. 2014;15(3A):1283–1292.

[8] Kazemi K, Eskandari, H. Effects of Salt Stress on Germination and Early Seedling Growth of Rice (*Oryza sativa*) Cultivars in Iran. African Journal of Biotechnology. 2011;10(77):17789-17792.

[9] Khan HA, Ayub CM, Pervez MA, Bilal RM, Shahid MA, Ziaf K. Effect of seed priming with NaCl on salinity tolerance of hot pepper (*Capsicum annuum* L.) at seedling stage. Soil & Environ. 2009;28(1):81-87.

[10] Lara TS, Lira JMS, Rodrigues AC, Rakocevic M, Alvarenga AA. Potassium Nitrate Priming Affects the Activity of Nitrate Reductase and Antioxidant Enzymes in Tomato Germination. Journal of Agricultural Science. 2014;6(2):72-80.

[11] Li Y. Effect of Salt Stress Germination and Seedling Growth of Three Salinity Plants. Pakistan Journal of Biological Sciences. 2008;11(9):1268-1272.

[12] Liu SG, Zhu DZ, Chen GH, Gao X, Zhang XS. Disrupted actin dynamics trigger an increment in the reactive oxygen species levels in the Arabidopsis root under salt stress. Plant Cell Rep. 2012;31:1219–1226.

[13] Özkaynak E, Orhan Y, Kargın İ, Tuncel M. Biber ve Domates Tohumlarında Organik Priming Uygulamaları. Black Sea Journal of Agriculture. 2020;3(4):301-307.

[14] Özkaynak E, Yüksel P, Yüksel H, Orhan Y. Karpuzda (*Citrullus lanatus* (Thunb.) Matsum. & Nakai) organik priming uygulamaları. Erciyes Üniversitesi Fen Bilimleri Enstitüsü Dergisi. 2015;30(2):149-155.

[15] Roby MHH, Sarhan MA, Selim KA, Khalel KI. Evaluation of antioxidant activity, total phenols and phenolic compounds in thyme (*Thymus vulgaris* L.), sage (*Salvia officinalis* L.), and marjoram (*Origanum majorana* L.) extracts. Industrial Crops and Products. 2013;43 (2013):827– 831.

[16] Rochalska M, Orzeszko-Rywka A, Seroka J, Najgrodzka A. Prımıng of Red Beet and Sugar Beet Seed Usıng The Infusıons Of Chamomıle And Sage. Journal of Research and Applications in Agricultural Engineering".2015;60(4):71-75.

[17] Ruttanaruangboworn A, Chanprasert W, Tobunluepop P, Onwimol D. Effect of seed priming with different concentrations of potassium nitrate on the pattern of seed imbibition and germination of rice (*Oryza sativa* L.). Journal of Integrative Agriculture. 2017;16(3):605–613.

[18] Sen A, Puthur JT. Influence of different seed priming techniques on oxidative and antioxidative responses during the germination of *Oryza sativa*

varieties. Physiol Mol Biol Plants. 2020;26(3):551–565.

[19] Shahi-Gharahlar A, Khademi O, Farhoudi R, Mirahmadi SF. Influence of Salt (NaCl, $CaCl_2$, $KNO_3$) Stress on Germination and Early Seedling Growth Traits of Cumin (*Cuminum cyminum* L.) Seed. Seed Science and Biotechnology. 2010;4 (1):37-40.

[20] Sivritepe N, Sivritepe HO, Eris A. The Effects of NaCl Priming on Salt Tolerance in Melon Seedlings Grown Under Saline Conditions. Scientia Horticulturae. 2003;97:229-237.

[21] Tatar N, Öztürk Y, Budaklı Çarpıcı E. NaCl Ön Uygulamalarının Farklı Tuz Seviyelerinde Çok Yıllık Çim (*Lolium perenne* L.)'in Çimlenme Özellikleri Üzerine Etkileri. Türk Tarım ve Doğa Bilimleri Dergisi. 2018;5(1):28–33.

[22] Varier A, Vari AK, Dadlani M. The subcellular basis of seed priming. Current Science. 2010;99(4):450-456.

Cilt 11, Sayı 2, Sayfa 70-75, 2022 Volume 11, Issue 2, Page 70-75, 2022

Araştırma Makalesi https://doi.org/10.46810/tdfd.1036402 Research Article

Türk Doğa ve Fen Dergisi
Turkish Journal of Nature and Science
www.dergipark.gov.tr/tdfd

# Preparation of Two Calix[4]arene-Functionalized Biopolymers and Evaluations of Their Extraction Abilities Against Cr(VI)/As(V) Anions

**Serkan SAYIN***

Giresun University, Faculty of Engineering, Department of Environmental Engineering, Giresun, Türkiye
Serkan SAYIN ORCID No: 0000-0003-0518-3208

**Corresponding author: serkan.sayin@giresun.edu.tr*

(Received: 14.12.2021, Accepted: 11.05.2022, Online Publication: 29.06.2022)

**Keywords**

Calix[4]arene,
Chitosan,
Cellulose,
Arsenate/dichromate,
Extraction

**Abstract:** Two calixarene-functionalized biopolymers (calixarene-functionalized chitosan and calixarene-functionalized cellulose) have been synthesized and duly characterized using FTIR, TGA and elemental analysis techniques. Furthermore, their anion extraction behaviors at various pH values have been evaluated toward dichromate and arsenate anions. Results indicated that calixarene-functionalized chitosan against dichromate ion exhibited higher extraction capability than calixarene-functionalized cellulose. Intriguingly, although a less extraction efficiency against dichromate anion was obtained by calixarene-functionalized cellulose, the arsenate anion extraction results showed that calixarene-functionalized cellulose is more effective ionophore than calixarene-functionalized chitosan.



# İki Kaliks[4]aren-Fonksiyonlu Biyopolimerlerin Hazırlanması ve Cr(VI)/As(V) Anyonlarına Karşı Ekstraksiyon Yeteneklerinin İncelenmesi

**Anahtar Kelimeler**

Kaliks[4]aren,
Kitosan,
Selüloz,
Arsenat/dikromat,
Ekstraksiyon

**Öz:** İki kaliksarene-fonksiyonlu biyopolimerler (kaliksaren-fonksiyonlu kitosan ve kaliksaren-fonksiyonlu selüloz) sentezlenmiş ve FTIR, TGA ve element analiz gibi teknikler kullanılarak uygun bir şekilde karakterize edilmişlerdir. Ayrıca, çeşitli pH lardaki anyon ekstraksiyon davranışları dikromat ve arsenat anyonlarına karşı incelenmiştir. Sonuçlar dikromat iyonuna karşı kaliksaren-fonksiyonlu kitosanın kaliksaren-fonksiyonlu selüloza göre daha büyük ekstraksiyon kabiliyetinin olduğunu gösterdi. İlginç bir şekilde, dikromat anyonuna karşı daha düşük bir ekstraksiyon verimliliği kaliksaren-fonksiyonlu selüloz ile elde edilmesine rağmen, arsenat anyon ektraksiyon sonuçları kaliksaren-fonksiyonlu selülozun kaliksaren-fonksiyonlu kitosana göre daha etkin iyonofor olduğunu gösterdi.

## 1. INTRODUCTION

In recent years, oxyanions such as dichromate and arsenate have become two of the top 20 most hazardous ions that cause serious water pollution in the world [1,2]. It has been estimated that about 140 million people who supply with arsenic contaminated drinking water face to its crucial health problems such as lung, bladder, kidney, skin cancers, ischemic heart disease, abdominal pain, cardiovascular disease etc. [3-6]. Due to its carcinogenicity and great toxicity, it has been recommended that a higher level of arsenic contaminated drinking water than 10 μg $L^{-1}$ should not be taken [5,7]. Water pollution based on dichromate compounds leakage leads similar serious issues to the environmental like arsenic [8]. Therefore, the U.S. Environmental Protection Agency (EPA) listed dichromate compounds, which are extensively used in various industries such as electroplating, leather tanning, metal finishing, steels fabrication, pigments, textile etc., in as "Group A" human carcinogen [9,10]. Excessive or long-term dichromate exposure can bring out chronic chromium poisoning, and cause severe damage to human health [10-12]. Hereby, the World Health Organization (WHO) have recommended the allowable limit contaminant level of dichromate in natural water as 0.05 mg/L [13,14]. In this sense, several methods such as chemical precipitation, reverse osmosis, ion exchanger, bio/physisorption [15], adsorption, electrodialysis etc. have been developed [10,16]. However, considering hazardous and high toxicity of these oxyanions, it is still

urgent to design an efficient and low-cost material for the removal of these anions to meet the standards of the contaminated water discharge.

Cellulose and chitin are available as the most abundant bio-sourced polymer in nature [17]. Chitosan, which is a deacetylated derivative of naturally abundant chitin [18], and its compounds have been focused attention, leading wide range of usage in various fields such as pharmaceutics, printing paper, textiles, medicine, health care products and agriculture with respect their great biocompatibility, low toxicity, shape flexibility, biodegradability, easy of processing, mechanical strength and efficient sorption properties [19-24]. Cellulose, which is a homopolymer comprised D-glucopyranose units [25], is also an important polysaccharide derivative like chitosan. Its unique features such as non-toxicity, biodegradable, renewable and biocompatibility makes cellulose attractive for industrial applications [26].

Over the years, a great deal of attentions has been devoted on calixarenes being a third generation of macrocycles due to their versatile three-dimensional structures, easy preparation and possible limitless functionalization with any kind of organic or inorganic substituents in their upper and lower rims [27,28]. Hereby, calixarenes have been successfully employed as the promising organic compounds for ion carriers, ion selective electrodes, catalysis applications, solid-phase support materials, enzyme-mimics, drug-delivery agents, gas sensors, and ion recognition [29-36].

In the present work, two biopolymers functionalized with calix[4]arene were prepared in order to use as potential ionophores for the removal of hazardous dichromate/arsenate ions from aqueous solutions. For this aim, the calix[4]arene dihydrazide derivative has been synthesized and then immobilized onto chitosan and/or cellulose biopolymer. Furthermore, the removal efficiencies of calix[4]arene-functionalized cellulose and calix[4]arene-functionalized chitosan towards dichromate/arsenate ions at different pH values have been investigated for the first time.

## 2. EXPERIMENTAL

### 2.1. Reagents and Instrumentation

A SRS OptiMelt MPA 100 instrument in a sealed capillary tube was used to determine melting points of compounds. NMR spectra of the compounds were recorded on a Bruker Avance III 400 MHz spectrometer. A Jasco FT/IR-6600 apparatus were employed to obtain ATR-FTIR spectra. Absorbance measurements were recorded on a Mapada UV-6100 PCS Double Beam UV-visible instrument. Elemental analyses were obtained using a Costech ECS 4010 analyzer. TLC analyses were performed on DC Alufolien Kieselgel 60 $F_{254}$ (Merck). All starting materials and reagents were purchased from Merck commercial source. Sodium salts of the anions were used in sorption studies. Doubly distilled water was used to prepare methyl violet solution ($4.5 \times 10^{-5}$ M ), ammonium molybdate solution ($3.15 \times 10^{-2}$ M) and HCl solution (6.85 M).

### 2.2. Synthesis

Literature procedures were used to synthesize the calixarene derivatives **1-3**, **Cel-iso**, **Chi-iso**, **Cel-Calix**, and **Chi-Calix** [35-38].

#### 2.2.1. Synthesis of *p-tert*-butylcalix[4]arene dihydrazine amide (3)

Yield: 1.6 g (53.3%); m.p.: 330-333ºC. IR (KBr): 1687 $cm^{-1}$ (C=O). $^1$H NMR (400 MHz $CDCl_3$): δ 1.02 (s, 18H, $Bu^t$), 1.26 (s, 18H, $Bu^t$), 2.15 (d, 4H, *J*= 1.6 Hz, $NH_2$), 3.42 (d, 4H, *J*=13.3 Hz, $ArCH_2Ar$), 4.11 (d, 4H, *J*=13.2 Hz, $ArCH_2Ar$), 4.63 (s, 4H, $OCH_2$), 6.92 (s, 4H, ArH), 7.10 (s, 4H, ArH), 7.70 (s, 2H, OH), 9.61 (brs, 2H, NH). Anal. calcd. for $C_{48}H_{64}N_4O_6$: C; 72.70, H; 8.13, N; 7.06 (%). Found (%): C; 71.58, H; 8.27, N; 7.01.

#### 2.2.2. General procedure for preparation of calix[4]arene-functionalized biopolymers (Chi-Calix and Cel-Calix)

Typically, a mixture of 0.2 g of calixarene derivative **3** and 0.6 g of biopolymer (**Chi-iso** or **Cel-iso**) in 10 mL of DMF was stirred at 70ºC. The reaction completion was monitored by IR in which the peak of isocyanate group at around 2260 $cm^{-1}$ needed to be disappeared. The reaction temperature was cool down, and the mixture was filtered off. Then, $CH_2Cl_2$ was used to remove excess of derivative **3**. The FTIR spectral data for **Chi-Calix** is as ATR $cm^{-1}$: 1651 (C=O). The FTIR spectral data for **Cel-Calix** is as ATR $cm^{-1}$: 1698 (C=O).

### 2.3. Dichromate/Arsenate Anion Extraction Studies

To estimate extraction capacities of calixarene-functionalized biopolymers toward arsenate and dichromate ions, a literature procedure was applied [2]. Generally, 10 mL of an aqueous solution of $Na_2Cr_2O_7$ or $Na_2HAsO_4$ ($1.0 \times 10^{-4}$ M) and 25 mg of calixarene-functionalized biopolymer (**Chi-Calix** or **Cel-Calix**) were shaken at 175 rpm, 25 ºC for 1 h. The residual concentration of dichromate and/or arsenate anion in aqueous phase was estimated using UV-vis spectrometer at 346 and/or 610 nm according to the literatures [2,39]. HCl and KOH solutions were carried out to adjust the pH values of aqueous solutions at 25 ºC. Eq. (1) was applied to calculate the extraction percentages (E %);

$$E\ \% = 100(A_0 - A)/A_0 \quad (1)$$

where $A_0$ and A are the concentrations of dichromate or arsenate ion before and after extraction.

## 3. RESULTS AND DISCUSSION

### 3.1. Synthesis and Characterization of Calixarene-functionalized Biopolymers

The main goal of this study is to fabricate the efficient and selective ionophores for the removal of toxic and highly danger arsenate and dichromate anions from aqueous solutions. For the goal, two calix[4]arene-functionalized biopolymers (**Cel-Calix** and **Chi-Calix**) were prepared according to the literature procedures (see **Scheme 1**) [38]. The structures of two calix[4]arene-functionalized biopolymers were determined using FTIR (ATR), TGA and elemental analysis techniques. The FTIR spectra attributed that the characteristic vibration bands of isocyanate units of **Cel-iso** (2272 $cm^{-1}$) and **Chi-iso** (2263 $cm^{-1}$) were disappeared when they were treated with the calix[4]arene-dihydrazide **3** in order to afford their corresponding biopolymers. Moreover, the FTIR spectra of **Cel-Calix** and **Chi-Calix** confirmed the existence of carbonyl groups in which a characteristic vibration bands of C=O units were obtained at 1698 and 1651 $cm^{-1}$, respectively. Findings address the confirmation of the conversion of isocyanate subunits to amide moieties. The elemental analysis of **Cel-Calix** and **Chi-Calix** also contributed to assess their structure. As seen in Table 1, elemental analysis data in which 9.24 and 3.41 % nitrogen contents were found respectively for **Cel-Calix** and **Chi-Calix** showed the consistency with the expected formulas.

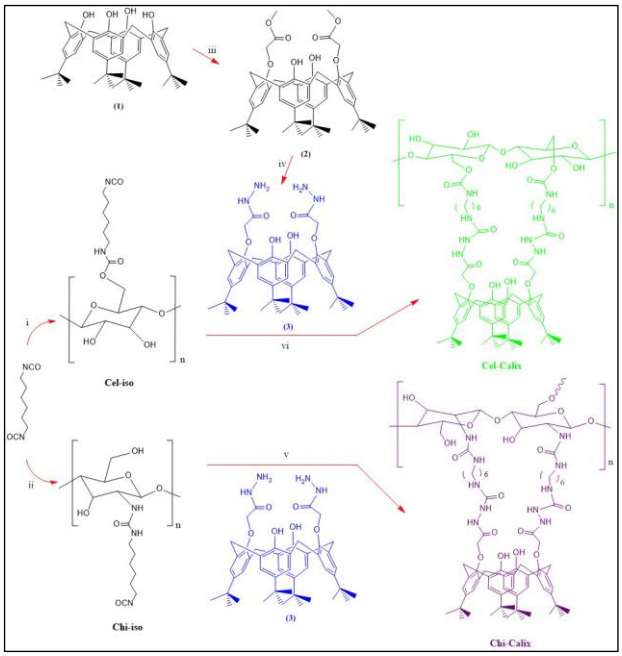


**Scheme 1.** Preparation of two calix[4]arene-functionalized biopolymers (**Cel-Calix** and **Chi-Calix**). Reaction conditions: (i) Chitosan, 70ºC; (ii) Cellulose, 70ºC; (iii) $K_2CO_3$, methylbromoacetate, reflux; (iv) Hydrazine, r.t.; (v) **Chi-iso**, 70ºC; (vi) **Cel-iso**, 70ºC.

**Table 1.** Elemental analysis for two calix[4]arene-functionalized biopolymers **(Cel-Calix** and **Chi-Calix)**

| | C(%) | H(%) | N(%) |
|---|---|---|---|
| **Cel-Calix** | 45.71 | 6.81 | 3.41 |
| **Chi-Calix** | 43.12 | 7.33 | 9.24 |

Further evidence for calix[4]arene-functionalized biopolymers came from their thermal behaviors. The experimental results are illustrated in **Figure 1** imply that **Chi-Calix** and **Cel-Calix** exhibit high thermochemical stability, as evidenced by the 4.2 % and a minor weight-loss respectively at 50-200 ºC, which are probably because of the loss of water and the external solvent molecules. Upon heating, the main weight loss of **Chi-Calix** was shown to be 62.3 % between the temperature of 200 and 525 ºC, while a 83.4 % for the decomposition of both calix[4]arene and biopolymer groups of **Cel-Calix** were observed within a broad temperature of 274 and 525 ºC.

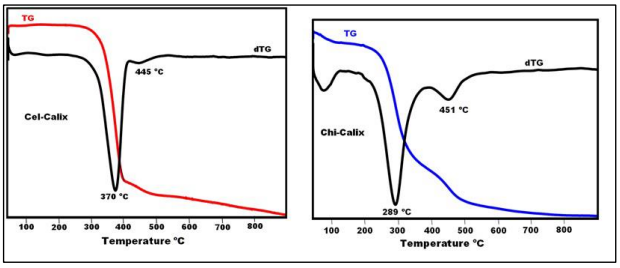


**Figure 1.** TGs and dTG curves of **Cel-Calix** and **Chi-Calix**.

### 3.2. Anion Extraction Studies

#### 3.2.1 Dichromate anion extraction behaviors of calix[4]arene-functionalized biopolymers

The dimeric $HCr_2O_7^-$ form of oxyanion species of dichromate ion becomes dominant when the pH value below of 6 in the solution [40]. So, this form of dichromate anion is capable to build hydrogen bonds with the ionophores. In view of the fact that, two calix[4]arene-functionalized biopolymers bearing amide moieties, which are able to perform the sites for hydrogen bonding as well as interaction with sodium cation [41], were employed as potential ionophores towards the sodium salt of dichromate at the pH ranges between 2.5 and 4.5.

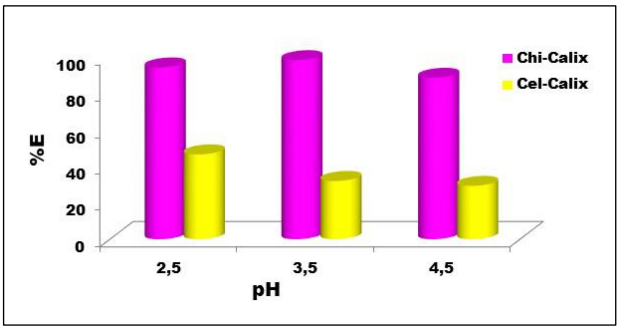


**Figure 2.** Extraction percentages of $HCr_2O_7^-$ anion by **Chi-Calix** and **Cel-Calix**. Solid phase= 25mg; aqueous phase, $Na_2Cr_2O_7$= $1.0x10^{-4}$ M at 25ºC for 1h.]

The dichromate binding efficiencies of two calix[4]arene-functionalized biopolymers were carried out using a solid-liquid extraction procedure. As illustrated in **Figure 2**, these ionophores are capable for the removal of dichromate anion from aqueous solution at the pH ranges between 2.5 and 4.5. Considering their rigid structures and containing amide moiety, which is

able to construct hydrogen bonding and interact with sodium cation, results were not a surprise. However, the maximum percentages of $HCr_2O_7^-$ anion by **Chi-Calix** and **Cel-Calix** were 46.6 and 98.4%, respectively. This result indicates that **Chi-Calix** exhibited higher extraction efficacy than **Cel-Calix** at low pHs (2.5-4.5).

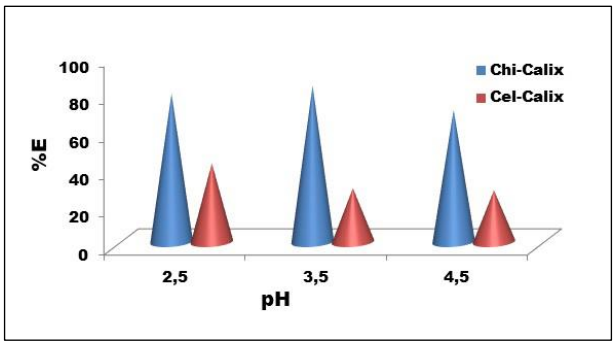


**Figure 3.** Percentage extraction of sodium cation by calix[4]arene-functionalized biopolymers at various pHs. Solid-phase, 25 mg **Chi-Calix**; aqueous-phase, $Na_2Cr_2O_7$= 1.0x10$^{-4}$ M at 25ºC for 1h.

To investigate the role of sodium cation on dichromate anion extraction by calixarene-functionalized biopolymers, the levels of residual sodium cation in the aqueous solution after extraction were estimated by atomic absorption. The results are shown in **Figure 3** indicate that the pronounced sodium extraction attributes an ion-pair mechanism in which the amide moieties of **Chi-Calix** and **Cel-Calix** interact with sodium cation.

### 3.2.2 Arsenate anion extraction behaviors of calix[4]arene-functionalized biopolymers

It is well known that the pH values of the solution affect the formation of arsenate species. For instance, the $H_2AsO_4^-$ form from the arsenate species occurs in the solution at a pH range of 3 and 6, while a higher pH value (8-11) in the solution leads the divalent $HAsO_4^{2-}$ form. The $H_2AsO_4^-$ and $HAsO_4^{2-}$ forms among the arsenate species are potential to construct the hydrogen bonding along with their electrostatic attraction features to the host molecules. Therefore, two calix[4]arene-functionalized biopolymers bearing amide moieties were employed as potential ionophores towards the sodium salt of arsenate at pH 5-8.

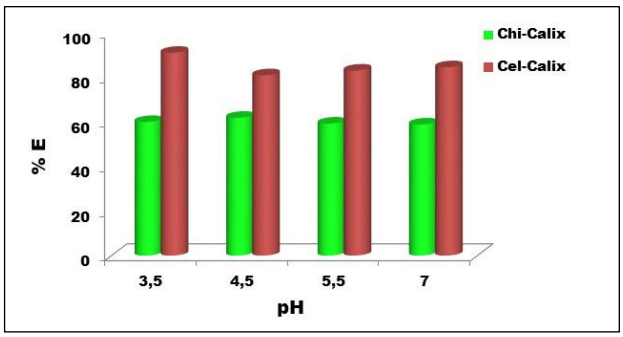


**Figure 4.** Extraction percentages of $H_2AsO_4^-$ anion with **Chi-Calix** and **Cel-Calix** at pH 3.5-7.0. (ionophore = 25 mg, aqueous phase, $Na_2HAsO_4$ = 1.0 x 10$^{-4}$ M (10 mL) at rt for 1 hour).

To assess the extraction binding characteristics of **Chi-Calix** and **Cel-Calix** towards arsenate anion at various pHs, a solid-liquid extraction procedure was performed. Typically, 25 mg of calixarene-functionalized biopolymer (**Chi-Calix** or **Cel-Calix**) and 10 mL aqueous solution of $Na_2HAsO_4$ (1.0 x 10$^{-4}$ M) interacted at 175 rpm and 25 ºC for 1 h. The percentages of the removed arsenate from aqueous solution were estimated using UV-vis spectrometer at 610 nm according to the literatures [2,39]. The extraction results of **Chi-Calix** and **Cel-Calix** in **Figure 4** indicate that both calix[4]arene-functionalized biopolymers provide effective extraction properties towards arsenate ions at pH 3.5-7.0. However, it was found that **Cel-Calix** exhibited higher extraction efficiencies than **Chi-Calix** at all pH values. The maximum extraction percentage of **Cel-Calix** towards $H_2AsO_4^-$ ion was 91.1% at pH 3.5, while a maximum extraction in 61.9% at pH 4.5 was obtained in the presence of **Chi-Calix**. The lowest values as 81 and 58.9% were received for **Cel-Calix** and **Chi-Calix**, respectively. Obtained results are in compatible with the data received from dichromate extraction by two calix[4]arene-biopolymers. Hence, findings clearly addresses that $H_2AsO_4^-$ anion with sodium cation was effective extracted as an ion-pair from aqueous solutions in the presence of ionophores (**Chi-Calix** and **Cel-Calix).** The proposed interaction of **Cel-Calix** with these anions is given in **Fig. 5**.

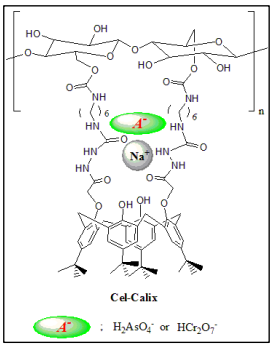


**Figure 5.** The proposed complexation phenomena of **Cel-Calix** with sodium salts of dichromate and arsenate ions.

## 4. CONCLUSION

In summary, two calix[4]arene-functionalized biopolymers (**Cel-Calix** and **Chi-Calix**) have been successfully prepared and characterized. Furthermore, the extraction capabilities of two calix[4]arene-functionalized biopolymers were evaluated with regard to arsenate and dichromate anions that are toxic and highly danger for human beings. The results showed that both calixarene-functionalized biopolymers exhibited considerable extraction properties for the removal of $H_2AsO_4^-$ and $HCr_2O_7^-$ ions at different pHs. Intriguingly, **Chi-Calix** showed higher affinity towards dichromate ion, while maximum extraction percentages for arsenate ion were obtained by **Cel-Calix**. Besides, the experimental results reflected that the extraction efficacies of calixarene-functionalized biopolymer against both anions were not depended on the pHs. Indeed, sodium cation detection experiments into residual aqueous solutions clearly illustrate that the ionophores (**Chi-Calix** and **Cel-Calix**) have an affinity

towards sodium ion, leading an efficient extraction of oxyanions as an ion-pair form from aqueous solutions.

**Acknowledgements**

I would like to thank the Research Foundation of Giresun University (FEN-BAP-A-160317-43) for financial support for this work.

**REFERENCES**

[1] Chen R, Zhang Z, Feng Z, Lei Z, Li Y, Li M, Shimizu K, Sugiura N. Batch study of arsenate (V) adsorption using Akadama mud: Effect of water Mineralization. Appl Surf Sci. 2010;256:2961-7.

[2] Sayin S, Ozcan F, Yilmaz M. Synthesis and evaluation of chromate and arsenate anions extraction ability of a N-methylglucamine derivative of calix[4]arene immobilized onto magnetic nanoparticles. J Hazard Mater. 2010;178:312-9.

[3] Weerasundara L, Ok Y-S, Bundschuh J. Selective removal of arsenic in water: A critical review. Environ Pollut. 2021;268:115668.

[4] Wei Y, Wei S, Liu C, Chen T, Tang Y, Ma J, Yin K, Luo S. Efficient removal of arsenic from groundwater using iron oxide nanoneedle array-decorated biochar fibers with high Fe utilization and fast adsorption kinetics. Water Res. 2019;167:115107.

[5] Watson M, Nikic J, Tubic A, Isakovski MK, Solic M, Dalmacija B, Agbaba J. Repurposing spent filter sand from iron and manganese removal systems as an adsorbent for treating arsenic contaminated drinking water. J Environ Manage. 2022;302:114115.

[6] Talukder ME, Pervez MN, Jianming W, Gao Z, Stylios GK, Hassan MM, Song H, Naddeo V. Chitosan-functionalized sodium alginate-based electrospun nanofiber membrane for As (III) removal from aqueous solution. J Environ Chem Eng. 2021;9:106693.

[7] WHO|WHO Guidelines for Drinking-Water Quality, fourth ed. World Health Organization, Geneva, 2011, ISBN 978-92-4-154995-0.

[8] Sayin S, Ozcan F, Yilmaz M. Two novel calixarene functionalized iron oxide magnetite nanoparticles as a platform for magnetic separation in the liquid–liquid/solid–liquid extraction of oxyanions. Mater Sci Eng. C 2013;33:2433-9.

[9] Basu D, Blackburn K, Harris B, Neal MW, Stoss FW. Health Assessment Document for Chromium. US Environmental Protection Agency, Office of Research and Development, Research Triangle Park, NC 1984.

[10] Jena SR, Choudhury J. 3D Metallo-organic coordination assembly-based anion-enriched supramolecular material for fast and efficient removal of Cr2O72-. J Hazard Mater. 2021;405:124242.

[11] Junejo R, Jalbani NS, Memon S, Kaya S, Erkan S, Serdaroğlu G, Palabiyik I M. Equilibrium, Thermodynamic, and Density Functional Theory Modeling Studies for the Removal of Dichromate Ions from Wastewater Using Calix[4]arene Modified Silica Resin. J Chem Eng Data 2021;66:1379-88.

[12] Sayin S. Synthesis of new anthracene-substituted calix[4]triazacrown-5 as highly sensitive fluorescent chemosensor and extractant against hazardous dichromate anion. Luminesc. 2021;36:1716-24.

[13] Zhang F, Du N, Li H, song S, Hou W. Sorbent effect on the sorption of Cr(VI) on a Mg6AlFe-layered double hydroxide and its calcined product in aqueous solutions. Colloid Polym Sci. 2015;293:1961-9.

[14] Fan L, Zhou B, Zhang S, Hu S, Mi X, Sun R, Wu Y. Adsorptive Removal of Low‐Concentration Cr(VI) in Aqueous Solution by Mg–Al Layered Double Oxides. Bull Environ Contam Toxicol. 2021;106: 134-45.

[15] Kozlowski CA, Walkowiak W. Removal of chromium(VI) from aqueous solutions by polymer inclusion membranes. Water Res. 2002;36:4870-6.

[16] Nawaz R, Ali K, Ali N, Khaliq A. Removal of chromium(VI) from industrial effluents through supported liquid membrane using trioctylphosphine oxide as a carrier. J Braz Chem Soc. 2016;27:209-20.

[17] Upadhyay U, Sreedhar I, Singh SA, Patel CM, Anitha KL. Recent advances in heavy metal removal by chitosan based adsorbents. Carbohydr Polym. 2021;251:117000.

[18] Ganji F, Abdekhodaie MJ. Chitosan–g-PLGA copolymer as a thermosensitive membrane. Carbohydr Polym. 2010;80:740-6.

[19] Wang W, Meng Q, Li Q, Liu J, Zhou M, Jin Z, Zhao K. Chitosan Derivatives and Their Application in Biomedicine. Int J Mol Sci. 2020;21:487.

[20] Zhao D, Zhu Y, Cheng W, Chen W, Wu Y, Yu H. Cellulose-Based Flexible Functional Materials for Emerging Intelligent Electronics. Adv Mater. 2021;33:2000619.

[21] Alves NM, Mano JF. Chitosan derivatives obtained by chemical modifications for biomedical and environmental applications. Int J Biol Macromol. 2008;43:401-14.

[22] Muzzarelli RAA. Chitins and chitosans for the repair of wounded skin, nerve, cartilage and bone. Carbohydr Polym. 2009;76:167-82.

[23] Ravi-Kumar MNV. A review of chitin, chitosan applications. React Funct Polym. 2000;46:1-27.

[24] Ta HT, Dass CR, Dunstan DE. Injectable chitosan hydrogels for localized cancer therapy. J Control Release 2008;126:205-16.

[25] Pandey A, Soccol CR, Nigam P, Soccol VT. Biotechnological potential of agro-industrial residues. I: Sugarcane bagasse. Bioresour Technol. 2000;74:69-80.

[26] Li J, Zhang L-P, Peng F, Bian J, Yuan T-Q, Xu F, Sun R-C. Microwave-Assisted solvent-free acetylation of cellulose with acetic anhydride in the presence of iodine as a catalyst. Molecules 2009;14:3551-66.

[27] Sayin S, Doğan V. Synthesis and properties of novel magnetic nanoparticles grafted with nitropyridine-substituted calix[4]arene derivative as Cr6+ extractant. Turk J Chem. 2015;39:130-8.
[28] Tekin M, Cevik E, Sayin S, Yildiz HB. Photocurrent and hydrogen production by overall water splitting based on polymeric composite Calix [n]arene/Cyanin Dye/IrO2 nanoparticle. Int J Hydrog Energy 2020;45:19869-79.
[29] Ramirez FdM, Serrano-Valero E, Varbanov S. Octaphosphinoylated para-tert-butylcalix[8]arene as an extracting agent for uranyl ions in an acidic nitrate medium: study of the extracted uranyl calixarene compound. J Radioanal Nucl Chem. 2020;323:651-62.
[30] Sayin S, Ozbek C, Okur S, Yilmaz M. Preparation of the ferrocene-substituted 1,3-distal p-tert -butylcalix[4]arene based QCM sensors array and utilization of its gas-sensing affinities. J Organomet Chem. 2014;771:9-13.
[31] Sayin S. Synthesis of New Quinoline-Conjugated Calixarene as a Fluorescent Sensor for Selective Determination of Cu2+ Ion. J Fluoresc. 2021;31:1143-51.
[32] Alizada M, Gül A, Oguz M, Kursunlu AN, Yilmaz M. Ion sensing of sister sensors based-on calix[4]arene in aqueous medium and their bioimaging applications. Dyes Pigm. 2021;184:108741.
[33] Jalbani NS, Solangi AR, Memon S, Junejo R, Bhatti AA, Yola ML, Tawalbeh M, Karimi-Maleh H. Synthesis of new functionalized Calix[4]arene modified silica resin for the adsorption of metal ions: Equilibrium, thermodynamic and kinetic modeling studies. J Mol Liq. 2021;339:116741.
[34] Ozyilmaz E, Ascioglu S, Yilmaz M. Calix[4]arene tetracarboxylic acid-treated lipase immobilized onto metal-organic framework: Biocatalyst for ester hydrolysis and kinetic resolution. Int J Biol Macromol. 2021;175:79-86.
[35] Gutsche CD, Nam KC. Calixarenes.22. synthesis, properties, and metal complexation of aminocalixarenes. J Am Chem Soc. 1988;110:6153-62.
[36] Collins EM, McKervey MA, Madigan E, Moran MB, Owens M, Ferguson G, Harris SJ. Chemically modified calix[4]arenes. Regioslective synthesis of 1,3-(distal) derivatives and related compounds.x-ray crystal structure of a diphenol-dinitrile. J Chem Soc Perkin Trans.1 1991;12:3137-42.
[37] Alekseeva EA, Bacherikov VA, Gren AI, Baukov YI. Synthesis of p-tert-Butylcalix[4]arene derivatives containing amino acid residues. Russ J Gen Chem. 2000;70:490-2.
[38] Ozyilmaz E, Sayin S. Preparation of New Calix[4]arene-Immobilized Biopolymers for Enhancing Catalytic Properties of Candida rugosa Lipase by Sol–Gel Encapsulation. Appl Biochem Biotechnol. 2013;170:1871-84.
[39] Sayin S, Ozcan F, Yilmaz M. Preparation and Application of Calix[4]arene Derivatives Bearing Pyridinium Units-Grafted Magnetite Nanoparticles for Removal of Dichromate and Arsenate Anions. J Macromol Sci, Part A: Pure Appl Chem. 2011;48:365-72.
[40] Sayin S, Yilmaz M. Synthesis of a new calixarene derivative and its immobilization onto magnetic nanoparticle surfaces for excellent extractants toward Cr(VI), As(V), and U(VI). J Chem Eng Data. 2011;56:2020-9.
[41] Ozcan F, Ersoz M, Yilmaz M. Preparation and application of calix[4]arene-grafted magnetite nanoparticles for removal of dichromate anions. Mater Sci Eng. C 2009;29:2378-83.

Cilt 11, Sayı 2, Sayfa 76-81, 2022 Volume 11, Issue 2, Page 76-81, 2022

Araştırma Makalesi https://doi.org/10.46810/tdfd.1106743 Research Article

Türk Doğa ve Fen Dergisi
Turkish Journal of Nature and Science
www.dergipark.gov.tr/tdfd

# Investigation of Microstructural, Mechanical and Corrosion Properties of Cu-10Sn Bronze Parts Produced by Selective Laser Melting

**Mustafa Naci TOP [1], Semih ÖZBEY [2], Batuhan SORUŞBAY[2], H.Özkan GÜLSOY [2*]**

[1] Marmara University, Institute Graduate Studies Pure and Applied Sciences, 34722, Göztepe-Istanbul, Türkiye
[2] Marmara University, Technology Faculty, Metalurgy and Materials Eng., 34722, Göztepe-Istanbul, Türkiye

Mustafa Naci TOP ORCID No: 0000-0002-8947-6245
Semih ÖZBEY ORCID No: 0000-0001-5582-9973
Batuhan SORUŞBAY ORCID No: 0000-0001-8108-1399
H.Özkan GÜLSOY ORCID No: 0000-0001-5366-5741

**Corresponding author: ogulsoy@marmara.edu.tr*

(Received: 21.04.2022, Accepted: 23.05.2022, Online Publication: 29.06.2022)

**Keywords**
Selective Laser Melting, Cu-Sn alloy, Microstructure, Mechanical properties, Corrosion resistance

**Abstract:** In this study, the production of full-density Cu-10Sn bronze parts by selective laser melting (SLM) technique and the examination of microstructural, mechanical and corrosion properties were carried out. Cu-10Sn pre-alloyed powders produced by gas atomization technique were shaped using SLM technique within selected parameters and then microstructural properties were determined. Depending on the microstructural properties, the mechanical and corrosion behaviors were determined. The obtained results were compared with similar bronze materials produced by conventional methods. Different characterization techniques were used for microstructural characterization. The microstructure of the Cu-10Sn alloy was observed to consist of dendritic primary α and δ-$Cu_{41}Sn_{11}$ phases. According to the mechanical test results of the samples produced at densities of 8.75 g $cm^{-3}$ at room temperature, the yield strength was measured as 420 MPa, the tensile strength was 578 MPa, the elongation was 32 % and the hardness value was 160.3 $HV_{0.2}$. For the electrochemical experiments, the corrosion rate of the samples was found to be 4.38 mpy. As a result of the productions and experiments, it was determined that the samples produced by the SLM method provide very good mechanical and corrosion properties compared to the literature.



# Seçici Lazer Ergitme Tekniği İle Üretilmiş Cu-10Sn Bronz Parçaların Mikroyapısal, Mekanik ve Korozyon Özelliklerinin İncelenmesi

**Anahtar Kelimeler**
Seçici Lazer Ergitme, Cu-Sn alaşımı, Mikroyapı, Mekanik özellikler, Korozyon direnci

**Öz:** Bu çalışmada, tam yoğunluklu Cu-10Sn bronz parçaların seçici lazer ergitme (SLM) tekniği ile üretilmesi, mikroyapısal, mekanik ve korozyon özelliklerinin incelenmesi gerçekleştirilmiştir. Gaz atomizasyon tekniği ile üretilmiş Cu-10Sn ön-alaşımlı tozlar, seçilen parametreler dahilinde SLM tekniği kullanılarak şekillendirilmiş ve sonrasında mikroyapısal özellikleri belirlenmiştir. Mikroyapısal özelliklere bağlı olarak mekanik ve korozyon davranışlarının belirlenmesi gerçekleştirilmiştir. Elde edilen sonuçlar geleneksel metotlar ile üretilmiş benzer bronz malzemeler ile karşılaştırılmıştır. Mikroyapısal karakterizasyon için farklı inceleme teknikleri kullanılmıştır. Cu-10Sn alaşımının mikroyapısının dendritik birincil α ve δ-$Cu_{41}Sn_{11}$ fazlarından oluştuğu görülmüştür. 8,75 g $cm^{-3}$ yoğunluklarda üretilen numunelerin oda sıcaklığında gerçekleştirilen mekanik deney sonuçlarına göre, akma mukavemeti 420 MPa, çekme mukavemeti 578 MPa, % uzama değeri 32 ve sertlik değeri 160,3 $HV_{0.2}$ olarak ölçülmüştür. Gerçekleştirilen elektrokimyasal deneylere göre numunelerin korozyon hızının 4,38 mpy değerlerinde olduğu görülmüştür. Gerçekleştirilen üretimler ve deneyler sonucunda SLM yöntemiyle üretilen numunelerin literatüre kıyasla oldukça iyi mekanik ve korozyon özellikleri gösterdiği belirlenmiştir.

## 1. INTRODUCTION

Cu-Sn alloys are traditionally used in the manufacture of musical instruments, artistic objects and engineering applications. In addition, Cu-Sn alloys are frequently used in electronics, aerospace and defense applications due to their high strength, superior wear resistance, high corrosion resistance, good weldability, high thermal and electrical properties. Other important application areas are heat exchangers, high precision springs and bearings, electronic fasteners and plastic deformation sensitive applications [1–5].

Owing to superior resistance to corrosion in seawater, Cu–Sn alloys have also been adopted in the marine industry as propulsion devices [2, 3]. In general, bronze with low level of Sn (less than 5 wt.%) intended for plastic working is widely used in electrical and electronic industries such as sensitive elements of pressure gauges and electrical connectors as well as high-precision springs. With the increase of Sn content, mechanical properties can be strengthened. When the Sn content exceeds 10%, alloy exhibit excellent mechanical properties, wear resistance and corrosion resistance [6]. Post-machining processes, such as forging, rolling, drawing, and/or bending, are essential for manufacturing precise and complex mechanical parts of alloys in desired shapes. However, the formation of the brittle δ phase in the high tin bronze alloy causes difficulties during plastic deformation. Therefore, the Cu–Sn alloys with tin content above 10%, termed high-tin bronze, is fabricated primarily by casting [3, 7]. In traditional casting technology, decrease in mechanical properties due to large grain size, shrinkage cavity and pores, the low solubility in the solid solution phase and serious grain boundary segregation, and the inability to produce complex parts in conventional powder metallurgy limits the production of Cu-Sn alloys. Compared with traditional casting technology, the novel-developed additive manufacturing (AM) technology can fabricate parts with complex structures with improved microstructure and mechanical properties, avoiding the defects introduced by casting technology [4]. Selective laser melting (SLM), a laser powder-bed fusion process, is one of the frontrunners in the accepted AM technologies. SLM, where production is done layer by layer, offers the ability to produce complex structural parts that have unchallenged design freedom, maximum material savings, high dimensional accuracy, and excellent surface finish. Using SLM, many engineering materials, including steels, Ni-alloys, Co-alloys, Ti-alloys, Al-alloys, high-entropy alloys, etc., have been successfully fabricated with properties comparable to those achieved in conventional processing methods [1, 8]. SLM also offers the possibility to produce metastable phases and microstructures due to its small size (µm size volume) melt pool and corresponding high cooling rates [9, 10].

Due to the layer-by-layer production of parts in the SLM technique, parts undergo complex thermal cycles. Rapid cooling rates with SLM cause nonequilibrium solidification, increase in solid solubility and finer grain size [11]. Moreover, the high thermal gradient and local inhomogeneous heating-cooling cycles result in a heterogeneous microstructure with high dislocation density and cellular structure [12, 13]. The unique microstructures developed during the SLM process allow the development of high-performance materials compared to their counterparts produced by conventional methods [11, 14, 15].

Due to copper's high thermal conductivity, the melt area experiences rapid heat dissipation and high local thermal gradients, resulting in delamination, layer curling, and part failure [16]. In addition, it has been determined that the production of copper alloys is relatively easy compared to pure copper [2, 11]. While alloying elements added to copper significantly reduce its conductivity, it widens the solidification range and lowers the Gibbs melting energy. As a result, sufficient time is provided for the molten metal to spread evenly over the previous layer to achieve good bonding with low porosity [16, 17]. With all this information, it seems possible to produce Cu-Sn bronze parts with the AM technique and to use them especially for marine applications.

In this study, Cu-10Sn bronze samples were produced by SLM technique to investigate the production of Cu-based alloys by additive manufacturing. The densities of the produced samples were measured according to the Archimedes principle. The microstructure, mechanical properties and corrosion behavior of the samples were examined and the findings were discussed in consideration of the literature. Experimental studies include scanning electron microscopy (SEM) and X-ray diffraction (XRD) analysis for initial powder morphology, microstructural evolution and analysis of fractured surfaces; Tensile tests and hardness measurements were performed to determine the mechanical properties, and electrochemical measurements were performed to determine the corrosion behavior.



## 2. MATERIALS AND METHODS

While preparing the samples, PM-BR101P (Powmet, Italy) spherical bronze powders (Cu-10Sn) produced by gas atomization, especially developed for laser melting applications, were used. Gas atomized powders are generally spherical in shape and exhibit high purity, fluidity and packaging properties [18, 19]. Powder morphology was visualized with FEI-Srion brand SEM and images are given in Figure 1. It is observed from that the particle shape of Cu-10Sn pre-alloyed powders is in spherical shape and the median particle size of the powders is suitable for using in AM applications. The powder surfaces are quite smooth and there is no satelliteing. Also, Malvern Mastersizer device was used to determine the particle size distribution of the powders. The physical properties of the powders are given in Table 1. The average particle size of the powders was found to be 50 µm. Phase analysis of the powders was performed on Rigaku brand D/MAX RINT 2200 (Japan) model XRD device.

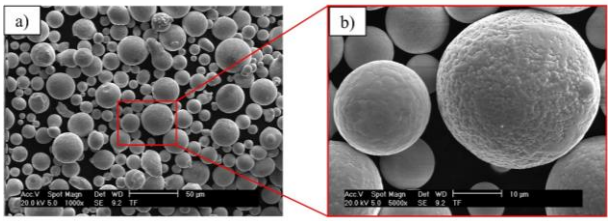


**Figure 1.** SEM images of Cu-10Sn powder: a) 1000 magnification, b) 5000 magnification.

**Table 1.** Physical properties of Cu-10Sn powders.

| Physical Properties | | |
|---|---|---|
| **Density, g cm$^{-3}$** | 8.77 | |
| **Apparent density, g cm$^{-3}$** | 3.90 | |
| **Tapped density, g cm$^{-3}$** | 4.20 | |
| **Particle Size Distribution, µm** | $D_{10}$ | 16 |
| | $D_{50}$ | 25 |
| | $D_{90}$ | 38 |

Two types of samples, whose images are given in Figure 2, to be used in tensile test and metallographic examinations, were produced under nitrogen atmosphere with SISMA-MYSINT100 PM (Italy) SLM device equipped with Yb-YAG, and the process parameters are given in Table 2. The energy density was calculated using Equation 1. During the production, the chess (5mmx5mm) scanning strategy was used as laser strategy.

$$E = \frac{P}{v * h * t} \qquad (1)$$

where the energy density E (J mm$^{-2}$) is a measure of average applied energy per unit volume of material, P is laser power (in W), v is laser scan speed (in mm s$^{-1}$), h is hatch spacing (in mm) and t is layer thickness (in mm) [8]. The samples were produced on a 10 cm diameter table, four bars of 10 mm diameter, 25 mm high for metallographic examinations, and two non-standard 70 mm length, 25 mm high bars to be used in the tensile test. The tensile test specimens were shaped by slicing into 2 mm thick pieces using a precision cutting machine. After grinding and polishing, samples surface roughness was made suitable for tensile testing. XRD analyzes were carried out on the building and scanning directions and the phases formed in different directions were analyzed. The samples to be used in metallographic examinations were electrolytically etched in a solution containing 50% HF and 50% distilled water for 5-10 s after the grinding and polishing. The samples were also examined in both directions at high magnifications using SEM. In the density measurements made using Archimedes principle, the average densities (at least 5 samples) were measured as 8.75 g cm$^{-3}$ (relative densities of 99.5%).

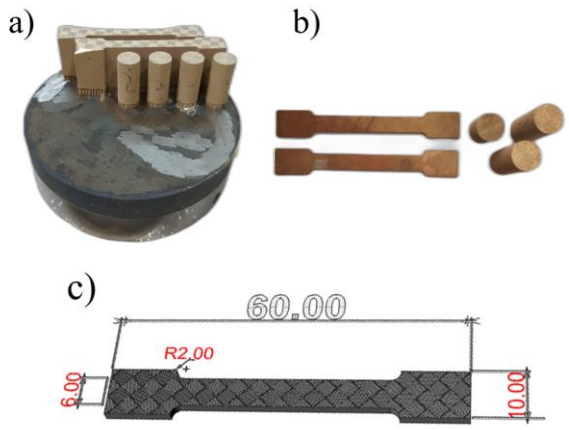


**Figure 2.** a) Sample images after SLM production, b) prepared samples for tensile test and metallographic investigation c) sample measurements prepared for the tensile test.

**Table 2.** SLM production parameters.

| Laser Power W | Scan Speed mm s$^{-1}$ | Hatch Spacing µm | Layer Thickness µm | Energy Density J mm$^{-3}$ |
|---|---|---|---|---|
| 110 | 1200 | 60 | 20 | 76 |

Microhardness measurements were made with FUTURE-TECH brand FM-310E (Japan) model microhardness device in both directions. Tensile tests were carried out on 10 specimens at a tensile speed of 25.4 mm/min with a Zwick-Z250 model device at room temperature. Tests were conducted as per the crosshead speed control method defined by ASTM E-8 standard. The fracture surfaces of the specimens that broke as a result of the tensile test were examined by SEM. The corrosion behavior of the samples was investigated in a standard 3-electrode system using a GAMR Interface 1000 (UK) potentiometer device in a seawater medium containing 3.5% NaCl. Saturated calomel electrode (SCE) was used as reference electrode and graphite electrode as counter electrode. The reliability of the experimental results was increased by repeating the mechanical tests on 5 different samples and the corrosion tests on 3 different samples.

## 3. RESULTS AND DISCUSSION

XRD analyzes of the powders and both building and scanning direction of the samples produced by the SLM method are given in Figure 3. When the XRD analyzes are examined, it is seen that the XRD results of the phases in the scanning direction and the powders are similar. In the both directions, the structure consists of α-Cu(Sn) and δ-$Cu_{41}Sn_{11}$ phases, while the construction direction consists of only the α-Cu(Sn) phase. The δ-$Cu_{41}Sn_{11}$ phase is formed as a result of rapid cooling in the scanning direction. [20].

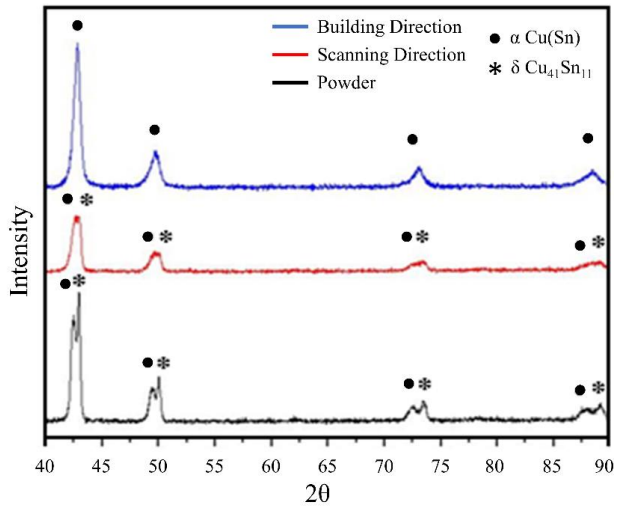


**Figure 3.** XRD analysis of the powders, and produced samples in the building and scanning direction.

In the SEM examinations carried out to determine the microstructures of the samples in the direction of building, it was determined that the rapid and local melting and cooling provided by the SLM technique causes very fine microstructures and very small porosities at the grain boundaries. SEM images taken from the building direction are given in Figure 4. In the building direction microstructure, especially the melting pool regions are visible and there are irregular grain boundaries between each melting pool.

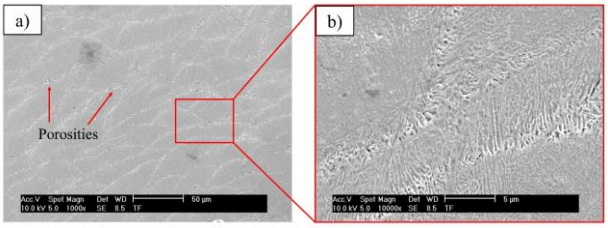


**Figure 4.** SEM images of the sample in the building direction: a) 1000 magnification, b) 10000 magnification.

As can be seen from high magnification SEM images, it is known that such cellular structures are due to rapid cooling and eutectic solidification. In the SEM examinations made in the scanning direction, it is seen that the δ-$Cu_{41}Sn_{11}$ phases are distributed in the microstructure, and the SEM images are given in Figure 5.

SEM image of the scanning direction given in Figure 6, it is seen that the microstructure consists of α + δ eutectoic (light color) and dendritic α (dark color) phases. In particular, the existence of very fine cellular structures consisting of α + δ phases has been observed. SEM investigations of building and scanning are in agreement with XRD analysis results.

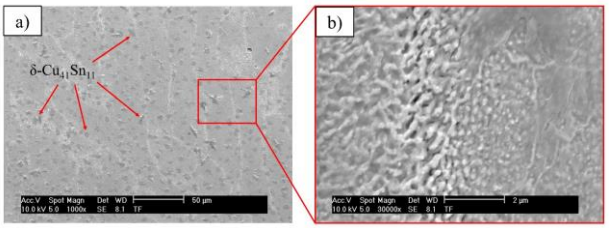


**Figure 5.** SEM images of the sample in the scanning direction: a) 1000 magnification, b) 30000 magnification.

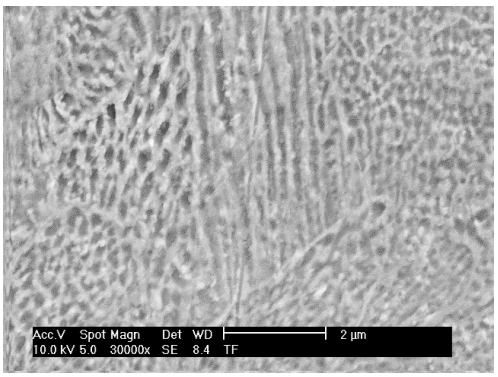


**Figure 6.** SEM image of the sample in the scanning direction: 30000 magnification.



As a result of the hardness measurements carried out in both directions, the highest and lowest hardness values in the building direction were 158.6 $HV_{0.2}$ and 150.6 $HV_{0.2}$; in the scanning direction, it was measured as 166.2 $HV_{0.2}$ and 161.7 $HV_{0.2}$. Although the hardness values are close to each other, the difference is due to the high hardness of the δ-$Cu_{41}Sn_{11}$ phases formed in the scanning direction [3].

The stress-strain graph obtained from tensile test is given in Figure 7, and it was observed that the sample showed an excellent combination of high strength (yield strength ~452 MPa, tensile strength ~578MPa) and ductility (32%). Compared to the Cu-10Sn alloys produced by the SLM technique in the literature, very high values were obtained. [2, 8, 21, 22]. Comparison of SLM production parameters is given in Table 3.

**Table 3.** Literature comparison of SLM production parameters.

| Alloy | Laser Power W | Scan speed mm $s^{-1}$ | Hatch Spacing µm | Layer Thickness µm | Energy Density J $mm^{-3}$ | Yield and Tensile Strength MPa | Reference |
|---|---|---|---|---|---|---|---|
| Cu-10Sn | 271 | 210 | 90 | 90 | ~159 | 220 / 420 | [2] |
| Cu-13Sn | 350 | 750 | 120 | 30 | 130 | ~404 / ~635 | [8] |
| Cu-10Sn | Variable | Variable | 120 | 30 | - | - / ~550 | [21] |
| Cu-10Sn | 95 | ~377, ~360, ~344 | 60 | 20 | 210, 220, 230 | ~386 / ~469 | [22] |
| Cu-10Sn | 110 | 1200 | 60 | 20 | 76 | ~452 / ~578 | Current Study |
| Cu-10Sn (Casting) | -- | -- | -- | -- | -- | 152 / 310 | [23] |

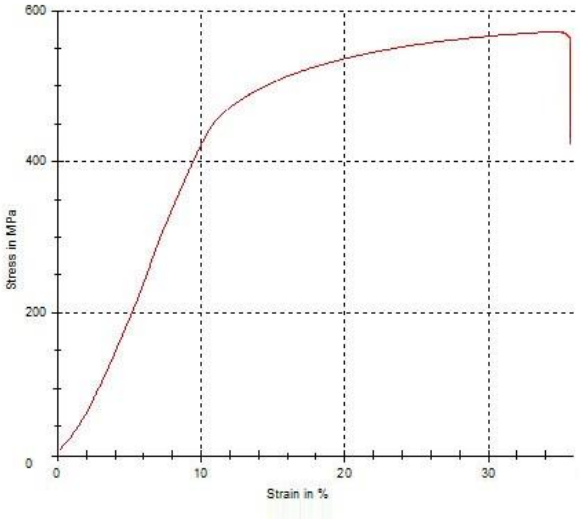


**Figure 1.** Stress-strain graph.

In order to interpret the fracture mechanisms of the samples as a result of the tensile tests, the fracture surfaces were examined by SEM and the images are given in Figure 8. As seen in Figure 8.b, there are dimples on the fracture surface, which are the biggest indication of ductile fracture. The large number of dimples in small size means that more surface energy is produced during fracture and therefore the strength of the material is higher. In addition, the size of the dimples is dependent on the size of the subgrains. [24]. The macropores in Figure 8.a, on the other hand, are thought to be formed as a result of ruptures especially from the edges of the melting pool.

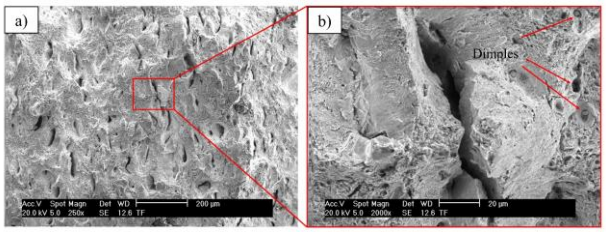


**Figure 2.** SEM images of the fracture surface: a) 250 magnification, b) 2000 magnification.

In Figure 9, decreasing in current density with the potential increasing has indicated that the protective layer has initiated to stably form on the sample surface. The formation of protective layer above 100mV is completely stable form and it remains with the potential increasing. Thus, it is known that the passive layer occurs on the material surface in the Tafel curve, the current density does not change with increasing potential. The data obtained by the Tafel method are given in Table 4. The corrosion rate was found to occur at 4,388 miles (1 mil=0.001 inch) per year.

Existing two and more phases in surface have sensitivity to galvanic corrosion in a corrosive media [25]. The full-density Cu-10Sn bronze parts produced by selective laser melting (SLM) technique has consist of primary α and δ-$Cu_{41}Sn_{11}$ phases. Phase distributions in the microstructure of Cu-10Sn bronze significantly affect the local corrosion development. Since primary δ-$Cu_{41}Sn_{11}$ phases higher corrosion resistance than primary α, primary δ-$Cu_{41}Sn_{11}$ phase acts as a cathode; on the other hand, primary α acts as anode [26]. Thus, the alpha phase, which is the anodic part, is significantly corroded. This has been emphasized in a previous similar study [27].

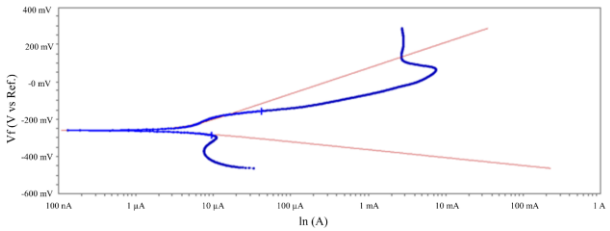


**Figure 3.** Tafel curve obtained from the corrosion test.

**Table 4.** Data obtained from the corrosion test.

| | |
|---|---|
| Beta A | 138,0e-3 V/decade |
| Beta C | 42.,50e-3 V/decade |
| $I_{corr}$ | 3,860 uA |
| $E_{corr}$ | -261,0 mV |
| Corrosion rate | 4,388 mpy |

## 4. CONCLUSION

Cu-10Sn bronze samples with almost full density (99.5%) were produced by SLM technique and their microstructure, mechanical and corrosion properties were examined and compared with other studies in the literature. As a result of XRD analysis, it was determined that α-Cu(Sn) and δ-$Cu_{41}Sn_{11}$ phases were formed in the scanning direction and α-Cu(Sn) phases in the building direction. As a result of the tensile, hardness and corrosion tests, the parts produced with SLM technique showed superior mechanical (yield strength 420 MPa, tensile strength 578 MPa, % elongation 32 and hardness value 160.3 $HV_{0.2}$) and corrosion properties (Corrosion Rate: 4.388 mpy). These findings prove that the complex shape and high strength Cu-10Sn bronze alloy can be produced effectively by SLM technique.



## Acknowledgement

This study (Project no: FEN-C-YLP-130219-0042) was supported by Marmara University.

## REFERENCES

[1] Li X, Ivas T, Spierings AB, Wegener K. Phase and microstructure formation in rapidly solidified Cu-Sn and Cu-Sn-Ti alloys. J Alloys Compd 2018;735: 1374–1382.

[2] Scudino S, Unterdörfer C, Prashanth KG, Attar H, Ellendt N, Unhlenwinkel V, et al. Additive manufacturing of Cu–10Sn bronze. Mater Lett 2015; 156:202–204.

[3] So S-M, Kim K-Y, Lee S-J, Yu Y-J, Lim H-A, Oh M-S. Effects of Sn content and hot deformation on microstructure and mechanical properties of binary high Sn content Cu–Sn alloys. Mater Sci Eng A 2020;796.

[4] Yang P, Guo X, He D, Shao W, Tan Z, Fu H, et al. Microstructure Twinning and Mechanical Properties of Laser Melted Cu-10Sn Alloy for High Strength

and Plasticity. Journal of Materials Engineering and Performance. 2022;31: 2624-2632.
[5] Mao Z, Zhang D, Wei P, Zhang K. Manufacturing Feasibility and Forming Properties of Cu-4Sn in Selective Laser Melting. Materials 2017; 10: 333.
[6] Mao Z, Zhang DZ, Jiang J, Fu G, Zhang P. Processing optimization, mechanical properties and microstructural evolution during selective laser melting of Cu-15Sn high-tin bronze. Mater Sci Eng A 2018; 721: 125–134.
[7] Park JS, Park CW, Lee KJ. Implication of peritectic composition in historical high-tin bronze metallurgy. Materials Characterization 2009; 60(11): 1268–1275.
[8] Karthik GM, Sathiyamoorthi P, Zargaran A, Park JM, Asghari-Rad P, Son S, et al. Novel precipitation and enhanced tensile properties in selective laser melted Cu-Sn alloy. Materialia 2020; 13: 100861.
[9] Prashanth KG, Scudino S, Klauss HJ, Surreddi K.B., Löber L, Wang Z, et al. Microstructure and mechanical properties of Al–12Si produced by selective laser melting: Effect of heat treatment. Materials Science and Engineering: A. 2014; 590: 153–160.
[10] Ma P, Prashanth K, Scudino S, Jia Y, Wang H, Zou C, et al. Influence of Annealing on Mechanical Properties of Al-20Si Processed by Selective Laser Melting. Metals 2014; 4(1): 28–36.
[11] Wang J, Zhou XL, Li J, Brochu M, Zhao Y. Microstructures and properties of SLM-manufactured Cu-15Ni-8Sn alloy. Additive Manufacturing. 2019; 31: 100921.
[12] Liu L, Ding Q, Zhong Y, Zou J, Wu J, Chiu Y, et al. Dislocation network in additive manufactured steel breaks strength–ductility trade-off. Materials Today 2018; 21: 354–361.
[13] DebRoy T, Wei HL, Zuback JS, Mukherjee T, Elmer J.W, Milewski J.O, et al. Additive manufacturing of metallic components – Process, structure and properties. Progress in Materials Science. 2018; 92: 112–224.
[14] Uchida S, Kimura T, Nakamoto T, Ozaki T, Miki T, Takemura M, et al. Microstructures and electrical and mechanical properties of Cu-Cr alloys fabricated by selective laser melting. Mater Des 2019; 175: 107815.
[15] Ventura AP, Marvel CJ, Pawlikowski G, Bayes M, Watanabe M, Vinci R, et al. The Effect of Aging on the Microstructure of Selective Laser Melted Cu-Ni-Si. Metallurgical and Materials Transaction A. 2017; 48(12): 6070–6082.
[16] Tran TQ, Chinnappan A, Lee JKY, Loc NH, Tran LT, Wang G, et al. 3D Printing of Highly Pure Copper. Metals 2019; 9: 756.
[17] Tiberto D, Klotz UE, Held F, Wolf G. Additive manufacturing of copper alloys: influence of process parameters and alloying elements. Materials Science and Technology. 2019; 35: 969–977.
[18] Irrinki H, Jangam JSD, Pasebani S, Badwe S, Stitzel J, et al. Investigation of 17-4 PH Stainless Steel Fabricated by Laser- Powder Bed Fusion. International Conference on Innovative Engineering Applications, CIEA 2018. Sivas.
[19] Irrinki H, Nath SD, Alhofors M, et al. Microstructures, properties, and applications of laser sintered 17-4PH stainless steel. J Am Ceram Soc 2019; 102: 5679–5690.
[20] Ludwig A, Grasser M, Schillinger W. Experimental Investigation on the Ternary Phase Diagram Cu–Sn–P. World of Metallurgy. 2012; 65: 117-125.
[21] Gu R, Yao X, Wang D, Hang H, Yan M, Wong KS. Selective Laser Melting of Cu–10Sn–0.4P: Processing, Microstructure, Properties, and Brief Comparison with Additively Manufactured Cu–10Sn. Advanced Engineering Materials. 2022; 24(2): 2100716.
[22] Deng C, Kang J, Feng T, Wang X, Wu P. Study on the Selective Laser Melting of CuSn10 Powder. Materials 2018; 11(4): 614.
[23] B05 Committee. Specification for Copper Alloy Continuous Castings. ASTM International. DOI: 10.1520/B0505_B0505M-12.
[24] Yao H, Tan Z, He D, Zhou Z, Xue Y, Chui L, et al. High strength and ductility AlCrFeNiV high entropy alloy with hierarchically heterogeneous microstructure prepared by selective laser melting. Journal of Alloys and Compounds. 2020; 813: 152196.
[25] Fu N, Tang X, Li D.Y, Parent L, Tian H. In situ investigation of local corrosion at interphase boundary under an electrochemical-atomic force microscope. Journal of Solid-State Electrochemistry. 2015, 19: 337-344.
[26] Šatovic D, Zulj L.V, Desnica V, Fazinic S, Martinez S. Corrosion evaluation and surface characterization of the corrosion product layer formed on Cu–6Sn bronze in aqueous Na2SO4 solution. Corrosion Science. 2009; 51(8): 1596-1603.
[27] Zeng C, Zhang B, Hemmasian A, Wen H, Yao H, Meng W.J, et al. Mechanical, thermal, and corrosion properties of Cu-10Sn alloy prepared by laser-powder-bed-fusion additive manufacturing. Additive Manufacturing. 2020; 35(7): 101411.

Araştırma Makalesi https://doi.org/10.46810/tdfd.1107332 Research Article

Türk Doğa ve Fen Dergisi
Turkish Journal of Nature and Science
www.dergipark.gov.tr/tdfd

# Investigation of Seismic Behavior of Buildings With Different Infill Wall Materials

**Pınar USTA**[1*]

[1] Isparta University of Applied Science, Technology Faculty, Civil Engineering Department, Isparta, Türkiye
Pınar USTA ORCID No: 0000-0001-9809-3855

**Corresponding author: pinarusta@isparta.edu.tr*

(Received: 22.04.2022, Accepted: 24.05.2022, Online Publication: 29.06.2022)

**Keywords**
Infillwalls, Earthquake, AAC, Conventional Brick, Reinforced Concrete

**Abstract:** Different masonry materials are commonly used construction materials for buildings. When the current situation of reinforced concrete structures under the earthquake effect is examined, it is seen that there are differences in the behavior of the reinforced concrete structures depending on the properties of the materials that are used in the reinforced concrete structures. The reason for this situation is related to the physical properties of the preferred material. The frame systems of reinforced concrete structures are completed with infill walls. Aerated autoclaved concrete and conventional brick materials are used as infill wall materials in most of the reinforced concrete structures built in Turkey. In this paper, the finite element program was used to analyze the current state of reinforced concrete structures with infilled walls under the earthquake effects. A reinforced concrete framed structure model was designed using the SAP2000 finite element program, two different materials were preferred in the model structure and four different model combinations were designed. The first two models are designed with infill walls, but the ground floor and the other models are designed with infill walls for the whole building. Nonlinear static pushover analyses were conducted, and base shear, displacement, and story drift values were obtained. All the results were presented by graphics. The data obtained from the model with Aerated autoclaved concrete material, which has a low unit volume weight under the effect of the earthquake, is healthier than the model with conventional brick material.



# Farklı Dolgu Duvar Malzemesine Sahip Binaların Deprem Davranışının İncelenmesi

**Anahtar Kelimeler**
Dolgu duvar, Deprem, Gazbeton, Tuğla, Betonarme bina

**Öz:** Binalarda yapı malzemesi olarak farklı yığma malzemeler yaygın olarak kullanılmaktadır. Betonarme yapıların deprem etkisi altındaki mevcut durumu incelendiğinde, betonarme yapılarda kullanılan malzemelerin özelliklerine bağlı olarak betonarme yapıların davranışlarında farklılıklar olduğu görülmektedir. Deprem etkisinde betonarme yapıların mevcut durumu incelediğinde betonarme yapıların kullanılan malzemelerin özelliklerine göre yapı davranışında farklılıklar meydana gelmiştir. Bu durumun sebebi tercihe dilen malzemenin fiziksel özellikleriyle ilişkilidir. Betonarme yapıların çerçeve sistemi dolgu duvarlarla tamamlanmaktır. Türkiye'de inşaa edilen betonarme yapılarda dolgu duvarlarda gazbeton ve tuğla malzemeler kullanılmıştır. Bu çalışmada, dolgu duvarlı betonarme yapıların deprem etkileri altındaki mevcut durumunu analiz etmek için sonlu elemanlar programı kullanılmıştır. SAP2000 sonlu elemanlar programı kullanılarak betonarme çerçeveli bir yapı modeli tasarlanmış, model yapısında iki farklı malzeme tercih edilmiş ve dört farklı model kombinasyonu tasarlanmıştır. İlk iki model dolgu duvarlı olarak tasarlanmıştır ancak zemin kat ve diğer modeller tüm bina için dolgu duvarlı olarak tasarlanmıştır. Doğrusal olmayan statik itme analizleri yapılarak taban kesme, deplasman ve kat öteleme değerleri elde edilmiştir. Sonuç olarak tüm sonuçlar grafiklerle sunulmuştur. deprem etkisi altında birim hacim ağırlığı düşük olan gaz beton malzemeli modelden elde edilen verilerin tuğla malzemeli modele göre daha sağlıklı olduğu tespit edilmiştir.

## 1. INTRODUCTION

Reinforced concrete skeleton (carcass) structures are often preferred due to the ease of construction and the rapid progress of the works, and generally, these frames are filled with wall infill panels (or) concrete blocks in most countries located in seismic zones. Masonry infills contribute significant lateral stiffness, strength, overall

ductility, and energy dissipation capacity. These elements act as compression supports between column and beam, transferring forces from one node to another. the infill walls increase the mass of the building whereas reducing the natural vibration periods. Past earthquakes show that infill walls have significant structural effects on the earthquake performance of the building. Reinforced concrete (RC) frame buildings with masonry infill and shear walls for elevators are commonly constructed around the world, including in seismic areas. this reinforced concrete (RC) frame buildings are usually encountered as commercial, industrial and multi-storey residential apartments. Masonry infill walls and shear walls for elevators are extremely effective in resisting lateral seismic loads on the building. Therefore, the use of masonry infill and shear walls for elevator in reinforced concrete frames changes the lateral load transfer mechanism responsible for the reduction in bending moments and increase in axial forces. The elements called infill walls that are constructed between the columns and beams of the reinforced concrete frame are usually made with a conventional brick wall, aerated autoclaved concrete, pumice, and concrete block. These infill walls, which are generally not considered in the design process, are considered non-structural components [1]–[4].

Infill walls contribute significantly to the strength and rigidity of structures, neglect of infill walls causes buildings to collapse. Masonry walls are used for functional and architectural needs in reinforced concrete buildings. The term infilled frame describes a composite structure consisting of a moment resisting reinforced concrete frame and infill walls. In these infill walls, filling materials such as traditional clay brick, concrete block, AAC block are used as building materials [5].

Infill wall panels are widely used also in our country due to aesthetic and functional demands. Most of the existing building stock in Turkey is under seismic risk. In this context, it is thought that a significant part of the existing structures will probably collapse or be severely damaged during a strong earthquake.

The most common type of damage in reinforced concrete and masonry structures is shear cracks caused by shear forces [6]. Masonry structures have low tensile strength compared to reinforced concrete structures and their energy consumption capacity against earthquake forces is also very low [7], [8].

In this context, it is thought that a significant part of the existing structures will probably collapse or be severely damaged during a strong earthquake. Literature studies also support this fact [9], [10]. Turkey, one of the most seismically active countries of the world in terms of its geological features, is situated on an active area surrounded by active faults [11]. Earthquakes in Turkey demonstrate that 92% of the our country's land is susceptible to earthquake risk [12]. The earthquakes that occurred in Turkey between 1990 and 2021 and the distribution of these earthquakes are shown in Figure 1 and Figure 2.

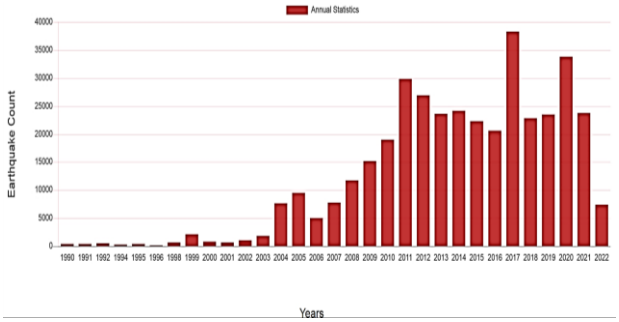


**Figure 1.** Earthquakes in Turkey between 1900-2022 [13]

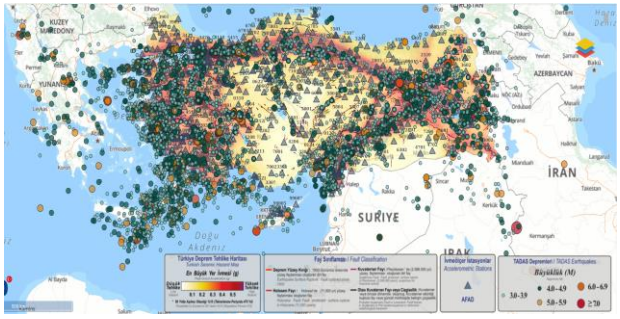


**Figure 2.** Turkey earthquake map and distribution of earthquakes [14]

Brick and stone have been used as building materials from past to present. As carrier material; While mostly brick material was used in the Seljuk period, stone was used in the Ottoman period. Brick is one of the most important building materials widely used to build walls and other elements, especially in the construction industry [6]. Brick is one of the most important building materials widely used to build walls and other elements, especially in the construction industry. However, the continued use of clay bricks in the construction industry leads to a large-scale loss of fertile topsoil in our country. This situation will inevitably create an environmentally destructive danger in the future. Environmental pollution from the brick production process contributes to global warming and climate change. Moreover, the air temperature can cause the brick surface to deteriorate due to frost damage, leading to global warming, which is now a global concern. Various types of blocks are used as an alternative to red bricks to reduce environmental pollution and global warming problems. Aerated autoclaved concrete blocks can be one of the solutions to replace traditional clay bricks [15].

Aerated autoclaved concrete is a material developed by Eriksson (1923) at the Royal Technical Institute in Stockholm, Sweden, and patented for production in 1924. Nowadays, Aerated autoclaved concrete is widely used in 135 countries on 6 continents [16]. Because Aerated autoclaved concrete wall panels are lightweight, highly thermally insulated, high fire protection, high sound insulation, low water absorption, environmentally friendly, and easy to apply [15].

As in different construction methods, it is necessary to verify whether the Aerated autoclaved concrete blocks used for structural purposes have sufficient and necessary resistance to seismic effects. Design rules for

structures constructed with Aerated autoclaved concrete blocks that can be used as load-bearing elements in walls have recently been included in the Turkish earthquake code [10].

Soft-storey buildings are multi-storey buildings with wide gates, commercial areas at ground level, and open space usually for parking. A soft storey may occur due to the lower rigidity of the first floor as a result of using less masonry infill walls on the first floor, or because the first may have a greater height than the other storey due to commercial reasons. [17]. Soft storey collapse is due to the high column strength demand of the first storey compared to the other storey. The presence of traditional brick infill walls sharing the forces on the upper storey and the fact that the upper storey is more rigid than the first soft storey effectively reduces the column forces. The lateral displacement of the entire structure is governed by the first soft storey of the building. [18].

Soft floor irregularity is seen in the ground floors designed for commercial use, when walls are not built in order to obtain wide, glazed spaces with high floor heights. If the infill walls on the ground floor work together with the load-bearing system and the ground floor, which has no walls, does not work together with the carrier system, relative displacements occur on the floor and a soft floor situation occurs [19] [20].

In reinforced concrete structures, due to the difference in stiffness between the ground floor and the first floor, large cross-sectional effects occur on the ground floor carrier columns. Great stresses occur in the ground floor columns due to earthquake forces and plastic hinges occur due to the growth of lateral displacements [19].

Choosing the normal storey heights less than the ground storey height, discontinuity of the infill walls, designing more spacious areas for service-oriented commercial spaces on the ground storey in the frame design of reinforced concrete buildings are led to soft storey irregularities. When the damage conditions in the buildings are examined after the earthquakes, it is seen that the soft storey irregularity prevents the buildings from being reliable and stable [20]–[22].

Examining the building damage in past earthquakes, it has been observed that typically buildings with no or very few walls on the ground storey, compared to the upper storey, suffered major damage at the ground storey level. Because the resistance of the ground storey, which is devoid of walls, against horizontal displacements is very low compared to the upper storey, which are rich in walls. Ground Storey with no walls and/or relatively large storey heights are the focal point of earthquake damage in buildings [22].

In order to reduce human losses, it is imperative to evaluate the performance of structures exposed to natural events such as earthquakes; and it is an issue that concerns the whole world [23]. This paper works presents a numerical study to investigate the effect of the masonry infill material on the seismic performance of an RC framed building subjected to dynamic loading considering the effects of the different masonry infill material. For this purpose, reinforced concrete building was modeled in four different ways by using the SAP2000 (ver. 23.0) finite element program [24]. The building was analyzed according to two different masonry infill materials, aerated autoclaved concrete and brick building materials, and whether the building has an infill wall on the ground storey or not .

Nonlinear static thrust analysis was performed on the reinforced concrete structure and the base shear force, structure displacement and storey drift values of the models were obtained. The values are compared and presented with graphs.

## 2. MODELLING OF INFILL WALLS

Various equivalent diagonal strut formulas and methods are available to find the width of compression struts. The diagonal braces were connected to the beam-column junction with a joint moment-free connection; thus they can only receive compression forces. The modeling of the infill wall can be done using the finite element method or the static equivalent strut approach. This is the model used in the study. In this type of modeling, the stiffness of the wall is considered in the loading plane. In infill walls placed in a lateral load-resistant frame, the stiffness and strength contribution of the infill are taken into account by modeling the infill as an equivalent strut approach. In this study, FEMA-356 [25] is used to find the width of compression struts.



The equivalent width of a diagonal compression strut, a, is given by:

$$w = 0.172\,(\lambda_1 H)^{-0.4} d_{inf} \quad (1)$$

$$\lambda_1 = \left[\frac{E_{inf} t_{inf} sin2\theta}{4 E_c I_{col} h}\right]^{0.24} \quad (2)$$

$$\theta = tan^{-1}\left(\frac{h_{inf}}{L_{inf}}\right) \quad (3)$$

From the above-given formula, the width of compression struts was calculated. Diagonal Strut Parameters are given in Figure 3.

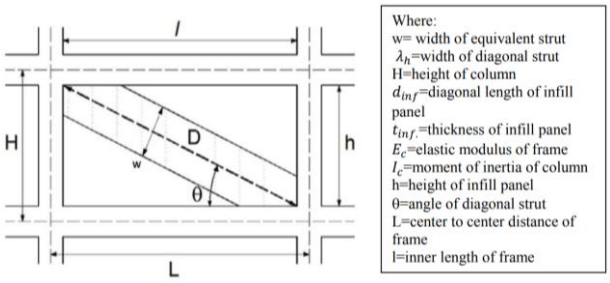


**Figure 3.** Diagonal Strut Parameters [26]

Mathematical models of these buildings were created by Sap 2000 finite element program. Afterward, strut elements representing the infill wall were added to these mathematical models and analyzed as a two-joint compression strut element, because the dominant

behavior was axial stressing of the infill panel provided in-between the two consecutive columns. The hinges properties were defined in SAP2000. The P-M2-M3 model was used to define the hinges in the columns, M3 model was used to define in the beam and an axial hinge was used for the struts. Strut element model is shown in Figure 4.

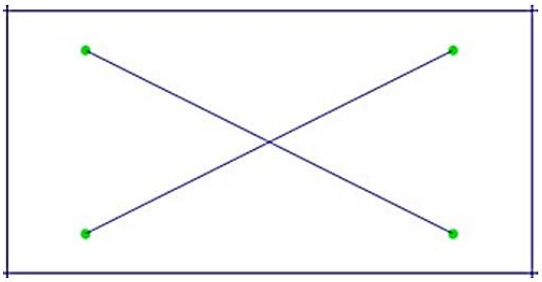

**Figure 4.** Strut element model

## 3. MATERIAL AND METHOD

In the study, the infill walls in the reinforced concrete frame were designed with conventional brick (CB) and aerated autoclaved concrete (AAC) filling materials. A total of four different model combinations were created. The first type model is consisting of an aerated autoclaved concrete infill wall from the ground to top (Model 1- AAC), the second type model is consisting of a conventional brick infill wall from the ground to top (Model 2- CB), the third type model is consisting of an aerated autoclaved concrete infill wall except for the ground floor (Model 3- AAC), the fourth type model is consisting of a conventional brick infill wall except for ground floor (Model 4-CB). The material characteristics used in modeling are given in Table 1.

**Tablo 1.** Material characteristics

| | *Aerated Autoclaved Concrete (AAC)* | Conventional Brick (CB) |
|---|---|---|
| Compressive Strength (f) | 3.5 MPa, | 5 MPa, |
| Modulus of Elasticity *(E)* | 8000 MPa, | 3500 MPa |
| Poisson ratio | 0.2 | 0.2 |
| Density | 5.3 kN/m$^3$ | 17.5 kN/m$^3$ |

The building is a reinforced concrete frame building structure. The model is formed by beams and columns whose joints connected to the ground story are made of fixed supports to be restrained in all directions The dimensions of the model building are 20.0 m x 20.0 m. The building has 7 storey including the ground storey. The height of each storey is 3 meters. The model is formed by beams and columns whose joints connected to the ground story are made fixed supports to be restrained in all directions.

The material and element dimensions of the model are shown in Table 2. The dimensions of the building and the elevation of the building are shown in Figure 5.

**Table 2.** Material and element dimensions of the model

| | Elements Properties |
|---|---|
| Concrete Grade | C30 |
| Steel Grade | S420 |
| Column Size | 50 cm x 50 cm |
| Beam Size | 30 cm x 40 cm |
| Slab thickness | 15 cm |
| Conventional Brick Struts | 23 cm x 56 cm |
| AAC Struts | 25 cm x 55 cm |

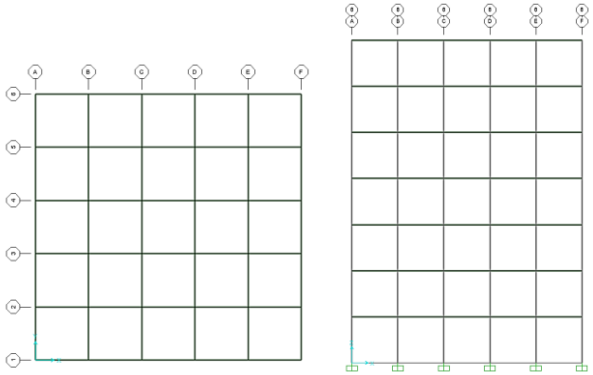

**Figure 5**. Plan and elevation of mid-rise building

Masonry infill walls consist entirely or partially of panels within the plane of the concrete frame bounded by columns and beams. In this study, the filled walls are modeled as equivalent diagonal strut model to make the structural analysis of the masonry infill wall frame system. Equivalent diagonal struts modeling of masonry fills in frames is extremely popular because of its simplicity and required a limited number of input parameters for the modeling. The building was modeled and analyzed using SAP2000 V23 finite element program. Finite element models of the building are given in Figure 6.

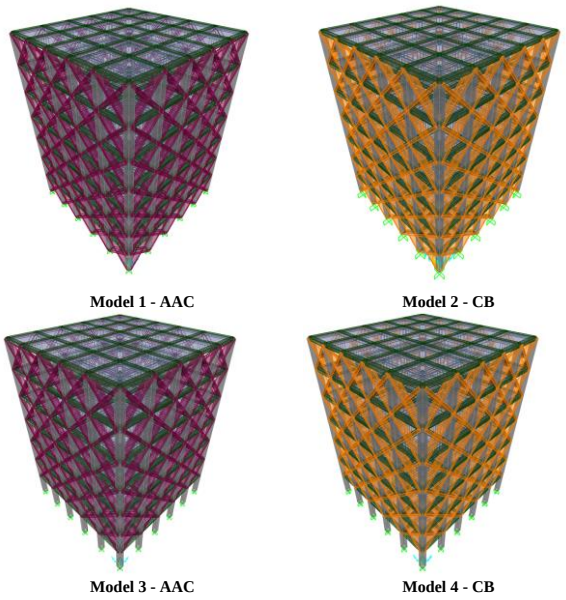


**Figure 6.** Models of aerated autoclaved concrete and conventional brick infill wall structures

The building is designed using the assumption that the floor systems serve as a rigid diaphragm. Infill walls are modeled as equivalent diagonal compression struts. In addition to live load and dead load, Conventional brick and aerated autoclaved concrete wall loads are also defined in the building. The building was designed for zone 2B. In the structure modeled in 3D, the infill walls were defined as two different materials, aerated autoclaved concrete and conventional brick, and the effect of the filling materials on the earthquake response of these type of structures were determined under both conditions.

## 4. ANALYSIS RESULTS

Pushover analysis is one of the important methods available to understand the behavior and vulnerability of structures subjected to earthquake loads. So, Nonlinear static pushover analysis was performed on the structure modeled in four different ways. This process was repeated for each combination with the Sap2000 (version 23) [24] program. As a result of the analysis, base shear force, top floor displacement values, and storey drift values obtained from four different models were found. First, the buildings modeled as infill walls from the ground to the top floor (Model 1- Model 2) were examined. Values of Model 1- Model 2 are given graphically in Figure 7, Figure 8, and Figure 9, respectively.

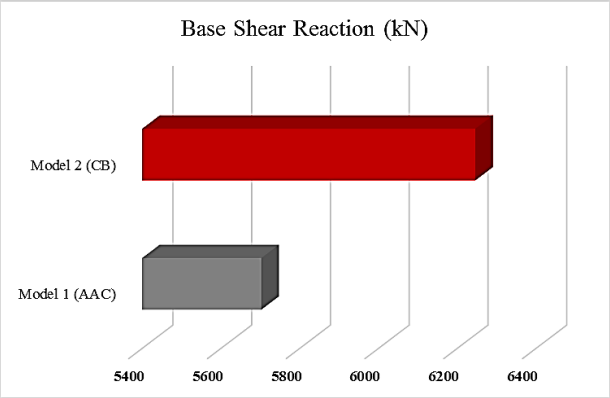


**Figure 7.** Base shear force of aerated autoclaved concrete (model 1) and conventional brick filled walls (model 2)

From Figure 7, it is seen that the base shear force value of the model with conventional brick material (Model 2) is higher than that of the model with aerated concrete block material (Model 1).

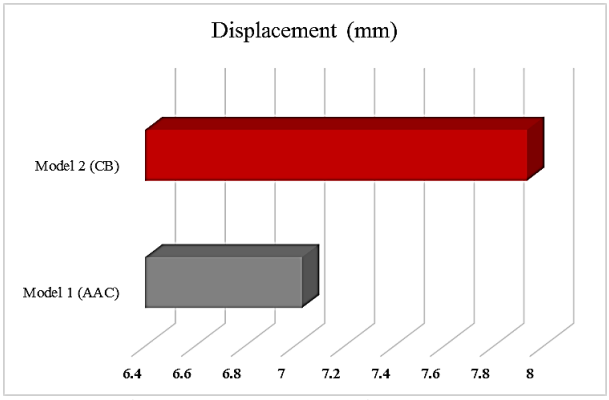


**Figure 8.** Top floor displacement values of aerated autoclaved concrete and conventional brick filled walls

Considering the top floor displacement values in model 1 and model 2, the displacement value in model 1 (conventional brick) is greater than model 2 (Aerated autoclaved concrete). When the storey drift values of the two models are compared (Figure 9) it is seen that the storey drift value of model 2 is higher due to the rigidity of the material it has.

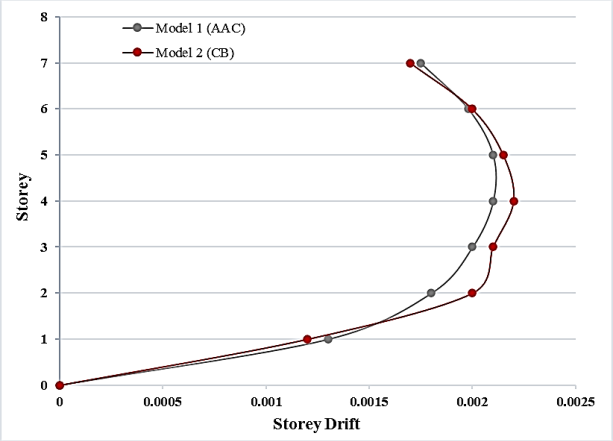


**Figure 9.** Storey drift value of Model 1 and Model 2

Secondly, static pushover analysis was performed for the building models Model 3 and Model 4, which are designed with no infill walls on the ground floor. The base shear force, top floor displacement, and storey drift values obtained from the static thrust analysis are given in Figure 10, Figure 11, and Figure 12, respectively.

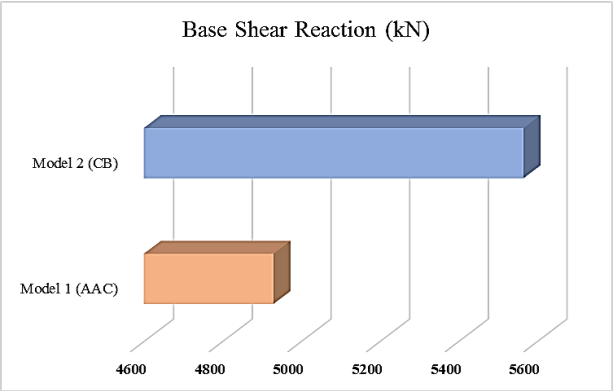


**Figure 10.** Base Reaction Forces of Models Without Ground Floor Infill Walls

As a result of the analysis, as seen in Figure 10, the base shear force value was found to be higher in Model 4 (conventional brick), similar to the ones in the filled model.

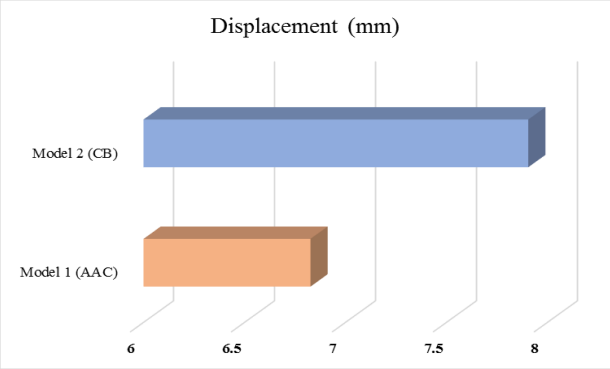


**Figure 11.** Top floor displacement values of models without ground floor infill walls

The peak displacement value of two different materials was found to be lower in Model 3 compared to Model 4.

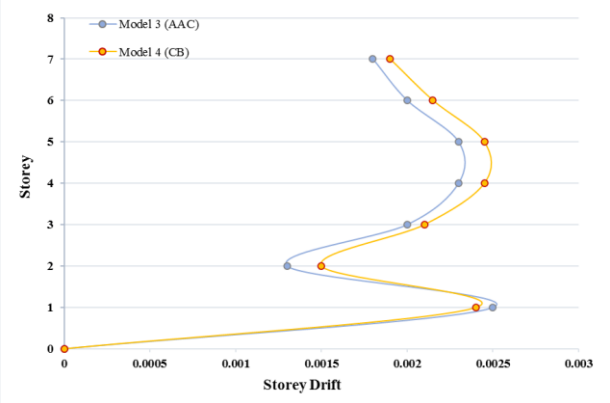


**Figure 12.** Storey drift values for models without ground storey infill walls

In the buildings modeled as the ground floor without walls, the storey drift values bounce on the ground floor where the stiffness was different, and the values were found to be higher in the conventional brick building material.

## 5. CONCLUSIONS

In this study, static pushover analysis of the building was conducted according to four different combinations, and the base shear force, displacement, and Storey drift value results were obtained for each model. The analyzes were conducted for 2 cases. First, model 1 and model 2, which have the same properties except for the filling wall material, were examined. Afterward, analyzes were conducted for Model 3 and Model 4. When the base shear force value obtained from Model 1 is compared with Model 2, the base shear force of the model with Aerated autoclaved concrete filling wall material was found 8.69% less. When the peak displacement values obtained from the same models are compared, 11.32% less displacement value was obtained in Model 1 (AAC) than in Model 2 (CB).

In the building models whose ground floor is designed without infill walls, the base shear force in Model 3 (AAC) was found to be 11.42% less than in Model 4 (CB). When the peak displacement values of the models are compared, 13.65% less displacement value was obtained in Model 3 (AAC) than in Model 4 (CB). Aerated autoclaved concrete has more rigidity than conventional brick. therefore, the storey drift values obtained from nonlinear analyzes are less in AAC filling wall material building models.

In addition, in Model 3 and Model 4, the drift ratio values on the ground storey are higher than the other storey, and soft storey behavior has emerged on the ground storey. This situation was caused by the using walls on the upper storey of the building and therefore the increased rigidity of the building.

To evaluate the infill wall materials in terms of "Soft Floor Behavior", when the models designed without infill walls on the ground storey are examined, Aerated autoclaved concrete gave slightly more negative values than conventional brick. In the design of the building, the designer should use shear and column sections that will provide sufficient rigidity on the ground storey to prevent soft storey for both materials.

As a result, the AAC block infill outperformed the Traditional brick infill in the RC frame. For reinforced concrete frames built in earthquake-prone areas, ACC block material is suitable to replace conventional bricks and can be used mainly as a substitute for traditional brick material. If we compare the performance of conventional clay bricks and AAC blocks were significantly superior.



## REFERENCES

[1] Flanagan RD, Bennett RM. In-plane Behavior of Structural Clay Tile İnfilled Frames. Journal of Structural Engineering. 1999;125(6):590–599.

[2] Hao H, Ma G, Lu Y. Damage Assessment of Masonry Infilled RC Frames Subjected to Blasting Induced Ground Excitations. Journal of Engineering Structures. 2002;24:799–809.

[3] Rajesh C, Kumar RP, Kandru S, Seismic Performance of RC Framed Buildings with and without Infill Walls. International Journal of Engineering Research & Technology (IJERT). 2014;3(10):281–289.

[4] Abd-Elhamed, A., Mahmoud, S. Effect of Infill Walls on Response of Multi Storey Reinforced Concrete Structure. International Journal of Civil, Environmental, Strcutural, Construction and Architectural Engineering. 2015; 9(5); 514-518.

[5] Goel K. Influence of Masonry Infill Walls on Seismic Performance of RC Framed Structures-A Comparison of AAC and Conventional Brick Infill. International Research Journal of Engineering and Technology (IRJET). 2015; 2 (6).

[6] Ural A., Çelik T. Gaziantep Nizip Tahtani (Leylek) Cami Yapısal Analiz Ve Değerlendirmesi. Uludağ Üniversitesi Mühendislik Fakültesi Dergisi. 2021; 26(1), 79-96.

[7] Çelik T., Tanrıverdi Ş. Farklı Çaplardaki Zıvanaların Kurşun ile Sabitlenmesinin Kayma Dayanımına Etkisi. Avrupa Bilim ve Teknoloji Dergisi. 2021; (24), 24-29.

[8] Tanrıverdi Ş., Çelik T. Farklı Dolgu Malzemeleri ile Sabitlenen Zıvanaların Yığma Taş Blokların Kayma Dayanımına Etkisi. Avrupa Bilim ve Teknoloji Dergisi. 2021; (25), 347-354.

[9] Cosgun C., Mangir A. Earthquake performance of collapsed school building under Van-Tabanli (Mw= 7.2) earthquake. Challenge Journal of Structural Mechanics. 2018; 4(4), 159-175.

[10] Usta P., Evci A. Using Reinforced AAC Panels to Against Earthquake Loads. International Symposium on Innovations in Civil Engineering and Technology. 2019; 435-445.

[11] Uysal N., Usta P., Bozdağ Ö. Structural Resistance of the Referenced Reinforced Concrete Structure under Earthquake and Wind Load in Mediterranean Region.Türk Doğa ve Fen Dergisi. 2022;11(1), e 142-150. Doi: 10.46810/tdfd.1060359.

[12] Onat Ö., Usta P. 20 Katlı Betonarme Yapının Farklı Perde Duvar Yerleşimlerine Göre Deprem Analizi. Avrupa Bilim ve Teknoloji Dergisi. 2021; (25), 363-369. Doi: 10.31590/ejosat.912625.

[13] AFAD, "Earthquake Statistic," https://deprem.afad.gov.tr/genelistatistikler (açık erişim;13.04.2021), 2022.

[14] AFAD, "Afet ve Acil Durum Yönetimi Başkanlığı, Türkiye Deprem Tehlike Haritaları (in Tukish)," 2021. https://www.turkiye.gov.tr/afad-turkiye-deprem-tehlike-haritalari (accessed Oct. 30, 2021).

[15] Rathore H.S., Maru S. Seismic Evaluation of AAC Block and Brick Wall Fully Infilled Building and Building Having Soft Storey at Different Floor as Per IS 1893-2016. International journal of scientific research in science, engineering and technology. 2018; 4.

[16] Jadhao V. P., Pajgade P. S. Influence of masonry infill walls on seismic performance of RC framed structures: a comparison of AAC and conventional brick infill. International Journal of Engineering and Advanced Technology. 2013; 2(4), 148-153.

[17] Bilgin H., Uruçi R. Effects of structural irregularities on low and mid-rise RC building response. Challenge Journal of Structural Mechanics. 2018; 4(2), 33-44. Doi: 10.20528/cjsmec.2018.02.001.

[18] Arunkumar S., Devi, G. Seismic demand study of soft storey building and it's strengthening for seismic resistance. Int. J. Emerg. Trends Technol. Comput. Sci. 2016;5(2), 52-57.

[19] Sandıkcı T. Investigaton of relationship between soft story and torsional irregularities in reinforced concrete buildings. Master's thesis, Karadeniz Technical, University Institute of Science and Technology., Trabzon, 2014.

[20] Tezcan S., Yazıcı A., Özdemir Z., Erkal A., Zayıf Kat-Yumuşak Kat Düzensizliği. 2007.

[21] Altuntop M.A., Analysis Of Building Structures With Soft Stories. Graduate School of Natural and Applied Sciences. İstanbul, 2007.

[22] Tezcan, T., Başaran, H., Demir, A., Bağcı, M. Yumuşak Kat Oluşumunda Duvar Etkisi ve Türk Deprem Yönetmeliğinin Konuya Yaklaşımı. Yapı Teknolojileri Elektronik Dergisi. 2013; 9(1), 29-38.

[23] Hoveidae, N., Fathi, A., Karimzadeh, S. Seismic damage assessment of a historic masonry building under simulated scenario earthquakes: A case study for Arge-Tabriz. Soil Dynamics and Earthquake Engineering. 2021; 147, 106732. Doi: 10.1016/j.soildyn.2021.106732.

[24] SAP 2000 Ver. 23, "Computer Program." Computers and Structures INC, Berkeley (CA, USA), 2006.

[25] FEMA-356, "Prestandart and commentary for seismic rehabilitation of buildings.," Washington (DC), 2000.

[26] Ahmed, A., Ali, A., Khalid, H., Ahmad, M. Role of masonry infill wall on the seismic behavior of typical four-storey building in Pakistan. In IOP Conference Series: Materials Science and Engineering. 2018; 414(1).

Araştırma Makalesi https://doi.org/10.46810/tdfd.1059408 Research Article

Türk Doğa ve Fen Dergisi
Turkish Journal of Nature and Science
www.dergipark.gov.tr/tdfd

# Determination of Biomass Energy Potential That Can Be Obtained from Agricultural and Animal Wastes of Konya Province

**Sinem KILIÇKAP IŞIK[1*], Sıraç YAVUZ[2]**

[1] Bingöl University, Faculty of Engineering and Architecture, Department of Mechanical Engineering, Bingöl, Türkiye
[2] Bingöl University, Faculty of Agriculture, Department of Animal Science, Bingöl, Türkiye
Sinem KILIÇKAP IŞIK ORCID No: 0000-0002-1044-5092
Sıraç YAVUZ ORCID No: 0000-0001-5878-8994

**Corresponding author: sinemisik@bingol.edu.tr*

(Received: 18.01.2022, Accepted: 31.05.2022, Online Publication: 29.06.2022)

**Keywords**
Energy, Biomass potential, Dry biomass amount, Biogas potential, Konya

**Abstract:** In the recent study, the annual biomass and biogas energy potential of Konya between 2011 and 2020 was determined according to the data obtained from the Turkish Statistical Institute (TSI). In 2020, throughout Turkey, 12.74% of biomass sources were produced in Konya. The total amount of dry biomass that can be obtained and its energy equivalent are 13.3 million tons and 62549.3 MWh in 2011, 19.5 million tons, and 91661.9 MWh in 2020, respectively. It has been determined that 11.6% of the biomass energy potential that can be obtained from grains across the country in 2020 is in Konya. Tuber plant production covers 22% of Turkey. In 2020, with 11649 MWh, the highest biomass energy potential was obtained in Cihanbeyli, and at least in Derebucak, with 47.7 MWh. In addition, it has been determined that 98.5 million $m^3$ of biogas from 13.4 million animals in 2011; and in 2020, 165.6 million $m^3$ of biogas can be obtained from 15 million animals. By evaluating the existing biomass and biogas energy potentials in Konya with this data that can be obtained, it is thought that it can have a very important biomass energy source for both the province and the country.



# Konya İlinin Tarımsal ve Hayvansal Atıklarından Elde Edilebilecek Biyokütle Enerji Potansiyelinin Belirlenmesi

**Anahtar Kelimeler**
Enerji, Biyokütle potansiyeli, Kuru biyokütle miktarı, Biyogaz potansiyeli, Konya

**Öz:** Bu çalışmada, Türkiye İstatistik Kurumu (TÜİK)'ndan alınan verilere göre Konya ili 2011-2020 yılları arasındaki yıllık biyokütle ve biyogaz enerji potansiyeli belirlenmiştir. 2020 yılında Türkiye genelinde biyokütle bitkilerinin %12,74'ünün üretimi Konya'da yapılmıştır. Elde edilebilecek toplam kuru biyokütle miktarı ve enerji eşdeğeri sırasıyla 2011 yılında 13,3 milyon ton ve 62549,3 MWh, 2020 yılında 19,5 milyon ton ve 91661,9 MWh'tir. 2020 yılında ülke genelinde tahıllardan elde edilebilecek biyokütle enerjisi potansiyelinin %11,6'sının Konya'da olduğu hesaplanmıştır. Yumru bitki üretimi ise ülke genelinin %22'sini kapsamaktadır. 2020 yılında 11649 MWh ile en yüksek biyokütle enerji potansiyeli Cihanbeyli ilçesinde, en az ise 47,7 MWh ile Derebucak ilçesinde elde edilmiştir. Ayrıca, ilde 2011 yılında 13,4 milyon hayvandan 98,5 milyon $m^3$ biyogaz; 2020 yılında ise 15 milyon hayvandan 165,6 milyon $m^3$ biyogaz elde edilebileceği belirlenmiştir. Elde edilebilecek bu veriler ile Konya ilindeki mevcut biyokütle ve biyogaz enerjisi potansiyelleri değerlendirilerek hem il hem de ülke için çok önemli biyokütle enerji kaynağına sahip olabileceği düşünülmektedir.

## 1. INTRODUCTION

Bioenergy, not only improves environmental sustainability; it also improves the sustainability of energy, agriculture, forestry, and other sectors [1]. The increasing population causes serious needs on both the energy requirement and the food sector. Because current fossil fuels are insufficient and the demand for energy use in industry is constantly increasing to meet needs, efforts for alternative and sustainable searches have increased [2-5]. Fossil fuels cause a continuous decrease in the resources used in energy production, environmental causes such as global warming and destruction of nature,

and pose a great threat to future generations. Therefore, alternative energy sources such as sustainable wind energy, geothermal energy, solar energy, and biofuel energy are all very important [6-8]. In addition, the evaluation of plant-based wastes and the reduction of emissions that cause global warming are important for biomass fuels.

Biomass is a general term used for all organic matter derived from plants and accepted as organic carbon. It has always been an important source of energy for humanity throughout history [9]. Biomass is important in meeting the needs of fuel and consumer goods, as well as providing a renewable fixed carbon source. Agricultural and forestry wastes, wood and annual crops, and municipal waste are some of the renewable energy sources [10]. It is recognized as the renewable energy source with the highest potential to contribute to the energy needs of both developed and developing economies worldwide [10-12]. In addition, energy from waste-based biomass can significantly contribute to the goals of the Kyoto Protocol in reducing greenhouse gas emissions (GHG) and mitigating the problems associated with climate change [10, 13].

Biomass can also be referred to as renewable organic materials from plants and animals, both living and dead. It can be directly burned to generate heat or converted into liquid or gaseous forms through various processes [14]. Plant sources, also known as energy plants, absorb more carbon dioxide ($CO_2$) than other plants, use less water, and are more drought resistant [15, 16].

Biomass still continues to be used for cooking and home heating in many countries around the world. Biomass fuels are used in transportation and electricity generation in some countries to reduce dependency on fossil fuels, pollution and GHG [14, 17]. Sources which are used for production of biomass energy; forest wastes (energy crops, various trees, etc.), oilseed crops (canola, sunflower, soybean, etc.), sugar and starch crops (potato, wheat, corn, sugar beet, etc.), fiber crops, protein crops, vegetables and the other agricultural wastes (branches, stems, straw, roots, bark, etc.), crop wastes, food processing wastes, animal manure, slaughterhouse wastes, urban wastes, industrial wastes, industrial and domestic wastewater [14].

And it is converted into energy in two ways: biochemical and thermochemical (Figure 1). Biogas is the process of producing fuel ($CO_2$, $CH_4$) by digesting biomass in a closed oxygen-free environment in the biomethanization process of biochemical transformations by microorganisms [18, 19]. Bioethanol is produced as a result of glucose or containing sugars which can be converted to glucose and the fermentation of biological resources (such as cellulose, starch, and sucrose) [19]. Plants with high bioethanol potential and widely used in its production; include barley, corn, potato, sugar beet, and wheat [20]. Gasification, one of the thermochemical processes, is a combustible gas process obtained by exposing biomass sources containing carbon atoms to high temperatures. Materials are burned by giving air in a controlled manner, such as methane, hydrogen, carbon monoxide, carbon dioxide, and nitrogen gases [19]. Pyrolysis is the most classical and easiest method applied to obtain gas using biomass. It is a series of physical and chemical events that occur when organic matter is heated up to 900 °C in an oxygen-free environment. As a result of this process, water, charcoal, organic compounds, tar, and gases are produced [21]. Direct combustion is the process of obtaining heat by burning the raw material. This process is the most classical method known and used since the discovery of fire. Chemical conversion, known as transesterification (esterification), is used to produce biodiesel by converting vegetable, and animal oils and greases to fatty acid methyl esters [17, 22-25].



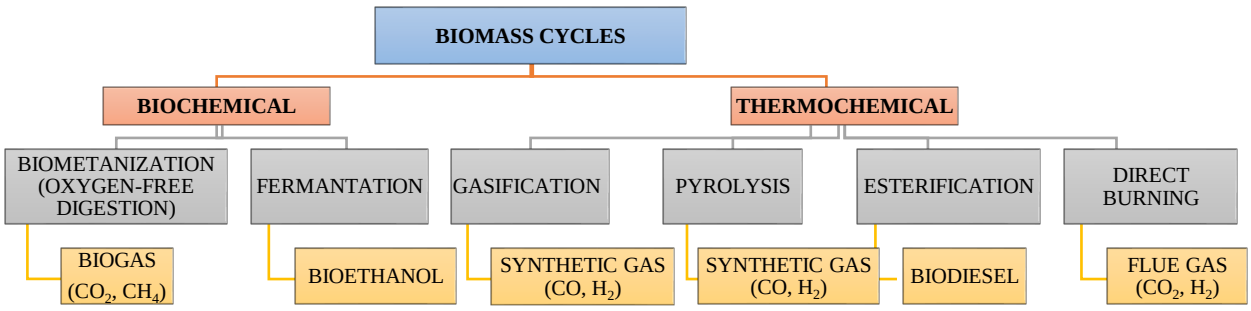


**Figure 1.** Biomass conversion systems [17].

In 2018, the global local supply of biomass was reported as 55.6 EJ (egza joules). The major part of this local supply (85%) consists of solid biomass sources, including wood chips, wood pellets and other biomass sources. In addition, in 2019, there were 1.9 billion $m^3$ of wood fuel produced worldwide [26]. Wood pellets are one of the fastest growing bioenergy sectors worldwide. Municipal and industrial waste sectors accounted for 5%, biofuels in liquid form accounted for 7%, biogas 3%. Between 2000 and 2018, the annual average growth rate of the bioenergy sector was 2%. Among all raw material sources, liquid biofuels were the fastest growing sector with a growth rate of 13%, followed by biogas with 9% (Table 1). In 2018, 637 TWh of electricity was produced from biomass worldwide. Of total generated power, 66% was obtained from solid biomass sources and 19% was obtained from municipal and industrial wastes [26].

**Table 1.** Globally where local biomass are supplied [28].

| Years | Municipal Waste | Industrial Waste | Solid Biofuels | Biogases | Liquid Biofuels | Total |
|---|---|---|---|---|---|---|
| **2000** | 0.74 | 0.49 | 40.5 | 0.29 | 0.43 | 42.5 |
| **2005** | 0.96 | 0.45 | 42.8 | 0.51 | 0.87 | 45.6 |
| **2010** | 1.18 | 0.77 | 45.1 | 0.85 | 2.53 | 50.5 |
| **2015** | 1.38 | 0.90 | 46.2 | 1.29 | 3.45 | 53.2 |
| **2016** | 1.42 | 1.04 | 46.9 | 1.30 | 3.58 | 54.3 |
| **2017** | 1.44 | 1.07 | 47.3 | 1.33 | 3.72 | 54.9 |
| **2018** | 1.45 | 1.13 | 47.6 | 1.36 | 3.98 | 55.6 |

Since the interest in renewable energy systems has increased rapidly in Turkey as well as all over the world in recent years, much research in this field has been conducted to determine biomass energy potentials. According to the data reported by the Ministry of Energy and Natural Resources, it is estimated that Turkey's biomass waste potential is approximately 8.6 million tons of equivalent petroleum (MTEP) [17]. Turkey, which meets its energy needs mostly from petroleum, natural gas and coal imports, paid approximately 50 billion USD in 2008 for these raw materials [27]. In order to encourage energy investments, the draft law on renewable energy sources was adopted and entered into force in 2011. It aims to increase the orientation towards renewable energy sources by giving the highest price guarantee to biomass energy with this law [27, 28]. Süleyman Demirel University, Renewable Energy Resources and Application Center, is carried out joint studies with public institutions on the pyrolysis of biomass [29]. Kurt and Koçer [19] reported that all of the cereals, legumes, industrial plants, oilseeds and tuber plants cultivated in the province of Malatya are produced on an area of approximately 145162 hectares, and the area has a total biomass potential of 3991966 tons. In addition, they calculated the average calorific value of dry biomass as 1596786 tons of equivalent petroleum (TEP). Topal and Topal [30] investigated the potential to produce biomass energy from agricultural products grown in Afyonkarahisar for five years (2006-2010). In the city center and its districts, the highest biomass energy in total is respectively obtained from cereal crops (2251-46960 MW), tuber crops (9-2483 MW), industrial plants (49-2326 MW), legumes (15-2105 MW), and oily plants. Seed crops (44-1688 MW) and forage crops (108-1526 MW). In the study investigating the biomass energy potential of the Eastern Anatolia region (Ağrı, Ardahan, Bayburt, Bingöl, Bitlis, Elazığ, Erzincan, Erzurum, Hakkari, Iğdır, Kars, Malatya, Muş, Tunceli, Van), it has been determined that an average of 47343313 tons of biomass potential can be obtained from a total planted area of 1721578 hectares. The average calorific value of dry biomass was found to be 19174042 TEP. The highest TEP rate was found in Erzurum with 2668021, and the lowest TEP rate was found in Hakkari with 218235 [31]. The potential biomass energy was calculated based on the data obtained from the agricultural products of the province of Elazig between the years 2000-2010. The total biomass energy potential of these products are, respectively; obtained from cereals (132083 MW), forage crops (10934 MW), legumes (8122 MW), industrial crops (6173 MW), tuber crops (1193 MW) and oilseed crops (443 MW) [32]. According to the data of 2016 considering the geographical structure and climatic conditions of Kars province, in the study conducted on the duration of staying indoors, it was calculated that there was 1948 tons/day of wet manure from 442575 cattle and 341 tons/day of wet manure from 567148 sheep and goats. Considering the whole year, it has been reported that the highest amount that can be produced from both bovine and ovine animals (1009723 heads) has the potential to produce 986121 tons of collectable waste manure, and 10171 tons/year of wet manure from 557330 poultry [33]. Demir et al. [34], compared the agricultural biomass energy potential of Mersin province proportionally with the Mediterranean and Turkey between the years 2005-2014. They reported the average dry biomass energy amount as 15.86% in Mersin/Mediterranean region and 1.93% MW in Mersin/Turkey. Kuş et al. [35], determined the annual average (2009-2013) biomass energy potential as 639000 TEP (7432 MW) in their study across the province of Iğdır. Field crops products constituted the majority of this potential. They also stated that the biomass energy potential of the province is equivalent to 3% of Turkey's average. Ekin et al. [36] assessed biomass energy production in the province of Şırnak, bovine and ovine numbers, and the products grown in the region's agricultural areas. They mentioned that 72% of the annual energy need in Turkey are met by importing and that fossil fuel sources that cause global warming constitute 70% of the electricity production in the country, causing environmental pollution. With the appropriate methods, it was concluded that biomass-based wastes and all industrial wastes can be converted into alternative fuels such as transportation fuel, electrical energy or gas, which the city needs.

Agriculture is carried out in approximately 67.7% of the total area of Konya province. The reason why agriculture is growing at such a high rate in Konya, which is known as the agricultural capital of our country, is the high amount of existing water potential and irrigable lands. Many types of vegetables and fruits are produced in Konya, especially field crops (wheat, barley, sugar beet, chickpeas, dry beans, green lentils, red lentils, potatoes, sunflowers, poppy, cumin, safflower, etc.). In addition, the province of Konya contributes to the development of animal husbandry and animal production of the country with its large pastures and plant production areas. It ranks among the top three in the country with the current numbers of bovine, ovine, and poultry. Çumra, Altınekin, Karapınar, Karatay, Ereğli, Kulu, and Cihanbeyli districts are among the districts with the highest agricultural potential in terms of irrigation opportunities of the lands [37]. According to the data of 2021 obtained from Turkish Statistical Institution (TSI), the districts of Kulu, Karatay and Sarayönü in barley production; Karatay, Karapınar and Kadınhanı in sunflower production; Çumra, Karapınar and Altınekin in sugar beet production; Ereğli, Karapınar and Karatay are leading in corn production [38]. In this research, the biomass and biogas energy

potentials of Konya province between the years 2011-2020 were determined and compared with the energy potential in Turkey.

## 2. MATERIAL AND METHOD

Konya province is located between 36° 22'N and 39° 08'N parallels and 31° 14'E and 34° 05'E meridians. The province, with an area of 40841 km$^2$ and 31 districts, is the largest province in Turkey. Konya province covers 5.21% of the country's surface area. In addition, Konya is in the 7th place in Turkey in terms of population. Its largest districts are Ereğli, Beyşehir and Akşehir. A continental climate prevails in Konya, with hot and dry summers and cold and warm winters. Besides its developing industry, Konya is also known as Turkey's granary [39].

In this study, data from the TSI between 2011 and 2020 was taken into account in order to determine the current biomass and biogas energy potential in Konya. Barley, rye, oat, canola, sunflower, safflower, potato, sugar beet, corn, poppy, fruits and vegetables were used to calculate the biomass energy potential. In the calculation of biogas energy potential, the presence of bovine, ovine and poultry was used. Equation 1-8 below is used to determine the average dry biomass amount, calorific value, and energy value that can be produced in Konya in a year. In addition, the assumptions used for biomass energy equivalents are given below [40].

| | | |
|---|---|---|
| 1 TEP (tons equivalent petroleum) | = | $10^7$ kcal<br>42 GJ<br>11630 kWh<br>11.630 MWh |

The following equations were used to determine the biomass energy value [19, 31, 32, 35].

$$BM_{min}=25*A \text{ [ton]} \quad \text{(Eq. 1)}$$
$$BM_{max}=30*A \text{ [ton]} \quad \text{(Eq. 2)}$$
$$BM_{mean}=(25+30)/2*A \text{ [ton]} \quad \text{(Eq. 3)}$$
$$ID_{min}=3800*BM_{mean} \text{ [kcal kg}^{-1}\text{]} \quad \text{(Eq. 4)}$$
$$ID_{min}=4300*BM_{mean} \text{ [kcal kg}^{-1}\text{]} \quad \text{(Eq. 5)}$$
$$ID_{mean}=(3800+4300)/2*BM_{mean} \text{ [kcal kg}^{-1}\text{]} \quad \text{(Eq. 6)}$$
$$ED_{mean} = ID_{mean}*10^{-7} \text{ TEP} \quad \text{(Eq. 7)}$$
$$ED_{mean}= ID_{mean}*10^{-7}*(11.63) \text{ MWh} \quad \text{(Eq. 8)}$$

The amount of wet manure that can be produced and biogas production differ according to the animal species. In this context, certain assumptions are made. The annual average amount of wet manure obtained from bovine, ovine, and poultry is, respectively, 3.6 tons, 0.7 tons and 0.022 tons. It is known that two-thirds of the wet manure is usable and the rest is lost by mixing with nature [41, 42].

The amount of biogas energy that can be produced from usable wet manure is as follows;

1 tons of usable bovine manure 33 m$^3$ year$^{-1}$,
1 tons of usable ovine manure 58 m$^3$ year$^{-1}$,
1 tons of usable poultry manure 78 m$^3$ year$^{-1}$'dır.
1 m$^3$ the electrical energy provided by biogas is 4.70 kWh, the heat energy is 4700-5700 kcal [42].

The cultivated areas of barley, rye, oat, canola, sunflower, safflower, potato, sugar beet, corn, poppy, fruit, and vegetable crops, which we use in calculating the biomass energy potential according to the data obtained from TSI, are given in Figure 2. In 2020, these plants were cultivated on a total of 707654.4 ha of land in Konya. These areas yielded 13897974 tons of product. In the same year, these crops were cultivated on an area of 6879313 ha throughout Turkey, and 109061582 tons of products were obtained. 12.74% of the nationwide production of the specified agricultural products is produced in Konya. Considering the data, the fact that a single province produces at such a high capacity and meets most of the needs in the country on its own shows that the biomass energy potential is quite high. Despite the fact that Cihanbeyli is the district with the highest amount of planting area, with 89934 ha in the same year, the production amount in the district was just 921033 tons. The district with the maximum production is Ereğli with 1871800 tons. In Ereğli, an area of 51771.1 ha was cultivated in 2020 (Figure 2).

In 2020, the districts with the highest production by product type were as follows: barley; in Cihanbeyli, oats; in Ilgın, canola; in Çeltik, sunflower; in Karatay, safflower; in Yunak, potatoes; in Karatay, sugar beet; in Karapinar, poppy; in Akşehir, corn, rye, fruit and vegetables; in Ereğli. In the province, sugar beet production was at its peak with 7228473 tons, and safflower production was made with at least 1812 tons. 31.4% of the sugar beet produced throughout the country is produced in Konya. In the same year, a maximum of 31177124 tons of vegetables and a minimum of 20542 tons of poppy were produced throughout Turkey.

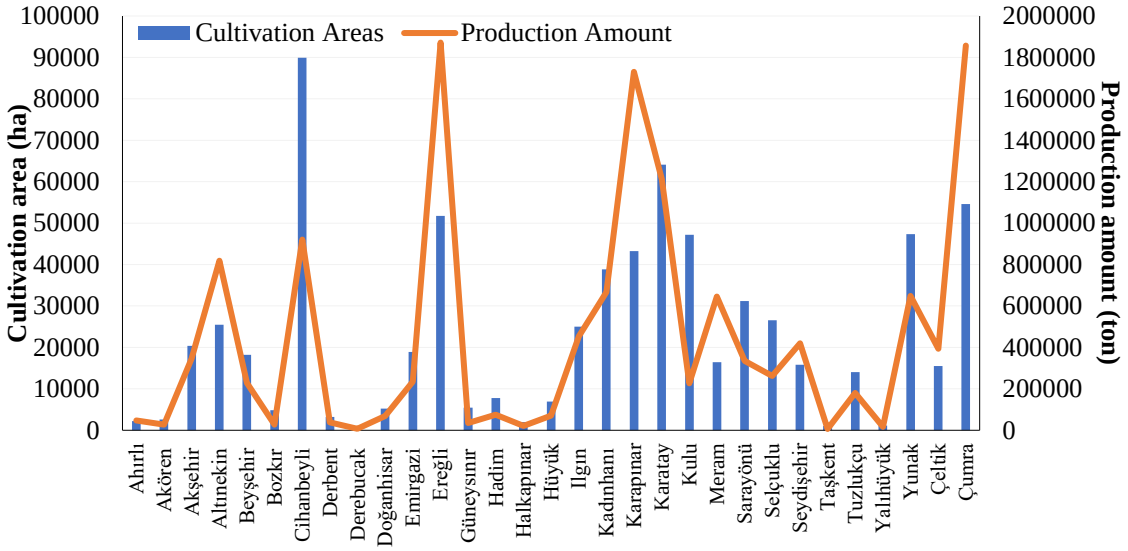


**Figure 2.** Total cultivation areas and production amounts by districts in 2020

In 2020, Konya's production rate to the country's production rate was for barley, rye, oat, canola, sunflower, safflower, potato, sugar beet, corn, poppy, fruit and vegetable crops as; 15.3%; 8.4%; 6.9%; 13.7%; 14.7%; 8.5%; 12.3%; 31.4%; 9.5%; 22.8%; 4.4% and 4.3%, respectively. Konya has grown the most barley, sugar beet and sunflower since 2011 (Figure 3). Every year, the highest production amounts were obtained from sugar beet, barley, and corn.

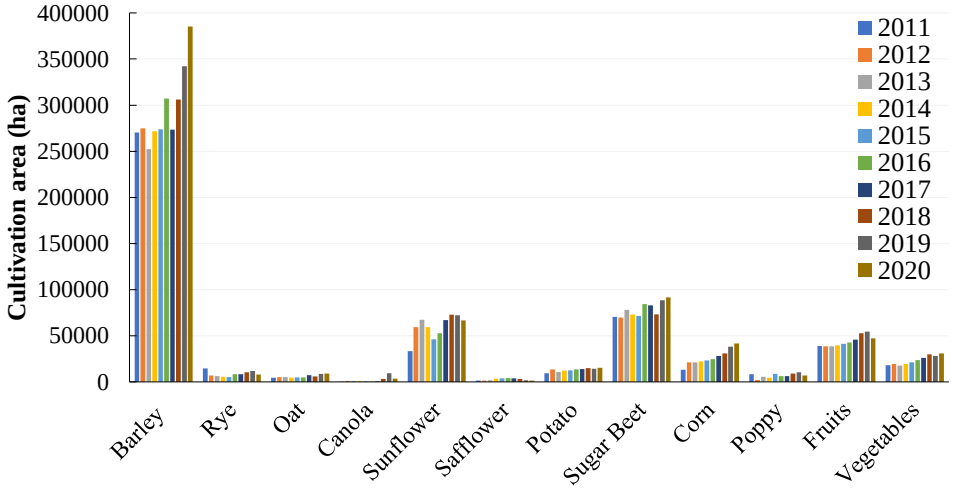


**Figure 3.** Cultivation area (ha) by year and crop type

Total plant production in Konya has generally shown an increasing trend every year since 2011 (Figure 4). While the product with the highest cultivation area was barley in all years, the product with the highest production was sugar beet. 31.4% of sugar beet production in Turkey is produced in Konya. According to the data received from TSI, as seen in Figure 4, approximately 9-13% of the total production in Turkey between the years 2011-2020 is met from the province of Konya.

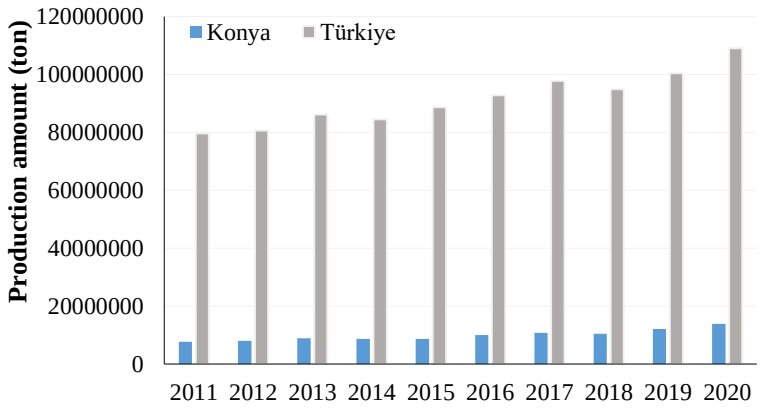


**Figure 4.** Total production amount in Konya by years (tons)

## 3. FINDINGS AND DISCUSSION

Cultivation areas of cereals, industrial plants, tuber plants, fruits and vegetables which are cultivated in Konya province and Turkey between 2011-2020 years that dry biomass amounts, calorific values, and energy values are given in Table 2. Konya's vegetative production areas account for 7.8% of the country's total cultivation area in 2011 and 10.3% in 2020. Since 2011, it has been observed that the amount of dry biomass that can be obtained and the energy value generally tend to increase. Between 2011 and 2020, there was an approximately 47% increase in total dry biomass in Konya and a 10.5% increase in Turkey.

**Table 2.** Change of total biomass energy potential by years

| Years | Cultivated Area | | Amount of Dry Biomass | | Calorific Value | | Energy Value | | Energy Value | |
|---|---|---|---|---|---|---|---|---|---|---|
| | ha | | $10^8$ ton | | $10^8$ kcal $kg^{-1}$ | | TEP | | MWh | |
| | Konya | Turkey | Konya | Turkey | Konya | Turkey | Konya | Turkey | Konya | Turkey |
| **2011** | 482898 | 6202076 | 0.132 | 1.71 | 537.8 | 6907.6 | 5378.3 | 69075.6 | 62549.4 | 803349.5 |
| **2012** | 513527.2 | 6108299 | 0.141 | 1.68 | 571.9 | 6803.1 | 5719.4 | 68031.2 | 66516.7 | 791202.7 |
| **2013** | 505806.4 | 6136232 | 0.139 | 1.69 | 563.3 | 6834.2 | 5633.4 | 68342.3 | 65516.7 | 794820.7 |
| **2014** | 516392.3 | 6234879 | 0.142 | 1.71 | 575.1 | 6944.1 | 5751.3 | 69441 | 66887.9 | 807598.4 |
| **2015** | 512676.8 | 6329910 | 0.141 | 1.74 | 571 | 7049.9 | 5710 | 70499.4 | 66406.6 | 819907.7 |
| **2016** | 572611.8 | 6343125 | 0.157 | 1.74 | 637.7 | 7064.7 | 6377.5 | 70646.6 | 74170 | 821619.5 |
| **2017** | 564183.2 | 6077700 | 0.155 | 1.67 | 628.3 | 6769 | 6283.6 | 67690.4 | 73078.2 | 787239.2 |
| **2018** | 612102.1 | 6266415 | 0.168 | 1.72 | 681.7 | 6979.2 | 6817.3 | 69792.2 | 79285.1 | 811683.2 |
| **2019** | 680296.2 | 6677508 | 0.187 | 1.84 | 757.7 | 7437.1 | 7576.8 | 74370.7 | 88118.2 | 864931.7 |
| **2020** | 707654.4 | 6879313 | 0.195 | 1.89 | 788.1 | 7661.8 | 7881.5 | 76618.3 | 91661.9 | 891071.4 |

To compare years according to the data obtained from TSI, it is understood that the year in which the most cultivation and energy is obtained in Konya is 2020 (Figure 5). In the province, cereals are the products that have the highest amount of dry biomass and energy value, while vegetables have the lowest amount of product groups. While the total amount of dry biomass was approximately 13.3 million tons in 2011, it increased to 19.5 million tons in 2020. The total biomass energy value that can be obtained was calculated as 62549.3 MWh in 2011 and 91661.9 MWh in 2020.

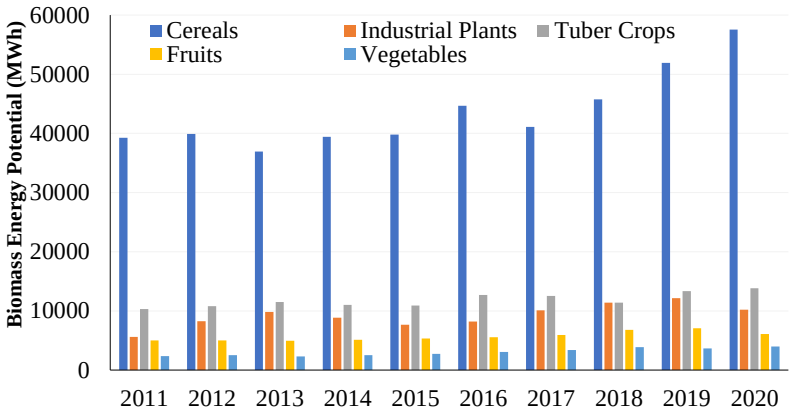


**Figure 5.** Biomass energy potential by product type and year

The biomass energy potential (MWh) to be obtained from cereals (barley, rye, oats, and corn), industrial plants (canola, sunflower, safflower, and poppy), tuber crops (potato, sugar beet), fruits, and vegetables in Konya and in Turkey is given in Figure 6. It has been calculated that the most biomass energy can be obtained from cereals in Konya and Turkey in 2020. While the energy that can be obtained from cereals is 496793.4 MWh in Turkey, it is 57525.7 MWh in Konya. Konya has the highest share with approximately 22% of the energy potential that can be obtained from tuber plants produced throughout the country. The share of biomass energy that can be obtained from vegetables produced throughout the country is occupied by the province of Konya, with approximately 4%. While the least biomass energy is obtained from tuber plants with 62966.02 MWh throughout the country, it is obtained from vegetables with 4000.6 MWh in Konya (Figure 6).

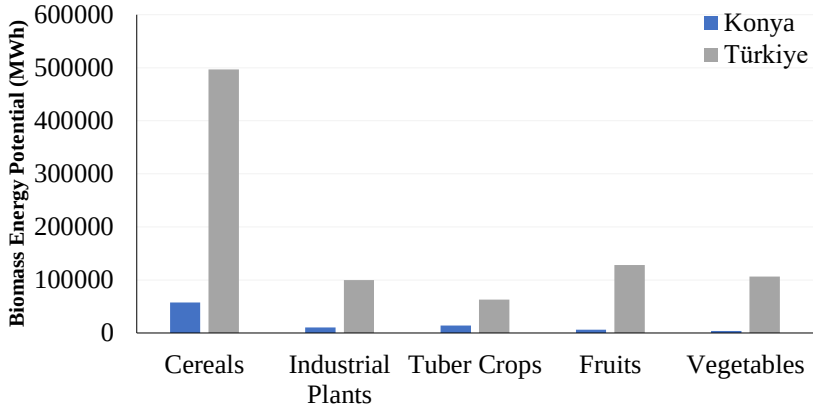


**Figure 6.** Biomass energy potential to be obtained according to the product type; comparison of Konya and Turkey for 2020

The biomass energy potentials obtained in 2020 by districts are given in Figure 7. The highest energy potential, with 11649 MWh, was obtained in Cihanbeyli district, where the cultivation area is also the highest, and the lowest energy potential was obtained in Derebucak district with 47.7 MWh.

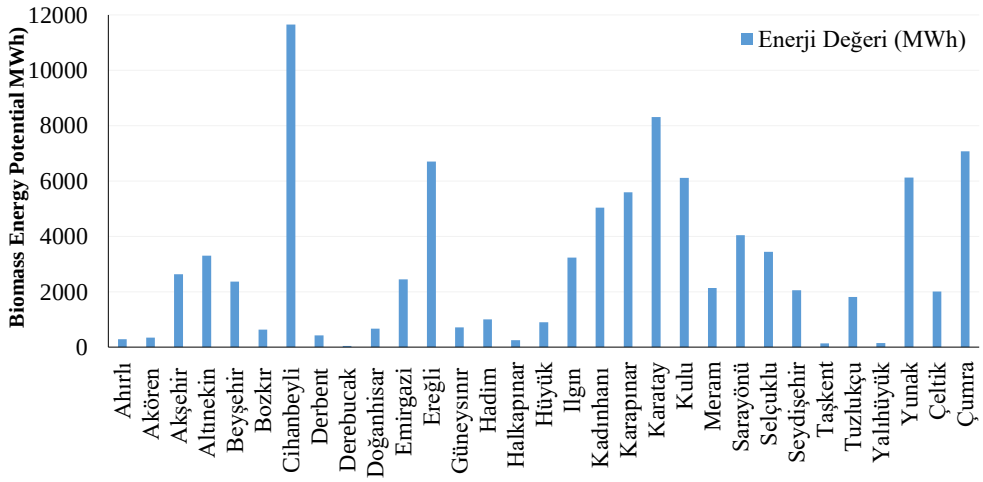


**Figure 7.** Total biomass energy potential in 2020 by districts

The biogas energy potential that can be obtained according to the total number of bovine, ovine and poultry in Konya between 2011-2020 years is given in Figure 8. Due to the rapid increase in the number of poultry in 2017 compared to other years, the highest number of animals was determined in 2017. Since 2011, there has been an increase of approximately 12% in the total number of animals and 68.1% in the biogas energy potential. The biogas potential that can be obtained has generally increased since 2011 and the maximum energy was obtained in 2020 with 165.6 million $m^3$.

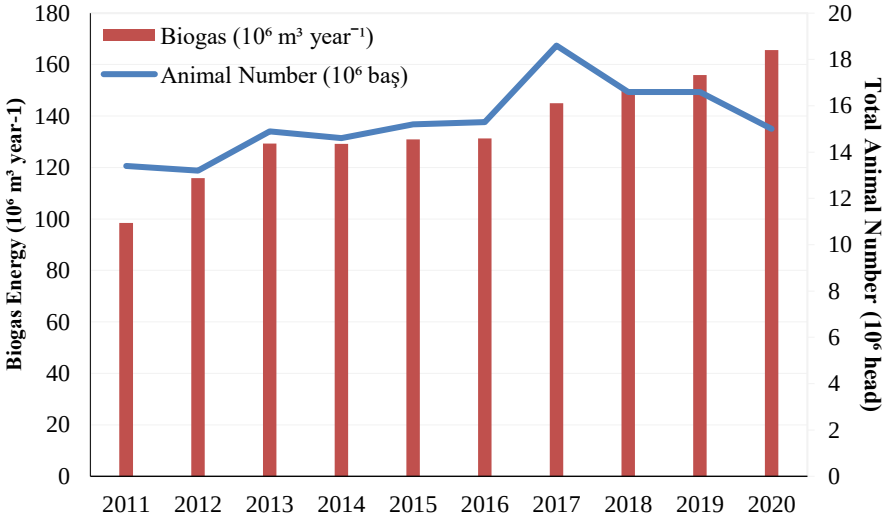


**Figure 8.** Total number of animals and biogas energy production potential in Konya province by years

The biogas, electricity and heat energy potentials obtained with the existing animal potential in Konya in 2020 are given in Table 3. It is seen that approximately 165.6 million $m^3$ of biogas energy can be obtained from the total livestock, including bovine, ovine and poultry, in 2020. According to the data received from TSI in 2020, Ereğli district with 176758 bovine, Karapınar district with 368150 ovine and Meram district with 3912225 poultry numbers are leading in Konya.



**Table 3.** Number of animals available in Konya province in 2020 and biogas energy potential to be obtained

| Animal type | Animal Numbers | Amount of Usable Manure | Biogas Potential | Electricity Energy Potential | Heat Energy Potential |
|---|---|---|---|---|---|
| | Head | $10^3$ ton $year^{-1}$ | $10^3$ $m^3$ $year^{-1}$ | $10^6$ kWh $year^{-1}$ | $10^{10}$ kcal $m^{-3}$ |
| Bovine (cattle, buffalo) | 963047 | 2311.3 | 76273.3 | 358.5 | 35.8 |
| Ovine (sheep, goat) | 2826236 | 1318.9 | 76496.8 | 359.5 | 35.9 |
| Poultry (hens) | 11234107 | 164.8 | 12851.8 | 60.4 | 6 |
| **Total** | **15023390** | **3795** | **165621.9** | **778.4** | **77.8** |

Konya has 7 biogas plants, 3 of which are in the Karatay district, 2 in the Çumra district, 1 in the Sarayönü district, and 1 in the Meram district. The biogas power plant located in the Çumra district, with 12 MW electrical energy production, is the largest one. In addition to energy production in existing biogas facilities, organic fertilizer production is also carried out [43]. The operation of large biogas power plants in Konya, developing in agriculture and livestock, will provide significant benefits for the province and our country.

## 4. CONCLUSION

In Konya province, the biomass energy potential that can be obtained from cereals, industrial plants, tuber crops, fruits and vegetables and the biogas potential that can be obtained from the presence of bovine, ovine, and poultry were determined. In 2011, 62549.3 MWh of energy was obtained from 13.3 million tons of dry biomass, and 91661.9 MWh from 19.5 million tons of dry biomass in 2020. It's concluded that every year, the most energy is obtained from cereals and the least energy is obtained from vegetables. When the 2011-2020 annual changes are compared, there has been an increase of 47% in the cultivation area and biomass energy potential, and an increase of 68.1% in the biogas potential. While Cihanbeyli is the district with the most cultivation areas in 2020, Ereğli is the district with the highest production yield. In the same year, it was calculated that 57525.7 MWh of energy could be obtained from cereals, 10217.7 MWh from industrial plants, 13815 MWh from tuber plants, 6102.9 MWh from fruits, and 4000.6 MWh from vegetables throughout the province. In addition, it has been determined that approximately 165.6 million $m^3$ of biogas energy can be obtained from the total livestock in 2020. In the province of Konya, approximately 613227.7 ha of land in 2011 and 307158.6 ha of land in 2020 remain uncultivated. Every year, there has been a decrease in the uncultivated area throughout the province and an increase in the cultivated area. It has been observed that there has been a decrease of approximately 50% in uncultivated areas since 2011. When compared with similar studies in terms of biomass energy potential; while the annual average biomass energy potential that can be obtained

from plant wastes in Konya is 73419 MWh, this value is 45228 MWh in Mersin [34], 7432 MWh in Iğdır [35], and 53801 MWh in Afyonkarahisar [30].

Konya has a unique opportunity to combine good agricultural land use practices with increasing environmental benefits through biomass production systems. The bioenergy industry can provide an opportunity to strengthen our economy and diversify markets in the agriculture and forestry sectors. There are no fossil fuel deposits such as petroleum, natural gas and uranium in Konya. So, Konya needs fossil fuel imports more than many provinces due to its huge geography and potential to become an industrial center. During the transition to new energy systems, new opportunities for heat (thermal energy), combined heat, power, and potentially the use of biomass for advanced biofuels or cellulosic ethanol are anticipated. Therefore, Konya province should be considered as a very good opportunity to obtain energy from biomass with its fertile agricultural products and infrastructure related to the livestock sector. The biomass energy that can be obtained in Konya has very important potential for Turkey. It is thought that the country's economy will be benefitted by transforming the waste potential in the province into energy with modern methods. Barriers to the production and use of biomass energy in Turkey should be removed. Incentives should be given by developing an appropriate biomass energy policy.

## ABBREVIATIONS

| | | |
|---|---|---|
| A | = | Cultivated area (ha) |
| $BM_{max}$ | = | Maximum amount of dry biomass (ton) |
| $BM_{min}$ | = | Minimum amount of dry biomass (ton) |
| $BM_{mean}$ | = | Mean amount of dry biomass (ton) |
| $ED_{mean}$ | = | Mean of dry biomass energy value (kcal kg $^{-1}$) |
| GHG | = | Greenhouse gases |
| $ID_{max}$ | = | Maximum calorific value of dry biomass (kcal kg $^{-1}$) |
| $ID_{min}$ | = | Minimum calorific value of dry biomass (kcal kg $^{-1}$) |
| $ID_{mean}$ | = | Mean of dry biomass calorific value (kcal kg $^{-1}$) |
| TEP | = | Ton equivalent petroleum |

## REFERENCES


[1] Ventura S, Hull S, Jackson R, Radloff G, Sample D, Walling S, Williams C. Guidelines for sustainable planting and harvest of nonforest biomass in Wisconsin. Journal of Soil and Water Conservation 2012;67(1):17A-20A.

[2] Kılıçkap S, Yıldız C, Çakmak G. Investigation of the efficiency of hot water solar collectors in Elazig climatic conditions. Dicle University Journal of Engineering 2015;6(2):103-110.

[3] Kılıçkap S, El E, Yıldız C. Investigation of the effect on the efficiency of phase change material placed in solar collector tank. Thermal Science and Engineering Progress 2018;5:25-31.

[4] Külcü N. Biogas as an alternative energy source. Erciyes University Graduate School of Natural and Applied Sciences Journal 1985;1:126-135.

[5] Işık S, Yıldız C. Improving thermal energy storage efficiency of solar collector tanks by placing phase change materials in novel finned-type cells. Thermal Science and Engineering Progress 2020;19:100618.

[6] Anonymous [Internet]. Renewable energy sources; 2014 [cited 2021 Dec 22]. Available from: http//www.ultraenerji.com

[7] El E, Argunhan Z, Çakmak G, Yücel HL, Yildiz C. Effect of the air flow rate of blower on the performance of solar still. J Therm Sci Technol, 2015;35(2):145-152.

[8] Sezek M. Using of industrial plants and plant residues as biofuel. Alinteri Journal of Agriculture Science, 2018;33(1):105-111.

[9] McKendry P. Energy production from biomass (part 1): an overview of biomass. Bioresource Technology, 2002;83(1):37-46.

[10] Bridgwater T. Biomass for energy. Journal of the Science of Food and Agriculture, 2006;86(12):1755-1768.

[11] Anonymous [Internet]. European Commission, energy for the future: renewable energy sources–White paper for a community strategy and action plan. communication from the Commission; 1997, COM (97) 599, Final of 26.11.97. EC, Brussels.

[12] Anonymous [Internet]. IEA, World Energy Outlook; 2000, IEA, Paris.

[13] Anonymous [Internet]. IEA Bioenergy. The role of bioenergy in greenhouse gas mitigation, Position paper; 1998, IEA Bioenergy, New Zealand.

[14] Anonymous [Internet]. 2021 [cited 2021 Dec 23]. Available from: https://www.1energysystems.com/renewable-energy-sources/

[15] Anonymous [Internet]. 2021 [cited 2021 Nov 21]. Available from: https://www.eie.gov.tr/

[16] Bayramoğlu T. Biomass energy and local economic development: a field study on biomass potential and economic impacts in tra1 region (Erzurum-Erzincan-Bayburt). Ataturk University Institute of Social Sciences. Doctoral Thesis (Unpublished).

[17] Anonymous [Internet]. 2021 [cited 2021 Dec 27]. Available from: https://enerji.gov.tr/bilgi-merkezi-enerji-biyokutle

[18] Işık S, Yavuz S. An overview of biofuels derived from biomass. European Journal of Science and Technology, 2022;34:193-201.

[19] Kurt G, Koçer NN. Biomass potential of Malatya city and energy production. Erciyes University Graduate School of Natural and Applied Sciences Journal, 2010;26(3):240-247.

[20] Melikoğlu M, Albostan A. Bioethanol production and potential in Turkey. Journal of the Faculty of Engineering and Architecture of Gazi University, 2011;26(1).

[21] Anonymous [Internet]. 2021 [cited 2021 Dec 29]. Available from: https://biyoenerjidergisi.com/biyokutle-donusum-teknolojileri/

[22] Prochnow A, Heiermann M, Plöchl M, Amon T, Hobbs PJ. Bioenergy from permanent grassland–A review: 2. Combustion. Bioresource technology, 2009;100(21):4945-4954.

[23] Suntana AS, Vogt KA, Turnblom EC, Upadhye R. Bio-methanol potential in Indonesia: forest biomass as a source of bio-energy that reduces carbon emissions. Applied Energy, 2009;86:215-221.

[24] Williams CL, Dahiya A, Porter P. Introduction to bioenergy and waste to energy. In Bioenergy. Academic Press. The United States, 2020;5-44.
[25] Işık S, Yavuz S. Investigation of biogas production potential from livestock manure by anaerobic digestion in Bingöl Province. Turkish Journal of Nature and Science, 2022;11(1):116-122.
[26] Statistics GB. World bioenergy association, 2020.
[27] Karayılmazlar S, Saraçoğlu N, Çabuk Y, Kurt R. Utilizations of biomass as an energy source in Turkey. Journal of Bartin Faculty of Forestry, 2011;13(19):63-75.
[28] Saraçoğlu N. Global climate change, bioenergy and energy forestry. Efil publishing house. Ankara-Türkiye, 2010;298.
[29] Üçgül İ, Akgül G. Biomass technology. Süleyman Demirel University Yekarum e-Journal, 2010;1(1).
[30] Topal M, Topal EIA. Determination of potential of biomass energy from crop plants as a renewable energy source: the case of Afyonkarahisar province (2006-2010) (025401)(1-11). Afyon Kocatepe University Journal of Science and Engineering Sciences, 2012;12(2):1-11.
[31] Koçer N, Ünlü A. Biomass potential of East Anatolia region and energy production. Fırat University Journal of Oriental Studies, 2007;5(2):175-181.
[32] Topal M, Topal EIA. On the biomass energy potential of Elazig province: 2000-2010. Journal of Mehmet Akif Ersoy University Institute of Science and Technology, 2012;3(2):21-30.
[33] Demir M. Potential and availability of biomass energy in Kars. Turkish Geographical Review, 2018;(68):31-41.
[34] Demir B, Kuş ZA, İrik HA, Çetin N. Agricultural biomass energy equivalent potential of Mersin province. Alinteri Journal of Agriculture Science, 2015;29(2):12-18.
[35] Kuş E, Yıldırım Y, Çokgez Kuş A, Demir B. Agricultural biomass potential and energy equivalent of Iğdır province. Iğdır University Journal of Institution Science & Technology, 2016;6(1):65-73.
[36] Ekin İ, Döner A, Keskin Aİ. Biomass energy: biomass energy potential of Şırnak province. Şırnak Energy and Mining Potential, Education publishing house, 2018;89-220.
[37] Anonymous [Internet]. 2020 [cited 2020 Dec 31]. Available from: http://www.kto.org.tr/tarim-449s.htm
[38] Anonymous [Internet]. 2021 [cited 2021 Dec 13]. Available from: https://www.tuik.gov.tr/
[39] Anonymous [Internet]. 2021 [cited 2021 Dec 13]. Available from: https://tr.wikipedia.org/wiki/Konya#cite_noteG%C3%BCncel_N%C3%BCfus_De%C4%9Ferleri-1
[40] Anonymous [Internet]. 2021 [cited 2021 Dec 13]. Available from: http://www.birimcevirme.org/
[41] Deniz Y. Biogas potential in Turkey and benefits of biogas. Rural Services Ankara Research Institute. Ankara, 1987.
[42] Akbulut A, Dikici A. Biogas potential and cost analysis of Elazig province. Fırat University Journal of Oriental Studies, 2004;2(2):36-41.
[43] Anonymous [Internet]. 2022 [cited 2021 May 23]. Available from: https://biyogazder.org/biyogaz-tesisleri/

Cilt 11, Sayı 2, Sayfa 99-106, 2022 Volume 11, Issue 2, Page 99-106, 2022

Araştırma Makalesi https://doi.org/10.46810/tdfd.808519 Research Article

Türk Doğa ve Fen Dergisi
Turkish Journal of Nature and Science
www.dergipark.gov.tr/tdfd

# $R^3_1$ Semi-Riemannian Uzayda 2-Cob Üreteç Kobordizm Örnekleri

**Muhsin İNCESU[1*], Sara IŞIK[2]**

[1] Muş Alparslan Üniversitesi Eğitim Fakültesi, Matematik Eğitimi ABD, Muş, Türkiye
[2] Muş Alparslan Üniversitesi Fen Bilimleri Enstitüsü, Muş, Türkiye
Muhsin INCESU ORCID No: 0000-0003-2515-9627
Sara ISIK ORCID No: 0000-0002-4058-3277

**Sorumlu yazar: m.incesu@alparslan.edu.tr*

(Alınış: 09.10.2020, Kabul: 31.05.2022, Online Yayınlanma: 29.06.2022)

**Anahtar Kelimeler**
Kobordizm, Birasyonel invaryant, Semi-Riemannian manifold, Kodaira boyutu, Regle yapı

**Öz:** Duggal ve Bejancu 1996 da yayınladıkları kitapta bir semi-Riemannian manifoldda lightlike (null) alt uzayın varlığını gösterdiler ve alt manifoldların geometrisi için ihtiyaç duyulan önemli bir boşluğu doldurdular. Semi-Riemannian manifoldlar için unireglelik, kodaira boyutu gibi birasyonel invaryantların yanında maximum lineer bağımsız lightlike vektörlerin sayıları olan k(U) değerlerinin de bir birasyonel invaryant olduğu vurgulanarak $R^3_1$ Semi-Riemannian Uzayda 2-Cob Üreteç kobordizmlere örnekler verilmiş, bunların kodaira boyutları ve k(U) invaryantları ifade edilmiştir.



# The Examples of Generators of 2-cob Cobordisms in Semi-Riemannian Space $R^3_1$

**Keywords**
Cobordism, Birational invariant, Semi-Riemannian manifold, Kodaira dimension, Ruled variety

**Abstract:** In their book published in 1996, Duggal and Bejancu demonstrated the existence of a lightlike (null) subspace in a semi-Riemannian manifold and filled an important gap needed for the geometry of submanifolds. In addition to birational invariants such as uniruledness and kodaira dimensions for Semi-Riemannian manifolds, in this study, by emphasizing the k (U) values which are the numbers of maximum linearly independent lightlike vectors, that are a birational invariance, the examples of generators of 2- Cob cobordisms are given in Semi-Riemannian Space R(3,1). Their codaira dimensions and k (U) invariants of these examples has been expressed.

## 1. GİRİŞ

Uzun zamandır simplektik geometride birasyonel denkliğin uygun bir kavramının ne olduğu gerçekten açık değildi. Simplektik geometride blow-up/blow-down gibi basit birasyonel operasyonlar biliniyordu[1,2]. Fakat esnek simplektik kategoride genel birasyonel fonksiyon kavramının açık bir genellemesi yoktu. Bu durum son zamanlarda zayıf faktörizasyon teoreminin geliştirilmesiyle büyük ölçüde değişmiştir [3] ki bu teoreme göre projektif manifoldlar arasındaki herhangi bir birasyonel fonksiyon blow-up ve blow-down ların (yukarı ve aşağı etkilerin) bir dizisi halinde ayrıştırılabilir [4].

Birasyonel geometrinin en temel kavramı unirregleliktir. Cebiro-geometrik bir şekilde bunun anlamı bir manifoldun cebirsel eğrilerle kaplanabilmesi demektir. Dikkat etmek gerekir ki, cebirsel geometrideki tanımı basit bir şekilde taklit ederek bu kavramı tanımlamak anlamsızdır [5] ve her noktadan geçen sabit sınıflarda bir simplektik kürenin olması da gerekir. Aksi takdirde her basit bağlantılı manifold uniregle olmalıdır [4].

Diğer yandan Kollar- Ruan'ın teoremiyle [6,7] bir uniregle projektif manifold, bir nokta arakesitiyle, sıfırdan farklı bir cins sıfır GW-invaryanta sahiptir. Bu nedenle, eğer bir nokta kısıtlaması dahil ederek sıfırdan farklı bir tür sıfır GW-invaryant varsa (M,w) simplektik manifolda unireglediz denir [4].

Duggal ve Bejancu 1996 da yayınladıkları kitapta bir semi-Riemannian manifoldda lightlike (null) alt uzayın varlığını gösterdiler [8,9,10] ve alt manifoldların geometrisi için ihtiyaç duyulan önemli bir boşluğu doldurdular. Bu kitabin yayınlanmasından sonra hedef, lightlike geometrideki yeni geometrik sonuçların ispatı ve lightlike geometrinin fizikteki uygulamaları oldu. Böylece geometrinin önemli bir boşluğu dolduruldu ve yeni bir çalışma alanı ortaya çıktı.

1942 yılında Moskova Üniversitesinde Lev Pontjagin, Charles Ehresmann sayesinde bir hücre alt bölümünü kullanarak Grassmann manifoldlarının homolojisini çalışmaya başlamıştır. Bu onun yeni önemli bir karakteristik sınıf oluşturmasına olanak sağlamıştır.[11]
1946 yılında Shiing-Shen Chern kompleks vektör demetleri için bir sınıf tanımlamıştır. [12] Chern göstermiştir ki kohomoloji yapısına sahip olan kompleks Grassmann manifoldlarını anlamak, reel Grassmann manifoldlarını anlamaktan daha kolaydır[11]. Chern temel makalesinde Hermitian manifoldları için karakteristik sınıflarının bazı inşaalarını vermiştir. [11].

## 2. MATERYAL VE METOT

**Tanım 1:** $R$ birimli ve değişmeli bir halka ve $R-\{0_R\}=R^*$, ikinci işlem $\cdot$ ye göre bir grup ise $R$ ye bir cisim denir [13].

**Tanım 2:** $R$ bir tamlık bölgesi olsun. $m1_R=0_R$ olacak şekilde bir $m>0$ tam sayısı varsa böyle $m$ lerin en küçüğüne $R$ nin karakteristiği denir. Eğer bu özellikte hiçbir $m>0$ bulunamıyorsa $R$ nin karakteristiği sıfır denir [13].

,

**Tanım 3:** R ve S tamlık bölgeleri verildiğinde, R den S ye 1-1 bir homomorfizma bulunabiliyorsa R, S içine gömülebilir veya S, R nin bir genişlemesidir denir [13].

**Tanım 4:** Eğer *K*, bir *L* cisminin alt cismi ise , o zaman *( L, K )* sıralı ikilisi, bir cisim genişlemesidir. $L/K$ olarak yazılabilir. *K* üzerinde vektör uzayı olarak *L* nin boyutu $[L:K]$ olarak yazılır. Bu boyutun sonlu olduğu durumda $L/K$ genişlemesinin kendisine sonlu denir [14].

**Tanım 5:** $M$ bir $C^\infty$ manifold olsun. $p\in M$ noktasındaki tanjant uzay $T_pM$ olmak üzere,

$$g_p: T_pM \times T_pM \longrightarrow R$$
$$(X_p, Y_p) \longrightarrow g_p(X_p, Y_p)$$

biçiminde tanımlı sabit indeksli, simetrik, bilineer, non-degenere $(0,2)$ tensörüne $M$ üzerinde bir metrik tensör denir [15].

**Tanım 6:** $M$ bir $C^\infty$ manifold olsun. $M$ bir $g$ metrik tensörü ile donatılmışsa, $M$ ye bir semi-Riemannian manifold denir [15].

**Tanım 7:** Bir $M$ Semi-Riemannian manifoldu üzerinde tanımlı $g$ metrik tensörünün indeksine semi-Riemannian manifoldun indeksi denir ve $indM$ ile gösterilir.

Eğer indeks ν ise $0\le \nu \le boyM$ dir. Özel olarak, $\nu=0$ ise $\forall p\in M$ için $g_p$, $T_pM$ üzerinde pozitif tanımlı bir iç çarpım olduğundan, $M$ bir Riemannian manifold olur. $\nu=1$ ve $n\ge 2$ olması durumunda ise, $M$ ye bir Lorentz manifoldu denir [15].

**Tanım 8:** $V$ sonlu boyutlu reel vektör uzayı, $V$ üzerindeki simetrik bilineer form

$$\gamma: V\times V\to R$$

R-bilineer fonksiyonu olsun. $V$ üzerinde tanımlı $\gamma$ simetrik bilineer formu

**(i)** $\nu\neq 0$ iken $\gamma(\nu,\nu)>0$ ise $\gamma$ pozitif tanımlıdır.

**(ii)** $\nu\neq 0$ iken $\gamma(\nu,\nu)<0$ ise $\gamma$ negatif tanımlıdır.

**(iii)** $\forall\omega\in V$ iken $\gamma(\nu,\omega)=0$ şartı sadece $\nu=0$ için sağlanıyorsa $\gamma$ ye non-degeneredir denir [15].

**Tanım 9:** $M$ bir Semi-Riemannian manifold olsun. $X_p\in T_pM$ olmak üzere,

**i)** $g_p(X_p,X_p)>0$ veya $X_p=0$ ise $X_p$ vektörüne spacelike,

**ii)** $g_p(X_p,X_p)<0$ ise $X_p$ vektörüne timelike,

**iii)** $g_p(X_p,X_p)=0$ , $X_p\neq 0$ ise $X_p$ vektörüne lightlike (null) denir [15].

$R^n$ n- boyutlu reel vektör uzayı olsun.

**Tanım 10:** Eğer bir $\{f_\tau(x),\tau\in T\}$ ailesi, $f_\tau(x)\in R[x]$ olmak üzere bulunabiliyorsa,

$$X=\{x\in R^n: f_\tau(x)=0,\forall\tau\in T\}\subset R^n$$

altkümesine $R^n$ nin bir afin manifoldu denir [16].

**Örnek 1**: $R$ de keyfi bir sonlu altküme bir afin manifolddur. Yani,

$$X=\{r_1,r_2,\dots,r_m\}\subset R$$

bir afin manifolddur. Çünkü,

$$X=\{x\in R:(x-r_1).(x-r_2)\dots(x-r_m)=0\}\subset R$$

yazılabilir [16].

**Önerme 1:** $X$, $R$ de bir afin manifold olsun. Bu takdirde $X$=$R$ veya $X=\emptyset$ ya da $X$, $R$ nin sonlu bir altcümlesidir [16].

**Örnek 2 :** $n = 2$ durumunda iki değişkenli polinomların sıfır yerleri olarak,

$X = \{(x,y) \in R^2 : f(x,y) = ax + by + c = 0\}$
kümesini alalım, burada $a,b,c \in R$ sabit sayılar olsun. Bu küme düzlemde bir doğrudur. Dolayısıyla keyfi doğru düzlemde bir afin manifolddur.

**Önerme 2:** Herhangi sayıda afin manifoldların arakesiti de bir afin manifolddur [16].

**Önerme 3:** $X_1, X_2$ afin manifoldlar ise $X_1 \cup X_2$ de bir afin manifolddur [16].

**Sonuç 1:** Sonlu sayıda afin manifoldun birleşimi de bir afin manifolddur.

Şimdi $R^n$ deki afin manifoldlarla bir topoloji oluşturacağız. $\Im$ ile $R^n$ deki tüm afin manifoldlar sistemini gösterelim. Yani,

$\Im = \{X : X \subset R^n \ \ bir\ Afin\ manifold\}$
olsun. Böylece

$$T1)\ \ R^n \in \Im$$
$$T2)\ \ \emptyset \in \Im$$
$$T3)\ \ \forall \tau \in T \text{ için } X_\tau \in \Im \text{ iken } \bigcap_{\tau \in T} X_\tau \in \Im$$
$$T4)\ \ X_1, \dots, X_m \in \Im \text{ için } \bigcup_{\tau=1}^{m} X_\tau \in \Im$$

dır. Dolayısıyla $\Im$ sistemi, $R^n$ de kapalı kümelerle oluşturulmuş bir topolojidir. Bu topolojiye Zarisski topolojisi denir [16].

$R^n$ deki sonlu sayıda noktadan oluşan keyfi bir altküme Zarisski topolojisine göre kapalıdır. Önerme 1 e göre n = 1 için $R$ deki Zarisski topolojisine göre R nin kapalı altkümeleri ancak $R, \emptyset$ ve sonlu altkümelerdir. Buna göre $R$ de [0,1] aralığı öklid topolojisine göre kapalı olmasına karşın Zarisski topolojisine göre kapalı değildir [16].

**Önerme 4:** $R$ de Zarisski topolojisi Housdorf topolojisi değildir [16].

**Tanım 11:** $X$ bir topolojik uzay olsun. Eğer, $X_1, X_2 \subset X$ kapalı altkümeleri, $X_1 \neq X \ \ X_2 \neq X$, iken $X_1 \cup X_2 = X$ olacak biçimde bulunabiliyorsa $X$ topolojik uzayına indirgenebilir denir. Aksi halde $X$ topolojik uzayına indirgenemez denir. [16].

**Örnek 3:** Zarisski topolojisine göre $R$ topolojik uzayı indirgenemezdir.

**Önerme 5:** $M$ topolojik uzayı indirgenemezdir ancak ve ancak $M$ deki keyfi iki boştan farklı açık kümelerin arakesiti boş değildir [16].

**Önerme 6:** $R^n$ indirgenemezdir [17].

**Önerme 7:** $U$ , $R^n$ de boştan farklı keyfi bir açık küme ise $\bar{U} = R^n$ dir. Yani $U$, $R^n$ de yoğundur [17].

**Önerme 8:** $B \subset R^n$ bir alt küme ve $f \in R[x_1, \dots, x_n]$ öyleki $f(x) = 0, \forall x \in B$ olsun. Bu takdirde $f(x) = 0$, $\forall x \in \bar{B}$ dir [16].
**Lemma 1:**( $R^n$ için Cebirsel Eşitsizliklerin Önemli Olmadığı Prensibi):

$p_i \in R[x_1, \dots, x_n]$ , $i$=1,…,$k$ sıfırdan farklı polinomlar olsunlar.

$$B = \{x \in R^n : p_i(x) \neq 0, i = 1, \dots, k\}$$

olsun. Bir $F(x_1, \dots, x_n)$ polinomu için $F|_B = 0$ ($\forall x \in B$ için $F(x) = 0$) ise, $F|_{R^n} = 0$ dir [16].

**Sonuç 2:** $p_i \in R[x_1, \dots, x_n]$ ,, $i$=1,…,$k$ sıfırdan farklı polinomlar ve

$$B = \{x \in R^n : p_i(x) \neq 0, i = 1, \dots, k\}$$

olsun. $f.g \in R[x_1, \dots, x_n]$ öyle ki, $f|_B = g|_B$ olsun. Bu takdirde $f|_{R^n} = g|_{R^n}$ dir.

**Tanım 12:** Bir $(C, \partial, \iota)$kobordizm *kategorisi* şu şartları sağlayan bir üçlüdür.

**1)** $C$ bir sonlu toplamlı ve başlangıç nesnesi $\emptyset$ olan bir kategoridir.

**2)** $\partial : C \to C$ funktörü $\partial\partial M = \emptyset$ (her $M \in C$ için) ve $\partial\emptyset = \emptyset$ şartını sağlayan toplamsal bir funktördür.

**3)** $\iota : \partial \to id$ funktörü, $id$ birim funktör olmak üzere toplamsal funktörlerin bir doğal transformasyonudur.

**4)** $C$ nin her zaman bir küçük $C_0$ alt kategorisi vardır öyle ki $C$ nin her elemanı, $C_0$ ın bir elemanına izomorfiktir.

Burada, kompakt diferansi-yellenebilir manifoldlar durumunda $\emptyset$ , bir boş manifold olarak ve $\iota$ da $M$ nin $\partial M$ yi içermesi olarak düşünülür. $D_0$ alt kategorisinin varlığı, Whitney gömme teoreminin, (her manifoldun $R^\infty$ un bir alt manifolduna izomorfik olması) biçimindeki ifadesiyle algılanır [18].

27 farklı durum için kobordizm problemlerinin bir listesini [19] de görebiliriz.

Kobordizm temel tanımı, şu denklik bağıntısıyla verilir.

**Tanım 13:** M ve N, n boyutlu iki kompakt manifoldlar olmak üzere, eğer n+1 boyutlu bir W kompakt manifoldu, sınırı M ve N nin ayrık birleşimi olarak yazılabilecek şekilde bulunabilirse M ile N ye kobordant, W ye de M ile N arasında bir kobordizm denir [20] (bkz. Şekil 1).

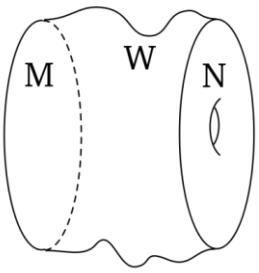


**Şekil 1:** Kobordizm (*W*; *M*, *N*).

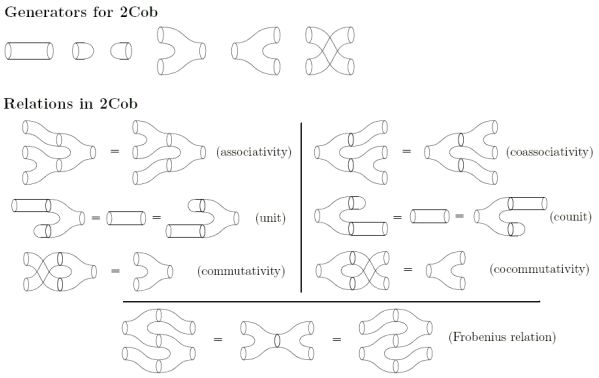


**Şekil 2:** 2 boyutlu kobordizmler için üreteçler ve onlarla üretilen denk kobordizmler

**Tanım 14:** Bir Semi-Rieamannian manifoldda maximum lineer bağımsız lightlike (null) vektörlerinin sayısına k(U) indexi denir [21].

**Önerme 8:**

$$k(U) = 0 \Leftrightarrow \begin{cases} U - spacelike, & boyU = 1 \\ U - spacelike, & boyU > 1 \\ U - timelike, & boyU = 1 \end{cases}$$

[21].

Cebirsel geometride, Kodaira boyutu κ (X), projektif bir X yapısının kanonik modelinin boyutunu ölçer. Bir cisim üzerinde tanımlı n boyutlu bir X düzgün cebirsel yapısının kanonik demeti, X in kotanjant demetinin n. nci dış kuvveti olan bir d tamsayısı için, $K_X$ in d. nci tensor kuvveti yine bir doğru demetidir.

$$K_X = \bigwedge^{n} \Omega^1_X$$

n-formlarının doğru demetidir. $d \geq 0$ için $H^0(X,K_X{}^d)$ global bölümlerin vektör uzayı, X düzgün projektif yapısının birasyonel invaryantı olmasından dolayı olağanüstü özelliğe sahiptir. Yani, bu vektör uzayı, daha düşük boyutlu alt kümelerin dışında X'e izomorfik olan herhangi bir düzgün projektif yapı için karşılık gelen uzay ile kanonik olarak tanımlanır. $d \geq 0$ için X in d.nci $P_d$ çoğul genusu (plurigenus), $K_X{}^d$ nin global bölümlerinin vektör uzayının boyutu olarak tanımlanır:

$P_d = dim\ H^0(X,K_X{}^d)$

Buna gore X in kodaira boyutu κ (X),

$$\kappa(X) = \begin{cases} -\infty, & eğer \ \text{her } d > 0 \text{ için } P_d = 0 \ ise \\ {}^{P_d}/_{d^k} & yı\ sınırlı\ yapan\ k\ ların\ minimumu, \quad diğer\ durumlarda \end{cases}$$

biçimninde tanımlanır. Böylece n boyutlu bir X projektif yapısının kodaira boyutu ya $-\infty$ dur ya da 0 ile n arasında bir tamsayı değeridir [25].

Cebirsel geometride $K$ -cismi üzerinde tanımlı bir cebirsel yapıya "ruled" denir, eğer o, bir projektif doğru ile $K$ üzerindeki bazı yapıların çarpımına birasyonel ise. Bir cebirsel yapı "uniruled" dir eğer, o bir rasyonel eğriler ailesi ile kaplanırsa. (Daha kesin bir ifadeyle, $X$ uniruleddir eğer, vardır bir $\gamma$ ve $\gamma \times P_1 \to X$ dominant rasyonel map öyle ki, Y ye projeksiyon boyunca etki etmez) [25].

Karakteristiği 0 (sıfır) olan bir cisim üzerindeki her uniruled yapı, -∞ kodaira boyutuna sahiptir. Tersi, en fazla 3 boyutta bilinen bir varsayımdır: karakteristiği sıfır olan bir cisim üzerindeki cebirsel yapının kodaira boyutu -∞ ise uniruled olmalıdır. Bununla ilgili şu ifade tüm boyutlarda bilinir: Boucksom, Dewailly, Pâun, ve Peternell gösterdi ki, karakteristiği sıfır olan bir cisim üzerindeki bir düzgün projektif $X$ yapısı, uniruleddir. ⇔ $X$ in kanonik demeti pseudo-effektive değildir (Yani, reel sayılarda tensörlendirilmiş Neron-Severi grubundaki, efektif bölenlerle elde edilmiş kapalı konveks koni içinde değil) [22,25]. Çok özel bir durumda karakteristiği sıfır olan bir cisim üzerindeki $P^n$ de derecesi $d$ olan bir düzgün hiperyüzey, uniruleddir ⇔ $d \leq n$ ise, (Aslında $P^n$ deki derecesi $d \leq n$ olan bir düzgün hiperyüzey Fano yapısındadır ve bundan dolayı, (unireglelikten daha güçlü olan) rasyonel bağlantılıdır) [25].

Sayılamayan cebirsel kapalı $K$- cismi üzerindeki $X$ cebirsel yapısı uniruleddir. ⇔ En az bir rasyonel eğri vardır öyle ki $X$ in her $k$ noktasından geçer. Tersine, bir $K$- sonlu cisminin cebirsel kapanışı üzerinde, cebirsel yapılar vardır ve bunlar uniruled değildir. Fakat bunların her $k$ noktasından geçen bir rasyonel eğri vardır ($p$ -tek alınmak üzere herhangi bir $F_p$ non-super singüler abelyen yüzeyinin Kummer yapısı bu özelliğe sahiptir) [23,25].

Uniruledlik bir geometrik özelliktir. Cisim genişlemeleri altında değişmezdir. Oysa ki ruled yapı böyle değildir. Pozitif karakteristikte uniruledlik çok farklı davranır. Özellikle genel tipte uniruled yüzeyler (hatta unirational) vardır. $p \geq 5$ olan $p$ asal sayıları için $\bar{F}_p$ üzerindeki $P^3$ de $x^{p+1} + y^{p+1} + z^{p+1} + w^{p+1} = 0$ yüzeyi bunun bir örneğidir [24]. Böylece uniruledlik, pozitif karakteristikte kodira boyutununun $-\infty$ olmasını ima etmez [25].

Kısaca özetlersek;

1 boyutlu eğriler için,

Düzgün projektif eğriler, $g = 0,1,\ldots$ gibi herhangi bir doğal sayı olan genuslarına göre ayrık olarak sınıflandırılır. Buradaki ayrık olarak sınıflandırma şu

anlamdadır: bir genus verildiğinde o genuslu eğrilerin indirgenemez bir moduli uzayı vardır.

Bir X eğrisinin Kodaira bayutu :

$K$=-∞ : genus 0 (projective line $P^1$): $K_X$ efektif değil, her $d>0$ için $P_d=0$
$K$=0 : genus 1(eliptik eğriler): $K_X$ aşikar demet, her $d \geq 0$ için $P_d=1$
$K$=1 : genus $g \geq 2$ (genel tipten eğri): $K_X$ geniştir (ample), her $d \geq 2$ için $P_d=(2d\text{-}1)(g\text{-}1)$

2, 3 ya da daha büyük boyutların sınıflandırmaları için bakınız [25].

## 3. BULGULAR

### 3.1. $R^3_1$ Semi-Riemannian Uzayda 2-Cob Üreteç Kobordizm Örnekleri

**Örnek 1:**
$R^3_1$ Semi- Rieamann alt uzayında bir kobordizm örneği olarak en temel kobordizmlerden pantolon şeklindeki kobordizmi göz önüne alalım. l doğrusu olarak {z = 4y+12; x = 0} doğrusunu ve $p$ parabolü olarak da {z =- $4y^2$; x = 0} parabolünü göz önüne alalım. l nin z > 0 olan kısmını z- ekseni etrafında döndürelim. Bu tam dönmede büyük çemberler oluşacağından pantolonun üst tarafında boşluklar oluşacaktır. Burada dönmeyi dönme açısına göre ilk 180 ve son 180 derecelik açılarla ayırıp ve küresel koordinatlar ile istenilen yüzeyi sağlayacak dönme açılarını sağlamak gerekir. Benzer şekilde $z \leq 0$ kısmını da; z = $z_0$ a karşılık gelen l doğrusu üzerindeki noktayı A ile, z = $z_0$ a karşılık gelen p parabolü üzerindeki noktayı da B ile gösterirsek, A noktasını, A ile B nin orta noktası etrafında xy- düzlemine paralel kalacak şekilde döndürelim. Bu döndürme sonucunda bir çember elde edilecektir. Bu çember hem l doğrusuna ve hem de $p$ parabolüne teğet bir çemberdir. Bu şekilde z değerlerine göre elde edilecek çemberler pantolon yüzeyinin uzun bacaklarını oluşturacaktır. Şimdi pantolonumuzu z>0 ve $z \leq 0$ göre ayıracak olursak 3 parça elde ederiz. Birinci parça z>0 a karşılık gelen dönel yüzey, ikinci ve üçüncü parçalar ise $z \leq 0$ a karşılık gelen biri diğerinin yansıması şeklinde iki pantolon bacağını oluşturan yüzeylerdir. Birinci dönel yüzeyi de parametrik ifadesini yazabilmek adına y≤0 ve y>0 olmak üzere tekrar ikiye ayırırsak, pantolon yüzeyini 4 parçaya ayırmış oluruz (Şekil 3).

Şimdi bu yüzeyin parametrik denklemini verelim:

**I yüzeyi:**

$a \in [0,1]$ ve $w \in [0,\pi]$ olmak üzere

$$X = 2cosw + a\left[\frac{3}{2}cos\left(-\frac{3}{2}\pi + 2(w-\pi)\right) - 2cosw\right]$$
$$Y = 2sinw + a\left[\frac{3}{2}sin\left(-\frac{3}{2}\pi + 2(w-\pi)\right) - 2sinw - \frac{3}{2}\right]$$
$$Z = 4(1-a)$$

biçiminde verilebilir. MATLAB ile bu yüzeyi çizersek Şekil 4-a'daki grafik elde edilir.

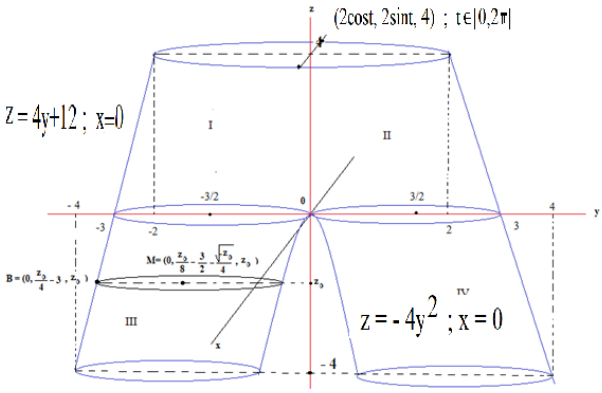


**Şekil 3:** {z = 4y+12; x = 0} doğrusu ve {z = -$4y^2$; x = 0} parabolü ile elde edilen kobordizm tasarım örneği

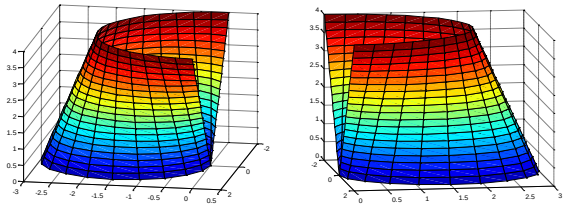

(a) (b)

**Şekil 4:** Pantolon tipi kobordizmin I ve II nolu parçası

**II Yüzeyi:**

$a \in [0,1]$ ve $w \in [\pi, 2\pi]$ olmak üzere,

$$X = 2cosw + a\left[\frac{3}{2}sin2w - 2cosw\right]$$
$$Y = 2sinw + a\left[-\frac{3}{2}cos2w - 2sinw + \frac{3}{2}\right]$$
$$Z = 4(1-a)$$

biçiminde verilebilir. MATLAB ile bu yüzeyi çizersek şekil 4-b deki gibi grafik elde ederiz.

**III Yüzeyi:**

$k \in [-4,0]$ ve $t \in [0,2\pi]$ olmak üzere,

$$X = \left[\frac{k}{8} - \frac{3}{2} + \frac{\sqrt{-k}}{4}\right]cost$$
$$Y = \left[\frac{k}{8} - \frac{3}{2} + \frac{\sqrt{-k}}{4}\right]sint + \left[\frac{k}{8} - \frac{3}{2}\right]$$
$$Z = k$$

biçiminde verilebilir. MATLAB ile bu yüzeyi çizersek şekil 5-a grafiği elde edilir.

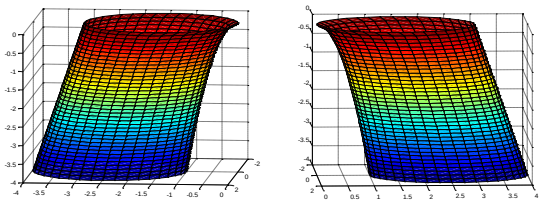

(a) (b)

**Şekil 5:** Pantolon tipi kobordizmin III ve IV nolu parçası

**IV Yüzeyi:**

$k \in [-4,0]$ ve $t \in [0,2\pi]$ olmak üzere

$$X = \left[\frac{k}{8} - \frac{3}{2} + \frac{\sqrt{-k}}{4}\right] cost$$

$$Y = \left[\frac{k}{8} - \frac{3}{2} + \frac{\sqrt{-k}}{4}\right] sint - \frac{k}{8} + \frac{3}{2} + \frac{\sqrt{-k}}{4}$$

$$Z = k$$

biçiminde verilebilir. MATLAB ile bu yüzeyi çizersek şekil 5-b grafiği elde edilir.

Şimdi bu dört yüzeyi birleştirirsek;

Z > 0 ve Y < 0 durumunda I yüzeyi;
Z > 0 ve Y > 0 durumunda II yüzeyi;
Z < 0 ve Y < 0 durumunda III yüzeyi;
Z < 0 ve Y > 0 durumunda IV yüzeyi;

biçiminde birleştirdiğimizde parametrik yüzey parçalı olarak şekil 6 daki gibi elde edilecektir.

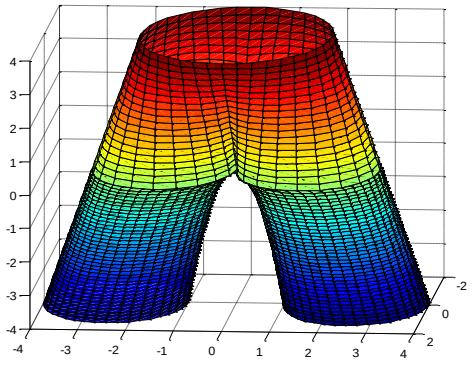

**Şekil 6:** Dört yüzeyin birleşimiyle elde edilen pantolon kobordizm örneği

Şimdi bu yüzeyin üzerindeki lightlike yada ışıksal vektörleri elde edecek olursak bunlar birer elips çiftleri oluşturacaklardır. Bu çiftler yukarıdaki kobordizm ile $X^2 + Y^2 - Z^2 = 0$ denklemiyle verilen uzay-zaman konisinin arakesitiyle bulunur. Bu eğrileri elde etmek için koninin parametrik denklemini de ifade edersek, u∈R, v∈[0,2π] olmak üzere parametrik denklem,

X(u,v)=ucos(v); Y(u,v)=usin(v); Z(u,v)=u;

biçimindedir. O halde arakesit grafiği aşağıdaki gibi olur:

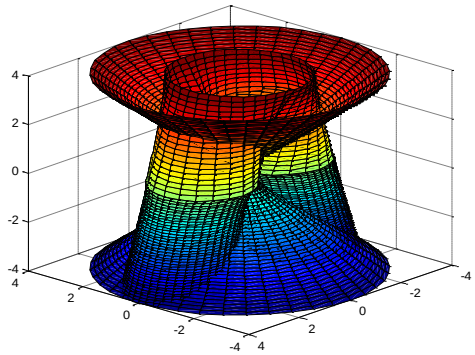

**Şekil 7:** Kobordizm üzerindeki lightlike (ışıksal) vektörler pantolon yüzeyi ile koninin arakesitini oluşturan elipsler

Bu elips çiftleri bir boyutlu manifold olduklarından boyutu 1 dir. O halde kobordizm üzerindeki lightlike yada ışıksal vektörlerin boyutu k(U)=1 olur. Bu da [21] e göre birasyonel kobordizm invaryantdır. Benzer şekilde, bu yüzeyler her biri karakteristiği sıfır olan complex cisim C üzerinde olduğundan örnekteki semi-Rieamannian manifoldun bir diğer birasyonel kobordizm invaryantı, kodaira boyutu $-\infty$ dur. Eğer yukarıdaki pantolon şeklindeki kobordizm yüzeyi tamamen space-like ya da tamamen timelike olsaydı bu durumlarda da k(u) invaryantı k(u)=0, kodaira boyutu yine $-\infty$ olurdu.

**Örnek 2:** Şimdi ikinci bir örnek olarak yine $R^3_1$ uzayında eğik boru şeklindeki bir kobordizm göz önüne alalım. Bu yüzeyin parametrik denklemi $u \in R$, $v \in [0,2\pi]$ olmak üzere,

$$X(u,v) = sinv$$
$$Y(u,v) = \sqrt[3]{u} - cosv$$
$$Z(u,v) = u$$

olarak alınabilir (Şekil 8).

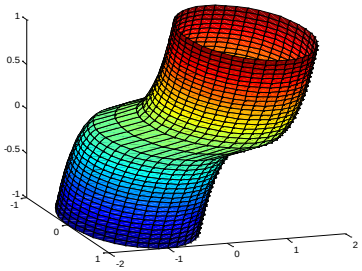

**Şekil 8:** Eğik boru şeklindeki kobordizm örneği

Şimdi bu yüzeyin üzerindeki lightlike yada ışıksal vektörleri elde edecek olursak bunlar bir hiperbol çifti oluşturacaklardır. Bu çift yukarıdaki kobordizm ile $X^2 + Y^2 - Z^2 = 0$ denklemiyle verilen uzay-zaman konisinin arakesitiyle bulunur. Bu eğrileri elde etmek için koninin parametrik denklemi yukarıdaki gibi, u∈R, v∈[0,2π] olmak üzere parametrik denklem,
X(u,v)=ucos(v); Y(u,v)=usin(v); Z(u,v)=u;

biçimindedir. O halde arakesit grafiği şekil 9 daki gibi olur:

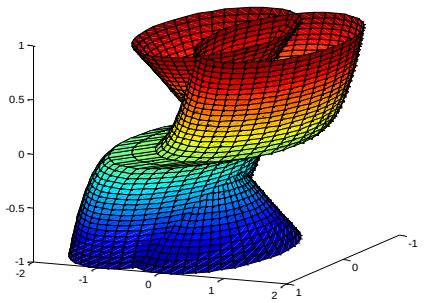

**Şekil 9:** Eğik boru kobordizmi üzerindeki ışıksal vektörler

Bu hiperbol çifti bir boyutlu manifold olduğundan boyutu 1 dir. O halde kobordizm üzerindeki lightlike yada ışıksal vektörlerin boyutu k(U)=1 olur. Bu da yine [21] e göre birasyonel kobordizm invaryantıdır. Benzer şekilde, bu yüzeyler her biri karakteristiği sıfır olan complex cisim C üzerinde olduğundan örnekteki semi-Rieamannian manifoldun bir diğer birasyonel kobordizm invaryantı, kodaira boyutu -∞ dur. Eğer yukarıdaki eğik boru şeklindeki kobordizm yüzeyi tamamen space-like ya da tamamen timelike olsaydı bu durumlarda da yine k(u) invaryantı k(u)=0, kodaira boyutu yine -∞ olurdu.

**Örnek 3:** Şimdi üçüncü bir örnek olarak yine $R^3_1$ uzayında düz boru şeklindeki yarıçapı 1 br. olan bir silindir kobordizmini göz önüne alalım. Bu yüzeyin parametrik denklemi $u \in R$ ve $v \in [0,2\pi]$ olmak üzere:

$$X(u,v) = cosv$$
$$Y(u,v) = sinv$$
$$Z(u,v) = u$$

biçimindedir. Bu yüzeyi de çizdiğimizde şekil 10 daki grafik elde edilir.

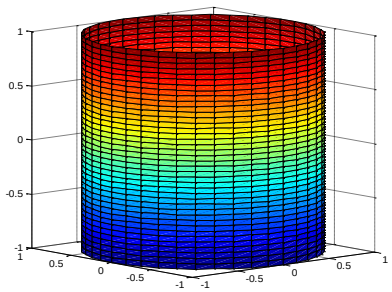

**Şekil 10:** silindir boru şeklindeki kobordizm örneği

Şimdi bu yüzeyin üzerindeki lightlike yada ışıksal vektörleri elde edecek olursak bunlar bir çember çifti oluşturacaklardır. Bu çift yukarıdaki kobordizm ile $X^2 + Y^2 - Z^2 = 0$ denklemiyle verilen uzay-zaman konisinin arakesitiyle bulunur. Bu eğrileri elde etmek için koninin parametrik denklemi yukarıdaki gibi, u∈R, v∈[0,2π] olmak üzere parametrik denklem,

X(u,v)=ucos(v); Y(u,v)=usin(v); Z(u,v)=u;
biçimindedir. O halde arakesit grafiği şekil 11 gibi olur. Bu çember çifti bir boyutlu manifold olduğundan boyutu 1 dir. O halde kobordizm üzerindeki lightlike yada ışıksal vektörlerin boyutu k(U)=1 olur. Bu da yine [21] e göre birasyonel kobordizm invaryantıdır. Benzer şekilde, bu yüzeyler her biri karakteristiği sıfır olan complex cisim C üzerinde olduğundan örnekteki semi-Rieamannian manifoldun bir diğer birasyonel kobordizm invaryantı , kodaira boyutu -∞ dur. Eğer yukarıdaki silindir şeklindeki kobordizm yüzeyi tamamen space-like ya da tamamen timelike olsaydı bu durumlarda da yine k(u) invaryantı k(u)=0, kodaira boyutu yine -∞ olurdu.

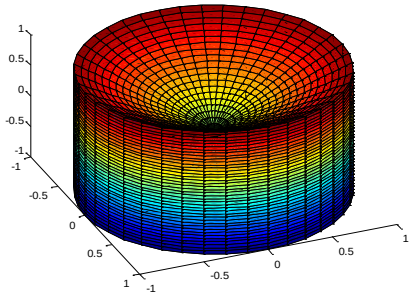

**Şekil 11:** Silindir boru kobordizmi üzerindeki ışıksal vektörler

**Örnek 4:** Dördüncü bir örnek olarak yine $R^3_1$ uzayında çift kanatlı hiperboloid şeklindeki timelike bir kobordizmi göz önüne alalım. Bu yüzeyin parametrik denklemi $v \in R,\ \vartheta \in [0,2\pi]$ olmak üzere:

$$X(u,v) = sinhv.cos\vartheta$$
$$Y(u,v) = sinhv.sin\vartheta$$
$$Z(u,v) = coshv$$

olur. Kartezyen denklemi de,

$Z^2 = X^2 + Y^2 + 1$

olur.

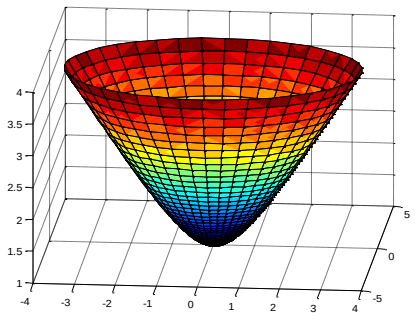

**Şekil 12:** çift kanatlı hiperboloidin üst yarısı şeklindeki kobordizm örneği

Şimdi bu yüzeyin üzerindeki lightlike yada ışıksal vektörler yukarıdaki kobordizm ile $X^2 + Y^2 - Z^2 = 0$ denklemiyle verilen uzay-zaman konisinin arakesitiyle bulunur. Eğer kobordizmi sınırlı olarak seçersek arakesit oluşmayacağından kobordizm üzerindeki lightlike yada ışıksal vektörlerin boyutu k(U)=0 olur.

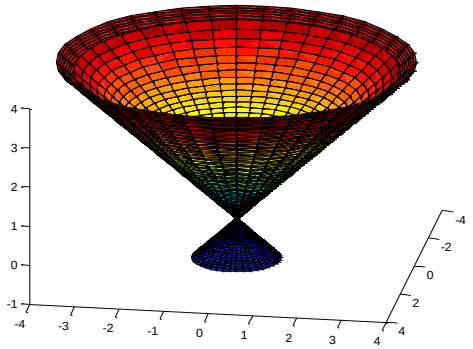

**Şekil 13:** Çift kanatlı hiperboloid kobordizmi üzerindeki ışıksal vektörler

**Teşekkür**

Bu çalışma Muş Alparslan Üniversitesi Bilimsel Araştırma Projeleri birimince desteklenmiştir. Proje no: BAP-18-EMF-4902-02.

**Yazarların Katkısı**

Bu çalışma sorumlu yazarın danışmanlığında diğer yazarın yüksek lisans tez çalışmalarından alınmıştır.

**KAYNAKLAR**

[1] Guillemin, V., Sternberg, S. Birational equivalence in the symplectic category. Invent. Math. 1989; 97: 485–522.
[2] McDuff, D., Salamon, D. Introduction to Symplectic Topology, 2nd edn New York: Oxford Math. Monogr. Oxford University Press;1998.
[3] Matsuki,K.:Lectures on factorization of birational maps. arXiv:math.AG/0002084
[4] Hu J., Li T-J., Ruan Y., Birational cobordism invariance of uniruled symplectic manifolds, Invent. math. 2008; 172: 231–275.
[5] Li, T.-J.,Existence of embedded symplectic surfaces. In: Geometry and Topology of Manifolds. Fields Inst. Commun.,47: 203–217. Am. Math. Soc., Providence, RI. 2005.
[6] Kollar J., Low degree polynomial equations: arithmetic, geometry, topology. European Congress of Mathematics, vol. I (Budapest, 1996). Prog. Math., 1998; 168: 255–288.
[7] Ruan Y.,Virtual neighborhoods and pseudoholomorphic curves. Turk. J. Math., 1999; 23: 161–231.
[8] Duggal K. L. and Bejancu, A., Lightlike submanifold of semi-Riemannian manifolds and its applications, The Netherlands: Kluwer Academic; 1996.
[9] Duggal K. L. and Şahin, B., Differential geometry of lightlike submanifolds, Birkhäuser: Verlag; 2010.
[10] Kupeli D. N., Singular Semi-Riemannian Geometry, Dordrecht:Kluwer Academic Publishers; 1996.
[11] Kocaayan H., Karakteristik Sınıfları, [Y.Lisans Tezi], İzmir: Ege Üniversitesi Fen Bilimleri Enstitüsü; 2012.
[12] Chern,S.S., Charecteristic classes of Hermitian manifolds, Annals of Mathematics, 1946;47(1):85-121.
[13] Çallıalp, F., Soyut Cebir, İstanbul: Birsen Yayınevi; 2009.
[14] Pierce, D. [internet], Galois Teorisi, Matematik Bölümü,*MSGSÜ,* 2018.Available from: *http://mat.msgsu.edu.tr/~dpierce/Dersler/Galois-Teorisi/galois-kurami-2018.pdf.*
[15] O'Neill B., Semi-Riemannian Geometry with Applications to relativity, San Diego-California: Akademic Press. Inc.; 1983.
[16] İncesu M., "Benzerlik Geometrisinde Noktaların Tam İnvaryantları Sistemi", [doktora tezi] , Trabzon: Karadeniz Teknik Üniversitesi, 2008
[17] Sağıroğlu Y., Parametrik Eğrilerin Afin Diferen-siyel İnvaryantları, [doktora tezi], Trabzon: Karadeniz Teknik Üniv. Fen Bilimleri Ens., 2002.
[18] Hirsch M.W., Graduate Text in Mathematics: Differential Topology, New York: Springer; 1976.
[19] Stong R. E., Notes on cobordism theory, Princeton N.J.: Princeton University Press; 1968.
[20] Thom, R., Qoelques propi_et es globales des varieties differentiables, *Commentari Mathematici Helvetici*, 1954; 28: 17-86.
[21] Ören İ., O(3,1)-Ortogonal Grubu için Noktaların İnvaryantları, [doktora tezi], Trabzon: Karadeniz Teknik Üniversitesi, 2007.
[22] Boucksom S., Demailly J.P., Paun M. and Peternell T., The pseudo-effective cone of a compact Kähler manifold and varieties of negative Kodaira dimension, J. Alg. Geometry 2013; 22 (2): 201-248.
[23] Bogomolov F., Tschinkel Y., Rational curves and points on *K*3 surfaces, Amer. J. Math., 2005;127 (4) : 825-835.
[24] Shioda T., An example of unirational surfaces in characteristic*p* . *Math. Ann.*, 1974; 211: 233–236.
[25] Wikipedia contributors. Ruled variety [Internet]. Wikipedia, The Free Encyclopedia; 2020 Apr 12, 13:29 UTC [cited 2020 Oct 9]. Available from: https://en.wikipedia.org/w/index.php?title=Ruled variety&oldid=950515178.

Cilt 11, Sayı 2, Sayfa 107-112, 2022 Volume 11, Issue 2, Page 107-112, 2022

Araştırma Makalesi https://doi.org/10.46810/tdfd.1084396 Research Article

Türk Doğa ve Fen Dergisi
Turkish Journal of Nature and Science
www.dergipark.gov.tr/tdfd

# Investigation of Wing Forms Through Mass and Wing Area Chart

**Seyhun DURMUŞ[1*]**

[1] Balikesir University, Edremit School of Civil Aviation, Balikesir, Türkiye
Seyhun DURMUŞ ORCID No: 0000-0002-1409-7355

**Corresponding author: drmsyhn@gmail.com*

(Received: 08.03.2022, Accepted: 06.06.2022, Online Publication: 29.06.2022)

**Keywords**
Wing loading, Wing Shapes, Scythe shaped wings, Wing structure, Wing morphology

**Abstract:** The wing loading parameter depending on the wing area and weight and the aspect ratio parameter, which is the wing shape factor, are the main parameters that determine the fixed-wing flight mechanics. In this study, the relationship between wing forms and flight style of 195 bird species was evaluated using wing area and mass scatter plot. The slope of the mass and wing area chart is proportional to the 1/wing loading. The results showed that birds with more wing area per unit mass tended to perform unpowered flight styles such as soaring and gliding; and birds with less wing area per unit mass tended to have powered flight styles, such as flapping and hovering. In general, it has been found that the slope of the trendline curve is more inclined tended to expend more energy in flight. Unlike the fixed-wing flight mechanics, hand-wings and arm-wings should also be examined to understand the flight mechanics of flapping wings as different effects occur during flapping flight in terms of the lift and thrust forces. In addition, scythe-shaped wings differ from high-speed wings in terms of the ratio of hand wing length/arm wing length according to their wing structure.



# Kütle ve Kanat Alanı Grafiğinden Kanat Formlarının İncelenmesi

**Anahtar Kelimeler**
Kanat yüklemesi, Kanat formları, Tırpan şeklindeki kanatlar, Kanat yapısı, Kanat morfolojisi

**Öz:** Kanat alanı ve ağırlığa bağlı olan kanat yükleme parametresi ve şekil faktörü olan en boy oranı parametresi, sabit kanatlı uçuşun mekaniğini belirleyen ana parametrelerdir. Bu çalışmada, 195 kuş türünün kanat formları ile uçuş tarzları arasındaki ilişki, kanat alanı ve kütle dağılım grafiği kullanılarak değerlendirilmiştir. Kütle ve kanat alanı grafiğinin eğimi 1/kanat yüklemesiyle orantılıdır. Sonuçlar, birim kütle başına daha fazla kanat alanına sahip kuşların, süzülme ve süzülme gibi enerji gerektirmeyen uçuş stillerine sahip olma eğiliminde olduğunu göstermiştir; ve birim kütle başına daha az kanat alanına sahip kuşlar, kanat çırpma ve havada asılı kalma gibi enerji gerektiren uçuş stillerine sahip olma eğilimindedir. Genel olarak, daha düşük eğri eğimli kuşların kural olarak uçarken daha fazla enerji harcadıkları belirtilmelidir. Çırparak uçuş sırasında kaldırma ve itme kuvvetlerinin oluşumu açısından farklı etkiler meydana geldiğinden, çırpma kanatlarının uçuş mekaniğini anlamak için sabit kanatlı uçuş mekaniğinin aksine el kanatları ve kol kanatları da incelenmelidir. Ayrıca kanat yapılarına göre tırpan kanatlar, el kanadı uzunluğu/kol kanat uzunluğu oranı bakımından yüksek hızlı kanatlardan farklılık gösterir.

## 1. INTRODUCTION

Size, shape, and structure are the main factors that determine the wing morphology. The first studies in the literature of bird wing morphology were made by German schools [1,2]. Savile [3] proposed wing forms that are still widely used today: elliptical wings, high speed wings, high aspect ratio (AR) wings, and slotted high lift wings. Savile classified the wing forms according to their shape and flight behavior and ignored the wing structure. Elliptical wings and high aspect ratio wings are shape-based designations. Although the designation of slotted high lift wings is related to flight, it is related to wing size, as high lift can only be achieved with long and wide arm wings. On the other hand, high-speed wings are a designation based solely on flight characteristics, regardless of size, shape, and structure. There is a strong relationship between wing forms and flight styles. For example, wings with a high aspect ratio provide high lift and thrust, and these wings are suitable for dynamic soaring and flap-gliding. Birds with slotted high lift wings have long-wide arm wings, and a large wing area, which is advantageous in thermal

soaring. Fast take-offs, tight maneuvers, short bursts of high-speed are the main flight characteristics provided by elliptical wings. The birds with high-speed wing forms do not have a specific flight style, although most forms of wings have their own unique flight style.

Rayner [4] did a correlation study between wing area and bird mass, showing that the general curve corresponds to square cube law (2/3) and hummingbirds shows a different curve slope from the general bird curve slope, again Corvidae shows a different curve slope from Passerines. Rayner has also attempted to decipher bird wing morphology using principal component analysis (PCA) via the AR and wing loading axes. Contrary to Rayner, Norberg [5] proposed the term relative wing loading (RWL) instead of wing loading. Norberg claimed that AR-RWL charts gave a more effective result in the distribution of wing morphology and flight styles, and classified groups of birds in terms of wing characteristics and flight patterns. Lockwood et al. [6] used convexity and pointedness parameters to investigate the effect of wingtip shape on detecting morphological adaptations to migration. They found that the migrants have relatively more pointed and more convex with larger AR. Videler [7] was the first to describe the unique wings of the common swift as a “scythe-shaped wing”. Videler [7] suggested that the swifts' slender and pointed hand-wing forms leading edge vortices (LEVS), that produce aerodynamic flow system that generates lift over a wide range of angles of attack.

The wing loading and aspect ratio are the main parameters studied to examine the effects of mass, wing size and shape factor on the fixed-wing bird flight. Unlike fixed-wing bird flight, hand-wings and arm-wings should be examined to understand the flight mechanics of wing flapping as different effects occur during flapping in terms of the lift and thrust forces flight. The wing loading parameter (the ratio of weight to wing area) is an aerodynamic parameter that allows us to understand the effect of both size and mass on flight characteristics. The second important parameter in fixed wing flight mechanics is the wing aspect ratio, which has an impact on gliding ability [8]. The wing aspect ratio parameter (ratio of wingspan squared to wing area) is a shape dependent aerodynamic parameter. The best glide rate is proportional to the square root of the aspect ratio, so a high aspect ratio is an indicator of the ability to glide [9]. Keast [10] suggested that short and low aspect ratio wings, which are usually found in resident species, are advantageous for rapid take-off.

As mentioned earlier, the flight mechanics of the flapping wing are different from the fixed wing bird flight. The arm wing is a part of wing close to the body, consisting of humerus, ulna, and radius bones with secondary and tertiary feathers. The hand wing is a part of wing close to the wingtip, consisting of the metacarpals and phalanges bones with the alula and primary feathers. The ratio of arm wing to hand wing affects the flight behavior and eco-morphology of birds, since during flapping the arm-wing determines lift ability of the wings, while the hand-wing determines thrust ability of the wings. Kruyt et al. [11] argued that the effect of aspect ratio is changed according to whether birds were flapping their wings or being in a fixed position. Again, Henningsson et al. [12] suggested that the efficiency of lift production during wing flapping is higher than that of gliding. Also, Muijres et al. [13] claimed that energy is more conserved in flap-gliding flight than in continuous flapping flight. Lilienthal [14] claimed that, during flapping, arm-wings (inner wings) create a lift force, hand-wings (outer wings) create thrust force and contribute to control and maneuverability. The mechanism of formation of the lift force and the thrust force in ornithopters supported this claim. Harmon [15] and Dvorak [16] corroborated this claim with tests conducted on flapping aerial vehicles, namely ornithopters.

In this study, it is aimed to investigate the effects of wing loading, shape, and size factors on bird flight styles in the mass wing area distribution chart of 195 bird species classified according to the 6 types of wing forms proposed in the method section.

## 2. MATERIAL and METHOD

Within the scope of the study, data on the body mass, wing area, aspect ratio, wingspan, and average wing chord length of 195 birds were collected. Biometry of bird data compiled from previous studies [8, 17, 18, 19, 20]. The wing size in birds is related to mass, and the study of scaling between mass and size is based on the idea that the unit length scale is proportional to mass to the power of 1/3. Therefore, the wing area is proportional to the mass the power of 2/3. The equation of correlation between wing area (S) and mass (m) can be written as in Eq. 1 where a is about 2/3, and c is a constant coefficient that varies according to bird groups [19, 21, 22]. The power of mass, denoted by a, determines the tendency of the wing size to grow relative to the mass and differs in groups of birds. Power correlation is used to decipher the relationship between bird mass and wing area in the charts provided in the result section of paper.

$$S = c.m^{2/3} \quad (1)$$

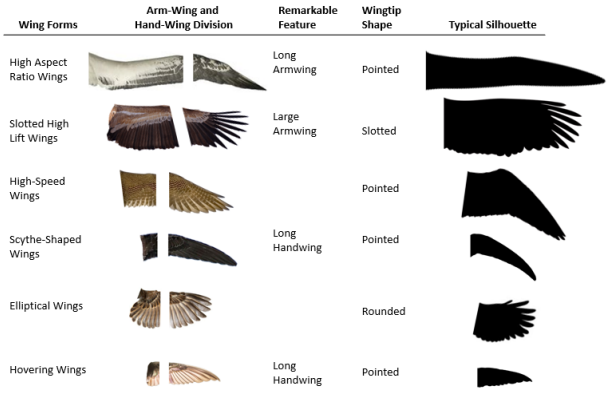


**Figure 1.** Structure properties of studied wing forms

To understand the criteria by which the wing forms are separated, the split wing structures and the wing

silhouettes used in the result charts are given in Fig.1. Photoshop tool was used to separate and scale the hand and arm wings.

The scythe-shaped wings and hovering wings of hummingbirds have a high ratio of length of hand-wing to length of arm-wing compared to typical high-speed wings. Therefore, in this study, these wing forms were not considered as a high-speed wing form as Saville did, but as separate wing forms. Swift and Hummingbirds are agile birds because their long hand-wings provide high thrust. The wings of hummingbirds are like the wings of swifts; however, the arm-wings are slightly thinner than those of the swifts, and their hand wings are slenderer than those the swifts. Swallows and Martins belong to the Hirundae family of the order Passeriformes, but their wing structure is more like the SSW (arm wings are short, hand wings are long). In scythe-shaped wings, the ratio of hand wing length/arm wing length is greater than that of typical high-speed wings, as shown in the Eq. 2.

$$\left(\frac{\text{Handwing Length}}{\text{Armwing Length}}\right)_{SSW} > \left(\frac{\text{Handwing Length}}{\text{Armwing Length}}\right)_{HSW} \quad (2)$$

The representation of the aerodynamic effects by wing position is shown in Table 1. The wing loading and aspect ratio are the main parameters examined to study the effects of mass, wing size and shape factor on the fixed-wing bird flight. Unlike fixed-wing bird flight, hand-wings and arm-wings must be examined to understand the flight mechanics of wing flapping.

**Table 1.** Aerodynamic factors according to avian wing position

| Wing Position | Parameter | Aerodynamic Factor |
|---|---|---|
| Fixed Wing | Weight | Wing loading |
| | Wing size | |
| | Wing shape | Aspect ratio |
| Flapping Wing | Wing structure | Arm-wings generate lift<br>Hand-wings generate thrust |

## 3. RESULTS

Wing area and mass distribution charts are useful in describing the effect of wing loading on flight behavior. The slope of the trendline in the mass and wing area graph is proportional to 1/(wing loading). In this study, regression analysis was performed between the bird mass and the wing area based on the wing forms. Fig. 2 shows the trend line curves of the bird mass relative to the wing area on a logarithmic scale for birds with 6 different wing forms.

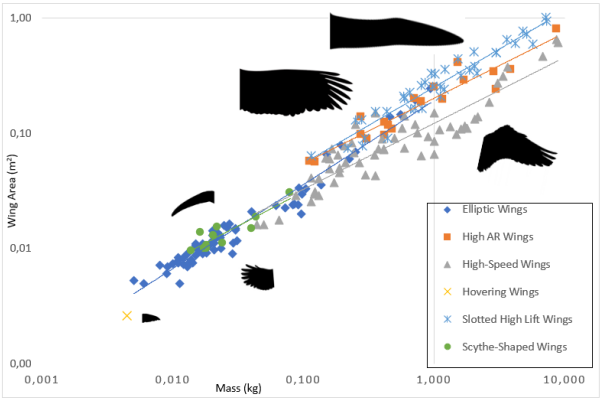


**Figure 2.** Distribution of wing size and mass according to wing forms. A base-10 log scale is used for all axes.

The power of the given mass that is "a" at Eq.1 differs in groups of birds. The trendline in all birds follows the 2/3 (0.66) rule, which has also been found in the literature, and the power of the mass calculated for 195 bird species in this study is 0.69. The trendline on the mass and wing area chart gives very consistent results in distinguishing between unpowered flight styles and powered flight styles. These results show how important the wing loading parameter is in flight mechanics. As can be seen from the Fig. 2, there is a relationship between low wing loading and unpowered flight strategies. In addition, it can be said that birds with the slope of the trendline curve is more inclined, as a rule, expend more energy when flying. Birds falling below the general trendline in Fig. 2 (Waterfowls, Galliformes and Anna's Hummingbird) often use powerful flight strategies, such as hovering or continuous flapping. In contrast, the birds that remain above the trendline are shown in Fig. 2 (Birds of prey, Falconiformes, high aspect ratio winged birds) often use unpowered flight strategies such as dynamic soaring, thermal soaring, or gliding.

The increase in wing area along with the increase in bird mass can be understood from the curve slopes of mass and wing area chart. The power equation of the trendlines gives the unit increase in wing area proportional to the bird mass. Fig. 3 shows the trendline equation of Corvidae wings, elliptical wings (EW) and slotted high-lift wings (SHLW). The curve-trend-line-equations show that the large members of Corvidae behaves like Accipitriformes, not Passeriformes. Large members of the Corvidae have transitional wing forms between the typical passerines with EW and the Accipitriformes with SHLW. Even though the family Corvidae belongs to the order Passeriformes, the wing forms of Ravens, Rooks and large Crows are similar to SHLW, that is the wings of Accipitriformes. Large members of Corvidae are capable of thermal soaring and gliding flight [23-25].

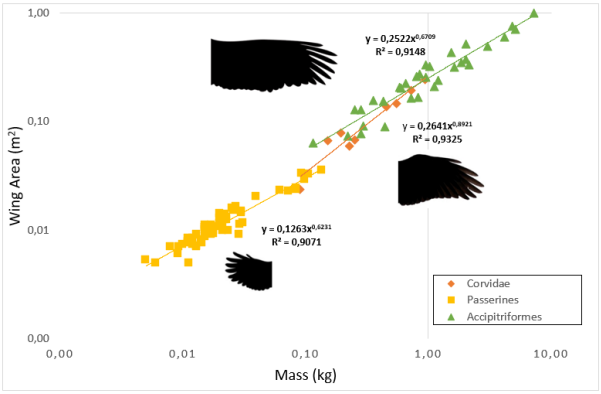


**Figure 3.** Distribution of wing size and mass of elliptical wings (EW) and slotted high lift wings (SHLW). A base-10 log scale is used for all axes.

Fig. 4 shows the wing area and the mass distribution curve of birds weighing more than 1 kg. The difference in curve slope between SHLW (birds of prey) and high-speed winged birds (HSW, waterfowls) is clearly visible. The most advantageous bird group in terms of wing area is SHLW, while the most disadvantaged bird group is HSW-waterfowls. Wing aspect ratio (AR) is important for gliding flight, while a large wing is important for soaring flight. For example, frigate birds with high aspect ratio wings (HARW) can use both thermal soaring because they have a large wing area, like SHLW, and dynamic soaring because their wing AR is high. The efficiency of lift production in the flapping flight is higher than in the gliding flight. This fact may explain why waterfowl (with a low wing loading) do not glide or flap continuously during migration. In addition, the wing aspect ratio (AR) is a decisive parameter on the ability to glide. For example, large birds with similar wing loading, albatrosses use dynamic soaring and ducks use continuous flapping.

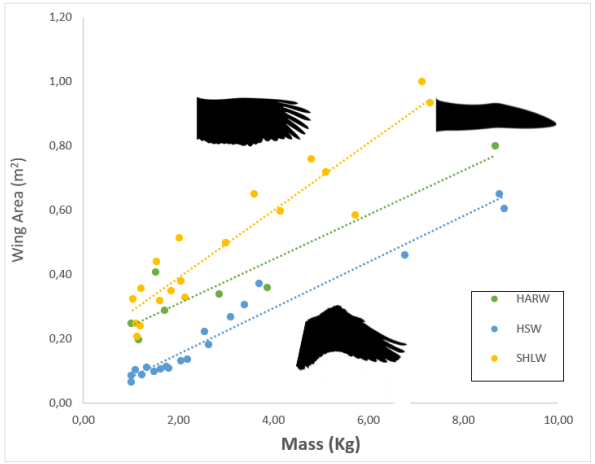


**Figure 4.** Distribution of wing size and mass of birds weighing more than 1 kg, where HARW is High Aspect Ratio Wings, HSW is High-Speed Wings, and SHLW is Slotted High Lift Wings.

High-speed wings (HSW) are the wing forms of the most heterogeneous groups of birds have. The Dunlin (*Calidris Alpina*) weighing 50 grams and the Whooper Swan (*Cygnus cygnus)* weighing 9 kg have the HSW form. Even though most wing forms have their own unique style of flight, this generalization is invalid in HSW forms. That is, birds with the HSW form may have one of several different flight styles, such as thermal soaring, gliding, or continuous flapping. Fig. 5 shows the distribution between mass and wing area for HSW type wing forms. The slope of the curve shown in Fig. 5 gives an idea of the flight styles: Falcons with the low slope trendline curve can perform gliding and thermal soaring flights. Medium-curve slope; the Shorebirds, Sandgrouse, and Columbiformes use short-term gliding and long-term flapping, while lowest-curve slope, divers and waterfowls need to flap continuously during migration. A striking result here is that large waterfowl, that is, geese and swans, have different curved slopes than small waterfowl, that is, ducks. Swans and geese have a relatively larger wing area per unit mass than ducks.

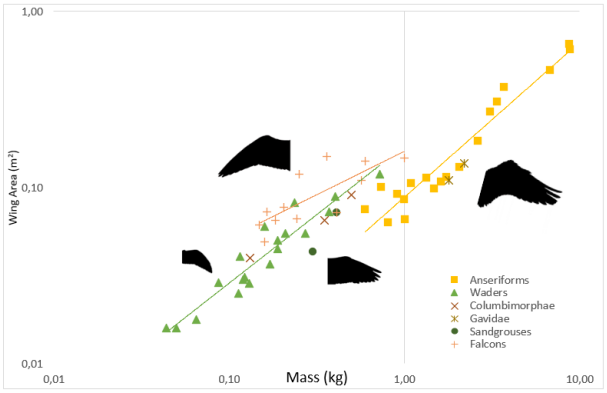


**Figure 5.** Distribution of wing size and mass of high-speed wing forms. A base-10 log scale is used for all axes

The difference between SSW and EW with similar wing area is due to the wing structure and shape rather than size, while the decisive difference between SSW and HSW depends on the wing size and wing structure. This is because the wingtips of the SSW are more pointed than the HSW, and the ratio of the (hand-wing length)/ (arm-wing length) is larger than the typical HSW. As can be seen from Fig. 6, the SSW has a similar wing area as the EW; however, the SSW has a higher AR, that is, the ability to glide(flap-gliding). Swifts have a smaller wing area than Falcons but have a relatively higher AR value. Falcons can sweep their wing shape in diving flight conditions, while Swifts can sweep their wing shape up to 60 degrees in cruising flight conditions [26,27].

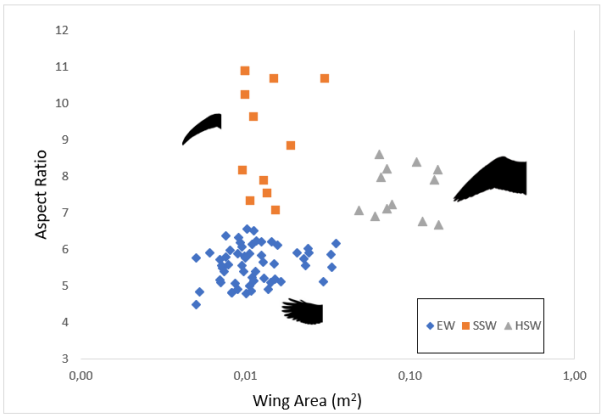


**Figure 6.** Distribution of aspect ratio and wing area of Elliptical Wings (EW), Scythe-Shaped Wings (SSW), and high-speed wings (HSW, only Falconiformes). A base-10 log scale is used for X axis.

Swifts are the fastest birds in cruising flight (non-diving flight), as the long-armed wings generate high thrust and the pointed wing tips reduce drag. On the other hand, wings with small arm-wings provide less lift, but they create extra lift by using leading edge vortices to compensate for this. These results indicate that the effects of wing structure on the flight form should be examined more, except for wing loading and AR, because features of the arm-wing and hand-wing have very significant effects on all flight styles except gliding and soaring. In addition, Passerines and swifts with similar wing loading but different AR have different flight styles. This is a phenomenon related to both the AR (gliding) and the wing structure (flapping).

## 4. DISCUSSION

The study, which claims that Savile's [3] bird wing forms are inadequate, suggested scythe-shaped wing form and hovering wing forms in addition to Savile's classification. The study examined the effects of wing loading in fixed-wing flight mechanics to explain the effect of wing structure on flight styles. The study examined the effects of wing loading on flight, as stated by Pennyquick [8]'s fixed wing flight mechanics, on the trendline slopes and showed the difference between gliding and non-gliding birds in charts. As a result of this study, birds with lower slope curves flapped their wings more often, it coincides with the proposal of lift production during wing flapping is higher than that of gliding of Henningsson et al. [12]. The study examined the effects of wing loading in fixed-wing flight mechanics to explain the effect of wing structure on flight styles. While the wing loading parameter is mainly taken into account in the mass wing area distribution charts given in the results. The most interesting result of this current study is that the groups of birds remain below the trendline curve given in Fig. 2 use powered (flapping, hovering) flight styles and the groups of birds remain above the trendline curve have unpowered flight styles (soaring, gliding). In fact, when Rayner's (1988) study is examined, this result is evident in the wing area-mass chart, but it was not expressed by Rayner [4]. It can also be seen in the results that birds with a lower curve inclination (due to the high wing load), as a rule, expend more energy in flight. Among the unpowered flight styles, the large wing area for soaring and the high aspect ratio for gliding stand out as prerequisites. Although most wing forms have distinctive flight style, the reason why birds with high-speed wing forms do not have a specific flight style has been questioned (see Fig. 5).

Lilienthal [14]'s arm-wings create a lift force, hand-wings create thrust force claim coincides with claim that the Swift's long arm wing plays a key role in reaching the highest speed in level flight. Since the effect of wing structure is more dominant in flapping wing flight, it is necessary to examine the arm-wings and hand-wings in detail. There are many studies on the flight style of swifts [26-29] however, there is no studies in the literature on the difference of swifts' hand-wings and arm-wings from the typical high-speed wings. In this study, based on the difference in wing structure, the wing form difference between scythe-shaped wing (SSW) and high-speed wings (HSW) was shown descriptively using photoshop, not quantitatively due to absence of experimental data.

This study supports the study of Videler [7] and suggests that the wings of Swift should be described as a scythe-shaped wing form, not a high-speed wing form. The distinction between the scythe-shaped wing form and the High-speed wing could be a potential research topic for future experimental research. Wang et al. [30] suggested that the ratio of feather length to total arm length could be used to evaluate the flight modes of Mesozoic birds. In that study, they suggested a high correlation between flight styles and the ratio of feather length to total arm length. Similarly, it is a very strong claim that the difference in flight style between scythe-shaped winged Swifts and high-speed winged Falcons is due to the ratio of the length of the hand-wing to the length of the arm-wing.

## REFERENCES

[1] Böker H Die biologische Anatomie der Flugarten der Vögel und ihre Phylogenie. Journal of Ornithology. 1927;75(2), 304-371.
[2] Lorenz K. Beobachtetes über das Fliegen der Vögel und über die Beziehungen der Flügel-und Steuerform zur Art des Fluges. Journal of Ornithology. 1933; 81(1), 107-236.
[3] Savile D B O. Adaptive evolution in the avian wing. Evolution. 1957; 11(2), 212-224.
[4] Rayner, J. M. . Form and function in avian flight. In Current ornithology. Springer, Boston, MA; 1988.
[5] Norberg, U. M. Vertebrate flight Springer-Verlag. Berlin, Germany; 1990.
[6] Lockwood, R., Swaddle, J. P., Rayner, J. M. Avian wingtip shape reconsidered: wingtip shape indices and morphological adaptations to migration. Journal of avian biology. 1998; pp. 273-292.
[7] Videler, J. J. Avian flight. Oxford University Press; 2006.
[8] Pennycuick, C. J. Measuring birds' wings for flight performance calculations. Bristol: Boundary Layer; 1999.
[9] Saarlas, M. Aircraft performance. John Wiley & Sons; 2006.
[10] Keast A. Wing shape in insectivorous passerines inhabiting New Guinea and Australian rain forests and eucalypt forest/eucalypt woodlands. Auk. 1996;113: 94 – 104.
[11] Kruyt J W, van Heijst G F, Altshuler D L, Lentink D. Power reduction and the radial limit of stall delay in revolving wings of different aspect ratio. Journal of the Royal Society Interface. 2015; 12: 20150051.
[12] Henningsson P, Hedenström A, Bomphrey R J. Efficiency of lift production in flapping and gliding flight of swifts. Plos one. 2014; 9(2), e90170.
[13] Muijres F T, Henningsson P, Stuiver M, Hedenström A. Aerodynamic flight performance in

flap-gliding birds and bats. Journal of theoretical biology. 2012; 306, 120-128.
[14] Lilienthal O, Lilienthal G. Birdflight as the Basis of Aviation: A Contribution Towards a System of Aviation. Longmans, Green; 1911.
[15] Harmon R L. Aerodynamic modeling of a flapping membrane wing using motion tracking experiments (Doctoral dissertation); 2008.
[16] Dvořák R. Aerodynamics of bird flight. In EPJ Web of Conferences. EDP Sciences; 2006. Vol. 114, p. 01001.
[17] Alerstam T, Rosén M, Bäckman J, Ericson P G, Hellgren O. Flight speeds among bird species: allometric and phylogenetic effects. PLoS biology. 2007; 5(8), e197.
[18] Bruderer B, Peter D, Boldt A, Liechti F. Wing-beat characteristics of birds recorded with tracking radar and cine camera. Ibis. 2010; 152(2), 272-291.
[19] Greenewalt C H. The flight of birds: the significant dimensions, their departure from the requirements for dimensional similarity, and the effect on flight aerodynamics of that departure. Transactions of the American philosophical society. 1975; 65(4), 1-67.
[20] Dunning Jr, J. B. CRC handbook of avian body masses. CRC press; 1993.
[21] Liu T. Comparative scaling of flapping-and fixed-wing flyers. AIAA journal. 2006; 44(1), 24-33.
[22] Mcmasters J. Reflections of a Paleoaerodynamicist. In 2nd Applied Aerodynamics Conference; 1986. p. 2167.
[23] KleinHeerenbrink, M., Johansson, L. C., Hedenström, A. Multi-cored vortices support function of slotted wing tips of birds in gliding and flapping flight. Journal of The Royal Society Interface. 2017; 14(130), 20170099.
[24] Serrano, F. J., Chiappe, L. M. Aerodynamic modelling of a Cretaceous bird reveals thermal soaring capabilities during early avian evolution. Journal of the Royal Society Interface. 2017; 14(132), 20170182.
[25] White, C. M., Tanner-White, M. Unusual social feeding and soaring by the Common Raven (Corvus corax). Great Basin Naturalist. 1985; 45(1), 21.
[26] Videler J J, Stamhuis E J, Povel G D E. Leading-edge vortex lifts swifts. Science. 2004; 306(5703), 1960-1962.
[27] Lentink, D., Müller, U. K., Stamhuis, E. J., De Kat, R., Van Gestel, W., Veldhuis, L. L. M., Van Leeuwen, J. L. How swifts control their glide performance with morphing wings. Nature. 2007; 446(7139), 1082-1085.
[28] Henningsson, P., Spedding, G. R., Hedenström, A. Vortex wake and flight kinematics of a swift in cruising flight in a wind tunnel. Journal of Experimental Biology. 2008; 211(5), 717-730.
[29] Muir, R. E., Viola, I. M. The leading-edge vortex of swift wings. BioRxiv. 2017; 099713.
[30] Wang X, McGowan A J, Dyke G J. Avian wing proportions and flight styles: first step towards predicting the flight modes of Mesozoic birds. PLoS One. 2011; 6(12), e28672.

Araştırma Makalesi https://doi.org/10.46810/tdfd.1113394 Research Article

Türk Doğa ve Fen Dergisi
Turkish Journal of Nature and Science
www.dergipark.gov.tr/tdfd

# Keratin Isolation Methods From Waste Goose Feather: An Effective Comparison

**Emel Çakmak**[1,2*]

[1] Aksaray University, Güzelyurt Vocational School, Department of Plant and Animal Production, Aksaray, Türkiye
[2] Aksaray University, Science and Technology Application and Research Center (ASUBTAM), Aksaray, Türkiye
Emel ÇAKMAK ORCID No: 0000-0002-6231-1950

**Corresponding author: emelcakmak@aksaray.edu.tr*

(Received: 06.05.2022, Accepted: 06.06.2022, Online Publication: 29.06.2022)

**Keywords**
Biomass, EDTA, $Na_2S$, Dissolution

**Abstract:** Conversion of biowaste into value-added material has attracted great interest lately. One of these materials is keratin, which is found in different structures such as nails, hair, beak, wool, feathers, claws and horns. Until now, keratin isolation has been carried out from waste wool, feather, hoof and hair. However, the development of effective techniques to obtain keratin without any damage to the secondary structure of the protein remains a challenging task. Herein, two distinct keratin isolation methods (sodium sulfide and ethylenediamine tetraacetic acid) were compared for the first time from Domestic Goose (*Anser domesticus*) waste feathers. The Kjeldahl method was used for the determination of crude protein by two methods from the obtained keratin powders and their antioxidant activities were conducted. According to our findings, keratin obtained from goose feathers using sodium sulfide showed higher yield (86.34%). On the other hand, the antioxidant activity of keratin obtained from the method prepared using ethylenediamine tetraacetic acid was found to be approximately three times higher than the other method, and our results proved that waste goose down could be considered as a potential source of keratin for further studies.



# Atık Kaz Tüyünden Keratin İzolasyon Yöntemleri: Etkili Bir Karşılaştırma

**Anahtar Kelimeler**
Biyokütle, EDTA, $Na_2S$, Çözünme

**Öz:** Biyoatıkların katma değerli malzemeye dönüştürülmesi son zamanlarda büyük ilgi görmektedir. Bu maddelerden biri de tırnak, saç, gaga, yün, tüy, pençe ve boynuz gibi farklı yapılarda bulunan keratindir. Şimdiye kadar atık yün, tüy, toynak ve saçtan keratin izolasyonu yapılmıştır. Bununla birlikte, proteinin ikincil yapısına herhangi bir zarar vermeden keratin elde etmek için etkili tekniklerin geliştirilmesi zorlu bir süreç olmaya devam etmektedir. Burada, Yerli Kaz (*Anser domesticus*) atık tüylerinden ilk kez iki farklı keratin izolasyon yöntemi (sodyum sülfür ve etilendiamin tetraasetik asit) karşılaştırılmıştır. Elde edilen keratin tozlarından ham protein tayini için Kjeldahl yöntemi kullanılmış ve antioksidan aktiviteleri belirlenmiştir. Bulgularımıza göre kaz tüyünden sodyum sülfür kullanılarak elde edilen keratin daha yüksek verim (%86,34) göstermiştir. Öte yandan, etilendiamin tetraasetik asit kullanılarak hazırlanan yöntemden elde edilen keratinin antioksidan aktivitesinin diğer yönteme göre yaklaşık üç kat daha yüksek olduğu tespit edilmiş ve sonuçlarımız atık kaz tüyünün ileriki çalışmalar için potansiyel bir keratin kaynağı olarak kabul edilebileceğini kanıtlamıştır.

## 1. INTRODUCTION

As one of the most abundant but underutilized protein sources, keratin is the main component of hair, nails, hooves, wool, horns and feathers [1, 2]. However, there are difficulties associated with the disposal and management of these valuable materials. Especially, feathers contain the largest amount of all keratinous waste and is produced largely from poultry processing [3]. Keratin-containing poultry feathers are a very irritating and troublesome waste product of the poultry industry due to their ultimate disposal which could be either parried by incineration or burying; thus, both of these have negative effects on the environment [4].

Keratin is a fibrous, structural protein that is formed by the juxtaposition of many types of amino acids [5]. However, keratin differs from other fibrous proteins in its higher cystine content. These cysteine amino acids have a

stronger structure due to their disulfide bonds [6]. It has a three-dimensional structure thanks to the disulfide bridges caused by cysteine molecules. Thanks to this cross-linked structure and its highly hydrophobic feature, keratin is insoluble in water, nor in nonpolar solvents. Namely, highly stable SS bonds could be denatured just by acid and base [7]. Keratin has a very active chemical structure, it can be easily reduced, oxidized and hydrolyzed thanks to the cystine molecule [5, 8]. Thus, the natural state of the protein is lost in strong inorganic acids or bases. Keratin also reacts with acids and bases, losing its original shape by hydrolysis [7].

It is critically important to develop effective techniques to isolate keratin without damaging this structure of proteins. The fundamental keratin isolation methods used for this purpose in the literature are physicochemical methods [9], enzymatic reactions by hydrolysis of the novel keratinase [10], alkali/acid handling [11], oxidation [12], reduction hydrolysis [13] and processing in ionic solutions [14]. Often used methods such as steam blasting used for the destruction of hard biomass or ionic liquids are high-cost, relatively energy-consuming and difficult to recycle [10]. 2-mercaptoethanol and sodium dodecyl sulfate are the most commonly used chemicals in keratin production [15]. Moreover, using them together with reducing agents such as urea and sodium bisulfite provides high efficiency keratin production in a short time [16]. However, 2-mercaptoethanol is not preferred due to its high cost. Conversely, the use of $Na_2S$ for keratin extraction with high yield is both more economical and commercially available [17]. In the meantime, EDTA acts as an emulsifier and helps the feather stay in dispersion at the peak level, a stable distribution was achieved [18].

Thus, the purpose of the current study was to evaluate two different methods for keratin extraction in terms of effectiveness and antioxidant activities for future product development. So, the feather hydrolysis using the $Na_2S$ and EDTA methods was preferred due to its low cost and simple hydrolysis herein.

## 2. MATERIALS AND METHODS

### 2.1. Sample Collection

Goose feathers were provided by a slaughterhouse in the province of Aksaray, Turkey.

### 2.2. Pre-treatment of the Feathers

Waste goose feathers collected from goose factories were washed three times with water, cleaned of blood and other dirty and left to dry in daylight. The fat compounds in the goose feather were annihilated by reflux with an organic solvent chloroform for 6 hours. After removing the goose feathers were separated to small pieces.

### 2.3. Extraction of the Feather's Keratin: *$Na_2S$ Method*

Degreased goose feathers (10 g) were stirred with 100 ml of distilled water, 3.0 N NaOH and 0.2 N $Na_2S$. The reaction was carried out in a water bath at 25 °C for 1.5 hours. All substances were dissolved in basic medium with the help of magnetic stirrer. Then, the pH of the keratin solution was adjusted to 4.2 with the help of dilute HCl solution to precipitate the keratin. These keratins were washed with acetone and filtered using a vacuum strainer. The resulting keratin was then dried in an oven at 50 °C for a night.

### 2.4. Extraction of the Feather's Keratin: *EDTA Method*

Dewaxed goose feathers (10 g) were blended with 100 ml of distilled water and 10 g of NaOH. The base was thoroughly dissolved by shaking and mixing by hand. After adding 0.15 g of EDTA to the solution, the keratin solution was poured onto it. This solution was then placed in a 40 °C bath where a stirrer was rotated for 2 hours. After the reaction was complete, neutralization was performed with HCl to pH 4.2. Afterwards, the precipitated keratin was firstly centrifuged, then washed with acetone and finally dried in an oven at 50 °C for 24 hours. At the end, the material was powdered and kept in a vacuum desiccator to be kept dry.

### 2.5. Kjeldahl Method

The Kjeldahl method was used to evaluate the nitrogen content of the dried hydrogel (1 g) by following method [19]. After determining the total nitrogen of the samples, the crude protein amount was calculated by a conversion factor of 6.25 to convert % nitrogen to % crude protein [20]. Each sample was analyzed in duplicate.



### 2.6. Antioxidant Activity

The antioxidant activities of keratin powders were determined by making minor modifications from Kaya et al. [21]. First, 10 mg of the keratin samples were weighed and placed in test tubes. Then, 1.0 mL of DPPH solution at 6 x $10^{-5}$ M concentration was added to each tube. The samples were incubated for 30 minutes at 25 °C in the dark. At the end of the incubation, the entire keratin solution was measured using a UV-Vis spectrophotometer at a wavelength of 517 nm. Analysis was performed in triplicate for each sample.

DPPH scavenging activities of keratin powders were calculated using the following equation:

$$Inhibition\ (\%) = ((Acontrol - Asample) / Acontrol) \times 100 \quad (1)$$

Acontrol is absorbance of the control, Asample absorbance of keratin powders+ DPPH.

### 2.7. Statistical Information

Three replicates were prepared for all of the antioxidant activity tests. The results of these analyses were given as means and their standard deviations (means±SD).

## 3. RESULTS AND DISCUSSION

Within the scope of this study, keratin extraction was targeted using 2 different methods from waste goose feathers, the protein yield of keratin particles calculated and the antioxidant activities of powdered keratins were compared. The stereomicroscopy images of extracted keratin particles and powders were shown in Figure 1.

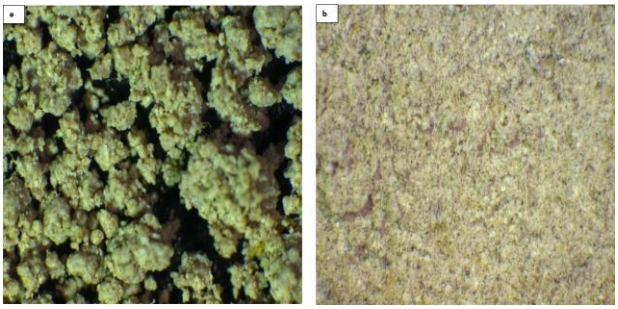

**Figure 1.** Stereomicroscopy images of keratin particles for Kjeldahl method (a) and powders for DPPH scavenging activity (b) extracted using goose feathers

As known, feathers contain 91% insoluble keratin and 1% oil; the rest is water [22]. For this purpose, firstly, the keratin oil was removed and then isolated from the insoluble goose down S-S cross-links that were broken in basic medium. An aqueous solution containing NaOH was used to break the keratin, disulfide bonds and provide solubility. Keratin was then precipitated with hydrochloric acid. Sodium sulfide ($Na_2S$) was chosen as the emulsifier in the first place because positive results were obtained with this chemical in many previous studies [23, 24, 25]. In general, physical conditions such as temperature, time, and concentration of reducing agent had a significant effect on the final yield of the isolated keratin [26]. Gül Çelik et al. found the best protein yield in $Na_2S$ (93.3%) compared to the extraction using only NaOH as a result of keratin extraction from chicken feathers [26]. Similarly, Pourjavaheri et al. found the yield as 88% in the extraction with sodium sulfide, but 66% with L-cysteine method [24]. Sharma et al. obtained the yield of keratin extracted with $Na_2S$ to be 80.2% under highly alkaline conditions [23]. Sinkiewicz et al. obtained 84% and 82% efficiency, respectively, by using mercaptoethanol and sodium bisulfite [27]; however, in our study, similar keratin yield was obtained at a lower cost. Gül Çelik et al. also proved that the yield increased as the temperature and time increased, and they observed the best yield at 60 °C [26]. Further, 25 °C obtained 87.6% efficiency [26] as in our study. Similarly, the previous study determined the optimum yield for keratin production within 2.5 hours at 23°C [5]. In Gül Çelik et al.'s study, the efficiency reached 90% as it was kept for 6 hours [26], however, in our study, 86% efficiency was achieved almost in one sixth of the time, which is a significant reduction in labor savings. Although, it has been shown in previous studies that alkaline hydrolysis takes longer to occur than acidic ones [25], but this study refuted this thesis.

Zeydanlı showed that the yield of powdered keratin obtained from feathers by EDTA method depends on the amount of feather, temperature, NaOH quantity, EDTA and hydrolysis reaction time [7]. Since the previous studies have shown that keratin yield is inversely proportional with increasing temperature [7, 23], reactions were carried out at 25 degrees and 40 degrees in the current study. Because excessive amount of EDTA concentration would be harmful to the product, it was used only 0.15 g. Similarly, conducted study has shown that by reducing the EDTA concentration, the efficacy is increased by half [7].

Looking at their antioxidant activities, keratin powders obtained using EDTA showed higher inhibition (65.21%) (Table 1, Figure 2). However, Alahyaribeik and Ullah (2020) obtained the best antioxidant activity from keratin by using sodium sulfite rather than 2-mercaptoethanol and mixture of sodium sulfite and SDS [25]. Mostly, the differences in inhibition activities of various keratin extraction methods are related to amino acid residues, various molecular weight of keratin, and production procedures [25]. Antioxidants possess an increasing interest due to their protecting functions in food and pharmaceutical products towards oxidative injuries and in the body and oxidative damage-intermediated pathological processes. Screening of antioxidant properties of plants and plant-derived agents necessitate suitable methodologies that address the machineries of anti-oxidant activities and emphasis on the kinetics of the reactions including the antioxidants. Several studies evaluating the antioxidant activity of various samples of research interest using different methods in food and human health have been carried out [28, 29, 30, 31, 32]. In our study we evaluated antioxidant activities of keratin by DPPH assay.

**Table 1**. DPPH radical scavenging activity of keratin powders obtained by two different extraction methods

| Methods | Inhibition (%) |
|---|---|
| $Na_2S$ | 24.14±5.79 |
| EDTA | 65.21±0.13 |

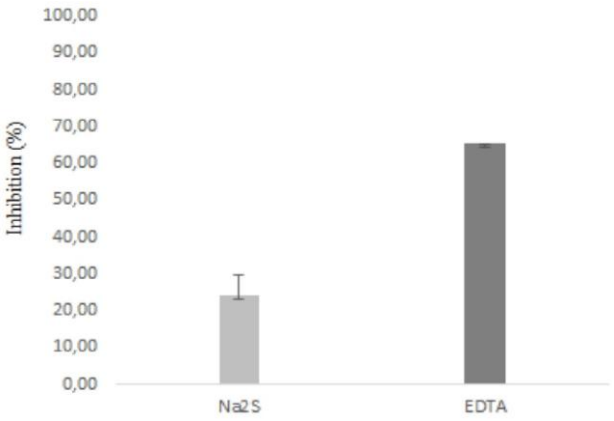


**Figure 2.** Antioxidant activities of keratins extracted by goose feathers determined by DPPH method

## 4. CONCLUSION

$Na_2S$ and EDTA were used during keratin extraction in this manuscript. The yield obtained from goose feathers extracted with $Na_2S$ and EDTA were 86.34% and 80.94%, respectively. The antioxidant activities of the powdered keratins obtained as a result of two extractions were

examined and detected as 24.14% and 65.21% for $Na_2S$ and EDTA, respectively. As a result, keratin extraction efficiencies were compared by using $Na_2S$ and EDTA chemicals separately and the best yield was obtained with $Na_2S$. It has been proven that the use of keratin can be increased with this study, which has high antioxidant activities especially for EDTA method. Considering the high protein structure of keratin, the addition of antioxidant activity strengthens the possibilities for further use in future for medical, tissue engineering and bioengineering studies.

## REFERENCES


[1] Sharma S, Gupta A. Sustainable management of keratin waste biomass: applications and future perspectives. Braz. Arch. Biol. Technol. 2016; 59.

[2] Shavandi A, Carne A, Bekhit AA, and Bekhit AE-DA. An improved method for solubilisation of wool keratin using peracetic acid. J. Environ. Chem. Eng. 2017;5:1977-1984.

[3] Adelere IA, Lateef A. Degradation of keratin biomass by different microorganisms. Keratin as a Protein. Biopolymer. 2019;123-162.

[4] Fan X. Value-added products from chicken feather fiber and protein [dissertation]. Auburn University ProQuest; 2008.

[5] Akkanat Ö. Keratin temelli biyokompozit sentezi [dissertation]. Istanbul Technic University; 2016.

[6] Schrooyen PM, Dijkstra PJ, Oberthür RC, Bantjes A, Feijen J. Partially carboxymethylated feather keratins. 1. Properties in aqueous systems. J. Agric. Food Chem. 2000;48(9), 4326-4334.

[7] Zeydanlı S. Keratın esaslı poli (akrilo nitril-ko-etilen glikol) sentezi ve karakterizasyonu [dissertation]. Istanbul Technic University; 2014.

[8] Bruice PY. Organic chemistry, 4th Ed., Prentice Hall, Upper Saddle River, NJ. Coll R.K; 2004.

[9] Tonin C, Zoccola M, Aluigi A, Varesano A, Montarsolo A, Vineis C, Zimbardi F. Study on the conversion of wool keratin by steam explosion. Biomacromolecules, 2006;7(12), 3499-3504.

[10] Su C, Gong JS, Ye JP, He JM, Li RY, Jiang M, et al. Enzymatic Extraction of bioactive and self-assembling wool keratin for biomedical applications. Macromol. Biosci. 2020;20(9), 2000073.

[11] Tsuda Y, Nomura Y. Properties of alkaline-hydrolyzed waterfowl feather keratin. Anim. Sci. J. 2014;85(2), 180-185.

[12] Buchanan JH. A cystine-rich protein fraction from oxidized alpha-keratin. Biochem. J. 1977;167(2), 489.

[13] Yamauchi K, Yamauchi A, Kusunoki T, Kohda A, Konishi Y. Preparation of stable aqueous solution of keratins, and physiochemical and biodegradational properties of films. J. Biomed. Mater. Res. An Official Journal of The Society for Biomaterials and The Japanese Society for Biomaterials. 1996;31(4), 439-444.

[14] Ghosh A, Clerens S, Deb-Choudhury S, Dyer JM. Thermal effects of ionic liquid dissolution on the structures and properties of regenerated wool keratin. Polym. Degrad. Stab. 2014;108, 108-115.

[15] Kamarudin NB, Sharma S, Gupta A, Kee CG, Chik SMSBT, Gupta R. Statistical investigation of extraction parameters of keratin from chicken feather using Design-Expert. 3 Biotech. 2017;7(2), 1-9.

[16] Poole AJ, Lyons RE, Church JS. Dissolving feather keratin using sodium sulfide for bio-polymer applications. J Polym Environ. 2011;19(4), 995-1004.

[17] Jones CB, Mecham DK. The dispersion of keratins. II. Studies on the dispersion of keratins by reduction in neutral solutions of protein denaturants. Arch Biochem. 1943;3, 193.

[18] Kalaoğlu Öİ. Tavuk tüyü keratininden tekstil elyaf eldesi [dissertation]. Istanbul Technic University; 2010.

[19] Bradstreet RB. Kjeldahl method for organic nitrogen. Anal. Chem. 1954;26:185-187.

[20] Salo-väänänen PP, Koivistoinen PE. Determination of protein in foods: comparison of net protein and crude protein (N × 6.25) values. Food Chem. 1996;57:27-31.

[21] Kaya M, Khadem S, Cakmak YS, Mujtaba M, Ilk S, Akyuz L, et al. Antioxidative and antimicrobial edible chitosan films blended with stem, leaf and seed extracts of *Pistacia terebinthus* for active food packaging. RSC Adv. 2018;8(8), 3941–3950.

[22] Schmidt W, Line M. Physical and chemical structures of poultry feather fiber fractions in fiber process development, Nonwovens. Conference, Atlanta, GA, USA. 1996. 135-140.

[23] Sharma S, Gupta A, Kumar A, Kee CG, Kamyab H, Saufi SM. An efficient conversion of waste feather keratin into ecofriendly bioplastic film. Clean Technol Environ Policy. 2018;20(10), 2157-2167.

[24] Pourjavaheri F, Pour SO, Jones OA, Smooker PM, Brkljača R, Sherkat F, et al. Extraction of keratin from waste chicken feathers using sodium sulfide and l-cysteine. Process Biochem. 2019;82, 205-214.

[25] Alahyaribeik S, Ullah A. Methods of keratin extraction from poultry feathers and their effects on antioxidant activity of extracted keratin. Int. J. Biol. Macromol. 2020;148, 449-456.

[26] Gül Çelik M, Hakan Morcali M, Ayhan Ziba C, Dolaz M. Valorization of chicken Feather waste: fabrication of keratin-chitosan biofilms. ChemistrySelect. 2021;6(9), 2189-2197.

[27] Sinkiewicz I, Śliwińska A, Staroszczyk H, Kołodziejska I. Alternative methods of preparation of soluble keratin from chicken feathers. Waste Biomass Valorization. 2017;8(4), 1043-1048.

[28] Kucukler S, Benzer F, Yildirim S, Gur C, Kandemir FM, Bengu AS, et al. Protective effects of chrysin against oxidative stress and inflammation induced by lead acetate in rat kidneys: a biochemical and histopathological approach. Biol. Trace Elem. Res. 2021;199(4), 1501-1514.

[29] Kucukler S, Darendelioğlu E, Caglayan C, Ayna A, Yıldırım S, Kandemir FM. Zingerone attenuates vancomycin-induced hepatotoxicity in rats through

regulation of oxidative stress, inflammation and apoptosis. Life Sci. 2020;259, 118382.
[30] Caglayan C, Kandemir FM, Darendelioğlu E, Küçükler S, Ayna A. Hesperidin protects liver and kidney against sodium fluoride-induced toxicity through anti-apoptotic and anti-autophagic mechanisms. Life Sci. 2021;281, 119730.
[31] Zengin G, Mahomoodally MF, Aktumsek A, Jekő J, Cziáky Z, Rodrigues MJ.et al. Chemical Profiling and Biological Evaluation of Nepeta baytopii Extracts and Essential Oil: An Endemic Plant from Turkey. Plants. 2021;10(6), 1176.
[32] Gulcin İ. Antioxidants and antioxidant methods: An updated overview. Arch. Toxicol. 2020;94(3), 651-715.

Cilt 11, Sayı 2, Sayfa 118-124, 2022 Volume 11, Issue 2, Page 118-124, 2022

Araştırma Makalesi https://doi.org/10.46810/tdfd.1078643 Research Article

Türk Doğa ve Fen Dergisi
Turkish Journal of Nature and Science
www.dergipark.gov.tr/tdfd

# The Effect of Different Steel Brace Types on Reinforced Concrete Frame System Retrofit

**Elif BORU[1*], Emine AYDIN[2]**

[1] Sakarya Uygulamalı Bilimler Üniversitesi, Teknoloji Fakültesi, İnşaat Mühendisliği Bölümü, Sakarya, Türkiye
[2] Sakarya Uygulamalı Bilimler Üniversitesi, Teknoloji Fakültesi, İnşaat Mühendisliği Bölümü, Sakarya, Türkiye
Elif BORU ORCID No: 0000-0003-1661-7673
Emine AYDIN ORCID No: 0000-0001-9191-5190

**Corresponding author: eorak@subu.edu.tr*

(Received: 17.03.2022, Accepted: 06.06.2022, Online Publication: 29.06.2022)

**Keywords**
Steel braces, Retrofit, Pushover analysis, Interstory drift.

**Abstract:** One of the common methods used as an alternative to shear walls in the retrofit of reinforced concrete (RC) structures is steel braces. The use of steel braces is preferred because of its rapid application as well as the increase in stiffness and strength. By using different types of braces in reinforced concrete frames, displacements can be reduced and properties such as structural performance, shear capacity, ductility, stiffness and strength can be increased. If the behavior characteristics of the hybrid system are known, the structural performance of the reinforced building can be predicted after the retrofit. In this study, the effect of different types of steel braces recommended in the Turkey Building Earthquake Code 2018 (TBEC-2018) on reinforced concrete building retrofit, was investigated. For this purpose, a 9-storey RC frame system was retrofitted using diagonal, X, inverted V, V and K type bracings. Considering the strength and stiffness results, an answer was searched for the question of which brace type had the best result in retrofit. The results obtained from the analyzes show that the X and K type bracings stand out in terms of strength and stiffness.



# Farklı Çelik Çapraz Türlerinin Betonarme Çerçeve Sistem Güçlendirmesine Etkisi

**Anahtar Kelimeler**
Çelik çaprazlar, Güçlendirme, İtme analizi, Göreli kat ötelemesi

**Öz:** Betonarme yapıların güçlendirmesinde perde yapımına alternatif olarak kullanılan yaygın yöntemlerden birisi de çelik çaprazlardır. Çelik çapraz kullanımı rijitlik ve mukavemet artışının yanı sıra hızlı uygulanabilmesi nedeniyle de dikkatleri çekmektedir. Betonarme çerçevelere farklı türden çaprazlar eklenerek yer değiştirmeler azaltılıp, yapısal performans, kesme kapasitesi, süneklik, rijitlik, mukavemet gibi özellikler iyileştirilebilir. Bir binayı güçlendirme sonrasında yeniden tasarlama, ancak yeni hibrit sistemin davranış özellikleri biliniyorsa mümkündür. Yapılan bu çalışmada Türkiye Bina Deprem Yönetmeliği 2018'de önerilen çelik çapraz türlerinin betonarme bina güçlendirmesi üzerindeki etkisi araştırılmıştır. Tasarlanan bir betonarme çerçeve sistem diyagonal, X, ters V, V ve K tipi çelik çaprazlar kullanılarak güçlendirilmiştir. Dayanım ve rijitlik sonuçları göz önünde bulundurularak güçlendirmede en iyi sonuç hangi çapraz türünde edilmiştir sorusuna cevap aranmıştır. Yapılan karşılaştırmalarda X ve K tipi çaprazların dayanım ve rijitlik açısından ön plana çıktığını göstermektedir.

## 1. INTRODUCTION

According to the principle of earthquake resistant building design, it is expected that the buildings will have adequate strength and stiffness to prevent them from collapsing and to increase the life safety for the inhabitants, under the influence of severe earthquakes. Steel braced frames are widely used to control the seismic performance of structures and improve lateral stiffness under severe horizontal forces such as earthquakes. In braced frames, proper bracing arrangements will increase lateral resistance and reduce internal forces, particularly bending moments in columns and beams [1-8]. Braced steel frames are divided into two, as central and eccentrically braced steel frames, depending on the arrangement of the braces [9]. Central braced frames are widely used for traditional structures due to their practical and economic advantages. The idea of using steel bracings in reinforced concrete structures has attracted more and more attention in recent years. When the previous studies are examined, it is seen that

the studies focused on either the external bracing of reinforced concrete frames or the internal bracing through intermediate steel frames [10-11].

Different methods are used to retrofit reinforced concrete structures [12-14]. When the studies in the literature are examined; In the retrofit of reinforced concrete structures, it has been tried to determine whether the best reinforcement method is a reinforced concrete shear wall or steel bracing by taking into account the interstory drift [15] .In steel buildings with regular and irregular geometry, the diagonal central steel bracing system has been found to have more energy absorption capacity than the inverted V central steel cross curtain system [16]. It has also been shown that when the beams of a steel braced frame with weak short columns are replaced, the inelastic behavior of the frame can be improved [10]. It has been tried to determine which is the best retrofitting method by using different bracing types related to the reinforcement of reinforced concrete structures [17]. When the mega braced configurations are examined, it is seen that the amount of steel for the structural elements and connections is lower. As a result, the reduction in construction cost makes mega braced frames attractive for use in seismic reinforcement applications [18]. Only tension braced frames (TOBFs) have poor seismic energy dissipation capacity and a compressed hysteresis behavior due to premature buckling of slender bracing members. The main concern in using the TOBF system is the determination of appropriate performance factors for seismic design. For this purpose, a series of predicted ground motions are applied and the safe design factor is obtained [5]. There are also studies examining the behavior of structures reinforced with both conventional central and composite steel bracing systems [19]. It has been found that the retrofit of low-rise reinforced concrete frames with steel X braces is beneficial to the performance of the frame columns in terms of many parameters. However, for medium and high-rise frames, the adverse effects of retrofit especially on the columns connected to the bracing system should be considered, and local retrofit of the columns should be done locally if necessary [20]. In the seismic performance of medium-height reinforced concrete buildings, a formula for fatigue has been developed considering the results of retrofit with different types of decentralized steel braces [21]. When looking at the experimental studies investigating the effect of adding different types of steel braces on the behavior of reinforced concrete moment-frames, strength, stiffness, crack expansion, ductility, energy loss and strength reduction factor of all frames were evaluated. Considering the ductility and strength reduction factor parameters, the results show that the decentralized brace has a better performance than the other specimens. However, when the hardness, strength and crack control parameters are evaluated, it is concluded that the behavior of the X brace is better [22].

In this study, it is aimed to determine which of the centric steel braces type, recommended in TBDY 2018 Section 9.5, gives the best results in retrofit of reinforced concrete frame. In the first stage of the study, a reference reinforced concrete frame with 9 floors and 3 spans was designed considering the TS500 and TBEC 2018 criteria. The necessity of retrofit the reference frame under the effect of a design earthquake is discussed. Performance analysis was performed by applying a single-mode pushover analysis at the decision stage. By using 6 different types of braces, the most suitable one in reinforced concrete frame retrofit was decided.

## 2. NUMERICAL STUDIES

In the study, the central steel bracing types recommended in TBDY 2018 Chapter 9, were used to retrofit a reinforced concrete frame. The reinforced concrete frame system has 9 floors and the building usage class is 3, the frame does not have any structural irregularities.

Analytical modeling of the framework and analyzes were performed in SAP2000 computer software [23]. The reinforced concrete frame system is retrofitted by using different steel brace types and cross sections. Modal and pushover analyzes were performed in Sap 2000 program. By comparing the analysis results, the answer to the question of which brace type is the most suitable for retrofitting was sought.

### 2.1. Numerical Model of RC Frame

The reinforced concrete frame used in the analyzes has 3 spans with a length of 4.5m. Story height is equal and 3m on all stories. S420 steel grade and C25 concrete grade were used in the design of the bearing elements. The effective section stiffnesses of columns and beams were applied as specified in TBEC 2018 Chapter 4. Column sections are 40x40cm and beam sections are 25x30cm (Figure 1). In the design of the frame, Turkey Building Earthquake Code 2018 [24] and TS500 Requirements for Design and Construction of Reinforced Concrete Structures [25] were taken into account. Controlled damage performance level (CD) has been achieved as stated in the TBEC 2018. Lumped plastic hinges are used in the analytical model.



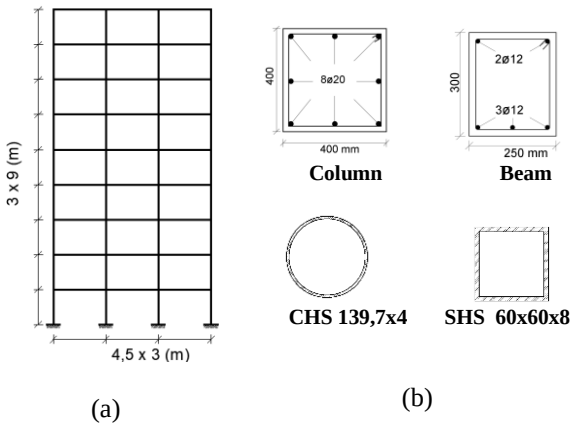


**Figure 1.** Reinforced concrete frame (a) numerical model (b) column, beam and braces cross-section details

Lumped plastic hinges are used in the analytical model. In this plastic hinge approach, it is accepted that the nonlinear behavior of column and beam elements occurs

in the most stressed end regions of the element under the influence of earthquake, and linear elastic behavior occurs outside of this. In column elements, plastic hinges are defined by the axial load and biaxial moment interaction, and in beam elements by the moment curvature relationship. In earthquake resistant building design, the ground motion at the location of the building and the earthquake loads acting on the building are calculated by using the elastic acceleration spectrum of the relevant location from the Turkey Earthquake Risk Map. It has been accepted that the earthquake level affecting the frame is Earthquake Ground Motion Level-2 (DD-2), and it is located in Sakarya University of Applied Sciences, Technology Faculty. The earthquake parameters used in the study are given in Table 1.

**Table 1.** Horizontal elastic response spectrum parameters of the frame

| Earthquake Parameters | |
|---|---|
| Soil classification | ZB |
| Building usage class ( BKS) | 3 |
| Building height class (BYS) | 5 |
| Seismic design category | 1 |
| Targe Building Performance Level | CD |
| $S_{DS}$ | 1.527 |
| $S_{D1}$ | 0.372 |

## 2.2. Determination of Seismic Performance of Reinforced Concrete

It has been determined whether the RC frame provides the performance level specified in TBEC 2018. At this stage of the study, it is aimed to determine whether the frame meets the performance target, which is the design condition, and to reveal the contribution of steel braces to the frame behavior. Buildings with a building height class of more than 2 must meet the controlled damage (CD) performance level according to TBEC 2018. At this performance level, the main goal is to avoid loss of life, so it is aimed to limit the damage to the bearing elements. In order to determine the performance level of the frame, Single-Mode Pushover Analysis was performed. One of the conditions for using unimodal pushover analysis is that the BYS must be greater than 5 and this condition is met. Another condition is that the ratio of the effective mass of the base shear force belonging to the dominant vibration mode of the building to the total mass of the building is at least 70%. Modal analysis was performed and it was determined that this condition was also met (Table 2). Finally, the condition that the torsional irregularity coefficient of the building is ηbi<1.4 is also met.

**Table 2.** Modal analysis results of the reference frame

| | Period (s) | Mass Participation (%) |
|---|---|---|
| Reference | 1.160 | 77 |

The pushover curve of the frame (Base shear force-Displacement) was obtained by single-mode pushover analysis. The modal capacity diagram of the frame was obtained by applying the transformation equations, specified in TBEC 2018 Chapter 5, to the pushover curve (Figure 5). By superimposing this diagram with the demand spectrum, the maximum modal displacement of the dominant mode, that is, the modal displacement demand of the frame, was found to be 0.27 m in the direction of the earthquake considered (Figure 2).

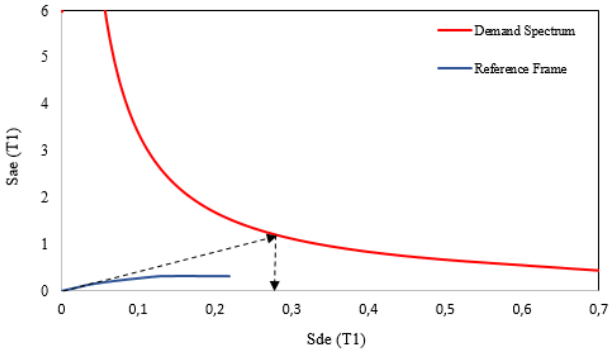


**Figure 2.** Modal capacity diagram of the reference frame

The calculated displacement demand was applied by the pushover analysis to the frame, and the plastic rotation values formed in the bearing system elements were obtained. While determining the performance level of the frame, it is necessary to determine the plastic rotation limits of the bearing elements and to check whether the rotation amounts in the sections as a result of the pushover analysis exceed these limits. According to TBEC 2018, the plastic rotation limits allowed for controlled damage (CD) and collapse prevention (GÖ) performance levels were calculated by using the yield and collapse prevention curvature values of the bearing elements (Figure 3).

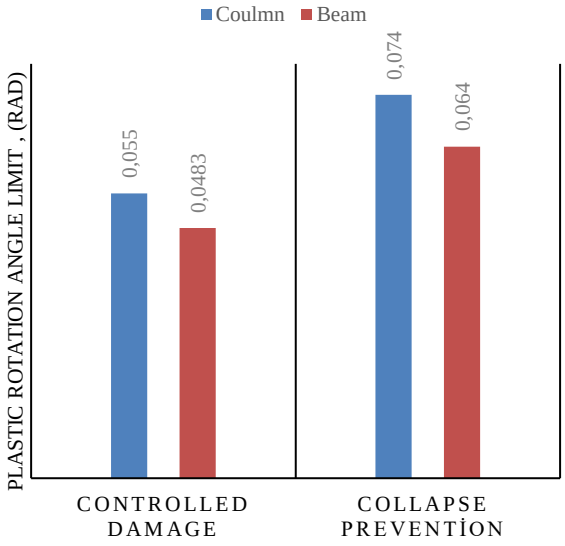


**Figure 3.** Plastic rotation angle limits of performance levels

The target displacement was applied to the frame by pushover analysis, and as a result, no hinges were formed in the columns, but plastic hinges were formed at the ends of some beams. When the plastic hinges rotation values were examined, it was determined that the CD performance level met the limit values. The rotation values of the 3 hinges with the highest rotation angles in the beams are given in Table 3.

**Table 3.** Highest plastic rotation angles in beams

| | Rotation Angle (Rad) | Controlled Damage (Θp, rad) | Collapse Prevention (Θp, rad) | Situation |
|---|---|---|---|---|
| Beam | 0.0175 | 0.0483 | 0.064 | Provides |
| Beam | 0.0173 | 0.0483 | 0.064 | Provides |
| Beam | 0.0173 | 0.0483 | 0.064 | Provides |

In the performance evaluation, it was determined that the plastic rotation values provided the CP performance level. After the performance evaluation, it was checked whether the interstory drift and second order effects meet the limits specified in TBEC 2018. It was determined that the effective relative interstory drift values for all stories exceeded the limit value. In the control of the second order effects, it was determined that the limit values given in the TBEC 2018 were exceeded, except for the first two floors.

### 2.3. Retrofit of The RC Frame With Centric Steel Braces

Although the designed RC frame provides the performance level required by the TBEC 2018, the relative interstory drift and second order effects have exceeded the limits. In order to limit the relative interstory drifts and second order effects, the frame is retrofit with centric steel braces. Diagonal, X, inverted V, V and K central diagonal braces given in TBDY 2018 were used for retrofit. S235 steel circular (CHS139.7x4) and square hollow section (Tube 60x60x8) are used diagonally, whose cross-sectional areas are very close to each other (Table 4).

**Table 4.** Properties of sections used in steel braces

| | Cross-section area ($cm^2$) | Moment of inertia ($cm^4$) |
|---|---|---|
| Circular hollow section | 16,96 | $7,68x10^{-3}$ |
| Square hollow section | 17,05 | $3,93x10^{-2}$ |

It is possible to retrofit reinforced concrete buildings with different types of steel braces. However, using the most suitable type of steel braces is important in terms of earthquake resistance and design cost. From this stage on, retrofit was made by using 5 different types of steel braces in order to determine the most suitable type of steel brace for retrofit (Figure 4). In the analytical modeling, nonlinear behavior is taken into account with the moment hinges defined at both ends of the steel braces. By taking the analysis results of the unretrofitted frame as a reference, the models were compared considering the performance levels of the frames and the results of the effective relative interstory drift.

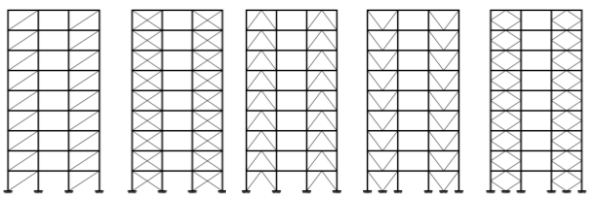

Diagonal Brace | X brace | Inverted V Brace | V Brace | K Brace

**Figure 4.** Steel braces used in reinforcement

## 3. ANALYSIS RESULTS

Numerical models of all reinforcement types were created in the Sap2000 computer package program and modal analysis was performed. As a result of the analysis, the mass participation in all retrofit models shows almost 100% agreement with each other in circular and square hollow sections. Since the mass participation rate of the 1st mode was more than 70%, the performance evaluation was continued with the single-mode pushover analysis method. Modal analysis results showed that X and K braces contribute more to structural stiffness than other brace types. It was determined that the results of the circular and square hollow section models were compatible with each other (Table 5).

**Table 5.** Modal analysis results of retrofitted frames

| Model | Circular hollow sections period (s) | Mass participation (%) | Square hollow sections period (s) | Mass participation (%) |
|---|---|---|---|---|
| Diagonal Brace | 0,37 | 78,5 | 0338 | 78,5 |
| X brace | 0,30 | 75,5 | 0,30 | 75,6 |
| Inverted V Brace | 0,32 | 77,0 | 0,32 | 77,0 |
| V Brace | 0,34 | 77,0 | 0,34 | 77,0 |
| K Brace | 0,31 | 74,6 | 0,30 | 74,3 |

After the modal analysis, static pushover curves were obtained for all models with pushover analysis and the curves were compared (Figure 5). When the curves are examined, it is possible to say that the appropriate retrofit process will increase the capacity of the structure.



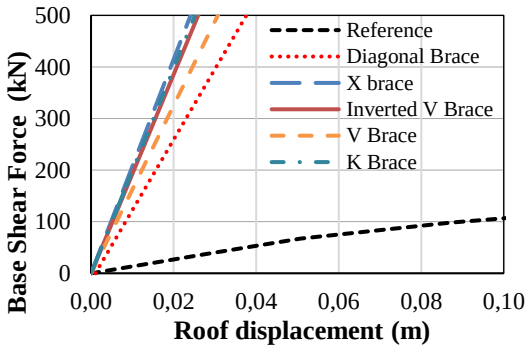


(a) Circular hollow section pushover curve

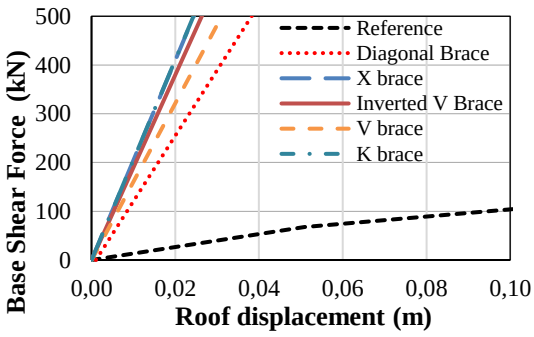


(b) Square hollow section pushover curve

**Figure 5.** Comparison of pushover curves (a) circular hollow sections (b) Square hollow sections

The displacement demands of all models were calculated by overlaying the modal capacity diagrams, obtained by the conversion of the static pushover curves, with the demand spectrum. The displacement demands of the circular and square hollow section models are the same except for the K braces. When the braces were compared among themselves, the two lowest displacement demands were obtained in the K and X braces (Figure 6).

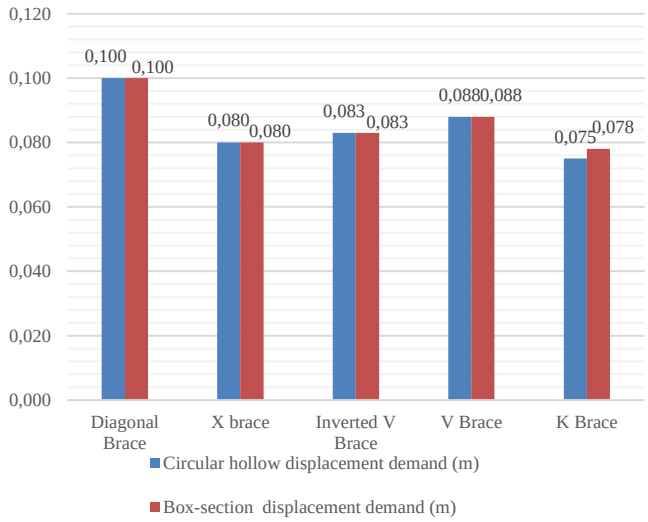


**Figure 6.** Target displacements of models

The displacement demands were applied to the all retrofitted models by pushover analysis and the plastic hinge rotation angles of the bearing elements were determined. When the results were examined, it was determined that the hinges were formed at the beam ends in all models. The maximum rotation angle values in the models are presented in Table 6. In the comparison, it was determined that the CP performance level was provided in all models and the result obtained was deemed appropriate in terms of design.

**Table 6.** Maximum plastic rotation angles in models as a result of pushover analysis

| Model | Circular hollow section hinge rotation (Rad) | Square hollow section hinge rotation (Rad) | Controlled damage rotation limit (Rad) | Situation |
|---|---|---|---|---|
| Diagonal Brace | 0.0045 | 0.0047 | 0.0483 | Provides |
| X brace | 0.0033 | 0.0031 | 0.0483 | Provides |
| Inverted V Brace | 0.0031 | 0.0030 | 0.0483 | Provides |
| V Brace | 0.0036 | 0.0036 | 0.0483 | Provides |
| K Brace | 0.0028 | 0.0030 | 0.0483 | Provides |

After the performance evaluation, it was determined that the main purpose of retrofit the frames was to limit the relative interstory drifts. For this reason, it has been checked whether the relative interstory drift values exceed the TBEC 2018 limit values. The reduced relative interstory drifts of all models were calculated and the maximum effective interstory drift values were obtained by using these values (Figure 7, Table 7-8). Maximum effective relative interstory drifts are limited to 0.008 in the TBEC 2018.

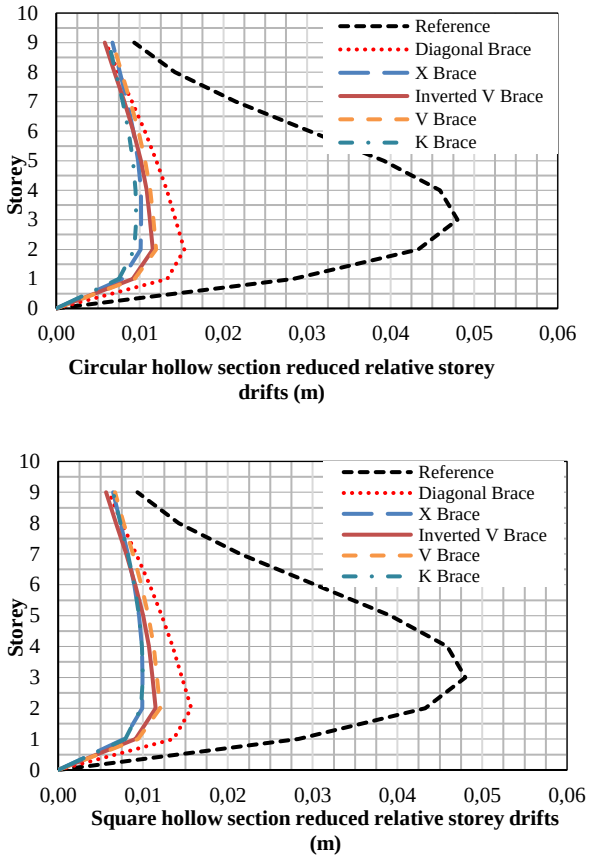


**Figure 7.** Reduced relative interstory drift values of all retrofit models

Relative interstory drift expresses, the ratio of the drift demands occurring at different stories in the case of horizontal drift. The effective relative interstorey drifts of the models provided the upper limit value, (0.008) given in TBDY 2018, for circular hollow section X and K braces. In circular hollow section models, there are drift values exceeding the limit value in X and K braces. In square hollowsection models, on the other hand, the relative interstory drift condition is satisfied only in the Inverted V braced model.

**Table 7.** Effective relative interstory drifts of circular hollow sections (m)

| Storey | Diagonal brace | X brace | Inverted V brace | V brace | K brace |
|---|---|---|---|---|---|
| 1 | 0.011 | 0.007 | 0.008 | 0.008 | 0.006 |
| 2 | 0.014 | 0.008 | 0.010 | 0.010 | 0.008 |
| 3 | 0.013 | 0.008 | 0.009 | 0.010 | 0.008 |
| 4 | 0.012 | 0.008 | 0.009 | 0.009 | 0.008 |
| 5 | 0.011 | 0.008 | 0.008 | 0.009 | 0.008 |
| 6 | 0.010 | 0.008 | 0.008 | 0.008 | 0.007 |
| 7 | 0.008 | 0.007 | 0.007 | 0.007 | 0.007 |
| 8 | 0.007 | 0.006 | 0.006 | 0.007 | 0.006 |
| 9 | 0.005 | 0.006 | 0.005 | 0.006 | 0.005 |

**Table 8.** Effective relative interstory drifts of square hollow sections (m)

| Storey | Diagonal brace | X brace | Inverted V brace | V brace | K brace |
|---|---|---|---|---|---|
| 1 | 0.027 | 0.011 | 0.006 | 0.008 | 0.008 |
| 2 | 0.041 | 0.014 | 0.008 | 0.010 | 0.010 |
| 3 | 0.046 | 0.013 | 0.008 | 0.009 | 0.010 |
| 4 | 0.044 | 0.012 | 0.008 | 0.009 | 0.009 |
| 5 | 0.037 | 0.011 | 0.008 | 0.008 | 0.009 |
| 6 | 0.029 | 0.010 | 0.007 | 0.008 | 0.008 |
| 7 | 0.020 | 0.008 | 0.007 | 0.007 | 0.007 |
| 8 | 0.014 | 0.007 | 0.006 | 0.006 | 0.006 |
| 9 | 0.009 | 0.006 | 0.005 | 0.005 | 0.006 |

## 4. RESULTS AND DISCUSSIONS

As a result of the performance analysis, it was determined that the plastic hinge rotations in the bearing elements did not exceed the CD limit given in TBEC 2018. After the performance analysis, the effective relative interstory drift values, which were required to be checked in TBEC 2018, were obtained. In the control, it was determined that the relative interstory drift limit value given in the earthquake code was exceeded at all floors in the reference model. In the next step, it is aimed to limit the relative interstory drift values of the reference frame. For this purpose, the reference frame was retrofit by using different types of centric steel braces (diagonal, X, inverted V, V and K braces). Circular and square hollow sections with close cross-sectional areas were used for retrofit.

While looking for an answer to the question of which brace retrofit is better, modal analysis results, displacement demands and effective relative interstory drift results are taken into account. When the modal analysis results are compared, it is an expected result that the highest period value will appear in the reference building (Table 6). Among the retrofit models, the results for both cross-section types almost overlap with each other. Among the steel braces, the period values of the models with X and K braces was lower than the other braces (Table 7). From this result, it was concluded that X and K brace types make the structure more rigid. From this result, it was concluded that X and K brace types make the structure more rigid.

When the displacement demands obtained under the effect of the design earthquake are examined, in the section type comparison, the results in circular hollow section models in K braces are 4% lower than in square sections. When bracing types were compared, it was determined that the lowest displacement demand was obtained in circular section K braced models, followed by the X braced model with a 6.7% higher value (Table 8).

The final comparison was made over the relative interstory drift values. As a result of the retrofit, it was determined that the relative interstory drift values decreased in all models. In the section type comparison, it was determined that lower relative interstory drift values were obtained in circular hollow section models in all brace types (Table 9). When bracing types were compared, it was concluded that the relative interstory drift values in the K braced models were lower than the other models, followed by the X model. Among the brace types, the best results were obtained in the K braced models, followed by the X braced models.

When the obtained results are evaluated in a general framework, it is concluded that the circular hollow section with the same area gives better results than the square section. Depending on the architectural features of the application, one of the K and X cross types can be preferred.

## REFERENCES

[1] Rahai AR, Alinia MM. Performance Evaluation and Strengthening of Concrete Structures with Composite Bracing Members. Constr. Build. Mater. 2004;22(10):2100–2110.
[2] Kasap H, Mert N, Sevim E, Şeber B. Perdeli-Çerçeveli Taşıyıcı Sistemli Binalarda Taşıyıcı Sistem Seçiminin Yapı Davranışı Üzerindeki Etkisinin İncelenmesi. Acad. Platf. J. Eng. Sci. 2015;3(1):48–55.
[3] Piroğlu F. Uzgider E. Mevcut Betornarme Yapıların Çelik Malzeme ile Güçlendirilme Yöntemleri. Türkiye Mühendislik Haberleri. 2005;(436);37–46.
[4] Celep Z, Kumbasar N. Deprem Mühendisliğine Giriş ve Depreme Dayanıklı Yapı Tasarımı. 7th ed. Beta; 2004.
[5] Nateghi F. Seismic Strengthening of Eightstorey RC Apartment Building Using Steel Braces. Eng. Struct. 1995;(17)6:455–461.
[6] Badoux BM, Jirsa JO. Steel bracing of RC frames for seismic retrofitting. J. Struct. Eng. 1990;116(1):55–74.
[7] Aydın E, Boru E, Betonarme Binaların Güçlendirilmesinde Uygun Merkezi Çelik Çapraz Yerleşiminin Belirlenmesi. Acad. Platf. J. Eng. Sci. 2020;8(2):286–294.
[8] Işık E, Özdemir M, Performance based assessment of steel frame structures by different material models. Int. J. Steel Struct. 2017;17(3):1021–1031.
[9] Özel AE, Assessing Effects of Type and Distribution of Eccentric Steel Braces on Seismic Vulnerability of Mid-Rise Reinforced Concrete Buildings. University of Gaziantep Graduate School of Natural & Applied Sciences; 2010.
[10] Rahimi A, Maheri MR, The effects of retrofitting RC frames by X-bracing on the seismic performance of columns. Eng. Struct. 2018;173: 813–830.
[11] Yaman Z, Ağcakoca E, Dairesel Kesite Sahip Merkezi Çelik Çaprazların Performans Analizi. Sak. Üniversitesi Fen Bilim. Enstitüsü Derg. 2018; 22(2):340–349.
[12] Baran M, Comparison Of Seismic Performances Of

Reinforced Concrete Frames Strengthened By Different Techniques. Latin American Journal of Solids and Structures. 2021; 18 (02).
[13] Aksoylu C, Kara N, Strengthening Of RC Frames By Using High Strength Diagonal Precast Panels. Journal of Building Engineering. 2020; 31(10):13-38.
[14] Aksoylu C, Sezer R, Investigation Of Precast New Diagonal Concrete Panels In Strengthened The Infilled Reinforced Concrete Frames. KSCE Journal of Civil Engineering. 2018; 22(1):236-246.
[15] İnce G, Tekeli H, İnce HH, Öcal C, Mercan K, Ulutaş H. Betonarme Çerçevelerin Düşey Bağ Kirişli Dışmerkez Çaprazlarla Güçlendirilmesi. in International Burdur Earthquake & Environment Symposium (IBEES2015) Uluslararası Burdur Deprem ve Çevre Sempozyumu; 2015.
[16] Çatalkaya H. Çok Katlı Bir Çelik Yapıda Değişik Çapraz Düzenlemelerinin Yapının Depremdeki Davranışına Etkilerinin İncelenmesi. İstanbul Teknik Üniversitesi; 2004.
[17] Yön B, Sayın E. Betonarme Perdeler ve Çelik Çaprazlarla Yapılan Güçlendirmelerin Karşılaştırılması. 6th International Advanced Technologies Symposium (IATS'11), Elazığ;2011. p. 237–242.
[18] Bush BTD, Jones EA, Jirsa JO. Behavior of RC Frame Strengthened Using Structural Steel Bracing. J. Struct. Eng. 1991;117(4):1115–1126.
[19] Maheri MR, Sahebi A, Use of Steel Bracing in Reinforced Concrete Frames. Eng. Struct.1997;19(12):1018–1024.
[20] TahamouliRoudsari M, Entezari A, Hadidi MH, and O. Gandomian, "Experimental Assessment of Retrofitted RC Frames With Different Steel Braces," Structures, vol. 11, no. June, pp. 206–217, 2017.
[21] Korkmaz KA, Çelik Çapraz Elemanlarla Güçlendirilen Betonarme Yapıların Deprem Davranışlarının İncelenmesi. Doğuş Üniversitesi Derg. 2007;8(2):191–201.
[22] Aydın E, Yapıların Deprem Davranışlarının İyileştirilmesi İçin Sönümleyicilerin ve Çelik Çapraz Elemanların Optimum Yerleşimi. İstanbul Teknik Üniversitesi, 2005.
[23] Computers and Structures INC. SAP2000.
[24] AFAD, TBDY 2018, Türkiye Bina Deprem Yönetmeliği. 2018.
[25] TSE, TS 500 Betonarme Yapıların Tasarım ve Yapım Kuralları. 2000.

Cilt 11, Sayı 2, Sayfa 125-129, 2022 Volume 11, Issue 2, Page 125-129, 2022

Araştırma Makalesi https://doi.org/10.46810/tdfd.1105343 Research Article

Türk Doğa ve Fen Dergisi
Turkish Journal of Nature and Science
www.dergipark.gov.tr/tdfd

# Detecting of Circular Knitting Fabric Defects Using VGG16 Architecture

**Kazım HANBAY**[1*]

[1] Inonu University, Department of Software Engineering, Malatya, Türkiye
Kazım HANBAY ORCID No: 0000-0003-1374-1417

** Corresponding author: kazimhanbay@gmail.com*

(Received: 18.04.2022, Accepted: 07.06.2022, Online Publication: 29.06.2022)

**Keywords**
Fabric defect,
Deep learning,
Defect detection

**Abstract:** Although the conventional image processing methods can detect fabric defects, fabric defect detection is an open research problem due to the diversity of defect types. In this paper, the feasibility of VGG16 deep learning architecture for fabric defect detection has been demonstrated. A new fabric defect database is used. The pre-trained model of VGG16 architecture on the new database is built. Thus, the training time of the model is reduced. The experimental results show that the VGG16 model outperforms the traditional Shearlet transform and GLCM methods.

# VGG16 Mimarisi Kullanılarak Yuvarlak Örgü Kumaş Hatalarının Tespit Edilmesi

**Anahtar Kelimeler**
Kumaş hatası,
Derin öğrenme,
Hata tespiti

**Öz:** Geleneksel görüntü işleme metotları kumaş hatalarını tespit edebilmelerine rağmen kumaş hatası tespiti hata tiplerinin çeşitliliği yüzünden açık bir problemdir. Bu çalışmada VGG16 derin öğrenme mimarisinin kumaş hatası tespiti için uygunluğu gösterilmiştir. Yeni bir kumaş hatası veri tabanı kullanılmıştır. Daha önceden eğitilmiş VGG16 mimarisi veri tabanı üzerinde inşa edilmiştir. Böylece modelin eğitim süresi azaltılmıştır. Deneysel sonuçlar VGG16 modelinin geleneksel Shearlet dönüşümü ve GLCM metotlarından daha iyi olduğunu göstermektedir.



## 1. INTRODUCTION

Today, the demand for fabric and fabric products is increasing. Fabric quality is a determining parameter in the demand for the product. Fabric defect control, which has traditionally been human-oriented, includes different problems. For example, labor costs, carelessness and mistakes cause important mistakes to be overlooked. Therefore, the importance of automatic fabric defect detection systems is increasing. With automatic systems, information about the location, size and type of the defects can be obtained. Some well-known types of circular knitting fabric defects are shown in Figure 1.

Until now, many different defect detection methods have been developed using image processing and machine learning methods. These methods can be examined in two main groups [1]: traditional image processing methods and convolutional neural networks (CNNs)-based methods. Traditional methods rely on extracting color and texture-based features of the fabric image. Regular texture breaks down when errors occur in fabric images with regular texture [2]. This degradation is also reflected in the extracted features. Well-known methods such as Fourier transform, histogram-based approaches [3], gray level co-occurrence matrix (GLCM) [4], and local binary pattern [5] are used to determine this distortion. In particular, metrics such as energy calculated on the image in GLCM-based methods emphasize the change in images with distortion [6]. Spectral methods such as Fourier transform and wavelet transform are used to detect fabric defects. On the other hand, Vermak et al. [7] analyzed the real and imaginary parts of the wavelet coefficients of the fabric image based on energy. Thus, they calculated detailed information about the defect. Shearlet transform was used to classify defects in terms of textural properties of fabric images in different scales and directions [8]. Thus, multi-scale methods have been developed that can effectively detect the presence of a defect. Thanks to the sensitive texture information provided by the Shearlet transformation, the defective pixel regions can be detected.

In recent years, it has been tried to detect difficult fabric defects by using deep learning algorithms. The ability of CNN-based methods to obtain high-level features from fabric images has enabled them to be used extensively in this field. Chen et al. [1] developed a defect detection system by using Gabor transform,

genetic algorithm and CNN architecture. By integrating Gabor kernels into the Faster R-CNN architecture, the feature calculation capability of the CNN architecture has been improved. On the other hand, Li and Li [9] developed a defect detection system with multi-scale training with the Cascade R-CNN model. Fabric images were analyzed at different resolutions with a multi-scale approach. Liu et al. [10] proposed a fabric defect detection system called DLSE-Net, using semantic information generated by connecting different network layers. Thus, instead of a single network layer, the entire network was optimized and information such as noise and background were tried to be distinguished from defects. In another study, a convolutional denoising autoencoder network was developed to detect fabric defects. By designing an architecture that can calculate the probability of defects, fabric defects can be successfully detected with the help of some prior knowledge [11]. The success of the CNN architecture has been improved with the mechanism called the pairwise-potential activation layer. In a CNN architecture designed to segment fabric defects and decide if there are faults, the network is split in two. [12]. The first part is segmentation and the second part is decision making. With this method, which can also work in real-time, a specific fabric defect detection-based deep learning architecture is proposed.

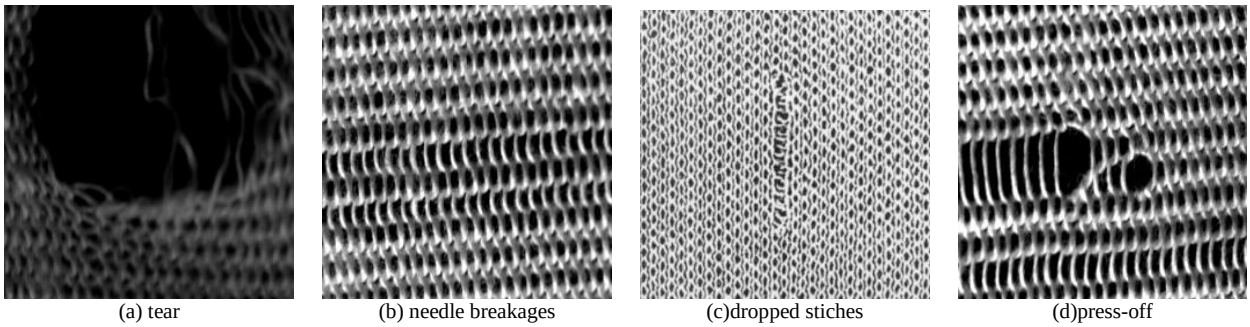

(a) tear (b) needle breakages (c)dropped stiches (d)press-off

**Figure 1.** Circular knitting fabric defects

With the use of deep learning methods, successful results have been obtained without the need to calculate complex hand-craft features. However, deep learning models have some limitations in fabric defect detection. For example, it is sometimes difficult to determine the size of the training dataset to obtain a good result. Especially when examining different types of woven and knitted fabrics, it is necessary to build databases containing fabric type-specific defects. This causes intensive labor and raw material loss in the fabric factory. Therefore, it is necessary to optimize the training data needs of existing deep learning models. For this purpose, it is necessary to work on CNN models that produce successful results with less training data. Existing studies mostly focused on woven fabric defects. However, there is a need for a CNN model that can produce successful results in knitted fabric types.

In this study, a deep learning-based defect detection system is proposed that can detect the types of defects frequently encountered in knitting fabrics produced on circular knitting machines. The results obtained by testing the performance of the VGG16 [13] CNN architecture in knitting fabric defects were analyzed. The database used is problem-specific and has been used in traditional image processing methods before. Thanks to this study, the performances of traditional methods and VGG16 deep learning architecture will be compared for the first time in detecting knitting fabric defects. Thus, detailed information will be given to the reader about the performance difference between the methods in the detection of knitting fabric defects.
In Section 2, information about the database used and the VGG16 network architecture is given. In addition, the traditional image processing methods used in the comparison are briefly mentioned. The experimental results are discussed in Section 3. In Section 4, some conclusions are presented.

## 2. MATERIAL AND METHOD

In this study, a database containing the types of defects frequently encountered in circular knitting fabrics has used. Defect detection has been made by using the created database both with traditional methods and VGG16 deep learning architecture. In this section, firstly, information about the database will be given. Then, the basic information and parameters of the methods used will be explained.

### 2.1. Fabric Dataset

Although there are different databases containing woven fabric defects in the literature, there is almost no database containing defects in circular knitting fabrics. In this study, the database developed by Hanbay et al. [8] has used. This database is constructed with video images obtained from the image acquisition mechanism installed on the circular knitting machine. A line-scan camera was used for image acquisition. The recording process was started by finely adjusting the line light source according to the line sensor position. Defective and defect-free fabric images were recorded in video form. Then, the database images were obtained by dividing each of them into 250×256 images. In the last case, a database consisting of a total of 13820 defective and defect-free fabric images was built. The database contains the most common fabric defects such as needle breakages, hole, press-off and gout. Some defect-free and defective images can be shown in Figure 2.

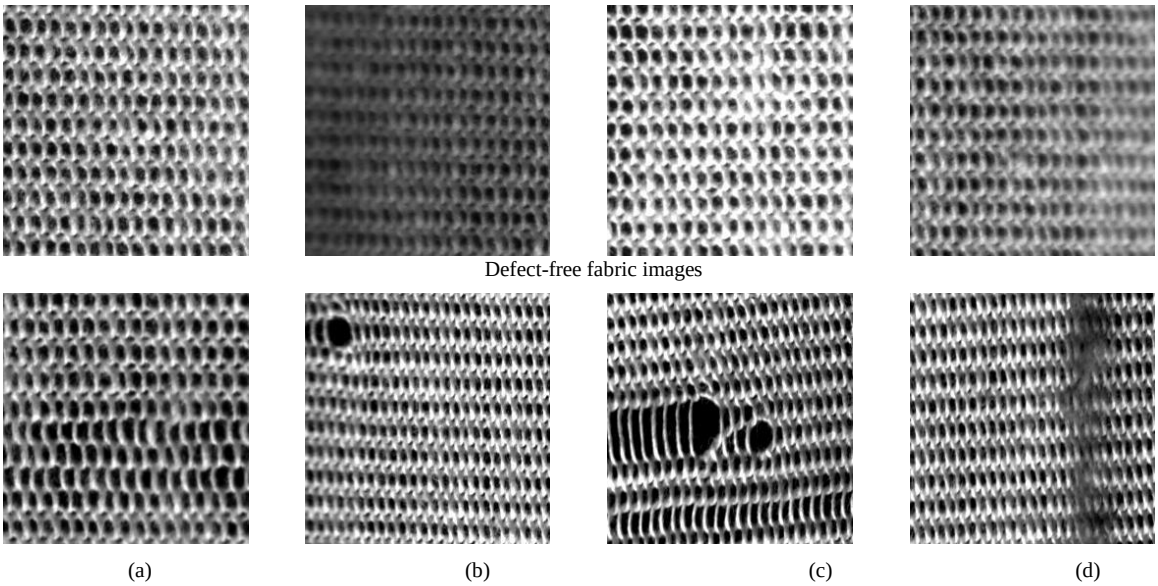


**Figure 2.** Examples of the popular defect-free and defective images. First row: defect-free fabric images. Second row: defective images (a) needle breakages, (b) holes, (c) press-off, (d) gout

### 2.2. VGG16 Network Construction

The VGG16 deep network used in this study generally consists of 5 block convolution layers. There are two convolution layers in the first two blocks and three in the last three blocks. The last three convolutional layers are fine-tuned layers. The step size of the convolution layer is 1 and each is 3×3. The size of the input layer is 224×224×3. There are max-pooling layers in every 5 blocks. The 5 maximum pooling layers have a step size of 2, each 2×2 in size. There are 3 fully connected layers. For training the VGG16 architecture, the BatchSize value is 32. Parameters are optimized with the Adam optimization method. VGG16 architecture is given in Figure 3.

The transfer learning approach is also used in this study. The main purpose of transfer learning is that convolutional weights are frozen during training. Weights are fixed and thus all parameters of the deep network are not trained. Fully connected layers are added to the deep model. Thus the transfer learning approach and the pre-trained weights of VGG16 architecture are used to solve fabric defect detection problems.

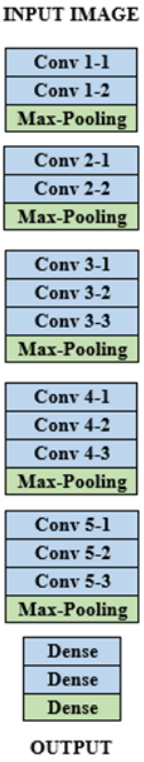


**Figure 3.** VGG16 architecture

### 2.3. Traditional Comparison Methods

The results obtained from the VGG16 architecture are compared with traditional image processing and machine learning methods. Thus the strengths and weaknesses of the method of the VGG16 architecture have been revealed. The study using the Shearlet transform on the same fabric database was used in the comparison [8]. The 1×24 feature vectors obtained from the Shearlet transform were classified by an artificial neural network. Another method used in

comparison uses GLCM features. Contrast, energy, correlation and homogeneity parameters were calculated from the GLCM information of the fabric image. By combining the obtained features, a feature vector with the size of 1×236 was obtained. The artificial neural network was used for classification.

## 3. EXPERIMENTAL RESULTS

In this section, VGG16 deep learning architecture is run on the fabric database containing circular knitting fabric defects. In addition, a comprehensive comparison was made by obtaining the results of traditional image processing methods. There are 3000 defective and 15320 defect-free fabric images in the database.

In the Shearlet transform method, feature vectors were created by analyzing images in different directions and scales. In the GLCM method, 4 different features of each image are calculated and combined into a single feature vector. The learning rate in VGG16 architecture is taken as 0.0001.

Table 1 shows the defect detection results of the VGG16 architecture. Very high classification success has been achieved with VGG16. Stable results are obtained for the other 3 parameters. The VGG16 architecture is trained faster with the transfer learning approach. In addition, the layer structure of the network has a structure to analyze fabric defects. In the first layers, the convolutional structure is used to characterize the defected pixel regions. Thus, the spatial location of the defect is revealed. The layer structure, which can make more precise calculations, is used for defect analysis and detection in the next layers.

**Table 1.** Classification results of VGG16 architecture

| Method | Precision | Recall | f1-score | Accuracy |
|---|---|---|---|---|
| Defected | 99.97 | 99.79 | 0.98 | 99.98 |
| Defect-free | 99.86 | 99.74 | 0.98 | 99.84 |

The Receiver Operator Characteristic (ROC) curve of the method is shown in Figure 4. ROC analysis is an indicator of the stable operation of the trained deep model. As can be seen from the ROC curve of defected fabric, fabric defects are stably and accurately distinguished.

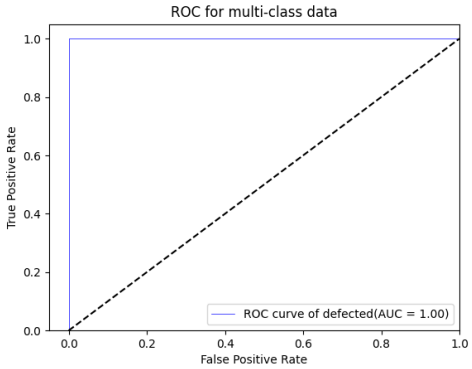


**Figure 4.** The ROC curve of VGG16 architecture

The data of the accuracy and loss function on the database of the VGG16 architecture are given in Figure 5. As can be seen, classification accuracy has steadily improved iteratively. In addition, the loss function curve has progressed iteratively and reached a reasonable level. Thus, the network has done the learning process without overfitting and in a determined manner.

In the last comparison, VGG16 architecture and traditional methods have been compared in terms of classification accuracy. The results obtained are shown in Table 2. Shearlet transform and GLCM features are classified by the artificial neural network. As can be seen from the results, the VGG16 model achieved better results. By obtaining high-level features of fabric images, defected pixels can be distinguished. Also, the proposed model is able to distinguish defect-free fabrics from defected ones. This prevents false positive results.



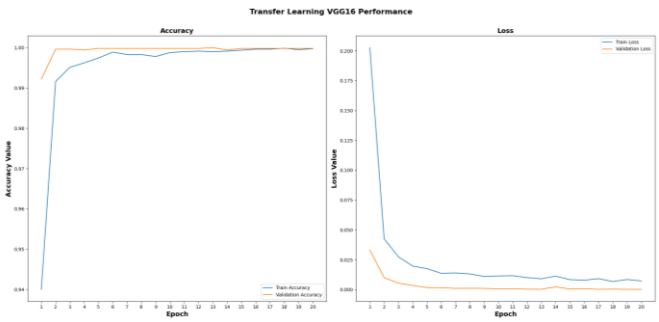


**Figure 5.** Classification accuracy (a) and loss function (b) of training and validation sets along with epochs

In the last comparison, VGG16 architecture and traditional methods have been compared in terms of classification accuracy. The results obtained are shown in Table 2. Shearlet transform and GLCM features are classified by the artificial neural network. As can be seen from the results, the VGG16 model achieved better results. By obtaining high-level features of fabric images, defected pixels can be distinguished. Also, the proposed model is able to distinguish defect-free fabrics from defected ones. This prevents false positive results.

**Table 2.** Classification results of VGG16, Shearlet transform and GLCM features

| Method | Accuracy (%) |
|---|---|
| VGG16 | 99.98 |
| Shearlet transform | 95.46 |
| GLCM | 93.00 |

## 4. CONCLUSION

In this study, the defect detection success of VGG16 deep learning architecture in circular knitting fabrics has been investigated. A new fabric database is used that has not been tested in the VGG16 architecture before. By making use of the positive contributions of the transfer learning approach, the training period has been kept to a minimum. The success of the method is also compared with two traditional feature extraction methods as Shearlet transform and GLCM method. The feature vectors of these traditional methods are classified by the artificial neural network. The experimental results show that the VGG16 architecture gives much better results than traditional methods in detecting fabric defects. In the future, it is considered to improve the convolution layers of the VGG16 architecture. Thus, it is planned to carry out studies for real-time use in fabric defect detection.

## REFERENCES

[1] Chen M, Yu L, Zhi C, Sun R, Zhu S, Gao Z, et al. Improved faster R-CNN for fabric defect detection based on Gabor filter with Genetic Algorithm optimization. Comput Ind. 2022.134:103551.

[2] Hanbay K, Talu MF, Özgüven ÖF. Fabric defect detection systems and methods—A systematic literature review. Optik (Stuttg). 2016 Dec 1;127(24):11960–73.

[3] Cuifang Z, Yu C, Jiacheng M. Fabric defect detection algorithm based on PHOG and SVM. Indian J Fibre Text Res. 2020;45:123–6.

[4] Zhu D, Pan R, Gao W, Zhang J. Yarn-Dyed fabric defect detection based on autocorrelation function and GLCM. Autex Res J. 2015. 15(3):226–32.

[5] Pourkaramdel Z, Fekri-Ershad S, Nanni L. Fabric defect detection based on completed local quartet patterns and majority decision algorithm. Expert Syst Appl. 2022 .198:116827.

[6] Zhang B, Tang C. A Method for Defect Detection of Yarn-Dyed Fabric Based on Frequency Domain Filtering and Similarity Measurement. Autex Res J. 2019 Sep 1;19(3):257–62.

[7] Vermaak H, Nsengiyumva P, Luwes N. Using the Dual-Tree Complex Wavelet Transform for Improved Fabric Defect Detection. J Sensors. 2016.–8.

[8] Hanbay K, Fatih Talu M, Özgüven ÖF, Öztürk D. Real-Time Detection of Knitting Fabric Defects Using Shearlet Transform. Tekst ve Konfeksiyon. 29(1):2019. 3-10.

[9] Li F, Li F. Bag of tricks for fabric defect detection based on Cascade R-CNN: https://doi.org/101177/0040517520955229. 2020.91(5–6):599–612.

[10] Liu Z, Huo Z, Li C, Dong Y, Li B. DLSE-Net: A robust weakly supervised network for fabric defect detection. Displays. 2021 Jul 1;68:102008.

[11] Ouyang W, Xu B, Hou J, Yuan X. Fabric Defect Detection Using Activation Layer Embedded Convolutional Neural Network. IEEE Access. 2019;7:70130–40.

[12] Huang Y, Jing J, Wang Z. Fabric Defect Segmentation Method Based on Deep Learning. IEEE Trans Instrum Meas. 2021;70:1–15.

[13] Simonyan K, Zisserman A. Very Deep Convolutional Networks for Large-Scale Image Recognition. In: 3rd International Conference on Learning Representations, ICLR 2015 - Conference Track Proceedings. International Conference on Learning Representations, ICLR; 2014. p. 1–14.

Cilt 11, Sayı 2, Sayfa 130-136, 2022 Volume 11, Issue 2, Page 130-136, 2022

Araştırma Makalesi https://doi.org/10.46810/tdfd.1001501 Research Article

Türk Doğa ve Fen Dergisi
Turkish Journal of Nature and Science
www.dergipark.gov.tr/tdfd

# Extraction of Bioactive Compounds in Wild Bilberry (*Vaccinium Myrtillus* L.) in The Eastern Black Sea Region With Different Techniques

**Evren ALTIOK [1], Sibel KACMAZ [2*], Duygu ALTIOK [2]**

[1] Giresun Üniversitesi, Mühendislik Fakültesi, Genetik ve Biyomühendislik Bölümü, Giresun, Türkiye
[2] Giresun Üniversitesi, Mühendislik Fakültesi, Gıda Mühendisliği Bölümü, Giresun, Türkiye
Evren ALTIOK ORCID No: 0000-0002-6437-5990
Sibel KACMAZ ORCID No: 0000-0003-3642-4940
Duygu ALTIOK ORCID No: 0000-0002-8503-2145

**Sorumlu yazar: sibel.kacmaz@giresun.edu.tr*

(Received: 27.09.2021, Accepted: 09.06.2022, Online Publication: 29.06.2022)

**Keywords**
Bilberry, Bioactive Compounds, Ultrasound Extraction, Microwave Extraction, Maceration

**Abstract:** Classical solvent extraction (CSE), solvent maceration (SM), ultrasound assisted extraction (UAE) and microwave assisted extraction (MAE) techniques were applied for the extraction of bioactive compounds of wild bilberry (*Vaccinium myrtillus* L.) fruit collected from the Eastern Black Sea Region in Turkey. Among these techniques, MAE is the most prominent in terms of total phenolics, total flavonoids and total anthocyanins yield in the extract. Total phenolics, total anthocyanin and total flavonoid content in MAE extract were determined as 1035 ± 16 mg gallic acid/100 g fresh bilberry weight (fw), 963 ± 7 mg cyanidin 3-glucoside equivalents/100 g fw and 150 ± 4 mg quercetin equivalent/100 g fw, respectively. Seven different anthocyanin compounds were identified in bilberry extracts. The effect of extraction techniques on the anthocyanin's distribution was revealed. Accordingly, malvidin-3-O-glucoside was found to be the most dominant anthocyanin in wild bilberry fruit.



# Doğu Karadeniz Bölgesindeki Yabani Çalıçileği (*Vaccinium Myrtillus* L.) Meyvelerinde Biyoaktif Bileşiklerin Farklı Tekniklerle Ekstraksiyonu

**Anahtar Kelimeler**
Yabani Çalıçileği, Biyoaktif Bileşikler, Ultrason Ekstraksiyonu, Mikrodalga Ekstraksiyonu, Maserasyon

**Öz:** Türkiye'de Doğu Karadeniz Bölgesi' nden toplanan yabani çalıçileği (*Vaccinium myrtillus* L.) meyvesinin biyoaktif bileşiklerinin ekstraksiyonu için klasik solvent ekstraksiyonu (CSE), solvent maserasyonu (SM), ultrason destekli ekstraksiyon (UAE) ve mikrodalga destekli ekstraksiyon (MAE) teknikleri uygulandı. Bu teknikler arasında ekstrakttaki toplam fenolik, toplam flavonoid ve toplam antosiyanin verimi açısından en iyi tekniğin MAE olduğu görüldü. MAE ekstraktındaki toplam fenolikler, toplam antosiyanin ve toplam flavonoid içeriği sırasıyla 1035 ± 16 mg gallik asit/100 g fw, 963 ± 7 mg siyanidin 3-glukozit eşdeğeri/100 g fw ve 150 ± 4 mg kuersetin eşdeğeri/100 g fw olarak belirlendi. Yabani çalıçileği ekstraktlarında yedi farklı antosiyanin bileşiği tanımlandı. Ekstraksiyon tekniklerinin antosiyanin dağılımı üzerindeki etkisi ortaya çıkarıldı. Buna göre, yabani çalıçileği meyvesinde en baskın antosiyaninin malvidin-3-O-glukozit olduğu belirlendi.

## 1. INTRODUCTION

Bilberry (*Vaccinium myrtillus* L.) is a wild fruit that can grow in temperate, Mediterranean or subtropical climate. With a water content of more than 80%, bilberry fruit is a good source of fiber, vitamins and minerals, and contains high levels of polyphenols, flavonoids, anthocyanins and other components that exhibit significant bioactivities. Associated with the antioxidant capacity of such different bioactive compounds that can prevent or slow oxidative processes, a diet rich in fruits and vegetables is reported to improve overall health and prevent cardiovascular diseases, neurodegenerative diseases, and different types of cancer [1]. Bilberry is one of the richest natural sources of anthocyanins, a large group of water-soluble flavonoids that give fruits, flowers and vegetables their characteristic blue/red color. Bilberry fruits contain 15 major anthocyanins, consisting of 5 anthocyanidin aglycones delphinidin, cyanidin, peonidin, petunidin, and malvidin, which are formed as 3- O-glycosides attached by galactose, glucose, and

arabinose [2-3]. In addition, other phenolic compounds it contains are molecules with at least one hydroxyl group attached to an aromatic ring and play a major role in plant metabolism [4]. However, all these compounds found in bilberry differ in content and composition depending on type of species, cultivation process, soil and climate conditions that affect plant growth. Although the composition and antioxidant activities of anthocyanins and phenolic compounds of bilberries grown in Europe, North America and Colombia have been investigated [5], there is lack of studies on the quantification and bioactivity of anthocyanins, phenolics and flavonoids of bilberry grown in Turkey.

Conventional phenolic compound extraction techniques include maceration and solvent extraction, which are highly efficient but require high solvent consumption and result in possible solvent toxicity [6]. In recent years, studies have focused on the discovery and design of extraction processes that will provide a safe and high-quality natural extract by higher yields in shorter extraction time, lower energy consumption and using renewable sources [4]. For this reason, anthocyanin and other phenolic compounds extractions from different fruits and plant materials such as sour cherry, grape seed, flax seed, potato peel, lemon peels, coffee, cherry laurel fruits and leaves and blueberry have been widely investigated by using environmentally friendly techniques such as ultrasound assisted extraction (UAE) [4] and microwave assisted extraction (MAE) [7] as an alternative to conventional solvent extraction and maceration methods. UAE is one of the modern methods used to extract bioactive compounds found in vacuoles of plant cells by the application of sound waves to a plant material/solvent mixture. It increases mass transfer by affecting cell permeability by different mechanisms. However, high-frequency ultrasound can tear the surface of the fruit, causing further leakage and pigment loss during process. Due to the possible changes in chemical structures and the high reactivity of the components, it may cause the formation of colorless or brown compounds [4]. MAE is an environmentally friendly technique with very few CO2 emissions and less solvent and time requirement. It works with two energy transfer mechanisms as dipole rotation and ionic conduction. Polar solvents that can effectively absorb electrical energy are more effective in microwave extraction. Besides, a high solvent performance due to high dielectric constant and dispersion factor ensures the effective impact of microwave in microwave extraction [7]. Considering all these, bilberry extraction techniques can significantly affect the amount and profile of phenolics, anthocyanins and flavonoids to be recovered.
The aim of this study is to evaluate the extraction of bioactive compounds from bilberry fruits grown in the Eastern Black Sea Region of Turkey. In this context, the effect of different extraction techniques such as classical solvent extraction (CSE), solvent maceration (SM), ultrasound assisted extraction (UAE) and microwave assisted extraction (MAE) on the yield of total phenolics, total monomeric anthocyanins and total flavonoids was determined. The anthocyanin profiles of the extracts were also assessed.

## 2. MATERIALS AND METHODS

### 2.1. Chemicals and Reagents

Ethanol and orthophosphoric acid (85% purity, HPLC grade) were purchased from Sigma Aldrich GmbH (Buch's, Switzerland). Water was deionized and filtered through a Millipore filter system (Millipore, USA) before use. All solvents, reagents and standards used were of analytical grade. The Folin-Ciocalteu reagent, sodium carbonate, sodium nitrite, aluminum chloride, sodium hydroxide, sodium acetate, gallic acid, hydrochloric acid-potassium chloride buffer and 2,2-diphenyl-1-picrylhydrazyl radical (DPPH) (95%) were purchased from Merck Company (Steinheim, Germany). Rutin and quercetin were purchased from Sigma Aldrich GmbH (Germany). Acetonitrile (HPLC grade) and acetic acid (99.8 %) were obtained from Merck (Darmstad, Germany). Formic acid was obtained from Fluka (Deisenhofen, Germany). Anthocyanin standards of delphinidin-3-O-glucoside chloride, delphinidin-3-O-galactoside chloride, petunidin-3-O-glucoside chloride, cyanidin-3-O-arabinoside chloride, cyanidin-3-O-glucoside chloride, malvidin-3-O-glucoside chloride and malvidin-3-O-arabinoside chloride were obtained from Merck (Darmstad, Germany).

### 2.2. Plant Material

Fresh, ripe wild bilberry (*Vaccinium myrtillus* L.) fruits were picked randomly from native habitat of the species in Giresun in Eastern Black Sea Region of Turkey in July, 2020. Whole fresh and ripe fruits were frozen and stored at -20 ± 1°C until use.

### 2.3. Extraction

Fresh bilberry fruits were crushed in a mortar to produce a thick puree which was subjected to four different extraction processes; classical solvent extraction (CSE), solvent maceration (SM), ultrasound assisted extraction (UAE) and microwave assisted extraction (MAE). For each extraction procedure, a 10 ±0.1 g puree was placed into a 50 ml flat-bottom flask and aqueous ethanol was added to the flask to a final ethanol concentration of 70% stoichiometrically to a final solid:liquid ratio as 1:20. The mixture was homogenized for a few minutes and used in the extraction process.

For CSE, the homogenate (sample-solvent homogeneous mixture) was extracted for 2 h by orbital shaking in the dark at room temperature. The samples were taken for the analysis at 10 min, 30 min, 1 h and 2 h. For SM, the homogenate was kept in the dark at +4 °C for 6 weeks and the sample was taken at the end of the extraction process. UAE procedure was carried out by treating the homogenate with ultrasound for the period of 5, 10- and 20-min using lab scale ultrasound water bath (53kHz-180-Watt, Kudos SK3310HP) at 40 ºC. MAE was performed in an ordinary house-hold microwave oven

(Inoksan GDM239DAH-S, Microwave output 800 W with the power of 2450 MHz). A Pyrex double-walled vessel where ice flakes were placed between the walls was used to keep the temperature below 60 °C during the application and to eliminate the risk of solvent loss by evaporation and any compound degradation due to rapid temperature rise. Container having homogenate was placed on a rotational plate in the middle of the oven and was treated by microwave irradiation for within three different times (2, 4, 6 minutes).

Three replicates of samples were prepared for each extraction procedure. Once the extraction process was completed, the suspensions were filtered through paper filter for removing the pulp and centrifuged at 3000 rpm for 5 minutes. The supernatants as crude extract were preserved at +4 °C in the dark until analysis.

### 2.4. Total Phenolics Quantification

The amount of total phenolic compounds in the bilberry extracts was determined by the Folin-Ciocalteu method described by Slinkard et al. [8] using gallic acid as a standard. The Folin-Ciocalteu reagent was prepared by diluting with distilled water (1:10, v/v). 0.5 mL crude extract sample was mixed with daily prepared 2.5 mL folin reagent and left to stand for 2.5 min at room temperature. Then, 1.25 mL of sodium carbonate solution (7% in deionized water) was added. This mixture was left for reaction for 40 minutes in the dark. The absorbance of the sample was measured at a wavelength of 725 nm with a UV-Visible spectrophotometer (MAPADA UV-6100PCS, China) with three replications. A standard curve of absorbance with respect to different concentrations of gallic acid standard (0–80 mg/L) was generated and used for calculation of concentration of total phenolics in the samples. The total phenol content was calculated as mg gallic acid (GA)/100 g fresh bilberry weight (fw) based on the standard curve of gallic acid.

### 2.5. Total Anthocyanins Quantification

A spectrophotometric pH differential method described by AOAC [9] was used for quantification of total anthocyanins content of bilberry extracts.

500 µL of extract solution was diluted with 2 mL of buffer solutions (potassium chloride buffer with pH 1.0 and sodium acetate buffer with pH 4.5) to prepare 2 different dilutions with different pH levels. The appropriate dilution factor was determined as a 1-part test sample and 4 parts buffer dilution with the absorbance at 520 nm and 700 nm within the linear range of the spectrophotometer (between 0.2 and 1.4 AU). The dilutions were kept in the dark at room temperature for 20 minutes and absorption of the solutions was measured at 520 nm and 700 nm against blank taken as water using a UV-Visible spectrophotometer. Total monomeric anthocyanin pigment concentration was expressed as cyanidin-3-glucoside equivalents (C3GE) and calculated using Eq. (1).

$$MA = \frac{[(A_{520}-A_{700})_{pH1.0}-(A_{520}-A_{700})_{pH4.5}]\times MW\times DF\times 10^5}{\varepsilon\times l}\times\frac{V}{m} \quad (1)$$

where MA is the total monomeric anthocyanin (C3GE, mg/100 g fw); A is the absorbance at different wavelengths for different pH buffers; MW is the molecular weight of cyanidin-3-glucoside (449.2 g/mol); DF is the dilution factor; ε is the molar absorptivity (L. mol-1.cm-1; 26900) of cyanidin-3-glucoside; l is the pathlength (cm); V is the total volume of solvent used in the extraction (L); m is the amount of fresh bilberry (g) and 105 is the conversion factor.

### 2.6. Total Flavonoid Quantification

Total flavonoid content was investigated by two different spectrophotometric methods in order to quantify the total flavonoid content and to estimate the major flavonoids based on the formation of aluminum-flavonoid complexes that exhibits the differences in type of flavonoid compounds [10].

In the first procedure, 1 mL of test extract was put into a 10-ml glass vial. After adding of 0.5 mL of each AlCl3 (2%, w/v), water, HCl (1 M), CH3COONa (1 M), the mixture was waited for 10 min at room temperature. The absorbance of all samples was measured at 425 nm using the UV-Vis spectrophotometer.

In the second procedure, 250 µl extract was taken into a 10-ml glass vial. 1.25 ml distilled water and 75 µl (5%) NaNO2 were added. The glass vial was waited for 6 min. Then 150 µl 10% (AlCl3) and 500 µl of NaOH (1M) and 275 µl distilled water was added. The absorbance of samples was measured at 510 nm using the UV-Vis spectrophotometer.

The content of flavonoid (mean of three determinations) was expressed as mg quercetin equivalent/100 g fw.

### 2.7. HPLC Analysis

Stock solutions of anthocyanin standards were prepared by weighing 5 mg of each standard into a 50 mL volumetric flask and adding 2 mL of HCl/methanol (2:98, v/v) followed by 10% phosphoric acid to a total volume of 50 mL and mixed. Stock solutions were stored at -40 ºC in glass vials until needed.

The bilberry crude extract obtained by different extraction techniques was concentrated by evaporating the solvent using a rotary evaporator (Hei-VAP, Heidolph Instruments, Germany) until as final solution amount of 2 grams was obtained. The solutions were stored in the dark at -40 ºC in glass bottles until analysis. It was thawed, brought to room temperature and vortexed before to HPLC analysis. A small amount of sample was taken from each solution, diluted 10 times with 5.5% acetic acid solution (Mobile phase A), passed through PTFE filter and injected to the HPLC.

The HPLC analysis was performed by Shimadzu SCL-10AVP HPLC system equipped with querternary pump, an autosampler, a column thermostat, UV/VIS detector

and system controller. Lab Solutions (LC Solution-Version 1.25) computer software was used throughout the analysis. Separation was achieved on a BISCHOFF ProntoSIL C18 column (4.6 mmx250 mm, 5 □m; Germany). The detection wavelength was set at 520 nm and flow rate was 1 mL/min. The injection volume was 20 µL. Mobile phase A was 5.5% aqueous acetic acid solution and mobile phase B was acetonitrile/water/formic acid=50:40:10 (v/v/v).

The gradient elution program was as follows: between 0 and 20 min, 2%–14% B; 20–40 min held at 14% B; 40–50 min increased to 15% B; 50–55 min increased to 19% B; 55–65 min raised to 20% B, 65–110 min washed and re-equilibrated with 2% mobile phase B.

### 2.8. Statistical Analysis

In this work, all experiments were carried out in triplicate and quantitative data are expressed as mean values of at least three analytical determinations with the respective standard deviation.

## 3. RESULTS AND DISCUSSION

The recovery of bioactive compounds of wild bilberry fruit grown in Giresun province was investigated by different extraction techniques. To analyze the effects of extraction method and time of extraction on the amount of total phenolics, total flavonoids and total monomeric anthocyanins in bilberry extracts different sets of experiments were designed and analyzed.

### 3.1. Total Phenol, Total Flavonoid and Total Monomeric Anthocyanin Contents

Four different extraction methods as microwave assisted extraction (MAE), ultrasound assisted extraction (UAE), classical solvent extraction (CSE), and solvent maceration (SM) methods were used to compare the total phenolic contents of bilberry extracts. Depending on the nature of the extraction method, total phenol content of the samples taken at different time of extractions is compared in Figure 1.

Extraction yield of phenolic compounds through MAE, CSE, UAE and SM differed accordingly the extraction technique and time of extraction where the highest total phenol content of the bilberry extracts were in the range of 750-1035 mg GA/100 g fw. Among these extraction methods, MAE was the most efficient method which yields highest amount of total phenols (1035 ± 16 mg GA/100 g fw) in just 2 minutes of extraction. There was no statistically significant difference in total phenol contents extracted over the longer MAE period. However, MAE method has some disadvantages. The major problem arises in MAE is to keep the temperature under controlled during the application.

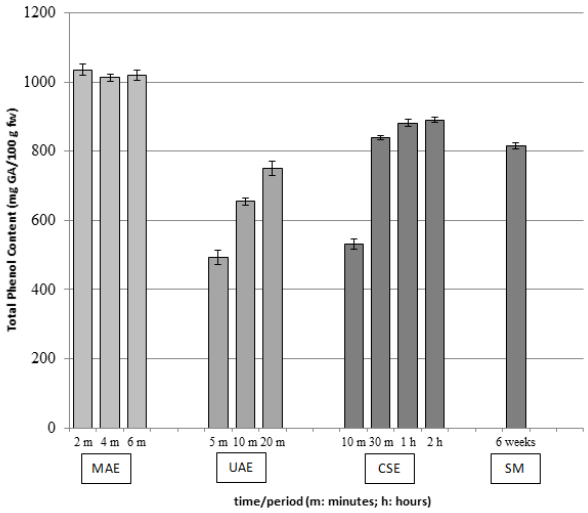


**Figure 1.** Total phenol content of the samples taken in MAE, UAE, CSE and SM extractions

In this study, although it was tried to be controlled by ice flakes at the double-wall vessel, the temperature was sometimes measured above 65 °C during the extraction process. This can be explained by the ability of the ethanol-water molecules to absorb microwave energy and rapidly pass it on in the form of heat to other molecules in solvents that can accelerate the extraction process in a way that no other technique can match. This mechanism is explained by the dissipation factor (tanδ), which is defined as the ratio of the dielectric loss (ε″) to the dielectric constant (ε′) of the solvent [11]. Accordingly, the rapid temperature rise in the bilberry matrix yields faster diffusion rate and provides faster extraction kinetics. However, compound degradation should be considered due to both the rapid temperature increase and possible chemical property changes occurred during the process. Closed vessel application requirement, high instrumental cost and safety are other disadvantages of the MAE. Total phenol content value of extract obtained by UAE was determined as 749 ± 20 mg GA/100 g fw. UAE is an alternative extraction method with some advantages such as moderate use of solvent and reproducibility. The mechanism underlying of the UAE is the formation of tiny bubbles in the solvent that collapse, causing the pressure and temperature changes and therefore enhancing the mass transfer of the natural components to the solvent. However, the UAE process can promote higher degradation rates of the compounds obtained by extraction, especially when it reaches temperatures above 75 ºC. This disadvantage can also reduce the extraction rate constant as a result of lower surface tension and increased vapor pressure of cavitation bubbles [6]. In the SM method performed at 4°C, however, the total phenol content in the solution was determined as 815 ± 10 mg GA/100 g fw, similar to the values obtained UAE method. Similar total phenol content was determined as 890 ± 8 mg GA/100 g fw for CSE. CSE is a well-known and highly efficient method that is easy to use at atmospheric pressure and ambient temperature, does not require sophisticated equipment and widely employed in a variety of industries. Total phenol content of the extracts in present study was higher compared with those reported for CSE method

which was applied under similar extraction condition for bilberries from Montenegro [12] where it ranged from 392 to 520, from Macedonia [13] where it was 393-706, from [14-15] where it was 890 ± 9, from North East Anatolia (Turkey) [16] where it was 679 ± 5 and also for bog bilberry from Finland [17] where it was 161 ± 1. When these values are compared, it can be said that the results vary according to the type of the bilberry, the region where it grows, the extraction technique used and application conditions. It has been reported that light intensity, photoperiod, temperature and growing location influence the level of total phenolics in berries and at altitude higher than 1500 m, higher amounts of total phenolics were observed [12].

In current study, total monomeric anthocyanin amount of MAE, UAE, CSE and SM extracts was determined as 903 ± 9, 832 ± 9, 762 ± 8 and 667 ± 5 mg C3GE/100 g fw, respectively. Total monomeric anthocyanin content of the extracts in other studies was reported for bilberries from Macedonia [13] where it was 151-507 and from North East Anatolia (Turkey) [16] where it was 164. Može et al. [18] reported the anthocyanin content of Slovenian bilberries as 1210 mg C3GE/100 g fw.

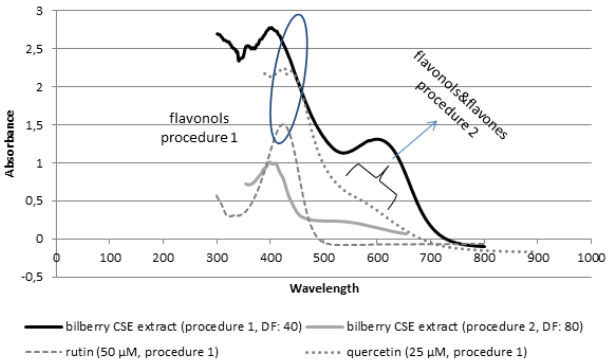


**Figure 2.** Absorption spectrum of Al-flavonoid complex of bilberry extracts, Al-rutin and Al-quercetin complexes of standards.

Total flavonoid contents were also determined in MAE, UAE, CSE and SM extracts as 150±6, 146 ± 5, 144 ± 3 and 114 ± 3 mg quercetin equivalent/100 g fw, respectively. The total flavonols of bilberry and bog bilberry from Macedonia was reported as 12.1 and 51 mg quercetin equivalent/100 g fw, respectively [13]. Neamtu et al. [19] evaluated the effect of solvent used during extraction of the flavonoids from wild bilberry fruit from South Carpathian Mountains in Romania and reported the flavonoids content in the range of 3.88-8.41 mg quercetin equivalent / g dry weight. Li et al. [20] found that the total flavonoid content of bilberry fruit grown in Nanjing as 13.5 mg quercetin equivalent / g dry weight. A recent study was performed to determine both anthocyanin and flavonoid contents of the different blueberry cultures (both cultivated and wild types) grown in North and South Black Sea region in Turkey [21]. It was reported that anthocyanin and flavonoid contents were determined in the ranges of 43.03-295.06 mg C3GE /100 g fw and 30.44-99.69 mg quercetin equivalent/100 g fw, respectively. The present study reveals that wild bilberry which grows native on high mountain pastures in Giresun almost 1.5 times higher flavonoid content and 2.5 times higher anthocyanin content than blueberries grows in same region. Two different procedures were applied to determine the flavonoid content of the bilberry extract according to Pekal et al. [10]. These procedures were based on the formation of aluminum-flavonoid complexes and exhibited significant differences depending on the type of flavonoids. From the flavonols group, quercetin and rutin were selected as model compounds to check the effect of both procedures' reaction environments. As seen from Figure 2, formed Al-quercetin and Al-rutin complexes with acetate salts (used in procedure 1), showed strong absorption band at 420 nm. But, only Al-quercetin complex exhibited weak absorption band at 560 nm. On the other hand, while flavone, luteolin-aluminum complexes showed absorption peak at 405-420 nm in the procedure 1, it shifted to 530-560 nm but to a lower absorption value when the procedure 2 was applied. For the flavonols group, strong absorption peak was seen at 420- 440 nm in procedure 1 [10], but differentiative absorbance peak at 510 nm was reported only for rutin in procedure 2. According to this information, absorption band was detected when procedure 2 applied to the bilberry extract, which indicates the presence of the rutin and/or luteolin. Stanoeva et al. [13] pointed out to high content of rutin, which constitutes 18% of the total flavonols present in bilberry.

### 3.2. Profiles of Anthocyanins

The anthocyanin profile of bilberry extracts varied according to the extraction technique applied. Typical anthocyanin profile of bilberry extract was given by HPLC chromatogram (Figure 3). The ratio of the peak area of anthocyanins, identified based on the retention time of available standards, to the sum of all anthocyanin peak areas was used to compare the effect of extraction methods on individual anthocyanin recovery (Table 1).



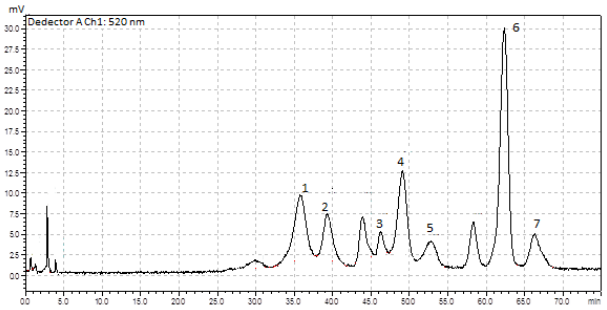


**Figure 3.** HPLC anthocyanin profile of bilberry extracts. 1. Delphinidin-3-O-glucoside; 2. Delphinidin-3-O-galactoside; 3. Petunidin-3-O-glucoside; 4. Cyanidin-3-O-arabinoside; 5. Cyanidin-3-O-glucoside; 6. Malvidin-3-O-glucoside; 7. Malvidin-3-O-arabinoside

Although the overall anthocyanin profiles are similar for all extracts, changes in individual anthocyanins are inconsistent and show different variability by the extraction method. Malvidin-3-O-glucoside has the highest proportion in all extracts but mostly in the CSE and SM extracts. It was reported that, malvidin possesses great antioxidant capacity [22], antihypertensive activity [23], and plays a role in controlling cellular activities

[24]. In these two methods, the bilberries are kept in direct contact with the solvent. As ultrasound and microwave effects were used in UAE and MAE, respectively, it increased the recovery of other anthocyanins in bilberry extract, and thus different distributions were observed in anthocyanin profiles. However, malvidin stands out with its high percentage distribution in these extracts as well. This can be attributed to microwave energy heating the solvent, increasing its interaction with the sample and accelerating the extraction of the extractable components. Other studies also support that microwave extraction reduces processing time compared to conventional extraction and provides higher yields with less solvent and energy requirements [25-26]. Apparently, delphinidin-3-O-glucoside and cyanidin-3-O-glucoside are also affected considerably. Heffels et al. [3] reported that individual anthocyanins in bilberry are arranged according to their polarity as delphinidin > cyanidin > petunidin > peonidin > malvidin. It seems that more polar anthocyanins show significant variances. Consequently, different extraction techniques lead to the different and variable anthocyanin proportions in the extracts.

**Table 1.** Anthocyanin proportions* in bilberry extracts

| | Extraction technique | | | |
|---|---|---|---|---|
| **Anthocyanin** | **UAE** | **MAE** | **CSE** | **SM** |
| Delphinidin-3-O-glucoside | 11.30 | 7.36 | 14.64 | 9.64 |
| Delphinidn-3-O-galactoside | 7.13 | 6.80 | 7.80 | 8.63 |
| Petunidin-3-O-glucoside | 1.48 | 1.55 | 2.15 | 1.48 |
| Cyanidin-3-O-arabinoside | 12.10 | 8.77 | 13.67 | 10.44 |
| Cyanidin-3-O-glucoside | 8.18 | 4.99 | 4.84 | 5.68 |
| Malvidin-3-O-glucoside | 27.63 | 24.29 | 35.97 | 37.64 |
| Malvidin-3-O-arabinoside | 5.26 | 4.10 | 6.27 | 5.60 |

* Values are expressed as % of total anthocyanins

## 4. CONCLUSION

The results we obtained have shown that the bilberry fruit, which spreads naturally in Giresun province, is a very rich source of natural bioactive compounds. Extraction methods were evaluated for the efficient recovery of these bioactive compounds and the effect of the extraction technique on anthocyanin distribution was revealed. MAE method was found to be very suitable extraction processes regarding the amount of total phenolics (1035 ± 16 mg gallic acid/100 g fresh bilberry weight (fw), flavonoids (150±6 mg quercetin equivalent/100 g fw) and anthocyanins (903 ± 9 mg C3GE/100 g fw) and the extraction time. Different anthocyanin proportions indicate that profile changes are due to different extraction techniques. Depending on the applied extraction technique applied, it was determined that different mechanisms affect the extraction performance of bilberry anthocyanins during the extraction process.

## ACKNOWLEDGMENTS

This study was supported by grants from Giresun University Scientific Research Projects Department (FEN-BAP-A-230218-27).

## REFERENCES

[1] Campero EV, Gomez Marigliano AC, Barrionuevo MJ. Physical, Chemical and Microbiological Characteristics of Tucuman Blueberry. Research & Reviews: J. Eng. Technol. 2017; 6(1): 20-7.

[2] Babova O, Occhipinti A, Capuzzo A, Maffei ME. Extraction of bilberry (*Vaccinium myrtillus*) antioxidants using supercritical/subcritical $CO_2$ and ethanol as co-solvent. J Supercrit Fluids. 2016; 107:358–63.

[3] Heffels P, Weber F, Schieber A. Influence of Accelerated Solvent Extraction and Ultrasound-Assisted Extraction on the Anthocyanin Profile of Different Vaccinium Species in the Context of Statistical Models for Authentication. *J. Agric. Food Chem.* 2015**;** *63* (34): 7532-38.

[4] Varo MA, Jacotet-Navarro M, Serratosa MP, Mérida J, Fabiano-Tixier AS, Bily A, Chemat F. Green Ultrasound-Assisted Extraction of Antioxidant Phenolic Compounds Determined by High Performance Liquid Chromatography from Bilberry (*Vaccinium Myrtillus* L.*)* Juice By-products. Waste Biomass Valorization. 2019; 10:1945–55.

[5] Garzón GA, Narváez CE, Riedl KM, Schwartz S.J. Chemical composition, anthocyanins, non-anthocyanin phenolics and antioxidant activity of wild bilberry (*Vaccinium meridionale Swartz*) from Colombia. Food Chem. 2010; 122, 980–86.

[6] Medina-Torres N, Ayora-Talavera T, Espinosa-Andrews H, Sánchez-Contreras A, Pacheco N. Ultrasound Assisted Extraction for the Recovery of Phenolic Compounds from Vegetable Sources. Agron. 2017; 7(47): 1-19.

[7] Routray W, Orsat V. MAE of phenolic compounds from blueberry leaves and comparison with other extraction methods. Ind Crops Prod. 2014; 58: 36–45.

[8] Slinkard K, Singleton VL. Total Phenol Analysis: Automation and Comparison with Manual Methods, Am J Enol Vitic. 1977; 28: 49-55.

[9] AOAC. Official Methods of Analysis. 18th Edition, Association of Official Analytical Chemists, Gaithersburgs, MD. 2006.

[10] Pekal A, Pyrzynska K. Evaluation of Aluminium Complexation Reaction for Flavonoid Content Assay. Food Anal. Methods. 2014; 9: 1776-1782.

[11] Kingston HM, Jassie LB. Introduction to Microwave Sample Preparation*: Theory and practice*. American Chemical Society, Washington, DC. 1988.

[12] Jovančević M, Balijagić J, Menković N, Šavikin K, Zdunić G, Janković T, Dekić-Ivanković M. Analysis of Phenolic Compounds in Wild Populations of Bilberry (*Vaccinium myrtillus L.*)

from Montenegro. J. Med. Plant Res. 2011; 5: 910–4.
[13] Stanoeva JP, Stefova M, Andonovska KB, Vankova A, Stafilov T. Phenolics and mineral content in bilberry and bog bilberry from Macedonia. Int. J. Food Prop. 2017; 20: S863-S83.
[14] Šavikin K, Zdunić G, Janković T, Tasić S, Menković N, Stević T, Đorđević B. Phenolic Content and Radical Scavenging Capacity of Berries and Related Jams from Certificated Area in Serbia. Plant Foods Hum. Nutr. 2009; 64: 212–7.
[15] Šavikin K, Zdunić G, Janković T, Gođevac D, Stanojković T, Pljevljakušić, D. Berry Fruit Teas: Phenolic Composition and Cytotoxic Activity, Food Res. Int. 2014; 62: 677–83.
[16] Colak N, Torun H, Gruz J, Strnad M, Hermosín-Gutiérrez I, Hayirlioglu-Ayaz S, Ayaz FA. Bog Bilberry Phenolics, Antioxidant Capacity and Nutrient Profile, Food Chem. 2016; 201: 339–49.
[17] Taruscio TG, Barney DL, Exon J. Content and Profile of Flavanoid and Phenolic Acid Compounds in Conjunction with the Antioxidant Capacity for a Variety of Northwest Vaccinium Berries. J. Agric. Food Chem. 2004; 52: 3169–76.
[18] Može Š, Polak T, Gašperlin L, Koron D, Vanzo A, Poklar Ulrih N, Abram V. Phenolics in Slovenian Bilberries (*Vaccinium myrtillus L.*) and Blueberries (*Vaccinium corymbosum L.*). J. Agric. Food Chem. 2011; 59(13): 6998–7004.
[19] Neamtu AA, Szoke-kovacs R, Mihok E, Georgescu C, Turcus V, Olah NK et al. Bilberry (*Vaccinium myrtillus L.*) extracts comparative analysis regarding their phytonutrient profiles, antioxidant capacity along with the in vivo rescue effects tested on a drosophila melanogaster high-sugar diet model. Antioxidants. 2020; 9(11): 1–33.
[20] Li C, Feng J, Huang WY, An XT. Composition of polyphenols and antioxidant activity of rabbiteye blueberry (*Vaccinium ashei*) in Nanjing, J. Agric. Food Chem. 2013; 61(3), 523–31.
[21] Okan OT, Deniz I, Yayli N, Şat IG, Öz M, Serdar G.H. Antioxidant activity, sugar content and phenolic profiling of blueberries cultivars: A comprehensive comparison, Not Bot Horti Agrobot Cluj. 2018; 46(2): 639–52.
[22] Pop R, Ştefănut M, Căta A, Tănasie C, Medeleanu M. Ab initio study regarding the evaluation of the antioxidant character of cyanidin, delphinidin and malvidin, Open Chem. 2012; 10(1): 180-6.
[23] Lee C, Han D, Kim B, Baek N. Baik BK. Antioxidant and anti-hypertensive activity of anthocyanin-rich extracts from hulless pigmented barley cultivars. Int. J. Food Sci. 2013; 48: 984-91.
[24] Huang W, Zhu Y, Li C, Sui Z, Min W. Effect of Blueberry Anthocyanins Malvidin and Glycosides on the Antioxidant Properties in Endothelial Cells, Oxid. Med. Cell. Longev. 2016; ID 1591803.
[25] Chan CH, Yusoff R, Ngoh GC, Wai-Lee KF. Microwave-assisted extractions of active ingredients from plants, J. Chromatogr. A, 2011; 1218 (37): 6213-25.
[26] Proestos C, Komaitis M. Application ofmicrowave-assisted extraction to the fast extraction of plant phenolic compounds. Lwt-Food Sci Technol. 2008; 41(4): 652–9.

Araştırma Makalesi https://doi.org/10.46810/tdfd.1095481 Research Article

Türk Doğa ve Fen Dergisi
Turkish Journal of Nature and Science
www.dergipark.gov.tr/tdfd

# Determination of Nutritive Value and *İn vitro* Gas Production of Some Triticale Varieties

**Özer KURT[1*]**

[1] University of Mus Alparslan, Faculty of Applied Science, Department of Animal Production and Technology, Mus, Türkiye
Özer KURT ORCID No: 0000-0002-6325-6201

**Corresponding author: o.kurt@alparslan.edu.tr*

(Received: 29.03.2022, Accepted: 09.06.2022, Online Publication: 29.06.2022)

**Keywords**
Chemical composition, Triticale, Varieties, *İn vitro* total gas

**Abstract:** The aim of this study was to determine the chemical composition, *in vitro* total gas production (TG), metabolisable energy (ME), and organic matter digestibility (OMD) of grains belonging to different triticale varieties. Variety crude ash (CA) contents range from 2.05 to 2.30%, ether extract (EE) contents range from 1.82 to 3.00%, crude protein (CP) contents range from 9.44 to 13.25%, and acid detergent fiber (ADF) and neutral detergent fiber (NDF) contents range from 2.51 to 4.50% and 15.15 to 17.65%, respectively. Total gas production *in vitro* ranged between 57.59 and 62.51 ml, with ME and OMD ranged between 11.69 and 12.55 Mj $kg^{-1}$ DM and 78.06 and 82.24%, respectively. While Bera and Tatlıcak 97 leap out in terms of ME, the Bera variety leap out in terms of OMD. The effects of varieties on chemical composition, *in vitro* TG, ME, and OMD of triticale grains were found to be significant ($P<0.05$). According to chemical composition and fermentation parameters, the Bera variety has high values in terms of CP, ME, and OMD can be recommended for grain production.



# Bazı Tritikale Çeşitlerinin Besleme Değeri ve *İn vitro* Gaz Üretiminin Belirlenmesi

**Anahtar Kelimeler**
Kimyasal bileşim, Tritikale, Çeşit, *İn vitro* toplam gaz

**Öz:** Bu çalışmada bazı tritikale çeşitlerine ait tanelerin kimyasal bileşimi, *in vitro* toplam gaz üretimi (TG), metabolik enerji (ME) ve organik madde sindirim derecelerinin (OMSD) belirlenmesi amaçlanmıştır. Çeşitlerin ham kül (HK) içerikleri %2.05-2.30, ham yağ (HY) içerikleri %1.82-3.00, ham protein (HP) içerikleri %9.44-13.25, asit çözücülerde çözünmeyen lif (ADF) ve nötr çözücülerde çözünmeyen lif (NDF) içerikleri sırasıyla %2.51-4.50, %15.15-17.65 aralığında yer almıştır. Çeşitlerin *in vitro* TG üretimleri 57.59-62.51 ml, ME ve OMSD dereceleri ise sırasıyla 11.69 - 12.55 Mj $kg^{-1}$ KM ve %78.06 ile 82.24 arasında değişmiştir. Metabolik enerji değeri bakımından Bera ve Tatlıcak 97, OMSD bakımından Bera çeşidi ön plana çıkmıştır. Tritikale tanelerinin kimyasal bileşimleri, *in vitro* TG, ME ve OMSD değerleri üzerine çeşitlerin etkisinin önemli olduğu görülmüştür ($P<0.05$). Kimyasal bileşim ve fermentasyon parametrelerine göre HP, ME ve OMSD bakımından yüksek değerlere sahip olan Bera çeşidinin tane üretimi için tavsiye edilebileceği belirlenmiştir.

## 1. INTRODUCTION

Triticale, which is obtained as a result of studies to determine new product groups in order to provide balanced and adequate nutrition for the rapidly increasing world population, is becoming more and more popular nowadays [1,2]. Triticale (*xTriticosecale Wittmack*) is a one-year cool-climate cereal that can be used in both human and animal nutrition and is obtained as a result of hybridization of wheat and rye [3,4]. Because of the low flour quality of the grains, they are generally allowed to be used in animal feed [5]. It has been stated that triticale is equivalent or superior to other grains in animal nutrition in terms of its important properties such as rapid growth and development, high dry matter rate, grain, dry and green herbage yield, fiber content, degree of digestion, protein rate, and high lysine content [6,7,8]. It has been reported that the feed value of its grain is equal to wheat and better than rye and barley [9]. Denek and Deniz [10] also emphasized that triticale can be evaluated as a feed equivalent to corn in ruminant nutrition. Therefore, it has been thought that determining the animal nutrition status of high-yield and quality varieties of triticale will increase the production potential. Although the triticale varieties have been

investigated in terms of chemical composition, there are limited studies on *in vitro* gas production, metabolisable energy and organic matter digestibility of these varieties. Recently, *in vitro* gas production, metabolisable energy and organic matter digestibility can be determined together with chemical compositions of the uninvestigated raw materials by using an *in vitro* gas production technique [11,12,13]. The aim of the current experiment was to evaluate the effect of variety on chemical composition, *in vitro* TG, ME, and OMD.

## 2. MATERIAL AND METHOD

### 2.1. Collection of Triticale Grain Samples

Triticale grain samples were obtained from agronomic trials carried out in the experimental area of Muş Alparslan University between 2020 and 2021. Samples of 11 triticale varieties were randomly collected from each block in the experimental plots with 3 replications. Collected samples were prepared by grinding to pass through a 1 mm sieve for chemical analysis and *in vitro* gas production.

### 2.2. Chemical Analyzes

Dry matter (DM), crude ash (CA), ether extract (EE), and crude protein (CP) contents of the grains were determined according to the method reported by AOAC [14]. ADF and NDF contents were determined by Van Soest et al. [15] according to the method reported. An *in vitro* gas production technique was used to determine the TG production of triticale grain samples [16]. Rumen fluid was immediately taken from sheep slaughtered in Kahramanmaraş animal market and placed in a thermos, and brought to the laboratory quickly so that microorganism activities could continue. Feed samples (0.2 grams) mixed with buffer solution were left for fermentation at 39 °C for 24 hours with rumen fluid obtained from sheep. Gas production is arranged according to standard feed and blind measurement. Metabolizable energy and organic matter digestibility of triticale grains were determined using the equations given below [17].

$$ME\ (Mj\ kg^{-1}DM) = 1.06+0.1570GP+ 0.084CP+0.220EE-0.081CA \quad (1)$$

$$OMD\ (\%) = 28.49+ 0.7967GP+ 0.325CP \quad (2)$$

GP: Gas production of 200 mg sample at 24 h incubation (ml)
CP: Crude protein (%)
EE: Ether extract (%)
CA: Crude ash (%)

### 2.3. Statistical Analysis

The data obtained in the study were evaluated statistically (Tukey 5%) using one-way analysis of variance (One-way ANOVA) [26].

## 3. RESULT AND DISCUSSION

The chemical compositions of triticale grains are given in Table 1. It was determined that the differences in the chemical compositions of the cultivars were significant. The CA contents of triticale cultivars ranged from 2.05-2.30%, the highest values in Karma and the lowest values in Ümran Hanım. The CA content of triticale grains was determined by Denek and Deniz [10], 1.71%, Alijošius et al. [18], 1.33-1.63%, Kowieska et al. [19], 1.8%, Umucalılar et al. [20], 1.9%. The EE contents of the cultivars ranged from 1.82-3.00%, the highest values in Tatlıcak 97 and the lowest values in Bc goran. The results obtained were higher than the findings of Denek and Deniz [10] (0.96%) and are similar to the findings of Umucalılar et al. [20] (2.00%) and Chrenková et al. [21] (1.70%). The CP contents of the cultivars ranged from 9.44-13.25% the highest values in Ümran Hanım, the lowest values in Presto. Krieg et al. [22] determined the CP content of 20 triticale lines ranged from 11.6 to 13.3%. Compared to the current study, similar findings were obtained except for only one variety (Presto). In similar studies, CP contents of triticale grains were determined, 9.00-16.26% [23], 10.5-14.6% [24], and 9.45-12.51% [18]. It is thought that these differences in CP content may be related to different climatic conditions, soil types, and fertilization. The ADF and NDF contents of triticale grains ranged from 2.51-4.50% and 15.15-17.65%, respectively. The current experiment's ADF and NDF contents of triticale cultivars were consistent with the findings of Dennett et al. [24], who discovered that the ADF contents of triticale lines ranged from 3.82-5.18% and the NDF contents ranged from 13.71-16.53%. Mut and Erbaş Köse [1] found that among 24 triticale genotypes, the ADF and NDF contents ranged from 2.44-3.59% and 17.5-19.1%, respectively. Alijosius et al. [18] found that ADF content ranged from 2.5-2.9% and NDF content ranged from 10.3-13.1% respectively.



**Table 1**. Chemical compositions of Triticale cultivars (% DM)

| Çeşitler | KM | HK | HY | HP | ADF | NDF |
|---|---|---|---|---|---|---|
| Alper bey | 93.05 | $2.12^{cd}$ | $2.72^{ab}$ | $11.88^{d}$ | $3.65^{abcd}$ | $17.65^{a}$ |
| Melih bey | 93.05 | $2.14^{bcd}$ | $2.74^{ab}$ | $12.91^{ab}$ | $4.50^{a}$ | $15.15^{e}$ |
| Karma | 93.20 | $2.30^{a}$ | $1.84^{c}$ | $11.76^{de}$ | $4.35^{ab}$ | $15.53^{de}$ |
| Ayşe Hanım | 93.21 | $2.15^{bcd}$ | $2.31^{abc}$ | $12.54^{bc}$ | $3.54^{abcd}$ | $17.36^{ab}$ |
| Bc goran | 93.30 | $2.26^{ab}$ | $1.82^{c}$ | $11.77^{de}$ | $2.51^{e}$ | $15.46^{de}$ |
| Bera | 93.34 | $2.26^{ab}$ | $2.12^{bc}$ | $12.16^{cd}$ | $3.84^{abc}$ | $15.86^{cde}$ |
| Özer | 93.34 | $2.29^{a}$ | $2.52^{abc}$ | $11.34^{ef}$ | $3.29^{cde}$ | $16.48^{bce}$ |
| Presto | 93.45 | $2.16^{bcd}$ | $2.61^{abc}$ | $9.44^{g}$ | $3.37^{bcde}$ | $15.46^{de}$ |
| Tatlıcak 97 | 93.48 | $2.18^{abcd}$ | $3.00^{a}$ | $11.19^{f}$ | $3.60^{abcd}$ | $17.49^{ab}$ |
| Ümran hanım | 93.49 | $2.05^{d}$ | $2.22^{abc}$ | $13.25^{a}$ | $2.83^{de}$ | $15.39^{e}$ |
| Esin | 93.56 | $2.25^{abc}$ | $2.17^{bc}$ | $11.44^{ef}$ | $3.48^{bcde}$ | $16.75^{abc}$ |
| SEM | 0.104 | 0.025 | 0.163 | 0.085 | 0.199 | 0.205 |
| Sig. | NS | ** | ** | ** | ** | ** |

abc Column means with common superscripts do not differ (P>0.05.) DM: Dry matter (%), CA: Crude ash (% of DM), EE: Eter extract (% of DM), CP: Crude protein (% of DM), ADF: Acid detergent fiber (% of DM), NDF: Neutral detergent fiber (% of DM), SEM: standart eror mean, Sig: Significant level, **: P<0.01, *: P<0.05, NS: Non-significant.

*İn vitro* TG, ME and OMD of triticale varieties were given in Table 2. The *in vitro* TG of the grains of Triticale cultivars ranged from 57.59-62.51 mL with the highest values in Bera and the lowest values in Özer.

Total gas production of triticale varieties determined in the current experiment was consistently higher than that reported by Umucalılar et al. [20] (75.5 ml) and Krieg et al. [22] (79.2 ml). The ME values of the cultivars ranged from 11.69-12.55 Mj $kg^{-1}$ DM, the highest values in Bera and the lowest values in Karma. ME values of triticale grains are 13.70 Mj $kg^{-1}$ DM [10], 13.3 Mj $kg^{-1}$ DM [7], 12.4 Mj $kg^{-1}$ DM [20], 14.0 Mj $kg^{-1}$ DM [22]. The OMD of triticale cultivars ranged from 78.06-82.24%, the highest values in Bera and the lowest values in Özer and Karma. The OMD contents of triticale grains were 89.09% [20], 77.94% [25] in similar studies.

**Table 2**. *İn vitro* total gas production, metabolizable energy and organic matter digestibilty of triticale cultivars.

| Çeşitler | TG (ml) | ME | OMD |
|---|---|---|---|
| Alper bey | $58.54^{e}$ | $12.01^{e}$ | $78.99^{f}$ |
| Melih bey | $60.51^{c}$ | $12.42^{ab}$ | $80.89^{bc}$ |
| Karma | $57.63^{f}$ | $11.69^{f}$ | $78.22^{g}$ |
| Ayşe Hanım | $59.43^{d}$ | $12.13^{cde}$ | $79.91^{de}$ |
| Bc goran | $61.59^{b}$ | $12.30^{bc}$ | $81.38^{b}$ |
| Bera | $62.51^{a}$ | $12.55^{a}$ | $82.24^{a}$ |
| Özer | $57.59^{f}$ | $11.79^{f}$ | $78.06^{g}$ |
| Presto | $60.48^{c}$ | $12.10^{de}$ | $79.74^{e}$ |
| Tatlıcak 97 | $61.75^{b}$ | $12.53^{a}$ | $81.32^{b}$ |
| Ümran hanım | $58.80^{de}$ | $12.06^{de}$ | $79.64^{ef}$ |
| Esin | $60.66^{c}$ | $12.20^{cd}$ | $80.53^{cd}$ |
| SEM | 0.143 | 0.036 | 0.127 |
| Sig. | ** | ** | ** |

abc Column means with common superscripts do not differ (P>0.05.) TG: Total gas, ME: Metabolizable energy, OMD: Organic matter digestibilty, SEM: standart eror mean, Sig: Significant level, **: P<0.01, *: P<0.05.

Cultivars have a significant effect on chemical composition, *in vitro* total gas production, ME, and OMD of grain. It has been determined that the Bera cultivar, which has high values in terms of HP, ME, and OMD according to chemical composition and fermentation parameters, can be used successfully in animal feeding. But before large implication, the grain yield of triticale grain should be tested. It is suggested that this study should be supported by in vivo studies.

## ACKNOWLEDGEMENT

We thank Assoc. Prof. Dr. Mehmet KARAMAN for carrying out the agronomic trial and providing triticale grains.

## REFERENCES

[1] Mut Z, Köse Erbaş ÖD. Grain yield and some quality properties of triticale genotypes. Anadolu Journal of Agricultural Sciences 2018;33(1):47-57.

[2] Dolgun C, Çiftçi Aydoğan E. Determination of yield and quality characteristics of some triticale genotypes in Bursa ecological conditions. KSU J. Agric Nat 2019;22(5):664-670.

[3] Demir İ, Aydem N, Korkut KZ, Şölen P. Triticale breeding studies in Turkey. Plant Breeding Symposium, 1979. İzmir: 22-25 Mayıs 1979, p.158-165.

[4] Mergoum M, Ryan J, Shroyer JP, Monem MA. Potential for adapting triticale in Morocco. Journal of Natural Resources and Life Sciences Education 1992;21(2):137-141.

[5] Keleş G. Nutritive Value of Morphological Components in Triticale Forage Harvested at Different Maturity Stages. Journal of Animal Production 2014;55(1):1-6.

[6] Fernandez-Figares I, Marinetto J, Royo C, Ramos JM, Garcia del Moral LF. Amino-acid composition and protein and carbohydrate accumulation in the grain of triticale grown under terminal water stress simulated by a senescing agent. Journal of Cereal Science 2000;32:249-258

[7] Glamočlıja N, Starčevıć M, Ćırıć J, Šefer D, Glıšıć M, Baltıć M, et al. The importance of triticale in animal nutrition. Ветеринарски журнал републике српске 2018;18(1).

[8] Biel W, Kazimierska K, Bashutska U. Nutritional value of wheat, triticale, barley and oat grains. Acta Scientiarum Polonorum Zootechnica 2020;19(2):19-28.

[9] Çiftçi İ, Yenice E, Eleroğlu E. Use of triticale alone and combination with wheat or maize: effect of diet type and enzyme supplementation on hen performance, egg quality, organ weights, intestinal viscosity and digestive system characteristics. Animal Feed Science and Technology 2003;105:149-161.

[10] Denek N, Deniz S. The determination of energy levels in some cereal grains used in ruminant diets by in vivo and *in vitro* methods. Turkish Journal of Veterinary & Animal Sciences 2004;28(1):185-193.

[11] Kaplan M, Üke Ö, Kale H, Yavuz S, Kurt Ö, Atalay Aİ. Effect of vegetative stages on potential nutritive value, gas production and methane of teff hay. Iğdır Univ. J. Inst. Sci. & Tech. 2016;6(4):181-186.

[12] Uslu OS, Kurt O, Kaya E, Kamalak A. Effect of species on the chemical composition, metabolisable energy, organic matter digestibility and methane production of some legume plants grown in Turkey. J App Anim Res 2018;46(1):1158-1161.

[13] Kurt O. Effect of variety on nutritive value and anti-methanogenic potential of oat grain. Progress In Nutrition 2021;23(3).

[14] AOAC. Official method of analysis. Association of Official Analytical Chemists, 15th ed., DC, USA, Washington; 1990. pp.66-88.

[15] Van Soest PV, Robertson JB, Lewis BA. Methods for dietary fiber, neutral detergent fiber, and nonstarch polysaccharides in relation to animal nutrition. J Dairy Sci 1991;74(10): 3583- 3597.

[16] Menke KH, Raab L, Salewski A, Steingass H, Fritz D, Schneider W. The estimation of the digestibility and metabolizable energy content of ruminant feedingstuffs from the gas production when they are incubated with rumen liquor *in vitro*. J Agric Sci (Camb), 1979; 93:217-222.

[17] Menke KH, Steingass H. Estimation of the energetic feed value obtained from chemical analysis and gas production using rumen fluid. Anim. Res. Dev. 1998, 28:7–55.

[18] Alijošius S, Švirmickas GJ, Bliznikas S, Gružauskas R, Šašytė V, Racevičiūtė-Stupelienė A, et al. Grain chemical composition of different

varieties of winter cereals. Zemdirbyste-Agriculture 2016;103(3).

[19] Kowieska A, Lubowicki R, Jaskowska I. Chemical composition and nutritional characteristics of several cereal grain. Acta Scientiarum Polonorum. Zootechnica 2011;10(2):37-50.

[20] Umucalilar HD, Coşkun B, Gülşen N. In situ rumen degradation and *in vitro* gas production of some selected grains from Turkey. Journal of animal physiology and animal nutrition 2002; 86(9-10):288-297.

[21] Chrenková M, Čerešňáková Z, Formelová Z, Poláčiková M, Mlyneková Z, Fľak P. Chemical and nutritional characteristics of different types of DDGS for ruminants. J Anim Feed Sci 2012;21(425):35.

[22] Krieg J, Seifried N, Steingass H, Rodehutscord M. In situ and *in vitro* ruminal starch degradation of grains from different rye, triticale and barley genotypes. Animal 2017;11(10): 1745-1753.

[23] Brandt DA, Brand TS, Cruywagen CW. The use of crude protein content to predict concentrations of lysine and methionine in grain harvested from selected cultivars of wheat, barley and triticale grown in the Western Cape region of South Africa. South African Journal of Animal Science 2000;30(1):22-25.

[24] Dennett AL, Wilkes MA, Trethowan RM. Characteristics of modern triticale quality: The relationship between carbohydrate properties, α-amylase activity, and falling number. Cereal Chemistry 2013;90(6):594-600.

[25] Kılıç Ü. Determination of some fermentation products and energy contents of some feed raw materials used in ruminant feeding using *in vitro* gas production technique. University of Ondokuz Mayıs; 2005.

[26] Mendeş M, Akkartal E. Comparison of ANOVA F and WELCH tests with their respective permutation versions in terms of type I error rates and test power. Kafkas Univ Vet Fak Dergisi 2010; 16 (5): 711-716.

Araştırma Makalesi https://doi.org/10.46810/tdfd.1120976 Research Article

Türk Doğa ve Fen Dergisi
Turkish Journal of Nature and Science
www.dergipark.gov.tr/tdfd

# Determination of the Effect of Harpin Protein on NaCl Salt Stress in Pistachio (*Pistacia vera* L.) Seeds

**Selçuk BİNİCİ[1]*, Civan ÇELİK[2], Fatma YILDIRIM[1], Adnan N. YILDIRIM[1]**

[1]Isparta Uygulamalı Bilimler Üniversitesi, Ziraat Fakültesi, Bahçe Bitkileri Bölümü, Isparta
[2]Isparta Uygulamalı Bilimler Üniversitesi, Ziraat Fakültesi, Bahçe Bitkileri Bölümü, Isparta
Selçuk BİNİCİ: ORCID NO: 0000-0002-2373-3990
Civan ÇELİK: ORCID NO: 0000-0002-1696-5902
Fatma YILDIRIM: ORCID NO: 0000-0001-7304-9647
Adnan Nurhan YILDIRIM: ORCID NO: 0000-0003-2526-040X

**Corresponding author: d.selcukbinici@gmail.com*

(Received: 24.05.2022, Accepted: 09.06.2022, Online Publication: 29.06.2022)

**Keywords**
*Pistacia vera*, Seedlings, Harpin protein, Salt stress, Antioxidant enzyme activity, Morphological development

**Abstract:** Drought and salinity are among the most important abiotic stress factors. Although there is a growing interest to the sustainability of fruit growing in arid and salty areas, there are not enough studies. Therefore, this study was carried out for the determination of the effects of harpin protein at different salt concentrations in Pistachio (*Pistacia vera* L.) seedlings. At the end of the treatment, there was a 10% decrease in plant height, 43% in root length. Superoxide dismutase, catalase and ascorbate peroxidase antioxidant enzyme activities increased by 56.65%, 410.36% and 343.48%, respectively. In addition, the amount of chlorophyll a, chlorophyll b, and chlorophyll a+b (respectively, 39.31%, 34.16%, and 36.12%) was decrease. In addition, it was determined that harpin applications protected the chlorophyll content related to photosynthesis, increased the diameter of the stem and root and decreased the stress enzyme activities. Thus, applications of harpin protein may be beneficial to increase tolerance to drought/salinity stresses in pistachio plants, especially in the early stages of seedling development. These findings may pave the way for future research on stress management in sustainable fruit growing in arid and semi-arid areas.



# Antepfıstığı (*Pistacia vera* L.) Çöğürlerinde Harpin Proteininin NaCl Tuz Stresi Üzerine Etkisinin Belirlenmesi

**Anahtar Kelimeler**
*Pistacia vera*, Çöğür, Harpin proteini, Tuz stresi, Antioksidan enzim aktivitesi, Morfolojik gelişme

**Öz:** Tarımsal üretimi ve verimliliği sınırlandıran en önemli abiyotik stres faktörlerin başında kuraklık ve tuzluluk gelmektedir. Kurak ve tuzlu alanlarda meyve yetiştiriciliğinin sürdürülebilirliği konusuna ilgi bulunmakla birlikte yeterli çalışma bulunmamaktadır. Bu nedenle bu çalışma, Antepfıstığı (*Pistacia vera* L.) çöğürlerinde harpin proteinin farklı tuz konsantrasyonlarındaki etkilerinin belirlenmesi amacıyla yürütülmüştür. Uygulama sonunda tuz konsantrasyonun artmasıyla birlikte bitki boyunda %10, kök uzunluğunda %43, yaş bitki ağırlığında yaklaşık olarak %40 oranında azalma meydana gelmiştir. Süperoksit dismutaz, katalaz ve askorbat peroksidaz antioksidan enzim aktiviteleri ise sırasıyla, %60, %410 ve %345 oranında artmıştır. Ayrıca klorofil a miktarı %39, klorofil b miktarı %34 ve klorofil a+b miktarı %36 oranında azalmıştır. Bununla birlikte harpin uygulamalarının fotosentezle ilişkili olan klorofil içeriğini koruduğu, gövde ve kök çapını artırdığı ve stres enzim aktivitelerini düşürdüğü saptanmıştır. Sonuçlar Antepfıstığı bitkilerinde özellikle çöğür gelişiminin hassas olduğu ilk zamanlarında kuraklık/tuzluluk streslerine toleransı arttırmak için harpin proteini uygulamalarının yararlı olabileceğini göstermiştir. Bu bulgular, kurak ve yarı kurak alanlarda sürdürülebilir meyve yetiştiriciliğinde stres yönetimi konusunda gelecekteki araştırmaların önünü açacaktır.

## 1. INTRODUCTION

Salinity is the second most important abiotic stress factors limiting agricultural production and productivity after drought in the world. About 20% of the cultivated lands in the world and about half of the irrigated lands are affected by salinity [1]. Salinization occurs in 1-1.5 million hectares of land in the world every year and causes about 12 billion dollars of income loss [2]. Salinity is generally defined by the concentration of soluble salts in the soil. Accordingly, 100-150 mg (0.10-0.15%) water-soluble salt per 100 g of soil is acceptable limit values, and when it exceeds 150 mg, the growth and development of many plant species is prevented. When the salt percentage rises to 0.65%, almost all cultivated plants cannot survive in these soils [3]. Salinization is an important issue particularly in arid and semi-arid climates due to insufficient precipitation as well as high evaporation. In addition, unconscious agricultural irrigation, insufficient drainage and high ground water play an important role in soil salinization [4]. In Turkey, which has arid and semi-arid climate, salinity and alkalinity problems are experienced in approximately 1.5 million hectares of irrigable agricultural lands (comprising 32.5% of irrigated lands). Especially in the Southeastern Anatolia Region, which has arid and semi-arid climate, irrigated areas have increased with the activation of the GAP project, but salinization has occurred in many areas as a result of unconscious irrigation. For example, as a result of wrong irrigation in the last 25-30 years in Şanlıurfa Harran Plain, saline areas have increased three times [2]. Again, the ground water, which is also a cause of salinization in the south of Şanlıurfa, rose up to 0.5 m, and therefore drying up in the orchards began [5].

Pistachio, namely *Pistacia vera* L., belongs to the genus Pistacia of the Anacardiaceae family of the Terebinthales order. The seeds of pistachio, which is one of the hard-shelled fruit types, are very rich in terms of unsaturated fatty acids, antioxidants, phenolic substances, vitamins and minerals [6]. Since its fruits can be stored for a long time, it has a strategic and economic value in the nutrition of human beings since ancient times. At the same time, it has ecological importance as it can be easily grown in barren and poor soils. It is grown in arid and semi-arid regions around the world [1]. *P. vera* can survive in areas with annual precipitation below 200 mm and withstand drought better than olive, almond, and fig species, which are considered typical xerophyte plants. It also tolerates salinity [1-7].

Turkey is one of the gene centers of pistachio, has suitable ecological conditions and is one of the first three countries (Iran, Turkey and USA) producing pistachios in the world. As a matter of fact, 474.004 tons of pistachios are produced in the world and Turkey ranks second with a production amount of 296.376 tons [8]. Quality and efficient pistachio production in our country is carried out in the Southeastern Anatolia Region, with the highest amount in the provinces of Sanliurfa and Gaziantep. Pistachio is propagated by grafting. The most widely used rootstock is *P. vera* seedlings [9].

It is known that high salt in the soil decreases production and causes some physiological issues in plants. It has been reported by different researchers that, high salt concentrations cause disruption of ion balance in cells, ion toxicity and osmotic stress, and produce reactive oxygen species (ROS) that damage DNA, lipids and proteins [10-11-12-13-14-15-16]. Therefore, molecular and enzymatic reactions developed by plants against biotic and abiotic stress conditions have recently been the focus of attention of researchers [11-13-17-18-19-20-21]. Plants perform some enzymatic and non-enzymatic mechanisms to avoid the harmful effects of ROS during biotic/abiotic stress [11]. One of these mechanisms is antioxidant enzyme activities. Antioxidant enzymes (superoxide dismutase (SOD), catalase (CAT), ascorbate peroxidase (APX) etc.) abolish the harmful effects of $H_2O_2$ accumulated in the cell during stress by catalyzing $H_2O$ and $O_2$ [20]. As a result, several biochemical reactions take place in the cell in terms of tolerance levels of plants under oxidative stress. Much research is needed to fully understand the mechanism of these reactions.

In recent years, researchers have focused on different amino acid and hormone applications in order to reduce the effect of stress in plants [22-23-24-25-26-27-28-29-30-31]. One of these amino acids is the harpin protein. Harpin is known as an acidic, glycine-rich, protease sensitive and heat resistant protein that is encoded by the hrpN gene of *Erwinia amylovora bacterium*, and also increases disease resistance in plants [32]. In addition, the harpin protein evokes a natural defense mechanism in plants [33]. Harpins activate the defense mechanism in plants by stimulating the expression of defense-related genes in the plant cell [34-35-36]. Indeed, Dong et al. [37] and Zhang et al. [38] reported that harpin increased drought tolerance by activating abscisic acid (ABA) signaling in *Arabidopsis*, and hrf1, the gene coding for harpin, provides tolerance against drought stress in rice. Almas [39] reported that antioxidant enzyme activities increase during drought stress in cotton, but plant activators reduce the level of oxidative damage caused by drought stress. Many studies have been conducted to determine the effect of harpin protein on yield and quality [40-41-42]. However, as a result of the literature review, it was seen that there are a limited number of studies examining the effects of harpin protein on plant growth and antioxidant enzyme activities under abiotic stress conditions.

The early stages of seedling development in arid and semi-arid soils is a critical stage when plants are exposed to a series of abiotic stresses. Plants exposed to salt stress are adversely affected by reduced growth and development. In this study, it was aimed to determine the morphological, biochemical and enzymatic activity levels of the plants with the salt stress relieving effect of different levels of salt stress and harpin protein applications in the seedlings obtained from the seeds of the *P. vera* L. species.

## 2. MATERIAL AND METHOD

This study was carried out in the glass greenhouse of Isparta University of Applied Sciences (ISUBÜ), Faculty of Agriculture, Department of Horticulture, in the vegetation period of 2021.

### 2.1. Material and Growing Conditions

In order to obtain the seeds, the seeds of the Siirt variety of pistachio were folded in boxes containing perlite, in a cold storage for 120 days at +4 ºC and 90-95% humidity. The seeds removed from the stratification were planted in 32x13 cm plastic tubes containing peat + perlite at a ratio of 1:1 and transferred to the side ventilated glass greenhouse. Maintenance procedures were applied to the emerging seedlings.

### 2.2. Salt Stress and Harpin Applications

When the seedlings were about two months old (03.08.2021), the applications were started. In order to create different salt stress in the experiment, three different concentrations of NaCl salt (40 mM, 80 mM and 160 mM) were given to the seedlings with irrigation water every five days according to the previously determined potted field capacity. In the experiment, the commercial dose of harpin protein (Messenger TM) was sprayed on the leaves 3 times, 15 days, 30 days and 45 days after salt applications. The experiment was terminated on the 50th day (22.09.2021). The experiment was set up according to the randomized plot design with 3 replications and 4 plants in each replication.

The irrigation water used in the experiment was evaluated as 1st class irrigation water [43]. Temperature and humidity in the greenhouse were measured with the HOBO UX100-003 Recorder. Temperature and air relative humidity values are given in Figure 1 and Figure 2, respectively.

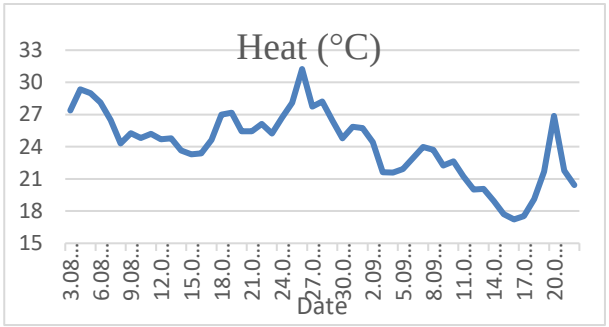


**Figure 1.** Daily average temperature values measured in the greenhouse of 2021 in August-September

In the study, seedling length (cm) and seedling stem diameter (mm) were measured as morphological growth parameters before and after the application. In addition, at the end of the application, seedlings were removed and plant fresh weight (g), stem fresh weight (g), root length (cm), root fresh weight (g), root dry weight (g), root diameter (cm), shoot number (piece/plant) and leaf area (mm2), leaf circumference (mm), leaf width (mm) and leaf length (mm) were measured.

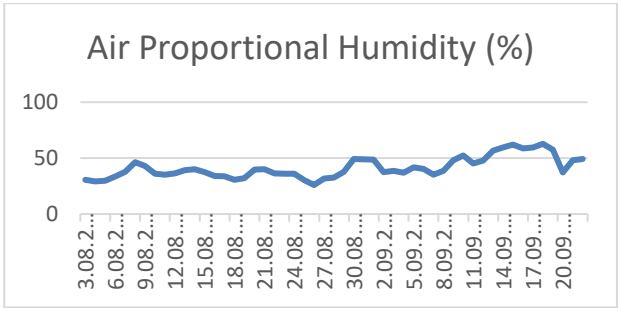


**Figure 2.** Daily average air relative humidity values measured in the greenhouse of 2021 in August-September

As physiological measurements, leaf stomatal conductivity (mmol/m2/s) and leaf temperature (°C) were measured with a porometer (Delta-T, Porometer-AP4) device before and after the application. As biochemical analyzes, chlorophyll content and APX, CAT and SOD antioxidant enzyme activity analyzes were performed in leaf samples taken before and after the application.

Chlorophyll content was determined according to the method developed by Zhang and Huang [44]. Results are expressed as mg/g.

Ascorbate peroxidase (APX) enzyme activity, APX enzyme activity Nakano et al. [45] according to the method specified. Accordingly, 4 g samples were weighed and analyzes were carried out in line with the researchers' practices. Results are expressed as mol/min/g protein.

Superoxide dismutase (SOD) enzyme activity, SOD enzyme activity Jiang et al. [46] was carried out according to the method specified. Accordingly, 10 g samples were weighed and analyzes were carried out in line with the researchers' practices. Results are expressed as U/mg protein.

Catalase (CAT) enzyme activity, CAT enzyme activity Beers et al. [47] according to the method specified. Accordingly, 10 g samples were weighed and analyzes were carried out in line with the researchers' practices. Results are expressed as U/mg protein.

The obtained data were subjected to one-way variance analysis method in MINTAB 17 statistical program. The resulting differences were determined according to the Tukey multiple comparison test, and the differences between the averages were shown with the help of different letters.

## 3. RESULT AND DISCUSSION

### 3.1. Morphological Development Characteristics

At the beginning of the first reaction given to salinity in plants is the slowdown and interruption of growth depending on the severity and duration of stress [48-49-50-51-52-53-54-55]. Harpin protein (Hpa 1) produced by bacterial blight induces a vegetative growth-promoting response by activating the ethylene signaling pathway,

increasing the rate of photosynthesis and increasing EXPANSIN (EXP) gene expression levels [42].

In the study, the mean values of seedling length and seedling stem diameter obtained from pistachio seedlings treated with salt stress and harpin protein, and statistical analysis results are presented in Table 1. There were no statistically significant differences ($p \leq 0.05$) between the treatments in terms of seedling length and seedling stem diameter (Table 1). At the end of the application, the longest plant height was measured in the control application (26.36 cm) and the shortest plant height was measured in the 160 mM NaCl application (23.66 cm). The largest diameter value in terms of seed stem diameter was determined in 40 mM NaCl+Harpin application (3.86 mm), followed by 80 mM NaCl+Harpin (3.57 mm) and 160 mM NaCl+Harpin (3.43 mm) applications., The seedling length and stem diameter change rates increased in all applications compared to the pre-application values. These increase rates in plant height and stem diameter varied according to the applications, and no significant correlation was observed. However, relatively low rates of change (9.28% and 28.73%, respectively) were detected at high salt concentration (160 mM) relative to the control. As a matter of fact, Ashraf et al. [56] stated that salt application reduced the plant height between 13.0% and 36.5%. On the other hand, 80 mM NaCl application in the study, relatively high change rates (28.73% and 52.25%, respectively) were detected in both seedling length and seedling stem diameter compared to the control, and it was observed that the growth continued relatively. These results indicate that pistachio tolerates salinity. This can be explained by the fact that the growth and development of plants are not adversely affected by maintaining the transport of mineral substances with water even under a certain degree of osmotic stress. Similar results were also found in a study on quince and pear rootstocks [55]. In addition, the application of 40 mM NaCl+Harpin had a relatively increasing effect on the stem diameter.

**Table 1.** The effects of salt stress and harpin protein treatments on seedling length (cm) and seedling stem diameter (cm) in pistachio seedlings

| Treatments | Seedling Length (cm) | | | Seedling Stem Diameter (cm) | | |
|---|---|---|---|---|---|---|
| | Before Treatment | After Treatment | Change (%) | Before Treatment | After Treatment | Change (%) |
| Control | 21.53±2.31 | 26.36±2.81 | +22.43 | 2.27±0.38 | 3.29±0.23 | +44.93 |
| 40 mM NaCl | 20.61±1.99 | 25.48±4.36 | +23.63 | 2.39±0.12 | 3.21±0.14 | +34.31 |
| 40 mM NaCl+Harpin | 24.41±2.68 | 25.04±1.99 | +2.58 | 2.45±0.35 | 3.86±0.30 | +57.55 |
| 80 mM NaCl | 19.11±0.96 | 24.60±1.62 | +28.73 | 2.22±0.17 | 3.38±0.32 | +52.25 |
| 80 mM NaCl+Harpin | 23.17±3.49 | 26.16±3.92 | +12.90 | 2.62±0.25 | 3.57±0.46 | +36.26 |
| 160 mM NaCl | 21.65±3.57 | 23.66±1.54 | +9.28 | 2.48±0.12 | 3.17±0.09 | +27.82 |
| 160 mM NaCl+Harpin | 20.69±2.10 | 24.61±0.91 | +18.94 | 2.37±0.29 | 3.43±0.10 | +44.72 |

*The difference between the means with different letters is significant at the $p \leq 0.05$ level.



The average values of plant fresh weight, stem fresh weight and shoot number and variance analysis results obtained from pistachio seedlings treated with salt stress and harpin protein are shown in Table 2. In the measurements made at the end of the experiment, there were statistically significant differences ($p \leq 0.05$) between the treatments in terms of plant fresh weight, stem fresh weight and shoot number. It was determined that plant and stem weight decreased with salt stress. The highest plant weight was obtained in the control application and the lowest in the application of 160 mM NaCl (12.51 g and 7.73 g, respectively) and it was determined that this application decreased the fresh plant weight by 38% compared to the control. In stem weight, the highest value was obtained in the application of 160 mM NaCl+Harpin (8.58 g), while the lowest value was determined in the application of 80 mM NaCl and 160 mM NaCl (4.04 g and 4.18 g, respectively). Salt applications reduced the stem weight by approximately 50% compared to the control. In a study conducted on pistachio, it was reported that the dry weight of shoots decreased significantly with the increase in salinity [7]. However, in this study, values close to control were obtained in harpin applications in terms of these properties. This may indicate that plants treated with harpin protein continue to absorb water from the soil and accumulate dry matter (Table 2). As a matter of fact, the stem diameters of the plants to which the harpin was applied were also found to be higher than the control (Table 1). In a study conducted on pepper, while harpin applications did not increase plant height compared to control, it increased the stem diameter relatively [57]. When the number of shoots was examined, there was a significant difference between the control and other treatments and the number of shoots decreased by half (Table 2). Harpin applications did not have an effect on the number of shoots.

**Table 2.** The effects of salt stress and harpin protein treatments on plant fresh weight (g), stem fresh weight (g) and shoot number (piece/plant) in pistachio seedlings

| Treatments | Plant Fresh Weight (g) | Stem Fresh Weight (g) | Shoot Number (piece/plant) |
|---|---|---|---|
| Control | 12.51±0.70a | 7.55±0.71ab | 3.23±0.25a |
| 40 mM NaCl | 8.96±1.50ab | 4.90±0.88bc | 1.50±0.50b |
| 40 mM NaCl+Harpin | 11.05±2.20ab | 7.37±1.35ab | 1.16±0.28b |
| 80 mM NaCl | 8.06±0.83ab | 4.04±0.92c | 1.50±0.50b |
| 80 mM NaCl+Harpin | 8.14±2.26ab | 5.14±1.43bc | 1.33±0.57b |
| 160 mM NaCl | 7.73±2.03b | 4.18±0.61c | 1.16±0.28b |
| 160 mM NaCl+Harpin | 11.67±0.53ab | 8.58±0.63a | 1.41±0.38b |

*The difference between the means with different letters is significant at the $p \leq 0.05$ level.

Average values of root fresh weight, root dry weight, root diameter and root length, and variance analysis results obtained from pistachio seedlings treated with salt stress and harpin protein are given in Table 3. Although decreases were detected in the wet and dry root weights with the effect of salt concentration in the study, it was determined that the difference between the applications was not statistically significant ($p \leq 0.05$). It was determined that the applications had significant effects on root diameter and root length, and statistically significant differences emerged ($p \leq 0.05$). The highest root diameter was obtained in 40 mM NaCl+Harpin, control and 80 mM NaCl+Harpin applications (6.19 cm, 6.17 cm and 5.62 cm, respectively). The lowest root diameter was found in 80 mM NaCl and 160 mM NaCl applications (4.38 cm and 4.49 cm, respectively) and these applications reduced the root diameter by approximately 28%. It has also been reported in other studies that salt stress reduces root growth [58-59-60 61-62-63]. However, in the study the root diameter promoting effect of harpin applications under salt stress was determined. In terms of root length, a statistically significant difference was observed only between the control and 160 mM NaCl application. However, relatively lower values were obtained in salt + harpin applications compared to the control application.

**Table 3.** The effects of salt stress and harpin protein treatments on root fresh weight, root dry weight, root diameter, and root length in pistachio seedlings

| Uygulama | Root Fresh Weight (g) | Root Dry Weight (g) | Root Diameter (cm) | Root Length (cm) |
|---|---|---|---|---|
| Kontrol | 4.18±0.57 | 2.28±0.27 | 6.17±0.10a | 39.86±1.03a |
| 40 mM NaCl | 3.77±0.64 | 1.90±0.35 | 5.15±0.25bc | 37.65±0.81a |
| 40 mM NaCl+Harpin | 3.67±0.98 | 2.09±0.11 | 6.19±0.49a | 33.85±1.23ab |
| 80 mM NaCl | 3.63±0.60 | 1.73±0.23 | 4.38±0.35c | 29.40±1.25ab |
| 80 mM NaCl+Harpin | 2.99±0.83 | 1.46±0.43 | 5.62±0.41ab | 35.48±2.37ab |
| 160 mM NaCl | 2.54±0.44 | 1.76±1.0 | 4.49±0.27c | 22.73±2.13b |
| 160 mM NaCl+Harpin | 3.42±0.68 | 1.56±0.60 | 5.02±0.04bc | 36.38±13.58ab |

*The difference between the means with different letters is significant at the $p \leq 0.05$ level.

The average values of leaf area, circumference, length and width obtained from pistachio seedlings that were treated with salt stress and harpin protein, and the variance analysis results are given in Table 4. In the measurements made at the end of the experiment, statistically significant differences ($p \leq 0.05$) were found between the applications in terms of leaf area, circumference, length and width (Table 4). Accordingly, it was determined that as the salt concentration increased, the leaf area decreased up to 51%. The highest leaf area was obtained from the control group (1071.50 mm2), and the lowest leaf area was obtained from 80 mM NaCl, 160 mM NaCl and 160 mM NaCl+Harpin applications (534.72 mm2, 515.90 mm2 and 534.80 mm2, respectively). Again, it was determined that there was a 27%, 23% and 40% reduction in leaf circumference, length and width, respectively, compared to the control. The highest leaf circumference, length and width were measured from the control group (122.80 mm2, 46.91 mm and 32.74mm, respectively). The lowest values were determined in 160 mM NaCl and 160 mM NaCl+Harpin applications. These results were similar to the findings of other studies on pistachio seedlings [7]. Also in the study, harpin applications at 40 mM and 80 mM salt doses had a healing effect on the leaf area. These results show that harpin has the potential to improve plant growth and salt tolerance by activating the plant defense mechanism. Indeed, harpin may exert its effect on plant growth and defense response through activation of transcription factors [64].



**Table 4.** The effects of salt stress and harpin protein applications on leaf area, girth, length, and width in pistachio seedlings

| Treatments | Leaf Area ($mm^2$) | Leaf Girth (mm) | Leaf Length (mm) | Leaf Width (mm) |
|---|---|---|---|---|
| Control | 1071.50±35.30a | 122.80±3.13a | 46.91±2.78a | 32.74±1.64a |
| 40 mM NaCl | 747.08±13.39c | 117.17±1.16b | 45.62±3.26a | 29.52±1.05ab |
| 40 mM NaCl+Harpin | 888.00±48.20b | 117.62±0.66ab | 45.48±3.15a | 25.96±1.95bc |
| 80 mM NaCl | 534.72±13.29d | 92.20±1.86c | 43.60±2.30a | 22.53±1.03cd |
| 80 mM NaCl+Harpin | 870.34±13.66b | 117.28±0.46b | 45.44±1.40a | 29.72±2.04ab |
| 160 mM NaCl | 515.90±19.70d | 89.86±2.92c | 35.94±2.29b | 19.83±1.50d |
| 160 mM NaCl+Harpin | 534.80±32.40d | 89.80±1.20c | 35.90±1.20b | 22.67±1.89cd |

*The difference between the means with different letters is significant at the $p \leq 0.05$ level.

### 3.2. Physiological Features

Average values and variance analysis results of leaf stomatal conductivity and leaf temperature obtained from pistachio seedlings treated with salt stress and harpin protein are given in Table 5. In the study, the differences between control and other salt and harpin applications at the end of the application in terms of stomatal conductivity were statistically significant ($p \leq 0.05$). The highest stomatal conductivity was measured in the control application (348.7 $mmol/m^2/s$) and the lowest in 160 mM NaCl (67.80 $mmol/m^2/s$) application. At the end of the experiment, only 5.17% decrease was observed in stomatal conductivity in the control group, while a significant decrease occurred in the combinations applied salt and harpin, varying between 40.48% (40 mM NaCl+Harpin) and 80.06% (160 mM NaCl) (Table 5). As the salt concentration increased, the stomatal conductivity gradually decreased. It has also been reported in many studies that salinity reduces stomatal conductivity [55-65-66]. The effect of harpin applications on stomatal conductivity was not significant. Romero-Arondo et al. [67] found that salt stress caused significant decreases in stomatal conductivity. However, they reported that combined applications with plant activators had higher stomatal conductivities. In this

study, higher values were obtained in combinations of 80 mM NaCl and 160 mM NaCl doses with harpin.

There was no statistical difference between the applications in terms of leaf temperature both before and after the application, and values at similar levels were obtained (Table 5). However, the leaf temperature, which was approximately 33.5 $^0$C before the application, decreased by approximately 14% at the end of the experiment and decreased to 28.5 $^0$C. As seen in Figure 1, it is thought that there is a decrease in the recorded greenhouse temperature before (29°C) and after the application (20°C), thus affecting the decrease in leaf temperature.

**Table 5.** The effects of salt stress and harpin protein treatments on leaf stomatal conductivity, and leaf temperature in pistachio seedlings

| Treatments | Stomatal Conductivity (mmol/m$^2$/s) | | | Leaf Temperature ($^0$C) | | |
|---|---|---|---|---|---|---|
| | Before Treatment | After Treatment | Change (%) | Before Treatment | After Treatment | Change (%) |
| Control | 367.7±100.40 | 348.7±25.3a | -5.17 | 33.700±0.890 | 28.54±0.20 | -15.31 |
| 40 mM NaCl | 500.5±53.70 | 188.7±78.5b | -62.30 | 33.447±0.731 | 28.61±1.57 | -14.46 |
| 40 mM NaCl+Harpin | 303.1±168.80 | 180.4±53.2b | -40.48 | 33.533±0.635 | 28.25±0.35 | -15.75 |
| 80 mM NaCl | 454.6±42.70 | 123.1±18.9bc | -72.92 | 33.827±0.270 | 28.92±0.57 | -14.51 |
| 80 mM NaCl+Harpin | 440.2±118.80 | 140.83±2.8bc | -68.01 | 33.593±0.277 | 28.57±0.46 | -14.95 |
| 160 mM NaCl | 340.1±67.20 | 67.80±12.8c | -80.06 | 33.393±0.643 | 28.81±1.44 | -13.72 |
| 160 mM NaCl+Harpin | 390.3±45.70 | 84.6±32.7bc | -78.32 | 33.807±0.580 | 29.14±1.52 | -13.80 |

*The difference between the means with different letters is significant at the p ≤0.05 level.

### 3.3. Biochemical Properties

Decreases in the amount of chlorophyll, which plays an important role in photosynthesis, affect growth and development of plant negatively by reducing carbohydrate synthesis. One of the most important parameters seen in plants under drought and salt stress is the decrease in total chlorophyll content. Indeed, it has been reported that chlorophyll degradation is an indicator of salt stress [68]. In the study, the mean values and variance analysis results of chlorophyll a, b, and a+b values obtained from pistachio seedlings treated with salt stress and harpin protein are given in Table 6. There were statistically significant differences between the treatments at the end of the experiment in terms of chlorophyll a, b and a+b contents (p≤0.05). Accordingly, while control and salt+harpin treatments were in the same statistical group, chlorophyll contents decreased significantly in only salt applied groups. Again, as the salt concentration increased, the chlorophyll a, b and a+b values gradually decreased. While the lowest chlorophyll

a contents were determined in the application of 160 mM NaCl (11.70 mg/g), the highest was determined in the control application (21.81 mg/g) (Table 6). At the end of the experiment, 160 mM NaCl application decreased chlorophyll a content by 39.31%, chlorophyll b content by 34.16% and chlorophyll a+b ratio by 36.12%. These results were in aggrement to the literature results reporting that salinity reduces chlorophyll content [55-69-70-71-72-73]. However, in this study, it was concluded that the application of harpin under salt stress preserved the chlorophyll contents. As a matter of fact, in a study conducted on pepper, it was reported that B. cinrea disease + harpin applications preserved chlorophyll content compared to only infected plants [74]. These results may show that harpin, an amino acid, plays a role in chlorophyll synthesis and degradation mechanisms. Indeed, in a previous study, it was stated that harpin modulates cell wall modifications, systemic resistance and gene expression related to the photosynthesis system [64].

It has also been reported in many studies that salt stress has negative effects on plants and that enzymatic and non-enzymatic antioxidants take part in the plant defense mechanism [69-70-71-72-73-75]. In the study, the mean values and variance analysis results of the antioxidant enzyme activities (APX, SOD and CAT) obtained from the pistachio seedlings treated with salt stress and harpin protein are given in Table 7. Before the application to the data obtained, variable results were obtained between the applications in the APX and CAT enzyme activities and were found to be statistically different (p≤0.05). However, these differences were not found to be significant. It is thought that this situation is caused by the differences in the current physiological mechanisms of the plants in the applications. However, statistically significant differences were found between the treatments in terms of all enzyme activities (APX, SOD and CAT) at the end of the experiment (p≤0.05) (Table 7). The lowest APX, SOD and CAT activities were in the control group (10.84 mol/min/g protein, 1.00 U/mg protein and 7.89 U/mg protein, respectively), and the highest was 160 mM NaCl application (49.37 mol/min/g protein, 2.71 U/mg protein and 27.28 U/mg protein, respectively). At the end of the experiment, an increase of 41.70% was observed in the APX enzyme activity in the control application, while an increase was determined between 103.77% (40 mM NaCl+Harpin) and 343.48% (80 mM NaCl) in applications. While there was an increase in SOD enzyme activity in 80 mM NaCl (8.97%) and 160 mM NaCl (56.65%) applications, decreases were observed in 40 mM NaCl and other salt + harpin combinations with control application. The highest decrease was found in the control group with 39.76%. The least decrease was 2.96% in 160 mM NaCl+Harpin application. Again, an increase of 4.50% was observed in the CAT enzyme activity in the control application, while an increase was observed between 67.22% (40 mM NaCl) and 410.36% (80 mM NaCl) in applications (Table 7). It has been determined that antioxidant enzyme activities increase with salt stress and the results of previous studies support our findings [69-70-71-72-73-77-78]. In the study, in general, harpin applications decreased antioxidant enzyme activities under salt stress. Especially, this decrease was more

pronounced in APX and SOD activities. As a matter of fact, while the SOD enzyme activity increased in 80 mM NaCl and 160 mM NaCl applications, there was a decrease in the harpin combinations of these applications. Similarly, Zhou et al. [76] reported that tomato seedlings treated with harpin protein under drought stress had lower CAT, SOD and APX antioxidant enzyme activities.

**Table 6.** The effects of salt stress and harpin protein treatments on chlorophyll contents

| Treatments | Chlorophyll a (mg/g) | | | Chlorophyll b (mg/g) | | | Chlorophyll a+b (mg/g) | | |
|---|---|---|---|---|---|---|---|---|---|
| | Before Treatment | After Treatment | Change (%) | Before Treatment | After Treatment | Change (%) | Before Treatment | After Treatment | Change (%) |
| **Control** | 16.21±6.32 | 21.81±1.49a | +34.59 | 27.46±10.24 | 35.35±246a | +28.73 | 43.67±16.56 | 57.17±3.95a | +30.91 |
| **40 mM NaCl** | 17.72±4.65 | 17.74±0.95b | +0.11 | 30.02±6.99 | 28.56±0.775b | -4.83 | 47.74±11.65 | 46.31±1.63b | -3.00 |
| **40 mM NaCl+Harpin** | 18.34±2.14 | 21.21±0.20a | +15.67 | 30.59±3.59 | 34.36±0.383a | +12.33 | 48.93±5.73 | 55.58±0.58a | +13.59 |
| **80 mM NaCl** | 19.41±0.92 | 14.96±0.88c | -22.91 | 32.702±0.98 | 25.06±0.246c | -23.34 | 52.11±1.90 | 40.03±1.10c | -23.18 |
| **80 mM NaCl+Harpin** | 17.53±2.83 | 20.96±0.86a | +19.57 | 29.25±4.91 | 34.07±1.355a | +16.49 | 46.78±7.74 | 55.03±2.22a | +17.64 |
| **160 mM NaCl** | 19.29±3.71 | 11.70±0.68d | -39.31 | 31.07±6.02 | 20.45±0.449d | -34.16 | 50.36±9.73 | 32.17±0.99d | -36.12 |
| **160 mM NaCl+Harpin** | 18.55±6.47 | 21.25±0.52a | +14.57 | 29.93±10.71 | 34.30±0.180a | +14.63 | 48.48±17.18 | 55.56±0.58a | +14.60 |

*The difference between the means with different letters is significant at the p ≤0.05 level.

**Table 7.** The effects of salt stress and harpin protein treatments on APX, SOD and CAT enzyme activity

| Treatments | APX (mol/min/g protein) | | | SOD (U/mg protein) | | | CAT (U/mg protein) | | |
|---|---|---|---|---|---|---|---|---|---|
| | Before Treatment | After Treatment | Change (%) | Before Treatment | After Treatment | Change (%) | Before Treatment | After Treatment | Change (%) |
| **Control** | 7.65±1.01d | 10.84±0.47d | +41.70 | 1.66±0.06 | 1.00±0.08d | -39.76 | 7.55±0.00a | 7.89±1.59d | +4.50 |
| **40 mM NaCl** | 15.43±0.37bc | 42.71±9.74ab | +176.80 | 1.62±0.13 | 1.51±0.07bc | -6.79 | 7.23±0.55a | 12.09±0.60cd | +67.22 |
| **40 mM NaCl+Harpin** | 11.67±1.53cd | 23.78±1.92c | +103.77 | 1.67±0.16 | 1.41±0.08c | -15.57 | 4.75±0.99ab | 10.05±0.71cd | +111.58 |
| **80 mM NaCl** | 7.29±1.63d | 32.33±2.09bc | +343.48 | 1.56±0.20 | 1.70±0.05b | +8.97 | 3.57±1.87b | 18.22±2.00b | +410.36 |
| **80 mM NaCl+Harpin** | 19.82±4.44a | 25.63±2.02c | +29.32 | 1.77±0.07 | 1.51±0.06bc | -14.69 | 6.94±1.04a | 13.16±2.16c | +89.63 |
| **160 mM NaCl** | 17.59±1.47b | 49.37±5.98a | +180.67 | 1.73±0.14 | 2.71±0.15a | +56.65 | 6.91±1.10a | 27.28±1.46a | +294.79 |
| **160 mM NaCl+Harpin** | 15.88±0.03bc | 35.91±1.16bc | +126.13 | 1.69±0.03 | 1.64±0.03b | -2.96 | 6.30±1.08ab | 20.19±1.75b | +220.48 |

*The difference between the means with different letters is significant at the p ≤0.05 level.



## 4. CONCLUSİON

Salt stress is one of the important abiotic stress factors in the world and in our country. Due to effects such as drought, wrong irrigation and fertilization programs, soluble salts cannot be washed in the soil and excessive salt accumulation occurs. This negatively affects plantyield and quality. Pistachio, constituting the plant material of this study, is the typical fruit type of Southeastern Anatolia Region and it tolerates drought and salinity. However, in addition to the arid and semi-arid climate of the Southeastern Anatolia Region, serious problems arise in the region such as the gradual salinization of many areas as a result of faulty irrigations. With the effect of increasing population and drought, researchers have made various applications in recent years to obtain plants resistant to biotic and abiotic stress conditions or to reduce the harmful effects of salt. This study was carried out in order to find an alternative way to these problems. For this, salt applications were applied to the pistachio seedlings for two months with different intensity and harpin applications were made in order to eliminate the effects of salt. According to the findings of the study, it is possible to say that the harpin protein in pistachio seedlings reduces the effect of salt stress relatively. This can be explained by the Hpa1-mediated regulation of plant growth and related physiological-molecular responses [42]. Indeed, in tomato, harpin has been shown to modulate the defense response and plant growth-related gene expression (via ethylene and ABA) by regulating the activity of the SlERF5 (ethylene-response factor 5) transcription factor [64]. In this study, it was determined that harpin applications protected the chlorophyll content related to photosynthesis, increased the diameter of the stem and root and decreased the stress enzyme activities. In addition, it can be said that the seedling rootstock used in the study can be used in salty soils and can tolerate salt up to a certain severity (40 mM NaCl and 80 mM NaCl). As a result, it has been demonstrated that harpin protein can be used to increase tolerance to drought/salinity stresses, especially in the early stages of seedling development in pistachio plants. These findings may pave the way for future research on stress management in sustainable fruit growing in arid and semi-arid areas.

## KAYNAKLAR


[1]. Hamed SB, Lefi E. Dynamics of growth and phytomass allocation in seedlings of *Pistacia atlantica* Desf. versus *Pistacia vera* L. under salt stress. International Journal of Agronomy and Agricultural Research (IJAAR). 2015;6(1):16-27.

[2]. https://topraktema.org/media/1409/07-tuzlanma.pdf erişim tarihi 26.04.2022

[3]. Dinç E. The spectrophotometric multicomponent analysis of a ternary mixture of ascorbic acid, acetylsalicylic acid and paracetamol by the double divisor-ratio spectra derivative and ratio spectra-zero crossing methods. Talanta. 1999 May 10;48(5):1145-57.

[4]. http://www.botes.com.tr/dokumanlar/013rizakanber.pdferişim tarihi 26.04.2022

[5]. Çetinkaya H, Kendal E, Sayar MS. Ekolojik tarım açısından güneydoğu anadolu bölgesi. Türk Bilimsel Derlemeler Dergisi. 2013;6(1):195-8.

[6]. Salas-Salvado´ J., Casas-Agustench P., Salas-Huetos A. (2011). Cultural and historical aspects of Mediterranean nuts with emphasis on their attributed healthy and nutritional properties. Nutrition, Metabolism and Cardiovascular Diseases. 21(1): 1-6.

[7]. Khalilpour M, Mozafari V, Abbaszadeh-Dahaji P. Tolerance to salinity and drought stresses in pistachio (*Pistacia vera* L.) seedlings inoculated with indigenous stress-tolerant PGPR isolates. Scientia Horticulturae. 2021 Nov 17;289:110440.

[8]. Food and Agriculture Organization (FAO) (2022). https://www.fao.org/faostat/en/#data/QCL. Erişim tarihi: 23.01.2022.

[9]. Özçağıran R, Ünal A, Özeker E, İsfendiyaroğlu M. Ilıman İklim Meyve Türleri Sert Çekirdekli Meyveler Cilt-I, Ege Üni. Ziraat Fak. Yayınları. 2004(553).

[10]. Zhu Z, Wei G, Li J, Qian Q, Yu J. Silicon alleviates salt stress and increases antioxidant enzymes activity in leaves of salt-stressed cucumber (*Cucumis sativus* L.). Plant Science. 2004 Sep 1;167(3):527-33.

[11]. Yasar F, Kusvuran S, Ellialtioglu S. Determination of anti-oxidant activities in some melon (*Cucumis melo* L.) varieties and cultivars under salt stress. The Journal of Horticultural Science and Biotechnology. 2006 Jan 1;81(4):627-30.

[12]. Yasar F. Effects of salt stress on ion and lipidperoxidation content in green beans genotypes. Asian Journal of Chemistry. 2007 Feb 15;19(2):1165.

[13]. Kusvuran S, Ellialtioglu S, Yasar F, Abak K. Antioxidative enzyme activities in the leaves and callus tissues of salt-tolerant and salt-susceptible melon varieties under salinity. African Journal of Biotechnology. 2012;11(3):635-41.

[14]. Dolatabadıan A, Sanavy SA, Chashmı NA. The effects of application of ascorbic acid (Vitamin C) on antioxidant enzymes activites, lipid peroxidant and proline accumulation of Canola (*Brassica napus* L.) under conditions of salt stress. Journal Agronomy and Crop Science. 2008:931-2250.

[15]. Li Y. Physiological responses of tomato seedlings (*Lycopersicon esculentum*) to salt stress. Modern Appl. Sci. 2009 Mar;3(3):171-6.

[16]. Chookhampaeng S. The effect of salt stress on growth, chlorophyll content proline content and antioxidative enzymes of pepper (*Capsicum annuum* L.) seedling. European Journal of Scientific Research. 2011;49(1):103-9.

[17]. Yasar F, Ellialtioglu S, Yildiz K. Effect of salt stress on antioxidant defense systems, lipid peroxidation, and chlorophyll content in green bean. Russian journal of plant physiology. 2008 Nov;55(6):782-6.

[18]. Amirjani MR. Effect of salinity stress on growth, mineral composition, proline content, antioxidant enzymes of soybean. American Journal of Plant Physiology. 2010;5(6):350-60.

[19]. Akyüz F, Yıldırım AN, Yıldırım F, Şan B, Karakurt Y, Çelik C, Önder S. Effects of water stress on leaf antioxidant enzymes activities and protein contents in five Prunus rootstocks. InXXX International Horticultural Congress IHC2018: International Symposium on Cultivars, Rootstocks and Management Systems of 1281 2018 Aug 12 (pp. 369-376).

[20]. Yıldırım F, Meltem Es, Binici S, Çelik C, Yıldırım A, Karakurt Y. Antioxidant Enzymes Activities of Walnut Nursery Trees to Drought Stress Progression. International Journal of Agriculture Forestry and Life Sciences. 2021;5(2):217-25.

[21]. Yıldırım A. N., Şan B., Yıldırım F., Çelik C., Bayar B., Karakurt Y. (2021b). Physiological and biochemical responses of almond rootstocks to drought stress. Turkısh Journal Of Agrıculture And Forestry, 45, 522-532.

[22]. Alian A, Altman A, Heuer B. Genotypic difference in salinity and water stress tolerance of fresh market tomato cultivars. Plant science. 2000 Mar 7;152(1):59-65.

[23]. Heuer B. Influence of exogenous application of proline and glycinebetaine on growth of salt-stressed tomato plants. Plant Science. 2003 Oct 1;165(4):693-9.

[24]. Faheed FA, Hassanein AM, Azooz MM. Gradual increase in NaCl concentration overcomes inhibition of seed germination due to salinity stress in *Sorghum bicolor* L.. Acta Agronomica Hungarica. 2005 Aug 1;53(2):229-39.

[25]. Sheteawi SA. Improving growth and yield of salt-stressed soybean by exogenous application of jasmonic acid and ascobin. International Journal of Agriculture and Biology (Pakistan). 2007.

[26]. Dhanapackiam S, Ilyas M. Effect of salinity on chlorophyll and carbohydrate contents of Sesbania grandiflora seedlings. Indian Journal of Science and Technology. 2010 Jan 1;3(1):64-6.

[27]. Hafez EM, Gharib HS. Effect of exogenous application of ascorbic acid on physiological and biochemical characteristics of wheat under water stress. International Journal of plant production. 2016 Oct 1;10(4):579-96.

[28]. Ahmadi FI, Karimi K, Struik PC. Effect of exogenous application of methyl jasmonate on physiological and biochemical characteristics of

*Brassica napus* L. cv. Talaye under salinity stress. South African Journal of Botany. 2018 Mar 1;115:5-11.

[29]. Ejaz B, Sajid ZA, Aftab F. Effect of exogenous application of ascorbic acid on antioxidant enzyme activities, proline contents, and growth parameters of Saccharum spp. hybrid cv. HSF-240 under salt stress. Turkish Journal of Biology. 2012 Nov 21;36(6):630-40.

[30]. Molaei S, Rabiei V, Soleimani A, Razavi F. Exogenous application of glycine betaine increases the chilling tolerance of pomegranate fruits cv. Malase Saveh during cold storage. Journal of Food Processing and Preservation. 2021 Mar;45(3):e15315.

[31]. Wang SY, Shi XC, Liu FQ, Laborda P. Effects of exogenous methyl jasmonate on quality and preservation of postharvest fruits: A review. Food Chemistry. 2021 Aug 15;353:129482.

[32]. Choi MS, Kim W, Lee C, Oh CS. Harpins, multifunctional proteins secreted by gram-negative plant-pathogenic bacteria. Molecular plant-microbe interactions. 2013 Oct;26(10):1115-22.

[33]. Fontanilla M, Montes M, De Prado R. Effects of the foliar-applied protein" Harpin (Ea)"(messenger) on tomatoes infected with Phytophthora infestans. Communications in agricultural and applied biological sciences. 2005 Jan 1;70(3):41-5.

[34]. He SY, Huang HC, Collmer A. Pseudomonas syringae pv. syringae harpinPss: a protein that is secreted via the Hrp pathway and elicits the hypersensitive response in plants. Cell. 1993 Jul 2;73(7):1255-66.

[35]. Andi S, Taguchi F, Toyoda K, Shiraishi T, Ichinose Y. Effect of methyl jasmonate on harpin-induced hypersensitive cell death, generation of hydrogen peroxide and expression of PAL mRNA in tobacco suspension cultured BY-2 cells. Plant and Cell Physiology. 2001 Apr 15;42(4):446-9.

[36]. Ichinose Y, Andi S, Doi R, Tanaka R, Taguchi F, Sasabe M, Toyoda K, Shiraishi T, Yamada T. Generation of hydrogen peroxide is not required for harpin-induced apoptotic cell death in tobacco BY-2 cell suspension culture. Plant Physiology and Biochemistry. 2001 Sep 1;39(9):771-6.

[37]. Dong HP, Yu H, Bao Z, Guo X, Peng J, Yao Z, Chen G, Qu S, Dong H. The ABI2-dependent abscisic acid signalling controls HrpN-induced drought tolerance in Arabidopsis. Planta. 2005 Jun;221(3):313-27.

[38]. Zhang C, Shi H, Chen L, Wang X, Lü B, Zhang S, Liang Y, Liu R, Qian J, Sun W, You Z. Harpin-induced expression and transgenic overexpression of the phloem protein gene AtPP2-A1 in *Arabidopsis* repress phloem feeding of the green peach aphid Myzus persicae. BMC plant biology. 2011 Dec;11(1):1-9.

[39]. Almas S. The effects of plant activators on drought tolerance of cotton (*Gossypium hirsutum* L.) genotypes grown in Gap region in Turkey (Doctoral dissertation).

[40]. Bednarz CW, Brown SN, Flanders JT, Tankersley TB, Brown SM. Effects of foliar applied harpin protein on cotton lint yield, fiber quality, and crop maturity. Communications in soil science and plant analysis. 2002 Apr 10;33(5-6):933-45.

[41]. Tezcan H, Akbudak N, Şeniz V. Effect of harpin protein on yield and fruit quality of pepper grown in greenhouse conditions. InIII Balkan Symposium on Vegetables and Potatoes 729 2004 Sep 6 (pp. 267-270).

[42]. Li X, Han B, Xu M, Han L, Zhao Y, Liu Z, Dong H, Zhang C. Plant growth enhancement and associated physiological responses are coregulated by ethylene and gibberellin in response to harpin protein Hpa1. Planta. 2014 Apr;239(4):831-46.

[43]. Esen M. Su stresi altında Chandler ve Fernor ceviz çeşitlerinin tüplü fidanlarının göstermiş olduğu tepkiler (M. Sc. dissertation).

[44]. Zhang Z, Huang R. Analysis of malondialdehyde, chlorophyll proline, soluble sugar, and glutathione content in *Arabidopsis* seedling. Bio-protocol. 2013 Jul 20;3(14):e817-.

[45]. Nakano Y, Asada K. Hydrogen peroxide is scavenged by ascorbate-specific peroxidase in spinach chloroplasts. Plant and cell physiology. 1981 Aug 1;22(5):867-80.

[46]. Jiang T, Jahangir MM, Jiang Z, Lu X, Ying T. Influence of UV-C treatment on antioxidant capacity, antioxidant enzyme activity and texture of postharvest shiitake *(Lentinus edodes*) mushrooms during storage. Postharvest biology and technology. 2010 Jun 1;56(3):209-15.

[47]. Beers RF, Sizer IW. A spectrophotometric method for measuring the breakdown of hydrogen peroxide by catalase. J Biol chem. 1952 Mar 1;195(1):133-40.

[48]. Shaheen S, Naseer S, Ashraf M, Akram NA. Salt stress affects water relations, photosynthesis, and oxidative defense mechanisms in *Solanum melongena* L. Journal of Plant Interactions. 2013 Mar 1;8(1):85-96.

[49]. Okkaoğlu H, Sönmez Ç, Şimşek Aö, Bayram E. Effect of salt stress on some agronomical characteristics and essential oil content of coriander (*Coriandrum sativum* L.) cultivars. Journal of Applied Biological Sciences. 2015;9(3):21-4.

[50]. Menezes RV, Azevedo AD, Ribeiro MD, Cova AM. Growth and contents of organic and inorganic solutes in amaranth under salt stress. Pesquisa Agropecuária Tropical. 2017 Jan;47:22-30.

[51]. Rahneshan Z, Nasibi F, Moghadam AA. Effects of salinity stress on some growth, physiological, biochemical parameters and nutrients in two pistachio (*Pistacia vera* L.) rootstocks. Journal of plant interactions. 2018 Jan 1;13(1):73-82.

[52]. Sahin U, Ekinci M, Ors S, Turan M, Yildiz S, Yildirim E. Effects of individual and combined effects of salinity and drought on physiological, nutritional and biochemical properties of cabbage (*Brassica oleracea* var. capitata). Scientia Horticulturae. 2018 Oct 20;240:196-204.

[53]. Inal A, Gunes A, Pilbeam DJ, Kadioglu YK, Eraslan F. Concentrations of essential and nonessential elements in shoots and storage roots of carrot grown in NaCl and $Na_2SO_4$ salinity. X-Ray Spectrometry: An International Journal. 2009 Jan;38(1):45-51.

[54]. Kapoor N, Pande V. Effect of salt stress on growth parameters, moisture content, relative water content and photosynthetic pigments of fenugreek variety RMt-1. Journal of Plant Sciences. 2015;10(6):210-21.

[55]. Aydınlı M. Armut yetiştiriciliğinde kullanılan farklı anaçların tuzluluğa toleranslarının morfolojik, fizyolojik ve biyokimyasal parametreler ile incelenmesi (Doctoral dissertation).

[56]. Ashraf M, Mukhtar N, Rehman S, Rha ES. Salt-induced changes in photosynthetic activity and growth in a potential medicinal plant Bishop's weed (*Ammi majus* L.). Photosynthetica. 2004 Dec;42(4):543-50.

[57]. Akbudak N, Tezcan H, Akbudak B, Seniz V. The effect of harpin protein on plant growth parameters, leaf chlorophyll, leaf colour and percentage rotten fruit of pepper plants inoculated with *Botrytis cinerea*. Scientia Horticulturae. 2006 Jun 29;109(2):107-12.

[58]. Abbas MA, Younis ME, Shukry WM. Plant growth, metabolism and adaptation in relation to stress conditions. XIV. Effect of salinity on the internal solute concentrations in Phaseolus vulgaris. Journal of Plant Physiology. 1991 Oct 1;138(6):722-7.

[59]. Franco JA, Esteban C, Rodriguez C. Effects of salinity on various growth stages of muskmelon cv. Revigal. Journal of Horticultural Science. 1993 Jan 1;68(6):899-904.

[60]. García LV, Marañón T, Moreno A, Clemente L. Above-ground biomass and species richness in a Mediterranean salt marsh. Journal of Vegetation Science. 1993 Jun;4(3):417-24.

[61]. Chartzoulakis KS. Photosynthesis, water relations and leaf growth of cucumber exposed to salt stress. Scientia Horticulturae. 1994 Sep 1;59(1):27-35.

[62]. Sivritepe N. Asmalarda tuza dayanıklılık testleri ve tuza dayanımda etkili bazı faktörler üzerinde araştırmalar (Doctoral dissertation).

[63]. Shannon MC, Grieve CM. Tolerance of vegetable crops to salinity. Scientia horticulturae. 1998 Nov 30;78(1-4):5-38.

[64]. Chuang HW, Harnrak A, Chen YC, Hsu CM. A harpin-induced ethylene-responsive factor regulates plant growth and responses to biotic and abiotic stresses. Biochemical and biophysical research communications. 2010 Nov 12;402(2):414-20.

[65]. Ashraf M. Some important physiological selection criteria for salt tolerance in plants. Flora-Morphology, Distribution, Functional Ecology of Plants. 2004 Jan 1;199(5):361-76.

[66]. Yılmaz E, Tuna Al, Bürün B. Tolerance strategıes developed by plants to the effects of salt stress. Celal Bayar University Journal of Science. 2011;7(1):47-66.

[67]. Romero-Aranda R, Soria T, Cuartero J. Tomato plant-water uptake and plant-water relationships under saline growth conditions. Plant science. 2001 Jan 5;160(2):265-72.

[68]. Chen BH, Huang JH. Degradation and isomerization of chlorophyll a and β-carotene as affected by various heating and illumination treatments. Food Chemistry. 1998 Jul 1;62(3):299-307.

[69]. Verma S, Mishra SN. Putrescine alleviation of growth in salt stressed *Brassica juncea* by inducing antioxidative defense system. Journal of plant physiology. 2005 Jun 14;162(6):669-77.

[70]. Ahmad P, Jaleel CA, Sharma S. Antioxidant defense system, lipid peroxidation, proline-metabolizing enzymes, and biochemical activities in two Morus alba genotypes subjected to NaCl stress. Russian Journal of Plant Physiology. 2010 Jul;57(4):509-17.

[71]. Maia JM, Costa de Macedo CE, Voigt EL, Freitas JB, Silveira JA. Antioxidative enzymatic protection in leaves of two contrasting cowpea cultivars under salinity. Biologia Plantarum. 2010 Mar;54(1):159-63.

[72]. Zhang M, Fang Y, Ji Y, Jiang Z, Wang L. Effects of salt stress on ion content, antioxidant enzymes and protein profile in different tissues of *Broussonetia papyrifera*. South African journal of botany. 2013 Mar 1;85:1-9.

[73]. García-Caparrós P, Hasanuzzaman M, Lao MT. Oxidative stress and antioxidant defense in plants under salinity. Reactive Oxygen, Nitrogen and Sulfur Species in Plants: Production, Metabolism, Signaling and Defense Mechanisms. 2019 Jul 18:291-309.

[74]. Akbudak N, Tezcan H. Bitkisel üretimde ve bitki korumada yeni bir etken madde: Harpin. Uludağ Üniversitesi Ziraat Fakültesi Dergisi. 2006;20(2):39-43.

[75]. Kumar S, Li G, Yang J, Huang X, Ji Q, Liu Z, Ke W, Hou H. Effect of salt stress on growth, physiological parameters, and ionic concentration of water dropwort (*Oenanthe javanica*) cultivars. Frontiers in plant science. 2021;12.

[76]. Zhou X, Chen Y, Zhao Y, Gao F, Liu H. The application of exogenous PopW increases the tolerance of *Solanum lycopersicum* L. to drought stress through multiple mechanisms. Physiology and Molecular Biology of Plants. 2020 Dec;26(12):2521-35.

[77]. Ayna A, Tunc A, Özbolat SN, Bengü AŞ, Aykutoğlu G, Canli D, Darendelioğlu E. Anticancer, and antioxidant activities of royal jelly on HT-29 colon cancer cells and melissopalynological analysis. Turkish Journal of Botany, 2021; 45(SI-2), 809-819.

[78] Özbolat SN, Ayna A. Chrysin suppresses HT-29 cell death induced by diclofenac through apoptosis and oxidative damage. Nutrition and Cancer, 2021; 73(8), 1419-1428.

Araştırma Makalesi https://doi.org/10.46810/tdfd.1097511 Research Article

Türk Doğa ve Fen Dergisi
Turkish Journal of Nature and Science
www.dergipark.gov.tr/tdfd

# Evaluation of Mechanical Performance of a Fe-Mn-Si Biodegradable Stent using Finite Element Simulations

**Nazim BABACAN**[1*]

[1] Sivas Bilim ve Teknoloji Üniversitesi, Mühendislik ve Doğa Bilimleri Fakültesi, Makine Mühendisliği Bölümü, Sivas, Türkiye
Nazim BABACAN ORCID No: 0000-0003-2173-8656

**Corresponding author: nazimbabacan@sivas.edu.tr*

(Received: 02.04.2022, Accepted: 14.06.2022, Online Publication: 29.06.2022)

**Keywords**
Biodegradable Stent, Fe–Mn–Si Shape Memory Alloy, Finite Element Analysis, Mechanical Performance

**Abstract:** Biodegradable metal stents are potential stent candidates as they dissolve in the body over time after fulfilling their mechanical duties and therefore do not pose a risk in the future. Fe-30Mn-6Si biodegradable alloy was found to be successful in the previous studies in terms of mechanical strength and biodegradability. In this study, the expansion and recoiling behavior of a stent made of Fe-30Mn-6Si alloy was investigated using finite element analyses. L605 Co-Cr and 316L stainless steel stents were also examined for comparison. Obtained results showed that novel FeMnSi stent exhibits lower equivalent stress than the counterparts. On the other hand, the lowest equivalent plastic strain and the highest radial elastic recoil value were observed in FeMnSi stent. Overall findings indicate that FeMnSi stent is moderately successful in terms of balloon-stent interaction.



# Fe-Mn-Si Biyobozunur Stentlerin Mekanik Performansının Sonlu Eleman Simülasyonları Kullanılarak Değerlendirilmesi

**Anahtar Kelimeler**
Biyobozunur stent, Fe-Mn-Si Şekil Hafızalı Alaşım, Sonlu Eleman Analizi, Mekanik performans

**Öz:** Biyobozunur metal stentler, mekanik görevlerini yerine getirdikten sonra zamanla vücut içerisinde çözüldükleri ve bu nedenle gelecekte bir risk oluşturmadıkları için potansiyel stent adaylarıdır. Önceki çalışmalarda, Fe-30Mn-6Si biyobozunur alaşımı mekanik dayanım ve biyolojik olarak parçalanabilirlik açısından başarılı olduğu görülmüştür. Bu çalışmada, Fe-30Mn-6Si alaşımından yapılmış bir stentin genleşme ve geri tepme davranışı sonlu eleman analizleri kullanılarak incelenmiştir. Karşılaştırma için L605 Co-Cr ve 316L paslanmaz çelik stentler de incelenmiştir. Elde edilen sonuçlar, yeni FeMnSi stentinin muadillerine göre daha düşük eşdeğer gerilme sergilediğini göstermiştir. Öte yandan, en düşük eşdeğer plastik gerinim ve en yüksek radyal elastik geri tepme değeri FeMnSi stentte gözlenmiştir. Genel bulgular, FeMnSi stentin balon-stent etkileşimi bakımından orta düzeyde başarılı olduğunu göstermektedir.

## 1. INTRODUCTION

Stents are used to open up coronary artery blockages by providing a structural support. These meshed tubes are often deployed by a balloon which is expanded with a pressure and placed inside the diseased region of the artery. Large plasticity is required for a balloon-expandable stent material to minimize the elastic recoiling effect when it is released in the vessel [1]. Co-Cr based and 316L stainless steel are among the most frequently used metal stent alloys owing to high strength, plasticity and biocompatibility [2, 3].

In recent years, as alternative to these permanent stents, biodegradable stents, that are resolved after providing scaffolding and therefore, no need to further usage after the healing is completed, have been developing by the scientists [4-6]. These new-generation stent type does not allow long-term complications, such as chronic inflammation, and physical irritation caused by the usage of permeant stents and thus, prevent the possible secondary surgeries for stent removal [7, 8]. Among the metal biodegradable stents, Mg-based, Zn-based and Fe-based alloys are seen as the most popular ones. Due to the relatively higher strength and lower degradation rate, Fe-based alloys have several advantages over their counterparts, such as using thinner strut thickness and

maintaining mechanical integrity for a longer period of time [9-11].

In the recent studies, Fe-(28-30)Mn-(5-6)Si (wt%) shape memory alloys were seen as a potential biodegradable stent candidate as a result of some corrosion and mechanical tests [12-15] and thus, it would be useful to investigate its mechanical response when it is inflated by the balloon by comparing with the performance of other reference stent materials.

One of the efficient methods to study and investigate the mechanical behavior of the stents without performing expensive tests is finite element (FE) analysis [16]. Stress evaluation and the determining the critical regions over the entire part are also possible in this method which are quite beneficial for designing. Many researchers investigated the mechanical performance of the stents by examining the effect of different parameters such as strut geometries, material properties and radial pressure were investigated by utilizing from FE methods [17-19].

In this study, it is aimed to examine the mechanical performance of a Fe-30Mn-6Si stent involving the deployment and recoiling stages by FE simulations. Equivalent stress and plastic strain values during these steps as well as recoiling ratio for this stent material were obtained and these values were compared with those of Co-Cr based and 316L stainless steel stents for better evaluation.

## 2. MATERIAL AND METHODS

### 2.1. Finite Element Model

Solid model of the stent was generated by SolidWorks software. 2D sketch was wrapped around a cylinder whose diameter equals to the stent diameter in order to create 3D model. The diameter and the length of the stent are 4.07 and 15.72 mm, respectively. Strut thickness was chosen as 60 µm. 3D model and the 2D sketch of a single unit are seen in Figure 1. The length of the bridge that connects the single units is 0.76 mm.

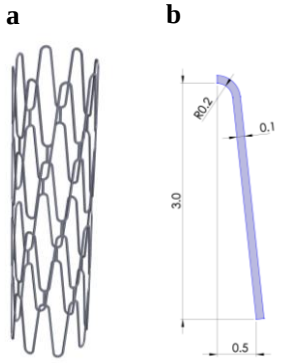


**Figure 1.** (a) Final 3D model of the stent, (b) Sketch for the single repeating unit of the design

A shell balloon element with a diameter of 3.85 mm and a thickness of 4 µm was added to the model. Since the stent geometry is symmetrical, 1/8 symmetry of the whole model was used to minimize the computational cost caused by excessive number of elements. FE model created by Ansys/Static Structural program is shown in Figure 2. The mesh of the stent was generated by hexagon dominant multizone method by defining the element size of 0.015 mm. Quadrilateral shell elements was used to create the balloon model and element size was chosen as 0.05 mm. The model consists of a total 65236 elements.

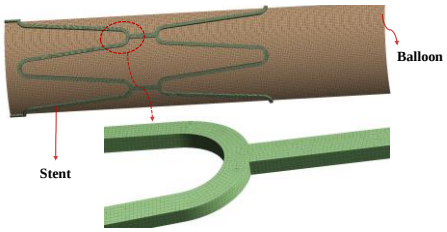


**Figure 2.** 1/8 symmetric finite element (FE) model. (A portion of the stent is magnified in the below to better view the FE mesh.)

A surface to surface frictionless contact between the interior surface of the stent and the exterior surface of the balloon was defined. Frictionless supports were applied from the surfaces as shown in Figure 3 as symmetry boundary conditions. 1 mm radial displacement was applied from the balloon surface as a loading and then, subsequently balloon was retracted to initial position.

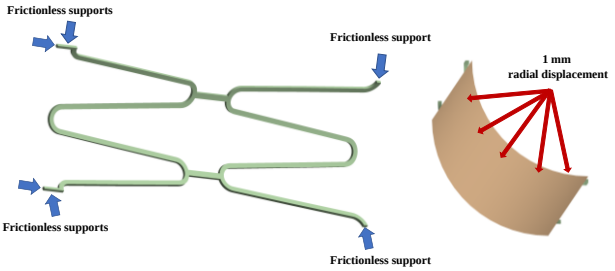


**Figure 3.** Applied boundary conditions in the FE model.

### 2.1. Material Properties

The balloon was assigned a Mooney-Rivlin hyperelastic material property. C10 and C01 material constants of Mooney-Rivlin 2 Parameter were defined as 1.06 and 0.114 MPa [20]. Multilinear isotropic hardening material model was used to define stent behaviors. While Mooney-Rivlin hyperelastic material model is suitable for materials that deform substantially elastically, multilinear isotropic hardening material model is very useful for alloys whose stress-strain data are obtained with experimental methods since it uses the plastic strain/yield stress points as data input. Stent material was chosen as Fe-30Mn-6Si, L605 Co-Cr and 316L stainless steel alloys in three different analyses. True stress-strain graphs in the literature (see Figure 4) were utilized to determine plastic strain-stress values and the material properties of the used alloys are shown in Table 1.

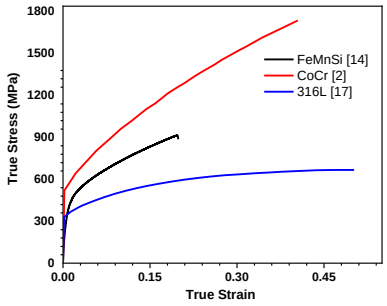


**Figure 4.** True stress-strain graphs adapted from literature to model Fe-30Mn-6Si, L605 Co-Cr and 316L stainless steel alloys

**Table 1**. Material properties of the alloys used as a stent material

| | FeMnSi [14] | L605 Co-Cr [2] | 316L [21] |
|---|---|---|---|
| **Young's Modulus (GPa)** | 120 | 240 | 201 |
| **Poisson's ratio** | 0.3 | 0.3 | 0.3 |
| **Yield Stress (MPa)** | 266 | 520 | 330 |

## 3. RESULTS AND DISCUSSION

### 3.1. Equivalent Stress Distribution

Von Mises (equivalent) stress distribution of three different stents, that are made of Fe-30Mn-6Si, L605 Co-Cr and 316L, after 1 mm radial displacement and springback stages are shown in Figure 5. Stress distributions seem to be independent from the material of the stent. While the maximum stress values are observed in Co-Cr stent, the minimum values are in FeMnSi stent both after loading and unloading. Stress concentrations occurred on the top and bottom surfaces of the crown radius parts after loading as seen in Figure 5(a, c and e). However, after unloading, i.e. after removing the balloon, there is no prominent stress values at the large portion of the stents and stress concentrations are seen in a very small region on the front and back side of the crown radius parts as exemplified by a highlighted image in Figure 5(b).

The stress values and distribution during the implantation of a stent is a critical parameter for a stent design. High stress that occurs in a large cross-section can be serious and the stent would fail. FeMnSi and 316L stents (as observed in Figure 5(a and c)) show lower stress values compared to Co-Cr stent. However, it should be noted that strength of Co-Cr alloy is relatively high and stress values do not exceed its ultimate tensile limit. Moreover, residual stress values at the outer surfaces of the stents are also important since high values can trigger corrosion [4, 22]. Therefore, low residual stress values seen in FeMnSi stent compared to its counterparts could be an advantage for it. Even though, biodegradable FeMnSi stent is desired to degrade by time, corrosion induced by stress concentration causes a non-homogenous degradation and breaks the integrity of the stent.



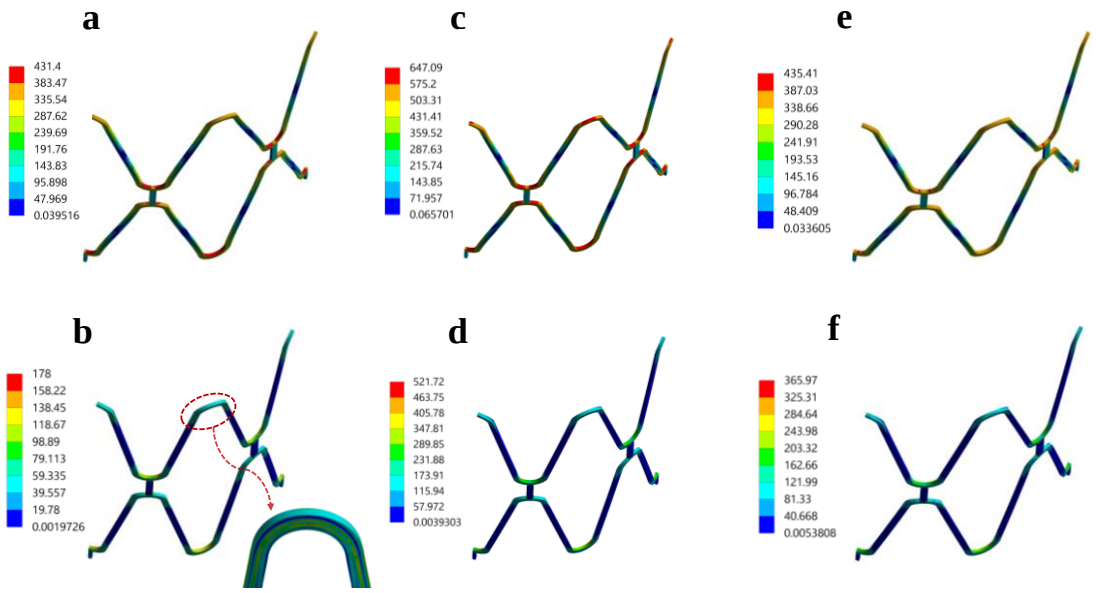


**Figure 5.** Equivalent stress distribution of (a, b) of Fe-30Mn-6Si, (c, d) L605 Co-Cr and (e, f) 316L stainless steel stents (a, c, e) after 1 mm radial displacement (b, d, f) after springback

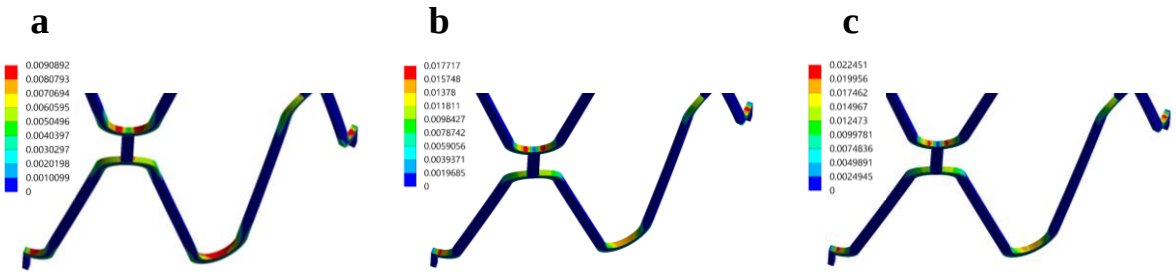


**Figure 6.** Equivalent plastic strain distribution of (a) Fe-30Mn-6Si, (b) L605 Co-Cr and (c) 316L stainless steel stents after 1 mm radial displacement

### 3.2. Equivalent Plastic Strain and Elastic Recoil

The equivalent plastic strains occurred after 1 mm radial deformation are presented in Figure 6 for all three stents. Since the plastic strains did not change after the expansion recoil, those results were not added. Plastification is found at the same regions where high stress values as seen in Figure 5(a, c and e). The highest plastic strains occurred in 316L stainless steel stent with a maximum value of 0.0224 mm/mm. Whereas, the maximum values of Co-Cr and FeMnSi stents are 0.0177 and 0.0091 mm/mm, respectively. Low elastic modulus value and the late onset of the plastic deformation in the FeMnSi stent resulted a lower plastic strain compared to other stents.

Plastic strains observed in the stents also influence the radial elastic recoil (ER) responses. Radial ER values were calculated and tabulated in Table 2 for each stent model by utilizing the FE results according to ASTM F2079-09 [23] as in Equation 1:

$$Radial\ ER = \frac{R_{load} - R_{unload}}{R_{load}}\ x\ 100\% \qquad (1)$$

where $R_{load}$ and $R_{unload}$ are the radius of the stent after the expansion and springback, respectively.

**Table 2**. Radial elastic recoil values for the analyzed stents

| Fe-30Mn-6Si | L605 Co-Cr | 316L |
|---|---|---|
| 17.05 % | 14.29 % | 10.90 % |

The highest elastic recoil value was obtained in the FeMnSi stent. It means that FeMnSi stent recovers more compared to other stents during the unloading and this behavior shows the higher flexibility of FeMnSi stent. Low plastic strain values seen in this stent is also related with the high elastic recoil behavior since these two responses have an opposite trend. Generally, a high value of elastic recoil is unfavorable for stent designs as the stent will not be exactly in the desired diameter in the final situation. However, there is no big difference between the degree of radial ER of the currently available L605 Co-Cr and potential Fe-30Mn-6Si stents. It should be mentioned that the radial ER values obtained in this study are higher than the design criteria (ER<4% [24]) of the stents. Nonetheless, a high value of expansion was applied in this study to see the mechanical strengths of the stents under extreme deformation and thus, higher radial ER values were obtained than the constraints. Therefore, it would be more sense to compare the ER values among the different stent materials not focusing the quantitative values.

## 4. CONCLUSIONS

In this study, mechanical response of the Fe-30Mn-6Si balloon expandable stent after the expansion and recoiling was investigated by using FE analyzes. The obtained equivalent stress and plastic deformation results as well as radial elastic recoil values for this stent were compared with those of L605 Co-Cr and 316L stainless steel stents.

The findings showed that lower stress values occurred in FeMnSi and 316L stents compared to Co-Cr stent. The lowest residual stress was seen in FeMnSi stent after recoiling which could be beneficial for the novel design due to the reduced risk of stress-induced corrosion. Owing to the lowest Young's modulus value and highest elasticity FeMnSi stent showed the lowest plastic strain and the highest radial elastic recoil compared to other stents. However, radial elastic recoil of the FeMnSi stent was found to be close to L605 Co-Cr stent. As a conclusion, the mechanical response of FeMnSi biodegradable stent was found to be promising by considering the balloon-stent interaction.

## REFERENCES

[1] Debusschere N, Segers P, Dubruel P, Verhegghe B, Beule M De. A finite element strategy to investigate the free expansion behaviour of a biodegradable polymeric stent. J Biomech. 2018;48(10):2012–8.

[2] Kumar A, Bhatnagar N. Finite element simulation and testing of cobalt-chromium stent: a parametric study on radial strength, recoil, foreshortening, and dogboning. Comput Methods Biomech Biomed Engin. 2021;24(3):245–59.

[3] Wang H, Wang X, Qian H, Lou D, Song M, Zhao X. The optimal structural analysis of cobalt-chromium alloy (L-605) coronary stents. Comput Methods Biomech Biomed Engin. 2021;24(14):1566–77.

[4] Galvin E, Brien DO, Cummins C, Donald BJ Mac, Lally C. A strain-mediated corrosion model for bioabsorbable metallic stents. Acta Biomater. 2017;55:505–17.

[5] Gu X, Mao Z, Ye SH, Koo Y, Yun Y, Tiasha TR, et al. Biodegradable, elastomeric coatings with controlled anti-proliferative agent release for magnesium-based cardiovascular stents. Colloids Surfaces B Biointerfaces. 2016;144:170–9.

[6] Xu C, Yin Z, Roy-Chaudhury P, Campos-Naciff B, Hou G, Schulz M. The development of a magnesium biodegradable stent: design, analysis, fabrication, and in-vivo test. Med Res Arch. 2020;8(9).

[7] Schinhammer M, Hänzi AC, Löffler JF, Uggowitzer PJ. Design strategy for biodegradable Fe-based alloys for medical applications. Acta Biomater. 2010;6(5):1705–13.

[8] Feng YP, Gaztelumendi N, Fornell J, Zhang HY, Solsona P, Baró MD, et al. Mechanical properties, corrosion performance and cell viability studies on newly developed porous Fe-Mn-Si-Pd alloys. J Alloys Compd. 2017;724:1046–56.

[9] Loffredo S, Paternoster C, Giguère N, Barucca G, Vedani M, Mantovani D. The addition of silver affects the deformation mechanism of a twinning-induced plasticity steel: Potential for thinner degradable stents. Acta Biomater. 2019;98:103–13.

[10] He J, He FL, Li DW, Liu YL, Liu YY, Ye YJ, et al. Advances in Fe-based biodegradable metallic materials. RSC Adv. 2016;6(114):112819–38.
[11] Donik Č, Kocijan A, Paulin I, Hočevar M, Gregorčič P, Godec M. Improved biodegradability of Fe–Mn alloy after modification of surface chemistry and topography by a laser ablation. Appl Surf Sci. 2018;453(March):383–93.
[12] Liu B, Zheng YF, Ruan L. In vitro investigation of Fe30Mn6Si shape memory alloy as potential biodegradable metallic material. Mater Lett. 2011;65(3):540–3.
[13] Drevet R, Zhukova Y, Malikova P, Dubinskiy S, Korotitskiy A, Pustov Y, et al. Martensitic Transformations and Mechanical and Corrosion Properties of Fe-Mn-Si Alloys for Biodegradable Medical Implants. Metall Mater Trans A. 2018;49(3):1006–13.
[14] Babacan N, Kochta F, Hoffmann V, Gemming T, Kühn U, Giebeler L, et al. Effect of silver additions on the microstructure, mechanical properties and corrosion behavior of biodegradable Fe-30Mn-6Si. Mater Today Commun. 2021;28(July):102689.
[15] Babacan N. Shape memory characteristics of silver-added Fe – 30Mn – 6Si Alloy. Trans Indian Inst Met. 2022;.
[16] Azaouzi M, Makradi A, Belouettar S. Numerical investigations of the structural behavior of a balloon expandable stent design using finite element method. Comput Mater Sci. 2013;72:54–61.
[17] Chen C, Xiong Y, Jiang W, Wang Y, Wang Z, Chen Y. Experimental and numerical simulation of biodegradable stents with different strut geometries. Cardiovasc Eng Technol. 2020;11(1):36–46.
[18] Kumar A, Bhatnagar N. Finite element simulation and testing of cobalt-chromium stent: a parametric study on radial strength, recoil, foreshortening, and dogboning. Comput Methods Biomech Biomed Engin. 2021;24(3):245–59.
[19] Britto JJJ, Venkatesh R, Prabhakaran R, Amudhan K. Design optimization of biomedical stent under the influence of the radial pressure using FEM. Mater Today Proc. 2021;39:1332–6.
[20] Cornell simulation YouTube channel [Internet] [cited 2022 May 20]. Available from: https://www.youtube.com/channel/UC8bXUXdcNDyFTIp6YVrtReg.
[21] Kim D-Y, Lee S-Y, Kim H-Y. Numerical evaluation and shape design of coronary artery stent. J Korean Soc Precis Eng. 2012;29(1):103–8.
[22] Chen Y, Shang X. Investigation on large elastoplastic deformation in expansion and springback for a composited bioresorbable stent. J Mech Behav Biomed Mater. 2021;119(February):104500.
[23] ASTM F2079-09(2017), Standard Test Method for Measuring Intrinsic Elastic Recoil of Balloon-Expandable Stents; ASTM International: West Conshohocken, PA, USA, 2017.
[24] Bowen PK, Drelich J, Goldman J. Zinc exhibits ideal physiological corrosion behavior for bioabsorbable stents. Adv Mater. 2013;25(18):2577–82.

Cilt 11, Sayı 2, Sayfa 156-160, 2022 Volume 11, Issue 2, Page 156-160, 2022

Derleme https://doi.org/10.46810/tdfd.995903 Review

Türk Doğa ve Fen Dergisi
Turkish Journal of Nature and Science
www.dergipark.gov.tr/tdfd

# Kanser Dostu MEIS Proteinleri

**Büşra ÇİMEN[1], Abdullah ASLAN[1*]**

[1] Fırat Üniversitesi, Fen Fakültesi, Biyoloji Bölümü, Moleküler Biyoloji ve Genetik Programı, Elazığ, Türkiye
Büşra ÇİMEN ORCID No: 0000-0003-3415-3390
Abdullah ASLAN ORCID No: 0000-0002-6243-4221

**Sorumlu yazar: aaslan@firat.edu.tr*

(Alınış: 15.09.2021, Kabul: 21.03.2022, Online Yayınlanma: 29.06.2022)

**Anahtar Kelimeler**
İnhibitör, Kanser, MEIS Proteini, Metastaz

**Öz:** Miyeloid kanser türünden ismini alan MEIS; enerji üretimini teşvik eden, ROS seviyelerini minimum düzeye indirmeye çalışan, kalp kası gelişim evresinde görev alan bir proteindir. Kanserli hücreler MEIS proteini metastaz için kullanmaktadır. MEIS proteini kanserli hücrelerde durdurmak amacıyla 'kanseri kendi silahıyla vurma' olarak tanımlanan MEIS protein inhibitörleri (MEISi) keşfedilmiştir. MEIS protein inhibitörleri göğüs ve pankreas gibi kanser türlerinden, %75 ve %95 gibi ciddi oranda kanserli hücrelerin yayılımını engellediği belirlenmiştir. Bu derlemede MEIS proteinlerinin; kanser türleri ve hastalıklar üzerindeki etkisi, MEIS inhibitörlerinin (MEISi) keşfi, kanser tedavisinde MEIS protein inhibitörlerinin önemiyle ilgili bilgilerden bahsedilmektedir.

# Cancer Friendly MEIS Proteins



**Keywords**
Cancer, Inhibitor, MEIS proteins, Metastasis

**Abstract:** MEIS, named after the type of myeloid cancer; It is a protein that promotes energy production, tries to minimize ROS levels, and takes part in the development phase of the heart muscle. Cancerous cells use the MEIS protein for metastasis. In order to stop the MEIS protein in cancerous cells, MEIS protein inhibitors (MEISi), which are defined as 'shooting the cancer with its own weapon', have been discovered. It has been determined that MEIS protein inhibitors prevent the spread of cancerous cells, such as 75% and 95%, from cancer types such as chest and pancreas. In this review, MEIS proteins; Information about the effects on cancer types and diseases, the discovery of MEIS inhibitors (MEISi), the importance of MEIS protein inhibitors in cancer treatment are mentioned.

## 1. GİRİŞ

Kanser; kontrolsüz hücre bölünmesi ve bölünme sonucunda meydana gelen hücrelerin yayılım göstermesi ile oluşan genel hastalıklara verilen isimdir. Moleküler seviyede kanserli hücreler kontrolsüz olarak bölünebilir fakat diğer doku ve hücrelere yayılma özelliği göstermeyebilir, bu tür tümörler bening\iyi huylu olarak isimlendirilmektedir. Cerrahi yöntemler ile tümörlü doku, normal dokudan ayrılabilmektedir. Primer dokuyu parçalayarak, lenf sistemi yardımıyla vücutta başka doku ve organlara ulaşabilen tümör hücreleri kanserleşmiştir ve malignant\kötü huylu tümör olarak isimlendirilmektedir. Bu tür tümör hücreleri, farklı doku tiplerinde sekonder tümör (metastaz) oluşturma özelliğine sahiptir. Kanser, gelişmiş ülkelerde kardiyovasküler hastalıklardan sonra ikinci sırada yer almaktadır. Kanser hastalığının öldürücü olması, kalıcı hasar meydana getirmesi (sakatlık vs) ve tedavilerinin yüksek maliyetli olması, ülke ekonomilerinde ağır kayıplara neden olmaktadır. Yapılan araştırmalarda önümüzdeki yıllarda ölüm sebepleri içerisinde kanser hastalığının birinci sırada yer alacağı tahmin edilmektedir. Dünya Sağlık Örgütü'nün araştırmalarına göre 2020'de her sene kanser hastalığı tanısı bırakılan kişi sayısı 17 milyon, 2030 senesinde 24 milyona ulaşacağı, 17 milyon kişinin aynı sene yaşamlarının sona ereceğini ve 2030'da ise 75 milyon kişinin kanser hastalığıyla yaşamlarını sürdüreceği tahmin edilmektedir [1].

Son beş yılda (2015-2019) dünyada 1 milyondan fazla kanserle ilgili çalışma yapılmıştır, fakat kanser hastalığına kesin bir çözüm bulunamamıştır. Bunun en büyük sebebi ise kanserli hücrelerin vücudumuzda bulunan faydalı proteinleri kendi menfaatlerine kullanmasıdır, bu proteinlerden biri MEIS proteinidir. Miyeloid kanser türünden ismini alan MEIS; enerji üretimini teşvik eden, ROS seviyelerini minimum

düzeye indirmeye çalışan bir proteindir. Ayrıca kalp kası gelişim evresinde de bu protein görev almaktadır. Kanserli hücreler MEIS proteini metastaz için kullanmaktadır [2]. MEIS proteinini kanserli hücrelerde durdurmak amacıyla 'kanseri kendi silahıyla vurma' olarak tanımlanan MEIS protein inhibitörleri (MEISi) Türk akademisyen Fatih KOCABAŞ tarafından keşfedilmiş ve bu çalışma Uluslararası Hemotoloji-Onkoloji ödülüne layık görülmüştür. Yapılan çalışmada MEIS protein inhibitörleri göğüs ve pankreas gibi kanser türlerinden, %75 ve %95 gibi ciddi oranda kanserli hücrelerin yayılımını engellediği belirtilmiştir. MEIS protein inhibitörleri ile ilgili çalışmalar hala devam etmekle birlikte, son zamanlarda kanserin yaylımını engelleyen heyecan verici bir buluş olarak değerlendirilmektedir [3].

### 1.1. MEIS 1 ve MEIS 2 Proteinleri

*MEIS 1*'in gen uzunluğu 137360 bp'dir, bu bölgede *MEIS 1*; LOC729348, LOC100507073, DNMT3AP1 (DNA metiltranferans 3A psödojen 1) ile beraber yer almaktadır. Kromozom üzerindeki MEIS 1 proteini 2p14 lokusunda bulunmaktadır [4]. MEIS 1 proteini 390 aminoasitten meydana gelmektedir, 43 KDa ağırlığına sahiptir. MEIS 1 (miyeloid ekotropik viral entegrasyon bölgesi 1), yapılan çalışmalar sonucunda miyeloid lösemi hücrelerinde viral entegrasyon bölgesi olarak belirtilmiştir. *MEIS 1* geni; homeobox genlerinin TALE ailesi sınıfında yer alan transkripsiyon faktörünü kodlamaktadır [5]. *MEIS 1*; PREP1, CREB1, GSK3, SALL4 gibi transkripsiyon faktörleri ile dolaylı veya doğrudan etkileşim içerisinde düzenlenmektedir [6]. MEIS 1 proteini; Hıf1a, SOX2, GATA1, CCND1, CCND3, PF4, ile farklılaşma ve çoğalma amacıyla etkileşim içerisindedir [7]. CREB proteinleri MEIS 1'in DNA'ya bağlanmasına yardımcı olmaktadır (CREB proteinlerine, GSK3 (Glikojen sentaz kinaz 3) proteinleri de eşlik etmektedir) [8]. MEIS 1 ile alakalı son 10 yılda yapılan çalışmalarda; kalp rejenerasyonunda, kök hücre fonksiyonu ve tümörgenezde önemli rollerinin olduğu belirtilmiştir [9]. N terminalindeki bağlanma alanlarından dolayı Pbx1 ve HOXA9 ile etkileşim içerisindedir. MEIS 1 TALE ailesinin üyesidir ve MEIS 2, MEIS 3'de bu ailenin diğer üyelerini oluşturmaktadır. MEIS 2 ve MEIS 3 proteinleri, MEIS 1 proteinine yüksek oranda benzerlik göstermektedir (MEIS 1 protein benzerlik oranı; MEIS 2 proteini için %83, MEIS 3 proteini için ise %66'dır) [10].

*MEIS 2* geni; homeobox genlerinin TALE ailesi sınıfında yer alan transkripsiyon faktörünü kodlamaktadır. *MEIS 2*; LOC110120842, LOC110120896, LOC110120905, LOC145845, MIR8063, CSNK1A1P1 ve C15orf41 ile aynı bölgede yer almaktadır. Ayrıca MEIS 2 proteini 15q14 kromozom lokusunda bulunmaktadır [11].

### 1.2. MEIS 1-MEIS 2 Proteinlerinin Etkileri ve Kanserle Olan İlişkileri

Embriyogenezde MEIS 1 proteini; hematopoez ve vasküler gelişimde, doğum sonrasında ise kemik iliğinde yer almaktadır [12]. Ayrıca bu protein; murin fetal karaciğerde, hematopoetik kök hücrelerde, fetal ve embriyonik dokularda, arka beyin –beyincikte, pankras adacıklarında, kolon, düz kas, ince bağırsakta, tükürük bezinde, uterusta, adrenal bezde, endometriyum gibi farklı doku tiplerinde bulunmaktadır [13].

MEIS 1 proteini hipoksi tümör markörleri olan Hif-1a ve Hif-2a ekspresyonunda pozitif olarak bir artışa sebep olmaktadır. Yapılan bir çalışmada MEIS 1 proteinin silinmesiyle, Hif-1a ve Hif-2a seviyelerinde azalma olduğu gözlemlenmiştir. Sonuç olarak ROS düzeylerinin ve apoptozun eş zamanlı olarak yükseldiği belirtilmiştir [9].

15q14 kromozomunda gerçekleşen delesyonlar bazı hastalıklara neden olmaktadır, örneğin; zihinsel engellilik, yüz dismorfizmi, konjenital kalp defekleri. Zihinsel engelli, yüz dismorfizmi ve konjenital kalp defekleri rahatsızlığı olan bazı hastalarda (toplam 23 hastada) yapılan çalışma sonucunda 15q14 kromozomu üzerinde bulunan *MEIS 2* geninin delesyona uğradığı ve *MEIS 2* genindeki delesyonun bu hastalıkların oluşumunda etkili olabileceği tahmin edilmektedir [14]. İnsan embriyonik kök hücrelerin (hESC) farklılaşmasına neden olan etkeni belirlemek amacıyla yapılan bir çalışmada CRISPR / CAS9 teknolojini kullanarak, embriyonik kök hücrelerde *MEIS 2* geni silinmiştir. Silinme sonrasında hESC'ler farklılaşma için uyarıldığında hemotopoez farklılaşmasında bozulmalar meydana geldiği gözlemlenmiştir. Sonuç olarak *MEIS 2*, *TAL1* genini hedefleyerek insan embriyonik kök hücrelerinin endotelyal hematopoetik geçişini düzenlediği belirtilmiştir [15]. Ayrıca farklı bir çalışmada MEIS 1 proteini lenfoblastik ve miyeloid lösemiden izole edilen kemik iliği hücrelerin ekspresyonunda artış gösterdiğinde, terminal farklılaşmanın bir uyarıcısı olan granülosit koloni uyarıcı faktörün etki mekanizmasını önlediği belirtilmiştir [16].

MEIS 1; HOXA7, HOXA9 ve HOXB3'ü eksprese eden hücre tiplerinde lösemi işlemini hızlandırmaktadır. NUP98-HOXA9 oluşturduğu kompleks MEIS 1 ile birlikte ifade edildiğinde, akut miyeloid lösemi oluşumu hızlandırmaktadır [17]. HOXA9 ve MEIS 1 kaspaz aracılı apoptoz oluşumunu ortadan kaldırabilmektedir [18].

MEIS 1'in küçük hücreli olmayan akciğer adenokarsinom kanser hücrelerindeki rolünü belirlemek için yapılan bir araştırmada MEIS 1'in, kanser hücrelerinin proliferasyonunu sınırlandırdığı ve kanser hücresinin proliferasyonunu kontrol edebilecek terapotik stretejiyi temsil edebileceği belirtilmiştir [19].

İnsan özofagus skuamöz karsinom hücre hattında (KYSE-30) *MEIS 1* geninin silinmesi sonucu hücredeki etkisinin araştırıldığı bir çalışmada ise silinen *MEIS 1* geninin KYSE-30 hücre hattında farklılaşmalara sebep olabileceği belirtilmiştir [20].

Omurgalılarda ürogenital kanal ve kolon dahil olmak üzere birçok vücut fonksiyonlarında görev alan HOXB13, prostat dokusunda da spesifik bir transkripsiyon faktörü olarak çalışmaktadır. HOXB13'de

tekrarlanan G84E gerçekleşen mutasyon prostat kanseri oluşum riskini arttırmaktadır. Prostat kanserinde HOXB13'de G8E4 mutasyonu sonucunda, MEIS 1 proteininin kanserli hücrelerdeki potansiyelini belirlemek amacıyla yapılan çalışmada; MEIS 1 proteininin HOXB13'ün ömrünün uzamasına, hücre proliferasyonu ve gen düzenlemesinde HOXB13'ün kanser teşvik edici etmenlerine yardımcı olduğu belirtilmiştir [21].

MEIS 1 proteini; pankreas kanseri hücrelerinde metastatik hücre yapışma molekülü olan Mcam'ın aktive etmede etkin rol oynamaktadır. Patel ve ark. [22] yaptıkları çalışmada; MEIS 1 proteinin ID1 aktivasyonu yoluyla malign periferik sinir kılıfı tümörlerinin ilerlemesi ve hayatta kalması konusunda yardımcı olduğu belirtilmiştir. Yokoyama ve ark. [23] yapmış oldukları farklı bir çalışmada ise; MEIS 1, Sytl1 ekspresyonunun artmasını sağlayarak lösemi hücrelerinin gelişimini sağladığı gözlemlenmiştir (Sytl1, CXCR4'ün hücre içi trafiğini belirlemektedir).

Fare lösemi dokusunda MEIS 2 protein miktarının yüksek olduğu belirlenmiştir. Transkripsiyon faktörü olan AML1-ETO'nun Run bölgesine MEIS 2 proteini sıkıca bağlanarak akut miyeloid lösemiyi (AML) tetiklediği yapılan çalışmalarla gösterilmiştir [24].

PTBP1, kolorektal ve böbrek gibi birçok farklı kanser türlerinde yüksek miktarda bulunmaktadır, ayrıca kanserin ilerlemesini de kolaylaştırmaktadır. PTBP1'in LN metastatik mesane kanserindeki etkisi belirlemek amacıyla Xie ve ark. [25] yaptıkları çalışmada, mesane kanserinin ilerlemesi aşamasında PTBP1'in katkısı olduğu, ayrıca MEIS 2 ve PKM'nin PTBP1 etkisiyle mesane kanserinin ilerlemesine katkıda bulunduğu sonucuna varılmıştır.

Denizkestanelerinin gelişim evresinde *foxQ2* geni önemli görevleri bulunmaktadır. Yaguchi ve ark. [26] yaptıkları çalışmada MEIS transkripsiyon faktörünün; *foxQ2* geninin ekspresyonunu koruyarak, nöroektoderm spesifikasyon\ farklılaşma aşamasını düzenlediği ve böylece denizkestanesinin türü olan Hemicentrotus *pulcherrimus'*un embriyo gelişiminde, ön- arka vücut ekseni oluşumuna katkı sağladığı belirtilmiştir.

Huzursuz bacak sendromu (Restless Legs Syndrom:RLS) sinir sistemi hastalıklarından birisidir. Genellikle akşam-geceleri bacaklarda ciddi olarak rahatsız edici ağrılara neden olmaktadır. Çoğul gebelik, böbrek hastalığı ve demir eksikliği anemisi RLS hastalığı görülme riskini arttırdığı tahmin edilmektedir. 2007 yılında büyük oranda yapılan çalışmalar sonucunda RLS hastalığıyla ilgili üç genomik bölge tanımlanmıştır. Bunlar; MEIS1, BTBD9 ve MAP2K5/SKOR1 bölgeleridir. RLS hastalığında MEIS 1'in etkisini belirlemek amacıyla yapılan çalışma sonucunda; MEIS 1 ve SKOR 1 arasında bağlantı olduğu, bu bağlantının RLS hastalığının gelişimine katkı sağladığı tahmin edilmektedir [27].Transkripsiyon faktörleri; tüm hücrelerde bulunan genlerin kontrolünden sorumludur, birçok protein kompleksleriyle birlikte çalışmaktadır. Çocukluk ve ergenlik döneminde sıklıkla görülen kemik tümörlerinden biri Ewing sarkoma hastalığıdır. Ewing sarkom hastalığına neden olan 'EWS-FLI1' olarak adlandırılan transkripsiyon faktörlerine sahip, sadece kemik tümöründe bulunan bir proteindir. Yapılan araştırmalarda MEIS 1 proteini transkripsiyonel düzenlemede EWS-FLI1 ile birlikte çalışarak, Ewing sarkoma hücrelerinin hayatta kalma konusunda yardımcı olan, süper güçlendirici bir onkogen olarak tanımlanmıştır [28]. Rett sendromu farklı nörolojik bozukluklar sonucu oluşan nörogelişimsel bir hastalıktır. Rett sendromu hastalarında; dil ve el kullanım becerilerinde gerileme, epilepsi, apraksik yürüme, zihinsel engellilik, otizm spektrum bozukluğu, solunumda sıkıntı, gastrointestinal sorunlar, skolyoz ve otonomik disfonksiyon, uyku bozukluğu gibi etkiler görülmektedir. Srivastava ve ark. [29] yapmış oldukları çalışmada *MEIS 2* genindeki bozukluklar Rett sendromunda olduğu gibi, otizm spektrum bozukluğu ve bozulmuş uyku düzenine neden olabileceği belirtilmiştir. Giliberti ve ark. [30] yapmış oldukları çalışmada ise; 10 yaşındaki erkek çocuğunda *MEIS 2* geninin mutasyona uğradığı ve bunun sonucunda da, nörogelişimsel bozukluklara olabileceği tahmin edilmektedir.

### 1.3. MEIS Protein İnhibitörleri (MEISi)

MEIS proteinin DNA'ya bağlanma özelliği bulunmaktadır. Kanserli hücreler DNA'ya bağlanan MEIS proteini sayesinde yayılım göstermektedir. MEIS protein inhibitörleri Fatih Kocabaş tarafından keşfedilmiştir [2].



Hedefe yönelik bir ilaç olarak tasarlanan bu moleküller (MEISi), DNA ile MEIS proteini arasındaki etkileşimi zayıflatarak kanserli hücrelerin yayılımını engellemektedir. Ayrıca MEIS proteinlerinin inhibitörleri hücre zarından geçebilme özelliği olan ve etkileşimini hücre içerisinde gösteren bir yapıya sahiptir. MEISi'leri; fare deneylerinde, ex vivo deneylerde insanların kordon kanında bulunan ve in vivo klinik araştırmalarda MEIS proteinlerinin inhibisyonunda etkili olarak hemotopoetik kök hücre ekspresyonunu arttırdığı, *P21, Hif1a* ve *Hif2a* genlerinin oranlarında düşme sağlayan ve MEIS proteinlerinin (MEIS 1, MEIS 2, MEIS 3) transkripsiyonel aktivasyonlarını önleyen kombinasyonu olarak tanımlanmaktadır. Bu inhibitörlerin bulunması aşamasında birçok farklı çalışmalar gerçekleştirilmiştir. Homeobox ailesi inhibitörlerinin kütüphanesi oluşturulmuştur, Autodock Vina ve PaDEL-ADV kullanılarak MEIS homedomain proteinine karşı silicoda milyonlarca küçük molekül taranmıştır. Ayrıca PubChem biyotahlil analiziyle sitotoksit ve kardiyotoksisiye sahip olmayan MEISi'nin belirlenmesini kolaylaştırmıştır [31].

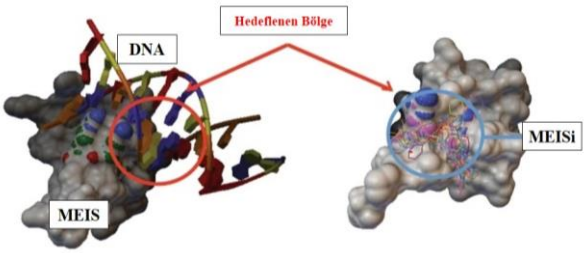


**Şekil 1.** MEIS-DNA etkileşim bölgesi ve MEISi ile engellenmesi [30].

MEIS inhibitörleri, yan etkisinin olup olmadığını gözlemlemek için ilk olarak fare üzerinde denenmiştir. Deney sonucunda herhangi bir sorun ile karşılaşılmamıştır. Ayrıca farelerin kök hücrelerini çoğalttığı gözlemlenmiştir [2]. Bulunan MEISi'lerinin kanser hücrelerinin yayılımına olan etkisini belirlemek amacıyla, özellikle MEIS proteinlerini kullanarak yayılım gösteren göğüs ve pankreas kanseri hücreleri üzerinde ilk olarak denenmiştir. Göğüs kanseri hücrelerini (T47D) %75 oranında yayılımını azalttığı, pankreas kanseri hücrelerinde (BxPC-3) ise %95 oranında yayılımını azalttığı belirtilmiştir. Fatih Kocabaş MEISi buluşunun ardında İsveç'te bulunan Uluslararası Hemotoloji- Onkoloji Derneği tarafından ödüle layık görülen ilk Türk akademisyen olmuştur [3].

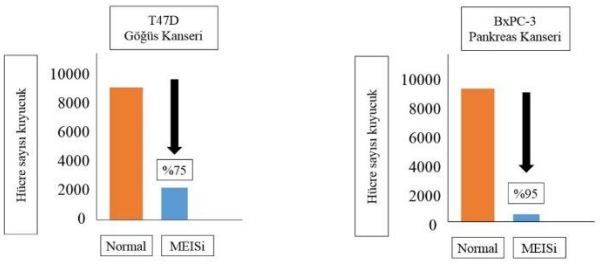


**Şekil 2.** MEISi'lerinin göğüs ve pankreas hücre yayılımına etkisi [3].

## SONUÇ

Fatih Kocabaş'ın MEIS protein inhibitörleri buluşunun ardından bu ürünü geliştirme amacıyla 'TÜBİTAK Genç Bireysel Girişim' 'TTGV' ve 'BIG BANG' yarışmalarında ''MEINOX ilaç teknolojisi'' isimli iş fikri ile katılmış ve kabul edilmiştir. Kocabaş ve ekibi; AR&GE çalışmasını ÜR&GE çalışmaları ile devam ettirerek bu çalışmanın yapılabilirliğini ve maliyet değerinin belirlenmesini amaçlamaktadır. Ayrıca bağımsız bilim insanlarının çalışmalarında kullanması amacıyla MEISi satışının yapılması planlamaktadır, böylece ÜR&GE çalışmalarına fon sağlanmış olacak ve katma değerinin ülkemizde kalacağı için ekonomiye katkısının olacağı düşünülmektedir [3].

Dünyada ölüm nedenleri içerisinde ikinci sırada yer alan kanser hastalığının metastaz oluşturmasını engellemek amacıyla geliştirilen bu inhibitörler, ilerde birçok farklı kanser türleri üzerindeki etkileri araştırılarak kanser alanındaki çalışmalarda çok önemli gelişmelere neden olacağı, ayrıca MEISi farklı hastalıklar üzerindeki etkisinin araştırılması planlanmaktadır.

## Bilgi

Bu derleme Fırat Üniversitesi Fen Bilimleri Enstitüsü Bünyesinde Biyoloji Bölümü, Moleküler Biyoloji Anabilim Dalında yüksek lisans semineri kapsamında sözlü olarak sunulmuştur.

## KAYNAKLAR

[1] Horozoğlu M. Uzman sistemler kullanılarak over (yumurtalık) kanseri tespiti. Selçuk Üniversitesi Fen Bilimleri Enstitüsü,Yüksek Lisans Tezi, Konya.; 2018.
[2] Kocabaş F, et al. Identfication of cardiogenic and hematopoetic MEIS Inhibitors. Poster SessionI-Basic Science-Cardiac Biology and Physiology, Session held on 20 april P69.; 2018.
[3] İnternet; 2021; Kasım 11. Erişim adresi: https://www.youtube.com/watch?v=zMpAnW9N6R4
[4] Sitwala KV, et al. HOX proteins and leukemia. Int J Clin Exp Pothol. 2008;1, 461-474.
[5] Crist RC, et al. A conserved tissue-specific homeodomain-less isoform of MEIS 1 is downregulated in colorectal cancer. Plos One. 2011;6, 1-7.
[6] Morgado E, et al. Flt3 is dispensable to the HOXA9/MEIS 1 leukemogenic cooperation. American Society of Hematology. 2007;109, 4020-4022.
[7] Wong P, et al. MEIS 1 İs an essential and rate-limiting regulator of MLL leukemia stem cell potential. Genes Dev. 2007;21, 2762-2774.
[8] Wang Z, et al. GSK-3 promotes conditional association of CREB and its coactivators with MEIS1 to facilitate HOX-mediated transcription and oncogenesis. Cancer Cell. 2010;17, 597-608.
[9] Kocabaş F, et al. Development of Small Molecule MEIS Inhibitors that modulate HSC activity. Scientific Reports. 2020; 10, 1-17.
[10] Aksöz M, et al. Emerging roles of MEIS 1 cardias regeneration stem cells and cancer. Current Drug Targets. 2018;19, 181-190.
[11] Louw J, et al. MEIS 2 Involvement in Cardiac Development, Cleft Palate, and Intellectual Disability. Amerıcan journal of medical genetics. 2015; 5, 1142-1146.
[12] Svingen T, et al. Altered HOX gene expression in human skin and breast cancer cells. Cancer Biology Therapy. 2003; 2, 518-23.
[13] Owens BM, et al. Hox and non-hox homeobox genes in leukemic hematopoiesis. Stem Cell. 2002; 20, 364-79.
[14] Verheije R, et al. Heterozygous loss-of-function variants of MEIS 2 cause a triad of. European Journal of Human Genetics. 2018;27, 278-290.
[15] Wang M, et al. MEIS 2 regulates endothelial to hematopoietic transition of human embryonic stem cells by targeting TAL 1. Stem Cell Research & Therapy. 2018;9, 1-13.
[16] Calvo KR, et al. MEIS 1a suppresses differentiation by G-CSF and promotes proliferation by SCF: potential mechanisms of cooperativity with Hoxa9

in myeloid leukemia. Proc Natl Acad Sci USA. 2001;23,13120-13125.
[17] Kroon E, et al. Defining roles for HOX and MEIS 1 genes in induction of acute myeloid leukemia. Mol Cell Biol. 2001;21, 224-234.
[18] Wermuth PJ, et al. MEIS 1-mediated apoptosis is caspase dependent and can be suppressed by coexpression of HOXA9 in murine and human cell lines. Blood. 2005;105, 1222-1230.
[19] Li W, Huang K, Guo H and Cui G. MEIS 1 regulates proliferation of non-small-cell lung cancer cells. J Thorac Dis. 2014; 6, 850-855.
[20] Mahmoudian RA, Bahadori B, Rad A, Abbaszadegan MR and Forghanifard MM. MEIS 1 knockdown may promote differentiation of esophageal squamous carcinoma cell line KYSE-30. Mol Genet Genomic Med. 2019; 7, 1-8.
[21] Johng D, et al. HOXB13 interaction with MEIS 1 modifies proliferation and gene expression in prostate cancer. Wıley The Prostate. wileyonlinelibrary.com/journal/pros. 2018.; 1-11.
[22] Patel Av, et al. An shrna screen ıdentifies MEIS 1 as a driver of malignant peripheral nerve sheath tumors. Ebiomedicine. 2016;9, 110- 119.
[23] Yokoyama T, et al. MEIS 1-mediated transactivation of synaptotagmin-like 1 promotes CXCL12/CXCR4 signaling and leukemogenesis. The Journal of Clinical Investigation. 2016;126, 1664-1678.
[24] Vegi NM, et al. MEIS 2 ıs an oncogenic partner in aml1-eto-positive aml. Cell Reports. 2016;16, 498-507.
[25] Xie R, et al. Polypyrimidine tract binding protein 1 promotes lymphatic metastasis and proliferation of bladder cancer via alternative splicing of MEIS 2 and PKM. Cancer Cell. 2019;449, 31-44.
[26] Yaguchi J, et al. MEIS transcription factor maintains the neurogenic ectoderm and regulates the anterior-posterior patterning in embryos of a sea urchin Hemicentrotus Pulcherrimus. Developmental Biology. 2018;444, 1–8.
[27] Catoire H, et al. A direct interaction between two restless legs syndrome predisposing genes: MEIS 1 And SKOR 1. Scientific Reports. 2018; 8, 1-9.
[28] Lin L, et al. Super-enhancer-associated MEIS 1 promotes transcriptional dysregulation in ewing sarcoma in co-operation with EWS-FLI1. Nucleic Acids Research. 2018.;1-13,Doi: http://creativecommons.org/licenses/by/4.0,
[29] Srivastava S, et al. Monogenic disorders that mimic the phenotype of rett syndrome. Neurogenetics. 2018;19, 41-47.
[30] Giliberti A, et al. MEIS 2 gene is responsible for intellectual disability cardiac defects and a distinct facial phenotype.2019.;Doi: https://doi.org/10.1016/j.ejmg.2019.01.017.
[31] Kocabaş F, et al. *Hematopoietic and cardiogenic MEIS ınhibitors that enhance cellular proliferation and HDR gene expression*. 5th International Congress of the Molecular Biology Association of Turkey (MolBiyoKon'17). 2017.; 8-10 September, Istanbul.